TATION PAGE

Form Approved
OMB No. 0704-0188

1. AGENCY USE ONLY (Leave blank)	2. REPORT DATE	3. REPORT TYPE AND DATES COVERED
	July 1994	Technical Report Mar 1990-Jul 1994

4. TITLE AND SUBTITLE

Omega Navigation System Course Book Vol I

5. FUNDING NUMBERS

23
DTCG-89-C-20008
Task Orders 90-0002, 91-0002, and 92-0004

6. AUTHOR(S)

P.B. Morris, R.R. Gupta, R.S. Warren, and P.M. Creamer

7. PERFORMING ORGANIZATION NAME(S) AND ADDRESS(ES)

TASC
55 Walkers Brook Drive
Reading, MA 01867

8. PERFORMING ORGANIZATION REPORT NUMBER

9. SPONSORING/MONITORING AGENCY NAME(S) AND ADDRESS(ES)

U.S. Department of Transportation
U.S. Coast Guard Navigation Center
7323 Telegraph Road
Alexandria, VA 22315

10. SPONSORING/MONITORING AGENCY REPORT NUMBER

2-D-5

11. SUPPLEMENTARY NOTES

12a. DISTRIBUTION/AVAILABILITY STATEMENT

NTIS Approved for Public Release
Distribution is Unlimted

12b. DISTRIBUTION CODE

13. ABSTRACT *(Maximum 200 words)*

This self-contained book on the Omega Navigation System is intended to provide theoretical and operational information needed by NAVCEN personnel to manage and maintain the Omega System. The book is composed of 13 chapters and seven appendices and can be used as a self-paced learning aid or in a classroom course environment. The course material addresses all major components of the Omega System, with emphasis placed on signal structure and utilization. Topics covered in the book include: Omega background, signal generation, navigation and propagation principles, operations, system performance evaluation, system utilization, and the future role of Omega in conjunction with other radionavigation systems. Several appendices are included to provide further detail on the material contained in the chapters.

14. SUBJECT TERMS		15. NUMBER OF PAGES
Omega History	Transmitting Stations	820
Signal Propagation	Navigation Principles	16. PRICE CODE
System Performance	Observed Signal Behavior	

17. SECURITY CLASSIFICATION OF REPORT	18. SECURITY CLASSIFICATION OF THIS PAGE	19. SECURITY CLASSIFICATION OF ABSTRACT	20. LIMITATION OF ABSTRACT
UNCLASSIFIED	UNCLASSIFIED	UNCLASSIFIED	UL

GENERAL INSTRUCTIONS FOR COMPLETING SF 298

The Report Documentation Page (RDP) is used in announcing and cataloging reports. It is important that this information be consistent with the rest of the report, particularly the cover and title page. Instructions for filling in each block of the form follow. It is important to ***stay within the lines*** to meet ***optical scanning requirements***.

Block 1. Agency Use Only *(Leave blank)*.

Block 2. Report Date. Full publication date including day, month, and year, if available (e.g. 1 Jan 88). Must cite at least the year.

Block 3. Type of Report and Dates Covered. State whether report is interim, final, etc. If applicable, enter inclusive report dates (e.g. 10 Jun 87 - 30 Jun 88).

Block 4. Title and Subtitle. A title is taken from the part of the report that provides the most meaningful and complete information. When a report is prepared in more than one volume, repeat the primary title, add volume number, and include subtitle for the specific volume. On classified documents enter the title classification in parentheses.

Block 5. Funding Numbers. To include contract and grant numbers; may include program element number(s), project number(s), task number(s), and work unit number(s). Use the following labels:

C	- Contract	**PR**	- Project
G	- Grant	**TA**	- Task
PE	- Program Element	**WU**	- Work Unit Accession No.

Block 6. Author(s). Name(s) of person(s) responsible for writing the report, performing the research, or credited with the content of the report. If editor or compiler, this should follow the name(s).

Block 7. Performing Organization Name(s) and Address(es). Self-explanatory.

Block 8. Performing Organization Report Number. Enter the unique alphanumeric report number(s) assigned by the organization performing the report.

Block 9. Sponsoring/Monitoring Agency Name(s) and Address(es). Self-explanatory.

Block 10. Sponsoring/Monitoring Agency Report Number. *(If known)*

Block 11. Supplementary Notes. Enter information not included elsewhere such as: Prepared in cooperation with...; Trans. of...; To be published in.... When a report is revised, include a statement whether the new report supersedes or supplements the older report.

Block 12a. Distribution/Availability Statement. Denotes public availability or limitations. Cite any availability to the public. Enter additional limitations or special markings in all capitals (e.g. NOFORN, REL, ITAR).

- **DOD** - See DoDD 5230.24, "Distribution Statements on Technical Documents."
- **DOE** - See authorities.
- **NASA** - See Handbook NHB 2200.2.
- **NTIS** - Leave blank.

Block 12b. Distribution Code.

- **DOD** - Leave blank.
- **DOE** - Enter DOE distribution categories from the Standard Distribution for Unclassified Scientific and Technical Reports.
- **NASA** - Leave blank.
- **NTIS** - Leave blank.

Block 13. Abstract. Include a brief *(Maximum 200 words)* factual summary of the most significant information contained in the report.

Block 14. Subject Terms. Keywords or phrases identifying major subjects in the report.

Block 15. Number of Pages. Enter the total number of pages.

Block 16. Price Code. Enter appropriate price code *(NTIS only)*.

Blocks 17. - 19. Security Classifications. Self-explanatory. Enter U.S. Security Classification in accordance with U.S. Security Regulations (i.e., UNCLASSIFIED). If form contains classified information, stamp classification on the top and bottom of the page.

Block 20. Limitation of Abstract. This block must be completed to assign a limitation to the abstract. Enter either UL (unlimited) or SAR (same as report). An entry in this block is necessary if the abstract is to be limited. If blank, the abstract is assumed to be unlimited.

OMEGA NAVIGATION SYSTEM COURSE BOOK

Volume I

U.S. COAST GUARD
OMEGA NAVIGATION SYSTEM CENTER

OMEGA NAVIGATION SYSTEM COURSE BOOK

Peter B. Morris
Radha R. Gupta
Ronald S. Warren
Paul M. Creamer

TASC
55 Walkers Brook Drive
Reading, Massachusetts 01867

July 1994

Document is available to the U.S. public through the
National Technical Information Service
Springfield, Virginia 22161

Prepared for

U.S. DEPARTMENT OF TRANSPORTATION
UNITED STATES COAST GUARD
Navigation Center
Alexandria, Virginia 22310

TECHNICAL REPORT DOCUMENTATION PAGE

1. REPORT NO.	2. GOVERNMENT ACCESSION NO.	3. RECIPIENT'S CATALOG NO.

4. TITLE AND SUBTITLE	5. REPORT DATE
Omega Navigation System Course Book	July 1994
	6. PERFORMING ORGANIZATION CODE TASC
7. AUTHOR(S) P.B. Morris, R.R. Gupta, R.S. Warren, and P.M. Creamer	8. PERFORMING ORGANIZATION REPORT NO.
9. PERFORMING ORGANIZATION NAME AND ADDRESS TASC 55 Walkers Brook Drive Reading, MA 01867	10. WORK UNIT NO. (TRAIS)
	11. CONTRACT OR GRANT NO. DTCG-89-C-20008 Task Orders 90-0002, 91-0002, and 92-0004
12. SPONSORING AGENCY NAME AND ADDRESS U.S. Department of Transportation U.S. Coast Guard Navigation Center 7323 Telegraph Road Alexandria, VA 22310	13. TYPE OF REPORT AND PERIOD COVERED Technical Report March 1990–July 1994
	14. SPONSORING AGENCY CODE

15. SUPPLEMENTARY NOTES

16. ABSTRACT

This self-contained book on the Omega Navigation System is intended to provide theoretical and operational information needed by NAVCEN personnel to manage and maintain the Omega System. The book is composed of 13 chapters and seven appendices and can be used as a self-paced learning aid or in a classroom course environment. The course material addresses all major components of the Omega system, with emphasis placed on signal structure and utilization. Topics covered in the book include: Omega background, signal generation, navigation and propagation principles, operations, system performance evaluation, system utilization, and the future role of Omega in conjunction with other radionavigation systems. Several appendices are included to provide further detail on the material contained in the chapters.

17. KEY WORDS		18. DISTRIBUTION STATEMENT
Omega History	Observed Signal Behavior	Document is available to the U.S. public through the National Technical Information, Springfield, Virginia 22161
Signal Propagation	System Synchronization	
System Performance	Data Analysis	
Transmitting Stations	Signal Phase Prediction	
Navigation Principles	Navigation Receivers	

19. SECURITY CLASSIF. *(Of This Report)*	20. SECURITY CLASSIF. *(Of This Page)*	21. NO. OF PAGES	22. PRICE
Unclassified	Unclassified		

F910 6/21/88

NOTICE

This document is disseminated under the sponsorship of the Department of Transportation in the interest of information exchange. The United States Government assumes no liability for its contents or use thereof.

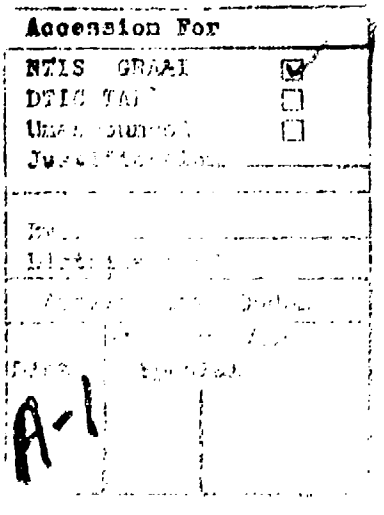

METRIC CONVERSION FACTORS

Approximate Conversions to Metric Measures

Symbol	When You Know	Multiply by	To Find	Symbol
		LENGTH		
in	inches	*2.5	centimeters	cm
ft	feet	30	centimeters	cm
yd	yards	0.9	meters	m
mi	miles	1.6	kilometers	km
		AREA		
in^2	square inches	6.5	square centimeters	cm^2
ft^2	square feet	0.09	square meters	m^2
yd^2	square yards	0.8	square meters	m^2
mi^2	square miles	2.6	square kilometers	km^2
	acres	0.4	hectares	ha
		MASS (weight)		
oz	ounces	28	grams	g
lb	pounds	0.45	kilograms	kg
	short tons (2000 lb)	0.9	tonnes	t
		VOLUME		
tsp	teaspoons	5	milliliters	ml
Tbsp	tablespoons	15	milliliters	ml
fl oz	fluid ounces	30	milliliters	ml
c	cups	0.24	liters	l
pt	pints	0.47	liters	l
qt	quarts	0.95	liters	l
gal	gallons	3.8	liters	l
ft^3	cubic feet	0.03	cubic meters	m^3
yd^3	cubic yards	0.76	cubic meters	m^3
		TEMPERATURE (exact)		
°F	Fahrenheit temperature	5/9 (after subtracting 32)	Celsius temperature	°C

*1 in = 2.54 (exactly). For other exact conversions and more detailed tables, see NBS Misc. Publ. 286, Units of Weights and Measures, Price $2.25, SD Catalog No. C13.10:286.

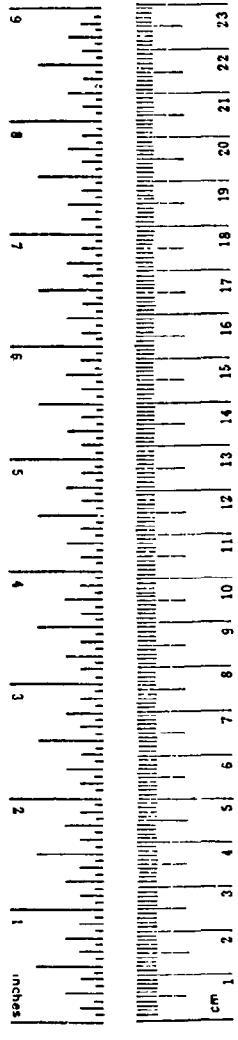

Approximate Conversions from Metric Measures

Symbol	When You Know	Multiply by	To Find	Symbol
		LENGTH		
mm	millimeters	0.04	inches	in
cm	centimeters	0.4	inches	in
m	meters	3.3	feet	ft
m	meters	1.1	yards	yd
km	kilometers	0.6	miles	mi
		AREA		
cm^2	square centimeters	0.16	square inches	in^2
m^2	squars meters	1.2	square yards	yd^2
km^2	square kilometers	0.4	square miles	mi^2
ha	hectares (10,000 m^2)	2.5	acres	
		MASS (weight)		
g	grams	0.035	ounces	oz
kg	kilograms	2.2	pounds	lb
t	tonnes (1000 kg)	1.1	short tons	
		VOLUME		
ml	milliliters	0.03	fluid ounces	fl oz
l	liters	2.1	pints	pt
l	liters	1.06	quarts	qt
l	liters	0.26	gallons	gal
m^3	cubic meters	35	cubic feet	ft^3
m^3	cubic meters	1.3	cubic yards	yd^3
		TEMPERATURE (exact)		
°C	Celsius temperature	9/5 (then add 32)	Fahrenheit temperature	°F

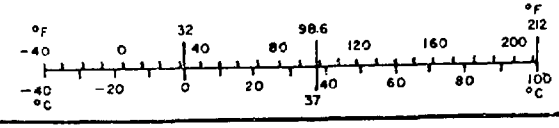

FOREWORD

This Omega Navigation System Course Book was prepared by TASC for the United States Coast Guard Navigation Center (USCG NAVCEN), Alexandria, VA under Contract DTCG23-89-C-20008, Task Orders 90-0002, 91-0002, and 92-0004. The course material was prepared over the period 1990-1994 in collaboration with Omega System specialists from NAVCEN. In the month that the final version of the Omega Course Book was published (July 1994), the name NAVCEN replaced the older name, ONSCEN (Omega Navigation System Center), which appears throughout the text of this book. Readers unfamiliar with the recent history of the Coast Guard administration of navigation programs should be aware of this name change when perusing the course material.

The principal authors of this Omega Course Book are from TASC: Peter B. Morris, who wrote Chapters 2, 3, 7, 8, 9, 11, and 12; Radha R. Gupta, who prepared Chapters 5 and 10; Ronald S. Warren, author of Chapters 1 and 4; and Paul M. Creamer, who wrote Chapter 13. These authors are also the primary contributors to Appendices A through G which follow the 13 chapters. Special recognition is given to long-time Omega researcher Eric R. Swanson who authored Chapter 6. Recognition is also extended to Joseph A. D'Appolito of TASC who wrote the appendix on Kalman filtering and David P. Frank, also of TASC, who contributed to Chapters 7 and 8. The text editing, graphics support, and formatting of the book were scrupulously overseen by Frances C. Sansalone of TASC. Finally, the authors wish to recognize the invaluable assistance and support of Vinicio Vannicola and other members of the NAVCEN staff who helped to make this book a reality.

PREFACE

The purpose of this book is to provide a self-contained presentation of theoretical and operational information needed to understand the characteristics, operation, and use of the Omega Navigation System. It is designed to be used as a self-paced learning aid or in a classroom environment by those primarily involved with operating and maintaining the Omega system. Therefore, it is structured and written in the format of a course book, rather than a reference book. It is assumed that the reader has a physics and mathematics background at the level of an associate of science degree, or higher.

The book includes 13 chapters with selected chapter-specific appendices and seven general appendices. Chapter-specific appendices are directed at the more advanced readers and contain additional technical details that are relevant to the specific chapter. The general appendices include supplementary material that expands upon selected topics addressed in the book and is intended to further enhance the understanding of the Omega system. The course material addresses all major components of the Omega system, with emphasis placed on signal structure and utilization. Topics include: Omega system development background, signal generation, navigation and signal propagation principles, system operations, system performance evaluation, system utilization, and the future role of Omega in conjunction with other radionavigation systems. An overview begins each chapter and appendix, followed by introductory material and the technical discussion. Abbreviations and acronyms are defined at the end of each chapter and appendix. Sample problems with solutions and problems to be solved by the reader appear throughout (answers are provided in a section following Appendix G).

Chapter 1 presents a general description of the Omega system, including the system signal characteristics, system capabilities and limitations, and system users. **Chapter 2** traces the history of the Omega system from its World War II origins to the present, including the development of Omega transmitting stations and receiving systems, user support, and system management. An overview of the station capabilities, equipment, and operational procedures is provided in **Chapter 3**, and **Chapter 4** presents a general overview of the fundamentals of position determination, which are applicable to all radionavigation systems, including Omega. A discussion of the hyperbolic and rho-rho techniques, Omega lanes and their resolution, and position determination using Omega phase measurements are also provided. **Chapter 5** describes the very low frequency signal propagation characteristics and concepts relevant to understanding Omega signal propagation characteristics. This includes a discussion of how the Omega signal characteristics vary as a function of the signal path properties and modal interference phenomena. Observed Omega signal behavior is addressed in **Chapter 6**. The sources, mechanisms, and characteristic signatures (magnitude/duration/shape) of the normal and anomalous signal behavior

are described as well as their impact on Omega navigation. This chapter also contains general guidance for identifying Omega signal behavior under normal and anomalous propagation conditions. **Chapter 7** discusses the synchronization of the Omega system, including internal/external synchronization measurements and sources, procedures, and performance. ONSCEN's data collection, analysis, and processing procedures are presented in **Chapter 8** together with a summary of the Omega Regional Validation Program whose objective was to confirm or modify predicted Omega system performance throughout the oceanic regions of the world. **Chapter 9** explains the need, development, and utilization of Omega propagation corrections (PPCs). The chapter focuses principally on the structure and calibration of the models and algorithms used to generate the PPCs. Omega Navigation System signal coverage products that have been developed from the early period of the Omega system to the early 1990s are identified in **Chapter 10**. This includes a discussion of the early version of the microprocessor-based coverage prediction system, called Omega ACCESS. The overall assessment, evaluation, and quantification of Omega system performance (availability) is addressed in **Chapter 11**. The chapter also discusses the early version of the Omega system performance assessment and coverage evaluation computer workstation, called PACE, which implements the system performance assessment algorithm. **Chapter 12** describes various uses of the Omega system signals and typical Omega signal processing techniques employed in modern receivers, along with the effects of noise on the receiving system. **Chapter 13** describes other global radionavigation systems and signals that are frequently used by multi-sensor (integrated) Omega receivers. Issues regarding the future of Omega in the context of existing and planned global radionavigation systems are also addressed.

The seven appendices provide additional details on material contained in the 13 chapters. **Appendix A** describes the models and algorithms available for predicting VLF signals, including those that have been used to generate the Omega signal coverage/ performance prediction products discussed in Chapter 10. **Appendix B** presents additional details on the Omega system availability index computational algorithm (described in Chapter 11), a version of which is used in the Omega system performance prediction computer workstation PACE. A detailed discussion of capabilities, features, and uses of PACE is given in **Appendix C**. Details of Kalman filter techniques (some of which have been applied in the Omega system synchronization procedure) are given in **Appendix D**. Omega synchronization uses GPS (Global Positioning System) signals to obtain accurate timing information to synchronize the Omega system stations. An overview of the GPS is given in **Appendix E**, and a discussion of typical GPS user equipment is given in **Appendix F**. **Appendix G** provides the transmitting station parameters, including system operational specifications, annual maintenance schedule, and transmitting antenna parameters.

TABLE OF CONTENTS

LIST OF FIGURES

LIST OF TABLES

CHAPTER 1

INTRODUCTION

Chapter Overview — This chapter presents a brief introduction and overview of the Omega Navigation System with an end-to-end, top-level view of the entire system. This overview provides a basis for understanding how the detailed information presented in the individual chapters in this book fits into the overall context of the system. A summary-level Omega tutorial is provided with references to the specific chapters where the details on the subject are contained. Section 1.1 presents an initial introduction to Omega in terms of the three major system elements. The transmitting system is introduced in Section 1.2, fundamental characteristics of Omega signal propagation are provided in Section 1.3 and Section 1.4 addresses the use of Omega signals by the end user. Problems, including both worked-out examples and those to be solved by the reader, are given in Section 1.5.

1.1 WHAT IS OMEGA?

Omega is a worldwide, internationally operated, ground-based radio navigation system, operating in the very low frequency (VLF) band between 10 and 14 kilohertz (kHz). Its purpose is to provide a continuous, medium accuracy aid to navigation intended primarily for air and marine en route oceanic navigation and domestic en route air navigation. The nominal fix accuracy of Omega is two to four nautical miles (nm). While not originally intended for land navigation or non-navigation purposes, Omega is being used in a number of terrestrial navigation/location and time/frequency dissemination applications. The Omega system consists of eight widely separated transmitting stations that emit continuous-wave VLF signals. An Omega receiver determines position from range measurements based on the phase of the received signals from two or more Omega stations, or by phase comparisons between signals of selected pairs of Omega stations, which produce intersecting lines of position.

Omega grew out of research in long-range electronic navigation systems, which took place during and after World War II. Operational Omega stations began broadcasting navigation signals in the early to mid-1970s, and the system reached its final eight-station configuration in 1982. Omega, the last letter of the Greek alphabet, was chosen as the name of the system because in the early system development in the 1950s, it was thought that 10 kHz was the lower end (longest wavelength) of the usable radio spectrum. The Omega System history is provided in Chapter 2.

The Omega System consists of three major elements:

- Transmitting System
- Signals in the Earth-Ionosphere Medium
- Receivers and Navigation Computers.

Although each of these major system elements is a separate entity, overall system performance and the ability to navigate satisfactorily with Omega depends on the performance of each element. This book addresses each system element and its important characteristics in detail. A complete understanding of the Omega System requires an understanding of the characteristics of all three system elements and their impact on navigation performance as viewed by the end user. This chapter provides a brief introductory overview of these system elements, referencing the chapters in this book that provide the appropriate details.

1.2 TRANSMITTING SYSTEM

The Transmitting System consists of the eight transmitting stations and the procedures required to maintain and synchronize these stations. The eight Omega stations are identified by a letter from A through H and are presented in Chapter 2. Omega is operated as an international partnership between the United States and Argentina, Australia, France, Japan, Liberia, and Norway. Each station is staffed and operated by agencies of the nation in which it is located. The Japanese Maritime Safety Agency is responsible for synchronization of the transmitted signals of all stations. The U.S. Coast Guard Omega Navigation System Center (ONSCEN) has operational control of the system and is responsible for engineering and logistics support of the station equipment. Overall coordination of operations and policy is governed by the International Omega Technical Commission, which is composed of one member from each of the partner nations that operate the Omega Stations.

The synchronization procedure integrates the otherwise autonomous stations into a system and makes it possible to use the signals to compute a position fix anywhere in the world where usable signals are available. All operational radionavigation systems (e.g., Omega, Navstar GPS, Loran-C) control the transmissions from each station so as to be synchronous. In simple terms, the ideal system would derive the signals for each transmitter from a single common frequency source. This would guarantee that each station would transmit its signal at exactly the same time with exactly the same phase. Because the physical separation of the Omega transmitter sites is thousands of miles around the world, it is neither practical nor realistic to use a single frequency source for all eight stations.

Each station actually derives its transmitted frequencies from cesium oscillators (a primary and back-up unit at each station). Cesium oscillators (commonly referred to as a clock or frequency standard) generate a frequency that is highly stable over long periods of time (better than 1 part in 10^{12} or a drift of 2.6 μsec/month). The synchronization procedure corrects (on a weekly basis) any small shifts in the transmitted signal phase at each station so that from the user's viewpoint all eight transmitters appear

to be operating from a single frequency source. Between the periodic synchronization corrections, the station clocks are stable enough to hold the phase of the transmitted signals within the allowable tolerance of ±2 microseconds relative to the mean epoch of the eight stations. The mean epoch of the system is synchronized to within ±1 microsecond of Coordinated Universal Time (UTC). Omega synchronization is addressed in detail in Chapter 7.

Primary components of the transmitting station include the timing equipment, VLF transmitter and the antenna system. As is discussed and illustrated in Chapter 2, three types of antennas are used today: valley-span, grounded tower, and an insulated tower. Only Hawaii and Norway use the valley span antenna. Three stations use the grounded tower antenna and three use the insulted tower antenna. All stations radiate a nominal power of about 10 kW. Because of differences in the antenna system efficiency at each site, the input power supplied by the transmitter ranges from 90 kW to 165 kW. The difference between the input power and the radiated power is dissipated in heat, primarily in the antenna ground plane.

All stations transmit four common frequencies: 10.2 kHz, 11.05 kHz, $11\frac{1}{3}$ kHz, and 13.6 kHz. In addition to these common frequencies, each station also transmits a unique frequency that can be used by a receiver to unambiguously identify the station. All frequencies are synthesized from the Cesium standard and controlled by the timing equipment. Transmissions are sequenced in a specified format (shown in Chapter 2) so that no two stations transmit the same frequency at the same time. This is to prevent confusing the receiver with simultaneous transmissions at the same frequency from multiple stations since there is no way to separate the received continuous wave signals for processing. A continuous wave is transmitted by each station at one of its five frequencies during each transmission segment for 0.9 to 1.2 sec with a 0.2 sec silent interval between segments. This complete format repeats every 10 sec. The sequence of frequencies transmitted by each station in each of the eight time segments is unique and provides the receiver with additional information for unique identification of the received signal. Additional details on the transmitting system are provided in Chapters 2 and 3.

1.3 SIGNALS IN THE EARTH-IONOSPHERE MEDIUM

The signal is "launched" by the antenna system into the atmosphere between the earth and the lower ionosphere, where it propagates in all directions for several thousand miles or, under some conditions, completely around the world. The ionosphere is a spherical layer of electrically charged particles (concentric with the earth), which bend and reflect the signals thus confining the signals to propagate

below the ionosphere, rather than traveling straight out into space. This region in which the signals propagate is referred to as the earth-ionosphere waveguide. The waveguide is illustrated and discussed in Chapter 5.

Ideally, Omega signals would travel with uniform intensity and phase in all directions through the waveguide. Unfortunately, VLF signals are influenced by various physical and electrical factors: the height of the waveguide, which varies regularly each day and over the year; ground conductivity, which varies by several orders of magnitude between seawater and ice; orientation of the signal path relative to the earth's magnetic field, which influences the propagation properties; and the physical laws and characteristics of radio waves. Because of these factors, the phase of Omega signals is not a simple, uniformly increasing function of distance from the transmitter as would be experienced in free space. Therefore, the user must apply propagation corrections to the phase measurements to obtain accurate position fixes with Omega (these are automatically applied by modern receiving equipment). Propagation corrections are referred to as PPCs and correct the measurements at the user location so that the corrected phase is close to what would be observed in free space. The perturbing influence of the earth on the signal is effectively removed; this greatly simplifies the position fix calculations since a simple phase vs. distance model applies under all conditions. The propagation predictions, of course, are not perfect and cannot correct for all of the disturbing influences of the real world. This is the primary reason why the advertised accuracy of Omega is 2 to 4 nm and not something much smaller. Development of the PPCs is presented in Chapter 9 and their use in the position fixing process is addressed in Chapter 4.

Detailed treatment of signal propagation theory for Omega is presented in Chapter 5 and observed signal characteristics are presented in Chapter 6, however, it is useful to introduce here some of the more physically intuitive concepts related to Omega signal propagation since the theory gets rather involved. A major influence on the signal propagation within the waveguide is the height of the waveguide, which is not constant. The waveguide in daylight has a height of about 70 km whereas its height in darkness is about 90 km, due to the absence of solar radiation. The phase of usable signals is the most predictable when the entire waveguide is in daylight or darkness, i.e., when the reflective boundary of the ionosphere is approximately constant along the path. The phase is less predictable on paths having both daylight and dark portions. For these paths, the corresponding PPCs are less accurate and the resulting fix accuracy of Omega tends to be somewhat worse.

Signal propagation becomes more complex when a path includes both day and night portions. When the sunrise/sunset line, or terminator, crosses the signal propagation path, the path is said to be in transition. The transition region is where the ionospheric height changes from its nighttime maximum to

its daytime minimum. In some cases this transition is rather abrupt relative to the signal wavelength and can introduce abrupt changes in the signal phase characteristic relative to the uniform predictable change in phase with distance from the transmitters. This means that if a user is stationary and observing the phase of a received signal, there could be a rapid change in the observed signal phase even though the receiver is not moving. Thus, if the user is moving, it may be difficult to differentiate between the change in phase due to vehicle motion and phase error induced by transition. This rapid change in phase can lead to a condition referred to as cycle jump or lane slip, which is addressed in detail in Chapter 6. The transition effect is less pronounced when the terminator intersects the propagation path at right angles and most apparent when the terminator crosses the propagation path very rapidly at a very shallow angle. In fact, for crossing angles of less than 5 deg it is generally recommended that the station be deselected and not included in the position fix calculation.

Knowledge of the signal phase velocity is necessary so the receiving equipment can make the transformation between measured phase and distance to the transmitter. At any of the transmitted frequencies, an Omega signal may propagate in several different modes, however, for most signal paths beyond about 1000 km from the transmitter, Mode 1 tends to be dominant. This is the fundamental mode of the Omega signal and the Mode 1 phase velocity is always used in the PPC algorithm that corrects the signal phase prior to the position fix calculation. This means that if the signal is not dominated by Mode 1, a significant error can be introduced into the fix calculations. Under this condition the signal is referred to as being modal and is not usable.

A figure of merit used to characterize the degree to which a signal is modal is the Mode 1 Dominance Margin (M1DM), which is a measure of Mode 1 strength relative to the total signal strength. For less sophisticated receivers, a M1DM of 6 dB is desired if the signal is to be considered usable. More sophisticated receivers can perform satisfactorily with a M1DM as small as 1 dB. It is difficult and usually impossible to detect a modal signal in an operational environment. Therefore, modal interference is generally predicted and signals that may be modal are deselected by the receiver or the operator. Modal interference exhibits the following characteristics; it is present at ranges less than 1000 km from the transmitter; it is most prevalent at night in areas northwest and southwest of the transmitter; it is particularly severe when a northwest/southwest path crosses the geomagnetic equator; and it always occurs at the transmitter antipode, which is the point on the globe directly opposite the transmitter.

Under conditions when the Omega signal travels around the world and can be received from the opposite direction, there is the possibility of "long-path" propagation. If the long-path signal strength is stronger than the short path strength (which is possible), the receiver will interpret the vehicle as moving

in the opposite direction. Long-path propagation is most likely to occur when the direct path is in all daylight and the long-path signal propagates west to east in darkness, particularly if the ground conductivity is higher on the long-path. The associated figure of merit for quantifying the severity of long-path propagation is the short- to long-path ratio and the recommended value is consistent with the M1DM: 6 dB for less sophisticated receivers and 1 dB for more sophisticated receivers.

The signal attenuation rate (the rate at which the signal strength decreases with distance along the path) is greater for sunlit paths than for night paths. The attenuation rate also increases as path ground conductivity decreases. Seawater paths have the highest conductivity and cause the least attenuation while paths transitioning fresh-water ice in regions such as Greenland and Antarctica exhibit the greatest attenuation rate. The earth's magnetic field has a pronounced effect on the attenuation rate. Signals propagating in the easterly direction experience the lowest attenuation rate the highest attenuation is experienced by signals propagating in the westerly direction.

Signal strength alone does not limit the utility of Omega. It is the level of the signal relative to the noise in the receiver bandwidth, generally assumed to be 100 Hz, that limits signal usability. Lightning discharges associated with thunderstorm activity around the world are the primary source of noise in the VLF band. The electrical discharges generate electromagnetic energy in the VLF band, which propagates like the Omega signal. At any moment hundreds of discharges occur randomly around the world; the receiver perceives this energy as noise relative to the desired Omega signal. The ratio of the signal level to the noise level in the receiver bandwidth, expressed in dB and referred to as the SNR, is the figure of merit used to determine whether or not a receiver can detect and satisfactorily process the Omega signal. These and other signal usability factors are addressed in Chapters 10 and 11.

Older receivers and many aircraft receiving systems require an SNR that is higher than about –20 dB (100 Hz) whereas modern receiving equipment, especially for marine applications, can provide usable phase measurements with an SNR as low as –30 dB (100 Hz). An SNR below these signal-access thresholds produces noise-induced errors in the phase measurements that render the station signal unusable for computing a position fix. It is important to note that the noise level, like the Omega signal level, is a complex function of time of day, location on the earth and the time of year. Although atmospheric noise is the dominant noise source, there are also sources of man-made noise that can further reduce the received SNR. Of particular importance in airborne applications is the placement of the Omega antenna on the aircraft and noise generated by other electrical equipment such as motors and generators. Refer to Chapter 12 for additional details on this subject.

1.4 RECEIVERS AND NAVIGATION EQUIPMENT

The typical user equipment suite consists of an antenna, receiver, and a navigation computer. The antenna system includes a loop (H-field) antenna, or a whip/blade (E-field) antenna and generally an antenna signal preamplifier. The antenna preamp feeds an analog input stage in most receivers. The output is sampled, or digitized, and the remainder of the receiver processing is digital. Older receiving equipment performed all of the processing with analog circuits that could not achieve the processing gain associated with modern digital processing techniques. This is why the SNR threshold for older receivers is typically assumed to be –20 dB, and –30 dB for modern equipment.

The receiver processing detects and tracks the received signals from each station and measures the phase of the signals relative to a local reference or oscillator. The number of frequencies simultaneously tracked depends on the particular receiver implementation. Also, as part of the processing, the receiver must identify the station that transmitted each of the frequencies in each transmission segment. The received signal is of no use if it cannot be associated with its transmission source because the goal is to obtain a measure of the range between the receiver and each transmitting station. Since the location (latitude and longitude) of the stations is accurately known, some form of multilateration with the indicated ranges is used in the navigation computer to determine the latitude and longitude of the receiver, or more precisely, the receiving antenna. Although this is a rather simplistic view, it serves to introduce the fundamental elements of the signal processing and position fixing/navigation process. A detailed presentation of navigation and position fixing with Omega is contained in Chapter 4.

At 10.2 kHz, the primary Omega navigation frequency, the signal wavelength is about 16 nm. In terms of range from a station, each wavelength, or cycle, is called a lane within which the signal phase varies from 0 to 360 deg. The receiver can only measure the phase of the Omega signal within a known lane; the range to the transmitter is equal to the number of whole lanes plus the fractional part of the lane indicated by the phase measurement. Therefore, as the platform moves, the receiver must "know" or keep track of the number of whole lanes. The lane count can be determined in various ways. One way is to compute the lane number at a location that is known with an accuracy of plus or minus half a lane and then increment (or decrement) the lane count as the receiver moves from one lane to the next. Obviously, use of the incorrect lane count (due to a lane slip) will introduce a significant error into the computed position.

A position fix can be determined by using two or more measurements of the range to the known locations of the transmitting stations. Conceptually, with two range measurements, a user's position can be located on a chart by determining the intersection of two circles with radii equal to the range measurements and centered on their respective transmitting station. This is called the direct ranging, or rho-rho,

mode of position fixing and the circles are referred to as lines of position (LOPs). Two circles will actually intersect at two points: the true fix point and an anomalous fix point. These two points are generally widely separated positions and it is usually straightforward to resolve the ambiguity. If a third range measurement is available, the rho-rho-rho mode is used, the equivalent of drawing a third circle to provide an unambiguous intersection of all three circles at the fix point. Multiranging with three or more stations is the preferred mode since the receiver does not require a precise reference oscillator (e.g., Cesium clock) that is needed to implement the rho-rho mode. Alternatively, the hyperbolic (range-difference) mode can be used if three stations are available.

In the hyperbolic mode of navigation, the receiver measures the difference in the signal phase between pairs of transmitters. The resulting LOPs are families of hyperbolas and the fix is established as the intersection of hyperbolas. Before the availability of efficient on-board digital computers, Omega navigation used precomputed hyperbolic LOPs plotted on paper charts. The receiver displayed the phase difference which was then plotted by the navigator on the chart to determine the position of the craft. Today, the fix determination process is fully automated and most navigation equipment uses all available signals to provide a best determination of craft position. These signals may even come from systems other than Omega, such as the Navy VLF Communications System or the Russian Alpha System, which is similar to Omega.

Most modern airborne Omega navigation equipment routinely uses the VLF communications signals to supplement Omega, particularly in regions where there is insufficient Omega signal coverage. Another mode of operation is differential Omega where a fixed monitor site is established at a known fixed location to determine the "error" in the received Omega signals. These errors are communicated to users in the vicinity of the monitor where they are used to correct the measurements made by the user's receiver with a resulting positioning accuracy of 0.3 to 1 nm. Omega is also used in integrated systems with inertial navigation and satellite navigation systems. Weather balloons use a very low cost Omega receiver that retransmits the Omega signals on another frequency to the ground-based receiving site to determine wind velocity profiles. Submarines use Omega because a hyperbolic position fix can be obtained while the submarine and the antenna are submerged. Although Omega has been the only operational radionavigation providing continuous global coverage for the past 20 years, the Navstar GPS system (Appendix E and Appendix F) is nearing operational status and according to the Federal Radionavigation Plan will replace Omega. Additional details on these and other position fixing modes are provided in Chapter 4 and Chapter 13.

1.5 PROBLEMS

1.5.1 Sample Problems

1. Each of the eight Omega stations derive the transmitted signal from a cesium beam frequency standard which acts as a precise clock. Before the advent of GPS, the stations were synchronized by adjusting the clock outputs based on reciprocal path measurements in which monitors at each station concurrently measure the phase at each end of the station baselines. From a qualitative viewpoint, why do you think these kinds of measurements would isolate the synchronization differences between the stations?

Answer:

In principle, a single-path phase measurement of one station's phase by the monitor at another station would, when corrected by the phase propagation delay over the interstation path, indicate synchronization offsets between the stations. However, in addition to propagation delay (based on some fixed phase velocity), Omega signals must be corrected by PPCs (propagation corrections; see Chapter 9). Although greatly refined, the PPCs have bias errors on the order of 7 to 10 microseconds, which, even if removed, leave random errors of about 4 to 6 microseconds, i.e., too much error to detect synchronization offsets less than or equal to 2 microseconds. It is shown in Chapter 7 that *differences* in reciprocal measurements tend to remove the PPC error but reinforce the synchronization error (offset).

2. Why do you suppose the silent interval (or guard time) between the signal transmissions in the Omega signal format was chosen to be 0.2 sec?

Answer:

The interval is designed for the worst possible case of interference in which a receiver located a few kilometers to the west of a station receives the "long-path" signal from that station, i.e., the signal propagating over the longer of the two arcs of the great circle connecting receiver and transmitter. In that case, the trailing edge of a transmission would reach the receiver after a time approximately given $2\pi R_E/c$, where R_E is the average earth radius (6367 km) and c is the free-space speed of light (about of x 10^5 km/sec), i.e., about 0.13 second. With a guard time of 0.2 sec, such a receiver would not see a pulse overlap, with a remaining 0.07 second before the onset of the next signal transmission.

1.5.2 Problems to be Solved by Reader

1. Give one or more reasons why a station signal might not be useful at the station's antipode.

2. Consider two 10.2 kHz signals dominated by the short-path Mode 1 component.

If Signal 1 propagates at night to the east over seawater and Signal 2 propagates during the day to the west over frozen tundra, which signal attenuates more rapidly as a function of distance?

3. Suppose the following set of criteria defines the signal usability:

   SNR (Signal-to-noise ratio) ≥ -20 dB (100 Hz bandwidth)

   S/L (Short-to-long path amplitude ratio) ≥ 6 dB

   M1DM (Mode 1 dominance margin) ≥ 6 dB

If the short-path signal level is 25 dB (relative to 1μV/M), the long-path signal level is 19 dB (relative to 1μV/m), the noise (100 Hz bandwidth) is 40 dB (relative to 1μV/m), and the M1DM is 8 dB, is the signal considered usable?

4. Why is the conductivity of seawater higher than the conductivity of fresh-water ice?

5. Given that the lane width of the 10.2 kHz signal is about 30 km, what is the lane width of the 13.6 kHz signal? If the two signals have the same phase at distance *r* from the station, what is the smallest incremental range (away from the station) required for the phase to again be the same?

6. What time of year would you expect the atmospheric noise to be the largest:

   Summer afternoon

   Winter night

CHAPTER 2

OMEGA SYSTEM HISTORY

Chapter Overview *— This chapter traces the history of the Omega system from its World War II origins to the present. The chapter begins with a historical sketch of Omega in Section 2.1, including the development of transmitting stations and receiving systems, user support, and system management. Section 2.2 explores the early work in VLF signal generation, control of signal stability, and signal propagation which demonstrated the viability of a long-range navigation system at VLF. Experimental VLF transmissions and prototype Omega transmitting stations are described in Section 2.3. Section 2.4 traces the evolution of Omega receiving systems used in surface, sub-surface, and air navigation. Finally, the changing role of user support in the evolution of Omega from a developing to a mature system is discussed in Section 2.5. Abbreviations and acronyms used in the chapter are given in Section 2.6 and references cited in the chapter are found in Section 2.7.*

2.1 INTRODUCTION

Very low frequency (VLF; 3 kHz to 30 kHz) stations have been broadcasting radio signals since the early part of this century. Prior to World War I, transmitting/receiving stations were located in The Netherlands, France, Indonesia, Germany, Wales, and the U.S. (New York, New Jersey, and Massachusetts). Between World War I and World War II more powerful stations with better transmitters were built in France, Great Britain (including Criggion and Rugby), and the U.S. (Annapolis, Maryland; Summit, Canal Zone; and Haiku, Hawaii). Eventually, commercial radio stations moved to higher frequencies (in the MF band: 300 kHz to 3 MHz) to gain higher data rates, leaving the VLF for mostly military stations whose missions emphasized security and long range over high data rate. Following World War II, VLF transmissions found applications in long-range dissemination of frequency and time, global navigation, and geophysical prospecting, as well as long-range, secure, reliable communications (Ref. 1). It was the early experiments in controlling long-range VLF signals during World War II that ultimately led to the present-day Omega System.

One of the earliest radio navigation systems, known as Gee, was proposed in 1937 and implemented in 1942 by a U.K. engineer, R.J. Dippy (Ref. 2). This system operated at 30 to 80 MHz and supported allied aircraft missions across the English Channel during World War II. Since Gee operated in the very high frequency (VHF) band, it was of relatively short range. Experimental systems in the U.S. about this time focused on lower frequencies to obtain the longer ranges required for navigation

support to troop convoys crossing the North Atlantic Ocean. These systems were used in a hyperbolic mode, i.e., the time difference-of-arrival for each pair of signals received was used to establish position. The transmissions were pulsed so that the differences in signal arrival times could easily be measured.

Some of the most active research in this area at the time was performed by a research engineer named John Alvin Pierce attached to Harvard's Cruft Laboratory. Pierce and others from the Radiation Laboratory at the Massachusetts Institute of Technology developed a medium-range (several hundred miles) hyperbolic system at 3 to 10 MHz in the hi ...ency (HF) band utilizing station-synchronized transmissions. This system beca ..e known as lo... ...ong RAnge Navigation) and, in the following years, acquired thousands of users.

Following World War II, Pierce proposed a hyperbolic system at 40 kHz with a 200 Hz modulation. An experimental system (known as Radux) was developed which differed from loran and Gee in that it was continuous-wave (CW), not pulsed. This meant that the navigational user measured the *phase* difference rather than the time difference. To extend the range of this system, a phase-stable 10 kHz signal was added to the Radux format in the early 1950s. The resulting system, known as Radux-Omega, was designed to use the 200 Hz modulation to resolve the (approximately) 8 nautical mile "lane"* of the 10 kHz transmission. This system, which was expected to provide 5 nm fix accuracy at ranges of about 3000 n.m., was tested at the Navy Electronics Laboratory (now called the Naval Command, Control, and Ocean Surveillance Center, NCCOSC) and the Naval Research Laboratory during the period 1954–1957. These tests showed that the Radux signal was stable within a few microseconds. The system as originally conceived never became operational because:

- The range of the 40 kHz signal was much less than that of the 10 kHz signal
- The measured position errors were greater than expected
- As a result of the 40 kHz range limitation, numerous stations would be required for a worldwide system.

In place of the 200 Hz modulation, lane identification was to be achieved through the use of multiple VLF CW transmissions at closely spaced frequencies. The transmission of CW VLF signals controlled by phase-stable oscillators then became known as Omega (Omega is the last letter in the Greek alphabet). The name "Omega" was chosen by Pierce to represent the "far end" of the radio spectrum usable for navigation (Ref. 3).

*In the hyperbolic mode of navigation, a lane corresponds to the distance interval between pairs of geographic points for which the phase difference (between two synchronized transmitting stations) differs by a cycle (360°).

Due to the high cost of constructing VLF antennas, the first experimental Omega stations were advantageously located at sites where VLF/LF communication station antennas were in place. Thus, in the late 1950s, experimental transmissions were broadcast from naval stations in San Diego, California (Chollas Heights), Bainbridge Island, Washington, and in the Haiku Valley on the island of Oahu in Hawaii. These stations transmitted on several frequencies in the VLF range and demonstrated many of the characteristic features of VLF signal behavior that are known today (see Chapter 6).

In the early 1960s, three additional experimental stations were established at Summit in the Canal Zone (Navy Communications Station), at Forestport, New York (Air Force test facility), and Criggion, Wales (British Post Office Station). The transmitting facilities at Chollas Heights and Bainbridge Island were closed following the decision to discontinue Radux-Omega. The resulting network of four stations was operated in the master/slave mode in which a slave (or secondary) station synchronizes its transmission to the master station signal.

Based on the success of the initial experiments with Omega signals, the U.S. Navy formed an Omega Implementation Committee in 1963, chaired by J.A. Pierce, to establish the transmitting, receiving, and operational characteristics of a worldwide Omega Navigation system. In 1966, the committee's final report (Ref. 4) was published and the U.S. Navy began preparing for implementation. The final report served as the basis for most of the characteristics of the system we now call Omega. An important exception was that few of the nations recommended by the committee for hosting station locations were represented in the final system configuration.

In 1966, the Criggion transmitter was relocated to Bratland, Norway, and the Summit transmitting equipment was moved to Trinidad in the West Indies. Both the Norway and Trinidad sites were outfitted with valley-span antennas that used natural formations (i.e., a fjord and a narrow valley) to attain the necessary antenna height. The master/secondary mode of operation was abandoned following introduction of stable atomic clocks/oscillators at the stations. The resulting four-station network* that transmitted precisely controlled frequencies in a particular format and operated in the so-called "absolute mode" (all stations operating independently) marked the beginning of the modern Omega System.

The U.S. Navy authorized full-scale implementation of the Omega System in 1968, based on the Omega Implementation Committee report. Program management, including station construction and funding, was assigned to a project office initially under the auspices of the Chief of Naval Materiel (PM-9) and later to Naval Electronics System Command (PME-119). In 1971–1972, under the terms of

*The stations were labeled as Station A — Norway, Station B — Trinidad, Station C — Hawaii, Station D — Forestport; this sequence was used in the frequency/time multiplexed transmission format.

Title 14, USC 82, operational duties were assumed by the U.S. Coast Guard's specially formed Omega Navigation System Operations Detail (ONSOD), although the Navy Project Office retained overall responsibility. One of ONSOD's primary functions at this time was coordinating station synchronization through the use of inter-station phase measurements. As construction of the eight final stations proceeded through the 1970s, ONSOD assumed the duties of engineering maintenance for those stations declared operational.

Except for the station located in Australia, all Omega stations in the final system configuration became fully operational during 1971–1976. Table 2.1-1 (from Ref. 5) lists the dates of operational commencement and bilateral agreement for each station of the final configuration. Separate bilateral agreements were negotiated between the U.S. and the six non-U.S. host nations regarding construction site, station operation, logistics, and finances. In most cases, the agreements were signed well before operations commenced. However, in the case of La Reunion, the station was in operation for more than five years before the Government of France formally signed the bilateral agreement. In August of 1982, the Australia station became operational, thus, completing the full configuration of eight stations. Figure 2.1-1 shows the location of the eight Omega stations in the final system configuration.

Representatives from the seven Omega station partner nations formed the International Omega Technical Commission (IOTC). The first IOTC meeting was held in June 1973 in Washington, D.C., but a formal charter was not drafted until 1980. The charter was formally adopted with all members' signatures in December 1981. Meetings were held more or less annually until 1986 when it was decided to hold IOTC and station manager conferences in alternate years.

Table 2.1-1 Important Dates for Stations in the Current Omega System Configuration

Station	Bilateral Agreement Signed	Station Declared Operational
A – Norway	November 1971	December 1973
B – Liberia	November 1973	February 1976
C – Hawaii (U.S.)	N/A	January 1975
D – North Dakota (U.S.)	N/A	October 1972
E – La Reunion (Fr.)	April 1981	March 1976
F – Argentina	December 1970	July 1976
G – Australia	September 1977	August 1982
H – Japan	August 1972	April 1975

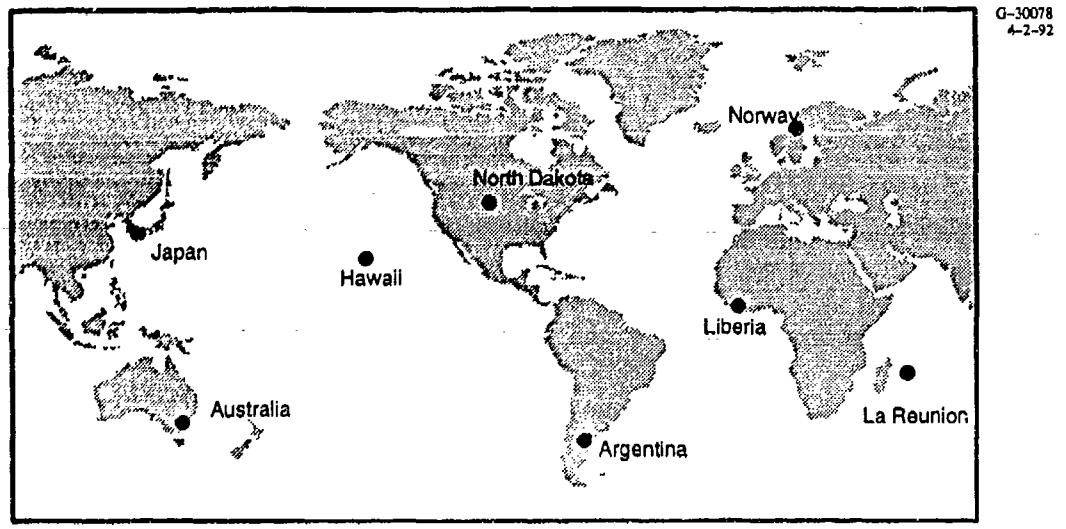

Figure 2.1-1 Present Omega Station Configuration

In 1977, the Japan Maritime Safety Agency assumed the duties of coordinating the synchronization of the station (internal and external). This helped to widen the international role for system operational support. Three years later, the U.S. Navy transferred system financial responsibility to the U.S. Coast Guard/ ONSOD, thus removing Omega operation from direct Department of Defense control. In 1986, ONSOD's name was changed to the Omega Navigation System Center (ONSCEN) and its facilities were relocated to the Coast Guard Information System Center (then known as Coast Guard Station Alexandria, Virginia).

2.2 EARLY EXPERIMENTS AND CONCEPTS IN VLF NAVIGATION

2.2.1 Signal Generation Stability

A major challenge in the early experimental transmissions of VLF signals for use in navigation was to achieve the necessary stability of the signal. For most kinds of signal modulation used in communication (e.g., frequency shift keying, FSK*), high signal stability is not crucial, since detection of a signal in a certain frequency interval (bandwidth) is all that is required.§ Also, most of the early navigation systems were pulsed systems in which only the timing (or time intervals) of the pulses is important. In a CW system, there is "nothing to hang your hat on" except the waveform itself which must therefore

*FSK is a modulation technique in which binary coded information (consisting of ones and zeros) is transmitted at two closely spaced frequencies.

§ The instability of signal generation accounts for a portion of the signal frequency spread over the received signal bandwidth.

be stable. To illustrate this concept, consider the phase of a VLF signal transmitted from a distant station (e.g., a thousand miles). A phase reading measured at a given location should not change with respect to a stable oscillator over a period of minutes unless the measuring location is changed (see Fig. 2.2-1). However, if the signal is not sufficiently stable, the detected phase wanders erratically even though the detection equipment remains fixed. If the measurements are made on a moving platform, it is impossible to distinguish the phase change due to an unstable signal from that due to platform motion. Thus, signal generation stability is an essential requirement for CW navigation systems.

An important milestone in the development of stabilized signal generation was achieved by Dr. Louis Essen of National Physical Laboratory in Great Britain (Ref. 3). Dr. Essen, who designed the first cesium beam resonator, designed a very precise crystal oscillator* known as a ring oscillator to stabilize the LF and VLF transmissions from the Rugby station in the U.K. In 1953, J.A. Pierce and others at Harvard began monitoring these signals which, at first, were transmitted daily for only one hour. Later, the 16 kHz transmissions were generated almost continuously, thus allowing measurements of cycle

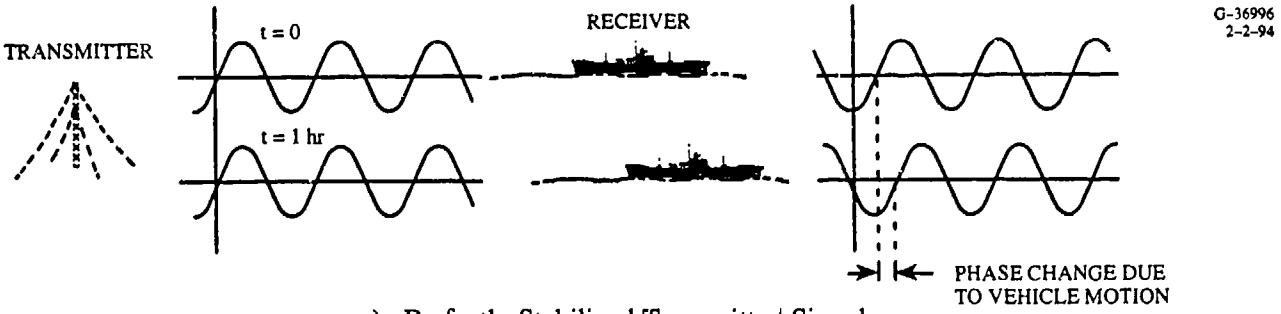

a) Perfectly Stabilized Transmitted Signal

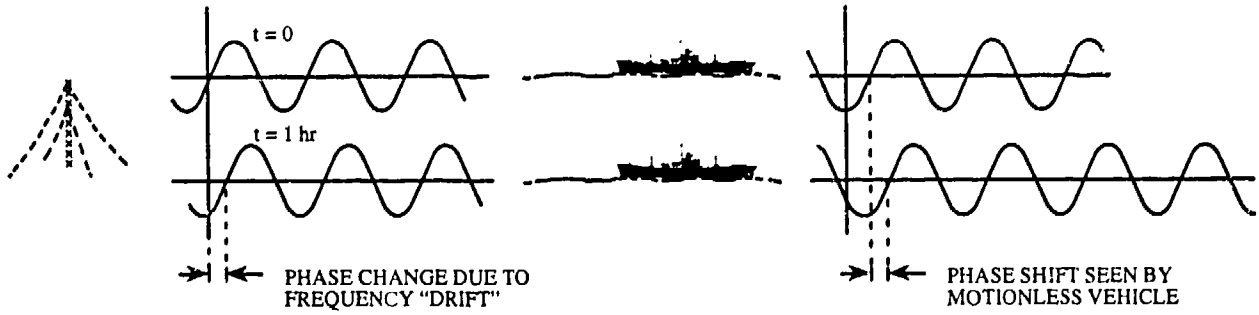

b) Imperfectly Stabilized Transmitted Signal

Figure 2.2-1 Effect of Unstable Signal Generation on Determining Vehicle Motion

* A crystal oscillator uses the natural mechanical oscillations of certain crystals to generate oscillations (of the same frequency) in electric signals.

changes in the measuring equipment. Ultimately, Pierce found that the day-to-day variation in the signal could be detected with an accuracy of about two parts in 10^{11}. To provide a feeling for what this stability means, consider a 16 kHz signal which has a period of $1/(16\times10^3)$ seconds, or 62.5 microseconds.* Since there are 8.64×10^{10} microseconds/day, an accuracy of 2 parts in 10^{11} means an error of about 1.7 microseconds/day or about 3% of the signal period in a day. This means that over a period of several days, a transmitted phase-stable signal could be tracked with high resolution and accuracy over long paths. This experiment also demonstrated that VLF signals could be transmitted with sufficient stability to permit navigation/position fixing.

2.2.2 Range of VLF Signal Propagation

The long ranges to which radio waves could be detected were not suspected until the discovery of the ionosphere. As early as 1839, C.F. Gauss speculated that electrical currents in the atmosphere caused the variations in the earth's magnetic field (Ref. 6). Later in 1860, Lord Kelvin also speculated that a conducting layer above the surface of the earth was responsible for atmospheric electricity (Ref. 7). The physical nature of such a conducting layer was not known, however, until after J.J. Thomson's discovery of the electron and its role in forming conductive gases (Ref. 8). G. Marconi's famous demonstration in 1901 that radio signals could be transmitted across the Atlantic Ocean implied that the radio waves were deflected towards the earth (see Fig. 2.2-2). In other words, simple refraction through the atmosphere as it was then known (at the lower altitudes) could not explain Marconi's achievement. A. Kennelly and O. Heaviside first suggested (in 1902) that free electrical charges in the upper atmosphere could reflect radio waves (Ref. 6). This was followed shortly by the suggestion that solar ultraviolet radiation acting on the neutral atmosphere was the source of the free charges. The existence of this so-called Kennelly-Heaviside layer was strongly doubted by many researchers until the experiments of Appleton and Barnett (Ref. 9) and Breit and Tuve (Ref. 10) in 1925–1926. These experiments, together with Chapman's pioneering work in solar control of the ionosphere in 1931 (Ref. 11), mark the beginning of ionospheric physics as a modern scientific discipline.

The existence of an ionosphere permits detection of radio signals at long ranges. This is especially true for the lower frequencies, which reflect from the ionosphere at large angles of incidence, thereby losing a relatively small fraction of the wave energy to the ionosphere. Thus, the signal undergoes multiple reflections from the ionosphere and the earth's surface between the transmitting source and the point of signal reception. At very low frequencies such as 10 kHz, the radio waves lose about half their energy

*The period of a signal is the time to complete one cycle and is the reciprocal of the frequency. A microsecond is 10^{-6} second.

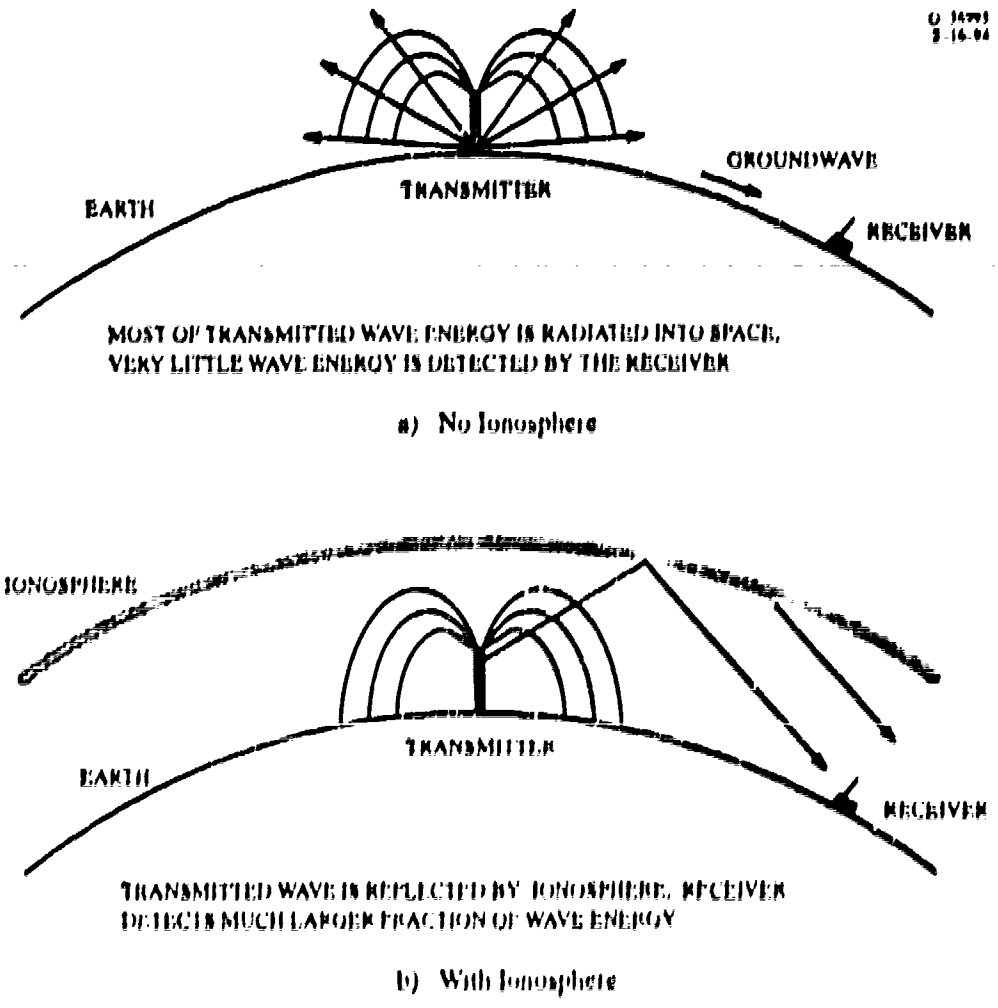

Figure 2.2-2 Effect of Ionosphere on Long-range Electromagnetic Signal Propagation

for each 1000 km of path length so that, with sufficient initial power, these signals can be detected at distances greater than halfway around the world. With no ionosphere, most of the radio wave energy would be radiated into free space, with only a small fraction being diffracted as a surface wave to ranges of less than 1000 km.

2.2.3 Experiments with Modulated VLF Signals

A fundamental drawback in navigating with a CW signal is that every wave period (in time) or wavelength (in space) is essentially identical and thus a specific wave period/wavelength cannot be "tagged" or identified. The phase of a signal can be measured between 0° and 360° but a given value of the phase, say 40°, may actually be 400° (360° + 40°), 760° (2 × 360° + 40°), etc., with respect to the

phase of the transmitted signal. This uncertainty (which amounts to an integral number of wavelengths) in relating the phase to a specific range from a transmitting station is referred to as lane ambiguity. Figure 2.2-3 shows an example of two receivers which measure the same phase (100°) although they are separated from the station by a different number of lanes (or cycles). One way to remove this ambiguity is to modulate the signal, i.e., the principal signal is transmitted as the carrier for a much lower-frequency CW signal. The period/wavelength of the lower-frequency modulating signal is much larger than that of the principal signal, so that the ambiguity is greatly reduced or eliminated. We will explain this method of reducing lane ambiguity, using the example of Radux

As mentioned in Section 2.1, the Radux system, which was the forerunner of Omega, employed a 200 Hz modulation frequency with a 40 kHz carrier signal. In this case, the modulating signal has a period of 5 milliseconds and a wavelength of about 1500 km (750 km in phase difference or hyperbolic mode). When Radux was proposed, this degree of ambiguity was tolerable, since it was assumed that all potential

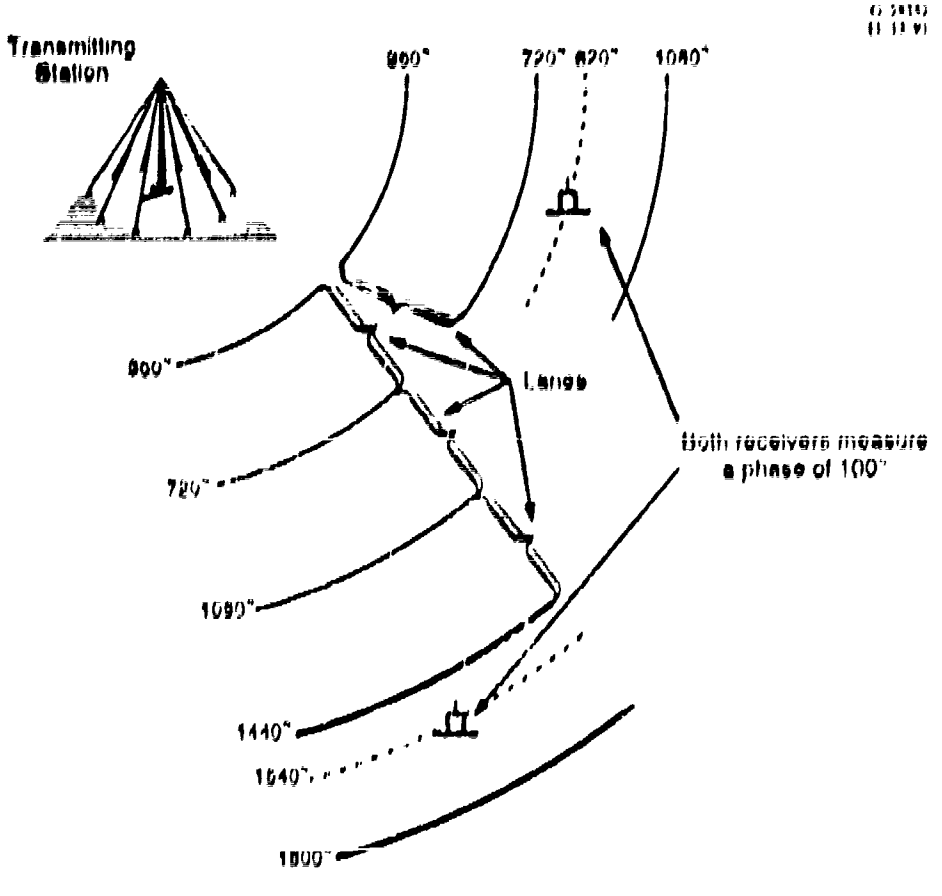

Figure 2.2-3 Equivalence of Phase Measurements in Different Lanes

users of the system knew their positions within a few hundred miles. The modulation frequency, however, cannot be made too low, because the phase measurement accuracy may not be sufficient to identify the correct carrier cycle. Thus, in the case of Radux, the ratio of the 200 Hz signal wavelength to that of the 40 kHz carrier is 200:1. This means that the 200 Hz phase measurement must be accurate to within 0.5% of a cycle. When the 10 kHz signal was added to the Radux format, the ratio of wavelengths was reduced to 50:1 so that the necessary phase measurement accuracy became 2% of a cycle. This greatly improved the probability of identifying the correct 10 kHz lane.

2.2.4 Unmodulated VLF Signal Generation

In the 1950s, as dead reckoning procedures improved and became automated, lane ambiguity became less of a concern for system planners (particularly in the military). Thus, the Radux 200 Hz modulation was dropped, marking the first use of unmodulated VLF signals for navigation and also the passage of Radux-Omega into a pure Omega system. Later, the resolution of ambiguities was improved by transmitting several closely spaced frequencies (from a few hundred hertz to a few kilohertz), whose differences served to provide a wider lane.

With the development of phase-stable signal generation techniques, described in Section 2.2.1, and experiments that demonstrated the long ranges attained by VLF signals, J.A. Pierce proposed a navigation aid which he called Draco (Ref. 3). This system would employ successive phase difference measurements on a moving platform as a means of dead reckoning. Such a system relies on tying changes in relative signal phase to changes in distance. Thus, when starting from a known location, Draco could be used to incrementally track a user along a desired route. This method works best when: (1) the successive measurement events are closely spaced in time (so that the path propagation conditions don't change), and (2) reasonably separated in distance (so that they are effectively independent). Among the platforms that use Omega for navigation, aircraft best satisfy these conditions. As a result, by the 1970s most aircraft units were outfitted with VLF navigation units, similar in principle to Draco.

2.2.5 Synchronized/Unsynchronized VLF Transmissions

In addition to stabilized signal generation and sufficiently long range, a VLF navigation system designed primarily for use in the hyperbolic mode must ensure that signals generated from each station are synchronized. Synchronizing signals from widely separated stations to an accuracy of about one microsecond was very challenging in the years before satellite dissemination of accurate timing signals. In the early 1960s, the experimental Omega stations were synchronized through the use of a master/secondary procedure (similar to that used in Loran). In this scheme, a secondary station synchronizes its

signal transmission to the phase of the received master station signal (including a fixed delay). This technique has the advantage of control by the master station but the disadvantage that the effective transmission time between the master and secondary station (as for any long path over which VLF signals are propagated) varies over the course of a day. Thus, a user receiving both master and secondary station signals would need to subtract the (nominal) master-secondary signaling time (and the fixed delay) before computing the phase difference. Differences between the actual and nominal signaling times would appear as synchronization errors.

In the late 1960s, the master/secondary operation was discontinued and very precise cesium beam frequency standards were installed to control the signal generation at each station (the "absolute" mode of system operation). With such stable frequency control, synchronization could be maintained for longer time intervals. A good cesium standard has a long-term stability of about 4 parts in 10^{13} which corresponds to a loss or gain of about one microsecond per month. Cesium standards are not easily adjusted, so that phase correction is usually implemented via an external device, called a phase shifter, located in the timer section of the station equipment suite. During the first few years of absolute mode operation, each station recorded the signal phase of the other stations and subtracted the best estimate of the inter-station propagation times (or phases) to determine the amount of the correction. Any significant changes in the phase recordings over a week were investigated as potential equipment failures. Later, this procedure became more systematized with the use of statistical estimation techniques. Moreover, the use of reciprocal path differences made the measurement of synchronization differences between station pairs more accurate.

2.3 FOUNDATIONS OF THE OMEGA TRANSMITTING STATION NETWORK

2.3.1 Early Transmitting Stations

As mentioned in Section 2.1, the first experimental Omega stations were advantageously sited at locations where VLF/LF communication station antennas were in place. Among the first stations to experiment with VLF transmissions for navigation purposes were those utilizing existing Naval VLF communication antennas in San Diego, California (Chollas Heights), Bainbridge Island near Seattle, Washington, and in the Haiku Valley on the island of Oahu in Hawaii. These stations were configured to transmit on several frequencies in the VLF band to determine the most stable frequency and, in general, to observe the diurnal behavior of the VLF signals. These stations transmitted low power (only a few hundred watts) but the signals were easily detected by the receivers collocated at each transmitter.

Most of these early transmitting stations were built to test the proposed Radux system, introduced in Section 2.1. For example, from 1951 to 1958, the Haiku station transmitted 40 kHz Radux signals with 200 Hz modulation. A single span across the Haiku Valley was used as an antenna while the Naval Station (NPM) concurrently transmitted communication signals from the other spans crossing the upper part of the Haiku Valley. Chollas Heights also transmitted Radux signals during this period using a three-tower antenna system. In addition, test transmissions at Chollas Heights were conducted at frequencies of 24, 52, and 72 kHz using the 200 Hz modulation. A third station, which was set up at the Naval Station in Bainbridge Island, Washington, transmitted only Radux signals (40 kHz with 200 Hz modulation) using a 20 kW transmitter. This triad of stations was used to test Radux operation and utilization in the hyperbolic mode. Data collected from a number of fixed and shipboard monitor sites demonstrated the stability and repeatability of the system (Ref. 12).

In 1958, Radux was expanded to include a VLF transmission (ultimately at 10.2 kHz) and the system name was broadened to Radux-Omega. The Haiku and Chollas Heights stations were reconfigured to transmit at pairs of frequencies (separated by 1 kHz) from 9.2 to 18.2 kHz (one transmission at about 7 kHz). Those signals, closely spaced in frequency, were used to test lane identification techniques. The 40 kHz Radux signal was eventually discontinued since its range was much smaller than that of the VLF signals. The idea of a global Radux system was also abandoned because the achievable position accuracy (~5 nm) was not consistent with expected requirements for a global U.S. Navy navigation system. With its relatively short range, the 40 kHz Radux signal would have required many expensive ground stations to establish a global system.

2.3.2 The Network of Master/Secondary Omega Stations

The San Diego/Haiku pair provided much useful information but could not demonstrate VLF hyperbolic navigation, which requires a minimum of three signals from physically separated stations. As a result, in the early 1960s additional stations were established at Forestport, New York; Summit, Canal Zone; and Criggion, Wales. Table 2.3-1 provides additional information on these stations which operated in the master/secondary mode (similar to Loran).

With the exception of Criggion, all stations were outfitted with the same type of transmitter equipment capable of delivering 100 kW of output power to the antenna (in the 10 to 14 kHz band). About the time that these stations were brought on-air, the experimental station in San Diego ceased operations, although monitoring of Omega signals continued for many years.

Table 2.3-1 Omega Station Network of the Early 1960s Operating in the Master/Secondary Mode

Station	Commenced Operations	Master/Secondary Status	Antenna Type	Effective Radiated Power Level
Haiku, Hawaii	[Previously existing site]	Master (1959–1961) Secondary (1961–1966)	Valley Span	2 kW
Forestport, New York	November 1959	Secondary (1959–1966)	Tower	100–300 W
Summit, Canal Zone	1961	Master (1961–1966)	Tower-supported "Valley Span"*	700–1000 W
Criggion, Wales	1963	Secondary (1963–1966)	Tower-supported "Valley Span"§	300–500 W

*The actual configuration consisted of active antenna spans suspended between six towers.
§Spans were anchored on 800′ hills on either side of the valley and supported by three 600′ towers based on the valley floor.

As a historical note, the station at Criggion was built during World War II to serve as a back-up to the VLF communication station at Rugby (GBR). The British feared that the Axis powers might destroy GBR which was farther south than Criggion and thus closer to the European continent. Fortunately, GBR survived the war and continues to transmit VLF information today.

2.3.3 Omega Implementation Committee Report

In 1963, an Omega Implementation Committee was formed by the U.S. Navy's Bureau of Ships to specify the requirements for a complete, worldwide Omega Navigation System, primarily for surface marine, but secondarily for airborne and submarine users. Committee members with expertise in VLF signal generation, VLF signal propagation, transmitting antennas, and receiving equipment included J.A. Pierce (chairman), W. Palmer, A.D. Watt, and R.H. Woodward. Based on their collective knowledge, perusal of observational data, experience gained with the experimental transmissions, and knowledge acquired from VLF communication station design and operation, these experts formulated and thoroughly described all major aspects of the Omega System.

The Committee's report (Ref. 4), published in May 1966, describes the basic principles of system utilization (including geometry), signal propagation, signal format, and system synchronization. It also provides initial specifications for the transmitting stations, system monitors, receivers, navigation charts, and "compensation graphs."

The report's section on system utilization covers use of the primary system frequency, station geometry, and additional frequencies for lane identification and resolution. It was generally considered that the principal usage of the system would be in the hyperbolic mode but use of the ranging mode* is also mentioned. A primary frequency near 10 kHz was proposed to minimize the contamination of the signal by the presence of higher-order modes§ (expected to be more extensive at higher frequencies). yet avoid the higher attenuation exhibited by lower frequency signals (whose wavelength is comparable to the height of the ionosphere). The authors believed that the greater cost to build a station at a lower frequency (10 kHz) was more than offset by the need for the wider lane provided by the lower frequency, so as to minimize lane ambiguity. The selection of 10.2 kHz as the primary Omega frequency apparently stemmed from the earlier Radux system that used a 0.2 kHz modulation frequency. It was thought at the time that the 10.0 kHz frequency use would be limited to precise standards, so that "beating" of the 10.2 kHz signal with the 10 kHz standard would permit acquisition of the modulating signal. In the 10–14 kHz band, the frequency whose ratio with 10.2 kHz is the "simplest" (i.e., involving the lowest integers) is 13.6 kHz, whose ratio with 10.2 kHz is 4:3. This provided a difference frequency of 3.4 kHz (whose lane width is three times that of 10.2 kHz, i.e., 24 n.m. in the hyperbolic mode) to assist in lane resolution. The ratio of 13.6 kHz to 10.2 kHz can also be expressed as 8:6 or 12:9 which suggests a third Omega signal frequency in the ratio 8:7:6 (11.9 kHz), 12:11:9 (12.467 kHz), or 12:10:9 ($11\frac{1}{3}$ kHz). The latter ratio was chosen to provide a frequency difference of $1.1\frac{1}{3}$ kHz ($11\frac{1}{3}$–10.2 kHz), which has a lane width of 72 nm (hyperbolic mode). The report also recommended that these signals be modulated to further reduce lane ambiguity. The report placed much emphasis on station geometry (for hyperbolic fixing) and lane resolution. The authors concluded that the RMS (Root Mean Squared) fix accuracy (accounting for all sources) would be half a mile in the day and one mile at night. They also concluded that the probability of correct lane identification would be 0.97 to 0.99 with the use of the 3.4 kHz difference frequency.

Because of its role in determining station location, designed transmitter power level, station synchronization, and the position error budget, VLF signal propagation was a very important consideration in the report. The principal propagation effects considered were: (1) the size of the region (defined as the near-field region) surrounding the transmitting station in which higher-order modes dominate or

*In the ranging mode of Omega navigation, phase measurements (rather than phase difference measurements) are processed.

§The Omega signal can be represented as the superposition (sum) of a number of modes. Use of the Omega signal for navigation, however, is predicated on the assumption that the signal is well approximated by a single mode (Mode 1); if strong higher-order modes are present, the signal cannot be used for navigation (see Chapter 5).

compete with the signal's Mode 1 component (see Chapter 5); (2) the east-west asymmetry in signal attenuation; and (3) signal attenuation over low-conductivity regions. As indicated above, the near-field region at 10 kHz, which is smaller than the near-field regions associated with the higher frequencies, was a major factor in the selection of that frequency. The report did not, however, mention signals with substantial higher-order modes *beyond* the near-field region of the transmitting station. In the years since the report was published, the discovery of extensive regions in which station signals contain higher-order modes on nighttime paths revealed what is perhaps the most significant propagation problem encountered in the use of Omega signals. For station placement, the authors recommended the middle latitudes to avoid both the east-west propagation asymmetry (effect (2) above) near the geomagnetic equator and the high signal attenuation over the low-conductivity areas located mostly in the polar regions. The proposed transmitting station power level was determined by first computing the minimum expected signal level (daytime westerly directed short-path signals) for a fixed power level of 1 kW, subtracting the maximum expected atmospheric noise level, and comparing with the minimum signal-to-noise ratio expected for a typical receiver. The deficit indicates the required power level in excess of 1 kW. This rather simple calculation yielded a required station-effective radiated power level of 10 kW, which served as a basis for the station transmitter and antenna specifications. Some 25 years later, the effective radiated power at all transmitting stations continues to be maintained at this figure of 10 kW.

The signal format proposed in the report is shown in Fig. 2.3-1 and for comparison, the current format is shown in Fig. 2.3-2. It is seen that, except for the precise value of the unique (station-specific) frequencies and the addition of the common 11.05 kHz frequency, the current format is the same as that recommended by the committee. The time/frequency multiplex format specified a pattern of time segment durations for each frequency transmitted by the stations. This pattern of frequencies and time durations permitted a unique identification of the transmitting station signals for receiver synchronization purposes.* The spacing between the segments (0.2 second) was selected to ensure that the signal from the most distant station dies away before the signal burst marking the next time segment from a nearby station begins.§ The committee proposed the unique frequency signals as an additional aid in station identification and, with a suitable imposed modulation, to further aid in lane identification/resolution. The proposed "central monitoring" scheme for station synchronization specified how phase data on reciprocal paths (e.g., Station A to Station B and Station B to Station A) should be used to

*The assumption is that the signal level is sufficient to permit discrimination of time segment durations differing by as little as 0.1 second.

§ A shorter time would also lead to problems in switching the antenna relays for the different frequency taps on the helix at the transmitting station.

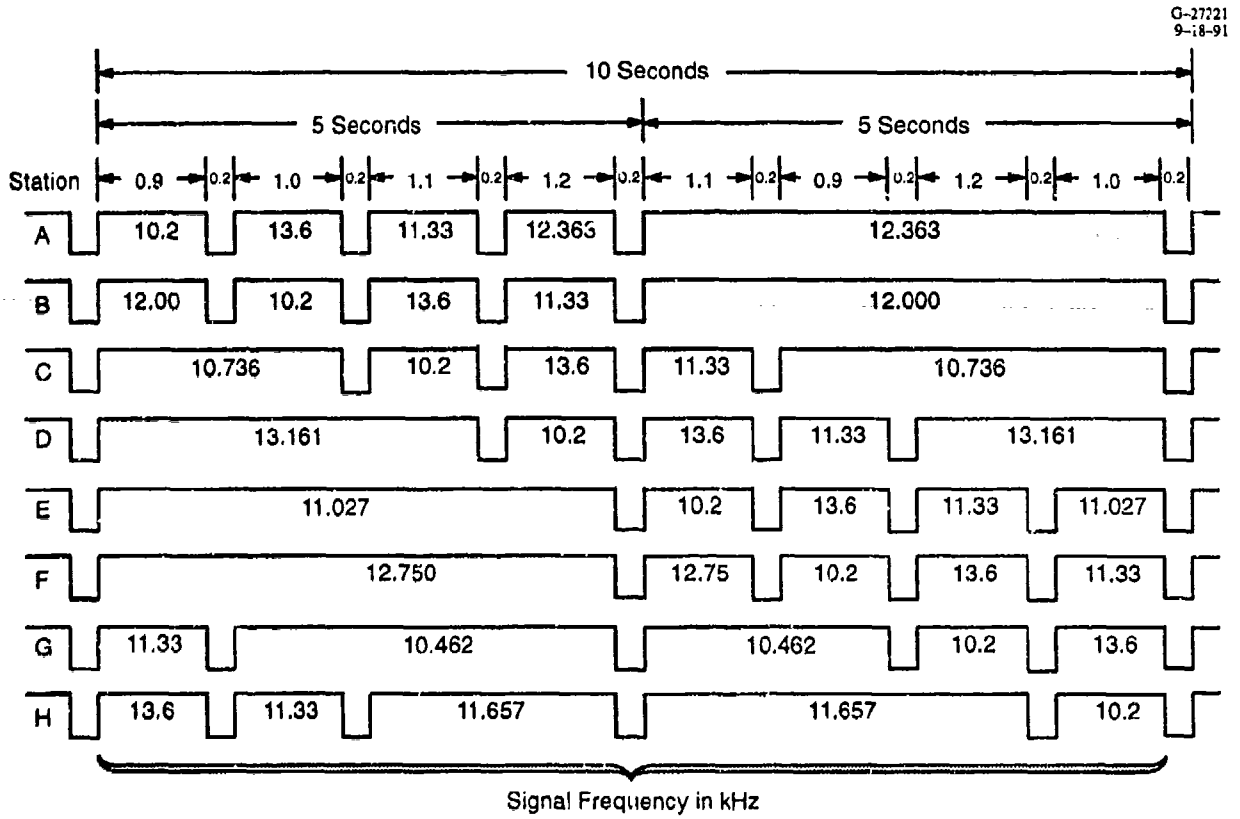

Figure 2.3-1 Omega System Signal Transmission Format as Originally Proposed

closely estimate station synchronization error. Although this estimation is now performed with a sophisticated software package, the general synchronization methodology now employed is essentially that described in the report.

4 The Network of Absolute Mode Omega Stations

Once the Omega Implementation Committee's final report was published, the U.S. Navy began preparing for implementation. In the same year, the Summit, Canal Zone transmitting equipment was moved to Chagaramus, Trinidad at the site of a valley span antenna. The Criggion, Wales equipment was temporarily relocated to Novika, in northern Norway before moving in 1967 to the current Omega location in Bratland, Norway. Eventually, new equipment, designed by the Naval Electronics Laboratory Center (NELC), was installed at the Bratland site. The site at Novika was later used for construction of a NATO (North Atlantic Treaty Organization) VLF communication station. The use of a fjord as a site for a valley span antenna at Bratland typified early stations that used such natural formations to attain the necessary antenna height. With the introduction of stable atomic clocks/oscillators at all stations, the master/secondary mode of operation was abandoned in 1966.

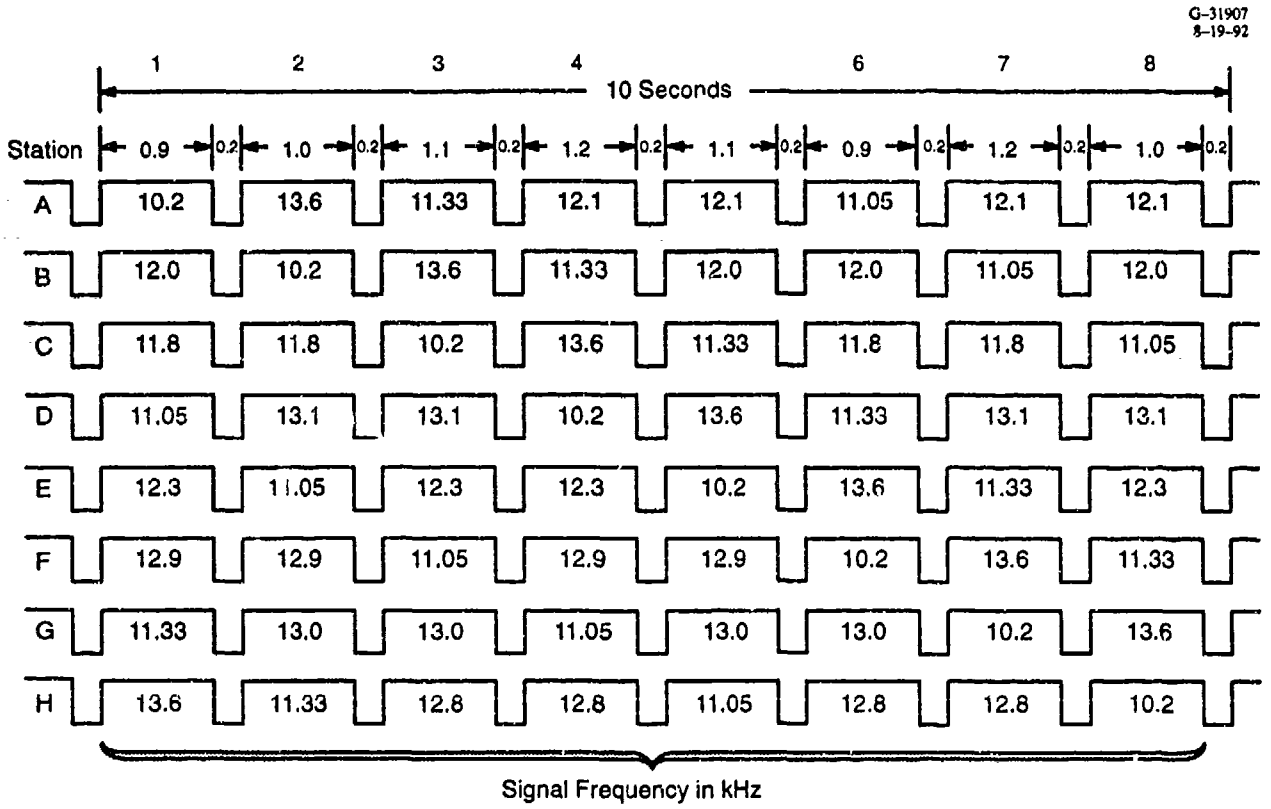

Figure 2.3-2 Current Omega System Signal Transmission Format

Table 2.3-2 provides an overall description of the resulting four-station network. Identical sets of transmitting equipment, consisting of input amplifier, driver amplifier, and power amplifier, were built for three of the four stations (Trinidad, Hawaii, and Forestport, New York). The Norway transmitter was a prototype version built by the Naval Electronics Laboratory. The stations were built and operated generally in accordance with the Implementation Committee's guidance. An important exception, however, was that none of the transmitted signals were modulated by a lower-frequency signal. The synchronization procedure recommended in the report was carried out by station personnel and controlled by the Naval Electronics Laboratory. The resulting four-station network transmitting precisely controlled frequencies according to the prescribed format marked the beginning of the modern Omega System.

Table 2.3-2 Omega Station Network of the Latter 1960s Operating in the Absolute Mode

Station	Commenced Operations	Monitor Station Location	Antenna Type	Effective Radiated Power Level
Bratland, Norway	March 1966	Hestmona, Norway	Valley Span	1–2 kW
Chagaramus, Trinidad	February 1966	Piarco, Trinidad	Valley Span	1 kW
Kaneohe,* Hawaii	[Previously existing site]	Makapuu, Hawaii Pyramid Rock, Hawaii Opana, Hawaii	Valley Span	2 kW
Forestport, New York	[Previously existing site]	Rome, New York	Tower	100–300 W

*Closest actual jurisdiction to station; Haiku is name of valley in which station is located.

2.3.5 Construction of Operational Stations

Following the Implementation Committee's report, negotiations were initiated with several nations regarding the siting of transmitting stations. Most of the committee's recommended sites did not become part of the final configuration of stations. Table 2.3-3 compares the recommended sites with the actual sites in the final configuration. Of course, it is difficult to make a one-to-one correspondence since each of the recommended site configurations represent different rotations (with respect to the earth) of equi-spaced network configurations. For example, Bouvet Island in the South Atlantic corresponds to either the current La Reunion or Argentina site, depending on the rotation of the station configuration.

Table 2.3-4 lists the stations in the full and final Omega network configuration. The table lists the date each station (in its present form) commenced operations, the location of the associated monitor site, and the station antenna type. Figure 2.3-3 illustrates the three primary types of Omega transmitting station antennas: grounded tower, insulated tower, and valley span.

Perhaps for economic reasons the Bratland site was retained as the A-station in the network. Portions of the antenna system were refurbished and new station equipment was installed prior to the formal operational on-air date of December 1973.

The station in Trinidad transmitted in the B-segment of the frequency/time multiplex format until the Liberia station became operational in 1976. At that time, Trinidad switched its transmission format to the G-segment of the pattern, where it remained until ceasing operation in December 1980. The Trinidad

Table 2.3-3 Recommended and Actual Sites for Omega Station Locations

Recommended Sites	Actual Sites
Balearic Island Spain Spitzbergen, Norway Western Ireland Hebrides Islands (U.K.)	Bratland, Norway
Nicobar Islands, India Tristan da Cunha (U.K.) Gulf of Oman (Iran) Windward Islands (U.K.)	Paynesville, Liberia
Galapagos Islands, Ecuador Marquesas Islands (France) Eastern Hawaii, U.S.	Kaneohe, Hawaii, U.S.
James Bay, Canada Leeward Islands (France/U.K.) Southern Texas, U.S. Aleutian Islands, U.S.	LaMoure, North Dakota, U.S.
Bouvet Island (Norway) Socotra Island (U.K.) Delagoa Bay (South Africa) Seychelles Islands (U.K.)	Plaine Chabrier, La Reunion, Fr.
Tierra del Fuego, Chile McMurdo Sound, Antarctica Chile (near 305 South) Bouvet Island (Norway)	Golfo Nuevo, Chubut, Argentina
East Cape, North Island, N.Z. Broome, Australia Southern South Island, N.Z. Auckland Islands, N.Z.	Woodside, Victoria, Australia
Aleutian Islands, U.S. Midway Island, U.S. Northern Luzon, Philippines Southwest Mindanao, Philippines	Shushi-Wan, Tsushima Island, Japan

site was discontinued primarily because a base rights agreement (between the governments of Trinidad and the U.S.) terminated in December of 1980. The decision to relocate the station in Liberia was made principally on political grounds. The Liberia antenna was a "grounded tower" (no large insulator at the base of the mast), the first of its kind in the Omega network.

The site in Hawaii was retained, again probably for economic reasons, although four additional spans were added and new transmitting equipment was installed prior to its designated operational date of January 1975. From 1972 to 1974, this station acted as a kind of system "headquarters," when ONSOD was located in nearby Kailua.

Table 2.3-4 Present Omega System Station Configuration

Letter Designation	Station	Commenced Operations	Monitor Station Location	Antenna Type/ Dimension	Position: * Latitude Longitude
A	Bratland, Norway	December 1973	Utskarpen, Norway§	Valley Span (2 spans)/ ~11,500 ft	66° 25′ 12.68″ N 13° 8′ 13.07″ E
B	Paynesville, Liberia	February 1976	Brewerville, Liberia	Grounded Tower/ 1400 ft	6° 18′ 19.26″ N 10° 39′ 51.85″ W
C	Kaneohe, Hawaii	January 1975	Wahlawa, Hawaii	Valley Span (6 spans)/ ~5,000 ft	21° 24′ 16.92″ N 157° 49′ 50.96″ W
D	LaMoure, North Dakota	October 1972	Dickey, North Dakota	Insulated Tower/ 1200 ft	46° 21′ 57.40″ N 98° 20′ 8.22″ W
E	Plaine Chabrier, La Reunion Island	March 1976	Riviere des Pluies, La Reunion Island	Grounded Tower/ 1400 ft	20° 58′ 26.90″ S 55° 17′ 23.62″ E
F	Golfo Nuevo, Chubut, Argentina	July 1976	El Tehuelche†	Insulated Tower/ 1200 ft	43° 3′ 12.79″ S 65° 11′ 26.81″ W
G	Woodside, Victoria, Australia	August 1982	Carrajung, Victoria, Australia	Grounded Tower/ 1400 ft	38° 28′ 52.42″ S 146° 56′ 7.06″ E
H	Shushi-Wan, Tsushima Island, Japan	April 1975	Ozaki, Tsushima Island, Japan	Insulated Tower/ 1500 ft	34° 36′ 53.06″ N 129° 27′ 13.12″ E

* Coordinates based on WGS-84 spheroid.
§ Established June 1991.
† Established September 1988.

In the late 1960s the D-station was planned for siting in Minnesota. However, efforts in the U.S. Congress to have the station located in North Dakota were successful. Being the first of the fully operational stations, the North Dakota antenna is of the older base insulator type.

The station in La Reunion commenced operations in 1976 but the French parliament did not formally approve the U.S.-France bilateral agreement until 1981. This station's antenna is the grounded tower type, modeled after the Liberia station antenna.

Of the stations constructed in the 1970s, Argentina was the last to become formally operational, although it transmitted signals at the three common frequencies long before the formal on-air date. Because it was originally planned to follow the North Dakota station in the on-air sequence, Argentina has a base insulator antenna, modeled after the North Dakota station antenna.

Up until 1970, the G-station had been planned for siting in New Zealand. However, a large public outcry followed reports that Omega was used by missile-carrying submarines and the station would be a target of the U.S.S.R. in the event of nuclear war between the two superpowers. The U.S. Navy then began negotiations with the government of Australia for a station located in that nation.

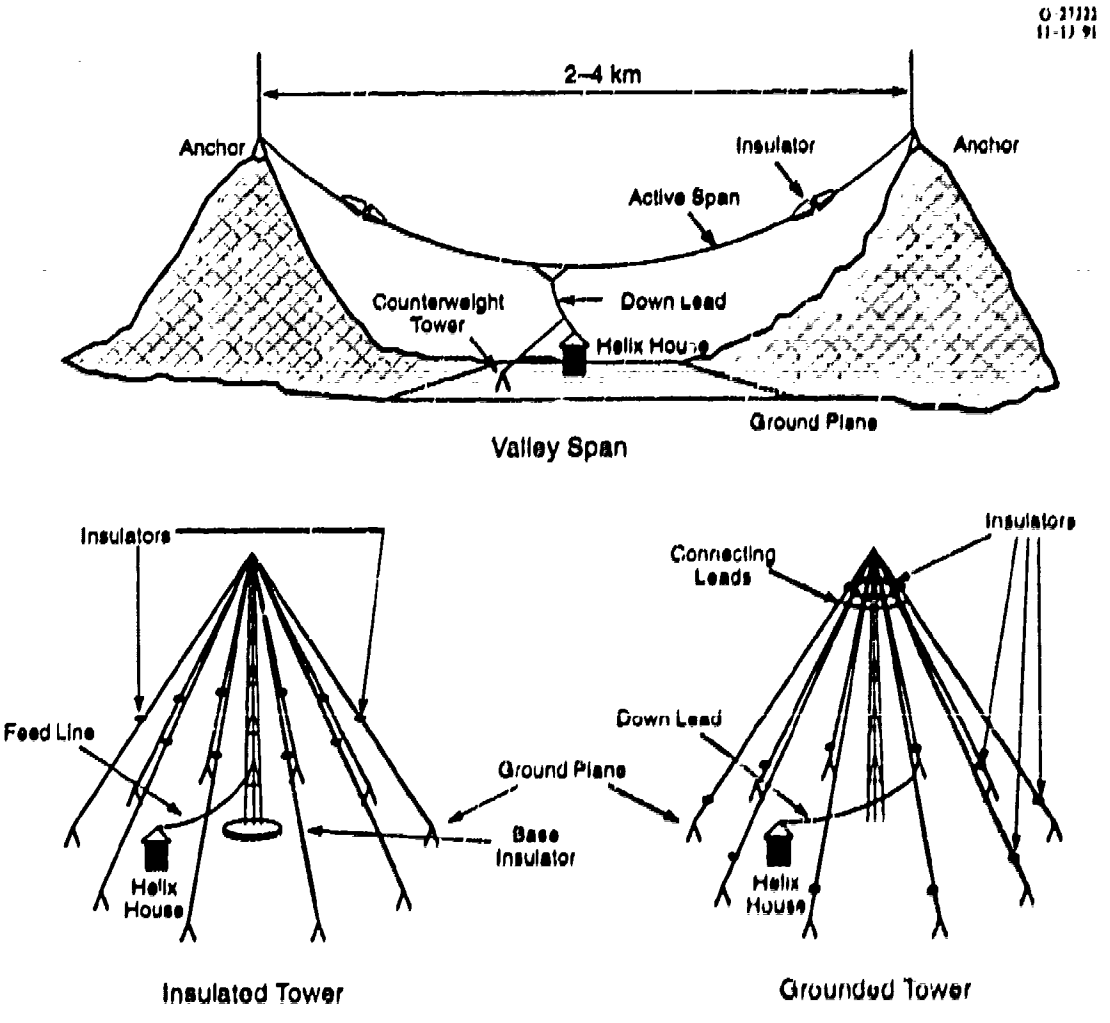

Figure 2.3-3 The Three Primary Types of Omega Antennas

Protests similar to those in New Zealand followed public disclosure of these negotiations. Debates in the Australian parliament continued for many months before being resolved in favor of pursuing an Australian station location. In the interim, alternative station locations in New Caledonia, New Hebrides, and other sites were studied. Construction of the Australia station was finally completed in 1982.

The Japan station commenced operations in 1975 with a specially designed cylindrical antenna centered over a base insulator. This antenna structure, located on the island of Tsushima, is so large that its guy wires are anchored on nearby islands.

2.4 EVOLUTION OF OMEGA RECEIVING SYSTEMS/USER PROFILES

2.4.1 First-generation Systems: Marine Receivers

Omega, as conceived by the U.S. Navy when it authorized implementation of the system, was primarily intended for marine users, both surface and sub-surface. Omega was seen as a navigation aid in the open ocean, far from coastal areas where existing radionavigation systems could be used. Moreover, the fact that Omega signals could be detected some tens of meters below the surface of the ocean (depending on the signal-to-noise ratio at the surface) made it useful as a navigation aid for submarines. The system was never considered accurate enough for weapons delivery from a submarine platform but was looked upon as an alternative navigation system for patrol craft.

The first operational Omega receivers were designed for shipboard platforms. These were large, bulky units with a long whip antenna, analog phase-difference measuring circuitry, and a strip-chart recorder to track lanes. Figure 2.4-1 (from Ref. 13) shows a block diagram of the AN/SRN-12, the first production-model receiver for U.S. Navy ships, designed in the mid-1960s. This receiver used all solid-state components (no vacuum tubes), considered an advanced feature at the time. The receiver tracked a single frequency so that separate units were required for multi-frequency use. Synchronization to the Omega time/frequency pattern had to be performed manually. The unit was configured to track signals from four stations and display three lines of position (LOPs)* with "nixie tube" lights. Two chart recorders were provided to furnish permanent records of the vessel's track and to maintain lane count.

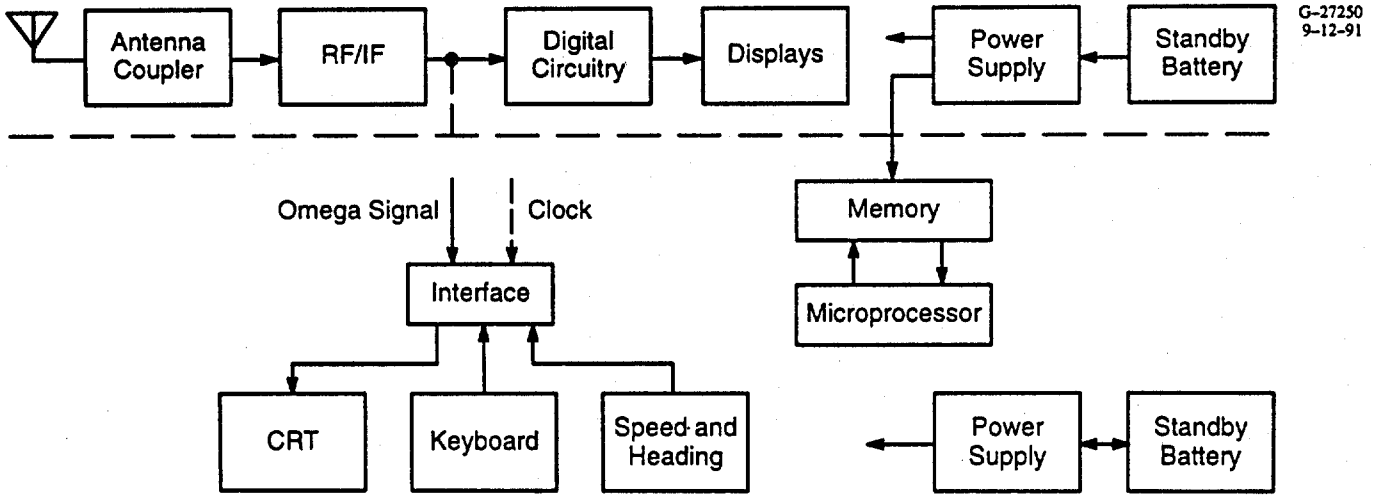

Figure 2.4-1 AN/SRN-12 Block Diagram

*An LOP for hyperbolic navigation is an imaginary curve on the earth's surface for which the phase difference between two station signals is a constant; the curve is a special kind of hyperbola on a spherical surface.

The first Omega receivers received a mixed reception from the (mostly U.S. Navy) users. Although some found it accurate and reliable, others did not and nearly all agreed that it demanded considerable time to operate. Manual synchronization to the Omega pattern (using blinking lights or headphones) was difficult and error-prone. Thick books of tables were consulted to obtain propagation corrections (known in the late 1960s as "skywave corrections") for the appropriate station/frequency signals. The propagation corrections were added to the displayed LOP values and the result plotted on large navigational charts overprinted with Omega LOPs. The chart recorders also had to be routinely checked to verify the correct lane identity.

The early receivers were "linear" in the sense that there was no limiting device for restricting the level of the input signal. In this type of receiver, the measured phase is very "clean," i.e., no phase irregularities are introduced by the receiver, but the detection circuitry is easily saturated by in-band noise bursts. Occasional noise bursts (usually caused by lightning discharges from both nearby and remote locations) generally result in only minor effects, but a series of such bursts can seriously degrade the phase tracking capability of such receivers.

The earliest operational Omega receiver designed specifically for submarine use was developed in 1967 (designated AN/WRN-3). This receiver was incompatible with existing VLF receiver antennas and was replaced in 1969 by the AN/BRN-4. Although a significant improvement over the AN/WRN-3, this receiver was still considered too large for the submarine environment and the time required to establish lane count (following loss of signals) was lengthy. The next version of the submarine Omega receiver (AN/BRN-7), produced in 1972, borrowed heavily from the technology used to develop the first *airborne* Omega receiver (see Section 2.4.2). This three-frequency, fully automatic receiver with a floating wire antenna was generally considered successful (especially in the Arctic) in spite of a scarcity of signals.* Operational evaluation by the U.S. Navy indicated position accuracies from a few hundred meters up to two miles at antenna depths of five meters (Ref. 14).

2.4.2 Second-generation Systems: Aircraft/Marine Receivers

Although the Omega military receiver development continued virtually uninterrupted through the late 1960s and into the early 1970s, the second full generation of Omega receivers for *civil* applications was introduced in the early to mid-1970s. These second-generation receivers utilized recent technological advances in microprocessors and high-performance, low-power CMOS circuits (Ref. 15). As

* Implementation of the full Omega system had just begun in 1972 so that only four station signals were available before 1975.

a result, the receivers were lighter, smaller, and easier to operate. Synchronization to the Omega pattern was automatic and, in most receivers, propagation corrections were calculated internally. More sophisticated lane resolution techniques were possible with a microprocessor-based system which resulted in greater accuracy.

Many of the advances that appeared in the second generation of Omega receivers were first employed in the development of the first operational Omega receivers for military aircraft. The receiver was designated the AN/ARN-99*and also served as the model for the AN/BRN-7 submarine receiver mentioned in Section 2.4.1. This receiver processed signals on all three common frequencies transmitted by the Omega system and contained a Kalman estimation algorithm for lane identification and position computation (see Chapter 4 and Appendix D). Propagation corrections were computed "on the fly" using an algorithm based on a model developed at the Navy Electronics Laboratory (Ref. 16). The receiver utilized a loop (H-field) antenna which was mounted in an electromagnetically quiet location on the aircraft skin. This type of antenna was generally superior to earlier blade (E-field) antennas in that it avoided "precipitation static," i.e., the noise due to charged particles picked up when passing through clouds or fog. To minimize in-band noise and improve signal detection, the signals were passed through a limiter and converted to narrowband intermediate frequencies. A latitude/longitude readout of position was also provided to save time for the pilot/navigator. Most of these features are still found in modern Omega receivers.

One factor that greatly enhanced the navigation capability of Omega receivers in the airborne environment was the inclusion of true air speed and heading data into the navigation solution. This "rate-aiding" of the Omega receiver provided important additional information which is sometimes critical in navigating through periods of poor Omega signal accessibility. Following each navigational update/solution, true air speed was compared with the Omega-computed ground track to determine the speed and direction of the winds aloft.

In the late 1970s, fully automatic receivers were offered for shipboard platforms. These receivers had features that were, in many ways, like their airborne counterparts; i.e., three-frequency signal processing, propagation corrections supplied from an internally executed algorithm, automatic pattern synchronization and lane identification, and a latitude/longitude readout. Most of these receivers were rate-aided with speed and heading provided by the ship's electromagnetic underwater log (EM log) and

*An earlier prototype version was known as AN/ARN-88.

compass. In spite of these advances, users reported problems which were traced to signal "self-interference," such as modal interference, cycle slip/jump, long-path dominance, etc. (see Chapters 5 and 6 for definition of these terms). As a result, hybrid systems that combined Omega and a satellite navigation system (using the TRANSIT satellite) became popular. These navigation systems advantageously combined the higher accuracy of the satellite fixes with the continuous navigation capability of Omega. Such systems were reportedly quite accurate and reliable (Ref. 15).

2.4.3 Modern Omega Receiving Systems

Several developments over the years from 1975 to 1990 contributed to improvements which led to the efficient, reliable, and accurate Omega-based navigation systems available today. Figure 2.4-2 illustrates a typical airborne Omega receiver system produced during this period. The system comprises a receiver processor unit that performs all computations, a control display unit that acts as a user (pilot) interface, and an antenna coupler unit.

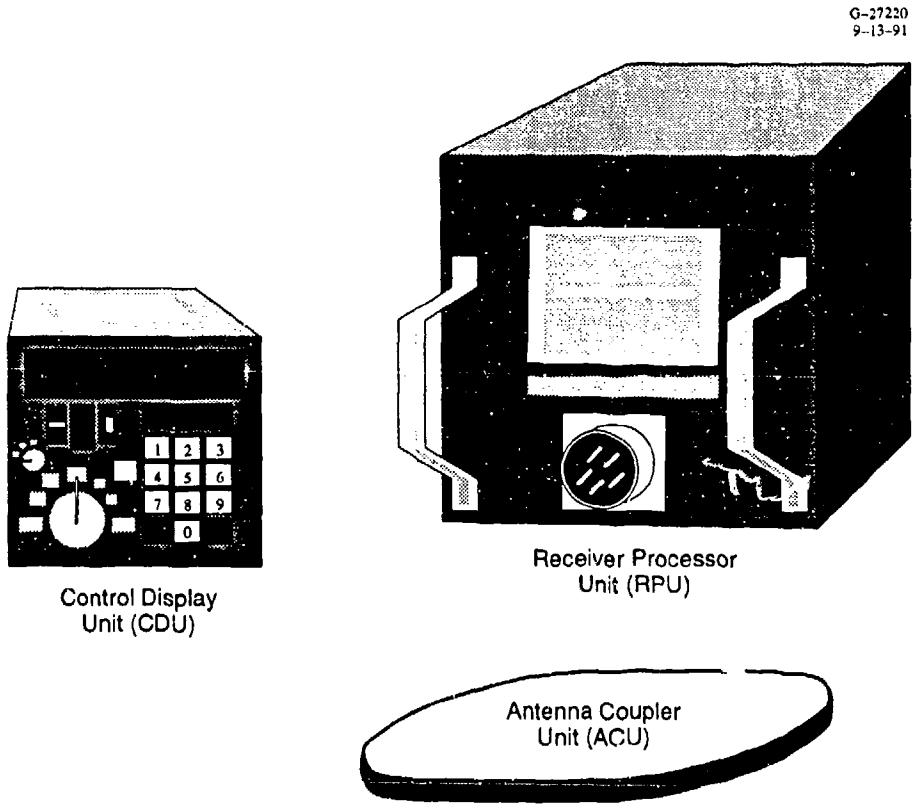

Figure 2.4-2 Typical Airborne Omega Receiver System used in the Early 1980s

One development during this period that was suggested by the earlier Draco system (see Section 2.2) was the utilization of the signals from the VLF communication stations for navigation. The carrier signals from these stations (a partial listing is provided in Table 2.4-1) are modulated with a minimum shift keying (MSK) format utilizing signals separated by 50 Hz. This small frequency separation yields a 3000 km phase difference "lane" which almost eliminates lane ambiguity. Unlike the Omega stations, the VLF communication stations are not synchronized, so that only phase changes from each station can be processed in a navigation mode. This means that VLF signal processing is used to *supplement* Omega navigation rather than acting as a substitute. Moreover, these communication signals are broadcast for national and international security purposes, so that stations can switch frequency, change modulation, or temporarily cease operation with no advance warning. Thus, although VLF signals serve a very useful supplementary function in many (mostly airborne) modern Omega receivers, they cannot play a primary navigational role because the VLF communication signals are *not* intended for navigation.

Another important development was the availability of improved signal prediction data. One of the most important sets of these data were propagation corrections, which, prior to 1974, were made available to the public solely in a tabular format. In 1974, the U.S. Coast Guard/Omega Navigation System Operations Detail (ONSOD) published a report explaining the basis of the algorithm and including a

Table 2.4-1 VLF Communications Stations*

Station ID	Location	Latitude	Longitude	Frequency (kHz)	Radiated Power (kW)
GBR§	Rugby, U.K.	52° 22′ N	1° 11′ W	16.0	45
JX§	Noviken, Norway	66° 58′ N	13° 53′ E	16.4	45
NDT†	Yokosuka, Japan	34° 58′ N	137° 01′ E	17.4	38
GQD§	Anthorne, U.K.	54° 55′ N	3° 16′ W	19.0	42
ICY§	Tavolara, Italy	40° 55′ N	5° 45′ W	20.27	43
NSS†	Annapolis, Maryland, U.S.	38° 59′ N	76° 27′ W	21.4	213
NWC†	Exmouth, Australia	21° 49′ S	114° 10′ E	22.3	1800
NPM†	Honolulu, Hawaii, U.S.	21° 25′ N	158° 09′ W	23.4	502
NAA†	Cutler, Maine, U.S.	44° 39′ N	67° 17′ W	24.0, 17.8	1200
NLK†	Jim Creek, Washington, U.S.	48° 12′ N	121° 55′ W	24.8	245
NAU†	Aguada, Puerto Rico (U.S.)	18° 23′ N	67° 11′ W	28.5	100

* This table lists most of the VLF stations whose signals are utilized by conventional Omega/VLF receiving systems; a complete list of VLF stations is given in Ref. 17.

§ Operated by the North Atlantic Treaty Organization (NATO).

† Operated by the U.S. Navy (USN).

computer program listing (Ref. 18). This allowed manufacturers to install a standardized PPC computational algorithm in a microprocessor-based receiver. An updated algorithm was published in 1980 (Ref. 19). Equally important were predictions of signal usability, usually in the form of coverage diagrams/maps, which showed the regions and times for which signals from each station should be used or avoided (see Chapter 10). This information was usually digitized and stored in the receiver serving as a reference file by a signal selection algorithm. This use of signal prediction data was made feasible by the continued development of smaller, faster, and higher-capacity microprocessors throughout the late 1970s and 1980s.

In the mid-1980s, "integrated" navigation systems which intelligently combined outputs from several navigation sensors, e.g., Omega and inertial navigation systems, began to displace single-sensor units, especially in aircraft. This idea was carried even further with "interoperable" units which combined the basic data (e.g., pseudo-ranges) from multiple systems into a single navigation output. This concept also provides protection for the user in the event that one of the systems becomes temporarily unusable or is phased out of service.

2.4.4 Changing Patterns in Users and Applications

As noted, Omega was primarily intended as a navigational aid for marine users. Thus, early emphasis was placed on the development of operational Omega receivers, such as the AN/SRN-12 for shipboard platforms. However, because of the inordinate amount of operator attention required, their comparatively low reliability, and the relatively few stations available in the 1960s and early 1970s, Omega marine receivers were not popular during this period, especially in the civil marine sector. Instead, marine users turned to TRANSIT satellite navigation systems in which fixes were obtained through Doppler measurements (i.e., measurements of the apparent signal frequency shift due to the relative velocity between the user and the satellite). The TRANSIT satellites provided accurate fixes (a few hundred meters for the two-frequency units) although the time between fixes ranged from two to six hours. Thus, by the time combined Omega/TRANSIT units (which were accurate, reliable, and required little operator attention) appeared in the late 1970s, the navigation system of choice for the marine transportation community was TRANSIT. Sub-surface use of Omega fared somewhat better since: (1) the users were entirely military and (2) the initial unit (AN/BRN-7) was based on an innovative aircraft design. Although expensive to produce, submarine Omega receivers have generally performed well over the past 20 years.

As explained in Section 2.4.2, the use of Omega receiver systems for aircraft grew rapidly during the second generation of Omega receiver development. Thus, from the outset, airborne Omega receivers enjoyed the reputation for requiring little operator attention, high reliability, and reasonably good accuracy. Supplemented with signals from the VLF communication stations and enhanced with signal selection/deselection algorithms and improved PPCs, airborne systems grew to dominate th Omega receiver markets in the 1980s. Following FAA certification of Omega on certain routes, many ot these systems were acquired by air carriers for their overseas flights. In the late 1970s, there were large acquisitions of Omega receivers for military aircraft, including the Navy's P-3 ASW (anti-submarine warfare) fleet and the Air Force's C-141 transports. The systems were less popular on general aviation aircraft, possibly because of their general confinement to continental regions, where more accurate systems, such as VOR/DME or loran were in place. Except for certain U.S. Army applications (Ref. 20), rotary wing aircraft have seen limited use of Omega receivers.

One non-navigational application of Omega signals, probably not foreseen during the early system implementation, was the tracking of meteorological balloons whose use developed rapidly in the 1980s. In these systems, balloon-borne radiosondes repeat Omega signals to a ground controller which tracks the balloon position and computes a wind speed profile with altitude. By using Omega signals, these expendable units are inexpensive and can be used practically anywhere on the globe. Recent figures (Ref. 21) indicate that over 100,000 of these units are deployed each year.

2.5 HISTORICAL DEVELOPMENTS IN OMEGA USER SUPPORT

Much of the early work in Omega involved testing the feasibility of a long-range VLF navigation system, including the stability of signal generation and the signals' day-to-day phase variation. Later work was primarily devoted to station construction and receiver development. Perhaps the earliest significant support provided to Omega users was the development of Omega charts and lattice tables by the U.S. Naval Oceanographic Office and later the U.S. Defense Mapping Agency. Following construction of the stations (except for Australia) in the latter part of the 1970s, Omega user support, principally by the U.S. Coast Guard, began to assume a more important role.

2.5.1 System Notifications and Communication

Because Omega is an open, freely accessible, global navigation system, it has always been a challenging task to notify its users of planned station off-airs, reduced power operation, insertion of new station signals, and other such critical information. The Omega Implementation Committee had recom-

mended that the suggested modulation frequencies (which were never implemented) be used to warn users of anomalous conditions, such as Sudden Ionospheric Disturbances (SIDs) or Polar Cap Disturbances* (PCDs) (see Chapter 6 for definitions of these terms). This recommendation was never implemented so that Omega operations personnel had to seek other ways to notify users.

When ONSOD was formed in 1971, an operations staff was appointed to coordinate system notifications and communications with stations, operating agencies, and users. Initially, notices of critical importance to Omega users were relayed through the Defense Mapping Agency (DMA). These notices included such events as:

- Imminent station off-air
- Occurrence of an anomalous event (e.g., PCD)
- Longer-term scheduled station off-air
- Reduction of station power
- Bringing a new station on-line.

In response, DMA issued warnings through a marine communications network in the Atlantic (HYDROLANT) and the Pacific (HYDROPAC) Ocean areas. DMA also disseminated the information in (hard-copy) Notices to Mariners and Broadcast Notices to Mariners. Local Notices to Mariners are issued by U.S. Coast Guard District Offices. As aircraft use of Omega increased, notices were also forwarded to the Federal Aviation Administration (FAA) which, in turn, sent out NOTAMs (Notices to Airmen) through its network of airports and regional offices.

Some anomalous events such as SIDs are relatively short, so that a warning message requiring many hours to deliver makes little sense. A PCD, on the other hand, can persist for several days, so that occurrence notifications are appropriate. In the 1980s, a procedure (currently in effect) was set up to increase the reliability of the PCD warnings. Stations on either end of transpolar paths (paths which transit the north or south geomagnetic polar regions[§]) are asked to report when the phase on these patns is depressed by more than 0.2 cycle for 1 to 2 hours. These reports are evaluated and compared with information from the Space Environmental Services Center (SESC) in Boulder, Colorado, and a warning message is issued by ONSCEN if all reports are consistent.

---

*Closely related to a Polar Cap Absorption (PCA) event.

[§]The geomagnetic polar regions are circular areas of approximately 1800 nm radius centered at the north and south geomagnetic poles.

Beginning around 1980, Omega status advisories and warnings were broadcast on frequencies of 2.5, 5, 10, and 15 MHz from HF broadcasting stations WWV in Fort Collins, Colorado and WWVH on the island of Kauai in Hawaii. A 40-second slot is provided at 16 minutes past the hour (WWV) and 47 minutes past the hour (WWVH) for information regarding station status, planned off-airs, and event warnings. Because of the widespread use of WWV/WWVH as a timing signal, it is thought that this mode of dissemination reaches the greatest number of Omega users.

Communications with the stations and operating agencies were initially by voice (telephone) and message (teletype). These were frequently difficult with remote stations such as Liberia or La Reunion. Message handling improved with the use of AUTODIN (AUTOmatic DIgital Network), a military communications system. Omega status messages are now sent to a variety of government sources via AUTODIN and commercial activities via telex on a weekly basis. In addition to warnings and planned station off-airs, these messages provide a detailed listing of station off-air times during the preceding week.

2.5.2 Propagation Corrections

ProPagation Corrections (PPCs) are indispensable for the proper use of Omega signals. The PPC is designed to adjust the received signal phase to a "nominal" model in which the phase is a fixed linear function of distance, independent of time or direction of signal propagation. The Implementation Committee recognized the need for "diurnal" corrections but recommended they be prepared and distributed in the form of "compensation graphs." Subsequently, it was found simpler for the shipboard navigator to use tables of corrections keyed to location (4° latitude × 4° longitude) and time (hour, half-month, and year). These tables were based on a model developed by the Naval Electronics Laboratory (now NOSC) and were produced by the Naval Oceanographic Office (later by DMA).

An ONSOD report (Ref. 18), widely distributed in 1974 explained the semi-empirical model of signal propagation (often referred to as the PPC model) on which the PPCs were based. The model combines results from complex theoretical calculations with observed signal phase data to achieve a physically based, data driven signal phase prediction algorithm. The report also presented the coded form of the algorithm so that anyone with a computer could produce PPCs at *any* point in space and time. This also had the advantage of establishing a standard PPC model whose performance is universally understood and documented

The model was recalibrated several times for specialized cases (local regions and global/single frequency) in the late 1970s. In 1980, however, an "official" three-frequency upgrade and recalibration of the model was produced. This recalibration was based on phase data collected at many locations around the world from 1965 to 1979. In 1977, ONSOD purchased specially-developed Omega monitors to provide a uniformly high-quality database for PPC model calibration. The monitor sets (MX1104) that were ultimately produced, however, were not fully deployed over the globe until the 1980s so that only a small fraction of the new monitor data was used in the 1980 PPC model recalibration. In addition, the 1980 model contained a new "term" (in the computation of predicted phase), which was exponentially dependent on year.* In the late 1980s, sufficient MX1104 data had been collected to provide a full global database for another PPC model recalibration. This high-quality data, together with reports of time-dependent phase errors in the 1980 model led ONSCEN (formerly ONSOD) in 1989 to initiate an effort to develop and calibrate a new PPC model.

2.5.3 Omega System Signal Prediction Products

Omega user information support products have evolved in consonance with a growing system, a changing user population, and advancing technology. Figure 2.5-1 provides a time-line for the development of the two principal categories of user information support products: coverage data and propagation corrections. For reference, other dates are also shown, including commencement of operation for each of the current stations and ONSOD/ONSCEN.

As noted above, most effort in the early 1970s was concentrated on station construction and bringing each new station's operations on-line. During this period, user support products emphasized information on new transmitting stations as they were brought into the system. Thus, for example, coverage information was intended to provide only "representative" data (e.g., local day, local night) on expected signal accessibility for each station and the system.

The marked shift in the Omega user/platform mix during the early 1970s also influenced the types of Omega user support information produced. As the Omega user community evolved from marine-dominated to airborne-dominated, corresponding changes were made in coverage information. Thus, for example, coverage conditions applicable to the marine user, e.g., portrayal of local-time signal coverage, were changed to those tailored to the airborne user, e.g., signal coverage for several global times.

---

* By 1990, ONSCEN determined that this term had grown beyond that projected in the 1980 calibration and was beginning to seriously degrade phase prediction accuracy. As a result, ONSCEN directed that the term be deleted from all PPC model software (Ref. 22).

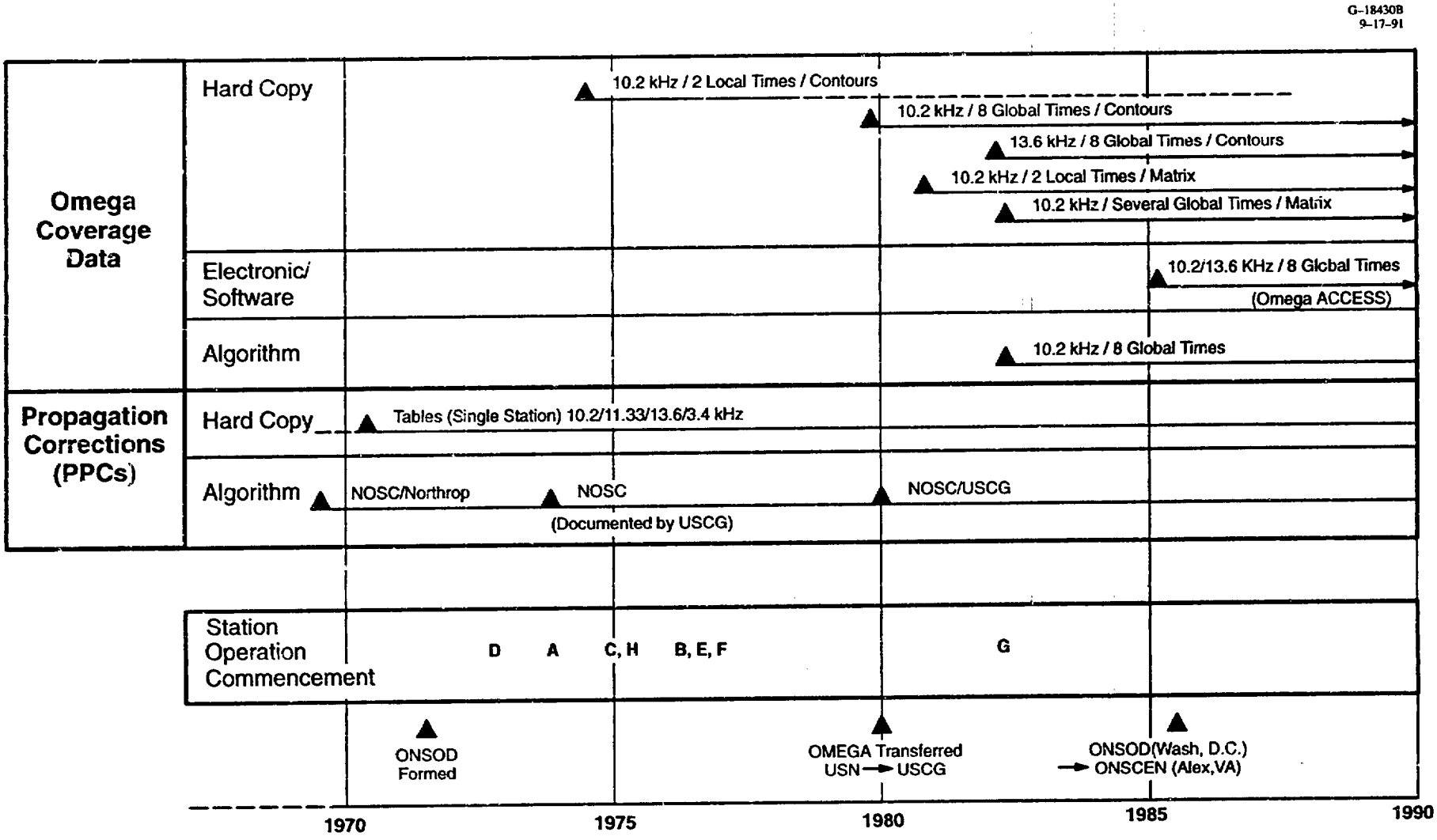

Figure 2.5-1 Evolution of Omega User Support Products

Advancing information display technology also changed the format and use of Omega user support information. As shown in Fig. 2.5-1, early coverage products were provided exclusively in hard copy. As microprocessor technology moved forward to make personal computers commonplace, coverage information was disseminated as a software package for use on a PC with a color graphics terminal. The electronic medium not only allows rapid access/efficient storage, but also permits use of other features, such as toggling and overlays to enhance understanding of the coverage characteristics.

Before Omega was declared fully operational, the system providers needed the fully operational system coverage information to evaluate Omega as a replacement for Loran-A and other similar radionavigation systems. In response to this need, the first coverage product, in the form of signal coverage diagrams, was developed in 1976. Due to changing Omega user population and requirements and improving Omega receiver/display technologies, the content and display of the information have undergone several improvements (see Chapter 10).

The first coverage information product consisted of two hard-copy coverage diagrams displaying the worldwide availability of coverage from the fully operational (eight-station) Omega system:

- For the primary Omega navigational signal frequency of 10.2 kHz
- For the "usable" signal access criteria consistent with known receiver characteristics
- At two local times having the supposed "worst" (local summer noon) and "best" (local winter midnight) local propagation conditions for the Omega signals.

The diagrams were developed using the best available theoretical Omega signal propagation models. These models have also undergone several improvements and have been used to develop later coverage products. Although the hard-copy diagrams were extremely complex to interpret and use, there was no other readily available way to display the coverage information with the available technology.

Later diagrams were constructed using improved coverage prediction models for eight fixed global times at 10.2 and 13.6 kHz. The eight times (0600 and 1800 UT in the months of February, May, August, and November) were selected to provide an adequate sample of the time-dependent global coverage using a manageable number of diagrams. Initially, these diagrams were provided in hard-copy format, but with the advent of inexpensive microprocessors, this coverage information was incorporated into Omega ACCESS (Automated Composite Coverage Evaluator of System Signals), a computer-based Omega coverage display and analysis product (see Chapter 10). This method of coverage display allows for greater flexibility in portraying signal coverage than hard-copy diagrams. Omega ACCESS was targeted for IBM PC/XT/AT machines with CGA color monitors with or without a mouse. Although the underlying signal coverage data

included only fixed threshold information, the use of color made the display more appealing. More importantly, the computer environment readily permitted the "compositing" of multiple single-station coverage diagrams to display system coverage under a variety of conditions.

The eight-time coverage diagrams were found to vary: (1) little from one computed month to the next, and (2) significantly between the two computed hours. As a consequence, the eight-time coverage information was useful, but not adequate to determine coverage between the two computed hours. It was recognized that 24-hour coverage information was necessary to properly characterize the Omega signal environment both as a prediction tool for users and as a means of system performance assessment.

In 1989, the Omega Navigation System Center (ONSCEN) sponsored development of a 24-hour-a-day, four-month worldwide database of signal coverage calculations at 10.2 and 13.6 kHz. This database was developed primarily as a component of the Omega System Availability Model, a model that establishes the framework for calculation of the overall Omega system availability (a system performance index), computed for a given scenario by means of a computer workstation known as PACE (Performance Assessment and Coverage Evaluation). This new coverage database not only expands the time domain of the signal coverage data by a factor of 12, but also spatially references the data in a matrix format of latitude/longitude cells. The 24-hour-a-day, four-month/two-frequency signal coverage database and some of the PACE features are included in an expanded version of Omega ACCESS, known as Omega ACCESS II.

2.5.4 Omega User Group

Users of most large, freely accessible navigation or communication systems eventually form user associations in order to obtain basic system information/access, make inquiries regarding future plans, and share experiences with other users. Omega is no exception to this process and has had an active user association in place since 1975. Until 1993 the group was known as the International Omega Association (IOA). In 1993, the organization sought to widen its scope and became the International Navigation Association (INA).*

*The INA address is:

International Navigation Association, Inc.
P.O. Box 2324
Arlington, VA 22202-0324
USA

In February 1975, the first planning meeting for an Omega support group was held. A link-up with the Wild Goose Association (WGA, the Loran-C user group) was briefly considered but rejected because of the perceived need for a distinctly international group. A constitution and set of bylaws were drafted and approved later that year. As stated in the original constitution, the mission of the IOA was to:

- Advance the cause of Omega as an international navigation aid
- Encourage the use of Omega by all segments of the international navigation community
- Disseminate information on the status of the system and developments related to it
- Provide an international forum for the exchange of information concerning Omega
- Work with other organizations for the advancement of the art of navigation
- Encourage standardization and the generation of specifications for all classes of Omega users.

The bylaws of the INA (adopted March 1993) incorporated most of these objectives but broadened their scope to include all long-range radionavigation systems. More than 300 representatives from the user, industry, government, and the academic communities attended the first annual IOA meeting in Arlington, Virginia in July 1976. The attendees included representatives from the U.S., Australia, Canada, England, France, and Norway (Ref. 23).

The annual meetings have been the chief focus of the IOA/INA's technical activity. In keeping with its charter, the IOA/INA has alternated meeting sites between U.S. and non-U.S. locations. Table 2.5-1 lists the IOA/INA annual meetings and locations through 1993. The meetings generally last one week and include several tutorial sessions, a full program of technical presentations, two user forums, a business meeting, and a navigation-related field trip.

Foremost among IOA/INA publications are the proceedings of the annual meetings (including transcripts of questions and comments), which serve as a primary archival source for Omega information. The INA also issues a newsletter several times during the year and maintains a bibliography of Omega publications. The INA is loosely affiliated with the Institute of Navigation and maintains an informal relationship with the WGA and the Institute of Electrical and Electronics Engineers. Finally, in keeping with its advocacy role, the INA encourages concerned users to communicate their support for the system to U.S. Department of Transportation which, together with the U.S. Department of Defense, publishes the Federal Radionavigation Plan. This plan, which is jointly signed by the Secretaries of Transportation and Defense, promulgates U.S. policy regarding the future roles of federally supported navigation systems. Current plans are that Omega will continue operation through at least the turn of the century.

Table 2.5-1 **International Omega Association/International Navigation Association Meeting Locations**

Meeting	Year	Location
IOA 1	1976	Arlington, Virginia
IOA 2	1977	Linthicum Heights, Maryland
IOA 3	1978	London, England
IOA 4	1979	San Diego, California
IOA 5	1980	Bergen, Norway
IOA 6	1981	Montreal, Quebec, Canada
IOA 7	1982	Arlington, Virginia
IOA 8	1983	Lisbon, Portugal
IOA 9	1984	Seattle, Washington
IOA 10	1985	Brighton, England
IOA 11	1986	Quebec City, P.Q., Canada
IOA 12	1987	Honolulu, Hawaii
IOA 13	1988	Munich, Germany
IOA 14	1989	Long Beach, California
IOA 15	1990	Benoa, Bali, Indonesia
IOA 16	1991	Vancouver, B.C., Canada
IOA 17	1992	Amsterdam, The Netherlands
IOA 18	1993	Orlando, Florida

2.6 ABBREVIATIONS/ACRONYMS

A	Omega Station Norway
ACCESS	Automated Composite Coverage Evaluator of System Signals
ACU	Antenna Coupler Unit
AN/ARN-88	Prototype airborne Omega receiver for U.S. Navy
AN/ARN-99	First-generation airborne Omega receiver for U.S. Navy
AN/SRN-12	First-generation shipboard Omega receiver for U.S. Navy
AN/WRN-3	Prototype submarine Omega receiver for U.S. Navy
AN/BRN-4	First-generation submarine Omega receiver for U.S. Navy
AN/BRN-7	Second-generation submarine Omega receiver for U.S. Navy
ASW	Anti-submarine Warfare
AUTODIN	AUTOmatic DIgital Network
B	Omega Station Liberia (formerly Trinidad)
C	Omega Station Hawaii
CDU	Control Display Unit
CRT	Cathode Ray Tube
CW	Continuous Wave
D	Omega Station North Dakota (formerly Forestport, NY)
DMA	Defense Mapping Agency
DME	Distance Measuring Equipment
E	Omega Station La Reunion
F	Omega Station Argentina
FAA	Federal Aviation Administration
Fr.	France
FSK	Frequency Shift Keying
G	Omega Station Australia
H	Omega Station Japan
HF	High Frequency
HYDROLANT	Hydrographic warnings for the Atlantic Ocean region
HYDROPAC	Hydrographic warnings for the Pacific Ocean region
Hz	Hertz
IF	Intermediate Frequency
INA	International Navigation Association
IOA	International Omega Association

IOTC	International Omega Technical Commission
kHz	Kilohertz
km	Kilometer
kW	Kilowatt
LF	Low Frequency
LOP	Line of Position
MF	Medium Frequency
MHz	Megahertz
MX1104	Omega monitor receiver used by ONSOD/ONSCEN
NATO	North Atlantic Treaty Organization
NOSC	Naval Ocean Systems Center
NOTAM	Notice to Airmen
N.Z.	New Zealand
ONSCEN	Omega Navigation System Center
ONSOD	Omega Navigation System Operations Detail
PACE	Performance Assessment and Coverage Evaluation
PCA	Polar Cap Absorption
PCD	Polar Cap Disturbance
PPC	Propagation Correction
RF	Radio Frequency
RMS	Root Mean Squared
RPU	Receiver Processor Unit
SESC	Space Environmental Services Center
SID	Sudden Ionospheric Disturbance
TRANSIT	U.S. Navy navigation satellite system
U.K.	United Kingdom
USN	U.S. Navy
VHF	Very High Frequency
VLF	Very Low Frequency
VOR	VHF Omni-directional Receiver
W	Watts
WGA	Wild Goose Association (Loran)
WWV	Timing signal broadcast station — Fort Collins, CO
WWVH	Timing signal broadcast station — Kauai Island, HI

2.7 REFERENCES

1. Watt, A., *VLF Radio Engineering*, International Series of Monographs in Electromagnetic Waves, Vol. 14, Pergamon Press, 1967.

2. Bowditch, N., *American Practical Navigator*, Publication No. 9, Defense Mapping Agency Hydrographic Center, 1977 Edition.

3. Pierce, J., *Memoirs of John Alvin Pierce*, Excerpts appearing in the IOA Newsletter, Special Edition, June 1988.

4. Pierce, J., Palmer, W., Watt, A., and Woodward, R., *Omega: A Worldwide Navigational System, System Specification, and Implementation*, Second Edition, Prepared for the U.S. Navy Department, Bureau of Ships and submitted through the Office of Naval Research. Published by Pickard & Burns Electronics, Waltham, MA, May 1966.

5. Thomson, LT R., U.S. Coast Guard Omega Navigation System Center, Alexandria, VA, private communication, June 1990.

6. Rishbeth, H., and Garriott, O., *Introduction to Ionospheric Physics*, Academic Press, 1969.

7. Chalmers, J., The first suggestion of an ionosphere, *Journal of Atmospheric and Terrestrial Physics*, Vol. 24, No. 219, 1962.

8. Thomson, J., *Conduction of Electricity Through Gases*, Cambridge University Press, 1906.

9. Appleton, E., and Barnett, H., Local reflections of wireless waves from the upper atmosphere, *Nature*, Vol. 115, pp. 333–334, 1925.

10. Breit, G., and Tuve, M., A radio method of estimating the height of the conducting layer, *Nature*, Vol. 116, p. 357, 1925.

11. Chapman, S., The absorption and dissociation or ionizing effect of monochromatic radiation in an atmosphere on a rotating earth, *Proceedings of the Physical Society*, London, Vol. 43, pp. 26–45, 1931.

12. Casselman, C., private communication, 22 July 1991.

13. Evans, D., and McCarthy, J., The automation of the AN/SRN-12: A new tool for the navy navigator, *Proceedings of the First Annual Meeting of the International Omega Association*, Arlington, VA, July 1976.

14. Wilkes, O., and Gleditsch, N., *Loran-C and Omega: A Study of the Military Importance of Radionavigation Aids*, Norwegian University Press, Oslo, 1987.

15. Perlowski, W., User acceptance of Omega in the marine community, *Proceedings of the Omega Workshop*, Atlantic City, NJ, May 1982.

16. Swanson, E., and Brown, R., Omega propagation prediction primer, *NELC* Technical Note TN 2102, 1972.

17. Kleinhans, C., Fixed VLF/LF Database, Technical Document 1965, Naval Ocean Systems Center, San Diego, CA, October 1990.

18. Morris, P., and Cha, M., Omega Propagation Corrections: Background and Computational Algorithm, Report No. ONSOD 01-74, December 1974.

19. Morris, P., and Swanson, E., New coefficients for the Swanson propagation correction model, *Proceedings of the Fifth Annual Meeting of the International Omega Association*, Bergen, Norway, August 1980.

20. Lawson, C., Jr., Wise, M., and Saganowich, J., Army Airspace Command and Control (A2C2), *Proceedings of the Eleventh Annual Meeting of the International Omega Association*, Quebec City, P.Q., Canada, August 1986.

21. Stratton, A., Report on Omega User's Survey Project, *Proceedings of the Fifteenth Annual Meeting of the International Omega Association*, Sanur, Bali, Indonesia, September 1990.

22. Wenzel, CAPT R., McManus, H., Casswell, R., and Vannicola, V., The 1980 Omega PPC model time should not be used, *Proceedings of the Fifteenth Annual Meeting of the International Omega Association*, Sanur, Bali, Indonesia, September 1990.

23. Sakran, C., Jr., The International Omega Association, Briefing given for the International Omega Technical Commission, June 1990.

CHAPTER 3

OMEGA TRANSMITTING STATIONS

Chapter Overview *— This chapter describes some important features of the Omega transmitting station network, including its operation as a coordinated system and the suite of equipment at each station. Following the chapter introduction in Section 3.1, the system operating policy and operational procedures are explained in Section 3.2. This section also contains a description of station maintenance procedures. Section 3.3 presents the Omega signal specification and other important system parameters and data. Section 3.4 provides an overview of the major equipment subsystems at each station: timing and control, transmitter, antenna tuning, and the antenna structure. Finally, the near-field behavior of the radiated signal and its relationship to antenna currents and other parameters are explained in Section 3.5. Sample problems and problems to be solved by the reader are found in Section 3.6. Abbreviations and acronyms used in the chapter are given in Section 3.7, followed by the cited references listed in Section 3.8.*

3.1 INTRODUCTION

The signals from the eight Omega transmitting stations shown in Fig. 3.1-1 provide continuous signal coverage over most of the globe. The signals are generated using electronics equipment that is virtually the same for all stations in the system; the station antennas, however, differ substantially. Because they radiate long-wavelength VLF signals, the antennas are the largest physical structures at the stations. Due to its size, the antenna structure often makes use of the local terrain, for example, in Norway, a portion of the antenna spans a fjord.

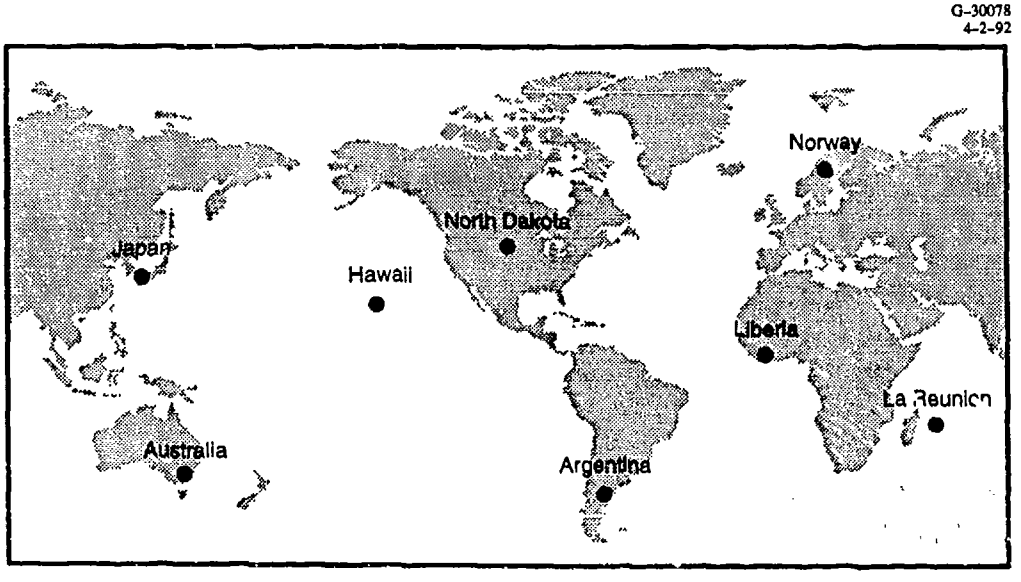

Figure 3.1-1 Omega Transmitting Station Network

Three types of antennas are employed in the Omega system: (1) grounded tower, (2) insulated tower, and (3) valley-span. Beyond the antenna, about 20 to 50 km from the effective phase center, each station has an associated signal monitoring facility. These unattended facilities perform several functions, including monitoring the performance of the associated station, providing data necessary to phase-synchronize the stations, and detecting the effects of solar-terrestrial events that cause anomalous shifts of the propagated signal phase.

Table 3.1-1 provides information on the eight Omega stations including the name of the municipality nearest to each transmitting station. The associated transmitting antenna types and their approximate dimensions are also included in the table.

The Omega signal transmission format is illustrated in Fig. 3.1-2. Across each of the eight rows in the figure is a 10-second sample of the signal frequencies transmitted by a particular station. Important features of this time/frequency multiplex format are:

- Four common signal frequencies are transmitted: 10.2, 11⅓, 13.6, and 11.05 kHz
- One unique signal frequency is transmitted by each station
- An interval of 0.2 second separates each of the eight transmissions
- The transmission periods vary in length.

Table 3.1-1 Omega Transmitting Station Locations and Antenna Types

STATION LETTER DESIGNATION	NEAREST MUNICIPALITY	ANTENNA TYPE (DIMENSION)	POSITION:* Latitude Longitude
A	Bratland, Norway	Valley Span (2 spans) (3505 m)	66° 25′ 12.68″ N 13° 8′ 13.07″ E
B	Paynesville, Liberia	Grounded Tower (427 m)	6° 18′ 19.26″ N 10° 39′ 51.85″ W
C	Kaneohe, Hawaii	Valley Span (6 spans) (1524 m)	21° 24′ 16.92″ N 157° 49′ 50.96″ W
D	LaMoure, North Dakota	Insulated Tower (366 m)	46° 21′ 57.40″ N 98° 20′ 8.22″ W
E	Plaine Chabrier, La Reunion Island	Grounded Tower (427 m)	20° 58′ 26.90″ S 55° 17′ 23.62″ E
F	Golfo Nuevo, Chubut, Argentina	Insulated Tower (366 m)	43° 3′ 12.79″ S 65° 11′ 26.81″ W
G	Woodside, Victoria Australia	Grounded Tower (427 m)	38° 28′ 52.42″ S 146° 56′ 7.06″ E
H	Shushi-Wan, Tsushima Island, Japan	Insulated Tower/ (457 m)	34° 36′ 56.05″ N 129° 27′ 13.12″ E

*Coordinates based on WGS-84 spheroid.

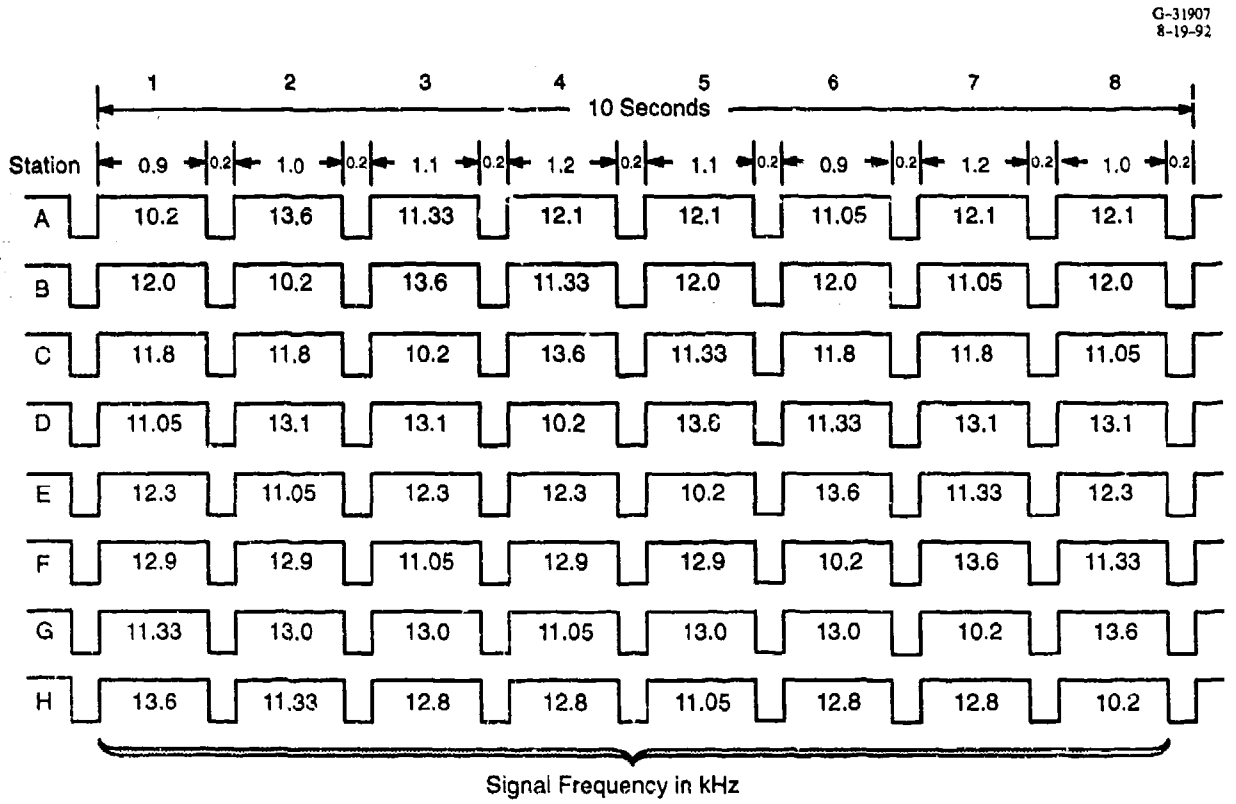

Figure 3.1-2 Omega Signal Transmission Format

The last feature makes it possible to synchronize a receiver to the format in the stand-alone mode of operation. For example, if a user determines that a 10.2 kHz transmission segment (repeated every 10 seconds) is 1.2 seconds in duration, then, according to Fig. 3.1-2, the transmitting station could be either Station D (North Dakota) or Station G (Australia). However, a measurement of the duration of the succeeding transmission segment at a frequency of 13.6 kHz would discriminate between Station D (1.1 seconds) and Station G (1.0 second).

At any given common frequency, Omega signals from each station are time-synchronized to each other to within an accuracy of about two microseconds. Moreover, the stations are also synchronized to within 1 to 2 microseconds of the UTC epoch (a specific time marker). Time-synchronization at each station is measured with respect to the station epoch, the point in time (repeated every 30 seconds) at which all station signal frequencies are aligned and the signal at the antenna is zero with the signal level (voltage) increasing positively. Thus, the Omega epochs at all stations have an average value (the mean system time) that is within 1 to 2 microseconds of the UTC epoch and a scatter of less than 2 microseconds. On a scale of seconds, however, Omega and UTC time formats significantly differ due to the injection of "leap" seconds. At 0000 UT on 1 January 1972, the Omega and UTC scales were identical

(on the scale of seconds). Since that time, however, leap seconds have been introduced into the UTC time scale on a nearly annual basis, while Omega does not include such leap seconds due to substantial coordination and procedural difficulties. Thus, as of 31 December 1993, Omega time leads UTC by 18 seconds.

At each station, the electronics equipment and supporting structures are usually described in terms of four major subsystems:

- Timing and control
- Transmitter
- Antenna tuning
- Antenna structure.

The timing and control subsystem is the "master" equipment group at the station since it provides the input signal at a precisely controlled frequency and phase. Control circuitry in this subsystem also governs the operation of equipment in other subsystems. The transmitter subsystem is responsible for signal amplification necessary to achieve worldwide coverage. The function of the antenna tuning subsystem is to efficiently match the amplified signal level/frequency with the antenna system impedance on a real-time basis. The antenna structure itself is designed to efficiently launch the signal into the earth-ionosphere waveguide.

Maintaining the operation of a full-time continuously operating navigation system within operational specifications is critically important and challenging. Wherever possible, redundancy has been incorporated into the station equipment design to mitigate critical component failures. Component replacement schedules are followed to minimize sudden failures. Maintenance requiring station off-air is planned well in advance during specific months to minimize coverage and availability deficiencies.

Section 3.2 presents the operating principles and guidelines followed by ONSCEN and the partner nations in their mission to operate and maintain the Omega stations and system. Much of the information in this section is obtained from Ref. 1. Signal specifications are given in Section 3.3 and a description of the four major equipment subsystems at each station is found in Section 3.4. Finally, a discussion of the fields in the vicinity of the station antennas, together with the antenna currents, limiting voltages and power levels, and pulse waveforms are presented in Section 3.5.

3.2 SYSTEM OPERATING POLICY AND PROCEDURES

3.2.1 Omega System Operating Policy

The Omega navigation system transmitting stations radiate phase-synchronized very low frequency (VLF) radio signals from eight stations that are more or less uniformly spaced over the surface of the globe. Under normal propagation conditions, the expected 95 percent radial two-dimensional position accuracy for a receiver with no previous estimate of location (but with knowledge of proper lane) is 3.6 km. for mostly daytime paths and 7.2 km for mostly nighttime paths. The system is intended to provide a 95 percent system availability, i.e., a probability of 0.95 that a user at any worldwide location and time can, with his properly functioning receiver, process three or more usable Omega signals to achieve successful navigation.

In terms of operating elements, the Omega system is composed of the eight transmitting stations, together with operating and support agencies of the partner nations, the Japan Maritime Safety Agency (JMSA), and the United States Coast Guard Omega Navigation System Center (ONSCEN). A representative from each operating agency is a member of the International Omega Technical Commission (IOTC), an advisory body that establishes and coordinates operating policy.

Under the direction of the Chief, Office of Navigation Safety and Waterway Services, U.S. Coast Guard Headquarters, the Commanding Officer, ONSCEN, is responsible for operational control of the Omega system. As the control element for Omega operations, ONSCEN issues directives and approves requests regarding operational status. Three of the most important operational functions exercised by ONSCEN are:

- Approval of specific off-air maintenance periods
- Calculating weekly synchronization data in parallel with MSA to ensure data integrity
- Issuing routine Omega status advisories and initiating navigational warnings due to external events that may adversely affect Omega navigation.

Station off-air requests usually concern specific dates for a station's annual maintenance and are made well in advance of the off-air time. Less frequent, but more urgent requests for station off-air stem from failure or imminent failure of one or more equipment items that require repair and replacement within a few hours to a few days. The back-up computation of synchronization corrections by ONSCEN is important in ensuring system accuracy/integrity (see Chapter 7). Advisories are issued for a station's

emergency scheduled off-air following approval of the off-air request. Warnings of polar cap disturbances (PCDs), which are detected by the station monitors and directly affect signal phase on transpolar paths, are broadcast through standard dissemination channels. Other operational functions performed by ONSCEN that are important but less urgent include:

- Monitoring overall system performance
- Acquiring, processing, and analyzing Omega signal data from a network of monitors and airborne data collection platforms
- Performing system maintenance engineering facility functions for Omega electronic equipment
- Coordinating logistic support for Omega stations
- Providing annual Omega training for station personnel
- Consulting with other national and international agencies on Omega activities of mutual interest
- Maintaining liaison with Omega equipment manufacturers.

Signal monitoring and data acquisition/analysis activities are crucial to the continuing evaluation of system performance (see Chapter 8). The annual training function performed by ONSCEN refers to a multi-week course on station operation and maintenance given at ONSCEN for selected personnel from each station. The last bullet listed refers primarily to ONSCEN's dissemination of new propagation correction (PPC) models or coverage information to receiver manufacturers and the subsequent feedback from them regarding the information's utility and accuracy.

3.2.2 Omega System Partner Nations

The Omega navigation system operates as an international partnership by a group of nations whose members benefit from Omega as a safe and reliable means of global navigation. Each station is staffed and operated by the country in which it is located, referred to as the partner nation. The operation and administration of the system is governed by a series of bilateral diplomatic agreements between each of the partner nations and the United States. Each agreement specifies the mutual responsibilities of the partner nation and the United States, including the degree of material, technical, and financial support required. Appended to the diplomatic agreements are technical agreements containing the technical and administrative details of station operations.

Each station is responsible for continuous transmission and monitoring of radiated Omega signals as specified in the Operations Bill (see Appendix G). A constant watch is maintained by each station to detect signal errors or propagation anomalies and insure proper operation. Each station provides on-the-job training to ensure qualified personnel and properly operating equipment.

Each partner nation is responsible for staffing, operation, and management of its transmitting station as specified in the bilateral agreement with the United States. This responsibility is carried out by an operating agency designated by the government of the partner nation. Additional coordination and support may be required from other agencies within the partner nation government. The operating agency normally acts as the partner nation's focal point for Omega matters. Table 3.2-1 lists the operating agencies associated with the eight stations.

Table 3.2-1 Omega Transmitting Stations and Operating Agencies

STATION	OPERATING AGENCY
A Norway	Norwegian Telecommunication Administration
B Liberia	Liberian Ministry of Transportation, Commerce, and Industry
C Hawaii (USA)	U.S. Coast Guard
D North Dakota (USA)	U.S. Coast Guard
E La Reunion (France)	French Navy
F Argentina	Argentine Navy
G Australia	Australian Maritime Safety Authority
H Japan	Japanese Maritime Safety Agency

In addition to operating Omega Station Japan, JMSA is responsible for synchronizing of the signal phase from all stations. The synchronization process consists of determining the phase offsets and corrections and applying the corrections at each station. The phase offsets are determined from daily satellite timing measurements and reciprocal path phase measurements. This weekly data is independently processed by both JMSA and ONSCEN who verify each other's results. JMSA issues the final corrections to the stations where they are implemented within a few hours of receipt.

3.2.3 Station Operational Procedures

Personnel at each transmitting station control the transmitted signal in terms of time, frequency, amplitude, and signal purity. The source signal (from the on-line cesium standard) is digitally processed to produce signals at the four common frequencies and one unique frequency according to the signal format assignment shown in Fig. 3.1-2. The signal time-frequency pattern for each station is given by the format assignment, and the signal amplitude is controlled so that the output radiated power is nominally 10 kW (see Section 3.5).

Each station maintains a 24-hour watch to ensure continuous, full-power transmission on each frequency at each time segment according to the Operations Bill (Appendix G). Training and frequent review of operational guidelines ensure that station personnel act to immediately restore signal transmissions following an equipment failure.

At each station monitor receiver (see Section 3.3.2), the signal phase data received from remote Omega stations is referenced to the signal transmitted by the local station and the results are used for synchronization reporting and anomaly detection. Phase data to support system synchronization includes both 10.2 and 13.6 kHz measurements on specific paths (remote stations) and times (UT hours). This is necessary so that 10.2 and 13.6 kHz reciprocal path information can be derived and entered directly into the synchronization program (see Chapter 7).

Received signal phase excursions from "normal" values exceeding 20 centicycles (cec) are immediately reported to ONSCEN since they may represent the onset of a polar cap disturbance (PCD; see Chapter 6). In this case, normal means the average of the phase data (path and hour) for the previous five days. The initial PCD report issued by the station includes the onset time, the path, and the current and reference phase values at 10.2 and 13.6 kHz. Following the initial PCD report, messages are sent to ONSCEN on a regular basis (same times as those used from synchronization data reporting) specifying the level (phase excursion) of the PCD. Remote data access (see Chapter 8) may also be used to monitor the PCD with much better time resolution. When all or nearly all PCD reports indicate excursions under 20 cec, ONSCEN instructs all reporting stations to cease further reports.

Table 3.2-2 shows the measurement times for synchronization data as well as for PCD reporting. Each measurement corresponds to a particular path-time in which the path is represented by a remote transmitting station and monitor receiver site, and the time is indicated by UT hour. All measurements are referenced to the time and phase at the station associated with the station monitor. In the case of Loran-C and GPS, the receivers are located in the Timing and Control Room at the station. The transmitting station codes are listed in the first column of the table and station monitor codes across the top. Measurement times (UT hours) for particular paths are indicated for the entire year or for designated monthly intervals. Path-times marked by a shaded cell indicate additional use for PCD reporting. As an example, the phase reading on the path from Station G (Australia) to ARGE2 (Argentina's station monitor) is measured (both for synchronization and PCD reporting purposes) at 0900 UT between April 1 and September 30 and at 2100 UT from October 1 to March 31. Note that Loran-C measurements are made at only three stations, whereas GPS data is recorded at all stations.

Table 3.2-2 Path-times for Synchronization Measurements

TRANSMITTING STATION	STATION MONITOR							
	NORWY	LIBER	HAWAI	NDAK	REUNI	ARGEI	AUSTS	JAPAN
A		1300	0500 (Oct-Mar) 1700 (Apr-Sep)		1100			1800
B	1300			1600	1000	1500		
C	0500 (Oct-Mar) 1700 (Apr-Sep)			2000			2400	0100
D		1600	2000			1700		1100 (Oct-Mar) 2200 (Apr-Sep)
E	1100	1000			1500	1800	0600	
F		1500		1700	1800	1800	0900	
G			2400		0500	0000		0400
H	1000		0100	1100 (Oct-Mar) 2200 (Apr-Sep)			0400	
Loran C	1200							0400
GPS	0816	0846	0916		0616	0646	0716	0746

3.2.4 Station Maintenance

The principal operational objective of the Omega Navigation System Center is to ensure, to the fullest possible extent, the continuous on-air and properly functioning status of all transmitting stations. If a station must be off-air, prompt advance notification of the event to the greatest possible number of users is a primary goal. The most serious danger to system users occurs when a station becomes disabled without any advance warning. To minimize this possibility, each station is authorized to go off-air for a particular month each year for maintenance and preventive maintenance.

Station off-air events are classified into three groups:

- Unscheduled off-airs
- Scheduled off-air (short advance notice)
- Annual maintenance off-air (long advance notice).

Unscheduled off-air events result from unforeseen circumstances -- usually equipment failure. Their individual occurrences may be considered random but compiled statistics indicate characteristics that can be tied to individual stations (see Chapter 11). Unscheduled off-airs of less than two minutes duration are not included in these statistics since they occur infrequently and most receiver time

constants are greater than one to two minutes so that they are "transparent" to the user. Because these events occur with either no warning or on extremely short notice to station personnel, no advance notification is given to system users. ONSCEN, however, is notified as soon as possible of the unscheduled off-air occurrence, including the probable time for resumption of on-air. If the projected off-air duration is sufficiently long, an advisory is issued. Total unscheduled off-air for a month varies from tens of minutes to several hours, depending on the station (Ref. 6).

Scheduled off-air events are, as the name implies, planned conditions under which a station ceases operation. These events usually occur when station personnel become aware of an imminent component failure that will cause the station to go off-air for more than 30 minutes. These types of off-airs are distinguished from the longer-term annual maintenance off-airs that are not scheduled on the basis of an imminent casualty. In these cases, "planned" refers to both the time at which the off-air begins and the off-air duration. The planning includes an advance notice of the off-air conditions (start time and duration) to system users although the amount of advance notice may vary considerably, depending on the urgency of the work to be done during the off-air. Typical advance notice for these events varies from 5 to 10 days, though it can be shorter or longer. Total monthly scheduled off-air durations vary from 30 minutes to a few days, depending on the station (Ref. 6).

A *station's annual maintenance* activity involves off-air periods having two main features:

- The off-air period for maintenance and repair occurs in a specific, distinct month for each station (see Fig. 3.2-2)
- The scheduled off-air period for annual station maintenance is planned well in advance so that system users are generally given 1 to 2 months' advance notice.

Any antenna, electronics, or structural maintenance or repair function that is not urgent is scheduled during the station's annual maintenance period. Because of the advance planning, several maintenance or repair projects can proceed in parallel during the off-air. Station personnel and contractors often work extra shifts during this period, although, when feasible, the station is sometimes brought on-air during a slack period, e.g., local night. The off-air period for annual maintenance cannot exceed one month (waived only under very exceptional conditions) but the actual period is generally much shorter, since stations are off-air only as long as equipment or safety considerations dictate. For most years, annual maintenance periods vary in duration from a few days to two weeks. Infrequent major projects, such as tower painting or replacing an antenna span, may require an entire month. The annual maintenance off-air schedule shown in Fig. 3.2-1 is based on such considerations as local climatic conditions, availability of maintenance contractors, operating agency budget cycles and cost ceilings, signal coverage and availability (see Chapter 6 of Ref. 6), and annual Omega training.

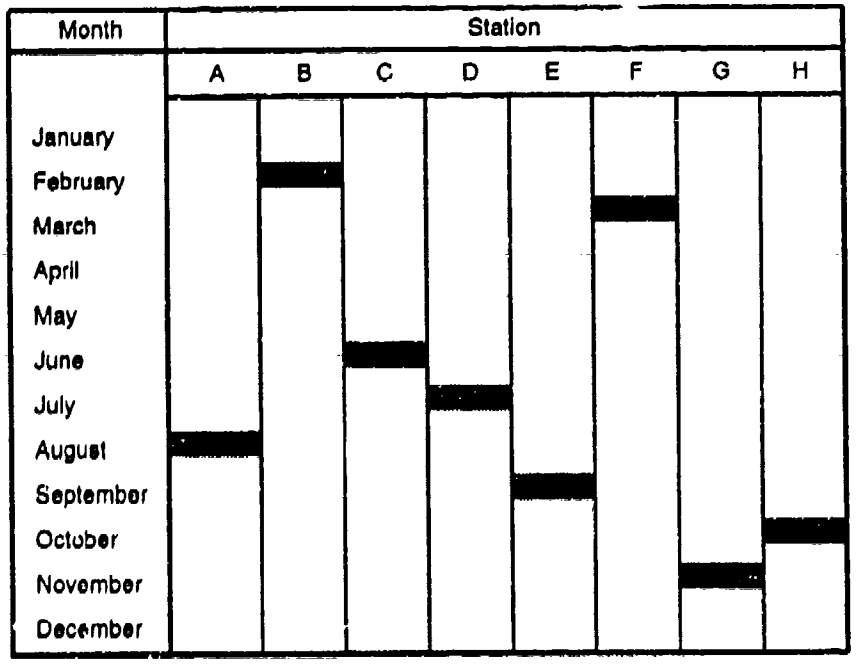

Figure 3.2-1 Omega Station Annual Maintenance Months

Off-air statistics based on historical data (Ref. 7) have been compiled for use in calculating the system availability index by means of the Performance Assessment and Coverage Evaluation (PACE) decision support tool (see Chapter 11 and Appendix C). In the system availability model, unscheduled off-air events at a station are modeled as random events, independent of off-air events at other stations. Scheduled off-airs are also modeled as random events (in terms of event knowledge by a user at the beginning of a month) but are *not* independent of scheduled off-air events at other stations. Because their occurrence time and duration are usually known at the beginning of a month, annual maintenance off-air periods are treated as deterministic (non-random) events in the system availability model (Ref. 6). In Chapter 6 of Ref. 6, an algorithm is described that determines the annual maintenance schedule that maximizes the overall system availability subject to the local station constraints (climatic conditions, etc.) listed.

3.3 SYSTEM PARAMETERS AND SPECIFICATIONS

3.3.1 Signal Transmission Format Assignment

The Omega signal transmission pattern (Fig. 3.1-2) has a time/frequency multiplex format in which a single frequency is transmitted by only one station at any given segment. Four common

frequencies (10.2, 11.05, 11⅓, and 13.6 kHz) are transmitted by all stations and, in addition, each station transmits a unique frequency for a total of 12 frequencies transmitted by the system. Each station transmits eight pulses approximately one second in duration within a time frame of ten seconds. The pulse durations (or widths) in the pattern vary so that detection of two signals, each with its associated frequency and pulse width uniquely determines the transmitting stations, thereby permitting receiver synchronization. A "guard" (or silent) time slot of 200 milliseconds (ms) separates each transmitted pulses.

Figure 3.3-1 illustrates the signal frequency/time format in a slightly different way than Fig. 3.1-2. Note that each station transmits 10.2, 11⅓, and 13.6 kHz in cyclical order, followed by five transmission pulses. The first two and last two of these five pulses are at the station's unique frequency, and the middle pulse is at 11.05 kHz. Both figures indicate how 10.2, 11⅓, and 13.6 kHz signals are shifted with respect to each other by one time segment. The 200 ms guard time ensures that any long path signal from the trailing edge of the pulse generated by a nearby station dies away before the station's short-path signal from the leading edge of the next pulse begins. Note that the unique frequencies differ by a minimum of 100 Hz which corresponds to the front-end bandwidth of conventional Omega receivers.

3.3.2 Locations of Transmitting Stations and Station Monitors

The eight Omega stations are located on the sovereign territory of seven nations, including the United States. Figure 3.1-1 shows the general locations of the stations on a world map. Note that the stations are distributed fairly uniformly over the globe.

Table 3.1-1 lists the station locations and coordinates that are given with respect to the WGS-84 datum. Antenna type/dimensions for each station are also listed since the antenna is the largest physical structure at an Omega station. Antenna structures are of three different types:

- Valley-span (Norway, Hawaii)
- Insulated tower (North Dakota, Argentina, Japan)
- Grounded tower (Liberia, La Reunion, Australia).

The types of antenna structures are listed in order of their technological evolution so that the valley-span is the earliest antenna structure and grounded towers are the most recent.

The monitor sites associated with each transmitting station have important operational functions as noted in Section 3.2.3. The monitor site is equipped with a Magnavox MX1104-MS Omega monitor receiver system which includes an antenna, pre-amplifier, receiver/processor, recorder, and modem (see Chapter 8 for more details on the basic receiver). The monitor data is transmitted via a data link to the

FREQUENCY (kHz)		TIME SEGMENT (sec)															
			<–0.9–>	0.2	<–1.0–>	0.2	<–1.1–>	0.2	<–1.2–>	0.2	<–1.1–>	0.2	<–0.9–>	0.2	<–1.2–>	0.2	<–1.0–>	0.2
	COMMON	10.2	A		B		C		D		E		F		G		H	
		13.6	H		A		B		C		D		E		F		G	
		11⅓	G		H		A		B		C		D		E		F	
		11.05	D		E		F		G		H		A		B		C	
	UNIQUE	12.1							A		A				A		A	
		12.0	B								B		B				B	
		11.8	C		C								C		C			
		13.1			D		D								D		D	
		12.3	E				E		E								E	
		12.9	F		F				F		F							
		13.0			G		G				G		G					
		12.8					H		H				H		H			
			10 seconds															

Figure 3.3-1 Omega System Frequency/Time Format

MX1104-LS unit for display at the station site. One of the most important functions of the monitors is collecting phase data used to compute station synchronization corrections (see Chapter 7). This phase data is also monitored (at the LS unit) to detect the onset of a PCD event for which navigational warnings are issued (Section 3.2.3). In the longer term, these monitors provide phase data for the global propagation correction (PPC) model and system performance evaluation using operational data analysis (see Chapter 8).

Important parameters for the station monitors are given in Table 3.3-1. The table lists the five-digit monitor code, the ID number used in the data processing, and the calibration channel selected, i.e., the station for which no data is recorded. The last three columns include the monitor location (closest municipality and country) and two coordinates based on the WGS-84 spheroid.

Figure 3.3-2 is a photograph of the enclosure for the station monitor facility at Utskarpen, Norway. Also shown is the antenna which is external to the enclosure.

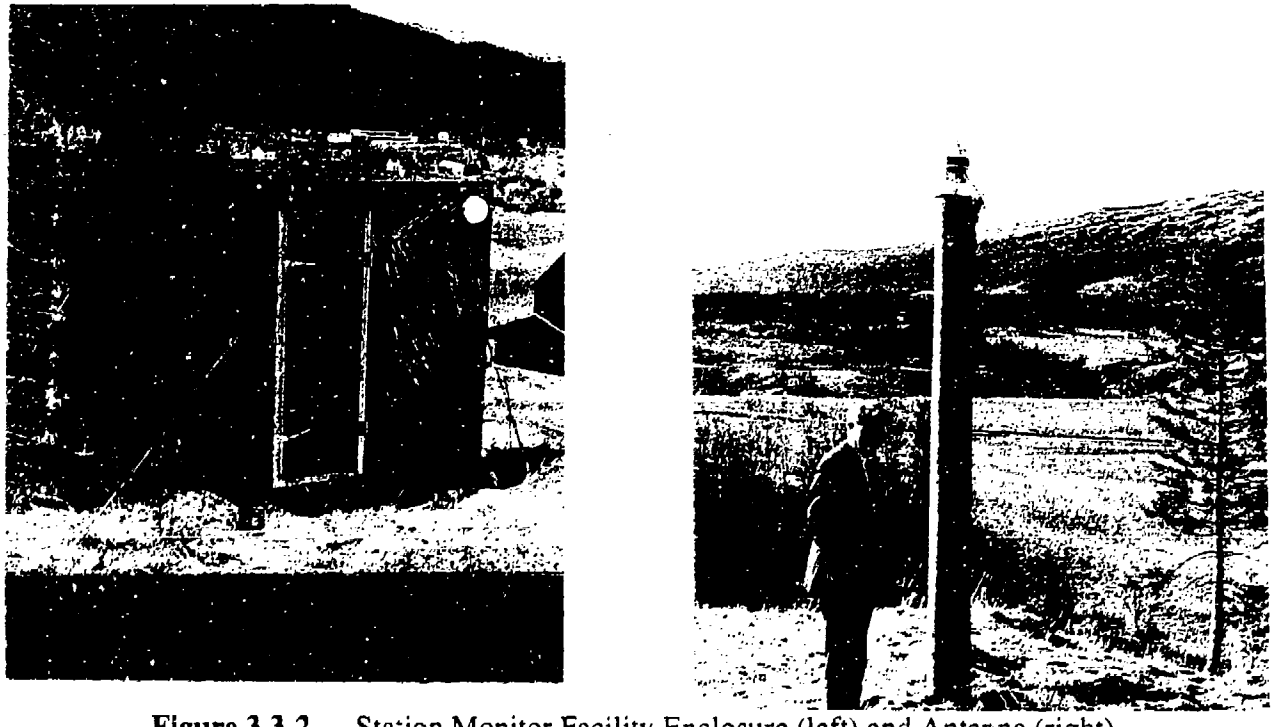

Figure 3.3-2 Station Monitor Facility Enclosure (left) and Antenna (right)

3.3.3 Signal Specification

The signals generated by an Omega transmitting station must be controlled in three principal domains: frequency, time, and signal quality. The signal transmission format depicted in Section 3.3.1 specifies the basic frequency/time structure for the signals radiated by each station and embodies the first signal specification:

Specification 1: The signals generated by each station shall be transmitted according to the time/frequency format given in Figure 3.3-1.

This specification governs the coarse-scale structure of the signal, i.e., the required timing intervals are specified only to about 100 milliseconds. The second specification refers to the behavior of the signal at the microsecond level and requires the introduction of additional concepts before it can be adequately described.

At each station, the signal is synthesized from the 1 MHz output of a cesium standard that has an intrinsic stability of about one part in 10^{12}. This means that, in terms of time, an initially correct cesium standard will be off by about 2.5 μsec in a period of one month. In terms of frequency, the cesium deviates by only about 0.01 Hz (with respect to the cesium standard frequency) in a month.

These ideas can be understood by noting that the signals generated by the station may be expressed as

$$E = A \sin(\omega t + \phi)$$

$$\phi = \alpha t$$

Table 3.3-1 Station Monitor Locations and Other Data

CODE DESIGNATION	ID NUMBER	CALIBRATION CHANNEL	MONITOR STATION LOCATION	POSITION*	
				LATITUDE	LONGITUDE
NORWY	53	G	Utskarpen, Norway†	66.2897°N	13.5502°E
LIBER	45	C	Monrovia Liberia**	6.3143°N	10.8172°W
HAWAI	29	F	Wahiawa, Hawaii	21.5209°N	157.9964°W
N$DAK	51	E	Dickey, North Dakota	46.5596°N	98.6386°W
REUNI	38	D	Riviere des Pluies, La Reunion Island	20.9086°S	55.5127°E
ARGE2	18	A	El Tehuelche,‡ Argentina	42.7533°S	65.1008°W
AUST$	22	A	Carrajung, Victoria, Australia	38.3355°S	146.6600°E
JAPAN	33	F	Ozaki, Tsushima Island, Japan	34.3247°N	129.2064°E

* Coordinates based on WGS-84 spheroid.
† Established June 1991.
‡ Established September 1988.
** Established at the American Embassy 24 February 1992.

where A is the amplitude, ω is the radian frequency, and ϕ is the phase. If $\phi = 0$ represents the condition of perfect synchronization by the station, then at the end of one month, ϕ will be about 2.5 centicycles (cec). Deviations of the phase, ϕ, associated with the cesium standard output are usually assumed to grow linearly in time, i.e.,

where α is sometimes called the "drift" rate. Combining these two expressions gives

$$E = A \sin(\omega t + \alpha t) = A \sin((\omega + \alpha)t)$$

Thus, α may also be considered a frequency bias, or, more commonly, an "offset." At 10.2 kHz, the typical offset for a cesium standard is therefore 10^{-12} cec/μsec, or 10^{-8} Hz.

Each station has three cesium standards in operation at all times. One of these is designated the on-line unit and the other two serve as backup units. Each cesium standard has a slightly different offset, or drift rate, so that over time, the phases of the three standards eventually diverge from each other. Several procedures are followed to reduce this divergence:

- Once each day, the phases of the back-up cesium standard outputs are aligned with the on-line cesium standard output; with the older timing and control equipment this procedure was known as "scoping"
- Frequency correction values for each cesium standard output, computed by the weekly synchronization program and known as "ACCUM" values, are inserted every four hours to minimize the computed offsets
- Cesium standards with large computed offsets ($\geq$0.3 μsec/day) undergo C-field adjustments, an off-line procedure which can sometimes be used to bring a standard back into specification.

The first procedure ensures that the off-line cesium standard output phases never diverge too far from the on-line standard output phase so that they can be immediately substituted, if the need arises. For example, if the maximum difference in the on-line/off-line standard offsets is 5×10^{-13} cec/μsec, then the maximum phase variation between the on-line and off-line units over one day is about 0.05 cec (10.2 kHz). The second procedure actively seeks convergence of on-line and off-line phase outputs to a system average (see Chapter 7). Typical ACCUM values are 0.01 to 0.05 μsec so that daily corrections of 0.06 to 0.30 μsec result from this procedure.

Omega epoch is defined as the regular occurrence of certain system "events" and is always implicitly characterized with respect to "true" time. For the purposes of Omega signal timing, true time is considered to be Coordinated Universal Time (UTC, often written as just UT), which is essentially

given by the output of the U.S. Naval Observatory Master Clock (USNO MC). At a station, Omega epoch refers to the coincidence of the zero phase point of all radiated signals at 30-second intervals. The zero phase point is the point at which the instantaneous vertical electric field of the transmitted signal is zero (going from negative to positive values) at the center of the antenna system.

To fix Omega epoch with respect to UTC (USNO MC), an initial Omega epoch is taken to be 0000 UT on 01 January 1972, when Omega time was coincident with UTC. Since that time, on the scale of seconds, Omega epoch has become earlier with respect to UTC so that the epoch of 0000 UT, 01 January 1994 lags Omega epoch by 18 seconds due to the insertion of leap seconds* into the UTC time scale during some of the intervening years. This gradual divergence of Omega system time and UTC is illustrated in Figure 3.3-3. On the scale of microseconds, however, Omega epoch is quite close to UTC.

Through reciprocal path measurements and indirectly through the use of external system data, the Omega synchronization procedure attempts to align all the station epochs (which differ slightly with respect to UTC). This synchronization is necessary because all navigation algorithms assume the stations' signals are radiated with precisely the same time/phase relationship. *Omega system time* is the

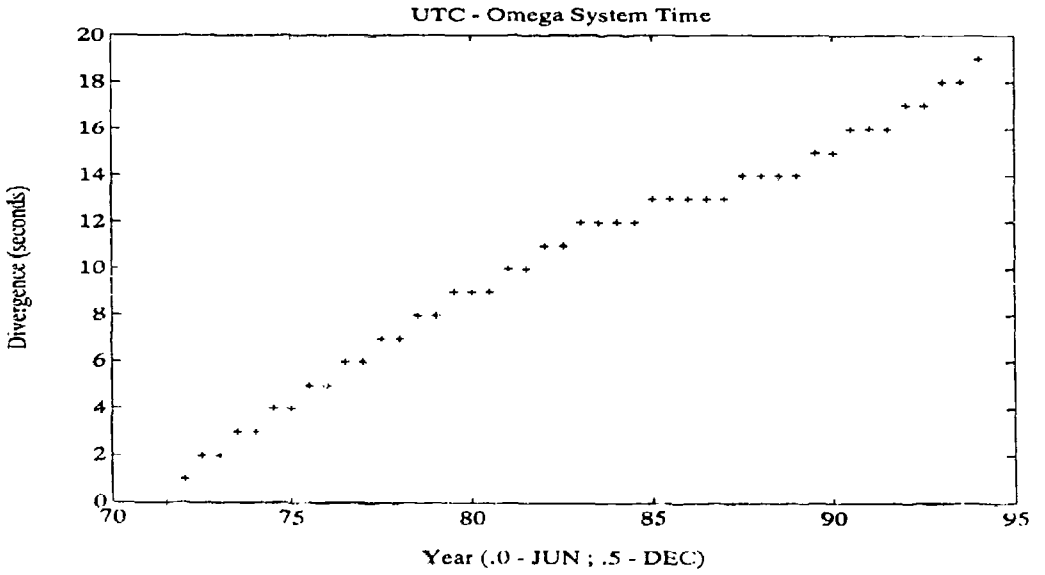

Figure 3.3-3 Divergence of Omega System Time and UTC Due to the Injection of UTC Leap Seconds

* Leap seconds are introduced at roughly 18-month intervals to account for the non-uniformity of the earth's rotation about its axis as measured with respect to atomic-referenced time (Ref. 9).

average of all the station epochs, measured with respect to true time. System-internal synchronization is achieved if all station epochs coincide with Omega system time. This leads to the following specification:

Specification 2: The epoch of each station shall not differ from Omega system time by a magnitude of more than 2.0 μsec, 95% of the time.

Ideally, the synchronization procedure is also designed to align Omega system time with UTC (USNO MC) at the microsecond level. Thus, if completely synchronized on an external basis, Omega standard time would lead UTC by 18.000000 seconds (as of 01 January 1994). This is achieved through the use of external system data (e.g., Loran-C and GPS) measured with respect to the cesium reference at each station. The alignment of Omega system time with UTC supports the increasing use of integrated or interoperable receiving systems which rely on a UTC time base (see Chapter 12). Thus, the need for external synchronization results in the following specification:

Specification 3: Omega system time shall not differ from the UTC epoch (at the microsecond level) by a magnitude of more than 1.0 μsec, 95% of the time.

Current usage indicates that, under normal operation, Omega system time is within 0.5 μsec of UTC (Ref. 3).

When it reaches the antenna, the source signal, which has been digitally processed and amplified, becomes less precisely defined (in frequency and time). Since the antenna is electrically short (compared to a half-wave dipole) and the grounding system has finite conductivity, the signal is radiated into the far field with only about 10 percent efficiency. At the beginning of a pulse segment, the signal is energized over a period of 5 to 40 milliseconds, which requires an average radiated signal bandwidth of about 30 Hz (see Section 3.5). The antenna tuning system implements a feedback control procedure which controls the zero phase point at the antenna by shifting the excitation drive to the transmitter (see Section 3.4.3). This control is governed by the following specification on the radiated signal:

Specification 4: The radiated phase of each Omega signal shall be controlled so that the phase error, when averaged over one minute, is less than one degree.

In this specification, the phase error refers to the feedback control loop error. The one-minute phase error averaging is included in the specification in recognition of the fact that most receivers have time constants of greater than 1 to 2 minutes, so that phase excursions (with zero mean) within a one-minute period have no navigational effect.

3.4 MAJOR SUBSYSTEMS

As the source of the signals detected and utilized by all Omega receiver systems, the eight Omega transmitting stations represent the core of the Omega system. As noted earlier, the electronics and mechanical equipment used at each station are virtually the same; the stations are primarily differentiated by their antennas and locations.

The equipment at each station is generally described as belonging to one of four functional groups or subsystems:

- Timing and control
- Transmitter
- Antenna tuning
- Antenna structure.

A functional diagram of these subsystems and some of their important interrelationships is shown in Figure 3.4-1. The primary functions of these subsystems are briefly described in Sections 3.4.1 through 3.4.4. More detailed information can be found in Reference 8.

3.4.1 Timing and Control Subsystem

The principal functions of the Timing and Control subsystem are signal generation and phase control as portrayed in Figure 3.4-2a. A photograph of the rack-mounted Timing and Control subsystem equipment is shown in Figure 3.4-2b. The signal source is a precision cesium beam frequency standard of 9.193 GHz with a stability of 1 to 5 parts in 10^{12}. Three cesium standards are used for frequency drift comparison and control, and are maintained as reserves in the event of failure of the on-line standard. The on-line cesium standard controls the frequency of a 5 MHz crystal oscillator whose output signal is frequency-divided to form a 1 MHz signal. The 1 MHz output is used to synthesize the reference carrier signals and generate keying pulses which define the time/frequency format. The carrier signals include

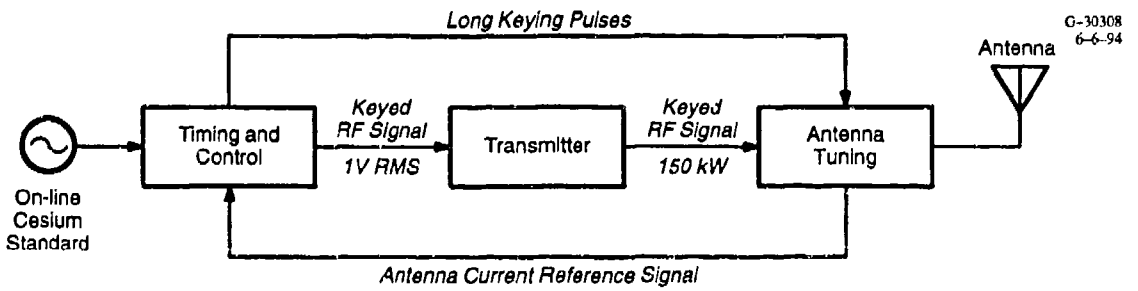

Figure 3.4-1 Major Functional Subsystems for Transmitting Station

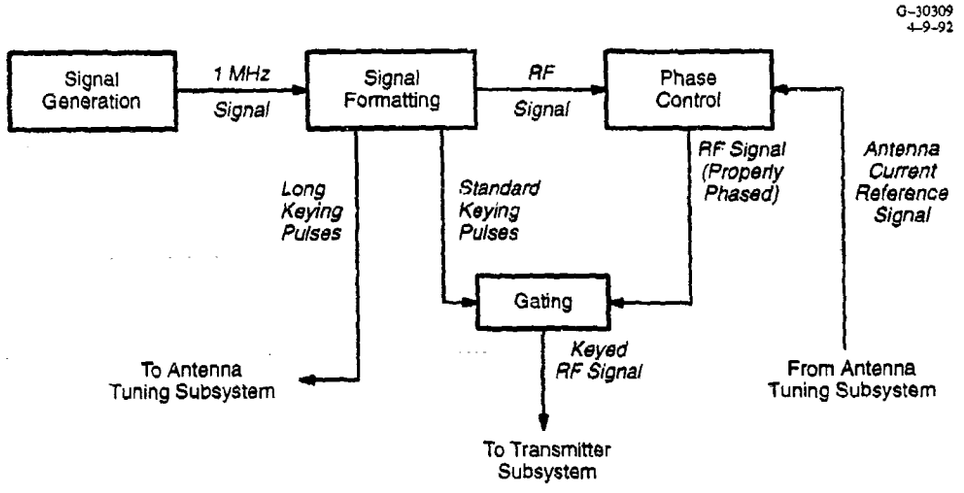

a) Functional Diagram of Timing and Control Subsystem

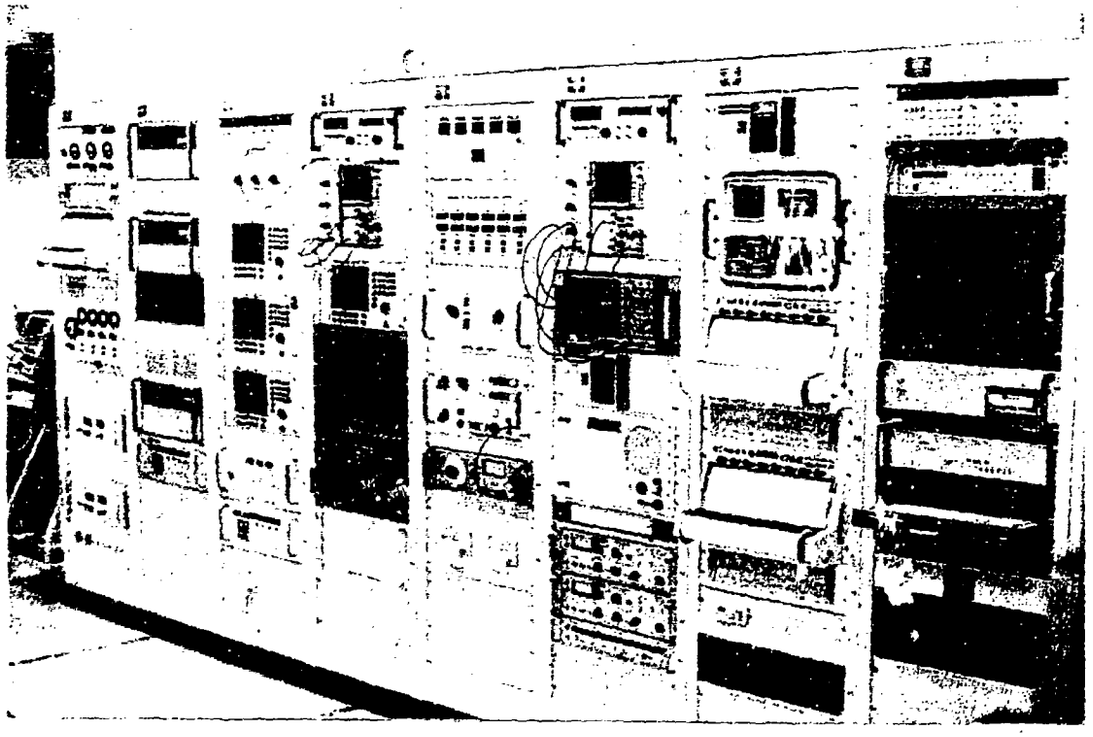

b) Timing and Control Subsystem Equipment at the Norway Transmitting Station

Figure 3.4-2 Timing and Control Subsystem

the four common frequencies at 10.2, 13.6, $11\frac{1}{3}$, and 11.05 kHz in addition to the station-unique frequency. Phase control is maintained by comparing the phase of the reference carrier signal to the phase of the signal fed back from the antenna tuning subsystem. The signal phase is advanced or retarded to ensure that its phasing at the antenna coincides with the appropriate UTC epoch. The carrier signals output from the phase control circuitry are gated into the transmitter subsystem in the proper sequence/ time interval by standard-length keying pulses developed during the format generation process. Also produced by the format generation are long keying pulses that precede and follow the standard keying pulses by 100 ms. These pulses are relayed to the Antenna Tuning subsystem to allow sufficient time for mechanical switching prior to the transmission of the keyed carrier frequency signal at that stage.

In terms of replacement precedence for the on-line cesium standard, one of the reserve standards (and its 1 MHz output) is denoted as the primary back-up and the other as the secondary back-up. As noted in Section 3.3.3, the 1 MHz outputs of the back-up standards are aligned with the on-line standard 1 MHz output once each day. These so-called "scoping" times are listed in Table 3.4-1.*

Table 3.4-1 Daily ACCUM Insertion and Scoping Times

		UT HOUR*																						
		00	01	02	03	04	05	06	07	08	09	10	11	12	13	14	15	16	17	18	19	20	21	22	23
STATION	A	16				16				16				16				16				16			
	B	46				46				46				46				46				46			
	C		16				16				16				16				16						
	D		46				46				46				46				46						
	E			16				16				16				16				16					
	F			46				46				46				46				46					
	G				16				16				16				16				16				
	H				46				46				46				46				46				

* For each entry, the number refers to a measurement 16 (46) minutes after the hour at the top of the column. ACCUM insertion times occur at all indicated times; scoping times are designed by a shaded entry.

3.4.2 Transmitter Subsystem

The Transmitter subsystem consists of those devices that amplify the signal generated in the Timing and Control subsystem (Figure 3.4-3). Figure 3.4-3b is a photograph of the bank of transmitter subsystem equipment. As shown schematically in Figure 3.4-3a, the carrier frequency signal from the Timing and Control subsystem is first raised to a level of 160 V RMS by the input amplifier. The driver

*New Timing and Control Subsystem equipment being installed (May 1994) at the stations includes the Omega Signal Generator (OMSGEN) and the Omega Signal Controller (OMSCON). Instead of using the oscilloscope method, alignment of the back-up clock units to the on-line units is now made by inserting the difference in the OMSGENS into the OMSCON. All information regarding these differences is transmitted to the other subsystem units via a communication ring.

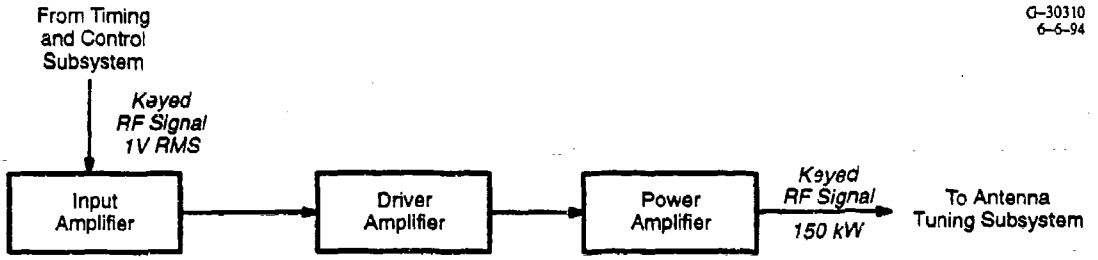

a) Principal Components of Transmitter Subsystem

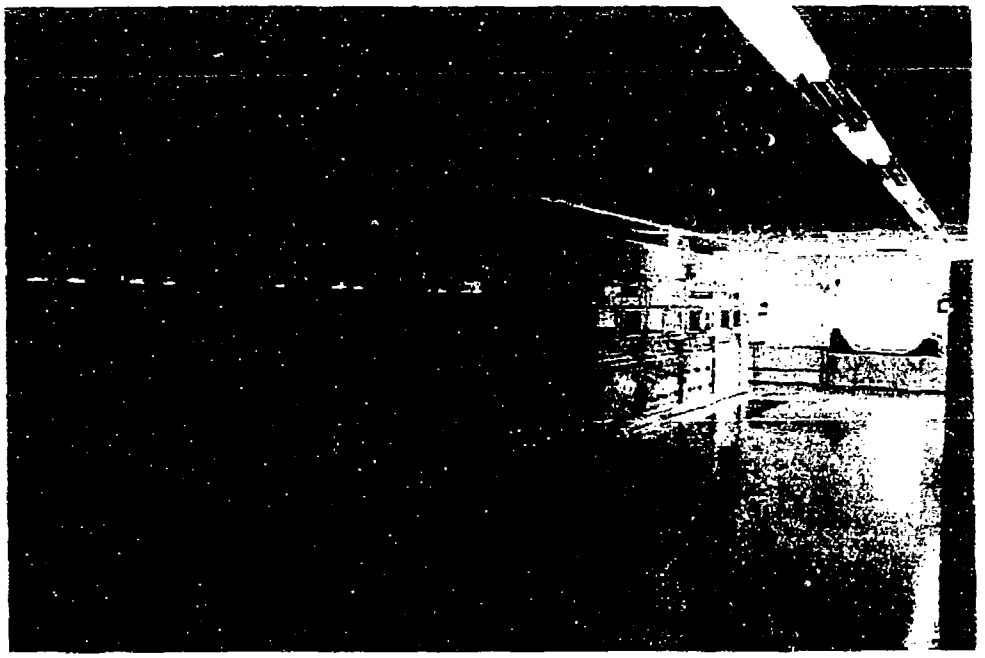

b) Transmitter Subsystem Equipment Showing Both Active and Spare Units

Figure 3.4-3 Transmitter Subsystem

amplifier further raises the signal level to a nominal 520 volts RMS and the final amplification is performed by the power amplifier which boosts the signal voltage and current to a peak power of 150 kW. Following this final amplification stage, the signal is fed to the Antenna Tuning subsystem.

For purposes of redundancy, two transmitters are located at each station. The non-operational transmitter is always in standby mode and can be rapidly switched on-line if needed. The standby transmitter can be energized for testing by directing its output to a "dummy load." Transmission into the dummy load is also sometimes used for maintenance purposes. To prevent arcing, the transmission line connecting the output of the transmitter to the antenna tuning subsystem is sealed and dehydrated (N_2 gas is used if the dehydrator fails). The transmitter uses 480 V three-phase electric power.

3.4.3 Antenna Tuning Subsystem

Figure 3.4-4 illustrates the functional stages of the Antenna Tuning subsystem. This subsystem is designed to tune the antenna at the carrier signal frequency by inductively matching the antenna to the input circuit. This ensures the maximum effective radiated power at the antenna for a given input signal power. The output signal from the Transmitter subsystem is taken from the secondary coil of the antenna matching transformer. The grounded side of the secondary is connected through a current transformer to

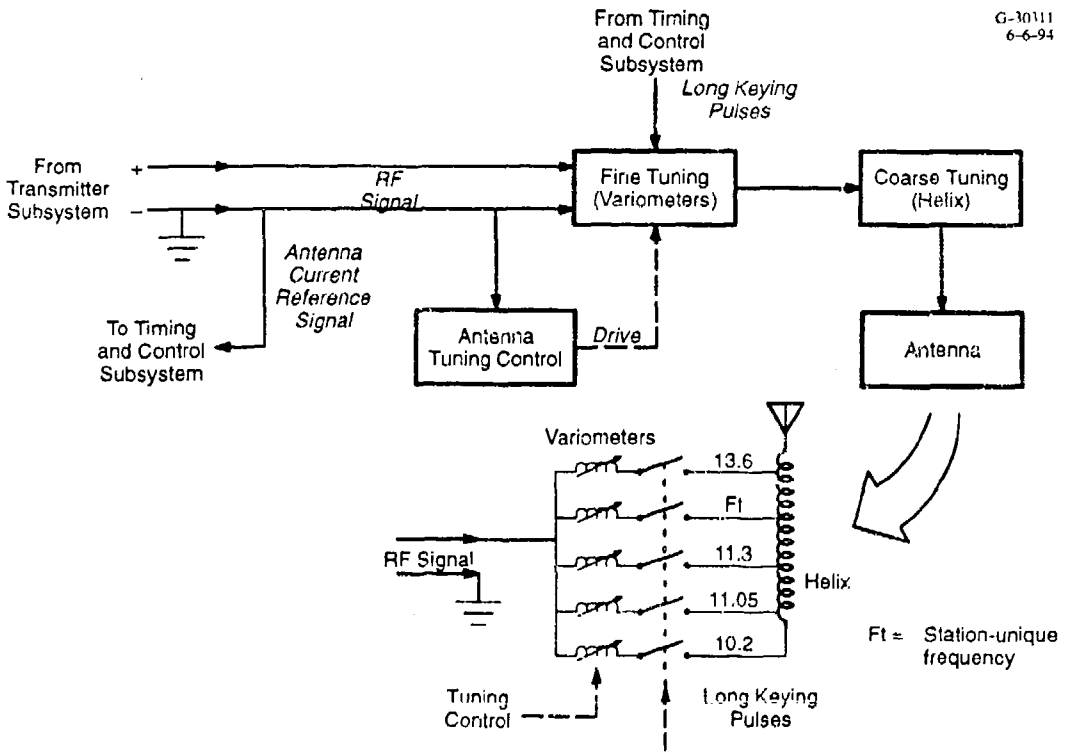

Figure 3.4-4 Functional Diagram of Antenna Tuning Subsystem

provide the antenna current reference signal used for phase control in the Timing and Control subsystem. The output of the current transformer is also passed to the antenna tuning control module. Based on the long keying pulses from the Timing and Control subsystem and the current samples received from the current transformer, the antenna tuning control first implements fine inductive tuning through the variometers.

The input to the antenna tuning control comes from the ground side of the secondary coil that is directly connected to the ground "mat," a collection of buried cables extending over a large area underneath the antenna (Ref. 3). Since the ground current varies as the effective antenna inductance changes (e.g., due to the effect of winds, temperature, or humidity on the antenna structure), this sign . acts as an external feedback in controlling the variometers.

The five variometers (plus one spare) are essentially adjustable induction coils, each of which is assigned to one of the keyed carrier frequency signals (see Fig. 3.4-4 and Fig. 3.4-5a). The antenna tuning control signal activates a mechanical drive that moves the variometer coil to the appropriate position for matching inductance. The long keying pulses activate antenna relays (through a power supply), which connect the appropriate variometer into the main antenna circuit. At the onset of the long keying pulses for the unique frequencies, *all* variometers (i.e., for all frequencies) are "gang-tuned" to minimize the drive motion required to tune each variometer. Each variometer, in turn, is fine-tuned during the period it is being used for transmission.

The RF signal is then transferred to the "helix," a large helical coil which acts as a coarse tuning device for the antenna. The helix is equipped with separate taps for each signal frequency transmitted. Since the lower frequencies require greater inductance (for impedance matching), the 10.2 kHz tap is at the bottom of the helix (see the photograph of the 10.2 kHz tap and the lower part of the helix in Fig. 3.4-5b), so that the signal inductance is generated for the entire helix; the higher frequency taps are therefore at higher positions. Finally, the RF signal is conducted to the antenna structure itself from which the signal is radiated.

3.4.4 Antenna Structure

As mentioned in Section 3.3.2, the structural feature that most differentiates Omega stations is the antenna structure. Two basic designs are utilized: tower and valley span. The tower antennas are further categorized in terms of grounded and insulated types. The three basic antenna design/types are illustrated in Fig. 3.4-6.

The valley-span antenna is a suspended cable system that advantageously uses the topography of a natural formation, such as a deep valley, fjord, or volcanic crater. One or more antenna cables strung

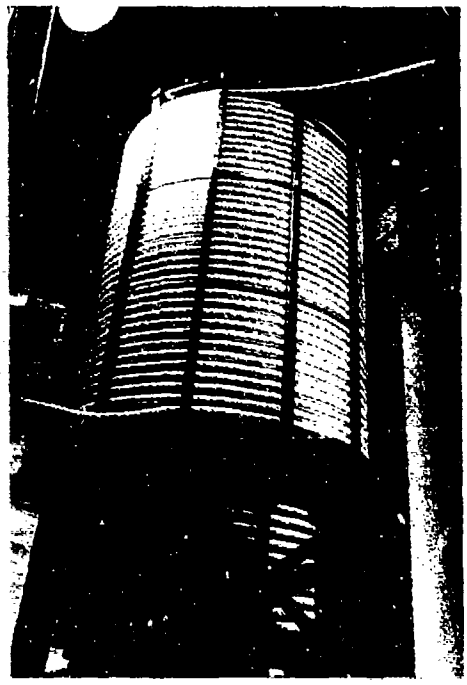

a) **Variometer Used for Fine Inductive Tuning**

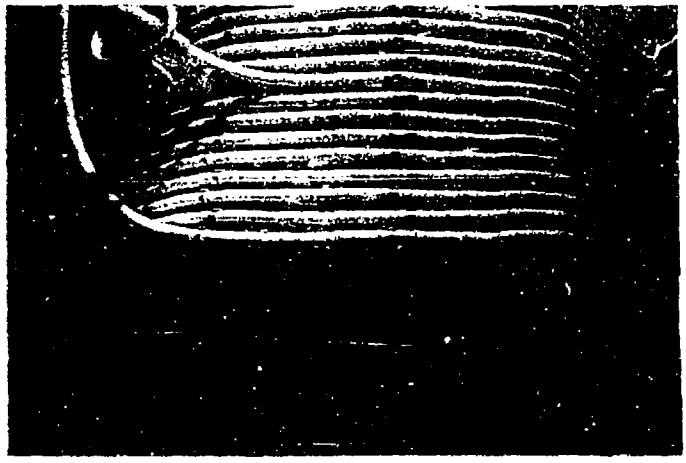

b) **Lower Part of Helix Showing Fixed Frequency Tap Providing Coarse Inductive Tuning**

Figure 3.4-5 Fine and Coarse Signal Tuning Equipment

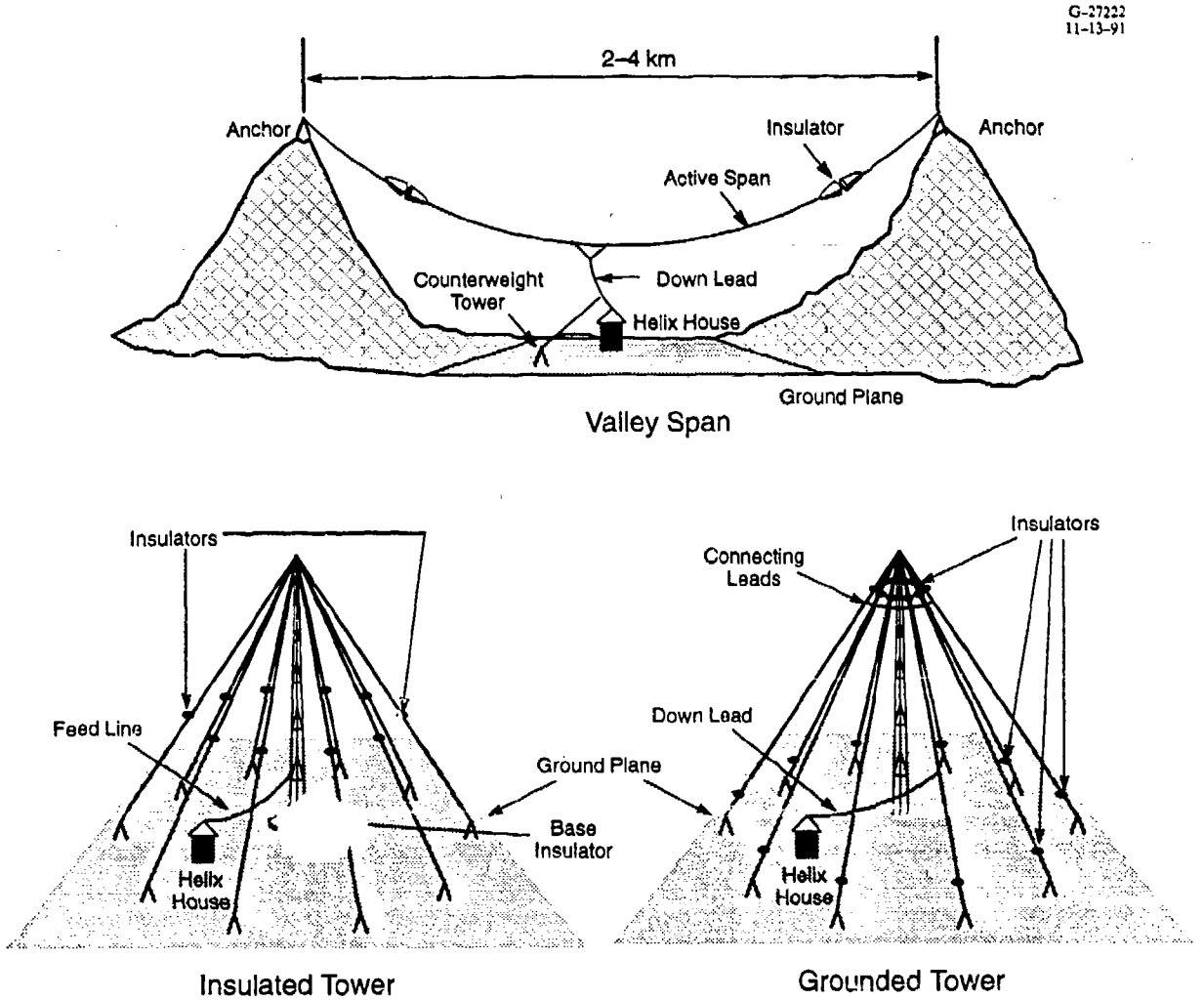

Figure 3.4-6 The Three Primary Types of Omega Antennas

across the open part of the formation are anchored on the surrounding ridges. The spans are connected by jumper wires and fed down through a downlead cage to the building housing the helix. A counterweighted pulloff cable system permits extension of the downlead under high wind conditions. A ground system, composed of buried conducting cables, extends outward from underneath the helix building. The density and length of the ground wires depend on the soil conductivity of the site. Figure 3.4-7 shows a mock-up of the Norway station's valley span antenna system. The two downleads are at the lower left in the figure and are pulled off to the left by the counterweight system. The two main spans are attached by anchors on both sides of the fjord.

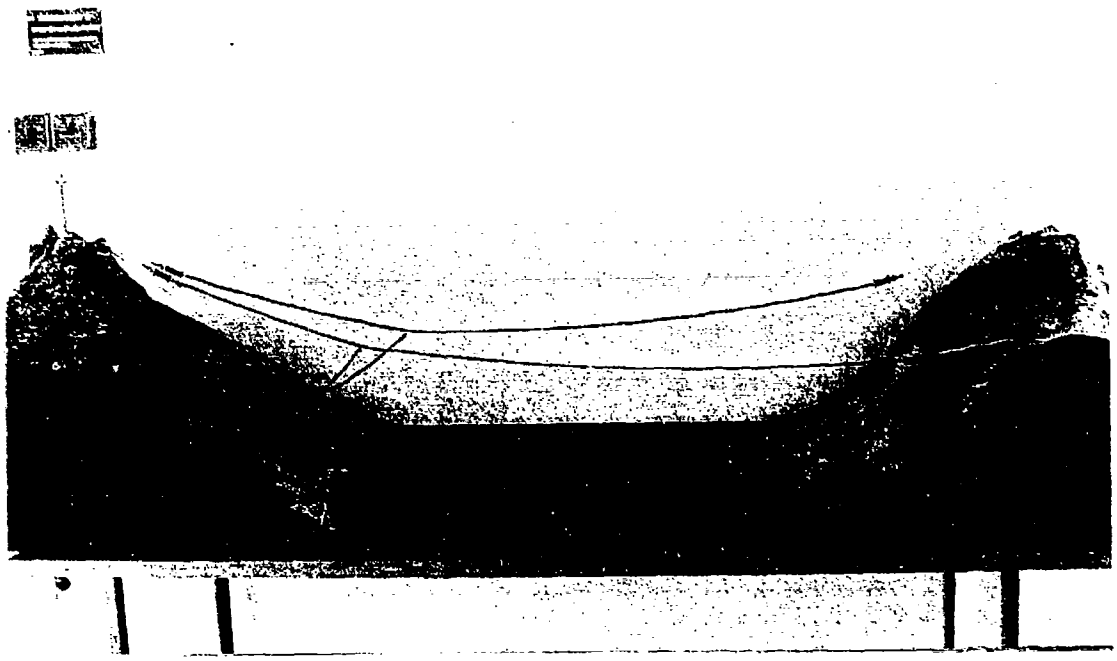

Figure 3.4-7 Mock-up of Valley Span Antenna System at the Norway Transmitting Station

A tower, or top-loaded monopole, is a vertically mounted structure supported by a number of guy wires. An insulated tower is isolated from the ground at the tower base by a large base insulator. Top-loading (i.e., creating additional capacitance between the top of the antenna and the ground) of the antenna is achieved by using cables electrically connected to the top of the tower. These cables (known as top-loading radials) are mechanically connected through insulators to secondary guy wires that provide support from the ground. Power is generally fed to the tower at a point directly above the base insulator. The antenna current flows up the structure and into the top-loading radials. A photograph of an insulated tower (at the Japan station) is shown in Fig. 3.4-8. The tower is so tall that some supporting guys are anchored on separate islands surrounding the main mast.

A grounded tower has a similar configuration except that it has no base insulator so that the tower structure itself is grounded. Top-loading radials are insulated at each end, joined together at the top, and are fed with a downlead extending from one of the radials to the helix. To achieve the same performance as the insulated tower antenna, the grounded tower antenna must be about 15 percent taller. Figure 3.4-9 is a photograph of a grounded tower antenna system at the La Reunion transmitting station.

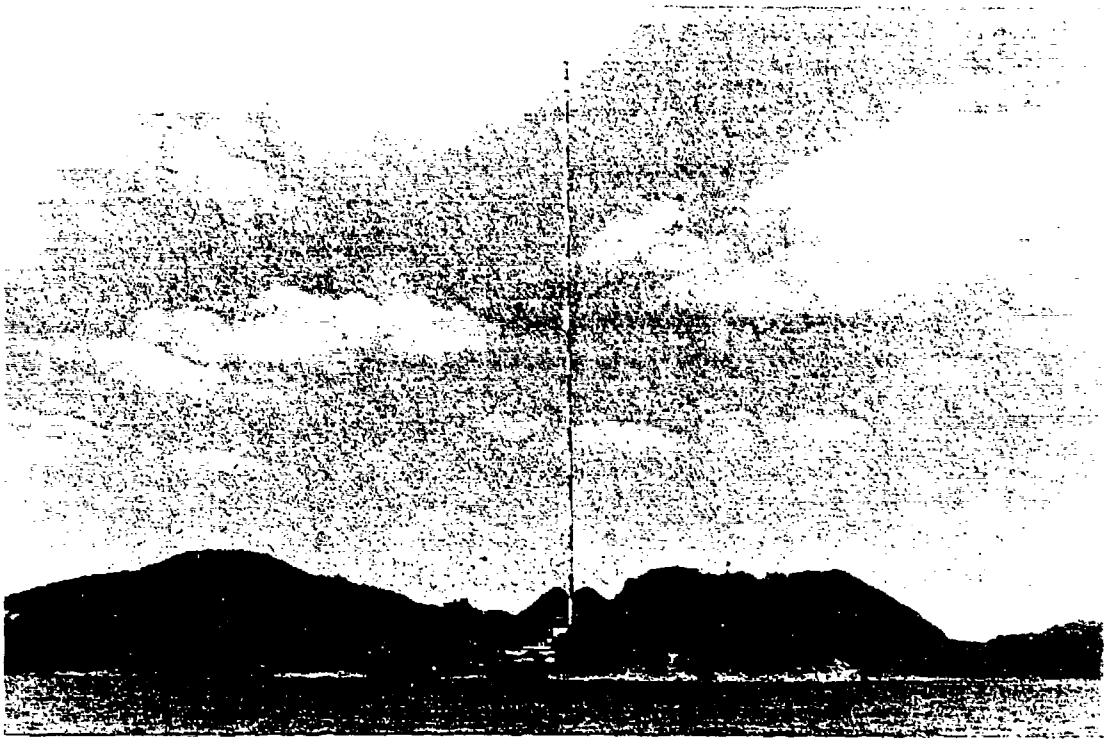

Figure 3.4-8 Insulated Tower Antenna System at the Japan Transmitting Station

3.5 RADIATED SIGNAL DATA

The signal structure in the vicinity of the station antenna is quite different than that for most receivers which sense the radiated field of the transmitted signal. The complexity of the signal near the station/antenna arises both from the signal itself, which contains many modes of approximately equal strength (see Chapter 5), as well as the local elements of the antenna structure, grounding system, and terrain conductivity.

3.5.1 Components of the Near-field Signal

To understand the signal behavior in the proximity of the station antenna, it is helpful to consider a simple model of the signal generation process (see References 4 and 5). Consider a vertical monopole antenna (equivalent to "half" of a center-fed dipole antenna) in which charge oscillates between the ground and the top of the antenna. The fact that Omega antennas are short compared to the signal wavelength leads to a relatively simple expression for the fields outside the immediate vicinity of the antenna, i.e.,

$$\mathbf{E} = \frac{iIh_e}{\omega} \cdot \left(\frac{k^2}{r} + \frac{ik}{r^2} - \frac{1}{r^3}\right) e^{ikr} e^{-i\omega t} \qquad (3.5\text{-}1)$$

Figure 3.4-9 Grounded Tower Antenna System at the La Reunion Transmitting Station

where I is the magnitude of the antenna current, h_e is the effective antenna height, ω is the radian frequency, k is the wave number ($2\pi/\lambda$, where λ = signal wavelength), t is the time, r is the distance of the receiver from the antenna on the (assumed flat) earth, and $\hat{z}$ is the unit vector pointing vertically upward. From this expression, the total signal field may be considered to be the sum of three component fields which are given as follows (in the same order as the terms in the parentheses in Eq. 3.5-1):

(1) Radiation field — varies as $1/r$

(2) Induction field — varies as $1/r^2$

(3) Electrostatic field — varies as $1/r^3$

The appearance of the i in the induction field term in Eq. 3.5-1 means that the phase of this field is shifted by $\pi/2$ radians or 90° (since $i = e^{i\pi/2}$) with respect to the other fields.

The electrostatic field is the strongest component at distances from the antenna up to about $1/k$, e.g., about 5 km at 10.2 kHz. For longer ranges, the radiation and inductive fields dominate the

electro-static field. At ranges greater than about 50 km, the radiation field is the only remaining significant component of the total signal field. The radiation field is, of course, the signal component required for navigation and all other uses of the Omega signal.

At the station monitors, which are located at ranges between 17 and 40 km from the transmitting antenna, the radiation field is dominant but the induction field introduces a perturbation which cannot be ignored for certain applications. Use of Eq. 3.5-1 and a simple phasor model show that the variation of the total signal field phase from the radiated signal field phase, $\delta\phi$ (due to the small but finite induction and electrostatic fields), is given by

$$\tan\delta\phi = \frac{kr}{k^2r^2-1} \tag{3.5-2}$$

where k and r are defined in connection with Eq. 3.5-1. Figure 3.5-1 shows several aspects of Omega signal phase behavior in the near field. The upper left panel shows the total signal phase delay as a function of distance from the transmitting station for 10.2, 11⅓, and 13.6 kHz. The total signal phase delay is composed of the nominal phase, kr (appearing in Eq. 3.5-1), and the variation $\delta\phi$, given by Eq. 3.5-2. In the near field, the wave number, k, is often assumed to have its free-space value, i.e., $k_0 = \omega/c$, and the resulting phase, k_0r, is called the free-space phase. The remaining three panels show the variation of the total phase from the free-space phase for 10.2, 11⅓, and 13.6 kHz. In each panel, the predicted value, i.e., $\delta\phi + (k-k_0)r$, is shown as a solid curve, while the measured values are indicated by small circles. Although somewhat lower than the predictions, most of the measurements, which are from the North Dakota transmitting station (Ref. 3), generally corroborate the theory.

3.5.2 Near-field and Antenna Parameters

The effective antenna height, h_e, appearing in Eq. 3.5-1, is determined by measuring the vertical component of the electric field amplitude, |E|, at several ranges from the transmitting antenna where the radiated field is effectively the sole contributor to the total field. For these cases, the magnitude of Eq. 3.5-1 may be written

$$E_z = \frac{Ih_e}{\omega}\frac{k^2}{r}$$

Expressed in dB, E_z is linearly related to log r, so that several measurements can be fit to a straight line whose slope can be used to determine h_e.

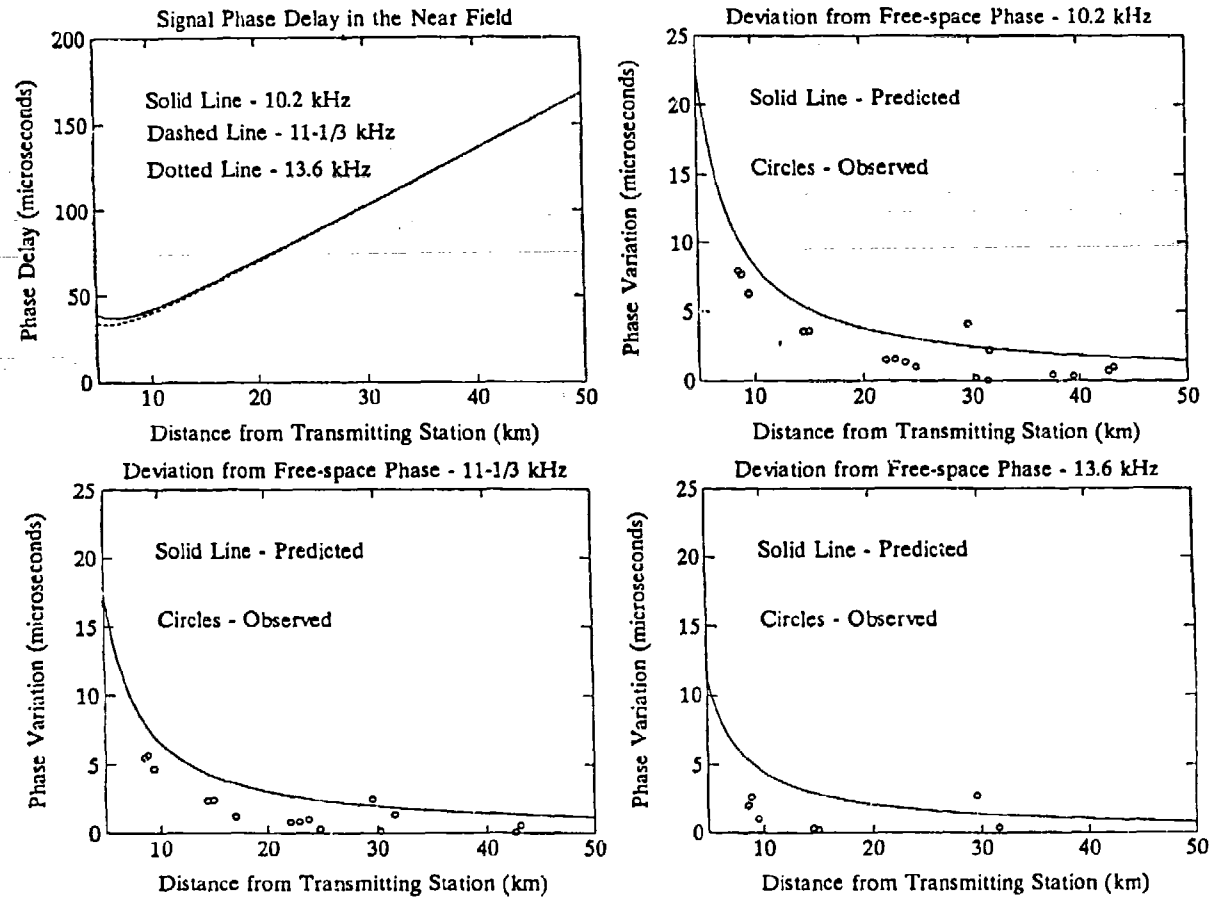

Figure 3.5-1 Signal Phase Behavior in the Near Field

With knowledge of the effective height, a quantity known as the radiation resistance can be calculated. Conceptually, the radiation resistance is the effective resistance associated with the antenna current that yields the effective radiated power. This resistance thus does not include those resistive elements that carry the input energy away as heat losses or other field components. From Reference 4, the radiation resistance (in ohms) for electrically short antennas is given as

$$R_r = \frac{P_r}{I^2} = 160\pi^2\left(\frac{h_e}{\lambda}\right)^2 \; ; \; h_e < 0.1\lambda \qquad (3.5\text{-}3)$$

where P_r is the effective radiated power (in watts). Note that this expression is valid for the Omega station antennas where, typically, $h_e \approx 0.01\lambda$.

Table 3.5-1 lists some of the important parameters associated with the station antennas. Note that the effective height is substantially shorter than the physical height listed in Table 3.1-1. The effective height generally increases slowly with frequency, and from Eq. 3.5-3, the radiation resistance increases more rapidly with frequency. In general, a larger effective antenna height means the antenna radiates more efficiently, and a greater effective radiated power is normally obtained.

Table 3.5-1 Measured and Derived Station Antenna Parameters

STATION	FREQUENCY (kHz)	EFFECTIVE HEIGHT (m)	RADIATION RESISTANCE (ohms)	ANT. SYST. RESISTANCE (ohms)	ANTENNA CAPACITANCE (μF)	BASE REACTANCE (ohms)
Norway	10.2	229	0.0957	1.230	0.0371	421
	11.05	231	0.1143	1.302	0.0374	385
	11⅓	233	0.1223	1.320	0.0393	368
	12.10	234	0.1330	1.396	0.0389	338
	13.6	242	0.1900	1.553	0.0408	287
Liberia	10.2	178	0.0576	0.916	0.0387	403
	11.05	182	0.0710	0.886	0.0398	362
	11⅓	183	0.0753	0.893	0.0413	350
	12.00	183	0.0844	0.868	0.0404	328
	13.6	183	0.1084	0.855	0.0442	265
Hawaii	10.2	169	0.0523	0.718	0.0460	339
	11.05	170	0.0620	0.751	0.0471	306
	11⅓	169	0.0646	0.750	0.0487	297
	11.80	168	0.0688	0.746	0.0478	282
	13.6	170	0.0936	0.769	0.0502	233
North Dakota	10.2	184	0.0619	0.429	0.0281	556
	11.05	184	0.0728	0.425	0.0282	510
	11⅓	184	0.0765	0.428	0.0292	496
	13.10	185	0.1034	0.453	0.0287	424
	13.6	185	0.1114	0.458	0.0288	406
La Reunion	10.2	163	0.0485	0.622	0.0406	384
	11.05	163	0.0569	0.631	0.0419	344
	11⅓	163	0.0602	0.635	0.0436	332
	12.30	168	0.0748	0.660	0.0440	294
	13.6	170	0.0942	0.685	0.0470	249
Argentina	10.2	193	0.0679	0.561	0.0277	563
	11.05	197	0.0827	0.541	0.0279	516
	11⅓	197	0.0875	0.566	0.0288	502
	12.90	196	0.1121	0.608	0.0284	435
	13.6	197	0.1258	0.558	0.0285	410
Australia	10.2	192	0.067	0.630	0.0396	394
	11.05	186	0.075	0.620	0.0407	354
	11⅓	189	0.080	0.620	0.0426	340
	13.00	191	0.108	0.650	0.0444	276
	13.6	192	0.120	0.660	0.0457	256
Japan	10.2	210	0.0805	0.705	0.0382	409
	11.05	209	0.0935	0.725	0.0380	379
	11⅓	209	0.0986	0.734	0.0400	362
	12.80	211	0.1279	0.765	0.0397	313
	13.6	211	0.1439	0.823	0.0402	291

The antenna system resistance is a measured quantity that includes the real part of the impedance in the antenna tuning system and includes the ground resistance. The measured capacitance of the antenna is associated primarily with the potential difference between the ground and the "top-hat" elements across the insulators. The capacitance, C, generally increases with frequency since the effective antenna area increases with decreasing wavelength. The base reactance (capacitive) is computed as $1/(\omega C)$.

3.5.3 Station Antenna Parameters

Table 3.5-2 lists the nominal and limiting antenna currents for each transmitted signal frequency at each station. The third column gives the antenna current (in Amperes) necessary to achieve the nominal 10 kW radiated power, i.e.,

$$\sqrt{\frac{10\text{kW}}{R_r}}$$

where R_r is the radiation resistance in ohms (see Table 3.5-1). This nominal antenna current is the target value the stations attempt to maintain during normal operation.

As the antenna current is increased, two electrical characteristics of the station limit its value. The first limitation is the transmitter output which cannot exceed 150 kW (see Section 3.4.2). The second restriction is on the base voltage, i.e., the potential difference between the exit bushing feedline and the ground. A base voltage exceeding 250 kV can lead to corona discharge and arc-over at the exit bushing, thus leading to radiated power loss and component damage. The fourth column of Table 3.5-2 shows the maximum antenna current that can be achieved based on the 150 kW transmitter output power limitation, which is calculated as

$$0.975\sqrt{\frac{150\text{kW}}{R_{as}}}$$

where R_{as} is the antenna system resistance in ohms (see Table 3.5-1). The factor of 0.975 accounts for a portion of the current shunted to ground through capacitive coupling at the helix bushing, leading from the antenna tuning system (with resistance R_{as}) to the antenna structure (Ref. 3). The fifth column in Table 3.5-2 gives the maximum antenna current that can be obtained without exceeding the 250 kV base voltage limitation and is calculated as

$$0.975\left(\frac{250\text{kV}}{X_b}\right)$$

Table 3.5-2 Limits on Output Parameters and Antenna Bandwidths

STATION	FREQUENCY (kHz)	ANTENNA CURRENT (AMPERES)			MAXIMUM RADIATED POWER (kW)	RISE TIME (msec)	BANDWIDTH (Hz)
		NOMINAL (P_r=10kW)	OUTPUT POWER LIMITED	BASE VOLTAGE LIMITED			
Norway	10.2	324	340	578	11.08*	9.0	35.4
	11.05	296	331	633	12.40*	7.5	42.4
	11⅓	286	329	662	13.20*	7.0	45.5
	12.10	275	320	721	13.60*		
	13.6	230	302	849	17.40*	4.0	79.6
Liberia	10.2	417	395	605	9.1*	13.0	24.5
	11.05	375	401	674	11.5*	10.5	30.3
	11⅓	364	400	696	12.1*	10.0	31.8
	12.00	344	409	743	14.2*		
	13.6	304	406	919	18.0*	6.0	53.1
Hawaii	10.2	437	446	719	10.5*	12.0	26.5
	11.05	402	436	797	11.9*	10.0	31.8
	11⅓	394	436	820	12.4*	9.5	33.5
	11.80	381	437	864	13.3*		
	13.6	326	430	1046	17.5*	6.0	53.1
North Dakota	10.2	402	576	438	11.8**	23.0	13.8
	11.05	372	579	478	16.6**	22.0	14.4
	11⅓	364	577	491	18.4**	19.0	16.8
	13.10	311	561	574	32.5**		
	13.6	300	558	600	34.6**	12.5	25.5
La Reunion	10.2	454	479	635	11.2*	13.0	24.5
	11.05	419	476	708	13.0*	11.0	29.0
	11⅓	408	474	734	13.6*	9.5	33.5
	12.30	366	465	829	16.3*		
	13.6	325	456	979	19.8*	6.0	53.1
Argentina	10.2	384	504	433	12.7**	19.9	16.0
	11.05	348	513	472	18.4**	16.5	19.3
	11⅓	338	501	486	20.6**	16.0	19.9
	12.90	298	484	560	26.2*		
	13.6	272	505	594	32.1*	10.5	30.3
Australia	10.2	386	476	619	15.9*		
	11.05	367	480	688	18.2*		
	11⅓	354	480	717	19.4*	N/A	N/A
	13.00	304	468	883	23.7*		
	13.6	289	465	953	27.7*		
Japan	10.2	353	449	596	16.4*	12.0	26.5
	11.05	327	443	643	18.3*	10.0	31.8
	11⅓	319	441	673	19.3*	9.5	33.5
	12.80	279	432	779	23.8*		
	13.6	264	416	838	25.2*	6.0	53.1

* Limited by 150 kW output power ** Limited by 250 kV base voltage

where X_b is the base reactance in ohms (see Table 3.5-1). The factor of 0.975 again accounts for the helix exit bushing current losses. The radiated power corresponding to the maximum allowed antenna current is listed in sixth column in Table 3.5-2. Notice that the maximum allowed antenna current is actually the

minimum of the values in columns four and five, i.e., the antenna current is limited by the most restrictive of the two criteria. A single asterisk attached to the entry indicates that the maximum radiated power (I^2R_r ; R_r = radiation resistance) is computed based on the maximum antenna current (I) resulting from the output power limitation. Two asterisks signify the base voltage limitation. Note that all but two stations have maximum output power (for most of the transmitted frequencies) which is limited by the maximum station transmitter output. Exceptions are North Dakota and Argentina which have (at most or all of the frequencies) high base reactances.

The last two columns of Table 3.5-2 provide information on the envelope of pulse waveform transmitted approximately once per second. Figure 3.5-2 shows the trace of the envelope of the pulse rise and decay for the $11^1/_3$ kHz signal from the North Dakota transmitting station as captured on an oscilloscope. The pulse rise and decay time profile is exponential in form so that the rise time is defined as the time required for the pulse envelope to reach $1-e^{-1}$ (i.e., about 63%) of its maximum value. The antenna bandwidth associated with the measured rise times is shown in the last column of Table 3.5-2. The bandwidth is computed by assuming the process has an exponential envelope with rise time τ; in this case it can be shown that the 3 dB bandwidth is $1/(\pi\tau)$. The bandwidths vary from 13.8 Hz for North Dakota (10.2 kHz) to 79.6 Hz for Norway (13.6 kHz). Bandwidth "resistors" (connected in parallel) were once installed (and later removed) at the North Dakota and Argentina stations (insulated towers) to effectively widen the antenna bandwidth by shortening the rise time. These were installed in response to users exploring pulse time-of-arrival techniques as a means of eliminating lane ambiguity.

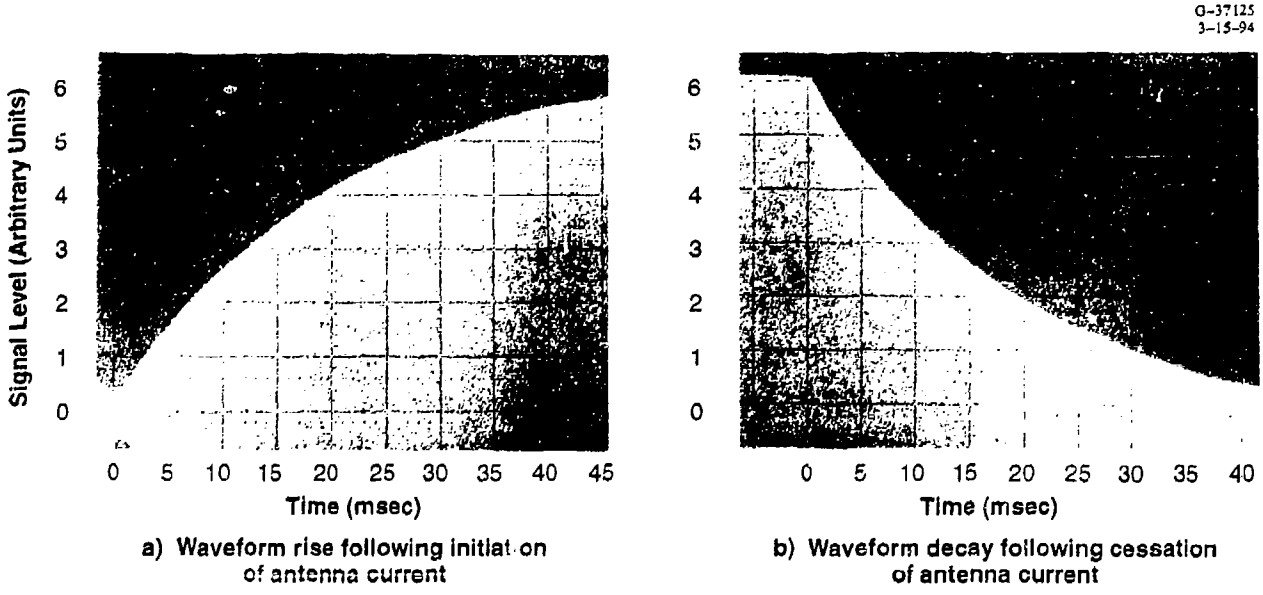

Figure 3.5-2 Pulse Rise (a) and Decay (b) of the $11^1/_3$ kHz Signal from the North Dakota Transmitting Station

3.6 PROBLEMS

3.6.1 Sample Problem

1. Equation 3.5-2 may be used to find the phase error (radiated field phase – total signal field phase) accounting for both the inductive field and the electrostatic field.
   a. What is the corresponding expression if only the perturbation due to the inductive field is taken into account?
   b. The shortest station monitor range is about 17 km (Liberia). What is the error in computing $\delta\phi$ at 10.2 kHz for this station monitor if the electrostatic field is ignored?

Solution:

a. The electrostatic field corresponds to the last term in Eq. 3.5-1. If this term is ignored, the phase error results from the desired (radiated) signal (which varies as k^2/r) in quadrature with the inductive field (which varies as k/r^2), so that

$$\tan\delta\phi = \frac{k/r^2}{k^2/r} = 1/kr$$

Note that this form is obtained from Eq. 3.5-2 in the limit of sufficiently long ranges so that $kr >> 1$.

b. For a 10.2 kHz signal at a range of 17 km, the free-space phase is

$$kr = \frac{2\pi \times 17 \text{ km}}{29.39118 \text{ km}} = 3.6342 \text{ radians}$$

where we assumed the phase velocity is the same as the speed of light in a vacuum. With this value, Eq. 3.5-2 yields for a phase error:

$$\delta\phi = 0.289 \text{ radian}$$

whereas the above expression (with no electrostatic field) gives

$$\delta\phi = 0.269 \text{ radian}$$

The difference is about 0.020 radian or 0.3 cec (also about 0.3 μsec).

3.6.2 Problems to be Solved by Reader

1. Which stations/frequencies have maximum radiated power levels that are limited by the 250 kV maximum base voltage requirement? In these cases, which antenna current is larger: the output power-limited current or the base voltage-limited current (see Table 3.5-2)? Why are the antenna currents for these limiting cases so much different than those at the other stations?

2. Assume that the pulse envelope has a rise time profile given by

$$S(t) = A\,(1 - e^{-t/\tau})$$

where A is the pulse envelope amplitude after the antenna has been fully energized and τ is the rise time defined in Section 3.5.3. Based on the data in Table 3.5-2, what is the time required for the 11⅓ kHz signal pulse envelope at the North Dakota station to attain 90% of its maximum value (A). Compare with Fig. 3.5-2.

3.7 ABBREVIATIONS/ACRONYMS

A	Norway transmitting station
ACCUM	Accumulative correction value inserted every 4 hours
ARGE2	Argentina's station monitor
AUST$	Australia's station monitor
B	Liberia transmitting station
C	Hawaii transmitting station
cec	Centicycle
D	North Dakota transmitting station
E	East (referring to coordinates); La Reunion (referring to transmitting stations)
F	Argentina transmitting station
ft	Foot
G	Australia transmitting station
GHz	Gigahertz (10^9 Hz)
H	Japan transmitting station
HAWAI	Hawaii's station monitor
Hz	Hertz
ID	Identification
IOTC	International Omega Technical Commission
JAPAN	Japan's station monitor
JMSA	Japanese Maritime Safety Agency
kHz	Kilohertz

km	Kilometer
kW	Kilowatt
kV	Kilovolt
LIBER	Liberia's station monitor
m	Meter
MHz	Megahertz (10^6 Hz)
ms	millisecond (also abbreviated msec)
MX 1104-LS	Omega Monitor System (local site)
MX 1104-MS	Omega Monitor System (monitor site)
N	North
N_2	Molecular Nitrogen
N$DAK	North Dakota's station monitor
NORWY	Norway's station monitor
ONSCEN	Omega Navigation System Center
PACE	Performance Assessment and Coverage Evaluation (workstation)
PCD	Polar Cap Disturbance event
REUNI	La Reunion's station monitor
RF	Radio frequency
RMS	Root-mean-squared
S	South
sec	seconds
UT	Shortened form of UTC
UTC	Coordinated Universal Time
V	Volt
VLF	Very low frequency
W	West
WGS-84	1984 World Geodetic Spheroid
µsec	microsecond
µF	microfarad

3.8 REFERENCES

1. Department of Transportation/U.S. Coast Guard, Omega Navigation System Operations Manual, COMDTINST M 16566.1A, December 1988.
2. O'Brien, A., Specification of the transmitted signal of the Omega Navigation System, *Proceedings of the Ninth Annual Meeting of the International Omega Association*, Seattle, WA, August 1984.
3. Vannicola, V., ONSCEN, private communication, October 1991.
4. Watt, A., *VLF Radio Engineering*, International Series of Monographs in Electromagnetic Waves, Vol. 14, Pergamon Press, 1967.
5. Jackson, J., *Classical Electrodynamics*, John Wiley & Sons, Inc., 1975.
6. Morris, P., Omega System Performance Assessment, Report No. CG-ONSCEN-01-89, March 1989.
7. "Omega Station Performance Statistics," Omega Navigation System Center, U.S. Coast Guard, Letter Correspondence to TASC, August 1988.
8. Omega Navigation System Equipment Maintenance Manuals (ONSEMM), ONSCINST M16566.3a, April 1990.
9. Klepczynski, W., U.S. Naval Observatory, Time Services Division, May 1994.

CHAPTER 4

FUNDAMENTALS OF OMEGA NAVIGATION AND POSITION FIXING

Chapter Overview *— This chapter presents position determination using measurements of radiowave signal propagation, based on distance from known locations, namely transmitting station locations. Although the focus is on Omega, the fundamentals are applicable to all radionavigation systems. A brief general introduction to navigation and position fixing is provided in Section 4.1. Section 4.2 presents a general overview of the general principles of position determination, which are applicable to most radionavigation systems, including Omega. These fundamentals are approached from the graphical, or geometric, point of view to provide a visual understanding of the position determination process. Both range-range and hyperbolic techniques are introduced. The relationship between distance and Omega signal phase is developed in Section 4.3. The concept of Omega lanes and the process of lane determination are also introduced, in addition to the use of PPCs, which permit a relatively simple propagation model used for Omega navigation. Section 4.4 defines the navigation coordinates and introduces the position determination process as one of coordinate conversion. The popular least-squares algorithm, which is employed by most modern equipment, is developed and used to illustrate a generic formulation and implementation of a practical position determination algorithm. The more common hybrid, or integrated systems, techniques involving Omega are presented in Section 4.5 and some of the most important issues associated with position accuracy are addressed in Section 4.6. Problems are contained in Section 4.7, abbreviations/acronyms are defined in Section 4.8 and the chapter references are identified in Section 4.9.*

4.1 INTRODUCTION

Navigation is the process of directing the movement of a craft from one location to another (Ref. 1). The craft can be any vehicle capable of purposeful motion. Navigation of a slow-moving craft typically involves answering the question, "Where am I?" At higher speeds encountered with aircraft, the questions may include, "Which way, and how far?" Although this process involves position, direction, time and speed, position is the most fundamental output of all navigation systems. Classically, position determination schemes have been classified (Ref. 1) as either *position fixing or dead reckoning*. Position fixing is the determination of the craft's location, relative to a specified coordinate or reference system, without reference to any former position of the craft. This contrasts with dead reckoning, which is the process of extrapolating a known position of the craft to some future position using measurements of direction of motion and distance traveled.

These classical definitions are often blurred by modern navigation equipment that generally integrates these two schemes, dead reckoning forming the basis for navigation, and position fixing being used to update the indicated position. If position fixes are only available infrequently, then dead reckoning is used between fixes to determine the position of the craft. On the other hand, dead reckoning is not necessary if nearly continuous position fixes are available or if it is not necessary to know the craft position between fixes.

The Omega system (Fig. 4.1-1) consists of eight transmitting stations strategically located around the world. Transmitting stations broadcast omnidirectional continuous wave signals, which are time multiplexed at 12 frequencies (see Chapter 3) in the VLF band: four common frequencies and a unique frequency for each station. An Omega receiver processes the phase of the received signals, at one or more of the frequencies, from two or more stations to determine the receiving antenna position in terms of latitude and longitude on the earth. *The process of transforming the measurements of Omega signals into indicated position is the focus of this chapter.* Understanding this process is not difficult

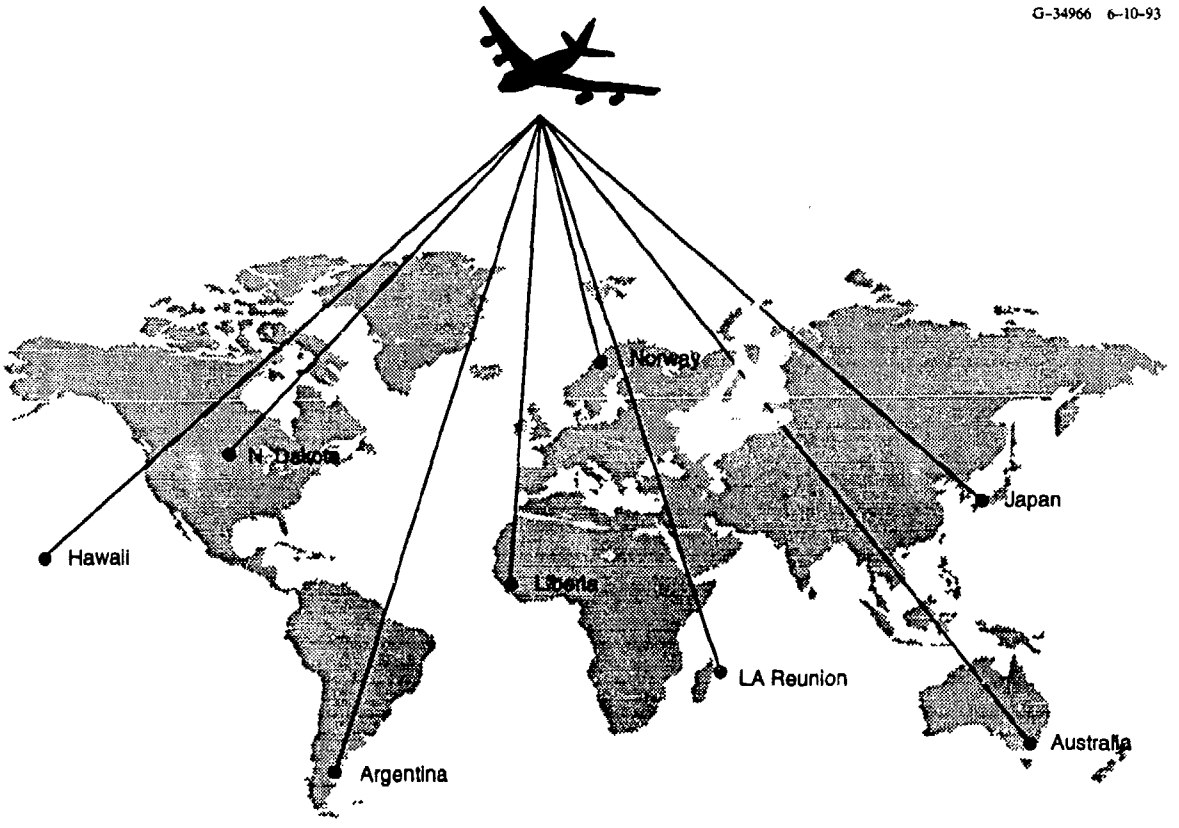

Figure 4.1-1 Omega System Geometry

once several fundamental concepts are understood. Each concept is introduced and explained in this chapter using basic terms and examples. These fundamentals are then used to develop a navigation algorithm that is typical of most modern receiving equipment. Specific algorithms used by actual equipment are not provided since they are generally considered to be proprietary to the manufacturer.

Position accuracy is the fundamental measure of navigation system performance and is defined as the difference, or error, between the true position of the craft and the position indicated by the navigation equipment. In an ideal world without noise and with no Omega signal propagation or measurement errors, assuming that the navigation algorithms are correct, no position error would occur. In the real world, however, numerous error sources contribute to system navigation error. Some of the errors can be controlled or their contribution to navigation error can be reduced to acceptable levels through mathematical algorithms and operational procedures. Other errors are simply a fact of the real world and serve to define the capability and accuracy of the Omega system. It is important to understand the source of these errors and their impact on both the formulation of the navigation algorithms and the resulting navigation error. Important sources of navigation error are introduced in this chapter along with the related concept of Geometric Dilution Of Precision (GDOP). GDOP is a commonly used figure of merit that characterizes the geometry-related position error caused by Omega signal phase measurement errors.

Navigation with Omega using modern equipment is often accomplished with multiple sources of positioning information to produce an integrated navigation solution. For example, most airborne Omega equipment supplements the Omega system signals with signals from the Navy VLF communications system. Most Omega navigation equipment can also use position information and velocity information from an independent source to initialize or aid the Omega navigation solution. Omega has also been integrated with inertial and satellite-based navigation systems to provide an integrated navigation solution. Because all navigation sensors and systems have performance and operational limitations, the process of integration attempts to exploit the positive aspects of each sensor or system to provide the best navigation solution. Some of the most common example of integrated systems are introduced and discussed in Section 4.5.

In this chapter, the primary focus is on providing a basic understanding of the process of position fixing using measurements of the distance (inferred from phase measurements), or change in distance from known locations like the location of Omega transmitting stations. Our goal is to develop a fundamental understanding of how the position of a craft can be determined using signals provided by the Omega system. This is fundamental to understanding how Omega is used for navigation in either a stand-alone or integrated mode.

4.2 BASIC PRINCIPLES

4.2.1 Fundamentals of Direct Ranging Position Fixing

Before getting into the specifics of position determination with Omega, it is instructive to review the fundamental principles of position fixing. All radionavigation systems, including Omega, depend on measuring or inferring by some means the distance from a known location to the craft's current position.

Assume for the moment that the earth is flat and the locations of three points (T_1, T_2 and T_3) are known on this flat earth. Further assume that we want to determine the position of the craft at point R_1. The geometry for this problem is illustrated in Fig. 4.2-1a. Assuming that there is some direct or indirect means for measuring the distance from T_1 to R_1, we can use this measurement to plot a constant *Line Of Position* (LOP_1), which in this case is a circle centered at T_1 (Fig. 4.2-1b). Position R_1 is somewhere on LOP_1, but a single (scalar) distance measurement is not sufficient to determine position in two dimensions. At least two independent measurements are necessary to locate the two-dimensional position of the craft. Assuming that a second measurement of the distance, from T_2 to R_1, can be obtained, a second

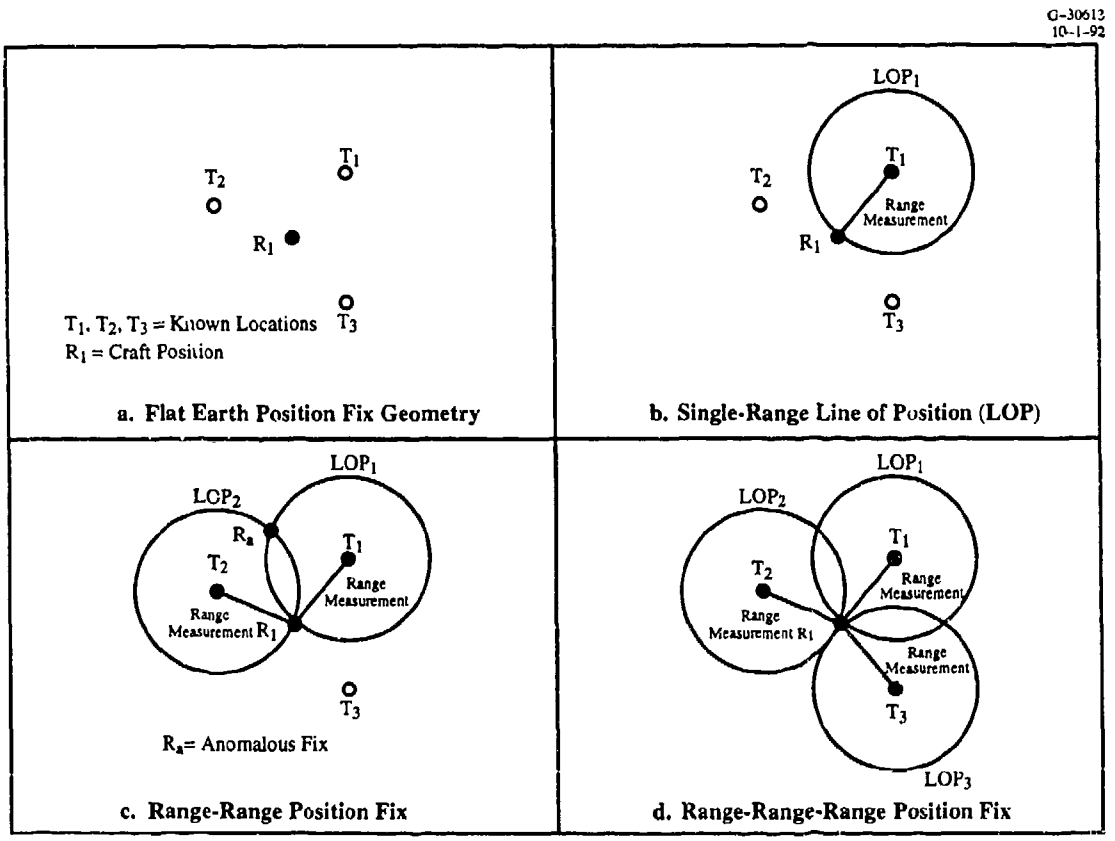

Figure 4.2-1 Fundamental Position Fix Geometry

LOP can be plotted and is shown as LOP_2 in Fig. 4.2-1c. Now, it is easy to see that the location of R_1 is at the intersection of LOP_1 and LOP_2. This is the basis for what is referred to as *range-range* (or rho-rho) navigation.

Also note in Fig. 4.2-1c that there is a second intersection of the two LOPs at R_a; this is called an *anomalous fix* since it is not the desired position. It is necessary to identify which intersection of the LOPs is the desired position. If the approximate location of R_1 is known and R_a is much farther away from R_1 than the error in this approximate knowledge of the location of R_1, then R_a is easily identified as an anomalous fix. One way to resolve the anomalous fix problem is to acquire a third range measurement from T_3 (Fig. 4.2-1d). Now the intersection of all three LOPs unambiguously identifies R_1. Also, this is the basis for what is referred to as range-range-range (or rho-rho-rho) navigation. Any number of independent range measurements can be used; this is referred to as a multilateration or multiranging navigation solution. Other methods for resolving anomalous fixes are available. It is generally not a problem in practice, particularly when navigating rather than position fixing. On a moving craft, the current indication of position is usually close to the previously indicated or known position and the ambiguity is easily resolved. Notice that if R_a is close to R_1, the range measurements in Fig. 4.2-1c are nearly collinear. This represents "poor geometry" and results in excessive navigation error treated this in the next section. [This simple example is the basis for position fixing with all radionavigation systems, including Omega!] In summary, the position determination process combines multiple measurements of the distance from known locations to ascertain the current position of the craft.

4.2.2 Real World Positioning Errors

If position fixing is really as simple as indicated in Section 4.2.1, why is it necessary to write books on the subject? The answer is, "because we live in a real world rather than the ideal world assumed in the preceding discussion." The most significant problem in the real world is uncertainty or "error." All measurements are subject to errors that cause the position indicated by the navigation equipment to be in error.

Returning to the simple example in Fig. 4.2-1, assume that the distance measurements have a *bias error* such that the measured distance is somewhat larger (or smaller) than the actual (true) distance. Now, instead of the three LOPs intersecting precisely at R_1 there are three distinct intersections (R_{13}, R_{23}, and R_{12}) near R_1, as illustrated in Fig. 4.2-2. We now must pick one of the three solutions or somehow combine the three solutions (e.g., using some form of averaging) to estimate R_1, given that R_1 is somewhere within the shaded region. In any event, the indicated position will probably be in error and the position-fixing process has become a bit more complicated. It is clear that some type of algorithm is necessary to automate the process.

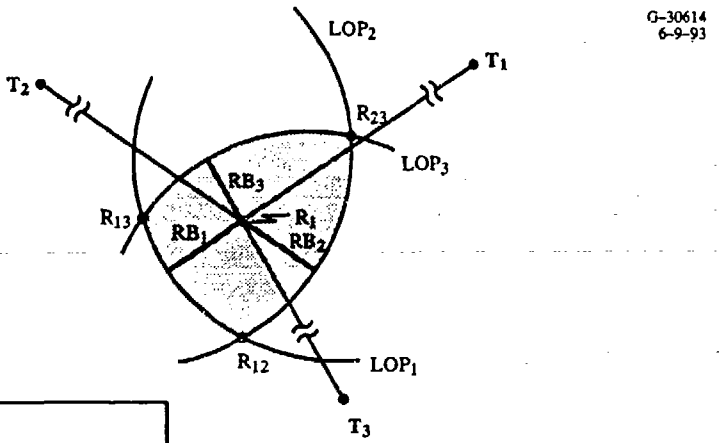

Figure 4.2-2 Range-Range-Range Fix with Bias Measurement Error

In addition to bias, or systematic, measurement errors, we must also contend with *random*, or *noise-like*, *measurement errors* in the real world. A random measurement error causes a "jitter" or "randomness" in the computed position. Again building on our simple example, assume that the measured distance includes a noise-induced error such that each time a measurement is made a slightly different value is obtained for the indicated range. The LOP crossings will differ for each measurement and the indicated craft position will change with each computation, even if the craft is stationary.

If the noise is a zero-mean random process (Ref. 2), the average of many range measurements (or position solutions) can be used to determine an average (mean) indication of position; this significantly reduces the error in the position fix. Effectively, this is done by the so-called navigation filters used in receiving equipment. If the craft is stationary, then averaging over many measurements is quite feasible, resulting in a dramatic reduction in the effect of random measurement errors (noise) on the position fix. However, the amount of "averaging" that can be performed on a moving platform is limited because each measurement is associated with a new position of the craft. Unless this motion of the craft is properly accounted for by the filtering algorithm, it may not be possible to distinguish *true motion* of the craft from the *apparent motion* caused by noise. Consequently, additional error can be introduced by averaging this dynamic effect. For example, an aircraft flying at 300 knots moves 500 feet in one second. Therefore, simply averaging several measurements over tens of seconds will introduce a significant error in the indicated position of the aircraft since the true position of aircraft is significantly different at each measurement.

Techniques to reduce the effects of dynamic errors on a moving platform include *rate aiding* of the measurement tracking process and the use of dynamic models in a Kalman filter (addressed in Appendix D). Rate aiding uses an external source of craft velocity, such as an air speed indicator in an aircraft, and a heading indicator, a compass, or an estimate of velocity derived from the changes in position as an indication of vehicle motion. Individual measurements that are separated in time can be related through dead reckoning; the current position is approximated by the previous position plus the integral of velocity over the time between measurements. If the time interval is small and the velocity is nearly constant, the integral is well approximated by the product of velocity and time between measurement. Differencing the dead reckoned position with the craft position derived from the Omega measurements yields an indication of the error. Because this error does not include the rapidly changing position of the vehicle, it can be averaged over several measurements and used to improve the indicated position of the craft. This process is expanded upon in Section 4.4. Kalman filtering is an advanced filtering technique that allows time-varying dynamics to be modeled and included in the filtering process. In spite of the available techniques for reducing the effect of noise, random positioning errors are associated with all practical real-world navigation systems. The size of these random errors often limits the utility of the system.

4.2.3 Geometry Effects

Along with measurement error, a related geometry effect is important in determining the fix error in radionavigation systems. Returning again to the example in Fig. 4.2-1, note that the LOPs can cross with a crossing angle between 0 and 90°. The LOP crossing angles depend on the relative position (geometry) of T_1, T_2, T_3 and R_1. In an ideal world the crossing angle would not be critical, except for the case where it approaches zero and the previously identified requirement to resolve the ambiguous fix becomes difficult.

In the presence of measurement errors, geometry has a profound effect on the position fix accuracy and is one of the most important characteristics that limits the performance of radionavigation systems. This is easily seen by looking at the uncertainty associated with determining the intersection of two LOPs in the presence of measurement noise. In Fig. 4.2-3, two LOPs (range-range position fix) are shown with a large crossing angle near 90° and also for a relatively shallow crossing angle near 0°. Assume that the measurement noise causes a random variation around the nominal (mean or average) value of the LOP. Further assume that the maximum variation in the indicated position of the LOP is $\pm\beta$. Because of this randomness in the measurement, the indicated location of the LOP crossing (position fix) can occur anywhere within the shaded area of uncertainty. Therefore, the size of this area of uncertainty is directly related to the position fix uncertainty.

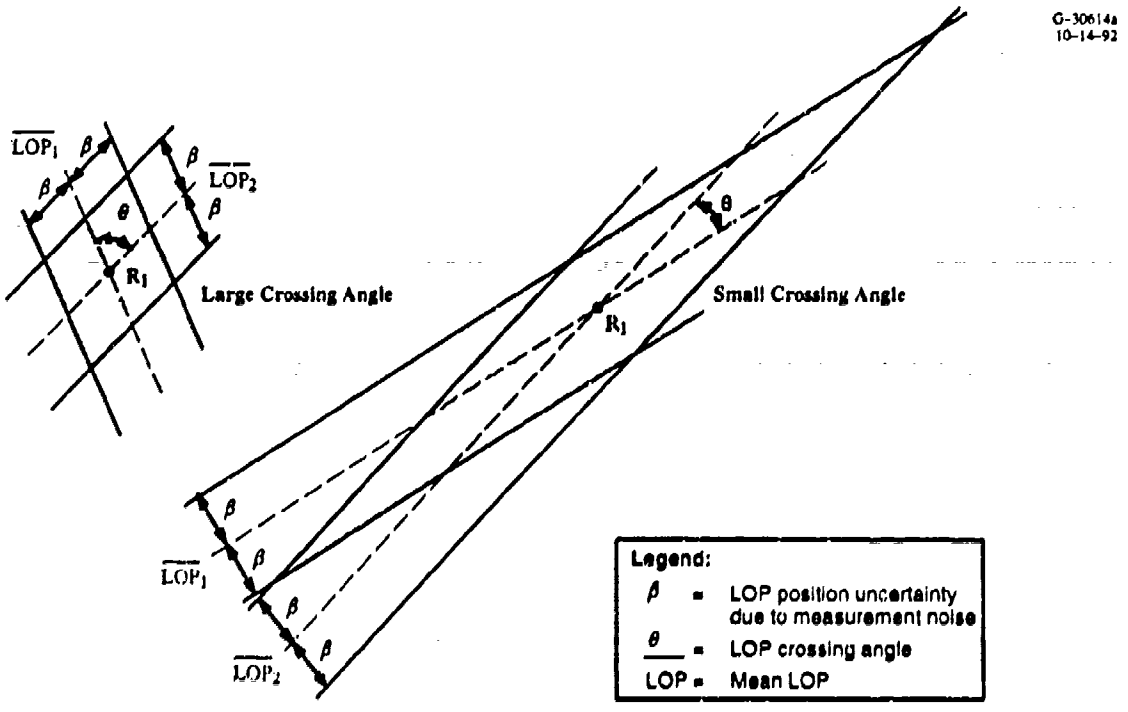

Figure 4.2-3 Range-Range Position Fix Uncertainty Regions Due to Range Measurement Noise as a Function of LOP Crossing Angle

If these two LOPs with the same associated fluctuation bounds of $\pm\beta$ happen to cross with a very shallow crossing angle, the associated area of uncertainty is now much larger than for the 90° crossing angle (see Fig. 4.2-3). Since the indicated position can fall anywhere within this uncertainty region, the resulting fix error also has the potential to be much larger. This geometric effect is captured numerically by a figure of merit called *Geometric Dilution of Precision* (GDOP), which is the ratio of position error divided by range measurement error. Therefore, a large GDOP is associated with large areas of uncertainty and the associated position error will be larger than the range measurement error. For example, a GDOP of 8 means that the position error will be about eight times larger than the range measurement error. Further discussion of GDOP is provided in Chapter 10 and additional insights are provided later in this chapter. Although this graphical interpretation of the effect of geometry on fix error is somewhat oversimplified, it captures the essence of the problem and provides a useful mental picture to support the associated mathematics addressed later in this chapter. Fix geometry must be accounted for in any practical navigation algorithm and the navigation user should be aware of poor geometry conditions that degrade navigation accuracy. Remember that range measurement errors cause position fix uncertainty (error) and poor geometry (large GDOP) magnifies the effect of the range error on the position fix error.

4.2.4 Range Measurement with Radiowaves

Thus far our simple example has assumed that it is possible to measure the distance from a reference point (T) to the desired fix point (R). The process of "measuring" this distance is fundamental to all radionavigation systems. The reference points are the known locations of the transmitting stations and the fix point is the location of the receiver antenna. No radionavigation system directly measures this distance. At best, the time it takes for a radiowave to propagate over the distance can be measured and the associated distance inferred from the "known" propagation velocity of the signal. The word known is in quotation marks because the precise propagation velocity of a radiowave is generally only available for a known uniform media; e.g., the propagation velocity in a vacuum (free space) is the same as the speed of light: 299,792.5 km/sec.

The presence of the earth introduces variations from free-space signal propagation that can be computed, but only if the electromagnetic properties of the path are known (see Chapter 5 for additional details). In most applications, the propagation velocity of the signal can be adequately approximated. Alternatively, the propagation velocity can be inferred from time or phase measurements over a known path and then used to estimate the distance on other paths with similar physical and electrical characteristics. This is in fact the basis* for determining the Propagation Corrections (PPCs) used to improve Omega accuracy (Chapter 9).

In general, there is a need to measure the time it takes for a radio signal to propagate over the desired distance so as to infer the distance. In the case of Omega, signal phase is the fundamental measurement. However, we must address some additional complications associated with phase measurements. These are referred to Section 4.3 and time is assumed to be the fundamental measurement in this section. If all transmitting stations are synchronized to transmit at precisely the same time, and the receiver has knowledge of this time, all that is necessary is to measure the time at which each signal is received and compute the distance to each transmitter using the known propagation velocity of the signal. Sounds too easy, right?

If all transmitters are synchronized to transmit at the same time, t_0, the time at which the signal is received, t, from each of three transmitters (1, 2, and 3) is

$$\begin{aligned} t_1 &= t_0 + t_{r1} \\ t_2 &= t_0 + t_{r2} \\ t_3 &= t_0 + t_{r3} \end{aligned} \qquad (4.2\text{-}1)$$

*For PPCs, the phase velocity (the apparent velocity of phase motion) is estimated.

where t_r is the signal propagation time. If t_0 is known, then any two measurements of t provide the necessary information to compute a rho-rho fix. However, if t_0 is unknown it introduces a bias in each measurement and the indicated position given by the crossing of any two LOPs will be in error, as illustrated in Fig. 4.2-2. Four fundamental approaches get around this problem: 1) use an external indication of t_0, 2) estimate t_0 using a known location, 3) estimate t_0 using additional independent measurements, and 4) employ the range-difference (hyperbolic) mode.

Approach 1 requires an accurate external clock (e.g., cesium frequency standard) that is synchronized at the stations and (conceptually) retains the value of t_0 for subsequent use by the receiver. *Approach 2* requires the craft to be positioned at a known location. The radionavigation fix is compared with the known location and the value of t_0 determined, which "forces" the indicated position to match the known location. This value of t_0 can then be used as the craft moves to their locations, assuming that t_0 does not change. *Approach 3* is based on the fact that a minimum of two range measurements is required to compute a rho-rho fix. If one or more additional measurements are available from other stations, the added information can be used to estimate t_0. Returning to the example illustrated in Fig. 4.2-2, t_0 will introduce a range bias (RB) of equal value in all three range measurements (R). If we can determine the value of the common range bias that must be removed to cause all three LOPs to cross at a common point, the effect of t_0 is eliminated. This is the basis for the rho-rho-rho mode of direct ranging and is easily extended to handle any number of multiranging measurements.

Historically, *Approach 4* has been the most popular due to its simplicity and low cost of implementation. Overcoming the need for the receiver to know when the transmitters transmit can be accomplished using the *range difference* or *hyperbolic mode*. The hyperbolic mode of navigation uses range differences rather than the absolute range to obtain a position solution. A minimum of three stations is required for a hyperbolic solution. Let us take a look at how the hyperbolic mode gets around the problem of the receiver needing to know when the transmission starts. Simply differencing the time that the signal is received from any two stations (Eq. 4.2-1) eliminates t_0 and provides a direct measure of the time difference (t_d):

$$\begin{aligned} t_{d12} &= t_1 - t_2 = t_{r1} - t_{r2} \\ t_{d13} &= t_1 - t_3 = t_{r1} - t_{r3} \end{aligned} \qquad (4.2\text{-}2)$$

Conceptually, the time difference can be measured by starting a stopwatch when one signal is received and stopping the watch when the second signal is received. Notice that the unknown time, t_0, drops out of the time difference expressions leaving only the differences between the signal propagation times. Multiplying the time differences by the signal propagation velocity yields a measurement of the *range difference*. Because of the popularity of the hyperbolic mode, further details are provided in the following section.

4.2.5 Hyperbolic Mode

The range difference approach is called the hyperbolic mode because the resulting LOPs are a family of hyperbolas (as compared to the circles associated with the direct-ranging mode), which are symmetric around the *baseline* (the direct path between the two station locations), as illustrated in Fig. 4.2-4. Note that the hyperbolic LOPs are easily constructed from the circular LOPs for each station by connecting the crossing points associated with equal differences between the LOPs from each station. The zero-difference LOP is the perpendicular bisector of the baseline because the time for the signal to propagate from T_1 is equal to the propagation time from T_2. Also, the *baseline extension* is important because it represents a region where a hyperbolic fix cannot be computed.

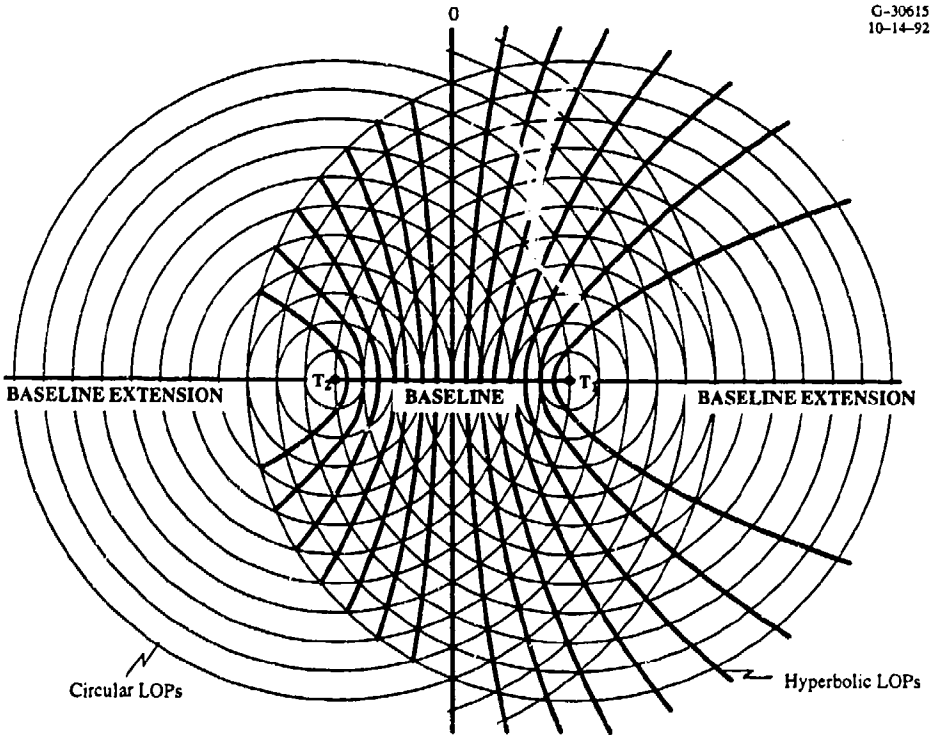

Figure 4.2-4 Hyperbolic Lines of Position

The hyperbolic LOPs for stations T_1 and T_2 are redrawn in Fig 4.2-5a to reduce the clutter associated with the constant-range circles. Notice that, unlike rho-rho LOPs that have a constant repetitive spacing, the spacing between the hyperbolic LOPs increases with increasing distance from the baseline. This is significant since it gives rise to an associated increase in the GDOP, which means reduced accuracy. It is important to recognize that the accuracy of a hyperbolic fix is not just a simple function of the LOP crossing angle, like in the rho-rho mode, but also depends on the relative spacing between the LOPs. This point is further illustrated in the following discussion.

As with the rho-rho mode, at least two hyperbolic LOPs are also required to determine position R_1. A second set of hyperbolic LOPs can be generated by using stations T_1 and T_3. The resulting hyperbolic LOPs that cross at R_1 are illustrated in Fig. 4.2-5b. Although T_1 is common to LOP_{12} and LOP_{13}, there is no requirement to select T_1 as the common station. Either T_2 or T_3 can be selected as the common station with the same resulting position and GDOP. This is counter-intuitive since the relative geometry of the LOPs is quite different. This point is illustrated by comparing Fig. 4.2-5b and Fig. 4.2-5c. The stations are identical in both cases but the hyperbolic LOPs crossing at R_1 have significantly different geometry, depending the common station. One may be inclined to conclude that selecting T_2 as the common station yields better LOP crossing geometry and hence a lower GDOP. This is not true! Both geometries provide identical GDOP. In practice, there may be slight differences in the fix error since the GDOP calculation assumes equal and unbiased error levels for each station.

It should be noted in passing that a four-station hyperbolic solution can be obtained if four stations are available. In this case the position fix and associated accuracy (GDOP) does depend on the particular station pairs selected. Because this is not a common mode of operation we will not address it further here. Aside from the case in which only range differences are available because of data collection or receiving equipment limitations, the four-station hyperbolic mode offers no advantage over the four-station direct ranging mode implemented with a least-squares algorithm. As with the range-range navigation mode, anomalous fixes can also occur in the hyperbolic mode and must be resolved by using techniques similar to those employed for range-range navigation.

4.2.6 Historical Position Fixing and Navigation

Before the availability of efficient on-board digital computers, navigation with Omega was accomplished by using precomputed hyperbolic LOPs plotted on paper charts. These charts were developed and published by Defense Mapping Agency (DMA) for use available Omega stations. Measurements made by a navigator using an Omega receiver were usually plotted on the chart to identify two or more LOPs. The intersection of these LOPs provided the position fix. This hyperbolic fix point could

G-30616
10-14-92

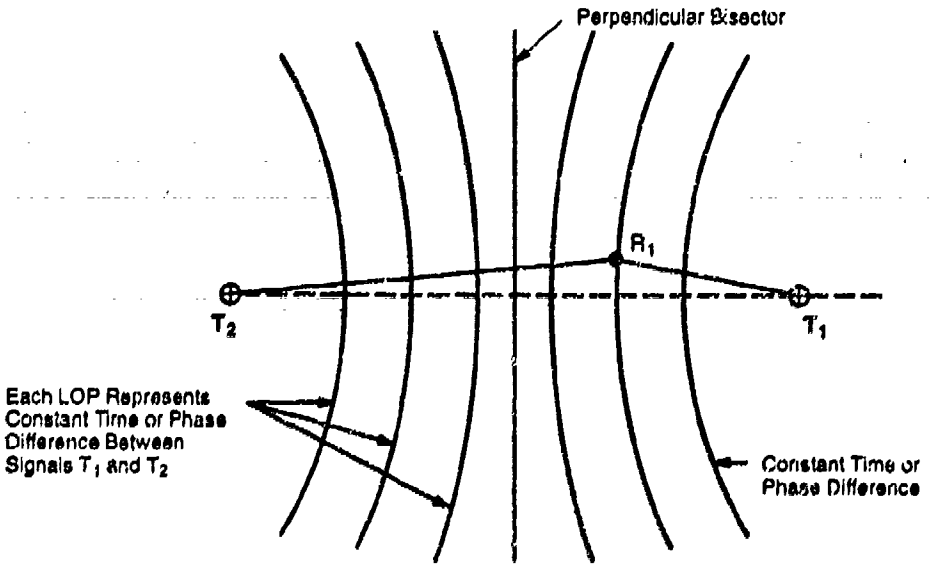

(a) Hyperbolic (Phase-Difference) LOPs for Station Pair T_1 T_2

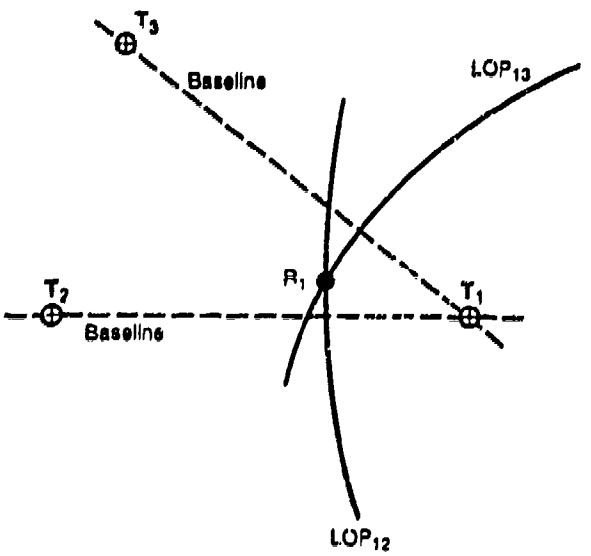

(b) Hyperbolic LOP Crossing (T_1 Common)

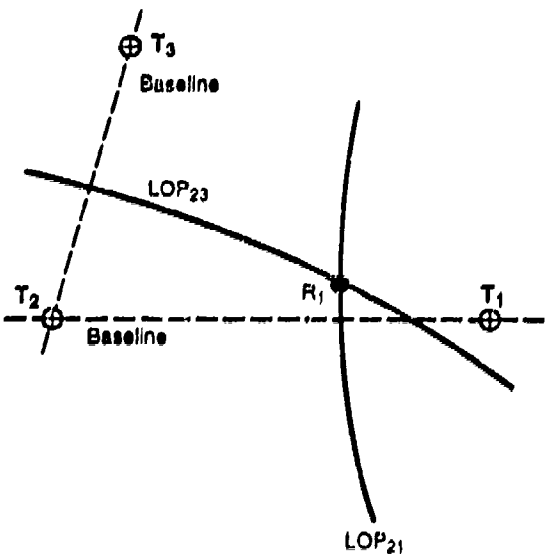

(c) Hyperbolic LOP Crossing (T_2 Common)

Figure 4.2-5 Hyperbolic Position-Fix Technique

then be related to the lines of latitude and longitude, or other navigational information, also plotted on the chart. This process was repeated periodically by the navigator to determine the track of the craft as given by the locus of fix points.

With the advent of microprocessors, Omega receiving equipment significantly improved. Paper charts are becoming a thing of the past as they are being replaced with electronic coordinate converters. Computer-based coordinate converters employ mathematical algorithms to process the measurement data and directly compute the latitude and longitude of the craft. Not only does this eliminate the manually intensive process of using paper charts, accuracy and overall capability of the receiving equipment are significantly improved. There has been a general trend to move away from the hyperbolic mode to the multi-ranging mode where all usable measurements from multiple stations are used to compute the fix rather than selecting just three stations. Fix algorithms and processing techniques are addressed in Section 4.4. However, it is important to have a basic understanding of the position fixing process first before getting immersed in the mathematical details. Keep in mind the picture of intersecting LOPs, either circular or hyperbolic, since this is the basis for all radionavigation techniques. A comparison of the important tradeoffs for the various techniques is summarized in Table 4.2-1.

At this point, it is important to have a basic understanding of the fundamental concepts of rho-rho, rho-rho-rho and hyperbolic position fixing using time (or range) measurements. The rest of this chapter expands upon these basic concepts to provide the details required to understand the real-world Omega system and signal characteristics, in addition to the practical implementation of vehicle navigation with Omega signals.

Table 4.2-1 Comparison of Navigation Fix Modes

ATTRIBUTE	NAVIGATION MODE		
	HYPERBOLIC	RHO-RHO	RHO-RHO-RHO
Accuracy	Better (under ideal conditions)	Good	Best
Geometry	Dilutes accuracy	Less effect	Same as rho-rho
Stations	Minimum of 3	Minimum of 2	Minimum of 3
Cost	Low	High	Medium
External clock	No	Yes	No

4.3 OMEGA SIGNAL PHASE AND DISTANCE RELATIONSHIPS

4.3.1 Signal Characteristics

An electromagnetic radiowave has sinusoidal characteristics in both time and space. The best visual analogy is to drop a stone in a pond and observe the waves (Fig. 4.3-1). The ripples in the radial direction form a *sinusoidal* (spatial) shape on the surface of the water that *appears* to move (*propagate*) away from the source of the excitation. There is no actual motion of the surface in the radial direction; a cork floating on the surface will bob up and down but does not actually move in the radial direction along with the waves. The motion of the waves at a fixed location in the water is up and down with a sinusoidal (temporal) motion at a certain *frequency*. The distance between the peaks (or troughs) of the waves is called the *wavelength*, which represents a *phase shift* of 2π radians (or 360°). This is a simple visual illustration of the temporal and spatial characteristics of a radiowave.

The above visualization can be represented mathematically:

$$E = E_0 \cos(\omega t - kd) \tag{4.3-1}$$

where:

$\omega = 2\pi f$; t = *time*; f = *frequency*

$k = 2\pi/\lambda$; d = *distance*; λ = *wavelength*

The quantity E_0 is the peak amplitude of the wave, ωt is the temporal portion of the phase and kd is the spatial component of the phase, which is the product of the *wave number, k, and the distance, d.*

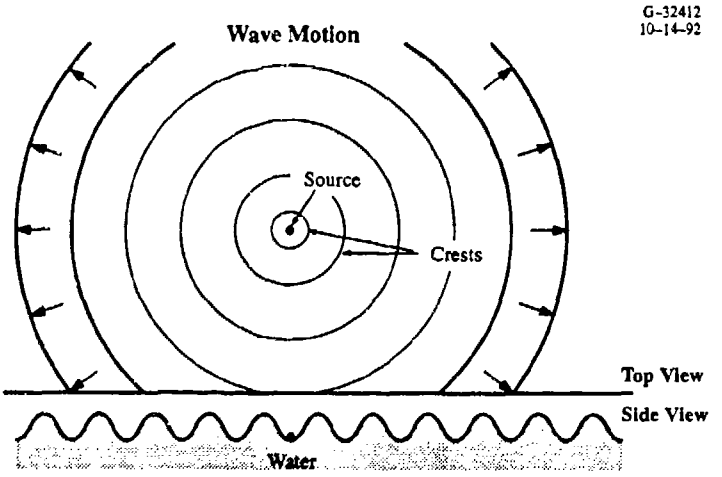

Figure 4.3-1 An Electromagnetic Wave Travels Through Space in Much the Same Manner as a Wave in Water

A plot of the sinusoidal wave is shown in Fig. 4.3-2 at three different values of time. The amplitude of the wave is plotted as a function of both phase on one horizontal scale and of the distance from the transmitter on a second scale. In Fig. 4.3-2, if the point P (defined as a constant-phase point) is observed as a function of time, it *appears* to move (propagate), just like the example of waves in the water, in the direction of propagation at the phase velocity (v). At a fixed distance from the transmitter, the signal amplitude exhibits a sinusoidal variation at frequency f with a peak amplitude of E_0 (see Chapter 5 for a complete discussion of signal propagation effects).

In Section 4.2 it is assumed that the fundamental measurement is the time it takes for the signal to propagate over the distance between the transmitter and the receiver. This is because it is easy for most people to think in terms of the time it takes to move a certain distance. In actuality, *Omega position fixing and navigation use the signal phase rather than time as the fundamental measurement.* Although some additional complications are associated with the use of phase, there should not be any confusion or loss of understanding of the position determination process since a direct relationship exists between the propagation time (or distance) and the phase of the signal. The objective of either type of measurement is to ascertain range, or distance, between the transmitter and the receiver, or the change in range relative to a previously known position. Figure 4.3-2 and a few simple equations illustrate this point.

The propagation velocity (v) of a radio signal is defined as:

$$v = f\lambda \tag{4.3-2}$$

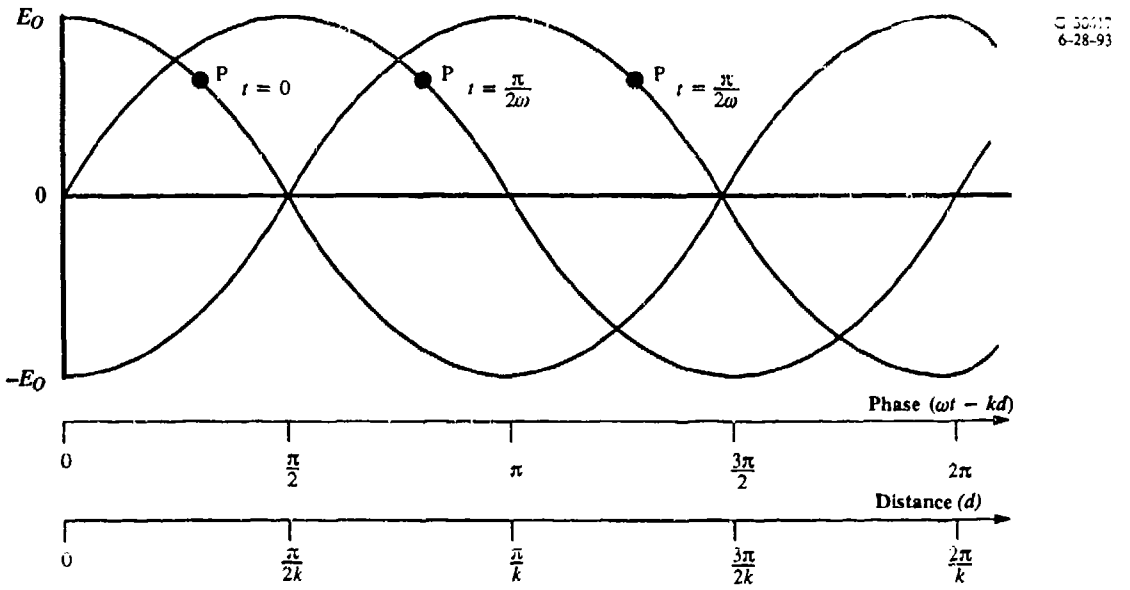

Figure 4.3-2 Sinusoidal Wave at Three Different Values of Time

where f is the frequency and λ is the wavelength of the signal. From Eq. 4.3-1, the relationship between the phase shift (ϕ), in units of radians, associated with a signal propagating over a distance d during the time interval t is:

$$\phi = kd = \frac{\omega d}{v} = \omega t \qquad (4.3\text{-}3)$$

where K is the wave number. It is easy to see from Eq. 4.3-3 how time, distance and phase are all related. Therefore, *the distance from the receiver to the transmitter can be inferred by measuring the shift, or change, in the signal phase at the receiver relative to the phase of the signal at the transmitter.*

As in the previous time measurement example where it is necessary to know the time at which the signal is transmitted, the *phase* of the signal at the transmitter location must be known or determined; alternatively, the hyperbolic phase difference approach can be used to get rid of the common unknown phase. Operationally, all eight Omega transmitting stations have a stable signal frequency and the transmitters are phase-synchronized. This is accomplished by using cesium frequency standards at each station and a phase shifter, which is periodically adjusted to correct the transmitted signal phase for any small drift in the cesium clock relative to the other stations and relative to an external time reference. The required periodic phase adjustment at each station is determined with the SYNC3 software (see Chapter 7), which processes signal measurements from each station to determine the required phase adjustments at each station.

At any given instant of time, the *cumulative phase* (kd) increases linearly with distance from the transmitting station and is equal to an integral number of cycles plus a fraction of a cycle. The sinusoidal spatial pattern repeats as the signal propagates away from the transmitter, as illustrated in Fig. 4.3-3. At each wavelength, or cycle, the wave repeats; this distance between repetitions is called an Omega *lane*. At the primary Omega frequencies of 10.2 kHz and 13.6 kHz, the respective wave lengths (lane widths) are approximately 16 nm and 12 nm. Omega lanes are an important concept and are fundamental to navigating with Omega. This important subject is treated in detail in Section 4.3.3.

The example in Fig. 4.3-3 shows a constant amplitude signal as a function of distance from the transmitter. This is not true in the real world, which is a lossy medium. The actual amplitude of a plane wave in a lossy medium is approximated by an exponential amplitude which decays with distance from the transmitter:

$$E_x = E_0 \, exp(-\alpha d) \cos(\omega t - kd) \qquad (4.3\text{-}4)$$

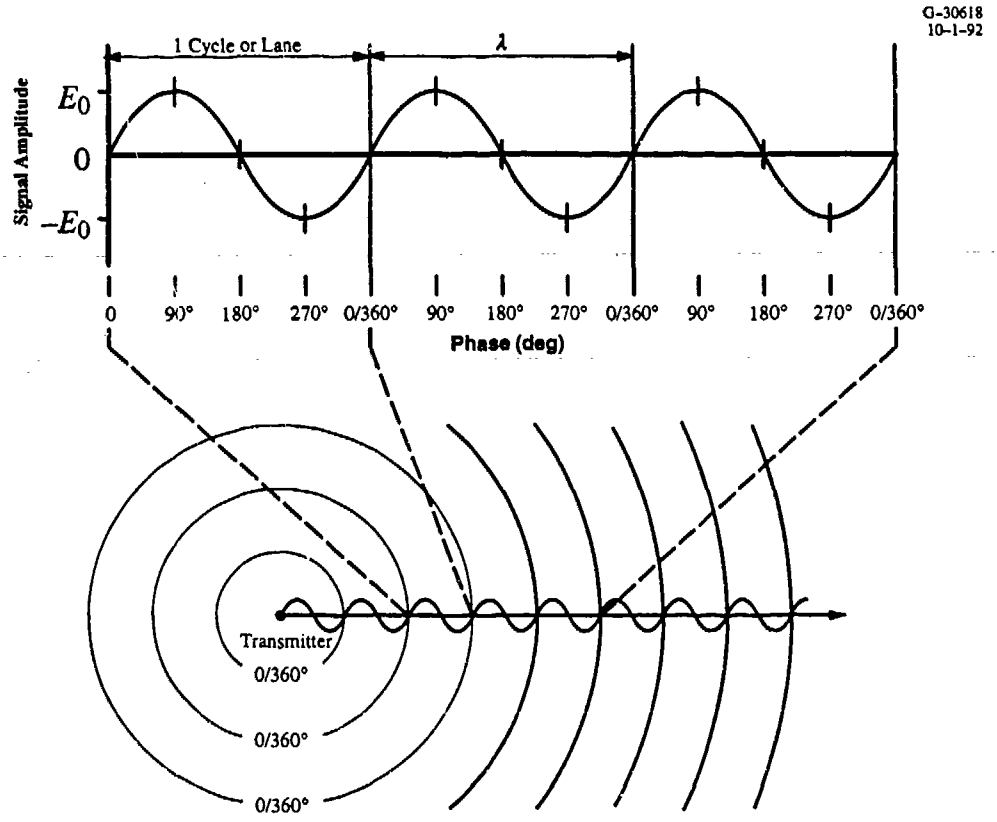

Figure 4.3-3 Omega Lanes Formed by Radio Waves

where α is the attenuation rate. Equation 4.3-4 is illustrated in Fig. 4.3-4. In the real world an additional reduction of the signal amplitude is a function of the distance from the transmitter due to geometry and is referred to as the "spreading factor" (see Chapter 5). The reduction in signal amplitude with distance from the transmitter does not directly impact the position fixing process, but it does influence the accuracy of the position fix. This is because in the real world it is necessary to contend with atmospheric noise, which limits the ability of the receiver to detect and measure the signal phase. If a signal level is very high compared to the noise level, the noise has little impact on fix accuracy. However, when the signal and noise levels are comparable, accuracy is degraded due to the noisy phase measurements. The limiting case, of course, is when the signal is buried in the noise and cannot be detected by the receiver. Although signal level and noise issues are extremely important when it comes to understanding Omega system availability and accuracy performance, they are of secondary importance to the fundamentals of position fixing. Only in the detailed consideration of the position fix algorithm design and implementation is it necessary to address these issues. The details of signal amplitude and noise effects, and the associated impact on the navigation fix, are addressed in Chapters 10 and 12.

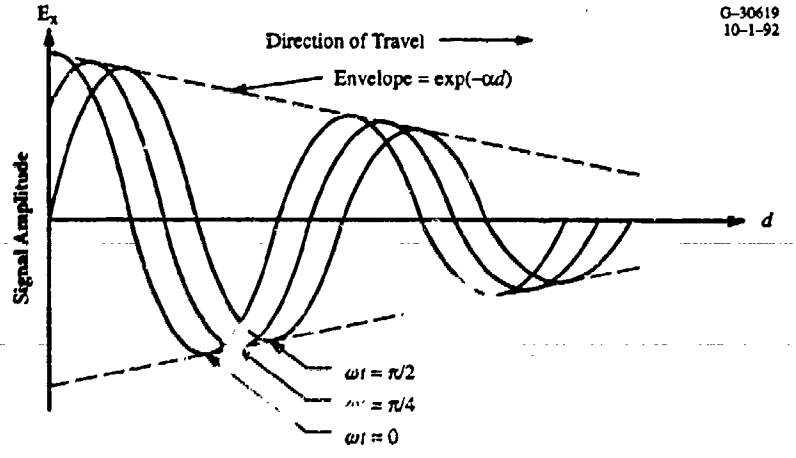

Figure 4.3-4 Plane Wave Propagation in a Lossy Medium

4.3.2 Propagation Corrections

Another real-world characteristic that impacts navigation accuracy and needs to be accounted for in the navigation solution is the fact that the true cumulative phase is not exactly a linear function of distance as suggested in Eq. 4.3-3. In reality, the wave number (k) is not constant in the presence of the earth and generally differs for each point along the signal propagation path. This means that the exact expression for the phase shift is a rather complicated integral of the wave number over the path. Fortunately, in practice, things are not as bad as this may lead one to believe. Using a single constant wave number yields a total *nominal phase* that is within about 0.2% to 2% of the the result of the path integral and real-world observations. *The simple nominal phase model given by Eq. 4.3-3 is the fundamental model used in most Omega receivers to characterize distance as a function of phase.*

Although an accuracy of one or two percent may be adequate for some applications, it is not sufficient to support the advertised Omega accuracy of 2 to 4 nm, 95% of the time. To obtain the advertised accuracy, the measured phase must be corrected in the receiver for the real-world effects by applying a PPC (propagation correction) to each phase measurement. After correction with the PPCs, the resulting corrected phase measurements correspond very closely to the nominal phase model. Therefore, for the purpose of position fixing or navigation calculations, there is no need to worry about the real-world phase complexities since it can be assumed that they are taken care of by the PPCs. The inability to provide perfect corrections of all real-world effects with the PPC produces a residual error which tends to be the major contributor to Omega position accuracy. The development and application of PPCs are addressed in Chapter 9.

4.3.3 Omega Lane Determination

Lane determination is important because the cumulative phase of the Omega signal at any point along the propagation path is an integer number of cycles (lanes) plus a fraction of a cycle, as illustrated in Fig. 4.3-2. Because of the 2π ambiguity associated with phase measurements, the receiver can only measure the fractional part of a cycle. In other words, that the phase varies from 0 to 360° (2π rad) in each and every lane (see Fig. 4.3-3). A receiver arbitrarily placed somewhere in the signal coverage region will indicate the phase within a lane. Therefore, without knowing the lane count it is impossible to determine the location of the receiver on the earth. It is necessary to determine the lane count (number of whole cycles) so that the total distance from the transmitter to the receiver can be determined.

There are three basic ways to determine the lane count and the associated coarse position. The *preferred way* is to start at a known location and let the receiver keep track of the lane count as the craft moves from the known position. This means that when the measured phase changes 360° and reads zero degrees, *a lane counter* is incremented (or decremented). Obviously, the accuracy of the initial known position must be no worse than plus or minus one-half of a lane width or the wrong initial lane may be selected. Most of the time this approach works just fine. However, there is always the possibility that the receiver will lose track of the lane count due to a power failure or a temporary loss of signal.

The *second way* to derive the lane count is to use another *independent positioning system*, such as a known surveyed location, a celestial fix or an electronic (e.g., Loran-C or radar) or visual means. This auxiliary fix must be accurate enough to identify the correct lane so that the Omega lane count can be reinitialized. At an operating frequency of 10.2 kHz, the lane width is approximately 16 nm in the direct ranging mode. Therefore, it is only necessary to know where you are with an accuracy of ±8 nm to determine the coarse lane count and then use Omega to refine this position within the known lane. The lane width for each of the common Omega frequencies is listed in Table 4.3-1. Both the direct ranging and hyperbolic (on the baseline) lane widths are provided.

A *third approach* is to use Omega *frequency differencing* to determine the lane count. One of the reason that Omega transmits at multiple frequencies is to support lane determination. Looking at the Omega navigation frequencies, it is important to observe that there is an integer relationship between these frequencies. For example, 10.2:13.6 is a ratio of 3:4. This means that the total width of three lanes at 10.2 kHz is exactly the same as the total width of four lanes at 13.6 kHz, a total of about 48 nm. A wavelength of 48 nm corresponds to a frequency of 3.4 kHz which is equal to the difference between

13.6 kHz and 10.2 kHz. Differencing the 10.2 kHz and the $11^1/_3$ kHz frequencies results in an equivalent lane width of 144 nm. The equivalent lane widths for selected difference frequencies are listed in Table 4.3-1. The lane widths and lane count are also illustrated in Fig. 4.3-5.

Table 4.3-1 Lane Width of Common Frequencies and Selected Difference Frequencies

FREQUENCY (kHz)	LANE WIDTH		
	RHO-RHO		BASELINE HYPERBOLIC (nm)
	km	nm	
10.2	29.5	16	8
13.6	22.1	12	6
$11^1/_3$	26.5	14.4	7.2
11.05	27.2	14.77	7.38
13.6–10.2 (3.4)	88.5	48	24
13.6–$11^1/_3$ ($2.2^2/_3$)	132.8	72	36
$11^1/_3$–10.2 ($1.1^1/_3$)	265.5	144	72
$11^1/_3$–11.05 ($0.28^1/_3$)	1062	576	288

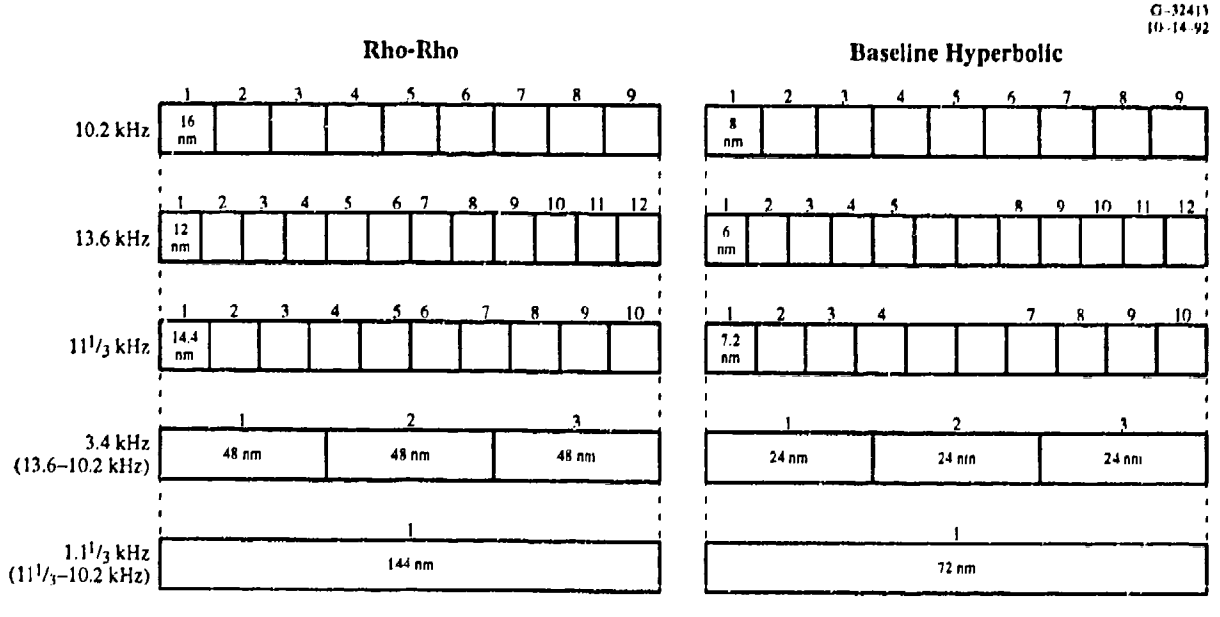

Figure 4.3-5 Lane Width as a Function of Omega Frequency

The receiver can easily synthesize the difference frequency using the primary frequencies. Given that a fix can be generated using the difference frequency, it is only necessary to know the approximate position of the craft with an accuracy of at least that corresponding to the larger width of the difference frequency lane. Generally, the maximum allowable error is defined to be half of the lane width to allow for the fact that the error could be positive or negative. The difference frequency fix is usually accurate enough to determine the primary frequency lane. The primary frequency is then used to determine the position of the craft.

In the hyperbolic, or phase difference, mode of operation the width of all lanes on the baseline is exactly one half of the lane width in the rho-rho mode (Table 4.3-1 and Fig. 4.3-5) This means that the lane width at 10.2 kHz is 8 nm and the 3.4 kHz difference frequency lane width is 24 nm. Using the 11.05 kHz signal with the $11\frac{1}{3}$ kHz signal yields a difference frequency with a hyperbolic lane width of 288 nm on the baseline. Apart from error considerations, this is generally sufficient to resolve the lane ambiguity in most operational situations.

The hyperbolic lanes are illustrated in Fig. 4.3-6. Each lane is defined by the contours of zero phase difference. The difference between two measured phase relationships defines an LOP within each and every lane established by the zero-phase contours. Again, since the LOP can lie within any lane, lane identification is extremely important. Note that unlike the direct ranging mode of operation, the width of the hyperbolic lanes is not constant. On the baseline the lane width is $\lambda/2$ where λ is the signal wavelength. However, the lane width widens with increased distance from the baseline.

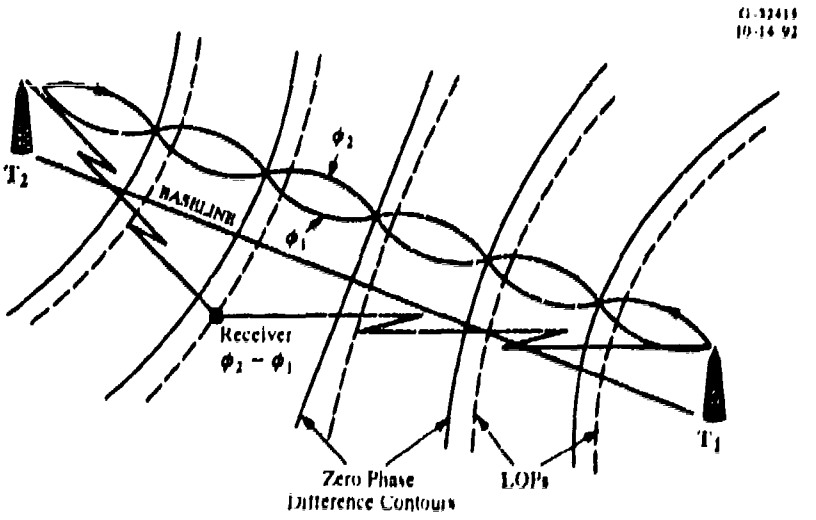

Figure 4.3-6 Hyperbolic Mode Lanes

In this section, we have tackled the important relationships between phase and distance. Also, the concept of Omega lanes has been identified along with various ways to determine the correct lane. This is important because Omega phase measurements only indicate craft position within a lane. If you are unsure of any of the fundamental concepts presented thus far, review this section before continuing. The next section expands upon these concepts and the basics given in Section 4.2 to address more details of position fixing and navigation with Omega.

4.4 OMEGA NAVIGATION/POSITION FIXING

Based on the fundamentals presented so far in this chapter, you should have a basic understanding of how Omega signals can be used to infer range (or change in range) from the transmitter to the receiver. What isn't clear at this point is *how* modern microcomputer-based equipment implements the navigation solution using signal phase measurements. This section "builds" a generic navigation algorithm by addressing each of the important elements that must be accounted for in a practical implementation. Knowledge of these elements is fundamental to a general understanding of modern methods and navigation equipment.

4.4.1 Phase Measurements

Before getting into the process of position fixing and navigation, it is instructive to look at how the phase of an Omega signal is actually measured. Most modern receivers use a phase-locked loop (PLL) to achieve both phase tracking and filtering of the received signal. A PLL (illustrated in Fig. 4.4-1) has a voltage-controlled oscillator (VCO) with a nominal frequency equal to the received Omega signal (e.g., 10.2 kHz, 13.6 kHz) and a phase comparator that produces a control signal in proportion to the difference between the phase of the signal and the VCO reference signal phase. This control signal is used to adjust the oscillator such that there is a nearly constant (average) relationship (0° or 90°, depending on the type of phase detector) between the reference signal and the signal. Under this condition, the PLL is said to be locked to the Omega signal and it will continue to track the nominal signal phase as the craft moves. Further, between Omega signal transmissions the PLL oscillator will continue to provide a continuous indication of the phase.

The continuous output from the PLL is quite useful because the Omega signal is not continuous at each frequency. As is shown in Chapter 3, each Omega frequency is transmitted for only 0.9 to 1.2 sec with a 0.2 sec silent interval between each segment. Also, all eight stations transmit at a different frequency during each of the eight segments. This means that the same frequency is never simultaneously transmitted by two stations and the receiver never receives a given frequency from more than

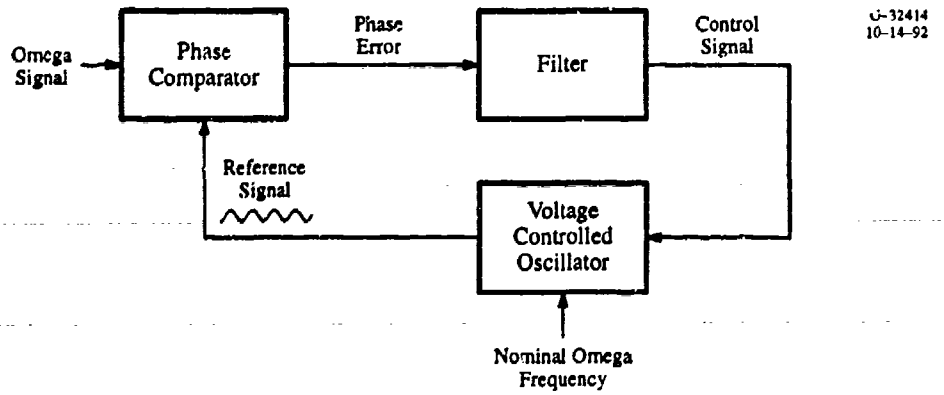

Figure 4.4-1 Typical Phase-Locked Loop (PLL)

one station at a time. The VCO used with the PLL is continuous and stable enough to maintain the frequency and phase over the 10-sec period of the Omega signal format. Visualize a receiver having a PLL for each frequency from each station. The outputs of these PLLs now provide continuous signals that are phase-synchronized to the received Omega signals every 10 sec using the approximately 1-sec frequency bursts transmitted by each station.

With relatively clean (phase-synchronized) continuous outputs from the PLLs, which are locked to the desired station signals, determination of the relative phase between these outputs is quite easy. A straightforward way to measure the relative phase in a digital computer is to simply use a counter to measure the time between zero-crossings for two signals and convert this count to the equivalent phase difference for hyperbolic. If a very stable oscillator or clock (e.g., cesium standard) is available to the receiver, then the phase comparison of the PLL outputs can be made relative to this reference to implement the rho-rho navigation mode.

4.4.2 Navigation Coordinates

Having acquired the desired phase measurements, it is necessary to convert them into an indication of position on the earth. Note that airborne applications are essentially the same as navigation on the surface of the earth, and no special consideration is given to the effect of altitude. This is because the nominal altitude is generally small relative to the radius of the earth. Also, Omega only supports two-dimensional position fixing since the signal propagation is confined to an essentially two-dimensional earth-ionosphere shell — altitude must be determined by other means. This contrasts with Navstar GPS (see Chapter 13), which provides a full three-dimensional fix capability.

The process of converting the phase measurements into position is actually a process of *coordinate conversion.* The Omega measurements and fixes are registered in station-centered circular (or hyperbolic) coordinates; the location of a craft on the earth is desired in the earth-fixed angular coordinates of latitude and longitude. Although this involves some geometry, the concepts are not difficult to understand. On the other hand, implementation of the "exact" equations to compute latitude and longitude in a computer is not straightforward since the equations do not lend themselves to a simple closed-form solution. Numerous computational techniques have been devised by receiver manufacturers to implement the position fixing and navigation solutions; most of the details of these solutions are closely held by this receiver manufacturers and are usually considered to be proprietary. The goal here is to generally understand the process, not to become an expert on the details of coordinate conversion. Therefore, we will focus is on fundamentals rather than on specific techniques and actual algorithms used in operational equipment.

Before getting into the mathematics and equations, it is necessary to have a clear picture of the navigation geometry. Thus far it is assumed that the earth is flat. A flat-earth assumption is acceptable over short distances (a couple of hundred miles) but not over the distances covered by Omega signals. The earth is generally represented by an ellipsoid of rotation around the earth's spin axis. A meridian section of the earth is illustrated in Fig. 4.4-2. This reference ellipsoid is a sphere that is flattened somewhat at the poles and bulges out at the equator. The radius of the earth at the equator is taken to be 3443.92 nm and the polar radius is about 11.5 nm less than the equatorial radius. This flattening (f) is generally expressed as the difference between the equatorial and polar radii divided by the equatorial radius, with a numerical value of 1/298.2. Although the flattening is relatively small (about 0.34% of the equatorial radius), accurate navigation calculations involving long distances (e.g., transmitter-to-receiver) on the surface of the earth make it necessary to account for the flattening effect.

The geoid is a mean sea-level approximation to the shape of the earth. However, the shape of the is not easily defined in a mathematical sense and is therefore not convenient for navigation calculations. For navigation with most radionavigation systems, position is reported with respect to the reference ellipsoid, which is an agreed-upon approximation to the geoid. Omega transmitting station coordinates are given in the World Geodetic System World Geodetic System 1984 (WGS-84). Note, however, that WGS-84 is not the only datum used for navigation, charts, and maps. Other commonly used datums include WGS-72 and the North American Datum 1927 (NAD-27). The relative offset (or error) between these systems is on the order of 10 to 20 m. This error is small compared to the advertised Omega accuracy of 2 to 4 nm.. The

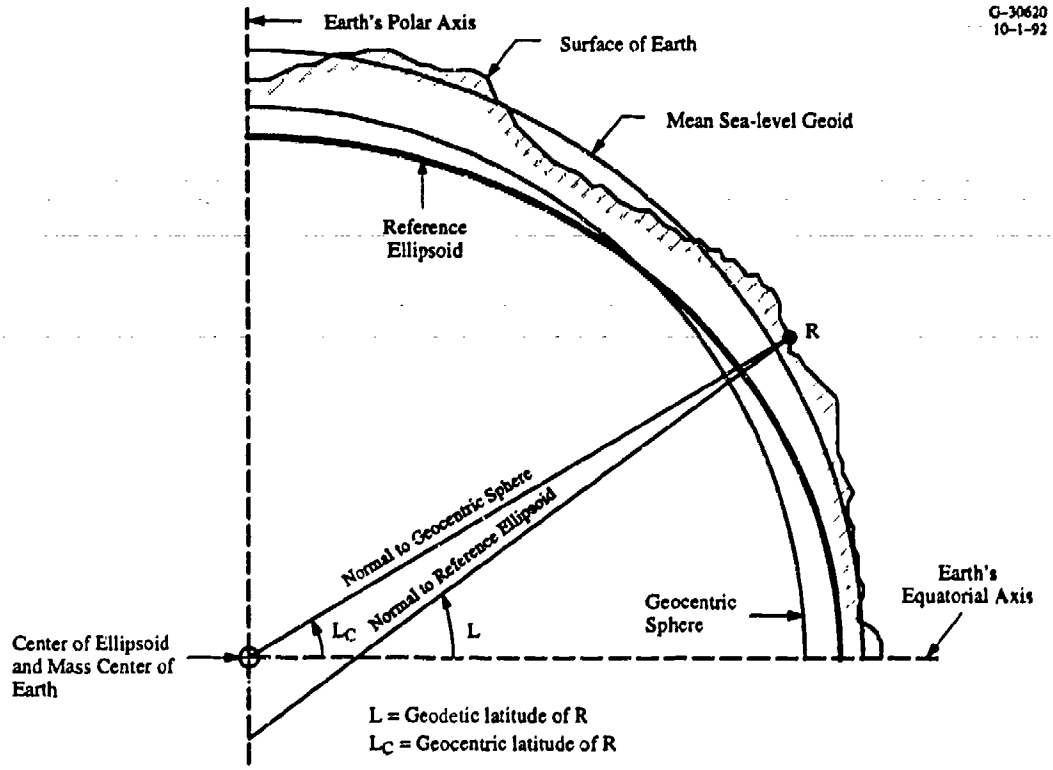

Figure 4.4-2 Meridian Section of Earth Showing the Reference Ellipsoid

geodetic spherical coordinates are the spherical coordinates of the normal to the reference ellipsoid. Geodetic coordinates are commonly used on maps and in the mechanization of dead reckoning system. Additional details on navigation coordinate systems are contained in Ref. 1.

The basic coordinate frame for earth navigation Longitude is shown in Fig. 4.4-3. A point on the earth is generally represented in *geodetic spherical coordinates,* Longitude which are the spherical coordinates of the normal (vector) to the reference ellipsoid. Longitude (Δ) is an angle measured from the Greenwich Meridian and is positive in the easterly direction; L is the latitude angle of the normal to the reference ellipsoid measured from the plane of the equator and is positive in the northerly direction. When traveling due north from the equator to the North Pole at a fixed longitude, latitude increases from 0° to 90°; in the southern hemisphere the sign changes and the south pole has a latitude of –90°. Moving in the easterly direction causes longitude to increase from 0° at the Greenwich Meridian to a full 360° as you travel around the earth and back to the starting point. Generally, East Longitude is defined from 0 to 180° and West Longitude is generally represented as a negative number from 0 to –180° (of course, 180° and –180° are exactly the same meridian).

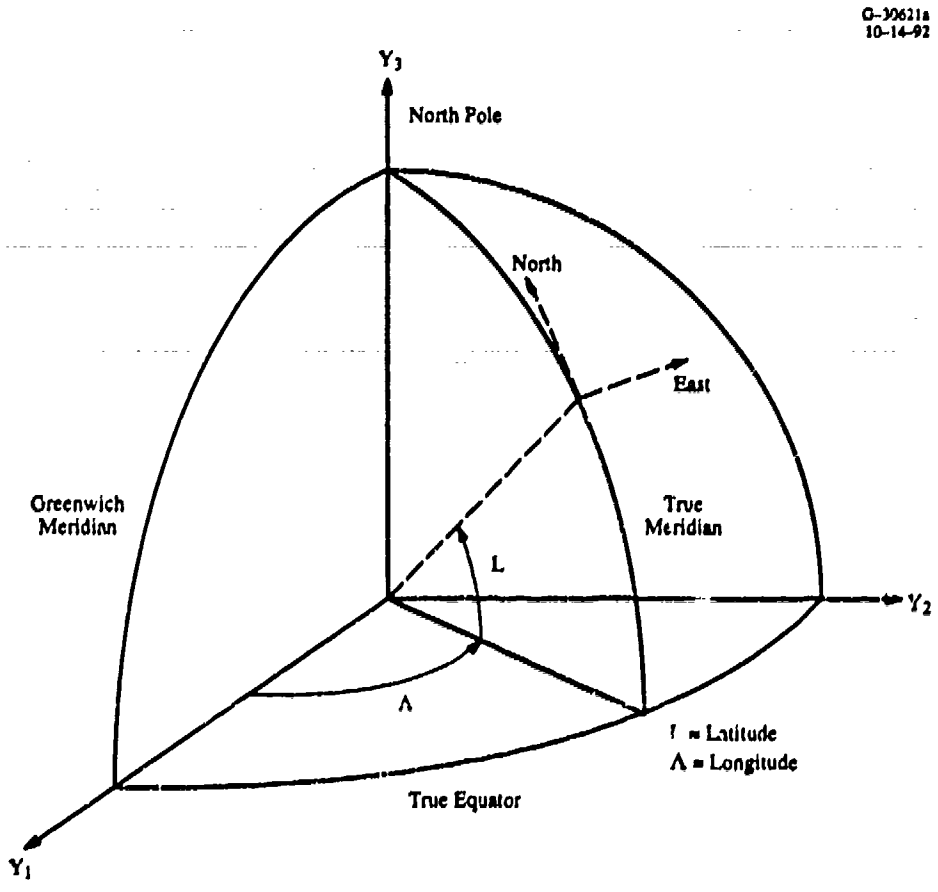

Figure 4.4-3 Navigation Coordinate Frame (Ref. 1)

4.4.3 Range Determination

Geodetic distance, d, between two points on the spherical earth can be computed with an accuracy of about 10 m or better, using the Andoyer-Lambert formula given in Table 4.4-1. The latitude and longitude of each Omega transmitting antenna is known from surveys. Given the range measurements (or range-difference measurements) inferred from Omega phase measurements, the problem at hand is to find a way to solve for the latitude and longitude of the receiving antenna using the relationship between range and position given by the nonlinear equation (Table 4.4-1) for distance, d. As can be seen, this is a coordinate conversion problem because we must convert the indicated position in range measurement coordinates into the latitude/longitude geodetic earth coordinates. Solving directly for L and Λ in terms of d is not a viable approach. Therefore, we need to explore other ways of computing position on the earth given multiple measurements of d from multiple known sites (transmitters).

Table 4.4-1 Andoyer-Lambert Formula

The geodetic distance, d, according to Andoyer-Lambert can be calculated with an accuracy of approximately 10 m using the following equations:

$$d = d_i + \varepsilon_i (rad)$$

where

$$\cos d_i = [\sin(L_r)\sin(L_t) + \cos(L_r)\cos(L_t)\cos(\Lambda_r - \Lambda_t)]$$

L_r = reduced latitude of receiver

L_t = reduced latitude of transmitter

Λ_r = longitude of receiver

Λ_t = longitude of transmitter

Reduced latitude $= \tan^{-1}[(1 - f)\tan L]$

L = geodetic latitude of receiver or transmitter

$$\varepsilon_i = \frac{f}{4}\left\{\frac{[\sin(d_i) - d_i][\sin(L_t) + \sin(L_r)]^2}{1 + \cos(d_i)} - \frac{[\sin(d_i) + d_i][\sin(L_t) - \sin(L_r)]^2}{1 - \cos(d_i)}\right\}$$

f = 1/298.2

One way to solve for geodetic position would be to start with an initial "best guess" of craft latitude and longitude, enter this best guess into the equation for d in Table 4.4-1 to calculate the associated range to each transmitter, and compare these calculated ranges with the Omega-based range measurements. If the guess is correct, the measured and computed ranges will be equal. If the guess is not correct, a new guess can be used with the goal of converging on the *indicated position* of the Omega receiver antenna. It is obvious that this process is quite tedious; even with a computer, it is not obvious how to pick the latitude and longitude values which will converge to the observed set of range measurements. Simply trying random numbers has no guarantee of convergence! Clearly, this is not a very practical approach and a better algorithm is required which can be implemented in a computer. Note that the result is referred to as the indicated position and not the true position. There are always errors associated with the measurements and the processing; *the indicated position is defined as the true position plus the error.* If there are no errors, then the indicated position is equal to the true position.

4.4.4 Linearizing the Process

The position determination process can be simplified and will lend itself to automation in a computer if we can find a *linear relationship*, or approximation, between the measured range and the position

(latitude and longitude) of the craft. A first-order series expansion of the range equation will provide a linear relationship between a small change (designated by Δ) in position and the associated change in the range to the transmitter. The desired linearized relationships between Δd, ΔL, and $\Delta \Lambda$ at a tangent point on the earth (L_r, Λ_r) are obtained by taking the partial derivative of d_i^* (Table 4.4-1) with respect to L_r and to Λ_r:

$$\frac{\partial d_i}{\partial L_r} = \frac{-\cos(L_r)\sin(L_t) + \sin(L_r)\cos(L_t)\cos(\Lambda_r - \Lambda_t)}{\sin(d_i)} \tag{4.4-1}$$

$$\frac{\partial d_i}{\partial \Lambda_r} = \frac{\cos(L_r)\cos(L_t)\sin(\Lambda_r - \Lambda_t)}{\sin(d_i)} \tag{4.4-2}$$

The partial derivatives given by Eqs. 4.4-1 and 4.4-2 are relatively simple linear relationships that can be evaluated numerically by substituting the latitude and longitude of the tangent point and the known transmitting station coordinates. These partials are generally quite accurate within about 200 nm of the tangent point. Therefore it is not necessary to know the exact position of the craft to compute the partials.

The location of the approximate latitude and longitude of the craft, if known (possibly the last computed position or a known reference), can be used for the tangent point. The measured range, as previously noted, can be derived from the cumulative phase by dividing by the familiar wave number, k. (Notice that k will have a numerical value that depends on the frequency and the desired units of range and phase.) Now d_i and the partial derivatives can be evaluated for transmitter i. The computed range (d_i) can be differenced with the measured range from transmitter i=1 to form Δd_1:

$$\Delta d_1 = \phi_1/k - d_1 \tag{4.4-3}$$

The offset in the current position of the craft (indicated by the range measurement) relative to the assumed tangent point is:

$$\Delta L_1 = \Delta d_1 / \frac{\partial d_1}{\partial L_r}$$

$$\Delta \Lambda_1 = \Delta d_1 / \frac{\partial d_1}{\partial \Lambda_r} \tag{4.4-4}$$

The corrected, or updated, craft latitude and longitude provided by the range measurement from transmitter i=1 is obtained by adding ΔL_1 and $\Delta \Lambda_1$ to L_r and Λ_r, respectively.

*Note that for purpose of linearization, the error associated with ignoring e_i in the partial derivative is negligible.

Although linearization provides a convenient and computationally attractive way to relate craft position to the measured range, recall that a single measurement of range only defines one of the desired LOPs. As shown in Section 4.2, range measurements from multiple transmitters must be processed to unambiguously determine the location of the craft. The objective is to solve for a single latitude and longitude that represents the best estimate of the true position (intersection of the LOPs) given the available measurements. Processing a second range measurement to determine a second LOP offset (Δd_2) will yield a second set of latitude and longitude offsets which may or may not match the position offsets given by Eq. 4.3-3 due to measurement errors and the linearization errors associated with the partial deviatives. Now it is necessary to combine the two sets of numbers to identify the best estimate of current craft position based on the available range measurements. In addition to accounting for the geometry of each measurement, it is also desirable to be able to account for phase measurement errors due to noise and unmodeled propagation effects, i.e., errors in the PPCs. Clearly, we need a computational algorithm to satisfy these requirements. The next section introduces the least-squares algorithm, which is the most commonly used solution to this problem. The least-squares algorithm is then applied in Section 4.4.6.

4.4.5 Least-Squares Algorithm Definition

Here is where the process of *position estimation is introduced.* Most modern receivers use a least-squares algorithm or a Kalman filter to estimate position. We will not present the details of deriving these algorithms here since the development and application of these algorithms is treated in Ref. 2 and Appendix D. Although the mathematics may appear formidable at first encounter, the concepts are really quite simple. A nice feature of these algorithms is their vector-matrix structure that allows any number of independent measurements to be included in the navigation solution. It is quite easy to incorporate phase measurements derived from more than one frequency from any or all of the transmitters. It is also rather straightforward to include measurements (i.e., the change in phase from a reference position) from the Navy VLF communications system to supplement Omega in areas of poor signal coverage. The least-squares algorithm involves using a set (or vector, Ref. 2) of measurements, z, which are linearly related to the unknown quantities (state vector, Ref. 2), x, by the expression

$$z = Hx + v \tag{4.4-5}$$

where H is the measurement matrix and v is a vector of additive measurement noise — this is the general formulation of the relationship between the measurement and the state vector. The goal is to compute an estimate of the vector of unknown quantities, denoted by $\hat{x}$, that minimizes the sum of the squares of the elements of the measurement error, i.e., the cost function

$$J = v^T v = (z - Hx)^T (z - Hx)$$

where the superscript T denotes the matrix transpose. The least-squares estimate is obtained (from Ref. 2) as

$$\hat{x} = (H^T H)^{-1} H^T z \tag{4.4-6}$$

where –1 denotes the matrix inverse. Note that the least-squares estimate of x is simply a linear scaling of the measurement vector, z.

Alternatively, a weighted least-squares estimate can be employed that allows non-uniform weighting of the measurements (e.g., in accord with the associated phase measurement noise) by minimizing the weighted cost function

$$J = (z - Hx)^T W (z - Hx)$$

to obtain the least-squares estimate

$$\hat{x} = (H^T W H)^{-1} H^T W z \tag{4.4-7}$$

Note that the weighted least-squares algorithm reduces to the least-squares algorithm when the weighting matrix, W, is the identity matrix (unity diagonal elements, zero off-diagonal elements).

The ability to weight the measurements from multiple stations allows the algorithm to place a lower dependence on questionable or noisy phase measurements; this de-emphasizes the contribution of the erroneous phase measurements to the position fix. Further, the weighting matrix can be used to account for noise that may be common (correlated) between two or more phase measurements. For example, if phase differences are used, there is a common element of phase measurement noise associated with the common phase measurement in each of the phase differences. Measurement noise weighting can be implemented by defining W to be the inverse of the phase measurement noise covariance matrix (R) defined as

$$R = E\left(vv^T\right)$$

where E() denotes expectation. If the measurement vector noise elements are independent, then the diagonal elements of R are simply the variance of the noise associated with each measurement and the off-diagonal terms of R are zero.

If desired, a relative indication of the measurement noise statistics (variance) can be obtained from the PLL (Section 4.3.1) and used to automatically weight the phase measurement. Note that the phase measurement noise level is not the same as the atmospheric noise at the antenna. Phase measurement noise is the residual phase jitter in the processed output of the PLL and tends to vary as a function of the inverse of the signal-to-noise ratio. Note that it is not required to use the inverse of R for W. It is possible to use W to weight measurements for other reasons, such as a signal that is suspected of being, or becoming, modal (see Chapter 5).

It may not be obvious, but we have identified the necessary pieces of the puzzle. It is simply a matter of defining the vector quantities and the elements of the least-squares algorithm matrices in terms of the previously defined scalar equations. Numerous techniques have been developed (Ref. 2) for implementing the least-squares algorithm in software, and they will not be addressed here. It is more important to understand how to define the elements of the matrices and to understand the relationship between the mathematics and the graphical interpretation of the fix process.

4.4.6 Least-Squares Fix Algorithm Implementation

Let us first look at the general direct ranging scheme where it is assumed that multiple range measurements are available from two or more transmitting stations. To implement this direct ranging scheme, the phase measurements are made relative to a common oscillator or local clock. This is generally a crystal oscillator, which does not have the long-term stability of the cesium (or rubidium) clock used in the rho-rho mode of operation. Although the crystal oscillator exhibits a phase drift (due to a frequency offset relative to the signal frequency), which is much larger than a cesium standard, the drift rate (frequency offset) is relatively constant over the Omega measurement period. This being the case, the navigation algorithm can be formulated to account for this clock drift and actually produce an estimate of the clock frequency error. This estimate is then used to correct the common clock error in each of the phase measurements.

For navigation with Omega, the three unknown quantities of interest are clock frequency error, latitude offset, and longitude offset. The position offset to be determined is the difference between the previous position and the new (i.e., current) position. It is assumed that the correct lane count is known and other techniques have been used to synchronize the measurements. Therefore, the least-squares solution is to be used to determine the change in position associated with the change in the measured phase as formatted in Section 4.4.4. A minimum of three range measurements are required to estimate

the three unknown quantities. In the case of rho-rho navigation with a cesium clock, clock drift is assumed to be negligible; it is not included as a state and is not estimated by the algorithm. Therefore, only two range measurements are required.

First, let us define the measurement vector, z, which is needed to compute a navigation offset in terms of the available range (derived from phase) measurements. Three measurements are assumed but the dimensionality can be easily increased to accommodate additional measurements:

$$z = \begin{bmatrix} \Delta d_1 \\ \Delta d_2 \\ \Delta d_3 \end{bmatrix} \tag{4.4-8}$$

where Δd_i is the measured offset, or change, in the range associated with transmitter i (cf. Eq. 4.4-3).

The frequency offset, $\Delta\omega_c$, of the clock is assumed to be constant (bias) between Omega measurements that occur every τ sec. Notice that if $\Delta\omega_c$ is known, it can be multiplied by τ to determine the phase error associated with this constant frequency offset during the time period τ. For the moment, assume that there is no bias phase error associated with the measurements and the measurement noise, v, is negligible.

The goal is to define a state vector, x, with states that can be related to the measurements and can be estimated with the least-squares algorithm to update the indicated location of the receiver:

$$x = \begin{bmatrix} \Delta L \\ \Delta \Lambda \\ \Delta\omega_c \end{bmatrix} \tag{4.4-9}$$

Estimates of the two position states (ΔL, $\Delta \Lambda$) will provide the desired corrections to be applied to the tangent position (L_r and Λ_r). An estimate of the reference frequency offset ($\Delta\omega_c$) can be used to correct for the associated clock-induced phase error in the measurements. The H-matrix is simply the partial derivatives (partials) of each of the station range (phase) measurements to be included in the navigation solution. These partial derivatives are obtained by evaluating Eqs. 4.3-1 and 4.3-2, using the known locations of the transmitting stations and the assumed location of the receiver, L_r and Λ_r.

Using the notation that the subscript "i" identifies t.. ..s associated with station i, the corresponding H for three stations is

$$H = \begin{bmatrix} \frac{\partial d_1}{\partial L_r} & \frac{\partial d_1}{\partial \Lambda_r} & \tau_1 \\ \frac{\partial d_2}{\partial L_r} & \frac{\partial d_2}{\partial \Lambda_r} & \tau_2 \\ \frac{\partial d_3}{\partial L_r} & \frac{\partial d_3}{\partial \Lambda_r} & \tau_3 \end{bmatrix} \tag{4.4-10}$$

Note that the known time between measurements (τ_i) for each measurement is included in the third column of H. Equations 4.4-8 and 4.4-10 can now be used in Eq. 4.4-6 (or Eq. 4.4-7) to estimate the state vector. Notice that this is the "best estimate" of the position offset and the clock frequency offset, given the available measurements. These estimates can be used to correct the indicated position in an iterative scheme, as shown in Section 4.4.7.

Implementation of the hyperbolic mode solution is also quite easy with the least-squares algorithm. Because the clock error can be ignored, (cf. Section 4.2.4) the state vector becomes

$$x = \begin{bmatrix} \Delta L \\ \Delta \Lambda \end{bmatrix} \tag{4.4-11}$$

and the measurement vector can be formulated as follows:

$$z = \begin{bmatrix} \Delta d_1 - \Delta d_2 \\ \Delta d_1 - \Delta d_3 \end{bmatrix} \tag{4.4-12}$$

It is quite easy to see that H becomes

$$H = \begin{bmatrix} \left(\frac{\partial d_1}{\partial L_r} - \frac{\partial d_2}{\partial L_r}\right) & \left(\frac{\partial d_1}{\partial \Lambda_r} - \frac{\partial d_2}{\partial \Lambda_r}\right) \\ \left(\frac{\partial d_1}{\partial L_r} - \frac{\partial d_3}{\partial L_r}\right) & \left(\frac{\partial d_1}{\partial \Lambda_r} - \frac{\partial d_3}{\partial \Lambda_r}\right) \end{bmatrix} \tag{4.4-13}$$

Note that although Station 1 is used as the common station, exactly the same result will be obtained if either of the other two stations is selected as the common station.

It is quite easy to see how any number of independent measurements can be included in the fix calculation by simply increasing the dimension (number of rows) of the measurement vector (and H). It is important that the measurements are independent or the required matrix inverse operation in the least-squares algorithm will be ill-conditioned and it will not be possible to obtain a solution. For example, simply entering the same measurement (from a single transmitting station at a single time) in each of the two or three measurement vector elements will not work. Also, the matrix inverse becomes ill-conditioned in cases with poor fix geometry, corresponding to a large GDOP (cf. Section 4.2.3), which is related to the lack of observability associated with the geometry.

The same geometry conditions that lead to LOP crossing angles near zero degrees also cause problems with the matrix inverse operation. For example, if two transmitting stations lie on the same great-circle path to the receiver, the geometry associated with these two measurements is not independent. In fact, as previously noted, this is the baseline or baseline extension of the two stations and it is not possible to compute rho-rho position fix. This follows from the matrix inverse definition:

$$A^{-1} = (\text{adj}A)/|A|$$

where $|A|$ is the determinant of the square matrix A, and adj$A$ is the adjoint (Ref. 2) of A. If $|A|$ equals zero, then the inverse of A does not exist. This means that no row or column of A can be a linear combination of the other rows or columns. Therefore, it is only necessary to examine the determinant of $H^{T}H$, which is the quantity that must be inverted in the least-squares algorithm, to determine if there is sufficient observability in the measurements to compute a position fix. Calculation of the inverse with a computer becomes ill conditioned as the determinant approaches zero.

4.4.7 Implementation

It is instructive at this point to integrate all of the individual pieces of the position determination process into a basic representative computer-based implementation. Again it must be recognized that each equipment manufacturer has its own proprietary approach to position determination and navigation with Omega. Special features of specific equipment such as waypoint navigation, external aiding, use of VLF signals, integration with other sensors, etc., all serve to dictate specific and possibly unique realizations of the position determination process. Also, it is beyond the scope of the text to address many practical issues and considerations associated with an operational implementation of the navigation algorithms. The following discussion is directed at tying together the fundamentals presented thus far in this chapter to summarize and illustrate the overall position determination process in the form of a representative implementation.

A generic implementation diagram for position determination with Omega is presented in Fig. 4.4-4. *This diagram supports the discussion in the following paragraphs.* All processing in the diagram proceeds from left to right and then loops back in an iterative manner. This means that determination of the new, or current, position uses variables (e.g., $\phi_{PPC}, H, \hat{\phi}_p, \Delta\hat{\phi}_f$) that are based on the previous known or computed craft position. Each of the inputs and variables are related to the important issues and considerations presented in this chapter.

The input on the left of the diagram (ϕ) is a vector of phase measurements from the receiver phase tracking and filtering function (e.g., as discussed in Section 4.4.1) The vector could contain any number of independent measurements, or could even contain phase difference measurements if they are appropriately handled by H. Note that ϕ is the phase within the current lane, not the cumulative phase.

The phase bias correction input (ϕ_b) is not necessary in all cases but is included to support the generic configuration. For example, if an external cesium reference is employed to implement range-range navigation, this bias correction could be used to correct for the phase offset between the cesium reference and the phase of the signals at the transmitting stations. Because even a cesium reference has unacceptably large phase drift over long missions, range-range navigation requires some type of periodic synchronization to estimate this phase offset (ϕ_b), generally not at the station but at some known geodetic

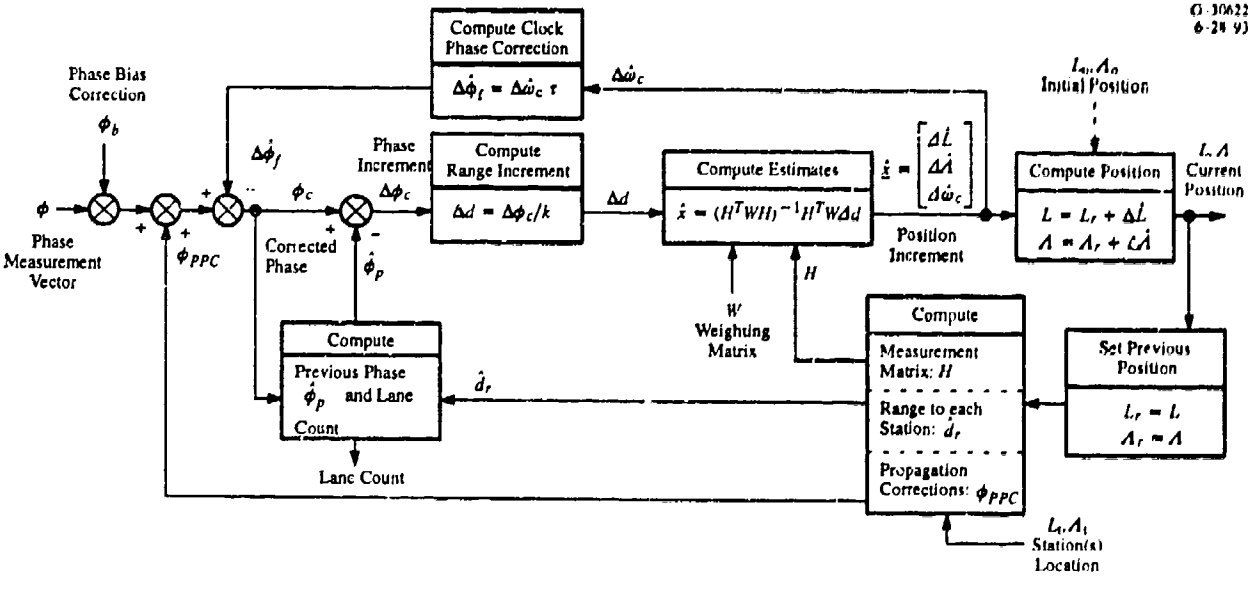

Figure 4.4-4 Position Determination Using Omega Phase

reference point or by using another position determination system. The accuracy of the phase bias estimate depends on the accuracy of the PPCs at the reference point; it should be obvious that the associated estimation errors will impact subsequent positioning accuracy.

The next step is to correct each element of the phase measurement vector with the appropriate PPC (Section 4.3.2), denoted as ϕ_{PPC} in Fig. 4.4-4. There appears to be a conflict here in that it is necessary to know the craft position in order to determine the PPC. This is true, but in practice it is only necessary to know the *approximate location* of the receiver to determine a sufficiently accurate PPC value. Therefore, the PPC is determined (using an algorithm or table look-up) from the best estimate of position, usually the most recent update of the navigation solution, which is identified in Fig. 4.4-4 as the Previous Position (L_r, Λ_r).

The measurement vector must be corrected for the frequency offset in the local oscillator of the receiver. This can be accomplished by taking the available frequency offset estimate provided by the least-squares fix algorithm and multiplying this frequency offset estimate by the time, τ, since the measurement was last processed. The clock phase correction, $\Delta\hat{\phi}_f$, is applied to the measurement vector; note that the clock frequency error is common to all elements of the measurement vector. Also, τ is shown as a vector so that the appropriate value can be is assigned to each element of the measurement vector. The result is a corrected phase measurement vector, ϕ_c, which corresponds to the "nominal phase" within a lane, as discussed in Sections 4.3.1 and 4.3.3.

Most Omega equipment processes the change in phase from an assumed or known previous location to determine the current position. Given the previous position (L_r, Λ_r) and the known locations of the stations (L_i, Λ_i), an estimate of the (previous) phase can be computed using the Andoyer-Lambert formula in Table 4.4-1. Differencing the corrected phase measurement ϕ_c with the estimate $\hat{\phi}_p$ provides an indication of the change in phase $\Delta\phi_c$ since the last measurement was processed. If this change in phase is relatively small, then the subsequent linearized processing of this change in phase by the least-squares algorithm to estimate the change in position ($\Delta\hat{L}, \Delta\hat{\Lambda}$) is generally quite accurate. This means that if L_r and Λ_r (the "set Previous Position" block in Fig. 4.4-4) are set equal to L and Λ, respectively, and a new value for $\hat{\phi}_p$ is computed, the resulting value of $\Delta\phi_c$ will be almost zero. In other words, $\hat{\phi}_p$ will be nearly equal to the corrected measurement, ϕ_c. Notice that this is an iterative scheme and additional iterations can be employed if $\Delta\phi_c$ is large and the linear assumptions do not hold. There are numerous ways to actually implement the equations in a computer to achieve computational efficiency.

The previous phase, $\hat{\phi}_p$, is computed in a block that is also assumed to keep track of the lane count. Again, there are a number of realizations of this process (see Section 4.3.3), the details of which are beyond the scope of this document. It is sufficient to note that ϕ_c can be used to keep track of the lane count, and/or the computed range based on the most recent position information can be used. When all else fails, the frequency differencing scheme discussed in Section 4.3.3 can be employed to determine the lane count.

The change in phase, $\Delta\phi_c$, is converted into a vector of incremental changes in range, Δd, by simply dividing by the wave number, k (cf. Eq. 4.3-3), which is then processed with a weighted least-squares algorithm (cf. Sections 4.4.5 and 4.4.6) to determine the corresponding change in latitude and longitude (position increment), along with updating the estimate of the frequency offset. The previous indication of position is updated (or corrected) with the position increments to produce an estimate of the current position. The previous position is then set equal to the current position and the indicated computations are performed to ready the iterative process for the next phase measurement. As previously mentioned, additional loops through the calculations can be made with the same phase measurement if convergence (i.e., $\Delta\phi \approx 0$) is not achieved in one pass. Note also that like the determination of ϕ_{PPC}, computation of the measurement matrix, H, uses the so-called previous position. Again, if the current and previous positions are close, the computational errors due to algorithm linearization are negligibly small and a single pass through the position calculations is sufficient.

Notice that if the craft position is known at some initial time or even at some time during the mission, this position (L_0,Λ_0) can be entered as the current vessel position (L,Λ) and used to determine the corresponding value of $\hat{\phi}_p$. The resulting value of $\Delta\phi_c$ now represents the phase offset between the measurement and the reference position. Conceptually, if this offset is excessively large, it could be subtracted from the bias correction (ϕ_b) to drive $\Delta\phi_c$ to zero. This corrected value of ϕ_b can now be used to correct subsequent phase measurements. In any event, the goal of the entire iterative process illustrated in Fig. 4.3-3 is to drive $\Delta\phi_c$ to zero. Under this condition, the current position yields a predicted (previous) phase that is equal to the corrected phase measurement. Again it must be recognized that this example is only one of many ways that a practical navigation algorithm for Omega may be implemented in a computer. It is, however, a viable mechanization and serves to illustrate the computational process.

4.5 HYBRID METHODS

The airborne digital computer has made multisensor navigation system integration commonplace. System integration is motivated by the fact that all navigation sensors and systems have inherent performance and/or operational limitations. Therefore, the goal of system integration is to exploit the synergy of various navigation systems and sensors to maximize overall navigation performance and to overcome the inherent operational limitations of individual systems.

As a *stand-alone navigation system,* Omega provides an advertised worldwide navigation capability, 24 hours a day with an availability in excess of 95% for most users. Using the best available PPCs, accuracy is on the order of 2 to 4 nm with a 95% probability. This level of system performance is sufficient to support a number of users, however, there are users and missions with navigation requirements which cannot be supported by Omega as a stand-alone system. The limiting factor may be operational requirements, accuracy, or both. In some cases Omega is used to aid another system and in other cases Omega is aided by another system or sensor. It is worthwhile to look at some typical system integration efforts involving Omega since they are an important part of achieving an overall appreciation for the use of Omega in modern navigation applications.

4.5.1 Omega Integration with Inertial Navigation

One of the earlier integrated applications of Omega was to aid an inertial navigation system (INS). Inertial navigation systems use inertial sensors (accelerometers and gyros) to sense the motion of a craft and to determine position. An INS is a rather sophisticated realization of a dead-reckoning system and has the desirable attribute of autonomous operation — in other words, it does not require external measurement information like signals from a transmitter. The INS has the desirable characteristic of providing continuous indications of craft position, velocity and attitude. Unfortunately, the INS also has the undesirable characteristic of unbounded growth in the navigation errors as a function of time. This means that after some period of time, the navigation error will become excessively large and the INS outputs are no longer suitable for navigation of the craft. A typical airborne INS has a position error growth rate of 0.5 to 1 nm/hr. Therefore, depending on the duration and accuracy requirements of the mission, it may be necessary to estimate and correct the INS error during the mission.

For applications aboard submarines or on certain aircraft, the self-contained capability of the INS is ideal; however, periodic navigation fixes from an external source are required to reset, or correct, the errors in the INS. This has been accomplished on both aircraft and submarines using Omega as the external position fix source. One significant attribute of Omega use on a submarine is that a hyperbolic

fix can be computed with a submerged antenna. This means that the submarine does not need to surface and give away its position to a potentially hostile observer. Further, the worldwide coverage of Omega means that submarine operating regions are not dictated by the availability of the external fix. The reasons for using Omega to aid airborne INS applications are quite similar. Certain military aircraft have a requirement to operate in any region of the world at any time of the day. It would not be prudent to depend strictly on Omega because there are regions and times at which modal interference or other propagation limitations make Omega signals unusable (see Chapters 5 and 6). Also, there is always a possibility that an Omega station will not be available due to equipment failure or even due to potential political and military hostilities. Therefore, continuous navigation information is obtained from the INS and periodic aiding of the INS is provided by Omega.

The heart of most modern multisensor navigation systems is the Kalman filter (see Appendix D). The Kalman filter can be considered to be a generalization of the least-squares algorithm presented in the previous section — under the appropriate assumptions and constraints, the Kalman filter reduces to a least-squares algorithm. The Kalman filter includes dynamic models of the errors associated with the navigation system(s) and sensors. Estimates of these errors and the associated navigation errors are obtained by processing the outputs of the navigation systems. These error estimates are then used to correct the indicated output of the navigation system. A representative block diagram for the integration of Omega with an INS is illustrated in Fig. 4.5-1. In this implementation, Omega is the external position fix source which is periodically used as a reference to correct the INS. Notice that the position outputs of both systems are differenced to form the input to the Kalman filter. This difference, or divergence, between the two outputs contains only errors associated with the two navigation systems. This is because the indicated position, and the associated rapidly changing dynamics, is common to both systems and cancels in the divergence. This simple difference operation is important because it provides the

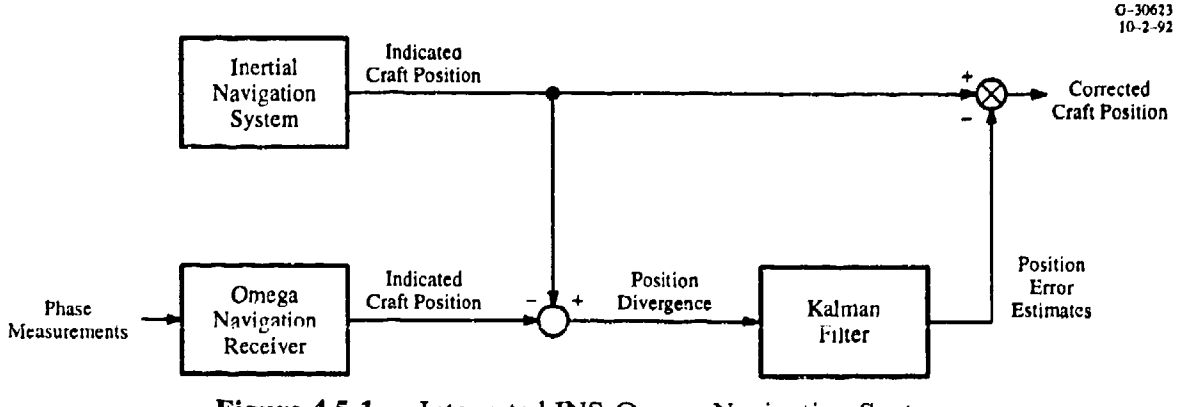

Figure 4.5-1 Integrated INS-Omega Navigation System

desired observability of the errors which typically have much slower (lower frequency) dynamics than the craft position information. The Kalman filter can process multiple measurements to realize the advantages of measurement averaging without incurring dynamic errors associated with the changing position of the craft.

Although this example uses an INS as the primary navigation system, this common architecture is used in many hybrid navigation systems. Estimates of position error are obtained and used to correct the indicated position output of the primary navigation system. In some implementations, Kalman filter estimates of component errors are used to correct errors within the navigation system. For example, estimates of INS gyro errors are often used to correct the gyro errors in the INS computer. Another possibility is to estimate Omega phase or clock errors and feed these estimates back to the Omega navigation receiver. The Kalman filter can also be used to initialize the Omega receiver and to support laning. These are all very specialized applications and the details will not be addressed here.

Notice that any number of independent navigation systems can be included in the architecture illustrated in Fig. 4.5-1. For example, Loran-C and NAVSAT could be included in this architecture by forming the associated divergences with the INS output and entering these additional divergences as inputs to the Kalman filter. Additional error states may be required in the filter, but the resulting estimates of position error will now be the optimal combination of information from all of the available indicators of position. The Kalman filter automatically exploits the synergy associated with multiple systems to provide the best single indication of position error; this is because the Kalman filter contains dynamic models of the error characteristics associated with each system. Also, if one of the systems is not available due to a failure or any other reason, the integrated system will still provide an indication of craft position based on the remaining available systems, although it will be somewhat degraded in accuracy.

4.5.2 Differential Omega

Another hybrid system is Differential Omega. In this configuration, an Omega reference receiver is located at a surveyed location. Because the geodetic location of the receiver is known, any difference between the position indicated by Omega and the known survey position is an error in the Omega-indicated position. Omega errors are both temporal and spatial in character. Temporal errors have a correlation time which is on the order of 15 to 30 min and spatial errors have a typical correlation distance on the order of 250 to 500 nm. This means that any receiver operating in the vicinity (less than the correlation distance) of the reference station will tend to see the same spatial errors as seen by the reference. The

correlation time provides an indication of the time period over which the error will not change significantly and the correction is expected to be valid. This dictates the minimum update rate of the differential corrections.

The differential system broadcasts the errors seen at the reference location over a communications link. These errors are received and used to correct the indicated position of the roving receiver. Although the corrections could be applied to the indicated position, the preferred approach is to correct the errors at the phase level before the position fix is formed. This is because the position fix error depends on the specific stations used to compute the fix and the associated implementation of the fix algorithm. Therefore, if the phase errors associated with each signal are determined and broadcast, each user can take maximum advantage of the corrected phase to determine position. Referring back to Fig. 4.4-4, the differential corrections can be entered as the Phase Bias Correction vector, ϕ_b.

Operational Differential Omega systems currently in place (1993) are tailored primarily to marine users, although a number of experimental systems have been tested. The correction information is normally broadcast using a 20 Hz modulation of low-frequency (285 to 415 kHz) radio beacon signals. Measured position accuracies vary from about 0.3 nm at about 100 nm from the reference station to about 1 nm at 500 nm from the reference station, 95% of the time (Ref. 3). As of 1990, 30 differential systems were operational throughout the world, including the Atlantic coasts of Europe and Africa, the Mediterranean Sea, the Caribbean, eastern Canada, India, and Indonesia (Ref. 4).

4.5.3 NAVSAT-Omega Integration

Omega has been integrated with NAVSAT (TRANSIT satellites). This was one of the earlier integrations of Omega (Ref. 5) with another radionavigation system. NAVSAT is a satellite-based navigation system with a positioning accuracy on the order of a fraction of a mile, as compared to the 2 to 4 nm accuracy of Omega.

Because of the polar orbits of the satellites, a fix is typically available only every 2 to 5 hr. Here is an example of a system with much higher accuracy than Omega but which may not support certain operational requirements because of the rather long interval between fixes. Therefore, NAVSAT can be used to periodically estimate the error in Omega and the corrected Omega can be used between NAVSAT fixes to provide improved navigation accuracy.

If the system is being used on a slowly moving ship, the Omega errors will not build up too rapidly and there will be a net improvement in position accuracy over the duration of the mission. In effect, NAVSAT permits the observation and correction of the Omega propagation errors at each NAVSAT fix. Because of the temporal and spatial correlation associated with Omega errors, the corrections are valid as simple bias corrections between NAVSAT fixes. This integration can be accomplished quite easily with a Kalman filter.

It should be obvious at this point that there are numerous advantages in performance and operational capability afforded by system integration to form a hybrid navigation system. The integrated performance has the potential to be better than any of the systems operating in a stand-alone operational mode. In practice, however, the accuracy of most integrated systems tends to be dictated by the highest accuracy source of position information. In many cases the operational advantages tend to outweigh the accuracy gains. The computational capability, high speed and relatively low cost of modern digital computers make such systems both practical and affordable.

Entire books are written on the subject of integration and hybrid systems. The objective here has been to simply present the basic fundamentals of practical integration techniques and to provide some operational system examples.

4.6 POSITION ACCURACY

Specifying the position determination accuracy obtained from the use of Omega signals is quite complex for a variety of reasons. First, it must be kept in mind that Omega is a worldwide navigation system so that accuracy depends on the region of operation and the associated geometry to the stations, time of day, available stations/signals, navigation equipment, external aiding (if used), integration with other equipment, and operational procedures. Position error data at fixed sites has been collected and analyzed (Ref. 6), but it is difficult to translate this information to specific navigation errors, where the space and time dependence of position errors are mixed and operational procedures are highly variable.

Omega position error can be traced to a variety of sources, including station synchronization offset, receiver dysfunction (e.g., lane slip/jump), operator mistakes (e.g., initialization coordinate insertion error), and temporal anomalies (e.g., a PCD). The predominant error source, however, is the propagation correction (or PPC). Recall that the PPC is a predicted quantity obtained from tables or algorithms, and is applied to the measured phase to transform from the highly complex, "real-world" phase variation to the "nominal phase" which varies linearly with distance.

The PPCs are obtained from a semi-empirical model/algorithm (see Chapter 9) of Omega signal phase behavior which is calibrated largely from phase measurements at globally distributed fixed Omega monitor sites. Analysis of these measurements can thus reveal important features of Omega phase behavior as well as provide insights into PPC error. A basic property indicated by these measurements is that, at a fixed location, Omega phase (and phase error) generally exhibits a larger variation over 24 consecutive hours than over a year at a given hour. Because the observed phase measurements show little systematic change over a month or half-month at a fixed hour, the average observed phase over 15 to 30 consecutive days is a robust aggregate measure of the phase for a given hour and specific month (or half-month). The predicted phase (obtained from the PPCs) over the same time period is nearly constant but often differs significantly from the average observed phase. This difference is referred to as the PPC *bias error*, which varies in magnitude from 0 to 30 cecs. Also occurring in this 15- to 30-day period at a fixed hour are random (non-systematic) day-to-day variations in the observed phase on the order of 1 to 5 cecs. Since these random variations (which are due to ionospheric fluctuations) are not reflected in the PPCs, they make up the *random component* of PPC error. Measurements also indicate that the random phase error due to ionospheric fluctuations is usually much larger than the phase error due to interfering noise in the signal processing bandwidth of the receiver (Ref. 7, Appendix A) which is typically 1 cec.

When processing phase measurements to determine position, the bias and random components of phase error produce corresponding bias and random components of position error. Transformation of the phase error to position error depends upon the individual phase errors of all signals processed by the fix algorithm and the geometrical configuration of the receiver and stations corresponding to the received signals. Because this is a rather complex process, simplifying approximations have been adopted by the user community to enable the approximate characterization of expected Omega accuracy. If the magnitude of the random phase errors is assumed to be the same for all signals received and the bias error is assumed to be zero, then the radial position error standard deviation (σ_p) can be obtained by multiplying the phase error standard deviation (σ_ϕ) by the GDOP figure of merit. For a least-squares method of position determination, in the multiranging mode, the following dimensionless form* of GDOP (Ref. 7, Appendix B) is obtained:

$$\text{GDOP} = \frac{1}{2}\left[\frac{\sum_{i=1}^{q-1}\sum_{j=i+1}^{q}\sin^2\left(\frac{\beta_i-\beta_j}{2}\right)}{\sum_{i=1}^{q-2}\sum_{j=i+1}^{q-1}\sum_{k=j+1}^{q}\sin^2\left(\frac{\beta_k-\beta_j}{2}\right)\sin^2\left(\frac{\beta_i-\beta_k}{2}\right)\sin^2\left(\frac{\beta_j-\beta_i}{2}\right)}\right]^{1/2}$$

*Dimensionless GDOP = $\sigma_p/(\lambda\sigma_\phi)$ where λ = signal wavelength.

where q is the number of usable signals received and β_i is the geographic bearing of the signal path to the i^{th} station (corresponding to the i^{th} usable signal). The GDOP becomes very large whenever at least $q-1$ stations have bearings which are nearly equal. Another interesting property is that the GDOP for q station signals is never greater than the GDOP for any subset (≥ 3 stations) of q. This means that, for least-squares position processing, the use of additional (usable) signals does not degrade, and most often improves, the resulting position accuracy. It is important to remember that GDOP is only a figure of merit and its utility for predicting position error given phase error is subject to the stated assumptions.

It is instructive to look at the position errors associated with actual phase measurements for different combinations of stations to illustrate the bias and random position errors, hour-to-hour variations in the position accuracy and the correlation of the observed error with the computed GDOP. Figure 4.6-1 illustrates the north/east position error derived from PPC-corrected phase data recorded at the monitor site in Hawaii, using the indicated stations. Each plot point represents the mean position error (using a least-squares algorithm) at a given hour of the day, based on an average of data recorded over 15 days. The indicated mean is the error that a user would expect to encounter at a given hour of the day during the first 15 days of January at the Hawaii monitor site. The open-circle plot points are local-day hours and the crosses are local-night hours; notice the shift in the grouping of day/night errors, which is characteristic of Omega.

The lower right panel of Fig. 4.6-1 also shows the standard deviation (radius of circle around each mean value) of the error at each hour, which illustrates the expected day-to-day variation of the position error at the given hour. Notice that the spread, or scatter, of the hourly mean error tends to be greater for station combinations with a larger GDOP. Also, the specific errors are a function of the stations used in the solution. Figure 4.6-1 is representative of the position error encountered by an observer on a stationary platform. A craft moving through the region would encounter these errors. However, as the craft moves away from Hawaii, the fix errors will change due to the spatial variation of the fix geometry and propagation conditions. Although the specific errors change along the track of the craft, the (statistical) characteristics of the errors will be similar to those illustrated in Fig. 4.6-1.

For moving vehicles performing navigation, the bias position error can be effectively removed by initializing at a known location, leaving only phase error due to noise during the initial segment of the mission (30 minutes to one hour). However, the paths from the stations to the receiver eventually change (both in space and time) enough so as to become decorrelated with the initialization conditions and the initial correction no longer applies. From the initialization time until the next position update, the Omega position solution is subject to phase bias and random errors and the associated magnification of

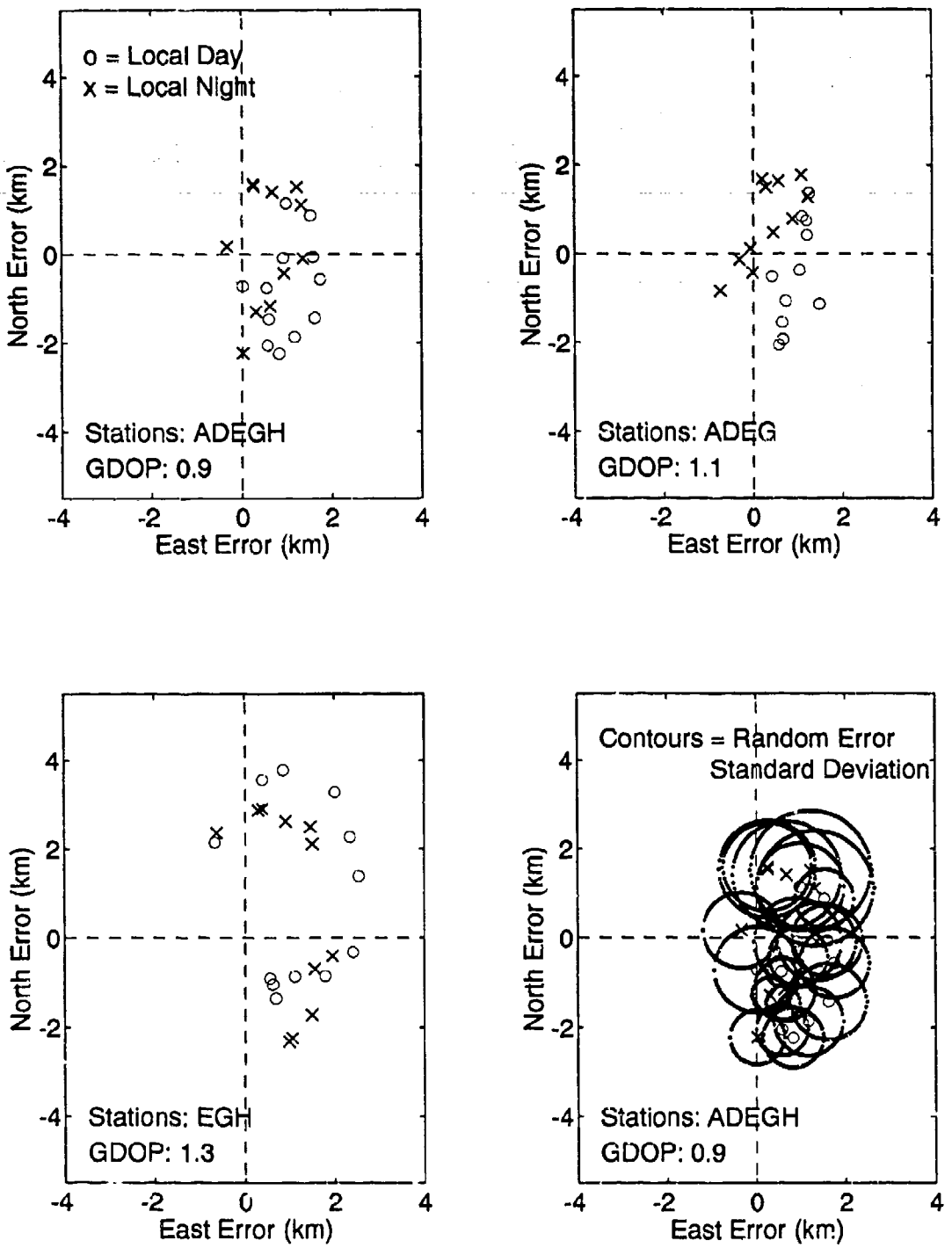

Figure 4.6-1 Position Error Using Phase Data Recorded During January at Hawaii Monitor Site (10.2 kHz)

these phase errors by GDOP. Omega-only accuracies have been reported for aircraft (measured when the aircraft comes under radar control at the termination of the flight) of 2.7 to 3.3 nm, 95% of the time (Refs. 8 and 9).

When integrated with navigation aids other than true air speed and heading, Omega receivers exhibit accuracy figures that differ considerably from those obtained in a stand-alone mode. In the usual case, Omega is combined with a sensor having an intrinsically higher absolute position accuracy, but providing data at discrete times. As a continuous navigation aid, Omega data provides incremental position data between the discrete times. In these cases, the accuracy of the integrated system (averaged over all times) depends on the length of the intervals between the discrete times, but will be bounded by the unaided Omega accuracy and the higher accuracy of the auxiliary sensor.

4.7 PROBLEMS

1. Given the indicated geometry with two transmitters, (T_1 and T_2) identify the receiver locations (A–F) that will provide:

   a. The best position accuracy
   b. The worst position accuracy

   Assume a range-range position-fix algorithm and assume that the errors associated with range measurements unbiased, random and uncorrelated with equal standard deviations. Base your decision on geometry (crossing angle) consideration and give your rationale for each selection.

   c. Is the accuracy at E expected to be better than the accuracy at B and why?

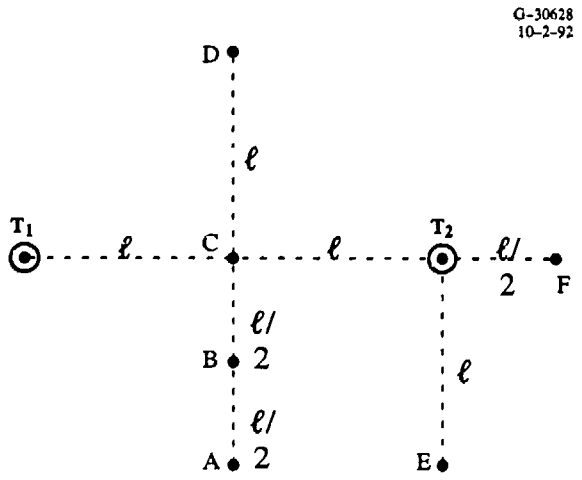

2. a. Using the geometry and definitions shown in the figure, show that the range-range GDOP is

$$\text{GDOP} = \frac{\sqrt{2}}{\sin\theta}$$

under the conditions:

$$\text{GDOP} = \frac{\sigma_p}{\sigma_\varepsilon}$$

Range measurement errors ε_1 and ε_2 are unbiased, random and uncorrelated

x, y are the rectangular coordinates of position.

Recall that $\sigma_p^2 = \mathrm{E}\left\{x_p^2 + y_p^2\right\}$ where E{ } denotes expected value

b. Use the GDOP formula to compute the GDOP for each user position indicated in Problem 1 and compare with your answers in Problem 1.

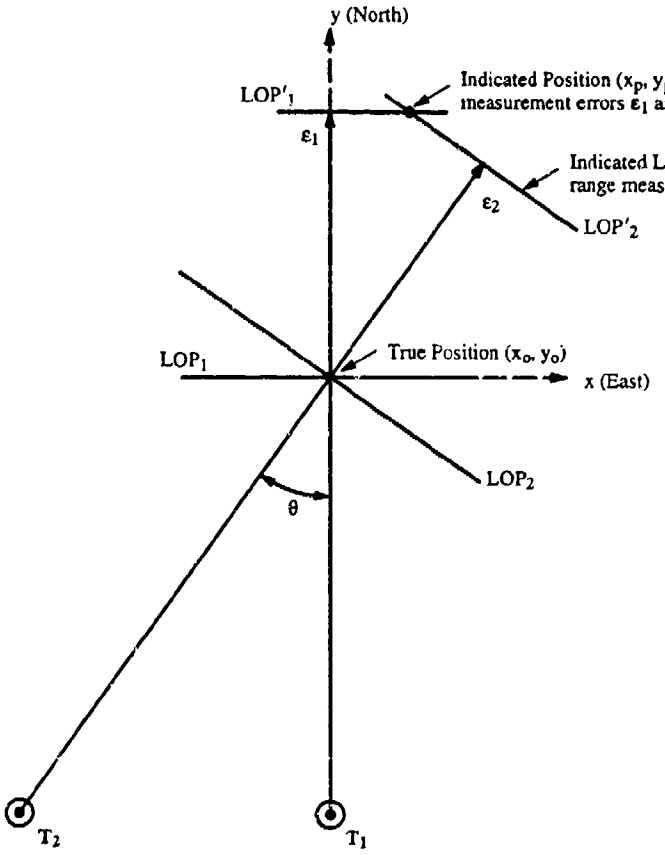

3. The hyperbolic GDOP for three range difference measurements with random, unbiased and uncorrelated errors on each range measurement is:

$$\text{GDOP} = \frac{\sigma_p}{\sigma_\varepsilon} = \frac{1}{\sqrt{2}\sin(\theta_3/2)} \sqrt{\frac{1}{\sin^2(\theta_1/2)} + \frac{1}{\sin^2(\theta_2/2)} - \frac{\cos(\theta_3/2)}{\sin(\theta_1/2)\sin(\theta_2/2)}}$$

where

σ_ε = standard deviation of the measurement error associated with each range

σ_p = standard deviation of radial position error

G-30625
10-2-92

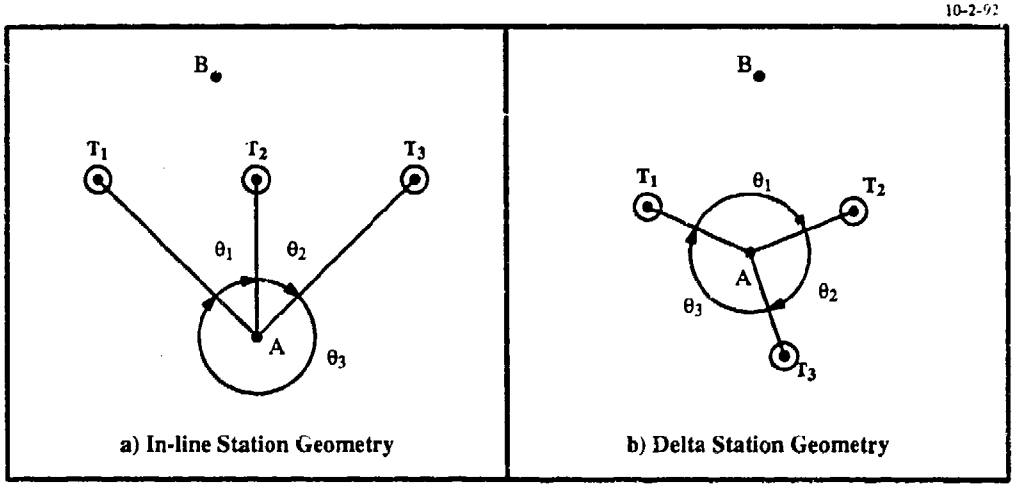

a) In-line Station Geometry

b) Delta Station Geometry

a. Assume that you are a navigator at point A and you want to navigate to point B using a hyperbolic navigation system. Which of the two station geometries (a or b) would you select and why?

b. What is the GDOP for the delta station geometry in (b) assuming that the station baselines are of equal length and you are located equal distance from each station? Is this the minimum GDOP for this station geometry? What is the GDOP if you are located on the midpoint of the $T_1 - T_2$ baseline? Confirm that a hyperbolic fix can be obtained on a baseline.

c. Based on the results obtained from (b), compare the hyperbolic GDOP with the range-range GDOP. Is the minimum range-range GDOP smaller or larger than the minimum hyperbolic GDOP?

4. Show why the lane width of Omega in the hyperbolic mode on the baseline is only half the corresponding lane width in the rho-rho mode. What happens to the hyperbolic lane width at all operating points that are not on the baseline.

5. Explain why Omega can be used aboard a submarine to compute a hyperbolic fix with a submerged antenna but cannot be used in the rho-rho mode. What is the approximate wavelength of the 10.2 kHz signal in the water. (Hint: the signal attenuation rate at 10.2 kHz in seawater is approximately 1 dB/ft and the signal phase shift is approximately 2 cec/ft. Due to refraction, the propagation direction is nearly vertical.)

6. Use the matrix formulation of the least-square position fix algorithm to show that a rho-rho fix cannot be determined a) on the baseline extension or b) by using two measurements from the same station. (Assume that the local clock is perfect.)

4.8 ABBREVIATIONS/ACRONYMS

cec	— Centicycles(s)
dB	— Decibel(s)
GDOP	— Geometric Dilution of Precision
Hz	— Hertz
INS	— Inertial Navigation System
kHz	— Kilohertz
km	— Kilometer(s)
kt	— Knot(s)
LF	— Low Frequency
LOP	— Line of Position
m	— meter
min	— Minute
Mm	— Megameter(s)
Navstar GPS	— Navstar (Satellite) Global Positioning System
nm	— Nautical mile
PCD	— Polar Cap Disturbance
PLL	— Phase-Locked Loop
PPC	— Propagation Correction
RMS	— Root Mean Squared
SNR	— Signal-to-Noise-Ratio
VLF	— Very Low Frequency

4.9 REFERENCES

1. Kayton, M. and Fried, W. (ed.), *Avionics Navigation Systems*, John Wiley and Sons, Inc., 1969.
2. Gelb, A., (ed.), *Applied Optimal Estimation*, The M.I.T. Press, 1974.
3. Nard, G.P., 1980's Differential Omega navigation and equipments, *Proceedings of the Fourth Annual Meeting of the International Omega Association*, San Diego, CA, September 1979.
4. Bourasseau, S., Differential Omega in Indonesia, *Proceedings of the Fifteenth Annual Meeting of the International Omega Association*, Sanur, Bali, Indonesia, September 1990.
5. Perlowski, W., User acceptance of Omega in the marine community, *Proceedings of the Omega Workshop*, Atlantic City, NJ, May 1982.

6. Hildebrand, V., Omega validation highlights, *Proceedings of the Fourteenth Annual Meeting of the International Omega Association*, Long Beach, CA, October 1989.

7. Morris, P., Omega System Availability as a Global Measure of Navigation Accuracy, Report No. CG-ONSCEN-05-90 (National Technical Information Service No. AD-A22?-492).

8. Reynolds, P., Plan American World Airways Omega experience, *Proceedings of the Fourth Annual Meeting of the International Omega Association*, San Diego, CA, September 1979.

9. Sakran, C., U.S. Navy flight test results with the LTN-211 ONS *Proceedings of the Sixth Annual Meeting of the International Omega Association*, Montreal, P.Q., Canada, August 1981.

CHAPTER 5

OMEGA SIGNAL PROPAGATION THEORY

Chapter Overview *— The signals radiated by an Omega transmitter reach a receiver by traveling (propagating) through the earth-ionosphere (EI) waveguide formed along the great-circle path from the transmitter to the receiver. The electromagnetic properties of the waveguide vary along the signal path. Furthermore, the earth's magnetic field makes the ionosphere a magnetized plasma which, in turn, introduces anisotropic behavior to Omega signals. This chapter presents VLF signal propagation concepts/mechanisms relevant to understanding Omega signal propagation characteristics. Section 5.1 gives an overview of the VLF propagation environment and discusses alternative approaches to describe and model VLF signal propagation behavior. The electromagnetic properties of the EI waveguide are reviewed in Section 5.2. Because of the complex nature of the EI waveguide, Section 5.3 presents waveguide propagation mechanisms for a rudimentary model of the EI waveguide. This includes waveguide-mode definition and development of the waveguide-mode equation. Section 5.4 applies the waveguide propagation mechanisms to an idealized EI waveguide with homogeneous properties, including a constant geomagnetic field. Section 5.5 describes an approach to approximate the real-world EI waveguide as a concatenated series of homogeneous segments and presents the signal field computation expressions for the real-world waveguide. As some readers may not be familiar with the fundamentals of basic electromagnetic theory needed to understand the subject material, three appendices to the chapter (Sections 5.6 through 5.8), containing these principles, may be consulted as needed. In particular, Section 5.6 describes the electromagnetic field units/dimensions and reviews the scalar/vector field representations and mathematical tools used to describe the fields. Section 5.7 reviews the basic electromagnetic principles and fundamentals relevant to wave propagation. Section 5.8 presents the equation for the electromagnetic field excited by a source in an EI waveguide. Abbreviations and acronyms are defined in Section 5.9, and the chapter references are identified in Section 5.10.*

5.1 INTRODUCTION

This chapter presents mode theory based VLF signal propagation concepts/mechanisms relevant to understanding Omega signal propagation characteristics. The concepts/mechanisms involve scalar and vector quantities. In this chapter, scalars are denoted by italic Greek or italic English characters such as α, θ, e, or E; vectors are represented by bold Greek or bold English characters, such as $\mathbf{H}$, or $\mathbf{e}$; while matrices are represented as upper-case roman English characters, such as R. Roman English letters are used for multiple character symbols that refer to standard functions, such as sin x, while numerical digits are always roman. Subscript and superscript variables, except for numerical digits, and coordinates axes appear in italics.

Omega is a long-range, ground-based radionavigation system operating in the very low frequency (VLF) band* between 10 and 14 kilohertz (kHz). The signals radiated by an Omega transmitter reach a receiver by propagating through the space between the earth's surface and the lower part of the ionosphere (the D-region). The space acts as a waveguide and is frequently referred to as the "earth-ionosphere" (EI) waveguide. VLF signal propagation in an EI waveguide is analogous to microwave propagation in a lossy waveguide. The height of the EI waveguide varies between about 70 km in day to 90 km at night. Because the waveguide height is comparable to VLF signal wavelengths, approximately 30 km at 10 kHz, the characteristics of a signal propagating along a transmitter-to-receiver path are functions of the electromagnetic properties of the boundaries of the EI waveguide formed along the signal path.

The spatial and temporal characteristics of a propagating signal along a path can be obtained by applying Maxwell's equations (see Section 5.7) to the path waveguide boundaries. The EI waveguide is a spherical waveguide with spatially varying ground conductivity of the earth's surface, and spatially and temporally varying ionospheric conductivity, along with the earth's spatially varying magnetic field (also called geomagnetic field) which affects the signal as it interacts with the ionospheric boundary. Exact electromagnetic field solutions in such a waveguide are extremely difficult to obtain. Several analytical approaches (with corresponding computer programs; see Appendix A) have been developed for determining approximate full-wave solutions§ for VLF signal propagation in the waveguide (Refs. 1 through 5). These approaches are based mostly on "wave-hop" theory (Ref. 6) or, by the mathematical equivalent, "mode theory" (Refs. 7 through 12).

The *wave-hop theory* represents a signal at a point (receiver) as a sum of the groundwave (i.e., the wave that results in the absence of ionosphere, as in the Loran-C system) and a series of "wave-hops" (also called skywaves) reflected from the ionosphere and earth's surface by successive wave-hops, as shown in Fig. 5.1-1. The wave propagation is described by wave-hops that are reflected according to the rules of geometric optics. In the figure, the received signal is composed of the groundwave (not shown) and three wave-hops (j = 1, 2, and 3). Note that wave-hop j is reflected j times from the ionosphere and

*The VLF band includes frequencies from 3 to 30 kHz.

§ A full-wave solution means Maxwell's equations have been applied to the problem without any approximations relative to the variability of electromagnetic properties of the wave propagation medium (Ref. 11). These properties can vary significantly for Omega signals over a distance of the signal wavelength. If, however, the path properties do not vary significantly over a wavelength, as is usually the case for the low- and high-frequency propagation signals, one could use the conventional ray or geometrical optics theory.

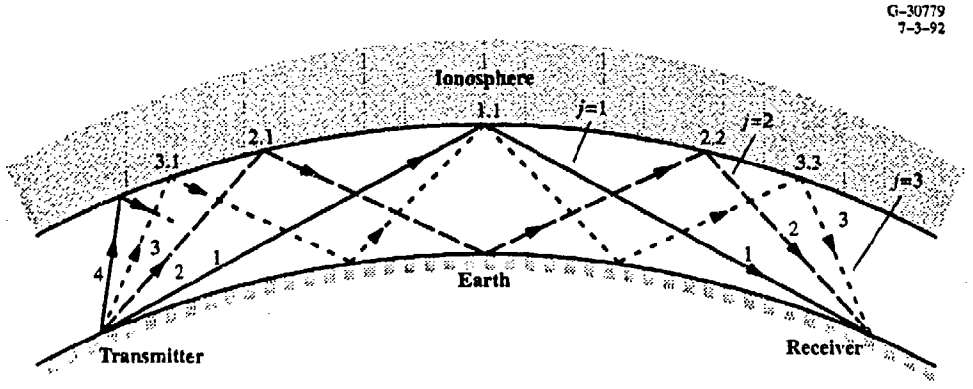

Figure 5.1-1 Diagrammatic Representation of Wave-hops

$(j-1)$ times from the earth's surface. This description is of particular interest when the distance (ϱ) between the transmitter and receiver is relatively short, e.g., ϱ<1000 km for Omega signals. For these short distances, it is usually enough to consider the wave-hops that have been reflected from the ionosphere two or three times. The number of wave-hops needed to represent a signal increases as ϱ increases. Because Omega is a long-range navigation system with signals propagating over distances of 10–15 thousand kilometers, currently available propagation algorithms based on wave-hop theory are not practical for Omega/VLF signal description.

Although elements of *mode theory* are not easily visualized as those of wave-hop theory, mode theory provides a useful model for certain characteristics of VLF propagation, such as "modal interference" (Section 5.5.2). In mode theory, the signal along a path is represented as a sum of the "normal or characteristic modes" of the EI waveguide formed along the path. A sketch of the electric field pattern of a VLF signal propagating in an EI waveguide is shown in Fig. 5.1-2. At short distances (500–2000 km), from a transmitter, called the "near-field region" of the transmitter, the signal field pattern (see Fig. 5.1-2) is generally complicated (irregular) due to the signal being a sum of several competing strong-amplitude modes of the waveguide. However, at longer ranges (several thousand kilometers from a transmitter) along most signal paths, the signal is dominated by its Mode 1 (the lowest-order mode) component as the signal's higher-order mode components are attenuated much more rapidly than Mode 1 component. The signal pattern is therefore much more regular (approximately Mode 1 signal pattern) at the longer ranges.

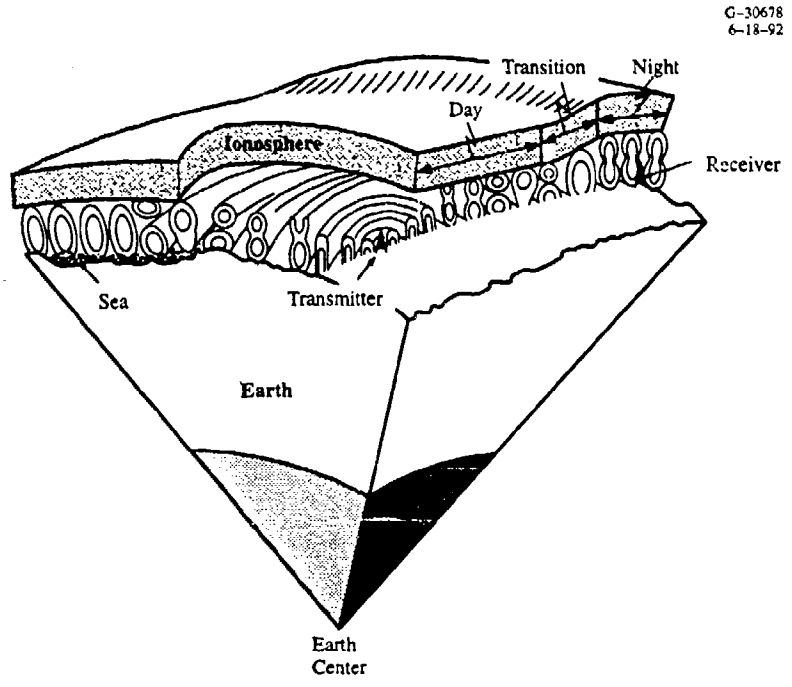

Figure 5.1-2 Electric Field Patterns Within the Earth-Ionosphere Waveguide

5.2 THE EARTH-IONOSPHERE WAVEGUIDE

From the Omega transmitting station source (antenna), Omega signal waves propagate outward inside the space between the earth's surface and ionosphere with circular wave fronts as shown in Fig. 5.2-1(a), assuming a spherical and homogeneous earth, and an isotropic and homogeneous ionosphere. The wave front is a constant phase surface. If a single point along any circular wave front is selected as a receiver, *a signal path* is defined between the transmitter and receiver as the shorter of the two great-circles arcs between the transmitter and receiver (see Fig. 5.2-1(b)). It is the electromagnetic properties of the earth's surface and the ionosphere medium along this path that determine the signalfield characteristics detected at the receiver.

Figure 5.2-2(a) shows a side view of the earth-ionosphere waveguide formed along a typical short path, *TR*, shown in Fig. 5.2-2(b). The path is a mixed-conductivity, mixed-illumination path. Path segments *TA*, *AB*, *BR*, have day, transition, and night illumination conditions, respectively. The next two subsections describe the electromagnetic properties of the lower and upper boundaries of the waveguide.

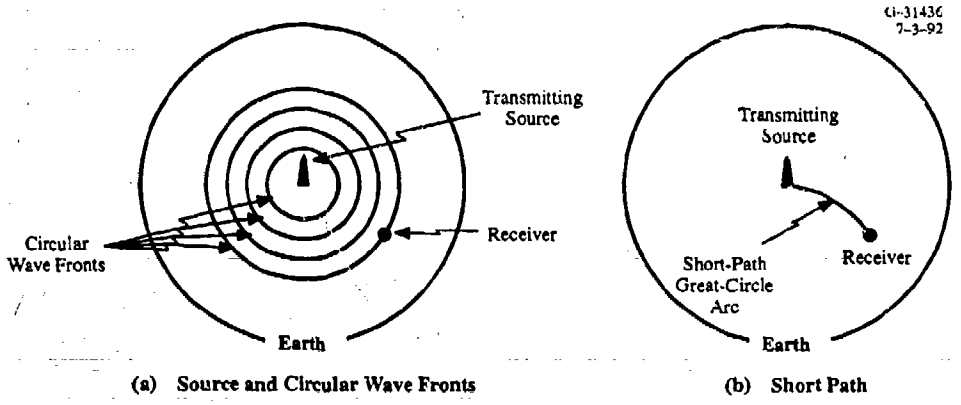

(a) Source and Circular Wave Fronts (b) Short Path

Figure 5.2-1 Transmitter Signal Path

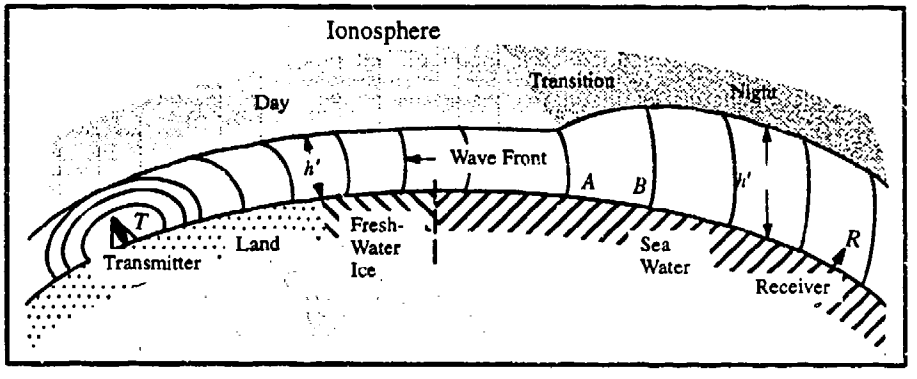

(a) Side view of the EI Waveguide Formed along the Path TR Shown in Fig. 5.2-2b

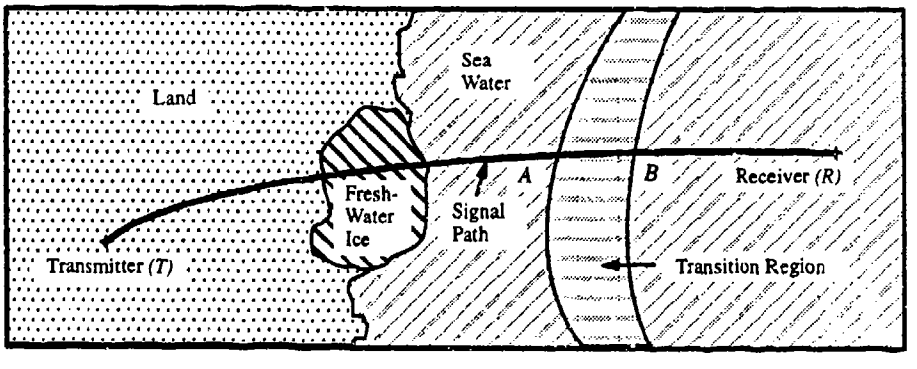

(b) An Example of Short-path Signal Path TR

Figure 5.2-2 Earth-Ionosphere Waveguide

5.2.1 The Lower Boundary — The Earth's Surface

The earth's surface consists of many different substances such as sea water, soil, and ice. The electromagnetic properties of the lower boundary are described by its two parameters: the ground conductivity,* σ, and associated relative permittivity, $\epsilon_r = \epsilon/\epsilon_0$.§ The conductivity relates the electric field to the electric current flowing in the earth's surface, and relative permittivity relates the electric field to the electric flux density in the earth's surface; see Section 5.7). These parameters vary with location on the earth's surface. Each parameter at a location is the average value of the local parameter over a distance of several skin depths† below the earth's surface (see Section 5.7). A worldwide, ten-level, ground conductivity map is available (Ref. 13) for use in the VLF signal calculations. The map is derived from empirical data, and theory wherever empirical data were unavailable. Typical values of the parameters for the various types of earth materials are given in Table 5.2-1.

Table 5.2-1 Typical Conductivity and Relative Permittivity of the Earth's Surface Materials

MATERIAL	CONDUCTIVITY, σ (mho/m)	RELATIVE PERMITTIVITY,* $\epsilon_r = \epsilon/\epsilon_0$	$\sigma/\omega\epsilon$
Sea water	4	80	9×10^4
Rich damp soil	10^{-2}	20	9×10^2
Dry soil	10^{-3}	10	1.8×10^2
Fresh-water (average lake)	10^{-3}	80	2.25×10^1
Permafrost (tundra)	10^{-4}	10	1.8
Fresh-water ice (Greenland ice)	10^{-5}	5	3.6

*Dimensionless quantity.

Note that the table includes values of $\sigma/\omega\epsilon$ of the earth materials for the signal frequency ($f = \omega/2\pi$) of 10 Hz. The $\sigma/\omega\epsilon$ is the ratio of "conduction current" and "displacement current" flowing through a material. The current through a pure resistor is the conduction current, while the current 'through' a pure capacitor is the displacement current (c.f. Ref. 19). A material is said to be a good conductor at the frequency $f(= \omega/2\pi)$ if it has $\sigma/\omega\epsilon >> 1$. From the table, we note that, except for

*Conductivity is proportional to the reciprocal of the resistance.

§ It is the permittivity relative to the free-space permittivity, ϵ_0 (= 8.854×10^{-12} farad/meter).

† At 10 kHz, the skin depths for sea water (σ = 4 mho/m), rich damp soil ($\sigma = 10^{-2}$ mho/m) soil, and fresh-water ice ($\sigma = 10^{-5}$ mho/m) are approximately 2.5, 50, 112, and 1590 meters, respectively (see Section 5.7.6).

the tundra and fresh-water ice regions, the earth's surface is a reasonably good conductor at Omega/VLF signal frequencies (10-30 kHz).

Notice that the ground conductivity of the earth's surface varies more than five orders of magnitude (i.e., 10^5) while the associated permittivity varies by an order of magnitude. The waveguide *modes* which have electric field vectors nearly perpendicular to the earth's surface carry most of the Omega signal energy and are most affected by the ground conductivity variations. The propagating signal in an EI waveguide is attenuated (i.e., the signal energy is lost due to path properties' effects) by as little as 0.5 dB (decibel) per 1000 km over sea water and as much as 30 dB per 1000 km over fresh-water ice. This large attenuation rate at Omega frequencies is the source of the term "Greenland shadow," especially in connection with the Norway Omega station signals, as observed in North America.

5.2.2 The Upper Boundary — The Ionosphere

The earth is surrounded by an ionized region above the neutral atmosphere called the ionosphere, which has an extremely important influence upon the propagation of radiowaves at very low frequencies as well as in other frequency bands. There are several sources of ionizing energy which tend to produce charged particles, ions, and free electrons from the neutral air molecules (Refs. 8, 9, 14, and 15). The fundamental source of ionization is the sun, with other stellar objects as secondary sources. Ion-neutral collision, excitation, recombination, and diffusion control the amount of ionization at a given location. The ionosphere extends from about 50 to 1000 km above the earth's surface. Since different solar radiation frequencies are most active as ionizing agents in different height regions, there are several ionospheric regions: the *D*-, *E*-, and *F*-regions. The ionosphere layers differ in several properties: constituent particle composition and density, principal sources of ionization and recombination mechanisms, and profiles (distribution with height) of particle density and collision frequency. Propagation of VLF radiowaves to great distances is made possible by the high reflectivity of the lower ionosphere, i.e., the *D*-region and the lower *E*-region which extend from 70 to 100 km above the earth's surface. The latter is due to the relatively sharp gradient of the electron density in the *D*-region of the ionosphere (see Fig. 5.2-3).

The structure of the ionosphere is quite sensitive to the net incident solar illumination. During the day, solar photoionization maintains a small but stable ionized component between 70 and 80 km. The amount of ionization depends inversely on the angle between the sun and the local solar zenith angle, i.e., the maximum ionization occurs at a solar zenith angle of 0 deg. For the nighttime ionosphere, the only major source of ionization is radiation scattered from the dayside, which has much smaller solar fluxes than direct solar radiation. As a result, the nighttime *D*-region almost entirely disappears, so that

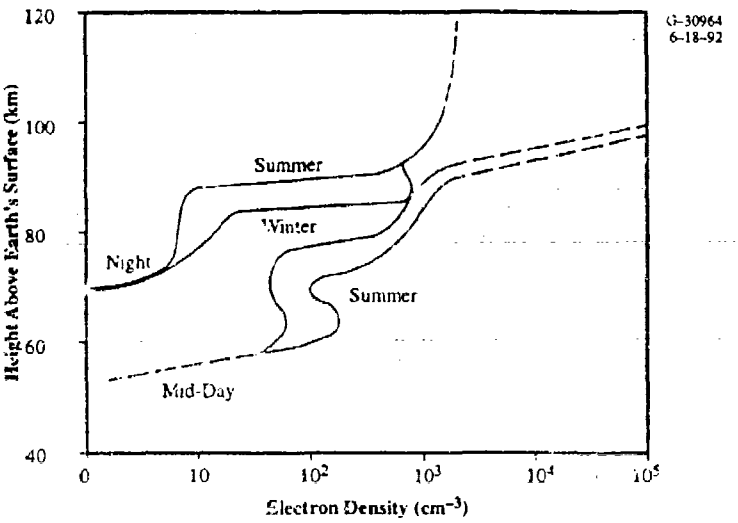

Figure 5.2-3 Electron Density for Sunspot Minimum Latitudes (Ref. 16)

VLF waves are effectively reflected from the bottom of the *E*-region (80 to 90 km). The solar control of the ionosphere is the source of the strong diurnal dependence of Omega/VLF signal propagation. The effective height of the EI waveguide increases 15–20 percent from day to night, leading to substantial differences in received signal characteristics over the same path.

The electron density and the effective electron collision frequency (average number per second with neutral particles) of the *D*-region determine the characteristics of propagating waves. The ionosphere is not, in general, homogeneous, especially in the direction perpendicular to the earth's surface where both the electron density and electron collision frequency vary with height. For VLF signal calculations, the *D*-region ionosphere is modeled by the following exponential height-dependent ionospheric conductivity profile (Refs. 5 and 7)

$$\omega_r(z) = 2.5 \times 10^5 \exp\left[\beta(z - h')\right] \qquad (5.2\text{-}1)$$

where z is the altitude (km) above the earth's surface; β is the ionospheric conductivity gradient (km^{-1}); and h' is a reference height (km), also called the reference reflection height. Typical values of h' are 70 km in day and 87 km at night, and β is 0.3 km^{-1} in day and 0.3–0.5 km^{-1} at night. The h' and β provide a convenient, but approximate, means of describing the *averaged* ionosphere conductivity, which is equal to $\varepsilon_0 \omega_r$,* approximately 10^{-6} mho/m. Thus, isotropic ionosphere is a very poor conductor at VLF, compared to sea water which has conductivity of 4 mho/m.

The above model is more a description of the mid-latitude ionosphere. The ionosphere in the higher-latitude (auroral/polar) and lower-latitude (equatorial) regions is quite different from the mid-latitude ionosphere. Some researchers have suggested the use of latitude-dependent h' and β values which are functions of season, in addition, to the solar illumination condition (Refs. 17 and 18).

The action of the earth's magnetic field on the constituent charged particles makes the ionosphere a magnetized plasma. This introduces *anisotropy* into the behavior of VLF signal waves interacting with the ionosphere, i.e., the signal propagation characteristics depend upon the direction of signal propagation, in addition to other isotropic ionospheric properties. Because of this anisotropy, a wave traveling from east to west (perpendicular to the geomagnetic field) is reflected much less efficiently from the ionosphere relative to west-east propagation. In contrast, signals propagating parallel to the geomagnetic field (i.e., north or south) are unaffected by a 180-degree shift in the signal propagation direction. Because the anisotropy is strongest on paths perpendicular to the geomagnetic field, this phenomenon in which signals propagating to the east having lower signal attenuation than those propagating to the west is often referred to as the "east-west effect."

Orientation and magnitude of the geomagnetic field are the parameters of interest to VLF signal propagation. The field orientation at a local path point is conveniently characterized by the local dip angle, D (or, alternatively, the local geomagnetic latitude, θ_m) and the local path azimuth, β_m (bearing from the geomagnetic north). Dip angle is the angle between the geomagnetic field vector and its horizontal component, Geomagnetic latitude and dip angle at a point are related to each other (based on an earth-centered dipole field) by the relationship: $2 \tan \theta_m = \tan D$. Figure 5.2-4 illustrates the dip angle and path azimuth at a local path point, P.

---

* ε_0 (= 8.854×10^{-12} farad/meter) is the permittivity (dielectric constant) of free space.

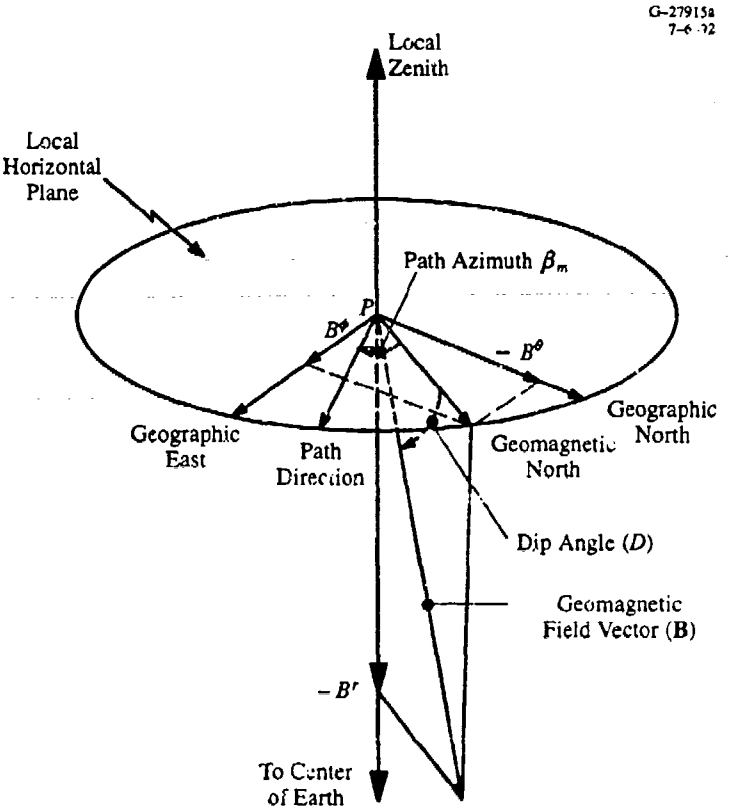

Figure 5.2-4 Path Azimuth and Dip Angle at Path Point P

5.3 GUIDED WAVE PROPAGATION

The earth-ionosphere waveguide is an extremely complex waveguide due to its spatially varying properties, some of which are also anisotropic, thus introducing propagation direction-dependent signal behavior. To better understand wave propagation phenomena in an EI waveguide, we will analyze a rudimentary model of this waveguide. The model to be considered is a waveguide with parallel boundaries (planes), each with uniform and isotropic properties; we will call the model the isotropic/planar waveguide. Specifically, in this section, we will describe what a "mode" is and develop the "mode equation" for an isotropic/planar waveguide. Also, we will present electromagnetic fields of the modes in this waveguide as well as in a special case of this waveguide. As the real-world EI waveguide has anisotropic properties, we will extend the isotropic/planar waveguide mode equation to the EI waveguide.

Note that waveguides, in general, are structures which guide propagation of radiowave signals. Everyday examples of waveguides are electrical transmission lines bringing electrical power or telephone service to homes and coaxial cables bringing TV information from the cable companies. In studying guided waves in a waveguide, it is common to classify the wave solutions (of Maxwell's equations) into the following types (Ref. 19):

- Waves *that contain* electric field but no magnetic field in the direction of propagation. Since the magnetic field lies in the transverse plane, they are called the *transverse magnetic (TM) waves*. They have also been referred to as *e-waves* or *waves of the electric type*.
- Waves *that contain* magnetic field but no electric field in the direction of propagation. These are known as the *transverse electric (TE) waves*, and have also been referred to as the *h-waves* or *waves of the magnetic type*.

In the EI waveguide, the ground-based vertical electric monopole antennas, such as the Omega transmitting antennas, excite mostly TM modes in the waveguide; while, airborne antennas with horizontal electric dipoles excite mostly TE modes in the waveguide. Figure 5.3-1 illustrates the vertical (denoted by the subscript V on a field quantity), transverse (denoted by the subscript T on a field quantity) and longitudinal (denoted by the subscript L on a field quantity) components of the electric (**E**) and magnitude (**H**) field vectors of the TM and TE modes. The figure also shows the height-dependence of $\mathbf{E}_V$ of TM modes and $\mathbf{E}_T$ of TE modes. Note that the electric field ($\mathbf{E}_V$) of the TM modes is largest at the ground while the electric field ($\mathbf{E}_T$) of the TE modes is zero at the ground.

The above is not the only way in which wave solutions may be categorized, but is a useful way in that any general field distributions excited by a source in a waveguide may be divided into a possibly infinite number of the above types with suitable amplitudes and phases. The *propagation constant*, also called *wave number*, of each of these waves tells how an individual wave changes its amplitude and phase as it travels down the guide, so that these waves may be superposed at any later position/time to

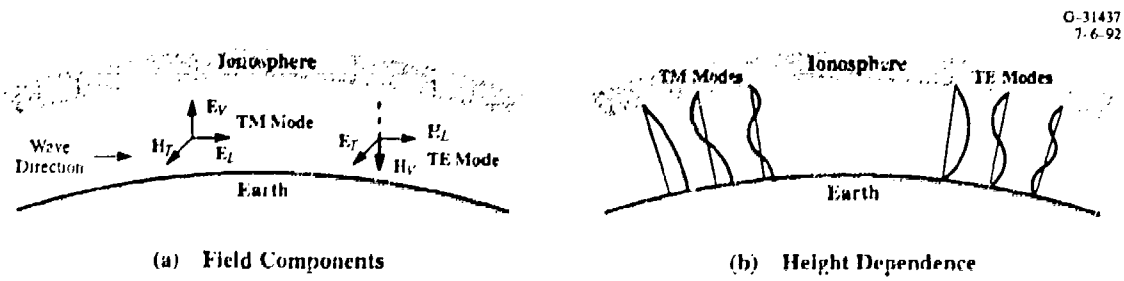

(a) Field Components (b) Height Dependence

Figure 5.3-1 Field Components and Height Dependence of TM and TE Modes of EI Waveguide (Ref. 20)

give the total resultant signal field. In principle, only one of the possible infinite number of these waves may propagate in the guide if it alone is excited and if guide conditions are favorable for its propagation.

5.3.1 Isotropic/Planar Waveguide

Consider an isotropic/planar waveguide, whose side view is shown in Fig. 5.3-2, with the lower boundary (an idealized planar earth's surface) at $z = 0$ and the upper boundary (an idealized planar ionosphere bottom) at $z = h$; the height h of the waveguide is two or more signal wavelengths, which means a minimum height of 60 km at Omega frequencies. The waveguide signal propagation direction is in $+x$ direction and the waveguide is infinitely long in the $\pm y$ directions and thus has no side walls. Both boundaries are assumed to have homogeneous (uniform) and isotropic properties, and the medium inside the waveguide is assumed to be free space (vacuum). Let the waveguide be excited by a small (relative to signal wavelength) vertical electric monopole antenna located at the earth's surface ($z = 0$) in the waveguide. The signal radiated by such a source is composed of the three parts: electrostatic, induction, and radiation. The first two parts dominate the total field for distances of up to one wavelength from the source (approximately 30 km at 10.2 kHz); beyond these distances, the third part dominates. The third, or the radiation part, provides the energy carried by the waves propagating in the waveguide. A further discussion of the source signal field components is given as an appendix to this chapter, Section 5.8.

The radiation part of the signal field has vertical electric field component of the form

$$\frac{1}{\rho}\cos(\omega t - k_0\rho)$$

where ρ is the radial distance from the source; $\omega = 2\pi f$; f = frequency; t = time; and k_0 ($= 2\pi/\lambda_0$) is the propagation constant in free space, where λ_0 is signal wavelength in free space. The radiated part of the

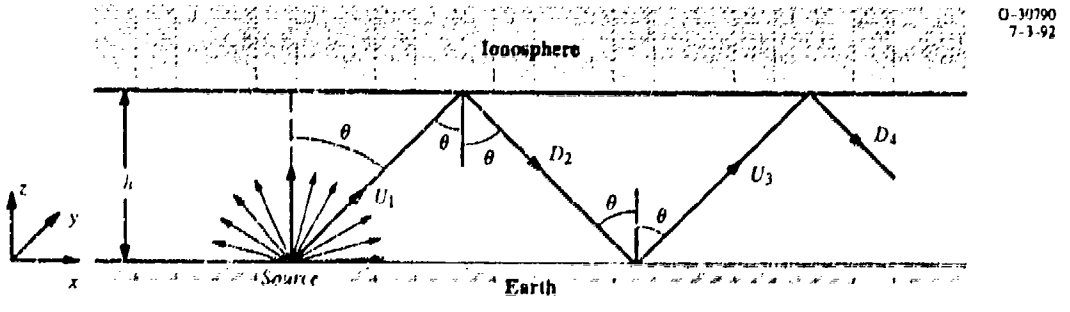

Figure 5.3-2 Planar Waveguide Geometry

signal field produces waves with approximately spherical wave fronts. By the time the waves are incident on the upper boundary (the ionosphere), the wave front radius of curvature is so large that the wave fronts can be considered approximately planar, as shown at points *A* and *B* in Fig. 5.3-3. Therefore, different points along the ionosphere boundary can be viewed to receive plane waves which appear to be coming at different incident angles from the source. For example, at points *A* and *B* in Fig. 5.3-3, the plane waves appears to be coming at incident angles θ_A and θ_B, respectively. Upon reflection from the ionosphere boundary, each of the incident plane waves undergoes successive reflections from the lower and upper boundaries of the waveguide as the wave moves down the waveguide.

There are certain plane wave incident angles for which the waveguide exhibits the "resonance condition," as described later in this section. That is to say, a plane wave incident at any of one of these angles leads to a propagating wave down the guide. This is due to phase coherence in the wave fronts of the reflected upgoing and downgoing plane waves in the guide (see Fig. 5.3-1). A plane wave, incident at any angle other than the resonance condition angles (e.g., at θ_C in Fig. 5.3-2) has negligible amplitude in the guide due to destructive interference between the phase fronts of the reflected upgoing and downgoing waves in the guide. Thus there is no resulting propagating mode for the plane wave incident at θ_C. The signal field "configuration," i.e., the spatial variations of the electromagnetic fields in the plane perpendicular to the waveguide propagation direction, of each propagating wave at a fixed time is called a *mode*, and the resonance condition is expressed as the *mode equation*.

For developing the resonance condition (Ref. 10), consider a plane wave, with the propagation constant k_0, incident at the ionosphere at an angle θ from the vertical (*z*-axis) as shown in Fig. 5.3-1. Let $R^g(\theta)$ and $R^i(\theta)$ be the reflection coefficients of the plane waves incident at the ground and ionosphere

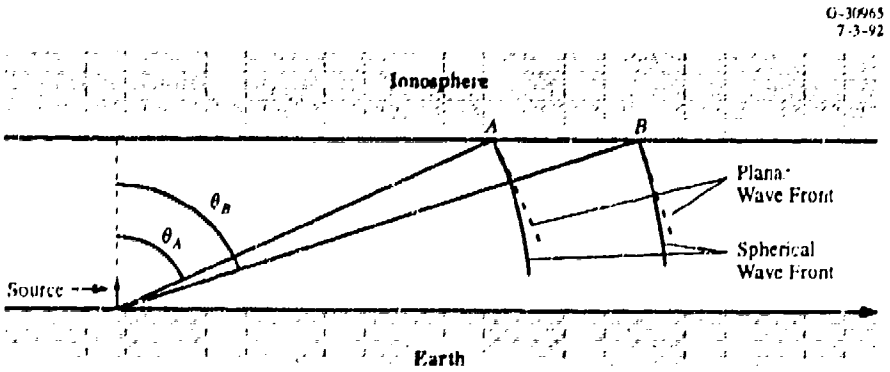

Figure 5.3-3 Spherical Wave Approximation By Plane Waves

boundaries, respectively, at an angle θ at either boundary. Furthermore, let the upgoing wave, U_1, in the waveguide has the field dependence, in complex notation, of the form

$$F_1 = F_0 \exp\left[i\omega t - \mathbf{k}\cdot\mathbf{r}\right] \tag{5.3-1a}$$

where exp $(i\omega t)$ is the assumed complex time dependence; $i = \sqrt{-1}$; F_0 is the amplitude of the wave; and the propagation constant vector, $\mathbf{k}$ called wave vector whose magnitude is called wave number) and distance vector $\mathbf{r}$ are given by

$$\mathbf{k} = k_0\,(\hat{\mathbf{x}}\,\sin\theta + \hat{\mathbf{y}}\,\cos\theta)$$
$$r = \hat{\mathbf{x}}\,x + \hat{\mathbf{y}}\,y$$

where $\hat{\mathbf{x}}$ and $\hat{\mathbf{y}}$ are the *unit vectors* along the x- and y- coordinate axes, respectively, of the rectangular coordinate system (see Section 5.6); x, y are the magnitudes of the distance vector $\mathbf{r}$ along the x- and y- coordinate axes; k_0 is the propagation constant (wave number) in free space. Substituting $\mathbf{k}_0$ and $\mathbf{r}$ in Eq. 5.3-1(a) gives

$$F_1 = F_0 \exp\left[i\omega t - ik_0(x\sin\theta + z\cos\theta)\right] \tag{5.3-1b}$$

Since all field quantities will have the same time dependence, we will henceforth drop the time dependence term from the field expressions, unless otherwise noted. When the upgoing plane wave U_1 meets the ionosphere boundary at $z = h$, it is reflected to produce a downgoing wave, D_2, with the field component

$$F_2 = F_{20} \exp\left[-ik_0\,(x\sin\theta - z\cos\theta)\right] \tag{5.3-2a}$$

At the ionosphere boundary ($z = h$) of the waveguide, F_2 must be equal to $F_1\ R^i(\theta)$ which requires that

$$F_{20} = F_0\ R^i(\theta)\ \exp\,(-2ik_0 h\cos\theta)$$

Therefore F_2 in terms of F_0 and $R^i(\theta)$ is given by

$$F_2 = F_0\ R^i(\theta)\ \exp\left[-ik_0(x\sin\theta - z\cos\theta) - 2ik_0 h\cos\theta\right] \tag{5.3-2b}$$

The downward wave D_2 is then reflected from the earth's surface boundary ($z = 0$) of the waveguide and gives rise to the upgoing wave U_3 in which the field component is

$$F_3 = F_{30} \exp\left[-ik_0(x\sin\theta + z\cos\theta)\right] \tag{5.3-3a}$$

At the earth's surface ($z = 0$) F_3 must be equal to $F_2\ R^g(\theta)$ which requires that

$$F_{30} = F_{20}\ R^g(\theta)$$

$$= F_0\ R^i(\theta)\ R^g(\theta)\ \exp\ (-2ik_0\ h\cos\ \theta)$$

Therefore F_3 in terms of F_0, $R^i(\theta)$, and $R^g(\theta)$ is given by

$$= F_0\ R^g(\theta)\ R^i(\theta)\ \exp\left[-ik_0(x\sin\ \theta + z\cos\ \theta) - 2ik_0 h\cos\ \theta\right] \qquad (5.3\text{-}3b)$$

For U_1, D_2, and U_3 waves to represent the upgoing and downgoing components of a self-consistent traveling wave in the waveguide (see Fig. 5.3-1), U_3 must be identical to U_1 except for a phase change* equal to an integral number (p) of 2π radians. Mathematically, it means that

$$R^g(\theta)\ R^i(\theta)\ \exp\ (-2ik_0 h\cos\theta)\ =\ \exp\ (-2i\pi p) \qquad (5.3\text{-}4)$$

where the reflection coefficients are complex quantities as described below

$$R^g(\theta) = |R^g(\theta)|\ \exp\ (i\phi^g) \qquad (5.3\text{-}5a)$$

$$R^g(\theta) = |R^i(\theta)|\ \exp\ (i\phi^i) \qquad (5.3\text{-}5b)$$

where ϕ^g and ϕ^i are real quantities. Equation 5.3-4 is the resonance condition for the propagating modes of the waveguide. It is a fundamental equation of mode theory and, in general, involves complex quantities. It has a unique complex angle solution, θ_p, for each integer value of p. The angle θ_p is commonly referred to as the *eigenvalue* or *eigenangle* of the p^{th} mode.

The mode equation, Eq. 5.3-4, is conveniently written as a set of the following two expressions, obtained by equating the magnitude and phase terms, respectively, of both sides of the mode equation (Eq. 5.3-4):

$$|R^g|\ |R^i|\ =\ \exp\left[-2k_0 h\left[\text{Im}\ (\cos\ \theta_p)\right]\right] \qquad (5.3\text{-}6a)$$

$$\phi^g + \phi^i\ -\ 2k_0 h\left[\text{Re}\ (\cos\ \theta_p)\right]\ =\ -2\pi p \qquad (5.3\text{-}6b)$$

where Re ( ) and Im ( ) are real part and imaginary part, respectively, of the quantities in the parentheses ( ); and | | denotes the magnitude of the quantity inside the bars | |. It is important to note that magnitude and phase of R^g and R^i in Eqs. 5.3-6a and 5.3-6b are dependent on the value of the physical angle

*The minus sign must be used in the physically real case since F_3 is one compete reflection farther along the propagation direction in the guide than F_1.

of incidence and therefore an iterative method must be employed to solve the mode equation. For a non-lossy waveguide, θ_p is a real quantity and thus the mode equation for the non-lossy waveguide is given by Eq. 5.3-6b.

A mode, as mentioned above, is formed by the upgoing and downgoing waves in a waveguide and thus the field polarization of the resulting mode signal fields is the same as that of the constituent upgoing and downgoing waves. Hence, like the plane waves, there are TE and TM modes in a waveguide. These modes, like the corresponding plane waves types, form a complete set of mathematical functions to describe a propagating signal at any point in an isotropic waveguide.

Mode Signal Field Components — A mode signal in the waveguide, as noted earlier, is the result of the upgoing and downgoing plane waves forming the mode signal, as shown in Fig. 5.3-1. The mathematical expressions for the upgoing (U) and downgoing (D) plane waves of a mode are

$$U = U^0 \exp\left[-ik_0(x\sin\vartheta + z\cos\theta)\right]$$

$$D = D^0 \exp\left[-ik_0(x\sin\theta - z\cos\theta)\right]$$

Applying Maxwell's equations (see Section 5.7) to the upgoing and downgoing waves of a mode, we get the electric field components (E_x, E_y, E_z) and magnetic field components (H_x, H_y, H_z) for the p^{th} TM and TE modes as listed below for the EI waveguide shown in Fig. 5.3-1.

The phasor expression for the field components of the p^{th} TM mode are (Ref. 19)

$$\begin{aligned} H_{yp} &= 2U_p^0 \cos(k_0 z C_p) \exp(-ik_0 x S_p) \\ E_{xp} &= 2i\eta_0 U_p^0 C_p \sin(k_0 z C_p) \exp(-ik_0 x S_p) \\ E_{zp} &= -2\eta_0 U_p^0 S_p \cos(k_0 z C_p) \exp(-ik_0 x S_p) \end{aligned} \qquad (5.3\text{-}7a)$$

The phasor expressions for the field components of pth TE mode are (Ref. 19)

$$\begin{aligned} E_{yp} &= -2iU_p^0 \sin(k_0 z C_p) \exp(-ik_0 x S_p) \\ H_{xp} &= \frac{-2iU_p^0}{\eta_0} \sin(k_0 z C_p) \exp(-ik_0 x S_p) \\ H_{zp} &= \frac{-2iU_p^0}{\eta_0} S_p \sin(k_0 z C_p) \exp(-ik_0 x S_p) \end{aligned} \qquad (5.3\text{-}7b)$$

where

p	=	Mode index	
U_p^0	=	p^{th} mode dependent field	
i	=	$\sqrt{-1}$	
θ_p	=	Eigenvalue (a complex quantity) of p^{th} mode	
C_p	=	$\cos\theta_p$	
S_p	=	$\sin\theta_p$	
u_0	=	$c=\left(\sqrt{\epsilon\mu}\right)^{-1}$ =	Velocity of light in an unbounded medium having the same dielectric properties as the waveguide propagation medium
η_0	=	$\sqrt{\mu/\epsilon}$ =	Characteristics impedance of an unbounded medium having the same dielectric properties as the waveguide propagation medium
k_0	=	$\frac{2\pi}{\lambda_0} = \frac{\omega}{u_0}$ =	Propagation constant (wave number) of the signal wave in an unbounded medium having the same dielectric properties as the waveguide propagation medium.

In the field component equations (Eqs. 5.3-7a and 5.3-7b), some of the field components have two subscripts, while other quantities have one subscript. For the two-subscript field components, the first subscript indicates the x, y, or z component of the field and the second subscript denotes the mode index of the field. For example, H_{yp} denotes the y-component of H-field for p^{th} mode.

We will now examine the spatial variations of the field components of the TM and TE modes in the waveguide shown in Fig. 5.3-1. The height (z)-dependence of the mode signal field components, called height-gain functions, is a cosine function in z for the TM modes and a sine function in z for the TE modes. As a result, the signal components at z = 0 (the earth's surface) are zero for the TE modes and maximum for the TM modes. Although this height-dependent behavior is derived for an idealized EI waveguide, it is very nearly the same for a real-world EI waveguide. This is the basis why Omega navigation employs the lowest-order TM mode for Omega navigation.

The x-dependence of the field components is given by

$$\exp\ (ik_0 S_p)$$

where S_p (= $\sin\theta_p$) is a complex quantity for lossy waveguides and is real for non-lossy waveguides. Incorporating the time dependence term exp ($i\omega t$), dropped earlier from the field equation, we get the x-dependence of the field components to be

$$\exp\left[i(\omega t - k_0 x S_p)\right]$$

For a lossy waveguide, the complex quantity

$$S_p = \left[\text{Real Part of } (S_p) + i \text{ Imagery Part of } (S_p)\right]$$

$$= Re\ (S_p) + i\ \text{Im}\ (S_p)$$

The x-dependence of the field components thus becomes

$$\underbrace{\exp\left[i[\omega t - k_0 x\ \text{Re}\ (S_p)]\right]}_{\text{First Term}}\ \underbrace{\exp[-k_0 x\ \text{Im}\ (S_p)]}_{\text{Second Term}} \tag{5.3-8}$$

The first term of Eq. 5.3-8 provides the phase velocity with which the mode propagates along the waveguide (the x-direcion); the second term describes the way the mode signal is attenuated exponentially with distance (x) along the waveguide as it propagates inside the waveguide.

If α_p is the signal attenuation rate and β_p is the propagation constant for the p^{th} mode, then

$$\alpha_p = k_0\ \text{Im}\ (S_p)\ \text{ neper/meter} \tag{5.3-9a}$$

$$\beta_p = k_0\ \text{Re}\ (S_p)\ \text{ radian/meter} \tag{5.3-9b}$$

The attenuation rate is sometimes expressed in decibels per megameter* (dB/Mm) of signal path length, as described by

$$A\ (\text{dB/Mm}) = 20\log_{10}\left[\exp\left(-10^6 \times \alpha_p\right)\right]$$

$$= -8.686\ k_0\ \text{Im}\ (S_p) \tag{5.3-10}$$

where $k_0 = 2\pi/\lambda_0$ and λ_0 is the wavelength in meters.

The phase velocity (u_p) of the p^{th} wave, denoted as u_{pp}, is given by

$$u_{pp} = \frac{\omega}{\beta_p} = \frac{\omega}{k_0 \text{Re}\ (S_p)} = \frac{u_0}{\text{Re}\ (S_p)} \tag{5.3-11}$$

To provide further insight of what the mode signal fields looks like, we will apply below the mode equation and the associated electromagnetic field formulas of the isotropic/planar waveguide developed above to the case where both of the waveguide boundaries are perfect electrical conductors (i.e., the waveguide boundaries have the conductivity, σ, equal to ∞); this is a typical microwave waveguide.

* 1000 km.

Perfectly Conducting Boundaries Isotropic/Planar Waveguide

For this waveguide, the reflection coefficients, given by Eqs. 5.7-6 and 5.7-7 (Section 5.7), become

$$R_e^g = R_e^i = 1 \text{ for TM modes}$$

$$R_h^g = R_h^i = 1 \text{ for TE modes}$$

For either TM or TE modes, the mode equation, Eq. 5.3-4, for the p^{th} mode, simplifies to

$$C_p = \cos\theta_p = \frac{p\pi}{k_0 h} = \frac{p\lambda_0}{2h} \tag{5.3-12}$$

The $p = 0$ mode has $C_p = 0$, $S_p = 1$, and $u_{p0} = u_0$. This ($p = 0$) is the *zeroth-order TM (TM_0) mode*, also called the *transverse electromagnetic TEM mode*. Note, from Eqs. 5.3-7a, that the electric and magnetic field vectors of the TEM mode are transverse to the direction of propagation. The phase velocity, u_{pp}, of the p^{th} TE or TM mode is given by

$$u_{pp} = \frac{u_0}{S_p} \tag{5.3-13}$$

It can be shown (Ref. 11) that the phase velocity of a mode is always higher than that in an unbounded medium having the same dielectric properties as those of the waveguide propagation medium.

An intuitive way of determining the phase velocity of a mode in a waveguide is by comparing the alternative ray path lengths travelled by the incident and reflected waves of the mode with the corresponding distance traveled by the mode signal along the guide direction. For example, in Fig. 5.3-4, we note that when the wave front of the plane wave moves from A to B in the wave propagation direction, it simultaneously travels through a distance EB along the guide. Since the wave velocity is u_0 along AB,

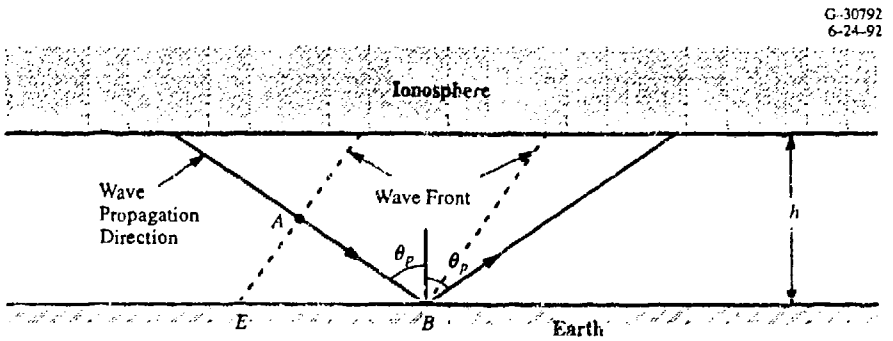

Figure 5.3-4 Phase Velocity and Wave Velocity Relationship Geometry

the phase velocity u_{pp} of the p^{th} mode signal is $u_0/\sin\theta_p$ ($= u_0/S_p$); it is the same expression as as Eq. 5.3-13. Note that the phase velocity of a mode is greater than the wave velocity u_0. Furthermore, as the mode index p increases, C_p (in Eq. 5.3-12) increases and thus S_p decreases, which causes the phase velocity (Eq 5.3-13) to increase with the mode index.

Note that Omega navigation is based on the assumption that received Omega signals are Mode 1 signals. It is the information on the relative phases, derived from the phase velocity of Mode 1, of the received signals which are needed to compute on Omega navigation position fix. However, in addition to the phase velocity, there is another velocity, called the *group* or *energy velocity*, which is the velocity at which the Omega signal wave-packet travels. The wave-packet is a series of approximately one-second-long pulses. Each of these pulses has characteristic rise and fall times. The time of detection of the leading edge of the pulse is determined by the group velocity of the signal. Once the signal pulse is established, about after 50–100 cycles the phase velocity of the received signal becomes the important parameter as it determines the phase of the received signal. The group velocity, u_{gp}, and phase velocity u_{pp}, of the p^{th} mode signal are related by (Ref. 19)

$$u_{gp} = \frac{u_0^2}{u_{pp}} \tag{5.3-14}$$

where u_0 is the velocity of light in an unbounded dielectric medium having the same dielectric properties as those of the waveguide propagation medium. The above relationship states that the group velocity is always less than or equal to the phase velocity which itself is always greater than or equal to u_0. In a non-dispersive medium (i.e., one where the phase velocity is independent of signal frequency), such as free-space, the phase velocity is the same as the group velocity of the signal.

Since the signal wavelength is proportional to the signal phase velocity, the *guide wavelength*, λ_{gp}, of the p^{th} mode in guide is given by

$$\lambda_{gp} = \frac{\lambda_0}{S_p} \tag{5.3-15}$$

Note that since $S_p < 1$, the guide wavelength of a mode is greater than the signal wavelength, λ_0.

Combining Equations 5.3-12 and 5.3-15 gives

$$\left(\frac{1}{\lambda_{gp}}\right)^2 = \left(\frac{1}{\lambda_0}\right)^2 - \left(\frac{p}{2h}\right)^2$$

which shows that for $\lambda_0 < \frac{2h}{p}$, λ_{gp} is imaginary and, hence, the mode associated with index p is evanescent.* There is a minimum *cut-off frequency*, f_{cp}, for the p^{th} mode, below which waves will not propagate in the waveguide. The cut-off frequency is

$$f_{cp} = \frac{pc}{2h} \tag{5.3-16}$$

where c is speed of light in free space.

The cut-off frequency for the mode with mode index $p = 1$ is, therefore, $f_{cp} = f_{c1} = c/2h$. Assuming, $h = 90$ km for the height of nighttime (D-layer) ionosphere boundary (see Section 5.2), we get $f_{c1} =$ 1.66 kHz indicating that $p = 1$ mode in this (90 km height) waveguide will not propagate below 1.66 kHz.

We will now illustrate the spatial dependence of the TM_1 mode of the example waveguide (i.e., perfectly conducting isotropic/planar waveguide). The instantaneous field expression for the TM_1 mode are obtained by: (1) substituting for C_p (Eq. 5.3-12) and S_p ($=1-C_p^2$) for the example waveguide in phasor field expressions of TM_p mode, Eq. 5.3-7a, (2) multiplying the resulting phasor expressions with the time dependence term, $\exp(i\omega t)$, and (3) taking the real part of the resulting product. Thus for p equal to one, we get

$$\begin{aligned} E_x(x,y;t) &= A_1 \sin\left(\frac{\pi z}{h}\right) \cos(\omega t - \gamma x) \\ E_z(x,y;t) &= \frac{\gamma h}{\pi} A_1 \cos\left(\frac{\pi z}{h}\right) \sin(\omega t - \gamma x) \\ H_y(x,y;t) &= \frac{-\omega\epsilon_0 h}{\pi} A_1 \cos\left(\frac{\pi z}{h}\right) \sin(\omega t - \gamma x) \end{aligned} \tag{5.3-17}$$

where

$$\gamma = \sqrt{k_0^2 - \left(\frac{\pi}{h}\right)^2} = \sqrt{\omega^2\epsilon_0\mu_0 - \left(\frac{\pi}{h}\right)^2}$$

$$A_1 = \frac{2i\pi}{\omega\epsilon_0}$$

---

*An evanescent mode is a *nonpropagating* mode with the fields decaying exponentially along the direction of the guide (Ref. 19).

Figure 5.3-5(a) illustrates the electric and magnetic field lines in the xy-plane at a fixed time. Note that the fields are independent of the y-coordinate as the waveguide is of infinite dimension along the y axis. The field lines in the waveguide repeat themselves for every one guide wavelength, λ_{g1}, change in distance along the waveguide and reverse their directions for every distance change of one-half the guide wavelength in the waveguide. The H field has only the y-component and its field lines are perpendicular to the xz-plane. The dots and cross inside the circles in the figure denote magnetic field lines are coming out of the paper (i.e., are along $+y$ direction) and going into the paper (i.e., they are along the $-y$ directions, respectively). The density of H_y lines vary as $\cos\left(\frac{\pi z}{h}\right)$ in the z-direction and as $\sin(\gamma x)$ in the x direction. In accordance with the boundary conditions, stated in Table 5.7-4 (Section 5.7), the H_y field lines induce surface currents and surface electric charge density at the waveguide conducting boundaries ($z = 0$ and $z = h$) of the waveguide. The z-dependence of the Mode 1 field components in the yz-planes at the points A and B along the guide is shown in Fig. 5.3-5(b). The entire field pattern moves along the $+x$ direction, with this so called phase velocity equal to ω/γ, as time elapses.

In summary, we note that at a perfectly conducting (i.e., $\sigma = \infty$) boundary of a waveguide, the electric field of the TM_1 mode is perpendicular to the boundary and the mode's magnetic field is parallel to the boundary (see Eq. 5.3-17). Similar TM_1 mode behavior occurs at a highly conducting boundary of a waveguide (i.e., $\sigma/\omega\varepsilon \gg 1$, see Section 5.2). Note that the lower boundary (the earth's surface) of the earth-ionosphere waveguide (which guides the propagation of Omega signals) is a highly conducting surface everywhere except over the permafrost and fresh water ice regions of the world. Therefore,

Figure 5.3-5 Electric and Magnetic Field Lines for TM_1 Mode Inside a Perfectly Conducting Parallel Plane Waveguide

electric field of an Omega signal (which is mostly the TM_1 mode) is nearly perpendicular, and its magnetic field is nearly parallel to the earth's surface everywhere in the world except over permafrost regions (in the northern part of Canada) and fresh-water regions (Greenland/Antarctica).

5.3.2 Geomagnetic Field Effects

Thus far in this section, we have analyzed and discussed the waveguide propagation environment free of the earth's magnetic field. Of course, the real-world EI waveguide has geomagnetic field which greatly influences the motion of the electrons in the *D*-region ionosphere, the upper boundary of the waveguide. As a result, the ionosphere appears as an anisotropic medium to a wave incident below the upper boundary. Consequently, the reflected and transmitted waves* from such an anisotropic boundary, as shown in Fig. 5.3-6, do not have the same wave polarization (i.e., orientation of the electric and magnetic fields of the wave; see Section 5.7-6) as the incident wave, but have elliptical polarizations which are independent of the incident wave polarization. An elliptically polarized wave (see Section 5.7.6) has electric field components both in the plane parallel (||) and perpendicular ($\perp$) to the plane of incidence (i.e., the plane perpendicular to the boundary which contains the incident wave propagation direction). To fully describe the reflection characteristics of an anisotropic ionosphere boundary relative

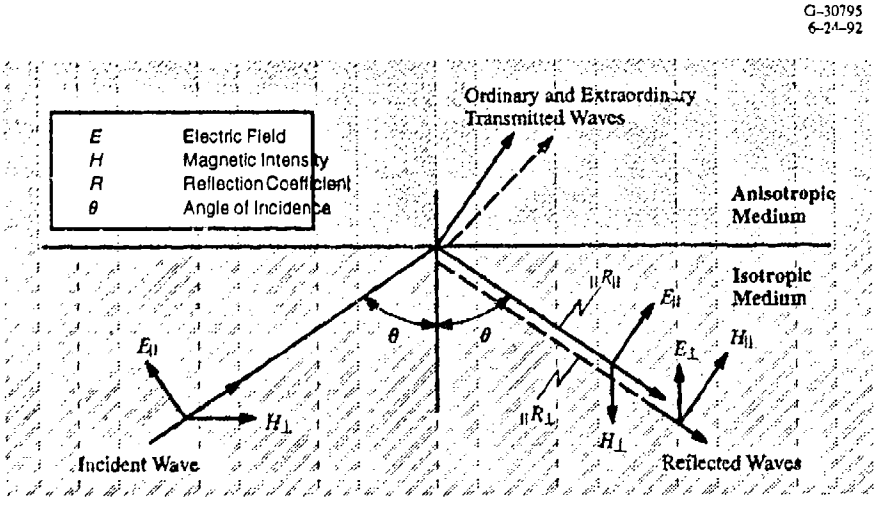

Figure 5.3-6 Incident, Reflected, and Transmitted Waves at Isotropic and Anisotropic Media Boundary

*For the case of isotropic medium, the reflecting and transmitted waves have the same wave polarization as the incident wave.

to an arbitrary polarized (linear, circular, or elliptical) incident wave, we need four reflection coefficients, instead of the two reflection coefficients ($_{\parallel}R^{i}_{\parallel}$ and $_{\perp}R^{i}_{\perp}$; See Section 5.7.7)* needed for an isotropic ionosphere. The reflection coefficients of an anisotropic ionosphere boundary are conveniently described by the following 2×2 matrix (Refs. 5 and 9)

$$\mathrm{R}^{i} = \begin{bmatrix} {}_{\parallel}R^{i}_{\parallel} & {}_{\perp}R^{i}_{\parallel} \\ {}_{\parallel}R^{i}_{\perp} & {}_{\perp}R^{i}_{\perp} \end{bmatrix} \tag{5.3-18}$$

The subscript on the left of reflection coefficient R^{i} indicates the parallel ($\parallel$) or perpendicular ($\perp$) polarization of the electric field of the associated incident wave; the subscript on the right of the reflection coefficient R^{i} indicates the parallel ($\parallel$) or perpendicular ($\perp$) polarization of the electric field of the reflected wave.

We will now determine the impact of allowing the upper boundary of the waveguide to be an anisotropic boundary due to the presence of the geomagnetic field. The resulting waveguide is henceforth called an anisotropic/planar waveguide. The mode equation for the anisotropic/planar waveguide is readily obtained by substituting§ the matrices R^{i} and R^{g} for R^{i} and R^{g}, respectively, in the isotropic/planar waveguide mode equation, Eq. 5.3-4. The resulting equation in the matrix notation is

$$\det \left\| \mathrm{R}^{g}\,\mathrm{R}^{i} - I \exp(-2i\pi p) \right\| = 0 \tag{5.3-19}$$

where "det $\| \|$" denotes the determinant of the quantity within the bars $\| \|$; I is a 2×2 identity matrix, and R^{g} is

$$\mathrm{R}^{g} = \begin{bmatrix} {}_{\parallel}R^{g}_{\parallel} & 0 \\ 0 & {}_{\perp}R^{g}_{\perp} \end{bmatrix} \tag{5.3-20}$$

On developing the determinant of Eq. 5.3-19, the mode equation becomes

$$\left({}_{\parallel}R^{g}_{\parallel}\ {}_{\parallel}R^{i}_{\parallel} - 1 \right)\left({}_{\perp}R^{g}_{\perp}\ {}_{\perp}R^{i}_{\perp} - 1 \right) - \left({}_{\parallel}R^{g}_{\parallel}\ {}_{\perp}R^{g}_{\perp}\ {}_{\parallel}R_{\perp}\ {}_{\perp}R_{\parallel} \right) = 0 \tag{5.3-21}$$

Note that the last term in the above equation is zero for an isotropic ionosphere boundary and the resulting equation is basically the same equation as the isotropic/planar waveguide mode equation, Eq. 5.3-4.

---

* Section 5.7.7 employs different notations for the reflection coefficients; specifically, $_{\parallel}R^{i}_{\parallel}$ and $_{\perp}R^{i}_{\perp}$ are denoted in Section 5.7.6 as R^{i}_{e} and R^{i}_{h}.

§ Note that the reflection coefficient of the earth's surface is not affected by the anisotropic nature of the ionosphere; the matrix representation for R^{g} in Eq. 5.3-19 is used for presentation convenience only.

As a consequence of the anisotropic ionosphere boundary, the mode solutions of the mode equation, Eq. 5.3-20, are no longer pure TE and pure TM modes but are *quasi-TE* and *quasi-TM* modes (Ref. 11). The electromagnetic fields of the quasi-TE and quasi-TM modes have relatively small longitudinal components (in the direction of wave propagation) which are not present in the case of pure TE and TM modes. The total signal in an anisotropic/planar waveguide is the mode-sum of the quasi-modes of the waveguide. Another consequence of the anisotropic ionosphere boundary of the waveguide is that the mode parameters (attenuation rate, phase velocity, excitation factor, and height-gain function) are dependent on signal propagation direction. This causes the so called east-west effect in the Omega/VLF signals, discussed in Section 5.4.

5.4 HOMOGENEOUS EI WAVEGUIDE

The inhomogeneous and anisotropic nature of the EI waveguide, coupled with its spherical geometry, makes it difficult to obtain an exact analytical solution to wave propagation in the waveguide. In the VLF literature, as mentioned Section 5.1, several analytical approaches have been proposed for obtaining approximate solutions to the problem. The most frequently used approaches are based on waveguide mode theory. Computational requirements of mode theory solutions limited the early application of the mode theory approaches to homogeneous EI waveguides such as, for example, a waveguide with an all day or all night ionosphere, and sea water for the earth's surface. Some of these approaches were later extended to mixed illumination waveguide (part day and part night) by considering the waveguide to be made of two homogeneous segments, one all day and the other all night (Ref. 5). With the availability of faster and less expensive computers, great strides have since been made to develop computationally efficient and accurate mode theory based approaches applicable to the EI waveguides with arbitrarily varying properties (Refs. 5, 12, and 20). These approaches usually partition the EI waveguide into a large number of "nearly" homogeneous segments and then determine waveguide-modes solution in each homogeneous segment, the individual segment solutions are then appropriately "connected" together to obtain signal propagation characteristics along the entire waveguide.

This section discussed the most frequently used mode theory based approach for determining VLF signal propagation characteristics in a homogeneous EI waveguide. This approach is extended in the next section to an inhomogeneous EI waveguide. Also, this section presents general relationships between the signal mode parameters and the signal path properties.

5.4.1 Signal Propagation Characteristics

The spherical geometry of the EI waveguide makes mode theory based VLF signal propagation prediction algorithms computationally cumbersome. However, reasonably accurate signal propagation predictions have been obtained using a first-order approximation for the spherical shell waveguide. In this approximation (Refs. 11 and 21), the spherical boundaries of the waveguide are replaced with flat boundaries and the refractive index of the propagation medium inside the waveguide (which is actually unity) is replaced by an artificial refractive index function which varies linearly with height above the earth's surface. We will consider below a parallel-plane approximation for the spherical waveguide boundaries.

Omega transmitting antennas are effectively electrically short vertical monopoles located at the earth's surface and they excite electric fields oriented mostly in the direction perpendicular to the earth's surface. Therefore, Omega-receiving antennas are either vertical electric dipoles (called whip or E-field antennas) which measure the vertical electric field, or loop antennas (called H-field antennas) which measure the horizontal component of the magnetic field. Note that the vertical electric field and horizontal magnetic field are components are of the same signal. Although, both E-field and H-field antennas measure the same signal, there are operational reasons (outside the scope of this chapter) for choosing one over the other type of receiving antenna.

We will therefore focus our discussion in this section to the reception of the vertical component of the electric field, from which the horizontal component of the magnetic field, if desired, can be readily obtained. Henceforth, in this chapter, for convenience, we will use *signal, signal field, field*, or *electric field* to mean the vertical component of the electric field of a propagating signal.

5.4.1.1 Total Signal -- Recall that a propagating signal in a waveguide can be described as a sum of the signals of the modes propagating in the waveguide. In general, an infinite number of modes can propagate. However, in practice, only a few lowest-order modes are needed to approximate a VLF signal, especially at Omega frequencies. If $E_{zm}(\varrho, z)$ is the signal of the m^{th} mode at radial distance ϱ from source (see Fig. 5.4-1) and at height z (above the earth's surface), the total signal E_z at ϱ and z, in general, is given by the "phasor-sum."

$$E_z(\rho) = \sum_{m=1}^{\infty} E_{zm}(\rho, z) \qquad (5.4\text{-}1)$$

Note that both E_{zm} and E_z are phasors, i.e., each has an amplitude and a phase and thus phasor algebra must be used in Eq. 5.4-1 (see Section 5.6).

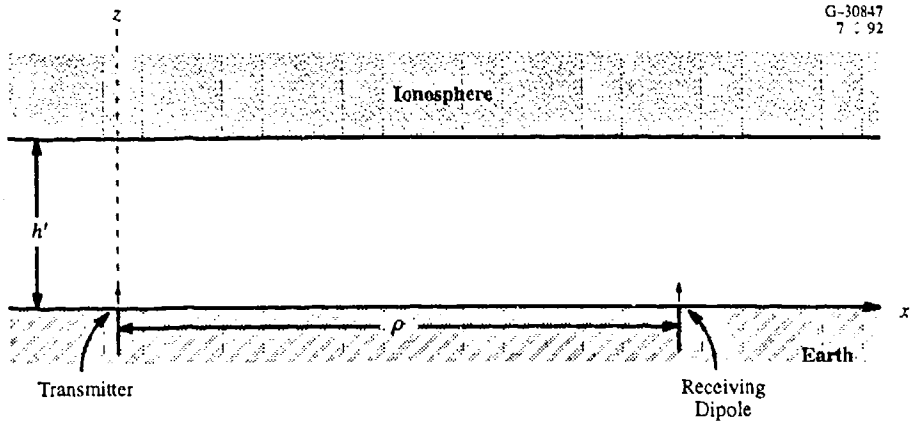

Figure 5.4-1 Homogeneous Earth-Ionosphere Waveguide

5.4.1.2 Individual Mode Signal — The mathematical steps involved in deriving the individual mode signal equation (Eq. 5.4-2) are tedious and can be found in Refs. 12 and 21. In a homogeneous and anisotropic EI waveguide, assuming the time dependence of the form exp ($i\omega t$), the signal field E_{zm} at a distance ϱ from the source and a height z is given by

$$E_{zm}(\rho,z) = \frac{-\eta_0 p_e f^{1/2} S_m^{3/2} A_{zm} G^r_{zm}(z) \exp(-\alpha_m \rho - i\gamma_m \rho)}{c^{1/2} h' (a \sin \rho/a)^{1/2}} \qquad (5.4\text{-}2)$$

where

η_0 = Characteristic impedance of free space

p_e = Current moment = $I_0 \ell_0 = (\lambda_0/40\pi)\sqrt{10P_r}$

I_0 = Source current magnitude

ℓ_0 = Length of the source dipole

P_r = Radiated power

f = Signal frequency

$G^r_{zm}(z)$ = height-gain function of the z-component of the electric field of the m^{th} mode evaluated at the receiver location (ϱ,z)

S_m = $\sin \theta_m$

θ_m = Complex angle (eigenvalue) of the m^{th} mode

c = Velocity of light in free space

h' = Reference height of the ionosphere reflecting boundary

a = Earth's radius

A_{zm} = Excitation factor of the z-component of the field of the m^{th} mode excited by the source (transmitter antenna)

$$\gamma_m = \frac{-2\pi f}{c}\left(1 - \frac{c}{u_m}\right)$$

$u_m = c/[K\ \{\ \mathrm{Re}\ (\sin\theta_m)\ \}\ ]$ = Phase velocity of the m^{th} mode at the earth's surface

$\alpha_m = Kk_0\ \{\ \mathrm{Im}\ (\sin\theta_m)\ \}$ = Attenuation rate of the m^{th} mode at the earth's surface

$k_0 = 2\pi/\lambda_0$

λ_0 = signal wavelength in free space

$K = [1-(h'/a)]^{-1}$

$[a \sin(\varrho/a)]^{-1/2}$ = Spherical spreading factor

Note that Re ( ) and Im ( ) are the real and imaginary parts, respectively, of the complex quantity inside the parentheses ( ).

We will now discuss the following items related to the signal field equations (Eqs. 5.4-1 and 5.4-2): mode parameters, waveguide modes, phasor-sum, and spreading factor.

Mode Parameters — The signal propagation characteristics of a mode signal are fully characterized by the four mode-specific parameters. These parameters have been described earlier in context of an isotropic waveguide in Section 5.3; they are briefly reviewed below:

Attenuation rate (α) — the spatial rate at which a mode signal dissipates (reduces) its energy in the waveguide.

Phase velocity (u) — the spatial velocity at which a mode signal wave front appears to propagate in the waveguide.

Excitation-factor (A_n) — a measure of relative efficiency with which a mode signal is excited in the waveguide by a source or received by an antenna in the waveguide; it is a complex quantity.

High-gain function ($G_n(z)$) — the variation of a mode signal field in the vertical (z) direction above the earth's surface.

In Section 5.4.3, the terms "phase velocity" and "phase velocity variation" mean the same thing. Mathematically, the phase velocity variation, Δu, is related to the phase velocity, u, by

$$\Delta u = \left(\frac{u}{c} - 1\right)\left(\frac{100}{\lambda_0}\right) \tag{5.4-3}$$

Δu has units of centicycles* per megameter of the signal path length. Thus, the two terms are related to each other via the constants: speed of light in free space, c, and the signal wavelength, λ_0). Δu is called the phase velocity variation because it is a measure of the variation of u from the free-space speed of light, c.

Waveguide Modes — In a waveguide, the modes are numbered with an integer mode index which increases according to the increasing value of the phase velocity of the modes in the waveguide. In this type of mode-numbering system, TM and TE modes are the even- and odd-numbered modes, respectively, of the waveguide, and Mode 1 is the lowest phase velocity TM (i.e., TM_1) mode. Mode 1 usually has the lowest attenuation rate and highest excitation factor amplitude; as a result, it is usually the strongest amplitude mode in an Omega signal.

Therefore, except in the "near-field" region of an Omega transmitting station and for paths with certain properties, Omega signals are adequately approximated by their Mode 1 components. It is this approximation feature which has made Omega navigation practical. The near-field region of a station typically extends from the station up to radial distances of 1000 km during day, and 2000 km at night. As will be seen in Section 5.4.3, certain nighttime paths with westerly-directed segments located at the lower geomagnetic latitudes exhibit signals which are not well-approximated by the Mode 1 component of the signal.

In the near-field region and along the special paths referred to above, 2–4 modes are usually needed to approximate an Omega signal. Omega navigation is therefore not recommended in the near-field as well as along the special paths. The number of modes needed for adequate signal approximation increases as the signal frequency increases; for example, typically 6–12 modes are needed to approximate a signal at twice the Omega frequency.

Phasor-Sum — An example of the phasor-sum of a multi-mode signal is shown in Fig. 5.4-2. For simplicity, the signal is assumed to be composed of two modes (Modes 1 and 2) whose signal field

*A centicycle (cec) is one-hundredth of a cycle.

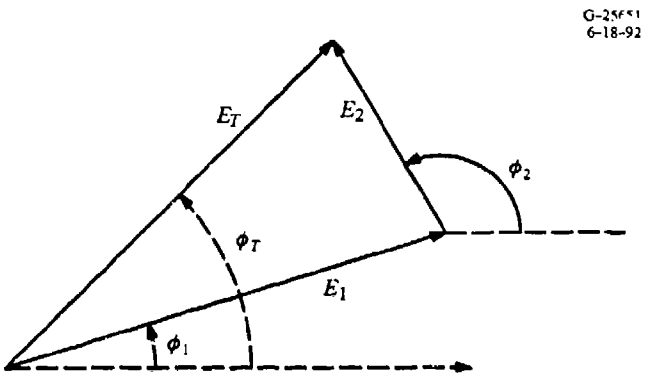

Figure 5.4-2 Example of Phasor Sum of the Signals: $E_1 \angle \phi_1$ and $E_2 \angle \phi_2$

phasors* are $E_1 \angle \phi_1$ and $E_1 \angle \phi_2$. Assuming the amplitude and phase of each mode (i = 1,2) signal are E_i and ϕ_i, respectively, the amplitude, E_T and phase, ϕ_T, of the total (mode-sum) signal are given by the phasor-sum expressions

$$E_T = \left[E_1 + E_2 + 2E_1E_2 \cos \phi\right]^{1/2}$$

$$\phi_T = \tan^{-1}\left[\frac{E_1 \sin \phi_1 + E_2 \sin \phi_2}{E_1 \cos \phi_1 + E_2 \cos \phi_2}\right] \qquad (5.4\text{-}4)$$

$$\phi = \phi_1 - \phi_2$$

When the signal is composed of many higher-order modes (e.g., Mode 2 and Mode 3, etc.), the phasor $E_2 \angle \phi_2$ can be thought as the phasor-sum of these higher-order modes.

Signal Spreading Factor — The spherical spreading factor, $[a \sin (\varrho/a)]^{-1/2}$, in the signal field equation, Eq. 5.4-2, is a direct consequence of the spherical geometry of the EI waveguide. The factor is correct everywhere except in the vicinity of the source as well as near the source antipode (i.e., the point geometrically opposite to the source on a spherical earth). A suitable approximation for the factor near the antipode can be found in Ref. 10.

The signal spreading causes the so-called "signal focusing;" we will present a heuristic explanation of the effect of the factor for the case of a homogeneous waveguide, in the absence of the geomagnetic field (Ref. 22). In such a waveguide, as the signal leaves the source (transmitter), it propagates outward from the source in circular wave fronts, as shown in Fig. 5.4-3. Note in the figure that as the

*The phasor notation $E_1 \angle \phi_1$ indicates a signal with amplitude E_1 and phase ϕ_1.

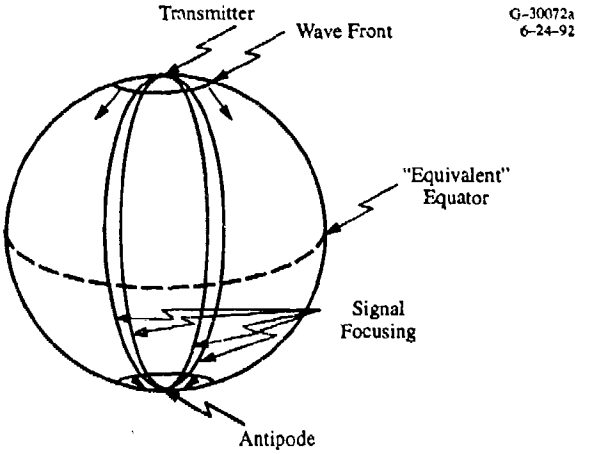

Figure 5.4-3 Propagation of Omega Signals on a Homogeneous, Isotropic Spherical Earth

wave fronts travel outward, they become larger and larger until they reach the "equivalent equator" (the equator corresponding to a source at the North or South Pole). At this point the signal energy per unit length of the wave front (due purely to geometry) is a minimum. Beyond the equator, the wave fronts diminish in size and the wave front energy density grows until the wave front converges at the source antipode. This increase in the wave front signal energy between the source equator and the source antipode leads to *signal focusing*.

The wave fronts, shown in Fig. 5.4-3, are circular only because we assumed homogeneous and isotropic signal propagation environment. In reality, however, the wave fronts are substantially non-circular, due to Anisotropy and inhomogeneity of the ionosphere and the non-uniform distribution of the earth's surface conductivity. This means that the total signal does not re-focus at a point (the source antipode), but in a more complex fashion, with a much smaller peak for the signal amplitude than at the source. An example of the signal focusing effect can be seen in Fig. 5.5-3 in Section 5.5.5.

5.4.2 Mode Signal Characteristics

This subsection first presents in graphical form general characteristics of selected Omega signal mode parameters as functions of the signal path properties (see Figs. 5.4-4 through 5.4-11). Following a discussion of the graphs, a broad summary of the general characteristics is presented.

The graphs are provided for the mode parameters: attenuation rate, phase velocity, and excitation factor amplitude. The phase velocity mode parameter is presented in two forms: (1) phase velocity variation (cec/Mm) in Fig. 5.4-5, which is $[(u/c)-1]\,(100/\lambda_0)]$ where u is the mode phase velocity, c is the

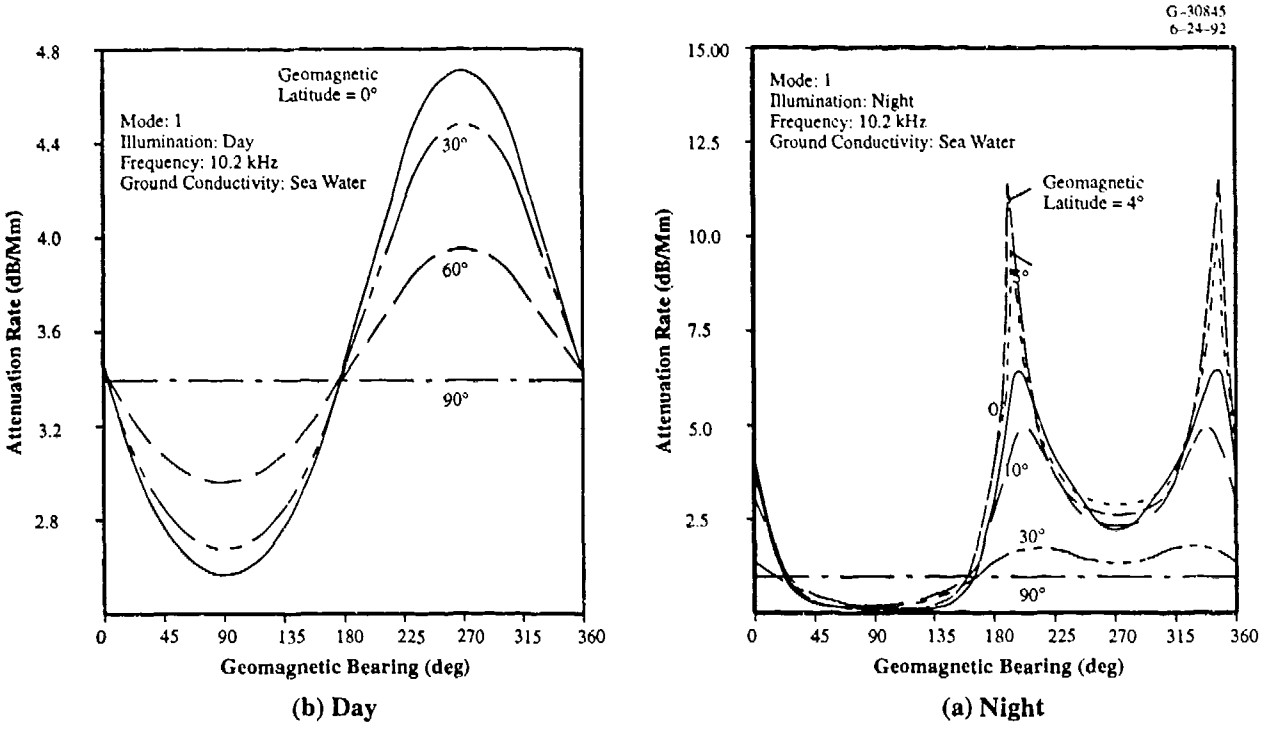

Figure 5.4-4 Mode 1 Attenuation Rate vs. Geomagnetic Bearing: Day and Night (Ref. 23)

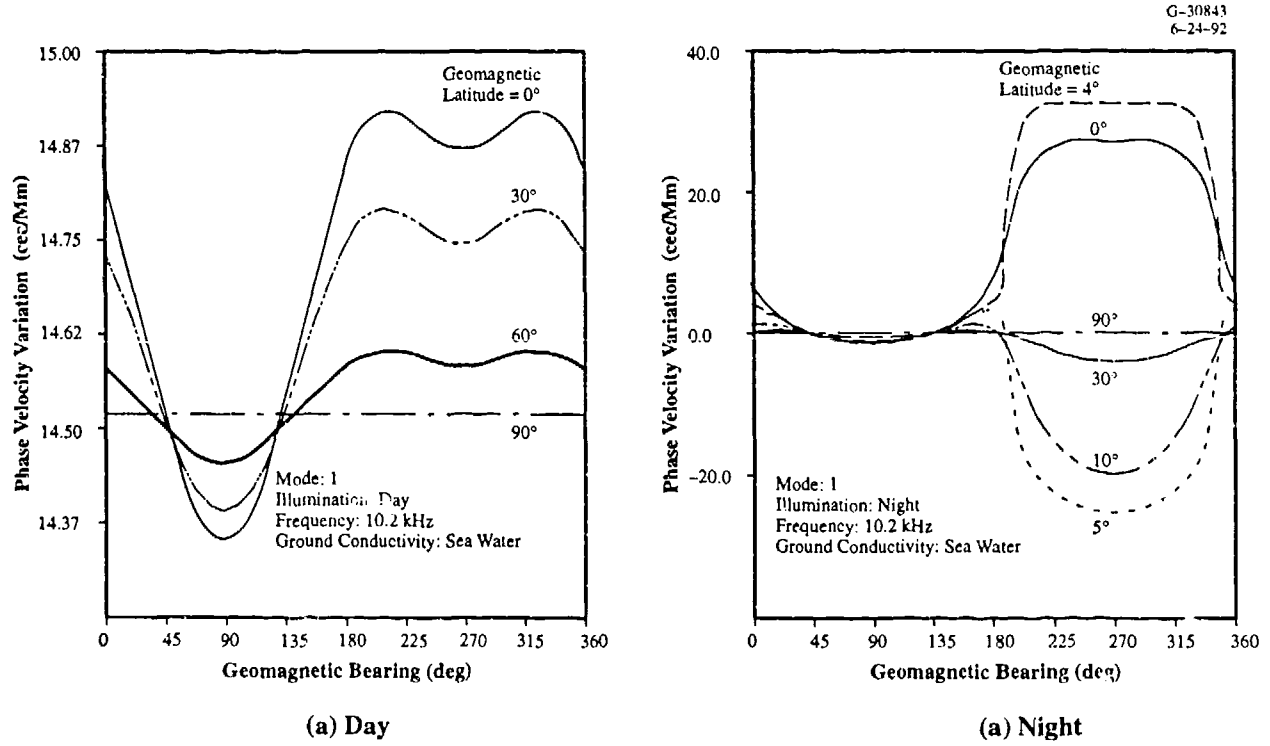

Figure 5.4-5 Mode 1 Phase Velocity Variation $[(u/c - 1)\ 100/\lambda_0]$ vs. Geomagnetic Bearing: Day and Night (Ref. 23)

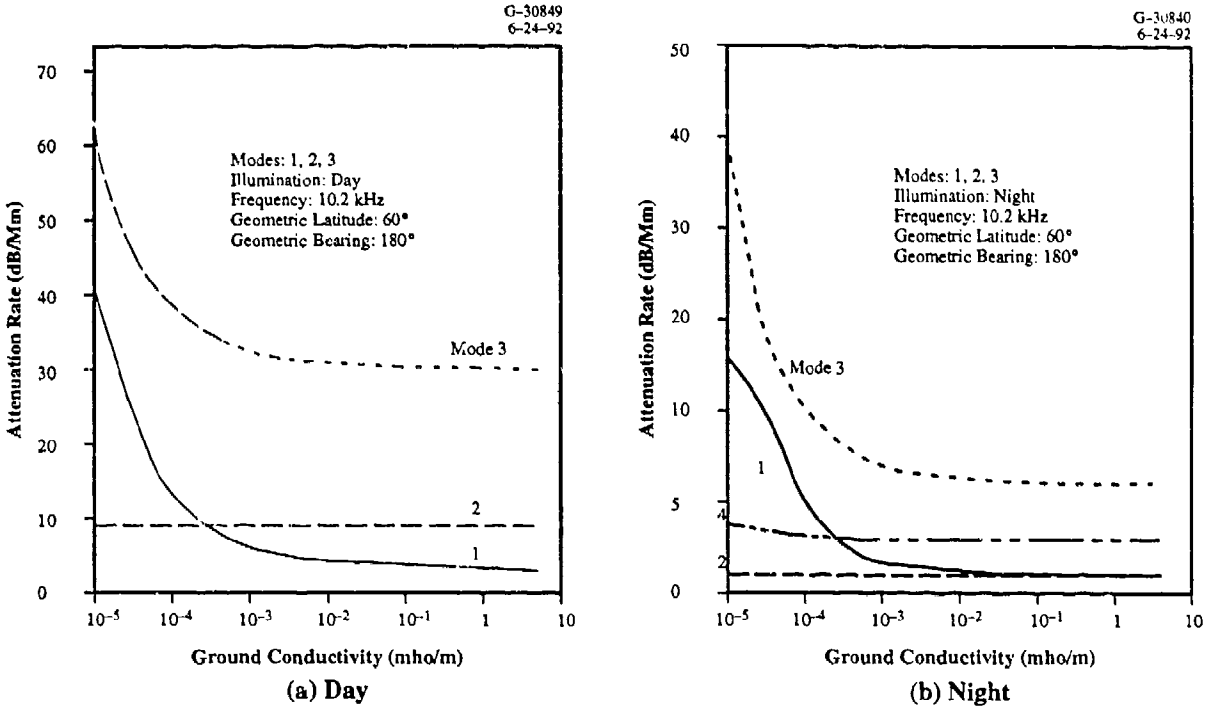

Figure 5.4-6 Attenuation Rate vs. Ground Conductivity: Daytime and Nighttime Modes (Ref. 23)

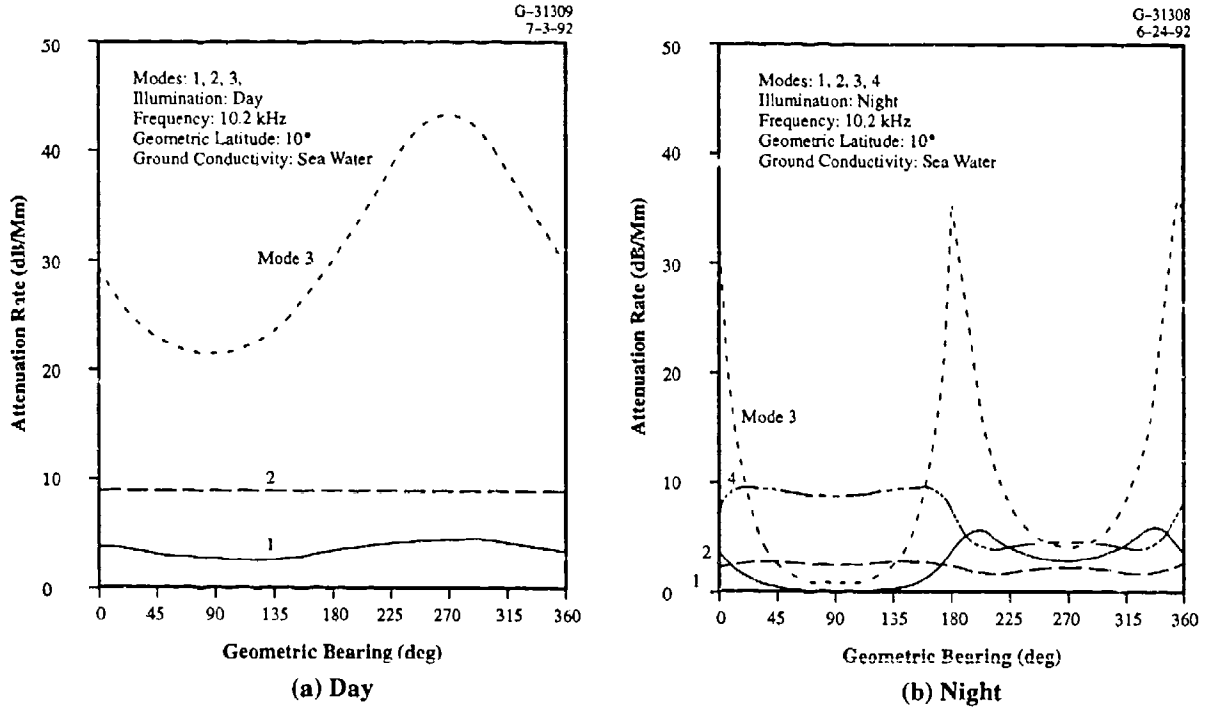

Figure 5.4-7 Attenuation Rate vs. Geomagnetic Bearing: Daytime and Nighttime Modes (Ref. 23)

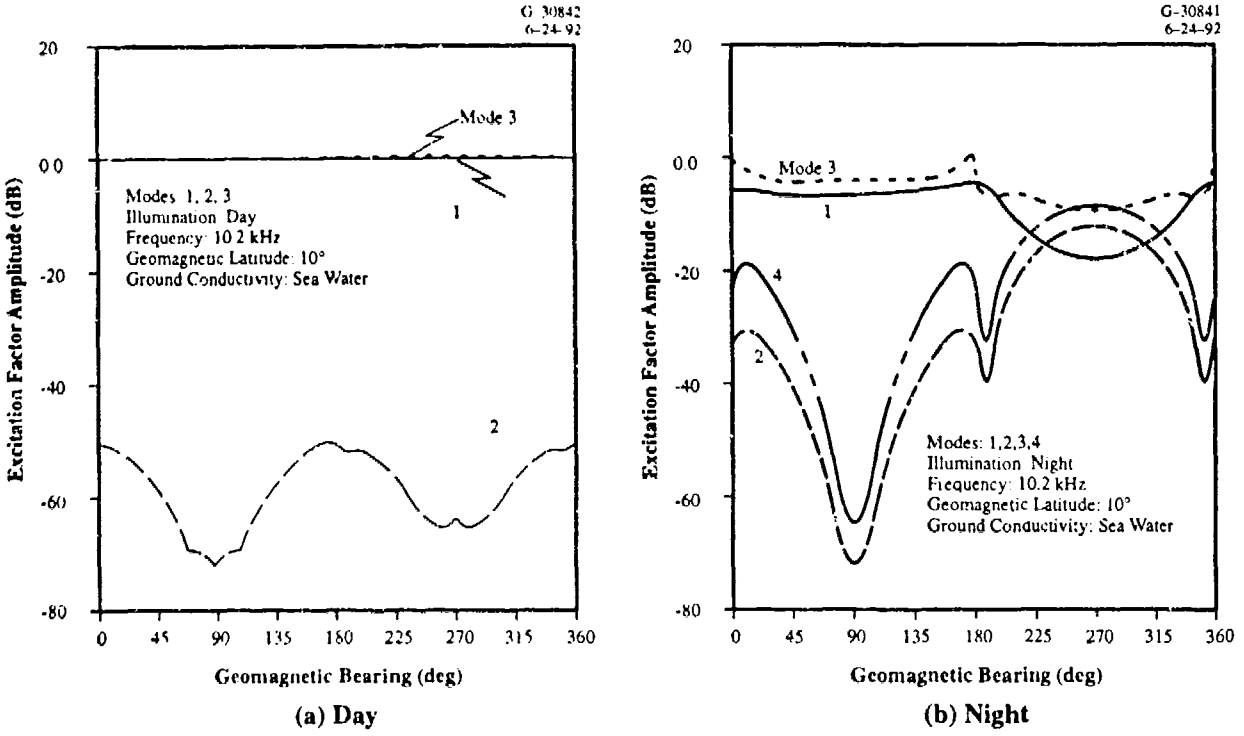

Figure 5.4-8 Excitation Factor Amplitude vs. Geomagnetic Bearing for Daytime and Nighttime Modes (Ref. 23)

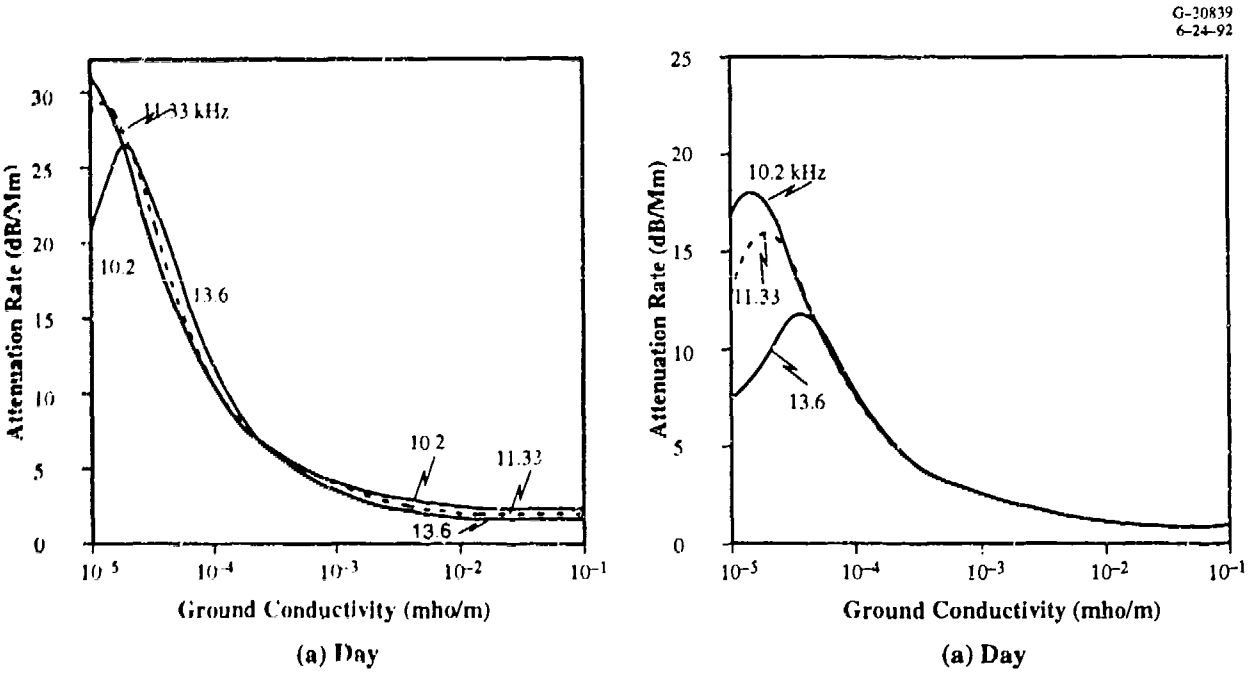

Figure 5.4-9 Daytime and Nighttime Mode 1 Attenuation Rate vs. Ground Conductivity: 10.2, 11.33, 13.6 kHz (Ref. 24)

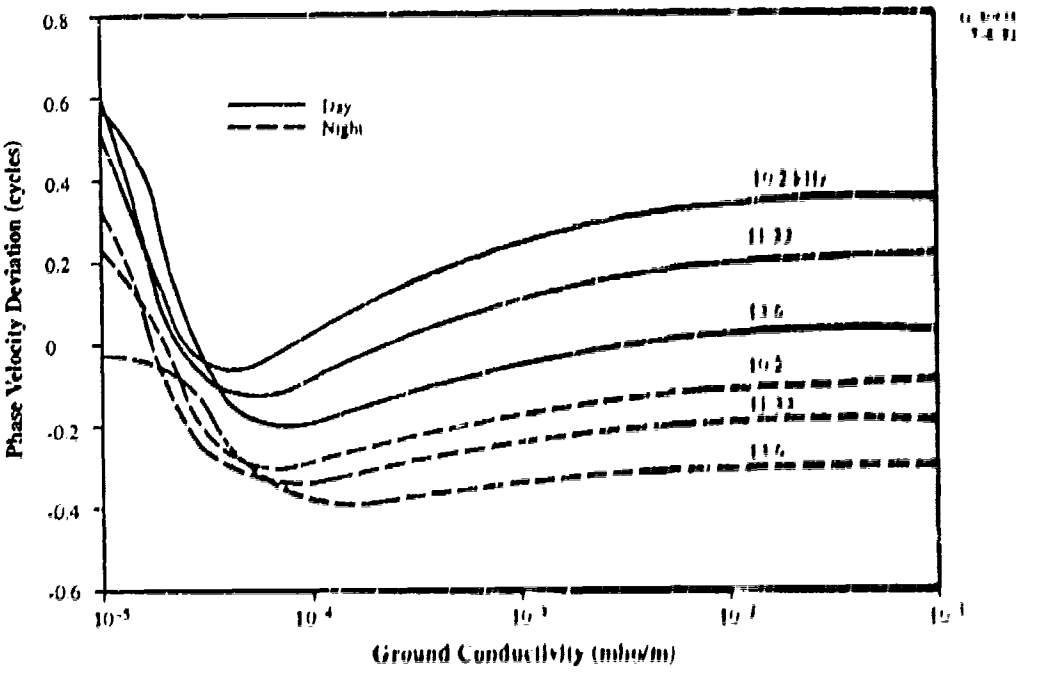

Figure 5.4-10 Daytime and Nighttime Mode 1 Phase Velocity Deviation (m/s − 1) vs. Ground Conductivity: 10.2, 11.33, 13.6 kHz (Ref. 24)

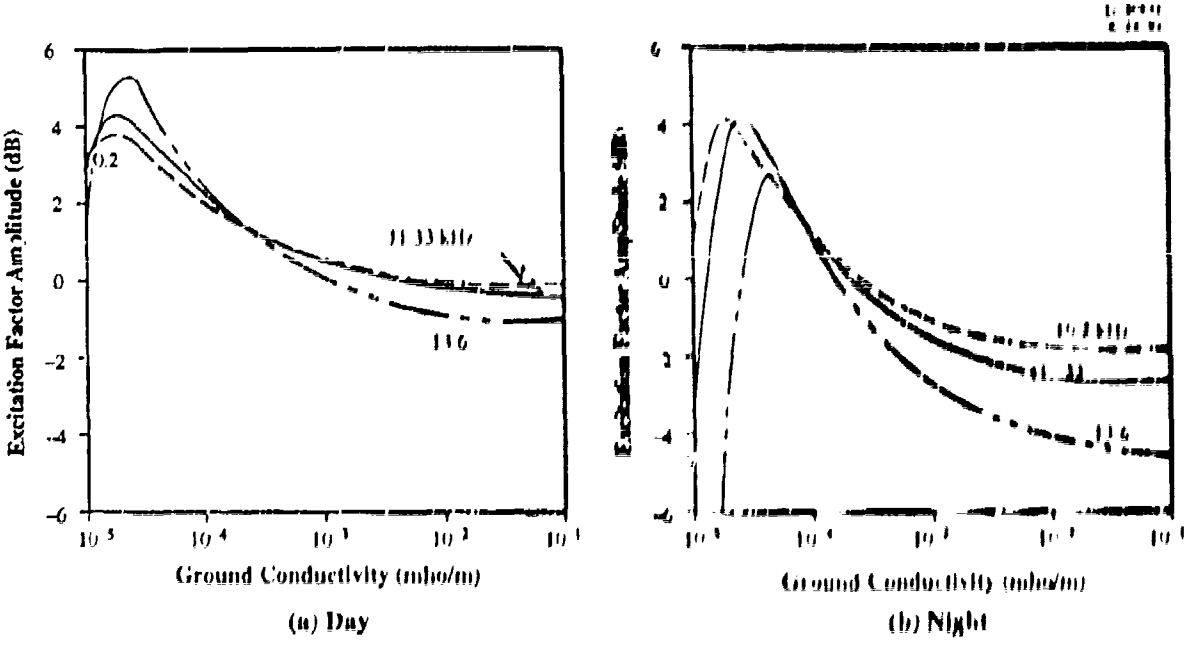

Figure 5.4-11 Mode 1 Excitation Factor Amplitude vs. Ground Conductivity 10.2 11.33, 13.6 kHz (Ref. 24)

speed of light in free space, and λ_0 is the signal wavelength in free space, and (2) phase velocity deviation (see) in Fig. 5.4-5, which is the phase velocity variation multiplied by the signal wavelength.

No plots are included for the height gain function mode parameter, as it exhibits the classical height dependence of antennas over a highly conducting ground, it is unity for all modes on the ground and is near unity for heights up to 10 km. The plots are given for mostly 10.2 kHz signal modes, as the mode parameters exhibit generally similar behavior at other Omega frequencies. Also, the plots are shown for mostly Mode 1, as Omega signals at most locations and times are Mode 1 dominated signals. Plots are provided for the day (solar zenith angle, χ, between 0 and 90 deg) and night ($\chi \geq 99$ deg) illumination conditions.

In the plots, the ionosphere is assumed to be characterized by an exponential ionospheric conductivity profile (see Eq. 5.2-1) with a reference reflection height, h', and a conductivity gradient, β. The h' values in the plots range from 70 to 74 km in the day time and 87 to 90 km at night, the β values are 0.3 km^{-1} in the day time and from 0.3 to 0.5 km^{-1} at night. The ground conductivity values in the plots range from the high value of 4 mho/m (sea water) to the very low value of 10^{-5} mho/m (ice cap such as in Greenland/Antarctica and northern parts of Canada). Recall that the in between conductivity values correspond to: 10^{-2} mho/m for damp soil, 10^{-3} mho/m for fresh water lakes and dry soil, and 3×10^{-4} – 10^{-4} mho/m for the permafrost region (see Table 5.2-1).

In the plots, the influence of the geomagnetic field is shown by its two parameters, the geomagnetic latitude (0–90 deg) and geomagnetic bearing (0–360 deg). Note that the mode parameter characteristics are symmetric in geomagnetic latitude about the geomagnetic equator. To relate geographic latitudes/longitudes to geomagnetic latitudes, Fig. 5.4-12 shows an overlay of geomagnetic latitude contours (with a earth centered magnetic dipole field) over a geographic Mercator projection of the world. The odd and even numbered modes in the plots are the TM (transverse magnetic) and TE (transverse electric) modes of the EJ waveguide. Furthermore, note that Mode 1 (the lowest order TM mode) is the mode of interest for Omega navigation.

Based on a review of the published mode characteristics information (Refs. 23 through 25), including the plots presented herein (Figs. 5.4-4 through 5.4-11), the influence of the various path properties on Omega signal mode parameters can be broadly summarized as follows:

Ground Conductivity Effects

- For common ground conductivities (between 10^{-3} and 4 mho/m), higher order modes are more heavily attenuated than lower order modes (see Fig. 5.4-6), which allows them to be neglected in signal computations, especially for long paths.

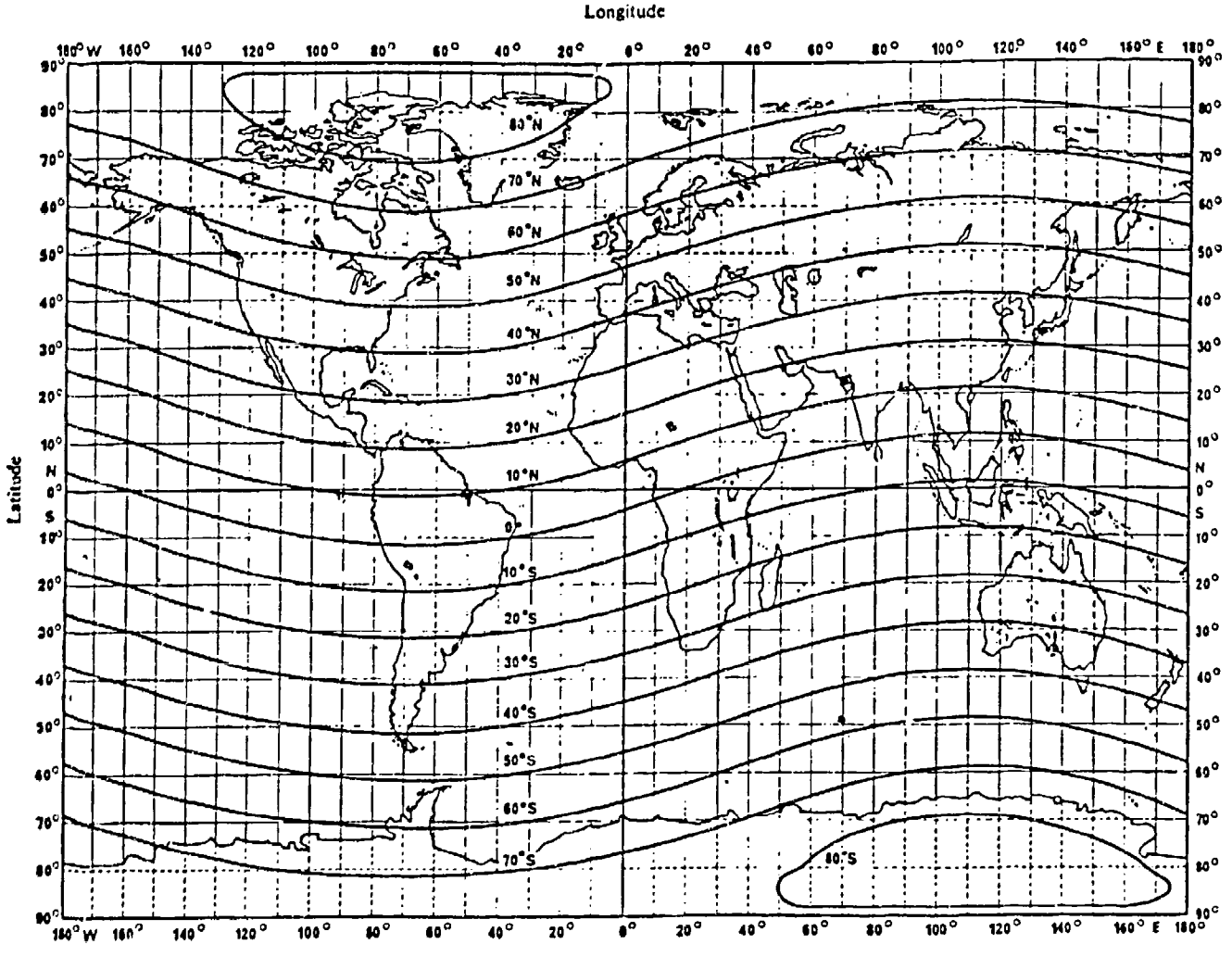

Figure 5.4-12 Geomagnetic Latitude Contours (Ref. 5)

- TE mode attenuation rate is virtually independent of the ground conductivity.
- TM modes have generally lower attenuation rates than TE modes for most common ground conductivities, but have higher attenuation rates over low-conductivity regions such as in Greenland/Antarctica and much of Canada (see Fig. 5.4-6).
- TM mode attenuation rates increase with decreasing ground conductivity and exhibit a broad maximum near the pseudo-Brewster angle (see Section 5.7) on the ground and then decrease with further decrease in the conductivity; the pseudo-Brewster angle peak occurs at higher conductivity values for higher frequencies (see Fig. 5.4-9, and Refs. 31 and 32). For example, at 10.2 and 13.6 kHz, the mode attenuation rate peak occurs over the conductivity range of 3×10^{-5} — 10^{-5} mho/m (fresh-water ice) and 3×10^{-4} — 10^{-4} mho/m (tundra), respectively.

- For common ground conductivities, excitation factor amplitude is usually higher for TM modes than for TE modes (see Fig. 5.4-11); as a result, Omega transmitting antennas excite TM modes much more strongly than TE modes. Within categories of TE and TM modes, higher-order modes are excited more strongly than lower-order modes.
- For common ground conductivities, phase velocity of modes usually decreases as conductivity decreases (Refs. 23 and 25).

Geomagnetic Field Effects

- During the daytime, parameters of all modes show little variation with geomagnetic latitude or path azimuth (see Figs. 5.4-4 through 5.4-11).
- At night, parameters of all modes show little geomagnetic latitude variation for easterly path azimuths, but a strong latitudinal variation for westerly path azimuths (see Figs. 5.4-4 through 5.4-11).
- Attenuation rate of most modes is usually greater for west than east (see Figs. 5.4-4, and Refs 31 and 32), the "east-west effect."
- Mode parameters of TM modes exhibit a reversal in their usual trends for the westerly path azimuths over a small band of geomagnetic latitudes around the geomagnetic equator (see Figs. 5.4-4, 5.4-5, and Refs. 31 and 32), for example, see Fig. 5.4-5(b) for the reversal in the phase velocity trend over the latitudes between 0 and 4 deg.

Mode 1 Frequency Dependence*

- For common ground conductivities, attenuation rate, phase velocity, and excitation factor amplitude usually decrease with increasing frequency (see Figs. 5.4-9 through 5.4-11).
- For low ground conductivities (i.e., conductivities between 10^{-5} and 4×10^{-4} mho/m), frequency dependence trends of mode parameters are mixed (see Figs. 5.4-9 through 5.4-11).

Ionospheric Effects

- TM modes are generally more strongly excited (higher excitation factor amplitude) than TE modes (see Fig. 5.4-8).
- Attenuation rates of most modes for easterly paths azimuths are higher during the day than at night (see Figs. 5.4-4 and 5.4-7).

---

*Over Omega signal frequencies.

- Attenuation rate and excitation factor amplitude of Mode 1 are higher for easterly path azimuths during day than at night, for westerly azimuths, the night values may be higher than the day values (see Fig. 5.4-4).
- Phase velocity of Mode 1 is generally higher during the day than at night (see Fig. 5.4-4).

The mode parameter characteristics for the transition illumination condition are generally somewhere between the day and night characteristics.

5.5 INHOMOGENEOUS WAVEGUIDE

5.5.1 Signal Field Equation

VLF signal propagation characteristics in an inhomogeneous waveguide, as alluded to in Section 5.4.1, can be obtained by approximating the waveguide as a concatenation of nearly homogeneous segments. Each segment is assigned path properties each of which is uniform along the segment and is the average value of the property along the segment. As a result, the path properties along the approximated waveguide undergo step changes at each of the interfaces between the homogeneous segments. The signal propagation characteristics along the approximated waveguide can then be conveniently obtained by applying the following three-step approach.

1. Solve the mode equation, Eq. 5.3-21, for the eigenvalues of the selected modes in each homogeneous segment and determine the corresponding mode parameters from the eigenvalues as per discussions in Section 5.4.2.
2. Express the total signal in each segment as a phasor sum of the signals of the selected modes, as per Eq. 5.4-1.
3. Obtain the signal propagating in the approximated waveguide by "connecting" the neighboring segment signal fields to account for the effects of mismatch in the path properties at the segment interfaces.

In Step 2, it is adequate to select the first two (and four) lowest order modes for day (and night) segments, as the higher order modes are attenuated much more rapidly than the selected modes. The segment properties mismatch at an interface causes the incident signal to scatter at the interface, i.e., the signal is reflected and transmitted at the interface. The presence of reflected signals is ignored in VLF signal computations as these signals are relatively much smaller than the incident or transmitted signals. Ignoring the presence of reflected signals, the mismatch in the path properties at an interface results in the incident signal energy being carried by modes whose eigenvalues differ from those of the incident

signal; as a result, the relative distribution of the signal energy among the component modes is different for the incident and transmitted signals at an interface. This phenomenon is known as *mode conversion (*or *scattering)* of signal.

A conceptual illustration of the mode conversion occurrence at an interface between the neighboring segments (1) and (2), with dissimilar path properties, is shown in Fig. 5.5-1. In this illustration, the incident and transmitted signals are assumed to be composed of Modes 1 and 2 only, and reflected signals are assumed to be zero. E_k^i and E_k^t $(k = 1,2)$ are the complex (phasor) values of the incident (i) and transmitted (t) mode signals associated with k^{th} mode at the interface; S_{jk}, is the complex mode conversion (or scattering) coefficient which is the ratio of the amplitude of j^{th} mode of the transmitted signal and the amplitude of k^{th} mode of the incident signal. Note, in Fig. 5.5-1, that as a result of the mode conversion, the relative energy distribution between Modes 1 and 2 of the transmitted signal is different than those of the incident signal.

For signal paths where the path properties are such that the mode eigenvalues vary slowly along the waveguide, the mode conversion effects at the segment interfaces are usually negligible and can be ignored. That is to say $S_{jk} \approx 0$ for $j \neq k$ in Fig. 5.5-1. In other words, there is no significant exchange (re-distribution) of energy among the modes at the mismatch interface. It is therefore reasonable to compute signal field along such an inhomogeneous waveguide using the homogeneous waveguide signal field equation, Eq. 5.4-2, with the use of the "average values" for both the attenuation rate and phase

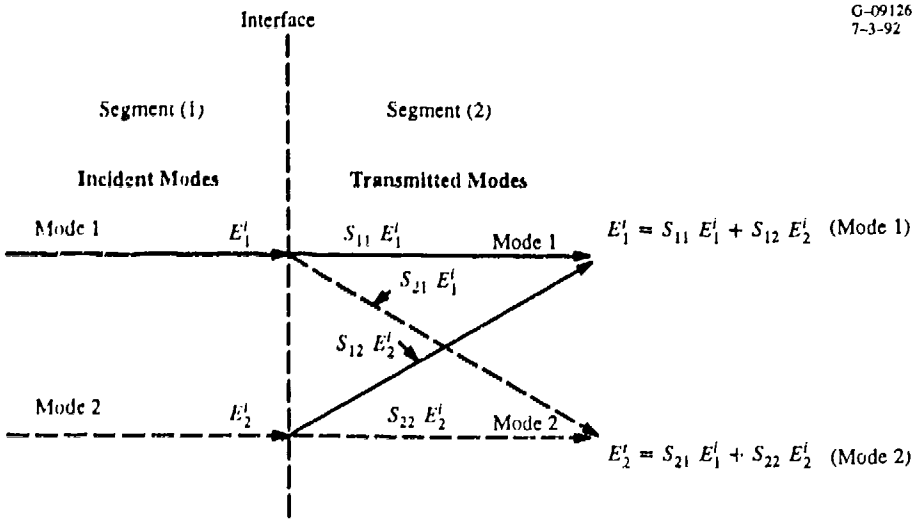

Figure 5.5-1 Mode Conversion Phenomenon Occurrence in a Two-Mode Signal (Reflected Modes are Not Shown)

velocity of the individual mode signals. That is, for a waveguide composed of N homogeneous segments each of $\Delta\varrho$ in length, the average attenuation rate, α_m, and average phase parameter, γ_m, of the m^{th} mode are

$$\alpha_m = \frac{1}{\varrho}\left[\sum_{n=1}^{N} \alpha_{mn}\,\Delta\varrho\right]$$

$$\gamma_m = \frac{1}{\varrho}\left[\sum_{n=1}^{N} \gamma_{mn}\,\Delta\varrho\right]$$

where α_{mn} and γ_{mn} are the attenuation rate and phase parameter, respectively, of the m^{th} mode along the n^{th} segment.

Furthermore, the transmitter and receiver locations may have different path properties, including the ionospheric reflection height which may be different due to differing solar illuminations at the locations. Therefore, the excitation term, A_{zm}, and the ionospheric reflection height, h', in the homogeneous waveguide signal equation, Eq. 5.4-5, must be modified to include the effects of both the transmitter and receiver locations properties on the excitation factor and waveguide height, as described below (Refs. 7 and 8):

$$A_{zm} \quad \text{Replaced by} \rightarrow \sqrt{A^t_{zm}\,A^r_{zm}}$$

$$h' \quad \text{Replaced by} \rightarrow \sqrt{(h')^t\,(h')^r}$$

where the superscript t and r refer to the transmitter and receiver locations, respectively. The result is a WKB*-type approximation (Refs. 5 and 21) signal field equation given below for the m^{th} mode of the signal propagating along the inhomogeneous waveguide:

$$E_{zm}(\varrho,z) = \frac{-\eta_0\,p_e\,f^{1/2}S_m^{3/2}(A^t_{zm}\,A^r_{zm})^{1/2}G^r_{zm}(z)}{c^{1/2}[(h')^t(h')^r]^{1/2}\left[a\,\sin\,(\varrho/a)\right]^{1/2}}\,\exp\left\{\sum_{n=1}^{N}\left[-(i\,\gamma_{mn}-\alpha_{mn})\,\Delta\varrho\right]\right\} \quad (5.5\text{-}1)$$

The total signal in the inhomogeneous waveguide is determined by the phasor-sum of the individual mode signals, as described by Eq. 5.4-1.

*Wenzel-Kramers-Brillouin.

For paths where mode eigenvalues are expected to change greatly along the waveguide, the signal cannot be adequately calculated using the WKB approximation. For such paths, mode conversion effects must be included in the signal calculations. Examples of greatly changing mode eigenvalues are:

1. At the sunset or sunrise terminator crossing along a path where the ionospheric properties change greatly
2. An abrupt change in ground conductivity along a path, such as from sea water to ice
3. Along nighttime, westerly-directed (path azimuth between 180 and 360 deg) segments located inside the geomagnetic equatorial belt (i.e., between ± 10 deg of geomagnetic equator).

We will now illustrate in Fig. 5.5-2, the spatial variations of the daytime and nighttime mode parameters and associated resultant signals along the signal path from the Hawaii Omega station to Guam. For the example path, both the daytime and nighttime signals are assumed to be composed of the first two lowest-order modes: Mode 1 (TM_1 mode) and Mode 2 (TE_1 mode). In the figure note that, as expected: (1) for each path illumination condition, Mode 1 has the lowest attenuation rate as well as lowest phase velocity, and (2) Mode 2 (higher-order mode) is excited relative to Mode 1 less strongly in day, and more strongly at night. In this example, the mode parameters vary slowly along the path. However, in general, they can vary greatly depending upon the path properties. For the example path, the total signal is basically Mode 1 during day; while, at night it is mostly Mode 2 for up to distances of about 2 megameters from the station, when it changes to the combination of Modes 1 and 2. The signal amplitude/phase vary gradually with distance during day but they exhibit oscillatory behaviors during night. The oscillatory behavior is due to "modal interference" phenomenon discussed in the next subsection.

5.5.2 Modal Interference

An Omega signal, as previously mentioned, consists of many modes. Except along paths with certain properties, and those inside the near-field region of the station, the signal amplitude along most paths at most times is dominated by the signal's Mode 1 component. The resulting signal is referred to as a Mode 1 dominated signal. In other words, the Mode 1 amplitude is much stronger than the amplitude of the phasor-sum of the higher-order modes (e.g., Mode 2, Mode 3, etc.) and thus the presence of the higher-order modes in the signal can be effectively ignored without any noticeable error in the resulting signal characteristics.

The near-field region of a station is a region where the signal is composed of several strong-amplitude modes. The region, as mentioned earlier, extends outward from the station up to 500 to 1000 km when the region is in daylight and increases usually to 1000 -2000 km when the region goes

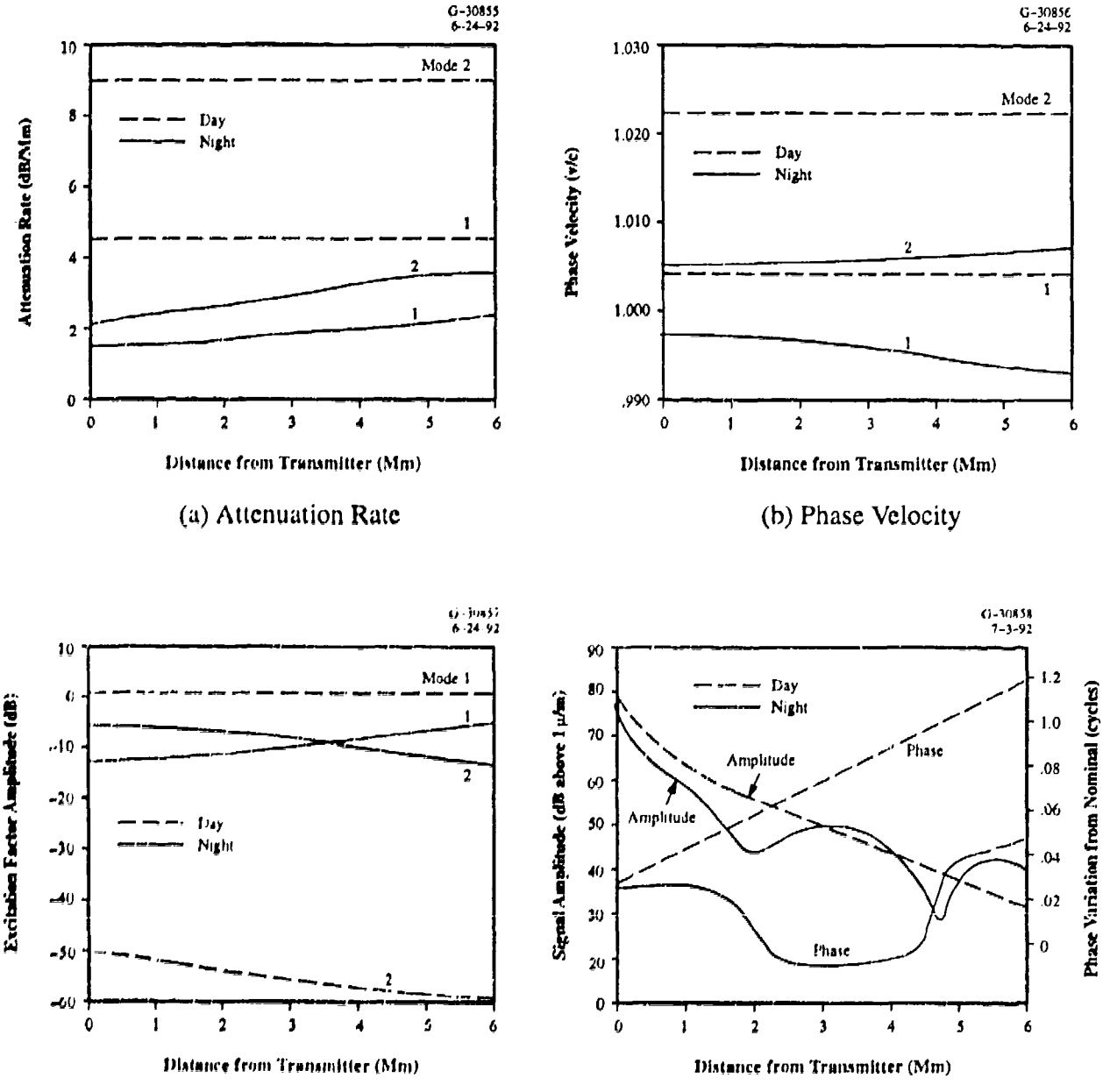

(a) Attenuation Rate

(b) Phase Velocity

(c) Excitation Factor Amplitude

(d) Signal Amplitude and Phase

Figure 5.5-2 Predicted Spatial Variations of Omega Signal Mode Parameters and Associated Signal Amplitude/Phase along Hawaii-to-Guam Signal Path: 10.2 kHz and Daytime/Nighttime Illumination (Ref. 3)

into darkness (night). Requiring special consideration are westerly directed paths with nighttime or transition illumination conditions. These are typically the radial paths emanating from a station (especially if located near the geomagnetic equator, such as the Hawaii, Liberia, and Japan Omega stations), with geographic bearing angles between about 210 and 330 degrees at the station.

Omega navigation is predicated on the assumption that received Omega signals are Mode 1 dominated signals. Therefore, an Omega receiver adjusts the measured phase of a received signal using a Mode 1 phase model (see Chapter 9) so that the adjusted-phase of the signal closely matches the reference phase derived from a linear phase vs. distance model embodied in the Omega navigation receivers. The lack of Mode 1 dominance in a signal, thereby not exhibiting the expected Mode 1 signal behavior, is called *modal interference* and the associated signal is referred to as being a "modal" or "modally-disturbed" signal. Thus a *modal signal* along a path is described by either of the following two characteristics (Ref. 26):

1. Composed of several competing strong-amplitude modes (which may or may not include Mode 1) which may alternately dominate the signal on different segments of the path, as shown in Figs. 5.5-3 and 5.5-4. Because of differing phase velocities of the modes, the signal amplitude/phase of the modal signal exhibits oscillatory behavior with distance.
2. Dominated by a single mode other than Mode 1 (e.g., Mode 2 or Mode 3) outside the station near-field region, as shown in Fig. 5.5-5. In this case, the phase is expected to vary linearly with distance (i.e., constant wave number* for the mode); however, the wave number can be significantly different from that of Mode 1.

In either type of modal signal, the phase can, and usually does, significantly differ from that of the Mode 1 phase and thus a modal signal is unsuitable for use in Omega navigation.

In all of the three modal signal examples, the signal behaviors are predicted by assuming that the signal is composed of the first four lowest-order modes. The paths in Figs. 5.5-3 and 5.5-5 are nighttime paths, while the path in Fig. 5.5-4 is a mixed-illumination path. In Fig. 5.5-3, note that the signal is modal (dominated by Mode 3) for distances of up to about five megameters from the transmitter and then beyond these distances, the signal is non-modal and its wave number is almost the same as the Mode 1 wave number. In this example, note that the increase in signal amplitude beyond ten megameters from the transmitter is due to the signal focusing effect discussed earlier.

In Fig. 5.5-4, the signal is dominated by its Mode 1 along the day and transition segments of the path, and Modes 1 and 3 along the nighttime segment of the path. This is an example of the day to night

*The wave number is the same as the wave propagation constant, k.

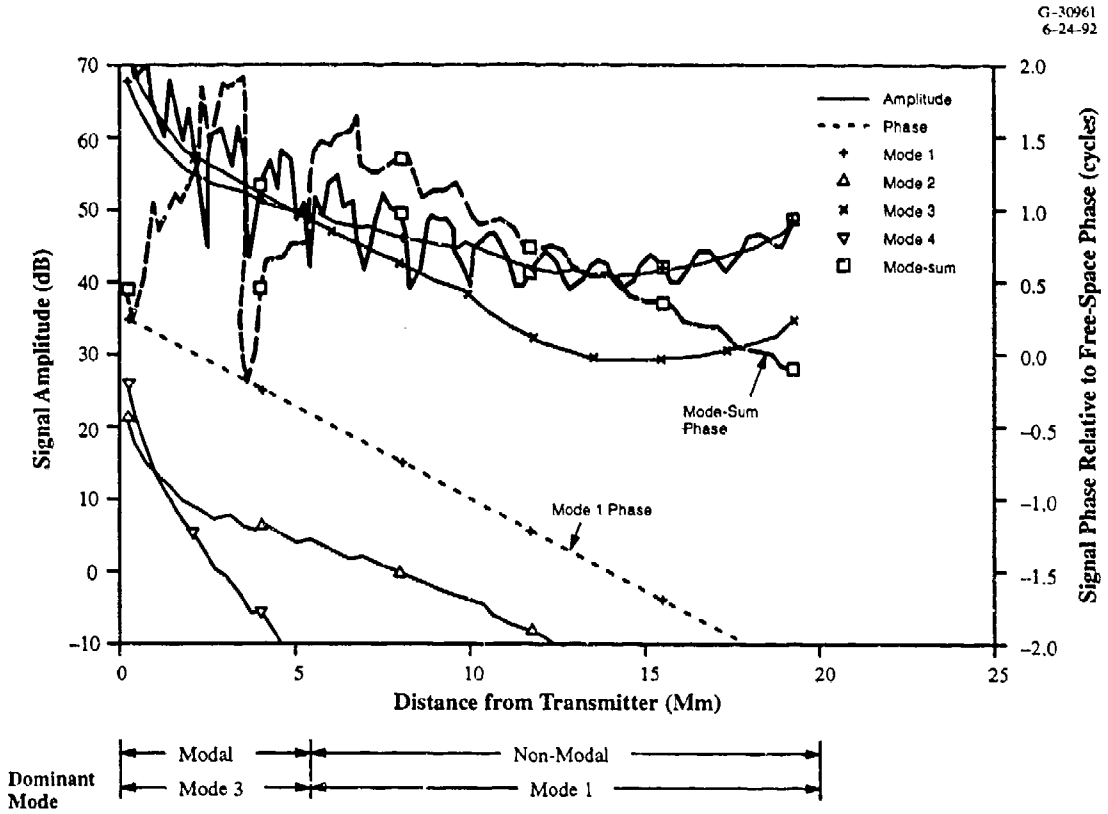

Figure 5.5-3 Example of Predicted Oscillatory Modal Interference Behavior: 13.6 kHz Signal along Nighttime Radial at Geographic Bearing of 105 deg from Liberia Omega Station (Ref. 26)

transition crossing along the path producing mode conversion effects in the signal due to rapidly changing ionospheric properties in the transition region. As a result, there is no Mode 3 of the magnitude comparable to Mode 1, and hence the signal along the nighttime segment is modal.

In Fig. 5.5-5, the signal is dominated along most of the path by Mode 2 and as a result the wave number of the signal differs significantly from that of the Mode 1 wave number. This kind of signal structure frequently happens along westerly-directed nighttime paths.

Examples of *non-modal* signals, outside the station near-field region are shown in Fig. 5.5-6(a) for a day path and Fig. 5.5-6(b) for a night path. These paths show the signal behavior typically observed along most worldwide Omega signal paths.

Modal interference at a path point is characterized as being "spatial" or "temporal" depending upon the solar illumination condition along the path between the station and the path point. Modal interference during the day (or night) illumination condition along a path is classified as *spatial* interference

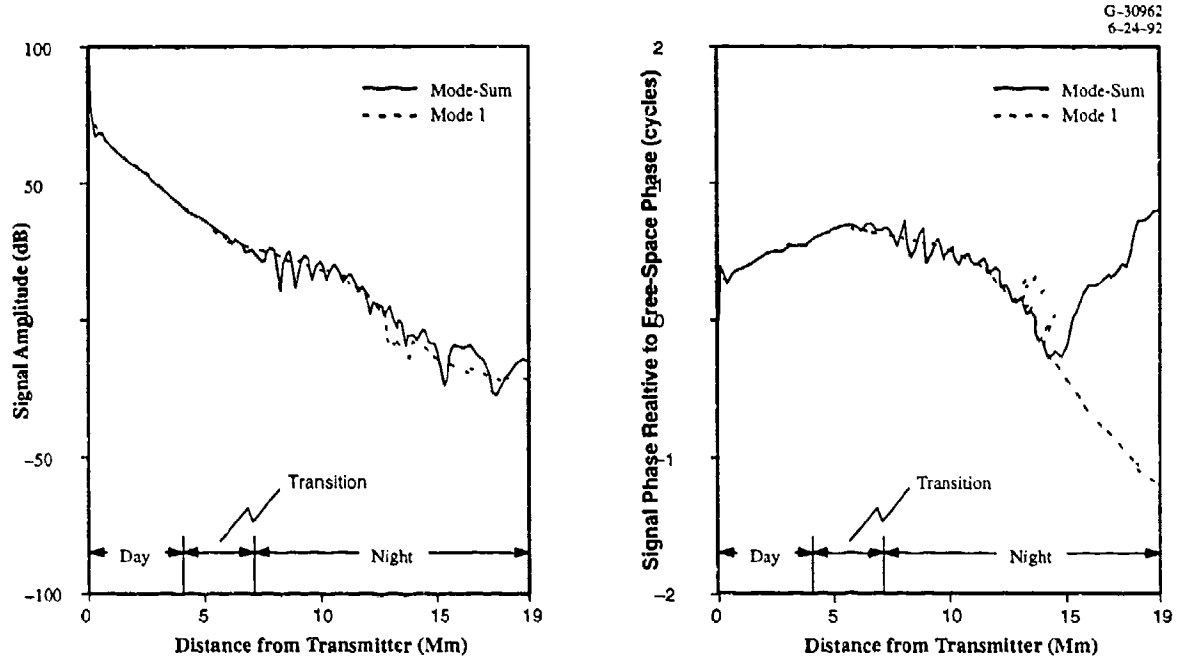

(a) Amplitude **(b) Phase**

Figure 5.5-4 Predicted Mode Conversion-Induced Modal Interference: 10.2 kHz Signal at 24 UT in August along Radial Path at 310 deg Geographic Bearing from Japan Omega Station (Based on Data Generated in Ref. 27)

if the degree of the interference at each path point is nearly the same during the day (or night) hours along the entire path (and thus depends only on spatial coordinates). The spatial interference is generally larger in magnitude and persists to longer distances along a signal path during night than in day. This can be seen by comparing amplitude/phase vs. distance behavior of the daytime and nighttime signals along the path in Figs. 5.5-6(a) and 5.5-6(b). Furthermore, the spatial modal effects are generally more severe both in magnitude and (spatial) extent along nighttime paths emanating from the Omega stations located at low geomagnetic latitudes. Examples of such Omega stations are Liberia, Hawaii, and Japan.

An example of the predicted temporal interference at a fixed location is shown in Fig. 5.5-7. The figure shows a diurnal plot of the predicted signal amplitude of the Liberia Omega station's 10.2 kHz signals received at the prediction point, *P*, which is ten megameters from the station along great-circle radial path emanating from the station at the geographic bearing of 240 deg. The signal path undergoes sunrise (and sunset) transition between the UT hours when the sunrise (and sunset) moves from Liberia (*L*) to the prediction point (*P*). Note in the figure, the signal is non-oscillatory for the UT hours corresponding to all-day or all-night solar illumination conditions along the path; and it becomes oscillatory

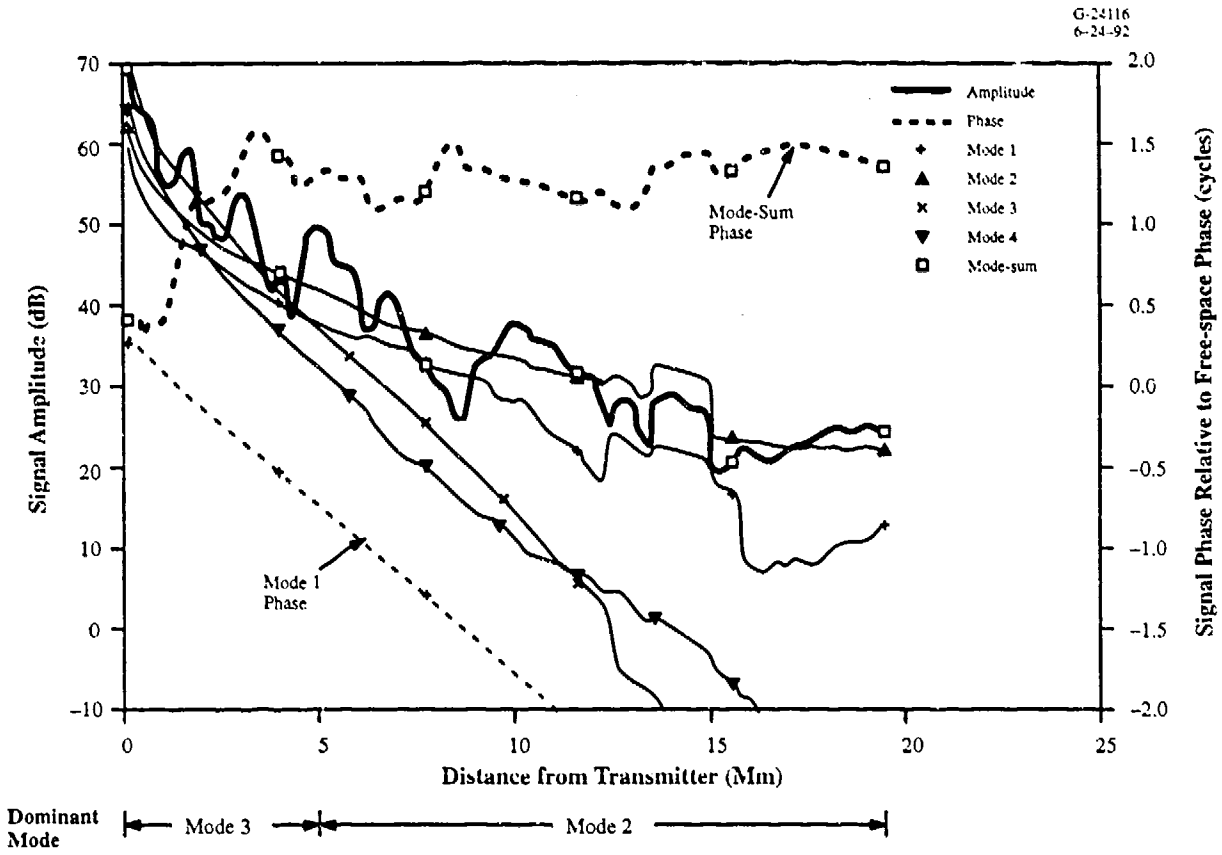

Figure 5.5-5 Predicted Severe Modal Interference by Higher-Order Mode Dominance: 13.6 kHz Signal along Nighttime Radial Path at Geographic Bearing of 300 deg from Omega Hawaii Station (Ref. 26)

for the UT hours for which the path has sunrise/sunset transition along it. An examination of the underlying mode structure of the signal (not shown in the plot) reveals that the signal is a: (1) predominantly Mode 2 signal for all-night path conditions, (2) combination of competing amplitude Modes 1 and 2 during transition illumination conditions along the path, and (3) predominantly Mode 1 signal for all-day path conditions. The transition path behavior is caused by signal mode conversion at the sunrise/sunset transition along the path.

As mentioned earlier, Omega navigation is based on the assumption that the received signal is a Mode 1 dominated signal. However, there is no practical way for a receiver to determine from measurements alone if the signal is, or is not, a predominantly Mode 1 signal. Therefore, *a priori* information is needed on the modal/non modal characterization of Omega signals prior to their use in Omega position-fix computations; otherwise the computed fix could be insignificant error.

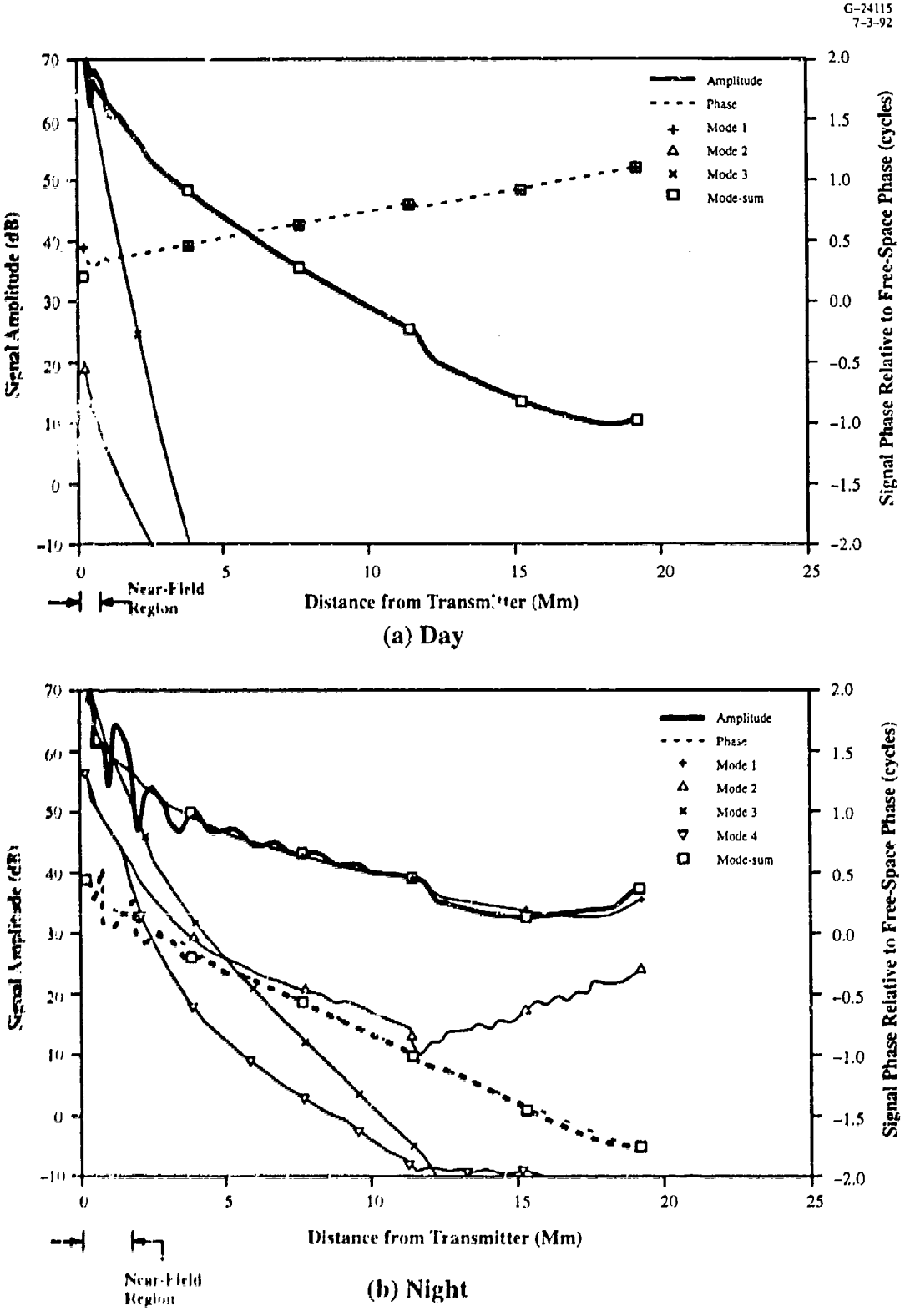

Figure 5.5-6 Predicted Non-Modal Signal: 13.6 kHz, Daytime and Nighttime Signals along Radial Path at 0 deg Geographic Bearing from Liberia Omega Station (Ref. 26)

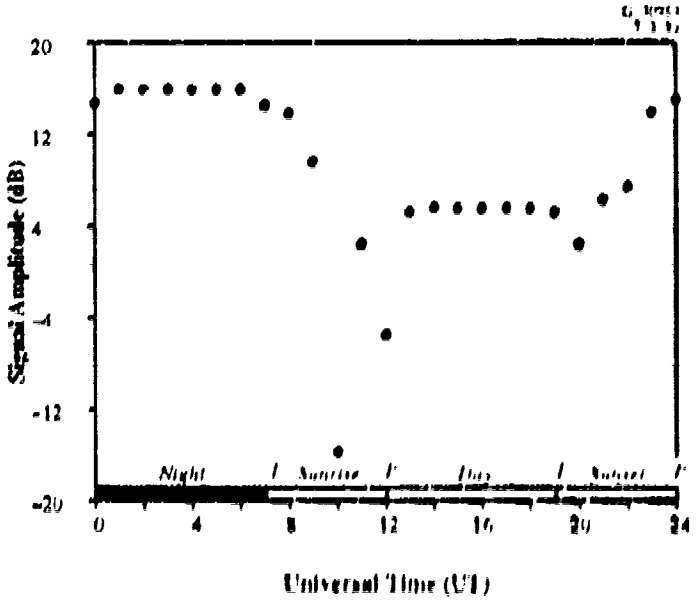

Figure 5.5-7 Predicted Temporal Modal Interference: 10.2 kHz Liberia Omega Station Signals at 10 megameters along the Station Radial at 240 deg Geographic Bearing at the Station (Based on Signal Coverage Data Developed in Ref. 27)

5.5.3 Omega Signal Propagation Characteristics Overview

This subsection summarizes the expected characteristics of Omega signals and their component modes (see Chapter 10; Refs. 26 and 28 through 30). The characteristics are:

1. Omega signal, in general, is a multi mode signal; however, Mode 1, the lowest order transverse-magnetic (TM) mode, is frequently the strongest amplitude mode of the signal.

2. Higher-order modes, compared to Mode 1, have greater signal attenuation rate and thus attenuate rapidly with increasing distance from a station, although they are usually more strongly excited at the station.

3. Mode 1 signal attenuation rate:

    a. Is lower at higher Omega frequencies, e.g., attenuation rate is usually highest at 10.2 kHz and lowest at 13.6 kHz.

    b. Is lower during night than during day, and is in between the day and night values during transition.

    c. Increases greatly with decreasing ground conductivity; it is lowest over sea water (the highest conductivity region) and highest over fresh water ice and permafrost regions (such as in Greenland/Antarctica and northern Canada).

d. Is higher toward the west than toward the east which leads to the east-west effect, which is often stated: "east is easy."

e. Is higher in the equatorial belt (between ± 10 deg geomagnetic latitudes) along westerly directed path segments.

4. A station signal is modal, i.e., has significant modal interference effects, whenever the signal is composed of either:

a. Several competing strong-amplitude modes and the resulting interference manifests itself as quasi-oscillatory variations in the amplitude/phase of the modal signal as a function of: (1) time at a fixed location, and (2) distance along radial path from the station at a fixed time.

b. A single higher order (i.e., non-Mode 1) dominant mode; the signal amplitude/phase behavior of such a modal signal is non-oscillatory in distance but is often unstable in time due to the higher sensitivity of the higher-order modes to temporal ionospheric variations.

5. An Omega station signal is usually modal:

a. In the station near-field region which typically extends from the station up to distances of 500–1000 km during day and 1000–2000 km at night.

b. Along paths having the following combination of path properties: nighttime illumination, westerly path azimuths (between 180 and 360 deg), and low geomagnetic latitudes (between ± 10 deg).

c. At and in close vicinity of the day/night terminator crossing along a path.

6. A station signal may be a long path signal (i.e., the long-path component of the signal is stronger than its short-path component) whenever:

a. The receiver is west of the station and therefore the short-path component may be much more attenuated than the long-path component.

b. The long path is composed of mostly the high ground conductivity regions (e.g., sea water and land) and the short path includes low-conductivity regions (e.g., Greenland/Antarctica); and thus the short-path component may be much more attenuated than the long-path component.

c. The long-path component includes the entire nighttime hemisphere, and conversely, the short path is an all-day path; as a result, the short-path component may be much weaker than the long-path component.

These signal characteristics as functions of path properties should prove useful to the reader in *a priori* determination of the potential usefulness of a given Omega station signal for navigation.

5.6 APPENDIX: REFERENCE MATERIAL

This appendix presents reference material pertaining to *units and dimensions* of electromagnetic quantities. It also introduces the mathematical tools used in this chapter to describe the electromagnetic

field propagation concepts and mechanisms (c.f. Refs 3 and 19). The tools are *vector analysis* and *complex notation* for harmonic (sinusoidal) time varying electromagnetic field quantities.

In this chapter, scalars are denoted by italic Greek or italic English characters such as α, θ, e, or E; vectors are represented by bold Greek or bold English characters, such as **H**, or **e**; while matrices are represented as upper-case roman English characters, such as R. Roman English letters are used for multiple character symbols that refer to standard functions, such as sin x, while numerical digits are always roman. Subscript and superscript variables, except for numerical digits, and coordinate axes, appear in italics.

5.6.1 Units and Dimensions

A measurement of any physical quantity must be expressed by a number followed by a unit. In this chapter we use the *rationalized MKSA* system of units, also referred to as the *rationalized International System of Units* (SI-units).* In this system, the quantities *length, mass, time,* and *current* are expressed in *meters (m), kilograms (kg), seconds (s),* and *amperes (A)*, respectively. From these units and the velocity of light in free space, it is possible to derive all other units used in this chapter.

5.6.2 Vector Analysis

In the study of electromagnetics, a great saving in complexity of notation is accomplished by using the notation of vector analysis. This section introduces vector notations and presents vector operations used in this chapter; the derivation of the results can be found in any electromagnetics textbook.

5.6.3 Definitions

A *scalar* is a quantity that is completely specified by its magnitude, positive or negative, together with its unit. Example of scalars are mass, time, charge, energy, etc. A simple extension of the idea of scalar is a *scalar field*, i.e., a function of position which is completely specified by its magnitude at all points in space.

A *vector* is a quantity which is completely specified by its magnitude and direction, and is denoted by boldface symbols, e.g., **A**, **B**, **e**. Force, velocity, acceleration, electric and magnetic field intensities are examples of the vector quantities. The generalization to a *vector field* gives a function of

*An equivalent system is the rationalized MKSC system which uses the *coulomb* (ampere × second), in place of the *ampere*, as the basic electrical unit. The system of units is said to be *rationalized* because the factor 4π does not appear in Maxwell's equations (the fundamental postulates of electromagnetism).

position which is completely specified by its magnitude and direction at all points in space. A vector is graphically represented by a directed straight-line segment of a length equal to the magnitude of the vector with its arrowhead pointing in the direction of the vector, as shown in Fig. 5.6-1.

Vector Sum and Difference — Two vectors are added by placing the tail of one vector at the head of the other, the sum being represented by an arrow from the tail of the first to the head of the second. This is illustrated in Fig. 5.6-2(b) for the two vectors shown in Fig. 5.6-2(a). The negative of a vector is a vector of same magnitude pointing in the opposite direction. To subtract one vector from another is the same as adding the first vector to a negative of the second vector. This is illustrated in Fig. 5.6-2(c) for the two vectors shown in Fig. 5.6-2(a).

In dealing analytically with vectors, it is convenient to refer them to some orthogonal "coordinate system." There are a number of orthogonal coordinate systems; we shall limit ourselves to the *right handed* Cartesian (rectangular) coordinate system*, where a vector is a sum of three "component vectors" directed along the x, y, and z axes, respectively. Let $\hat{x}$, $\hat{y}$, and $\hat{z}$ be three such orthogonal component vectors with unit magnitude (called *unit vectors*), as shown in Fig. 5.6-3. The vector $\mathbf{A}$ can then be expressed as

$$\mathbf{A} = \hat{x}\, A_x + \hat{y}\, A_y + \hat{z}\, A_z$$

Figure 5.6-1 Graphical Representation of Vector

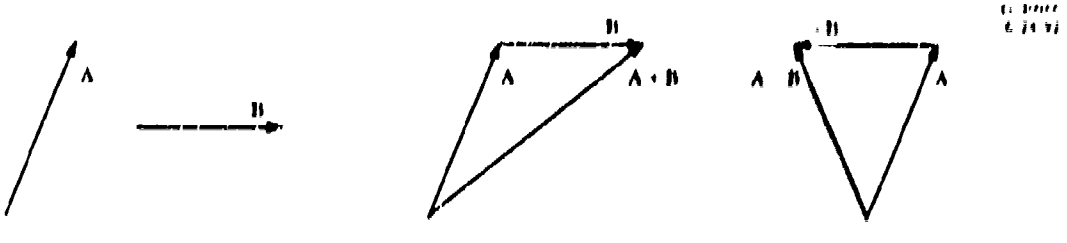

(a) Vectors A and B (b) The Sum A + B (c) The Difference A − B

Figure 5.6-2 Sum and Difference of Two Vectors

*The coordinate system is said to be *right-handed* if rotation of the x axis into the y axis would advance a a right-handed screw in the positive z direction. If rotation would advance a right handed screw in the negative z direction, the coordinate system is said to be *left handed*.

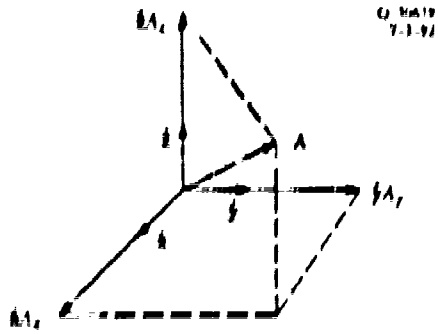

Figure 5.6-3 Components of a Vector in Rectangular Coordinates

where A_x, A_y, and A_z are the projections of the vector **A** on the three coordinate axes (x, y, and z). The scalar quantities A_x, A_y, and A_z are referred to as the *rectangular* or *Cartesian components* of the vector **A**. The magnitude of the vector **A** in terms of its rectangular components is indicated by vertical bars, $|\,|$, surrounding the vector, as illustrated below

$$A = |\mathbf{A}| = (A_x^2 + A_y^2 + A_z^2)^{1/2}$$

When adding and subtracting vectors, their components can be added and subtracted separately, as follows

$$\mathbf{A} + \mathbf{B} = \mathbf{C} = \hat{x}\,(A_x + B_x = C_x) + \hat{y}\,(A_y + B_y = C_y) + \hat{z}\,(A_z + B_z = C_z)$$

Vector Multiplication — We now define two kinds of vector multiplication. The first type is a *scalar product*, also called *inner* or *dot product*, of two vectors and is written as

$$\mathbf{A} \cdot \mathbf{B} = A_x B_x + A_y B_y + A_z B_z = AB \cos\theta = \mathbf{B} \cdot \mathbf{A}$$

where A and B are the magnitudes of the two vectors and θ is the angle between them as shown in Fig. 5.6-4. If **A** and **B** are collinear (i.e., have the same orientation), then $\mathbf{A} \cdot \mathbf{B} = AB$ since $\theta = 0$ deg; but if they are perpendicular to each other, then $\mathbf{A} \cdot \mathbf{B} = 0$ since $\theta = 90$ deg.

The second type of vector multiplication is a *vector product* or *cross product* of two vectors. This is another vector, given by

$$\mathbf{A} \times \mathbf{B} = \hat{x}\,(A_y B_z - A_z B_y) + \hat{y}\,(A_z B_x - A_x B_z) + \hat{z}\,(A_x B_y - A_y B_x)$$

$$= \hat{n}\,AB \sin\theta = -\mathbf{B} \times \mathbf{A}$$

where $\hat{\mathbf{n}}$ is a unit vector perpendicular to the plane containing **A** and **B**, as shown in Fig. 5.6-5. The direction of $\hat{\mathbf{n}}$ is given by the "right-hand rule" which states that the direction of $\mathbf{A} \times \mathbf{B}$ is that in which a right-hand screw would advance if rotated in the same manner.

Derivatives of a Vector — There is a derivative in vector analysis, closely related to each of the two kinds of multiplication just discussed. The vector-like differential operator ∇ (del) has the following form in rectangular coordinates

$$\nabla \equiv \hat{\mathbf{x}} \frac{\partial}{\partial x} + \hat{\mathbf{y}} \frac{\partial}{\partial y} + \hat{\mathbf{z}} \frac{\partial}{\partial z}$$

When ∇ operates on a vector **A** in the dot product sense, the result is a scalar quantity called the *divergence (div) of* **A** and is given by

$$\text{div } \mathbf{A} \equiv \nabla \cdot \mathbf{A} = \frac{\partial A_x}{\partial x} + \frac{\partial A_y}{\partial y} + \frac{\partial A_z}{\partial z}$$

If ∇ operates on A in the cross product sense, one obtains the *curl* (or *rotation) of* **A**, which is a vector quantity. In rectangular coordinates, the curl takes the following form

$$\text{curl } \mathbf{A} \equiv \nabla \times \mathbf{A} = \hat{\mathbf{x}} \left(\frac{\partial A_z}{\partial y} - \frac{\partial A_y}{\partial z} \right) + \hat{\mathbf{y}} \left(\frac{\partial A_x}{\partial z} - \frac{\partial A_z}{\partial x} \right) + \hat{\mathbf{z}} \left(\frac{\partial A_y}{\partial x} - \frac{\partial A_x}{\partial y} \right)$$

The operator ∇ can also be applied to a scalar quantity ϕ, which is a function of x, y, and z. The result is the *gradient (grad) of* ϕ and in rectangular coordinates it is the vector

$$\text{grad } \phi \equiv \nabla\phi = \hat{\mathbf{x}} \frac{\partial \phi}{\partial x} + \hat{\mathbf{y}} \frac{\partial \phi}{\partial y} + \hat{\mathbf{z}} \frac{\partial \phi}{\partial z}$$

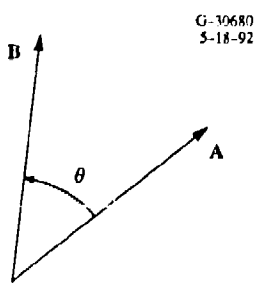

Figure 5.6-4 Vectors **A** and **B**

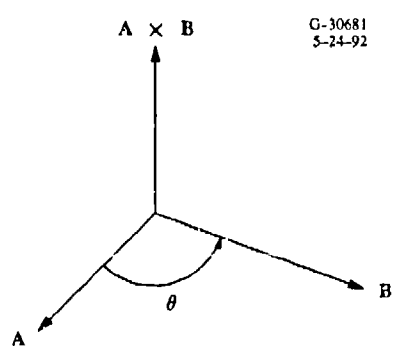

Figure 5.6-5 Vector Product Geometry

Repeated application of the differential operator ∇ to a vector or a scalar is sometimes required in electromagnetic field theory. The following relations are of special interest:

$$\nabla \cdot \nabla\phi \equiv \nabla^2\phi \equiv \frac{\partial^2\phi}{\partial x^2} + \frac{\partial^2\phi}{\partial y^2} + \frac{\partial^2\phi}{dz^2}$$

$$\nabla \times \nabla \times \mathbf{A} \equiv \nabla(\nabla \cdot \mathbf{A}) - \nabla^2 \mathbf{A}$$

$$\nabla \cdot \nabla \times \mathbf{A} \equiv 0 \quad \text{for all vectors } \mathbf{A}$$

$$\nabla \times \nabla\phi \equiv 0 \quad \text{for all scalars } \phi$$

The operator $\nabla \cdot \nabla = \nabla^2$ (Laplace's operator) is a scalar quantity and is extensively used in the electromagnetic theory. The expression $\nabla^2\mathbf{A}$, in rectangular coordinates, is

$$\nabla^2\mathbf{A} \equiv \nabla(\nabla \cdot \mathbf{A}) - \nabla \times \nabla \times \mathbf{A} = \hat{\mathbf{x}}\,(\nabla^2 A_x) + \hat{\mathbf{y}}\,(\nabla^2 A_y) + \hat{\mathbf{z}}\,(\nabla^2 A_z)$$

Complex Notation — When the time variation of a function such as voltage or electric field is harmonic (sinusoidal), *complex notation* is used to simplify mathematical analysis. The basis for this is *Euler's identity*

$$\exp(i\omega t) = \cos(\omega t) + i \sin(\omega t)$$

where $i = \sqrt{-1}$, ω ($= 2\pi f$) is the angular frequency, f is the frequency, and t is time. This gives a relation between real sinusoidal functions and the complex exponential function.

Consider a sinusoidally varying scalar quantity, such as voltage $u(t)$, of the form

$$v(t) = |V_0| \cos(\omega t + \phi) = \sqrt{2}\ |V| \cos(\omega t + \phi)$$

where $|V_0|$ and $\sqrt{2}\ |V_0|$ are the *peak* and the *rms (root-mean-square)* value of the *instantaneous voltage* $v(t)$, respectively; and ϕ is the phase. Note that specification of a sinusoidal quantity requires the knowledge of its three parameters: amplitude, frequency, and phase.

In complex notation, $v(t)$ would be interpreted according to

$$v(t) = \sqrt{2}\ \mathrm{Re}\ [V \exp(i\omega t)]$$

where $V = |V| \exp(i\phi)$ is called the *complex quantity*, and the notation Re[ ] stands for "the real part of" of the complex quantity inside the brackets [ ].* Another name for V is the *scalar phasor quantity* and it has both a magnitude and a phase. Thus, in complex notation, V is the complex voltage corresponding to the instantaneous voltage $v(t)$.

Throughout this chapter, we use complex notation for the electromagnetic field quantities which are interpreted according to the rules of *complex algebra* presented in this subsection. Frequently, the time dependence factor is not written out explicitly for sinusoidally varying field quantities, since the same time dependence is common to all field expressions.

Field vectors that vary with space coordinates and are sinusoidal functions of time can be similarly represented by "vector phasors" that depend on space coordinates but not on time. As an example, we can write a time-harmonic **e** field referring to cos ωt time reference§ as

$$\mathbf{e}(x,y,z\,;t) = \mathbf{E}_0(x,y,z)\cos(\omega t + \phi) = \sqrt{2}\,\mathbf{E}(x,y,z)\cos(\omega t + \phi)$$
$$= \mathrm{Re}\,[\mathbf{E}_0 \exp(i\omega t)] = \mathrm{Re}\,\sqrt{2}\,[\mathbf{E}\exp(i\omega t)]$$

where $\mathbf{E}_0$ and $\mathbf{E}$ are the peak and rms complex-vector (phasor-vector) fields containing information on direction, magnitude, and phase. The rectangular component of **e**, e_j ($j = x,y,z$), in complex notation, is

$$e_j(x,y,z\,;t) = \sqrt{2}\,\mathrm{Re}\left[E_j \exp(i\omega t)\right]$$
$$= \sqrt{2}\,\mathrm{Re}\left[|E_j| \exp i(\omega t + \phi)\right]$$

where the scalar phasor $E_j = |E_j| \exp(i\phi)$.

5.7 APPENDIX: RADIOWAVE PROPAGATION PRINCIPLES

This section presents the basic concepts in electromagnetic field theory relevant to radiowave propagation in a waveguide. Specifically, it presents Maxwell's equations (the basic electromagnetic theory postulates), wave equations, and reflection and refraction of waves. The material in this appendix is extracted from basic textbook on electromagnetic theory (e.g., Refs. 19 and 31 through 36).

---

* The convention $v(t) = \sqrt{2}\,\mathrm{Im}\,[V \exp(i\omega t)]$ can also be used, where Im [ ] stands for the imaginary part of the quantity within the brackets [ ].

§ If the time reference is not explicitly specified, it is customarily taken as cos ωt.

5.7.1 Basic Concepts

Electromagnetic phenomena can be described in terms of the *free* electric charge density ϱ, a scalar quantity, and the five vector quantities listed in Table 5.7-1. These *quantities* are related by two distinctly different set of equations. The vector pairs **J** and **E**, **E** and **D**, and **H** and **B** are assumed to depend linearly on each other (linear media); no time or space dependence is involved. These relations are known as the *constitutive relations* (Section 5.7.3) and depend on the properties of the medium in which the electromagnetic field exists. The second set of relations is the basic postulates of the electromagnetic

Table 5.7-1 Fundamental Electromagnetic Vector Quantities

VECTOR QUANTITY	SYMBOL	UNIT
Electric field intensity	**E**	volt/meter (V/m)
Electric flux density (Electric displacement)	**D**	coulomb/meter^2 (C/m^2)
Magnetic field intensity	**H**	ampere/meter (A/m)
Magnetic flux density	**B**	weber/meter^2 (Wb/m^2)
Current density	**J**	ampere (A)

theory, called *Maxwell's equations* (Section 5.7.2). They involve derivatives in time as well as in the space. At interfaces between media with different electromagnetic properties, the field quantities on either side of the interface are related through the *boundary conditions* or *relations* (Section 5.7.4). The actual fields in a certain region are also dependent on the source or sources of these fields. To determine the electromagnetic fields for a given problem, proceed as follows.

(a) Obtain a set of *elementary solutions* to Maxwell's equations together with the constitutive relations, typically represented in the form of plane electromagnetic waves.

(b) Find the combination of elementary solutions that satisfy the boundary conditions; these *partial solutions* or *modes* are specific for the region and usually form an enumerable but infinite set. (An enumerable set is a set whose members can be enumerated, i.e., assigned numbers 1, 2, 3 . . .)

(c) Select the set of partial solutions that matches the distribution of sources at hand.

In the following subsections, we apply the procedure outlined above to develop expressions for the electromagnetic fields of propagating radiowave signals.

5.7.2 Maxwell's Equations

The basic laws of electromagnetics are summarized by the four Maxwell's equations whose derivative forms and equivalent integral forms are given in Table 5.7-2.

In Maxwell's equations, $\nabla \cdot$ is the *divergence operator* (see Section 5.6.2.4); $\nabla \times$ is the *curl operator* (see Section 5.6.2.4); $\frac{\partial(\ )}{\partial t}$ is the partial derivative of the quantity within the parentheses ( ) with respect to time t; $\oint_v$ is the volume integral over the volume V; $\oint_S$ is the surface integral over the

Table 5.7-2 Maxwell's Equations

BASIC LAW	DIFFERENTIAL FORM	INTEGRAL FORM
Gauss's law	$\nabla \cdot \mathbf{D} = \varrho$	$\oint_s \mathbf{D} \cdot d\mathbf{s} = \oint \varrho \, dv = Q$
Ampere's law	$\nabla \times \mathbf{H} = \mathbf{J} + \frac{\partial \mathbf{D}}{\partial t}$	$\oint_c \mathbf{H} \cdot d\mathbf{l} = \int_s \left(\mathbf{J} + \frac{\partial \mathbf{D}}{\partial t}\right) \cdot d\mathbf{s} = I + \int_s \frac{\partial \mathbf{D}}{\partial t} \cdot d\mathbf{s}$
Faraday's law	$\nabla \times \mathbf{E} = -\frac{\partial \mathbf{B}}{\partial t}$	$\oint_c \mathbf{E} \cdot d\mathbf{l} = -\int_s \frac{\partial \mathbf{B}}{\partial t} \cdot d\mathbf{s} = -\frac{d\phi}{dt}$
No isolated magnetic charge	$\nabla \cdot \mathbf{B} = 0$	$\oint_s \mathbf{B} \cdot d\mathbf{s} = 0$

closed surface S; $\oint_C$ is the contour integral over the closed contour C; $d\mathbf{l}$ is the path (contour) element along the contour C; $d\mathbf{s}$ is the surface element over the surface S; and dv is the volume element of volume V. Note that $d\mathbf{l}$ and $d\mathbf{s}$ are based on the convention that $d\mathbf{l}$ encircles $d\mathbf{s}$ according to the "right-hand" rule* (see Fig. 5.7-1) and $d\mathbf{s}$ points outward for a closed surface (see Fig. 5.7-2).

Gauss's law states that the electric flux flowing out of any closed surface is equal to the charge, Q, enclosed; i.e., the electric flux lines begin and end on electric charge. Note that the Gauss's law is a direct

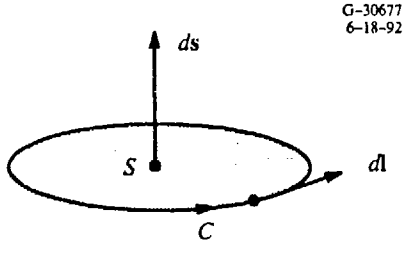

Figure 5.7-1 $d\mathbf{l}$ and $d\mathbf{s}$ on an Open Surface S and Contour C

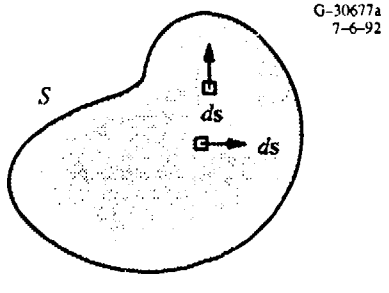

Figure 5.7-2 $d\mathbf{s}$ on a Closed Surface S

*The rule is that the fingers on one's right hand point in the direction of $d\mathbf{l}$ and the thumb points in the direction of $d\mathbf{s}$.

consequence of *Coulomb's law* which states that the force between two charged particles is proportional to the product of the charges of the two particles and inversely proportional to the square of the distance between the particles.

Ampere's law states that the line integral of the magnetic field about a closed path is equal to the total current, I, flowing through the surface bounded by the path. Note that the *current density* may consist of a *conduction current density*, $\sigma \mathbf{E}$, caused by the presence of an electric field $\mathbf{E}$ in a conductive medium with conductivity σ and a *convection current density* $\rho \mathbf{u}$ due to motion (with a velocity $\mathbf{u}$) of the free charge distribution ρ. The surface integral of $\mathbf{J}$ is the current, I, flowing through the open surface S.

Faraday's law states that the line integral of the electric field about a closed path is equal to the negative rate of change of the magnetic flux ϕ flowing through the path. This means that the changing magnetic field induces "emf" (voltage) in a path surrounding the field.

The last of the four Maxwell's equations states that the surface integral of magnetic field, or total magnetic flux flowing out of a closed surface, is zero. This expresses the fact that magnetic charges have not been found in the nature.

As a consequence of the *conservation of charge*, the charge density, q_v, and the current density, $\mathbf{J}$ are related by the *equation of continuity* which is

$$\nabla \cdot \mathbf{J} = -\frac{\partial q_v}{\partial t}$$

The principal of conservation of charge, like the principle of conservation of momentum, is a fundamental postulate or law of physics. It states that the electric charge is conserved; that is, it can neither be created nor be destroyed.

5.7.3 Constitutive Relationships

To solve an electromagnetic field problem, we need, in addition to Maxwell's equations, the following *constitutive relationships*, which specify the properties of the medium in which the field exists. Table 5.7-3 lists the constitutive relationships between the field pairs $\mathbf{E}$ and $\mathbf{D}$, $\mathbf{H}$ and $\mathbf{B}$, and $\mathbf{J}$ and $\mathbf{E}$ in free space (vacuum) as well as in an isotropic/linear dielectric medium. In the relationships, ε_0 is the permittivity, also called dielectric constant, of free space ($= 8.854 \times 10^{-12}$ farad/meter); μ_0 is the permeability of free space ($= 4\pi \times 10^{-7}$ henry/meter); ε_r is the relative permittivity, or relative dielectric constant (a dimensionless quantity); μ_r is the relative permeability (a dimensionless quantity); σ is the conductivity (mho/m). Note that the free-space medium is a special case of isotropic/linear medium

where $\varepsilon_r = 1, \mu_r = 1$, and $\sigma = 0$. In an isotropic/linear medium, the two vectors in any of the constitutive relationships (e.g., between **J** and **E**) are oriented in the same direction and are related to each other via the scalar properties $(\varepsilon, \mu, \sigma)$ of the medium.

Table 5.7-3 Constitutive Relationships

MEDIUM	RELATIONSHIP BETWEEN		
	D and **E**	**B** and **H**	**J** and **E**
Free space	$\mathbf{D} = \varepsilon_0 \mathbf{E}$	$\mathbf{B} = \mu_0 \mathbf{H}$	$\mathbf{J} = 0$
Isotropic/linear dielectric	$\mathbf{D} = \varepsilon \mathbf{E} = \varepsilon_r \varepsilon_0 \mathbf{E}$	$\mathbf{B} = \mu \mathbf{H} = \mu_r \mu_0 \mathbf{H}$	$\mathbf{J} = \sigma \mathbf{E}^*$

*Ohm's law.

In the case of an *anisotropic/linear dielectric medium*, such as the magnetized plasma which is the upper boundary medium of the earth-ionosphere waveguide, the dielectric constant and conductivity may be different for different directions of the electric field as a result the dielectric properties, ε and σ, and this they are tensor quantities (Ref. 19). As a result, **D** and **J** depends on all three components of **E**.

For *harmonically (sinusoidally) time-varying fields* (i.e., exp $(i\omega t)$ time dependence), the dielectric constant (permittivity) is, in general, a complex quantity and expressed as:

$$\varepsilon = \varepsilon' - i\,\varepsilon''$$

where both ε' and ε'' may be functions of frequency.

The ratio $\varepsilon' / \varepsilon''$ expressed by Eq. 5.7-1, is called *loss tangent* because it is a measure of power loss in the wave propagation medium

$$\tan \delta_c = \frac{\varepsilon''}{\varepsilon'} \approx \frac{\sigma}{\omega \varepsilon'} \qquad (5.7\text{-}1)$$

Note that the *speed of light* in a lossless medium is $(\varepsilon\mu)^{-1/2}$ which in free space reduces to $(\varepsilon_0 \mu_0)^{-1/2}$. Furthermore, the *index of refraction, n* of an isotropic medium is $\sqrt{\varepsilon_r \mu_r}$ (a dimensionless quantity). In the case of a *lossy* medium (i.e., $\varepsilon'' \neq 0$), n is a complex quantity. In free space, n is unity since $\varepsilon_r = \mu_r = 1$.

On the basis of Eq. 5.7-1, a medium is said to be good conductor if $\sigma >> \omega\varepsilon'$, and a good insulator (dielectric) if $\omega\varepsilon' >> \sigma$. Thus, a material may be a good conductor at VLF but may have the properties of a lossy dielectric at very high frequencies. For example, for a moist ground which has the relative dielectric constant of about 10 and conductivity of 10^{-2} mho/meter, the loss tangent is 1.8×10^4 at 10 kHz,

which makes the moist ground a relatively good conductor. At 10 GHz (10×10^{12} Hz), the loss tangent is 1.8×10^{-3} and thus the moist ground at 10 GHz behaves like an insulator.

5.7.4 Boundary Conditions

The field equations, described in Section 5.7.2, are valid at points in space in whose neighborhood the physical properties of the medium vary continuously. However, at any surface separating one medium from another, there occur sharp changes in the medium parameters ε, μ, and σ. These changes result in discontinuous field quantities across the discontinuity between the two media. In solving electromagnetic field problems, we need *boundary conditions*, listed in Table 5.7-4, to relate the electric and magnetic fields on the two sides of a discontinuity. The boundary conditions are obtained by applying Maxwell's equations at the two adjacent points, one on each side of the discontinuity. In the table, each field quantity has two subscripts. The first subscript t or n denotes the tangential or normal component of the field, respectively, and the second subscript (1 or 2) indicates the medium to which the field component belongs.

From the boundary conditions table (Table 5.7-4), we note that the tangential component of electric field, E_t, and normal component of magnetic flux density, B_n, are always continuous at the interface between any two media (see Fig. 5.7-3). For the case of *source-free interface*, both the tangential component of magnetic flux intensity, H_t, and the normal component of electric flux density, D_n, are continuous. Whenever there are sources, i.e., non-zero surface charge density, source i.e., $\varrho_s \neq 0$ (and non-zero surface current density, source, i.e., $j_s \neq 0$), D_n (and H_t) are discontinuous at the interface by the amount equal to the electric (and magnetic) field source magnitude. From the table, note that for a perfect conductor, there can be no electric and magnetic fields inside a conductor.

Table 5.7-4 Boundary Conditions for Electric and Magnetic Fields

Media 1 and 2	Tangential Component of Electric Field (E_t)	Normal Component of Electric Flux Density (D_n)	Tangential Component of Magnetic Flux Density (H_t)	Normal Component of Magnetic Flux Density (B_n)
σ_1, σ_2 arbitrary ($\sigma \neq \infty$)	$E_{t1} = E_{t2}$	$D_{n1} = D_{n2}$	$H_{t1} = H_{t2}$	$B_{n1} = B_{n2}$
Medium 1 is a perfect conductor ($\sigma_1 = \infty$) with current sheet density j_s and charge density ϱ_s at the interface between media	$E_{t1} = 0$ $E_{t2} = 0$	$D_{n1} = 0$ $D_{n2} = \varrho_s$	$H_{t1} = 0$ $H_{t2} = j_s$	$B_{n1} = 0$ $B_{n2} = 0$
$\sigma_1 = \sigma_2 = 0$; $j_s = 0$	$E_{t1} = E_{t2}$	$D_{n1} = D_{n2}$	$H_{t1} = H_{t2}$	$B_{n1} = B_{n2}$

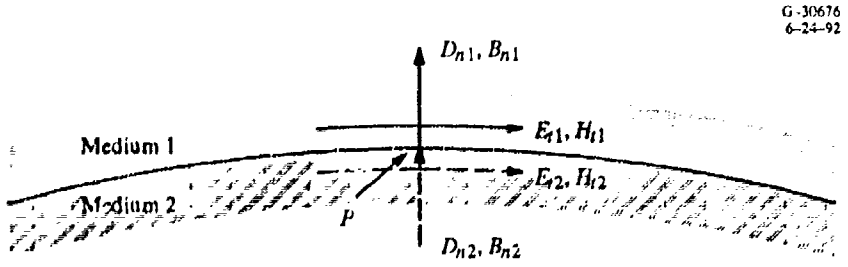

Figure 5.7-3 Field Components at point P on th ce Between Media 1 and 2

5.7.5 Wave Equations

We will now consider applying Maxwell's equations to wave propagation in an *unbounded, homogeneous, isotropic, and linear medium with no sources (current or charges).* For harmonic time dependence of the wave field quantities (from which an arbitrary time dependent field quantities can be easily derived by the principle of superposition), Maxwell's equations reduce to the following *homogeneous vector wave equations*, also called *homogeneous vector Helmholtz equations*:

$$\nabla^2 \mathbf{E} + k^2 \mathbf{E} = 0$$
$$\nabla^2 \mathbf{E} + k^2 \mathbf{H} = 0$$

where ∇^2 is the Laplacian operator (see Section 5.6.2), $k^2 = \omega^2\varepsilon\mu = (\omega^2\varepsilon_0\mu_0)(\varepsilon_r\mu_r) = k_0^2\varepsilon_r\mu_r = k_0^2 n^2$; $\omega = 2\pi f$, f is the signal frequency, and n is the refractive index of the medium. The constant k is called the *propagation constant* (or *wave number*). In free space ($\varepsilon_r = \mu_r = 1$)

$$k = k_0 = \omega\sqrt{\varepsilon_0\mu_0} = \frac{\omega}{c}$$

where c is the speed of light in free space.

In the Cartesian coordinates, the *rectangular components* of $\mathbf{E}$ and $\mathbf{H}$ satisfy the *scalar wave equation* or *Helmholtz equation*

$$\nabla^2\psi + k^2\psi = 0 \qquad (5.7\text{-}2)$$

where ψ is any scalar component of $\mathbf{E}$ or $\mathbf{H}$. We can construct electromagnetic fields by choosing solutions to Eq. 5.7.2 for E_x, E_y, and E_z, or H_x, H_y, and H_z. Note that all fields that satisfy Maxwell's equations also satisfy the wave equations. The converse is not true. A pair of field vectors $\mathbf{E}$ and $\mathbf{H}$ that satisfy wave equations constitute admissible electromagnetic fields only if at the same time they satisfy Maxwell's equations. Furthermore the fields must behave properly at the boundaries in accordance with the boundary conditions listed in Table 5.7-3. If the wave propagation region is unbounded, attention must also be paid to the field behavior at infinity (see radiation condition in Ref. 35).

5.7.6 Plane Waves

The harmonic plane wave solution of Maxwell's equations is of both theoretical and practical importance in understanding Omega/VLF signal wave propagation, as the electromagnetic fields of very general form can be represented by a superposition of harmonic plane waves. A plane wave is a particular solution of Maxwell's equations, with the electric field **E** (similarly, the magnetic field **H**) in the same direction and same phase over each of the infinite planes perpendicular to the direction of wave propagation. The equiphase surface of a wave is called *wave front* or *phase front*. A *plane wave* is uniform when the amplitudes of **E** and **H** are constant over the equiphase surfaces. First, we will consider plane wave propagation in a non-conducting (lossless) medium and then in a conducting (lossy) medium. Finally, we will discuss reflection and refraction of plane waves from a planar boundary.

Non-Conducting Medium — The medium is assumed to be isotropic and linear. In this medium, consider a uniform plane wave characterized by a uniform E_x (constant magnitude and constant phase) over plane surfaces perpendicular to the z axis of the rectangular coordinate system. Note that the field E_x is a phasor and depends only on the z coordinate. For this case, the solution of the wave equation, Eq. 5.7-2, is

$$E_x(z) = E_x^+ \exp(-jkz) + E_x^- \exp(jkz) \qquad (5.7\text{-}3)$$

where E_x^+ and E_x^- are arbitrary (in general, complex) constants that are determined by the boundary conditions and k is the propagation constant in the medium.

Now let us examine what the first phasor term on the right-hand side of Eq. 5.7-3 represents in real time. Based on the complex notation representation described in Section 5.6 and assuming that $E_x^+ = E_0^+$ to be a real constant (zero phase at $z = 0$), the instantaneous dependence of E_x^+ is given by

$$\begin{aligned} E_x^+(z,t) &= \mathrm{Re}\left[E_x^+ \exp(-jkz) \exp(j\omega t)\right] \\ &= E_0^+ \cos(\omega t - kz) \end{aligned} \qquad (5.7\text{-}4)$$

Eq. 5.7-4 has been plotted in Fig. 5.7-4 for several values of time t. At $t = 0$, $E_x^+(z,0) = E_0^+ \cos kz$ is a cosine curve with an amplitude E_0^+. At successive times, the curve effectively travels in the positive z direction. We have, then, a traveling wave. If we fix our attention on a particular point (a point of a particular phase) on the wave, it seems to move with a velocity v_p, called *phase velocity*, which is given by

$$v_p = \frac{dz}{dt} = \frac{\omega}{k} = \frac{1}{\sqrt{\mu\varepsilon}} = \frac{c}{\sqrt{\mu_r \varepsilon_r}} = nc$$

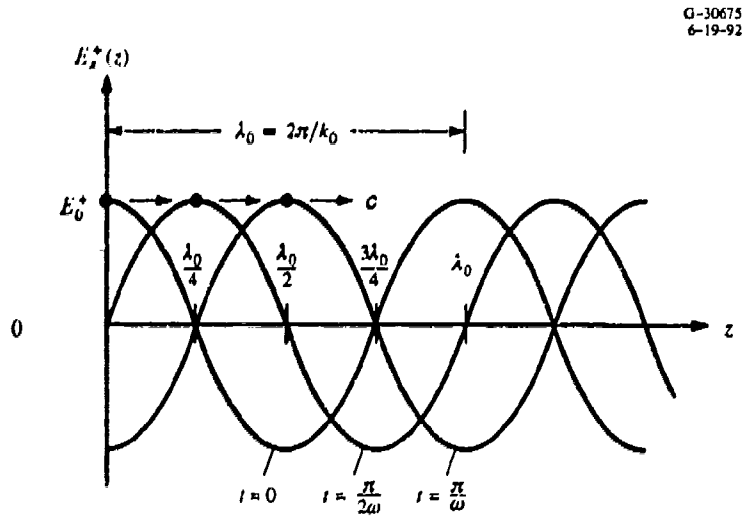

Figure 5.7-4 Wave Traveling in Positive z Direction: $E_x^+(z,t) = E_0^+ \cos(\omega t - k_0 z)$ for Several Values of Time t.

Note that in the free space, $\varepsilon_r = \mu_r = 1$, and hence $n = 1$ and $v_p = c \approx 3 \times 10^8$ meters/second.

The *wavelength*, λ, of a wave is defined as a distance (see Fig. 5.7-4) in which the phase of the wave increases by 2π radians at any instant. Thus, $k\lambda = 2\pi$, or

$$\lambda = \frac{2\pi}{k} = \frac{2\pi v_p}{\omega} = \frac{u_p}{f} = \frac{c}{f\sqrt{\mu_r \varepsilon_r}}$$

In free space, the wavelength $\lambda \Rightarrow \lambda_0 = c/f$. Note that the wavelength is used as a measure of whether a distance is long or short. At Omega frequencies (10–14 kHz), the wavelength in free space is approximately 30–21.5 km, whereas the free-space wavelength at 1000 kHz is only 0.03 km. Thus, a distance of 1 km is very short at Omega frequencies but very long at 1000 kHz.

It is obvious, that the second phasor term on the right-hand side of Eq. 5.7-3 represents a sinusoidal wave traveling in the --z direction with the same phase velocity as u_p. If we are concerned only with the wave traveling in the +z direction, then $E_0^- = 0$. However, if there are discontinuities in the wave propagation medium, reflected waves (i.e., E_0^-) traveling in the opposite direction must also be considered in the electromagnetic field solution of Maxwell's equations, as we will see later.

The magnetic field **H** associated with E_x can be found by solving Maxwell's equations. Thus for the case of the electric field $E_x^+(z,t)$ in Eq. 5.7-4, the rectangular components of the associated magnetic field **H** phasors are

$$\begin{aligned} H_x^+ &= 0 \\ H_y^+ &= \frac{1}{\eta} E_x^+(z) \\ H_z^+ &= 0 \end{aligned} \tag{5.7-5}$$

where $\eta(=\sqrt{\mu/\varepsilon})$ is called the *intrinsic impedance* of the medium. In free space ($\varepsilon = \mu_r = 1$)

$$\eta \Rightarrow \eta_0 = 120\pi \simeq 377\ \Omega \text{ (ohms)}$$

Because η is real in a non-conducting medium, $H_y^+(z)$ is in phase with $E_x^+(z)$ and thus we can write the instantaneous expression for **H** as

$$\begin{aligned} \mathbf{H}(z,t) &= \hat{\mathbf{y}}\, H_y^+(z,t) = \hat{\mathbf{y}}\, \mathrm{Re}\left[H_y^+(z)\exp(i\omega t)\right] \\ &= \hat{\mathbf{y}}\, \frac{E_0^+}{\eta} \cos(\omega t - kz) \end{aligned}$$

Hence, for a uniform plane wave the ratio of **E** and **H** is the *intrinsic* or *characteristic impedance* of the medium. We also note that **H** is perpendicular to **E** and that both are normal to the direction of propagation. Figure 5.7-5 shows an instantaneous picture of **E** and **H** fields in a traveling uniform plane wave. Note that our specification of $\boldsymbol{E} = \mathbf{x}\, E_x$ as an electric field parallel to the x axis is not as restrictive as it appears, inasmuch as we are free to designate the direction of **E** as the $+x$ direction, which is normal to the direction of propagation $\mathbf{u}_z$.

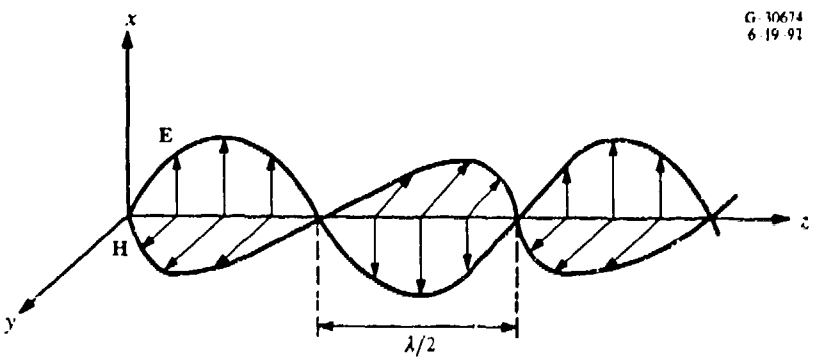

Figure 5.7-5 Instantaneous Picture of **E** and **H** in a Traveling Wave

The plane wave described by Eqs. 5.7-4 and 5.7-5 is a *linearly polarized* wave; its electric field vector is at all times in the same (i.e., x) direction. Figure 5.7-6a shows the direction of the electric field of a *linearly polarized* wave traveling out of page (positive z direction). In general, the electric field of a wave traveling in the z direction may have both an x component and a y component, as suggested in Fig. 5.7-6b. In this general situation, the wave is said to be *elliptically polarized*. At a fixed value of z, the electric field $\mathbf{E}$ rotates as a function of time, and the tip of the vector field traces out an ellipse. Two extreme cases of elliptical polarization correspond to *circular polarization* as shown in Fig. 5.7-6c, and *linear polarization* as shown in Fig. 5.7-6a. For the circular polarization, $E_1 = E_2$; while, for the linear polarization $E_2 = 0$. Note that the $\mathbf{H}$ field vector of a plane wave lags the $\mathbf{E}$ field vector by 90 degrees and has the same polarization (linear, circular, or elliptical) as the $\mathbf{E}$ field. The polarization is said to be *right-handed* if the instantaneous electric field vector rotates in the direction of fingers of the right hand when the the thumb points in the direction of propagation. The polarization is said to be *left handed* if the instantaneous field vector rotates in the opposite direction.

Conducting Medium — In a conducting medium, the wave equation and its plane wave solution have the same general form as in a non-conducting (loss-free) medium. However, the propagation constant k is now a complex quantity and is given by

$$k^2 = \omega^2\mu\epsilon = \omega^2\mu\epsilon' \left(1 - \frac{j\sigma}{\omega\epsilon'}\right)$$

$$k = k' - jk''$$

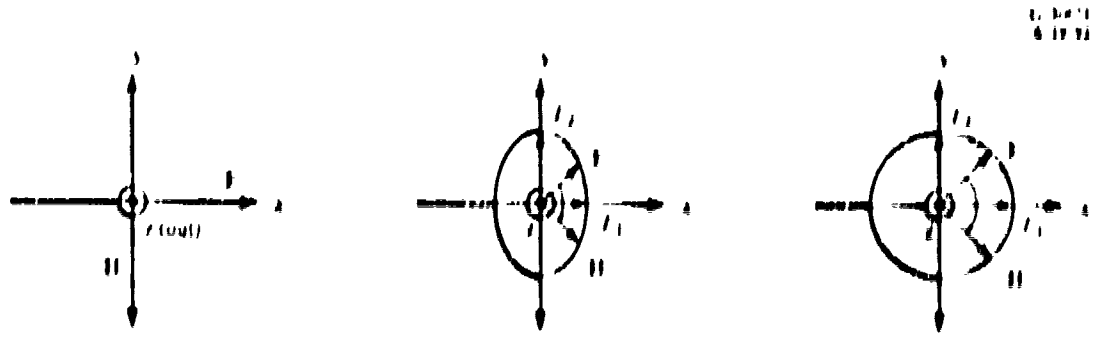

a) Linear Polarization b) Elliptical Polarization c) Circular Polarization

Figure 5.7-6 Plane Wave Polarizations

$$k' = \omega\left\{\frac{\mu\epsilon'}{2}\left[\sqrt{1+\left(\frac{\sigma}{\omega\epsilon'}\right)^2}+1\right]\right\}^{1/2}$$

$$k'' = \omega\left\{\frac{\mu\epsilon'}{2}\left[\sqrt{1+\left(\frac{\sigma}{\omega\epsilon'}\right)^2}-1\right]\right\}^{1/2}$$

where k' is the *intrinsic phase constant* and k'' is the *intrinsic attenuation constant*. There are several lossy media of interest to us for which Table 5.7-4 lists the approximate expressions for phase and attenuation constants (k' and k'').

Table 5.7-5 Wave Number ($k = k' - j\,k''$)

MEDIUM*	k'	k''
Perfect dielectric (no loss; $\sigma = 0$)	$\omega\sqrt{\mu\epsilon}$	0
Good dielectric (low loss; $\epsilon' >> \epsilon''$)	$\omega\sqrt{\mu\epsilon'}$	$\frac{\omega\epsilon''}{2}\sqrt{\frac{\mu}{\epsilon'}}$
Good conductor (high loss; $\sigma >> \omega\epsilon$)	$\sqrt{\frac{\omega\mu\sigma}{2}}$	$\sqrt{\frac{\omega\mu\sigma}{2}}$

*No magnetic losses.

The field impedance η is also a complex quantity in a lossy medium. The phase velocity of a plane wave in a lossy medium is

$$u_p = \frac{\omega}{Re\,(k)} = \frac{\omega}{k'} = c\left[\frac{\mu_r\epsilon'_r}{2}\sqrt{1+\left(\frac{\sigma}{\omega\epsilon'}\right)^2}+1\right]^{-1/2}$$

and the wavelength is

$$\lambda = \frac{2\pi}{k'} = \frac{u_p}{f}$$

The fields of a wave propagating along the z-axis towards $z = +\infty$ will be attenuated by a factor $\exp(-k''z)$ when the medium is lossy. If we define the field impedance as

$$\eta = |\eta|\exp(j\zeta)$$

then the fields are given by

$$E_x^+ = E_0^+ \exp(-k''z)\cos(\omega t - k'z)$$

$$H_y^+ = \frac{E_0^+}{|\eta|} \exp(-k''z)\cos(\omega t - k'z - \zeta)$$

Due to the phase angle ζ, the **E** and **H** fields of the wave are not in phase. Figure 5.7-7 illustrates the effect of attenuation in a wave of this type. Note that the *envelope*, (the curve connecting minima and maxima of the waves) is proportional to exp $(-k''z)$.

For the case of a high conductivity medium ($\sigma >> \omega\varepsilon'$), as displayed in Table 5.7-4, we have

$$k' = k'' = \sqrt{\frac{\omega\mu\sigma}{2}}$$

$$|\eta| = \sqrt{\frac{\omega\mu}{\sigma}}$$

$$\zeta = \frac{\pi}{4}$$

$$\lambda = \frac{2\pi}{k''} \quad \frac{2\pi\sqrt{2}}{\sqrt{\omega\mu\sigma}}$$

Thus, for a high conductivity medium, the attenuation constant is very large and **H** lags **E** by 45 deg, and the wavelength is very small compared to the free-space wavelength. For example, at the Omega signal

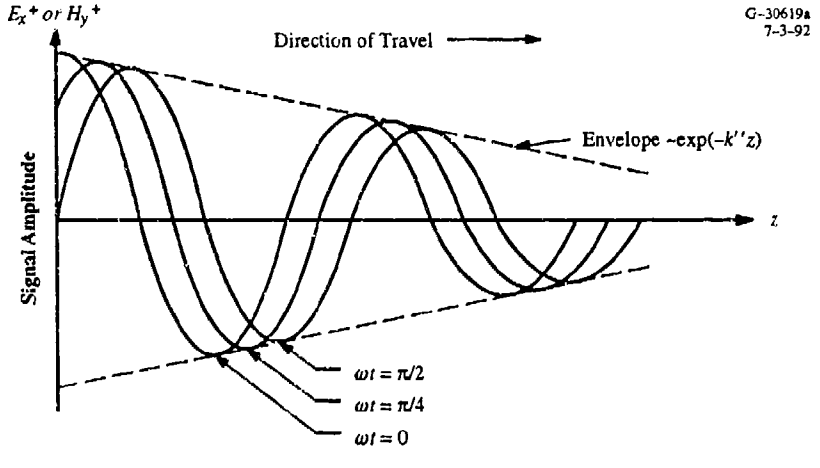

Figure 5.7-7 E_x^+ or H_y^+ in a Plane Wave Traveling Along the z-Axis in a Lossy Medium

frequency of 10.2 kHz, the wavelength is approximately 29.4 km in free space and 15.6 meters in sea water ($\sigma >> \omega\varepsilon'$), a difference between the two wavelengths of about a three orders of magnitude.

A wave starting at the surface of a good conductor and propagating inward is very quickly damped (absorbed) to insignificant values. The wave field is localized in a thin surface layer; this phenomenon is known as *skin effect.* The distance in which a wave is attenuated to 1/*e* (i.e., 36.8 percent) of its initial value is called the *skin depth or depth of penetration,* δ. This is defined by the condition that $k''\,\delta = 1$, or

$$\delta = \sqrt{\frac{2}{\omega\mu\sigma}} = \frac{1}{k''} = \frac{\lambda_{gc}}{2\pi}$$

where λ_{gc} is the wavelength in the good conductor. The frequency dependence of the skin depth of the various soils/materials forming the earth's surface is shown in Fig. 5.7-8. In the figure, note that the skin depth of Omega signal waves (10–14 kHz) is approximately:

1. 2.5 meters in sea water ($\sigma = 4$ mho/m), which means Omega signals attenuate very rapidly in sea water. For example, the signal is attenuated more than 99 percent over a distance of about 15 meters in sea water and therefore Omega navigation is limited to several meters of depth below the sea surface.

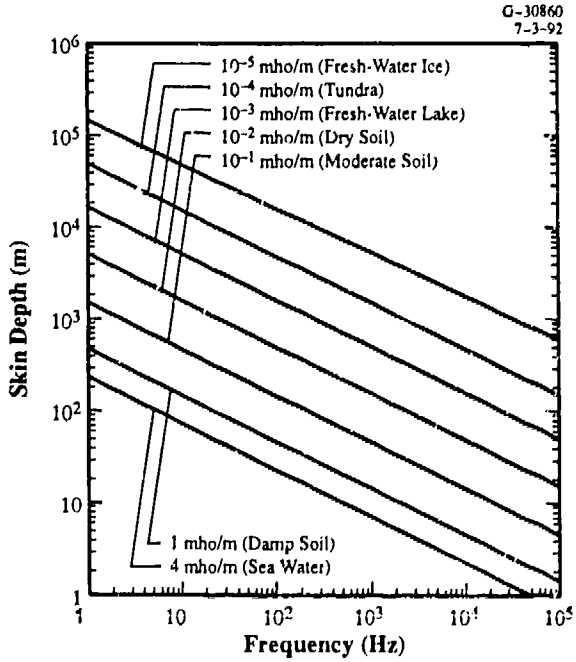

Figure 5.7-8 Skin Depth vs. Frequency for Various Earth Materials

2. 1600 meters in a fresh-water ice region ($\sigma = 10^{-5}$ mho/m) such as Greenland/ Antarctica, which means that Omega signals attenuate very slowly in an ice cap region and therefore Omega navigation is possible under the polar ice cap.

5.7.7 Reflection and Refraction of Plane Waves

Omega signals propagate from a transmitter to a receiver by successive reflections from the earth's surface and the ionosphere boundary of the earth-ionosphere waveguide. Therefore, in this subsection we will discuss reflection and refraction of plane waves incident on a planar boundary between two dissimilar media, as illustrated in Fig. 5.7-9. Let the *incident wave* (in medium 1) make an angle θ_i with the y axis (the normal to the boundary), the *reflected wave* (in medium 1) makes an angle θ_r with the y axis, and the *transmitted wave* (in medium 2) make an angle θ_t with the negative y axis. Note that the transmitted wave is the *refracted wave* and θ_t is the *angle of refraction*. As mentioned in Section 5.7.5, the incident signal, in general can have an arbitrary polarization (linear, circular, or elliptical). For our discussion, we will assume that the incident signal has the most general polarization, i.e., elliptical. We can consider such a wave to be composed of two linearly polarized waves, one with the electric field

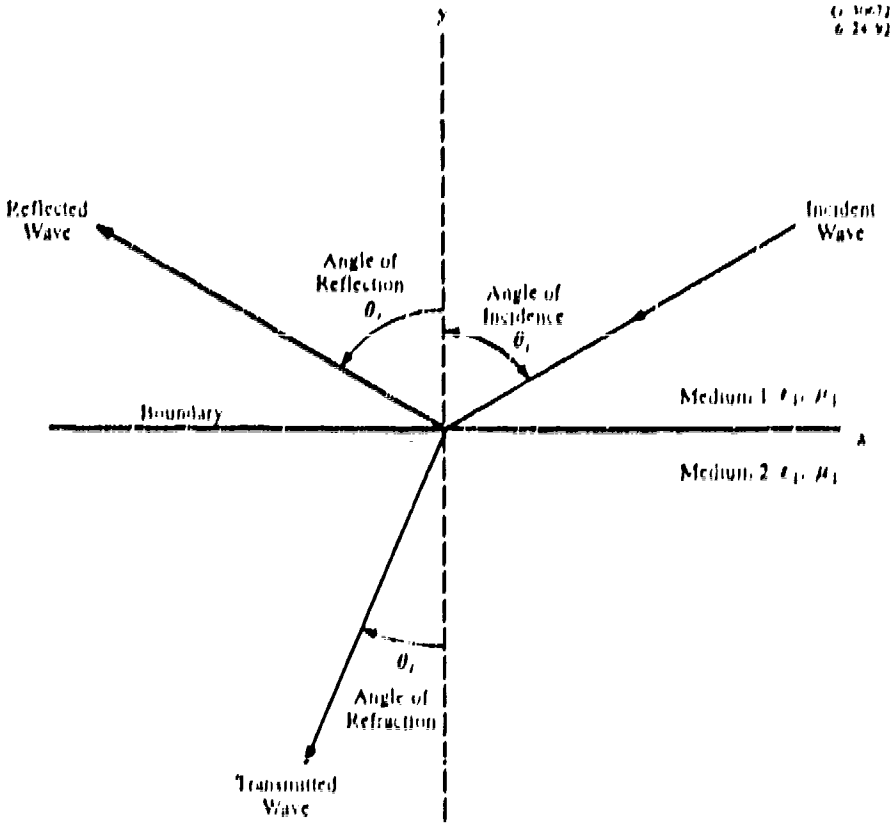

Figure 5.7-9 Plane Wave Incidence Geometry

vector parallel to the plane of incidence and the other with the electric field vector perpendicular to plane of incidence. The *plane of incidence* is a plane containing the wave propagation direction and the normal to the boundary between the two media. The waves with the electric vector field parallel and perpendicular to the plane of incidence are commonly referred to as the *e-wave* or *transverse magnetic (TM) wave,* and *h-wave* or *transverse electric (TE) wave,* respectively

At the boundary between the two media, the electromagnetic fields of the incident, reflection, and refraction waves must satisfy the boundary conditions listed in Table 5.7-3; as a result, we get

$$\theta_i \text{ (angle of incidence)} = \theta_r \text{ (angle of reflection)} \tag{5.7-6a}$$

$$\left(\sin \theta_i / \sin \theta_t\right) = \left(n_1 / n_{2)}\right) \tag{5.7-6b}$$

where n_1 and n_2 are the refractive indices of media 1 and 2, respectively; the second relationship, Eq. 5.7-6b, is familiar in optics and is known as Snell's law.

For Omega/VLF signal propagation, two types of two-medium boundaries are of interest. The first type is the boundary between air (medium 1) and ground (medium 2), similar to the air-ground boundary of the EI waveguide. The second type is the boundary between air (medium 1) and magnetized plasma (anisotropic medium 2), similar to the air (magnetized) ionosphere boundary of the EI waveguide. Therefore, we will present below the reflection and transmission (refraction) coefficients for the case where both media are isotropic, homogeneous, and conducting. As the reflection and refraction formulas for the second type of boundary, the air-(magnetized) plasma, are quite complex, we will give a qualitative discussion of the reflection and transmission of the waves form such a boundary.

CASE I: Reflection and Refraction at the Boundary Between Two Isotropic Media

The reflection coefficient R and the transmission coefficient T for the plane wave incident at the boundary $y = 0$ in (see Fig. 5.7-9) are obtained by applying of the boundary conditions at the boundary. There are given in the first row of Table 5.7-3, which considers σ_1 and σ_2 as arbitrary quantities. As a result, for an incident e wave, the reflection coefficient, R_e, and transmission coefficient, T_e, are given by (Ref. 10)

$$R_e = \frac{n_2^2 \cos \theta_i - n_1\left(n_2^2 - n_1^2 \sin^2 \theta_i\right)^{1/2}}{n_2^2 \cos \theta_i + n_1\left(n_2^2 - n_1^2 \sin^2 \theta_i\right)^{1/2}} \tag{5.7-7a}$$

$$T_e = \left(1 + R_e\right)\left(\cos \theta_i / \cos \theta_t\right) \tag{5.7-7b}$$

Similarly, for an incident h wave, we get the reflection coefficient, R_h, and the transmission coefficient, T_h, given by

$$R_h = \frac{n_1 \cos\theta_i - \left(n_2^2 - n_1^2 \sin^2\theta_i\right)^{1/2}}{n_1 \cos\theta_i + \left(n_2^2 - n_1^2 \sin^2\theta_i\right)^{1/2}} \tag{5.7-8a}$$

$$T_h = 1 + R_h \tag{5.7-8b}$$

Recall that the refractive index, n_ℓ, for the medium l (= 1,2) is given by

$$n_\ell = (\varepsilon'_\ell/\varepsilon_o)(1 + i \tan\delta_{c\ell})$$

$$\tan\delta_{c\ell} = \sigma_\ell/(\omega_\ell \varepsilon')$$

where ε'_ℓ and $\delta_{c\ell}$ the real part of the permittivity and loss tangent of l^{th} medium. The reflection coefficients are also called the *Fresnel reflection coefficients.*

For the case where medium 2 is a highly conducting medium ($|n_2|>>1$ because $\sigma >> \omega\varepsilon'$)

$$R_e \text{ and } R_h \Rightarrow (-1)$$

$$T_e \text{ and } T_h \Rightarrow 0$$

Note that the above expressions for the reflection and transmission coefficients are consistent with the boundary condition (see Table 5.7-3) which requires that the tangential component of the electric field vector must vanish on the surface of perfect conductor ($|n| = \infty$ because $\sigma = \infty$). For the case of a TM plane wave incident at a plane dielectric (lossless) boundary, the incident angle at which there is no reflection from the boundary is called the *Brewster angle* for the TM waves. Similarly, there is a Brewster angle for the TE waves. However, if both media are non-magnetic (i.e., $\mu_1 = \mu_2 = \mu_0$), there is no Brewster angle for the TE waves. If the dielectric medium is a lossy medium, the Brewster angle is a complex angle in which the real part of the incident angle yields the *smallest* reflection from the boundary. The physical incident angle associated with the Brewster angle condition for a lossy medium boundary is called the *pseudo-Brewster angle* (Ref. 35).

For the air-ground boundary, the reflection coefficients have the following general characteristics, an example of which is shown in Fig. 5.7-10 (Ref. 36).

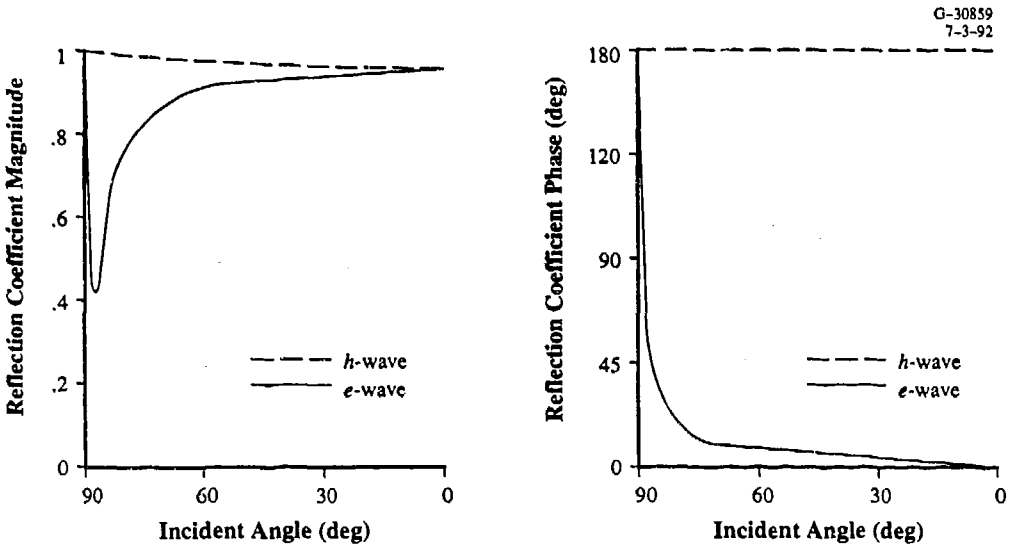

Figure 5.7-10 Reflection Coefficients for an Air-Ground Boundary with the Ground Conductivity of 10^{-4} mho/m (Ref. 36)

TE Wave Reflection Coefficient

1. The magnitude of reflection coefficient increases regularly with increasing angle of incidence and with increasing frequency; the magnitude is higher when the ground conductivity is greater and the frequency is lower.
2. The phase of reflection coefficient is always in the proximity of 180 deg.

TM Wave Reflection Coefficient

1. The magnitude of reflection coefficient first decreases with increasing angle of incidence, θ, until θ has attained a critical value, the "pseudo-Brewster incident angle;" the magnitude then passes through a minimum after which it increases very rapidly towards the grazing incidence (θ = 90 deg) to the boundary.
2. The angle θ corresponding to the minimum value of the reflection coefficient is smaller when the conductivity is greater.
3. The phase of the reflection coefficient starts at a very low value at normal incidence (θ = 0 deg) a[illegible] then increases very slowly until θ reaches in the neighborhood of pseudo-Brewster incidence, after which it approaches 180 deg for the grazing incidence.

CASE II: Reflection and Refraction at the Boundary Between Free-Space and Anisotropic Plasma

This case d[illegible] Case I in that now medium 2 is anisotropic (magnetized plasma). Note that in Case I, where [illegible] are isotropic, an incident TE wave gives rise to a reflected wave with the

same properties (i.e., another TE wave); similarly, an incident TM wave causes a reflected TM wave. However, in Case II, the anisotropic medium causes the reflected wave to be elliptically polarized (i.e., having both TE and TM wave components as shown in Fig. 5.3-6), independent of whether the incident wave is TE or TM wave.

Furthermore, the anisotropic plasma medium has a double-valued refractive index. As a consequence, there are two transmitted waves for each incident wave (Ref. 15). They are (nearly) circularly polarized in opposite sense and are called the *ordinary* and *extraordinary waves*. The ordinary name comes from the fact that for a vertically incident wave, the ordinary wave behaves as though there is no magnetic field in the anisotropic medium. We will not present the reflection coefficient expressions for this case as these expressions are quite involved and can be found in any book on wave propagation in magnetized media (cf., Ref. 15).

5.8 APPENDIX: ELECTROMAGNETIC FIELD COMPONENTS OF A TRANSMITTING SOURCE

Consider the transmitting source to be a small (relative to the signal wavelength), vertical, electrical monopole on the surface of a flat, perfectly conducting earth (see Fig. 5.8-1(a)). Assuming a uniform current $I(t) = \sqrt{2}I\cos\omega t$ (where I is the rms current) along the monopole of effective height h_e*, the resulting rms electric and magnetic fields at the distance ρ (meters) from the monopole are given by (Ref. 8).

$$E_z = \frac{Ih_e}{2\pi\epsilon_0}\left[\underbrace{\frac{1}{\omega\rho^3}}_{\text{Electrostatic}} + \underbrace{\frac{i}{u_0\rho^2}}_{\text{Induction}} - \underbrace{\frac{\omega}{u_0^2\rho}}_{\text{Radiation}}\right]$$

$$H_\phi = \frac{Ih_e}{2\pi}\left[\underbrace{\frac{i}{\rho^2}}_{\text{Induction}} - \underbrace{\frac{\omega}{u_0\rho}}_{\text{Radiation}}\right]$$

where E_z is the rms vertical electric field (volt/meter), H_ϕ is the rms tangential magnetic field (ampere/meter), ε_0 is the free-space permittivity ($=8.854\times10^{-12}$ farad/meter) u_0 is the speed of light in free space ($\approx 3\times10^{10}$ m/s), $\omega = 2\pi f$, f is the signal frequency, and $i = \sqrt{-1}$.

*It is the integral of the electric current $I(t)$ over height and divided by the base current, $(\sqrt{2}I)$.

It is interesting to note the effects of distance upon the various components (electrostatic, induction, and radiation) of E_z and H_ϕ. At $\varrho = \lambda_0/2\pi$ (note that $v_0 = f\lambda_0$ where λ_0 is the signal wavelength), the induction and radiation components are equal. Beyond one wavelength, the radiation component dominates and its E_z and H_ϕ fields decay as $(\varrho)^{-1}$. Figure 5.8-1(b) shows the distance dependence of E_z and H_ϕ for distances of up to one wavelength from the source. In this figure, it can be seen that for $0 \leq \varrho/\lambda_0 < 1$, all three components are contributing; while, for $\varrho/\lambda_0 < 0.1$, the electrostatic component term dominates. The *far-field* components of the electric and magnetic fields are related by $E_z = -\eta_0 H_\phi$ where η_0 ($\approx 120\pi$) is the characteristic impedance of free space.

Assuming that P_r is the power (watt) radiated by the monopole whose effective height, h_e, is small relative to the signal wavelength (i.e., $h_e < 0.1\,\lambda$), the rms value of the vertical electric field E_z at a distance ϱ (meters) is approximately given by (Ref. 8).

$$E_z \approx \frac{9.5P_r^{1/2}}{\varrho} \quad \text{(volt/meter)}$$

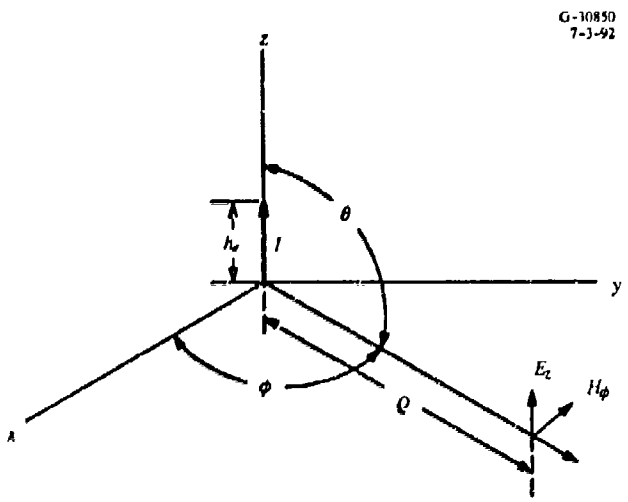

(a) Source Geometry

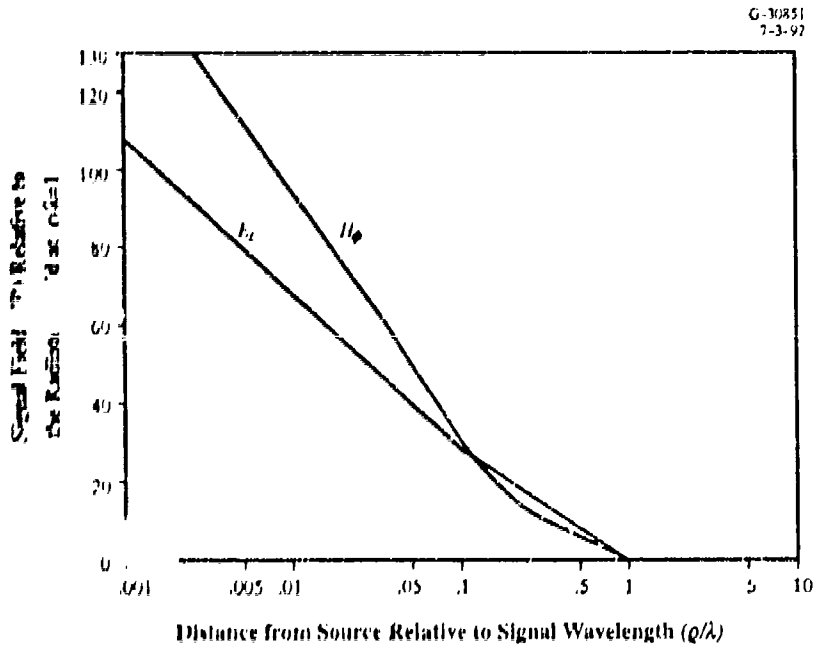

(B) Electromagnetic Fields

Figure 5.8-1 Electromagnetic Fields of an Electric Dipole (Ref. 8)

5.9 ABBREVIATIONS/ACRONYMS

cec	Centicycle (one-hundredth of a cycle)
dB	Decibel
deg	Degree
EI	Earth-Ionosphere
GDOP	Geometric Dilution of Precision
GHz	Gigahertz
hr	Hour
kHz	Kilohertz
km	Kilometer
mho/m	mho per meter
Mm	Megameter
PPC	Propagation Correction
rms	Root-Mean-Square
TE	Transverse Electric
TEM	Transverse Electromagnetic
TM	Transverse Magnetic
VLF	Very Low Frequency
UT	Universal Time

5.10 REFERENCES

1. Jones, T.B., and Mowforth, K., A review of the analytical techniques for determining the phase and amplitude of a VLF radio wave propagating in the earth-ionosphere waveguide, *AGARD Conference Proceedings* No. 305, AGARD-CP-305, 21–25 September 1981, Brussels, Belgium.
2. Cheng, D.H.S., A survey of some mathematical models of the very low frequency wave propagation, Goddard Space Flight Center, Report No. X-521-70-425, December 1970.
3. Gupta, R.R., Omega Navigation System VLF signal propagation, TASC, Technical Report TR-343-15, November 1975.
4. Gupta, R.R., Two-frequency 24-hour/4-month Omega signal coverage database development, TASC, Technical Report TR-5351-5-2, September 1988.
5. CCIR International Radio Consultative Committee), Propagation in Ionized Media, Volume VI, Report No. 895-1, Geneva, 1986.
6. Berry, L.A., and Herman, J.E., A wave hop propagation program for an anisotropic ionosphere, Telecommunications Research Report OT/ITS RR11, April 1971.
7. Wait, J.R., and Spies, K.P., *Characteristics of the earth-ionosphere waveguide for VLF radio waves*, National Bureau of Standards, NBS Technical Note No. 300, December 1964.
8. Watt, A.D., *VLF Radio Engineering*, Pergamon Press, Oxford, 1967.
9. Wait, J.R., *Electromagnetic Waves in Stratifield Media*, Second Edition, Pergamon Press, Second edition, 1970.
10. Galejs, J., *Terrestrial Propagation of Long Electromagnetic waves*, Pergamon Press, Oxford, 1972.
11. Budden, K.G., *The Waveguide Mode Theory of Wave Propagation*, Logos Press, London, 1961.
12. Pappert, R.A., Gossard, E.E., and Rothmuller, I.J., A numerical investigation of classical approximations used in VLF propagation, *Radio Science*, Vol. 2, No. 4, April 1967.
13. Morgan, R.R., Preparation of a worldwide VLF effective conductivity map, Westinghouse Electric Corporation, AD 669917, March 1968.
14. Ratcliff, J.A., *An Introduction To The Ionosphere & Magnetosphere*, Cambridge University Press, London, 1972.
15. Davies, K., *Ionospheric Radio Waves*, Blaisdell Publishing Co., Waltham, Mass., 1969.
16. Deeks, D.G., D-region electron distributions in middle latitudes deduced from reflection of long radio waves, *Proceedings of Royal Society*, A291, 1966.
17. Morfitt, D.G., Effective electron density distributions which describes VLF/LF propagation data, Naval Electronics Laboratory Center, NELC TR-141 (AD 738846), 1977.
18. Ferguson, J.A., Ionospheric profiles for predicting nighttime VLF/LF propagation, Naval Ocean Systems Center, NOSC TR530 (ADA085399), February 1980.
19. Cheng, D.K., *Field and Wave Electromagnetics*, Second Edition, Addison-Wesley Publishing Company, 1990.

20. Kossey, P.A., Lewis, E.A., and Field, E.C., Relative Characteristics of TE/TM waves excited by airborne VLF/LF transmitters, AGARD Conference Proceedings, AGARD-CP-305, September 1981.

21. Gupta, R.R., Theoretical background of IPP-2, TASC, Technical Report TR-343-2, February 1973.

22. Morris, P.B., and Gupta, R.R., Omega Navigation Signal Characteristics, *Navigation, Journal of Institute of Navigation*, Vol. 33, No. 3, Fall 1986.

23. Gupta, R.R, Graphical display of Omega signal modal parameters, TASC, Engineering Memorandum EM-2650 (Vol. I), September 1987.

24. Morris, P.B. and Cha, M.Y., Omega propagation corrections: Background and computational algorithm, Omega Navigation System Operations Detail (ONSOD), ONSOD-01-74, December 1974.

25. Gupta, R.R., Graphical display of Omega signal modal parameters, TASC, Engineering Memorandum EM-2650 (Vol. II), September 1987.

26. Gupta, R.R., and Morris, P.B., Overview of Omega Signal Coverage, *Navigation, Journal of Institute of Navigation*, Vol. 33, No. 3, Fall 1986.

27. Gupta, R.R., Omega/VLF signal coverage database development, TASC, Technical Information Memorandum TIM-5834-3-1, January 1991.

28. Gupta, R.R., Mode Interference Studies: (Volume I) Transmitter-excited interference, TASC, Technical Report, TR-343-10, November 1970.

29. Gupta, R.R., Graphical Display of Omega day/night 10.2 kHz signal radial profiles, TASC, Engineering Memorandum EM-2855 (Volumes A through H), November 1990.

30. Gupta, R.R., Graphical Display of Omega day/night 13.6 kHz signal radial paths, TASC, Engineering Memorandum EM-2855 (Volumes A through H), November 1990.

31. Harrington, R.F., *Time-harmonic Electromagnetic Fields*, McGraw-Hill Book Co., New York, 1961.

32. Ramo, S., Whinnery, J.R., and Van Duzer, T., *Fields and Waves in Communication Electronics*, John Wiley and Sons, New York, 1965.

33. Reitz, J.R., and Milford, F.J., *Foundations of Electromagnetic Theory*, Addison-Wesley Publishing Co., Reading, MA, 1960.

34. Kraus, J.D., and Craver, K.R., *Electromagnetics*, McGraw-Hill Book Company, Second Edition, New York, 1973.

35. Stratton, J.A., *Electronic Theory*, McGraw-Hill Book Co., New York, 1941.

36. Picqueard, A., *Radiowave Propagation*, John Wiley & Sons, New York-Toronto, 1974.

CHAPTER 6
OBSERVED SIGNAL BEHAVIOR

Chapter Overview — This chapter addresses the observed behavior of Omega signals based on a synthesis of observed and predicted behavior. Section 6.1 introduces important features of Omega signals. Sections 6.2 and 6.3 describe the normal signal behavior. Section 6.2 presents typical features of Omega signals that lead to useful navigation. Section 6.3 describes conditions that are "normal" (i.e., occur daily) but lead to coverage limitations. Abnormal signal behavior, particularly that associated with solar flares, is discussed in Section 6.4. Interrelationships between Omega signals at different frequencies are further addressed in Sections 6.5 and 6.6, which also introduce the concept of Composite Omega. Sections 6.7 and 6.8 summarize observed Omega signal behavior as interpreted by theory and identify some general tendencies. Problems, including worked-out examples and those to be attempted by the reader, are found in Section 6.9. Abbreviations/acronyms used in the chapter are defined in Section 6.10 and chapter references are listed in Section 6.11.

6.1 INTRODUCTION

This chapter addresses observed Omega signal behavior – its interpretation and explanation. Although the signal phase is of primary interest it is worthwhile to first list the general properties of the Omega signal and some of the conditions that must be satisfied to make measurements.

As with any radionavigation signal, the characteristics of Omega signals are described in terms of the following signal attributes: amplitude, phase, direction of arrival, and polarization. Observation of these quantities depends on the circumstances and equipment of the observer. Observers range from scientists with special equipment constructed especially for the signal property being studied to navigators using highly integrated receivers who are concerned almost exclusively with derived position information. All classes of observer must contend with observations made under both normal (geophysically quiescent) conditions and those measured during ionospheric disturbances. An additional concern is adequate observing conditions, i.e., good signal to noise ratio and absence of interference.

In this section, most attention will be directed to phase characteristics, particularly those of "well behaved" signals received under quiescent ionospheric conditions. Since Omega is a phase measurement system, position accuracy depends on the characteristics of these "useful" signals. Fortunately, they are undisturbed more than 95 percent of the time.

Although it is central to system accuracy, phase is not the only important signal attribute. If a signal cannot be received because of extraordinarily high local noise, locally generated interference, or high signal attenuation, its properties are moot. Such circumstances may make navigation impossible and, thus, signal and/or noise levels would be "most important" at that time and place. Fortunately, with good receiver installations, such circumstances are rare. Another important signal attribute is self-interference, which may render the signal from a particular station unusable. An example is long-path interference in which the signal propagated from the station over the short great-circle path is contaminated by, or even dominated by, the signal propagated over the long great-circle path. Quite obviously, interpreting a signal as propagated over the wrong path usually causes gross error.

Complexities aside, the basis of Omega is that it *must* be possible to relate phase changes in a receiver to position changes on the ground. Indeed, an absolute relationship between phase measurement and position normally exists. Severe self-interference may destroy this relationship at certain times and places, so that the measured phase becomes a random number not uniquely related to position or position changes (see Section 6.3.8). Thus, a discussion of "useful" phase characteristics is confined to explaining phase variation over paths with a single dominant mode.

This focus on single-mode phase variation leads to an understanding of Omega very much simpler from that which would generally follow from direct application of Maxwell's equations. The basic notion is that of a plane wave with a phase velocity that may change slowly in time and space with day/night ionospheric variations, changes in ground conductivity, etc. This model is used not only because of its comparative mathematical simplicity, but also because it *must* apply if the signals are to be considered useful. It has the great advantage of allowing propagation characteristics to be modeled using well-known parameters such as path location and orientation, rather than electromagnetic boundary conditions in the ionosphere, which are poorly known. However, the powerful full-wave models and computational techniques are especially needed and useful in answering the key question as to which signals are "useful."

6.2 NORMAL BEHAVIOR -- USEFUL SIGNALS

6.2.1 The Path

Experience in electromagnetics teaches two things: (1) there is no such thing as perfect shielding, and (2) lacking perfect shielding, everything everywhere affects anything anyplace. We have all looked out on a scene when, eventually, a window, windshield or something assumes a perfect alignment

to reflect the sun. We may even find ourselves casting shadows by the reflected light. A previously unremarkable part of the scene has just become a major contributor of radiation incident on us. That is, the object has now become part of an effective "path." The lesson is that it is always conceivable that some unusual set of circumstances combine to reflect, refract, or focus electromagnetic energy along a path quite different from what one ordinarily expects. With that in mind, one usually expects Omega signals to follow a great-circle path.

A difference between the example with the windshield and Omega signals is the wavelength. Although it is easy to find manmade components that are large with respect to light wavelengths, it is difficult to find or assemble structures that are comparable in size to the 30 km wavelength of 10.2 kHz Omega signals. This quite properly suggests that Omega signals will usually be received without the sometimes troublesome reflections from structures often found at higher frequencies. However, it does not ensure Omega reception via the great-circle path. Also, natural features, e.g., coastlines and the day-night terminator, can easily be large with respect to a wavelength.

If there is a marked asymmetry between conditions right and left of a propagation path, the great circle path assumption should be questioned. Basic principles of electromagnetics and optics, such as Fermat's Principle*, do, indeed, apply to Omega signals. However, in the absence of extremely anomalous conditions, one does not expect that path deviations would be sufficient to cause phase variations much different than those expected on a great-circle path. Thus one expects the steady state propagation calculations based on great-circle paths to be relatively accurate. However, if the day-night terminator intercepts the path, the apparent diurnal pattern or direction of arrival could be different from that predicted by steady-state, great-circle calculations.

An important concept is that of the *effective propagation path.* From the hop theory of radio propagation (Chapter 5, Section 5.1), it is apparent that no energy reflected directly over a receiver will reach the receiver. Rather, the rays that contribute primarily to the signal at a remote point are those launched and received more or less tangentially. For *D*-region ionospheric heights, a tangential launch corresponds to a first ionospheric interaction at about 9 degrees of arc (1000 km) from the transmitting source. As this is an absolute limit in hop theory, a smaller figure, such as 6 or 7 degrees (700 to 800 km) is expected for a typical path shortening. (In waveguide theory, calculations of the size of the first

*Sometimes referred to a Fermat's Principle of Least Time but used here in the more modern sense wherein the path traced by a beam of electromagnetic energy represents a minimum, inflection, or even a maximum in time. A modern statement is: Any path from A to B whose length is stationary with respect to a variation of path, and only such a path, is an actual path from A to B.

oblique Fresnel zone lead to similar results). Effectively, a portion of the first (or last) 6 degrees comprises the excitation (or de-excitation) region while in the mid-path the signal phase is modeled by incremental phase velocity or wave number contributions along the great-circle path. The notion of an effective path is developed more extensively in Chapter 9 (cf. Fig. 9.3-2).

The distinction between total geometric path and effective path is especially important when it is remembered that 7 degrees of arc on an east-west path corresponds to about a half hour at the equator and more elsewhere. Thus the distinction is especially obvious when considering diurnal phase change. Figure 6.2-1 shows a portion of a hypothetical diurnal phase variation near sunrise on the eastern end of an approximately east-west path. Once the terminator begins its transit through the mid-path region, the diurnal rate of change will be on the order of 10 cec/Mm* depending on path details. For an equatorial east-west path, the 15 degree/hour rotation rate of the earth corresponds to 1667 km/hour. Thus the slope of the diurnal change is 17 cec/hr but can be much higher for a north-south path. The consequence of a half-hour error in estimating the transition onset time is indicated by the dotted line in Fig. 6.2-1. The solid line shows the situation with the transition beginning with the start of mid-path illumination at point B, that is, when the sun illuminates the area at the effective eastern path end. (Ref. 1 describes the situation in more detail, especially in Fig. 4.)

Experimental evidence supporting the notion of an effective path may be obtained as follows. First, examine the start of sunrise on a north-south path when the illumination occurs simultaneously at

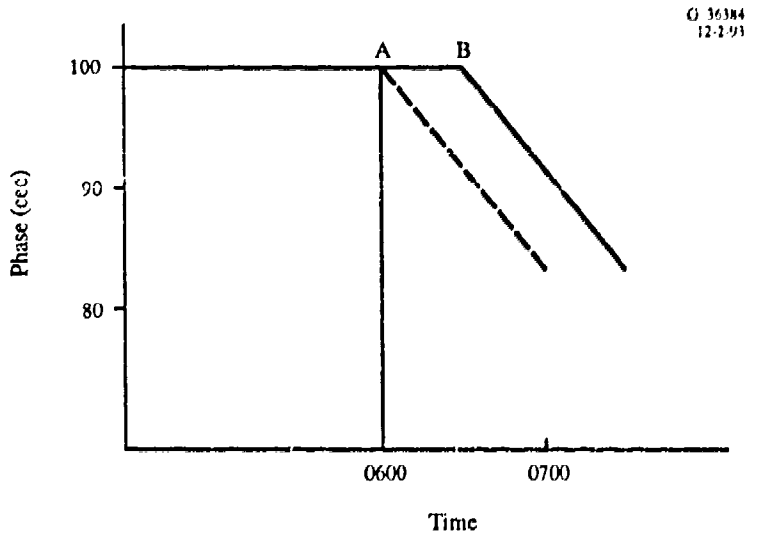

Figure 6.2-1 Phase Behavior at Start of Sunrise on a Long East-West Path

*Mm is the abbreviation for megameter, a 1000 km unit of distance.

all points on the path. This time, corresponding to points A or B in Fig. 6 2-1, can be determined to an accuracy of 1 to 3 minutes using a continuous analog recording. Then, compute the solar zenith angle corresponding to this start of sunrise. [As calculated, this angle corresponds to the moment when the sun's first feeble rays strike the ionosphere from *underneath* (98°).] Use this defining zenith angle to determine where sunrise begins on an east-west path. As expected, the answer turns out to be about 6 degrees as shown in Table 6.2-1 (from Ref. 1).

Table 6.2-1 End-Path Size from Phase Recordings

PATH	NUMBER OF MEASUREMENTS (Days)	SUNRISE END-PATH SIZE (degrees of arc)
Norway – New York	22	6.1
Trinidad – Norway	18	7.0
Hawaii – Trinidad	8	6.1
Hawaii – New York	31	2.7
Hawaii – San Diego	6	7.0
New York – Trinidad	32	8.5
New York – Hawaii	23	4.2
Median	22	6.1

6.2.2 Specific Spatial Behavior On Radial Paths

Radial paths, i.e., those directly outward from stations, are the most easily analyzed. While of little direct value to system calibration, great insight can be gained from examining signal variation over a few specific paths under simplified but real conditions. This means that while path orientation, magnetic field, and ground conductivity may vary along the path, the variation is relatively slow. In measuring signals along radial paths, it is more convenient to examine signal amplitude rather than phase. While phase varies rapidly along a path and is difficult to measure and reference to exact position, amplitude is readily measured and varies more slowly so that it is easily referenced to approximate positions. Further, the character of the amplitude variation relates closely to the character of the phase variation; a simple amplitude variation will correspond to a single dominant mode and, hence, a simple phase variation.

Figure 6.2-2 shows amplitude variation measured on an aircraft flying from the La Reunion transmitting station on a southwest bearing during daytime conditions. As can be seen, variation is quite smooth except at a distance near 300 km from the transmitting station. This range corresponds roughly to the skywave-groundwave interference expected by ray-hop theory. Note that, within the region very

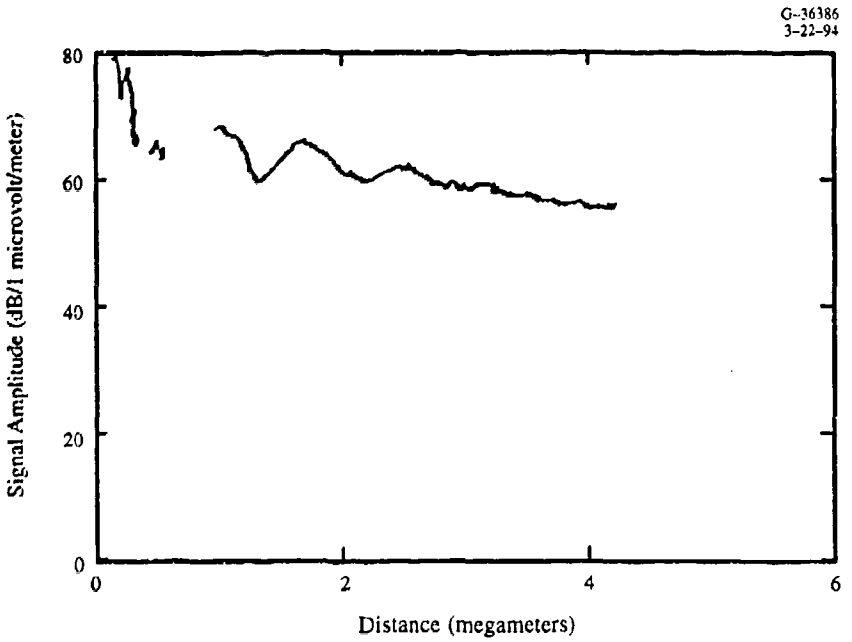

Figure 6.2-2 10.2 kHz Omega La Reunion Signal Amplitude Along a Nearly Radial Path (235°–253° Geographic Bearing) During Path Day (0705–1310 UT)

close to the transmitting station, propagation is essentially by groundwave. At greater distances along the path, a dominant first mode is established and variation is again uniform.

Figure 6.2-3 depicts a similar situation except that the path is nearer the magnetic equator and the signal is at a higher frequency. The variation is more pronounced showing the presence of a slight competing mode even out to a range of 2 Mm and beyond. The character of the amplitude variation indicates effective interaction between a dominant mode and a single competing mode. In this case, it is possible to relate peak amplitude deviations to peak or root-mean-square phase deviations. For the 5 dB maximum-to-minimum amplitude variation occurring at a range of about 2 Mm, an associated maximum phase deviation of about 4 cec is obtained.*

Figure 6.2-4 is similar to Fig. 6.2-2 except that the signal amplitude is measured at night. The severe fade at 400 km is sufficient to suggest the possibility of cycle slipping (cf. Section 6.3.8). However, as range increases, interference rapidly dies out. This is a good example of a mid-latitude path becoming dominated by a single mode at night.

*Computation is straightforward, however, a convenient nomograph is derived and given in Ref. 35. It relates relative mode strength, size of observed maximum-minimum fades, peak phase deviation and RMS phase deviation for two competing modes.

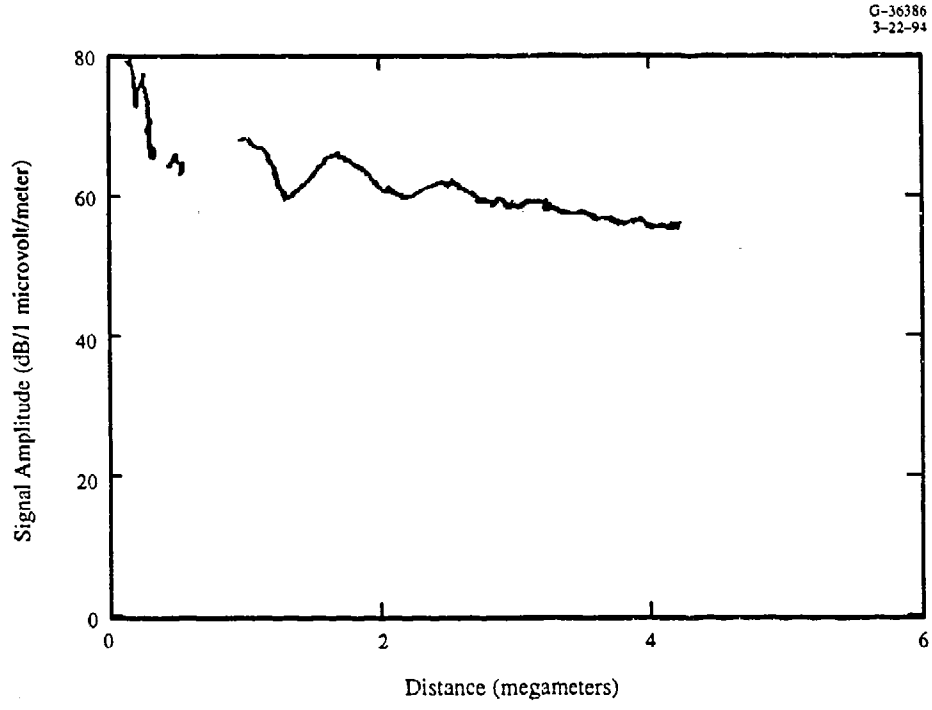

Figure 6.2-3 13.6 kHz Omega Hawaii Signal Amplitude Along a Radial Path (64° Geographic Bearing) During Path Day (1510–2340 UT)

Figure 6.2-5 illustrates a case of severe interference. It shows interference at night on a westbound path not on the geomagnetic equator but in the lower mid-latitudes. Interference between modes is severe and the signal is considered unusable for navigation even though the amplitude is reasonably high. It may be compared with computations shown in Fig. 5.5-5. While the curves show differences, as might be expected from variations in flight azimuths as well as from routine night-to-night ionospheric variations, both indicate severe interference.

6.2.3 General Spatial Behavior

This section addresses spatial variation of signal behavior particularly as is needed for system calibration. Discussion of these variations provides a basis for development of Propagation Corrections (PPCs) as is discussed in Chapter 9. The interpretation developed here is appropriate for the explanation of well-behaved signals useful for navigation, that is, most Omega signals. A unified approach is used in which all aspects of spatial variation are addressed simultaneously.

Spatial variation is best considered by first restricting other variations as much as possible. This means selecting data free from the effects of geophysical disturbances. A second selection is by considering measurements during only two diurnal conditions: "day" and "night." In discussing propagation,

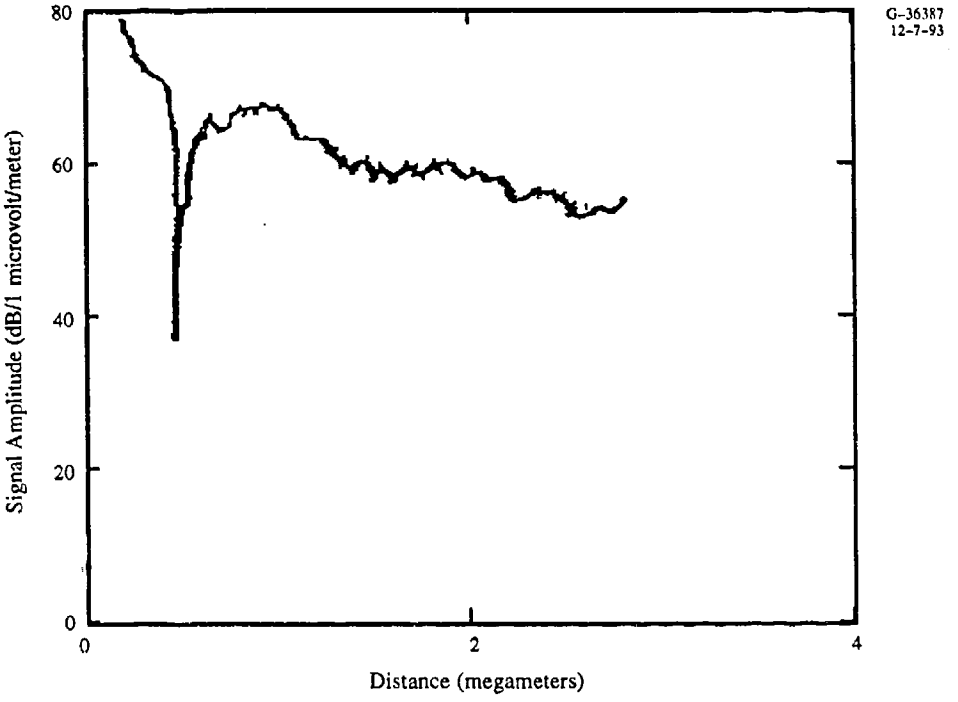

Figure 6.2-4 10.2 kHz Omega La Reunion Signal Amplitude Along a Radial Path (253° Geographic Bearing) During Path Night (1440–2105 UT)

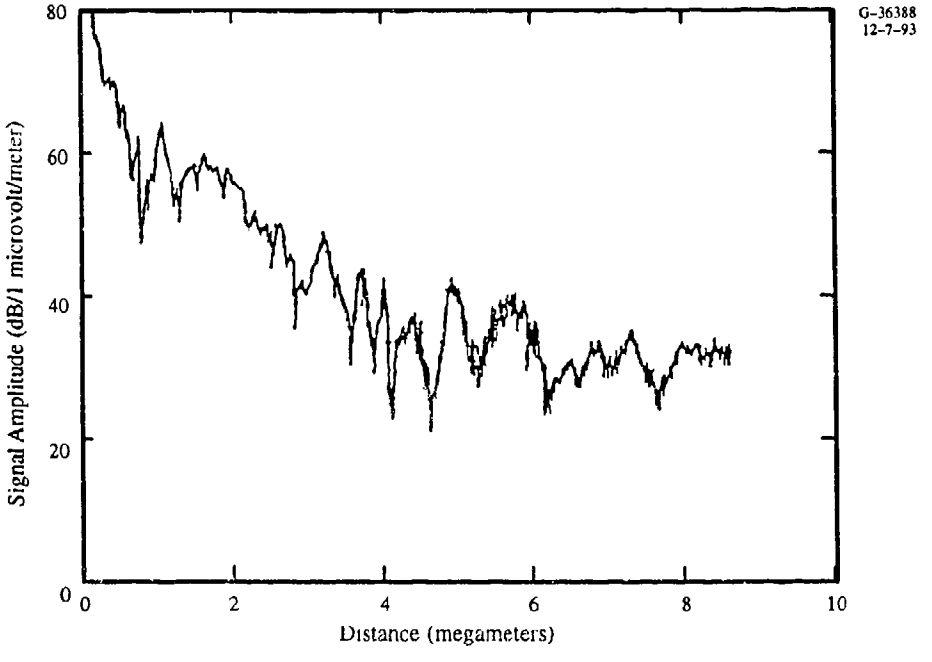

Figure 6.2-5 13.6 kHz Omega Hawaii Signal Amplitude Along a Nearly Radial Path (273°–281° Geographic Bearing) During Path Night/Sunrise (1235–1840 UT, 0905–1425 UT, 0755–1525 UT)

"day" means that an entire propagation path or paths is illuminated while "night" means that the path or component paths are entirely dark. A further restriction is to those measurements corresponding to propagation by Mode 1. From Section 6.2.2, spatial variation may be treated as if signals actually propagate over great-circle paths. A further convenience is that the point-to-point variation of propagation parameters along typical paths is usually small. For example, even a change from sea water to land typically corresponds to a change of phase velocity of only a few parts in 10^4. Also, for the selected day or night periods, point-to-point ionospheric variations are comparably small. These are the required conditions supporting a model incorporating path averaging wherein the resultant signal characteristics can be explained by incremental variations attributed to characteristics along a path. (This method is also used in the full-wave computational models mentioned in Chapter 5, Section 5.1.) In mathematical form, this model not only provides a means of predicting signal characteristics, it also provides a means of determining the sensitivity of Omega signals to the various parameters through regression analysis on an appropriate database (Ref. 2).*

Within the constraints of this model of spatial variation, it is important to realize that there is no essential difference between a phase measurement and a phase-difference measurement. Both reflect a mathematical combination of incremental phase shifts over a variety of propagation conditions. There is, perhaps, a tendency to regard a single radio propagation path as a "thing" of unique physical importance while a phase-difference is considered a mathematical artifact. This is simply not true. Indeed, the resultant phase over a simple path on the real earth represents propagation over a variety of conditions so the measurement cannot be associated with any single condition — any more or less than a phase-difference could. Our thinking perhaps gets muddled by oversimplifying to an idealized earth that is both homogeneous and isotropic; the real world is neither.

Thus, in a sense, phase and phase-difference measurements are interchangeable as data for the study of spatial phase variation. This is indeed fortunate as phase-difference measurements are easy to make while direct phase measurements are extraordinarily difficult. Direct phase measurement requires not only a local clock precisely synchronized to the transmitter, it also requires an antenna arrangement free from coupling to local objects. Such coupling can distort phase measurements by nearly 90° but will affect all signals similarly so that phase differences are not perturbed (Ref. 3).

*Applied to phase prediction over a signal path, the mathematical development referred to here is covered in Chapter 9.

A difficulty in making meaningful phase or phase difference measurements is the need for accurate reference survey. Since Omega navigation utilizes signal phase or phase-difference, it is not surprising that measurements of these quantities are very sensitive to the position of the receiver. A hyperbolic instrumental accuracy of one centicycle at 10.2 kHz corresponds to a displacement of 150 meters on the baseline connecting the pair of stations. Even today, reference data on which maps are based may not be that good. This is particularly true when it is remembered that the position of importance is the receiver with respect to the station(s) which may be on different continents. Presently, the Global Positioning System (GPS) provides the best reference.

Within the interpretive framework outlined above, each signal measurement is associated with particular defined incremental geophysical/electromagnetic conditions such as ground conductivity, geomagnetic latitude, path orientation, etc. Further, regression analysis of this set of measurements reveals particular sensitivities of Omega signals to each of the various conditions. Essentially, this is the means of calibrating the spatial variation of Omega signals. Two especially good features of the approach are: (1) there is a means of improving calibration through acquisition of more data and repeated regression analysis, and (2) the required path parameters, e.g., path orientation with respect to the geomagnetic field, are known. The latter circumstance is particularly desirable when contrasted with approaches requiring ionospheric electron de..sity profiles that are not well known. An undesirable aspect, perhaps, is that the entire system calibration problem is addressed at once. This makes it difficult for the student to grasp the various aspects separately.

The results of regression analysis can, however, be displayed as phase velocity variations with respect to the various parameters, e.g., ground conductivity. One can also display phase velocity variation as a function of direction for various geomagnetic latitudes. This shows that signal behavior is much more sensitive to small changes in path conditions during the night than during the day and much more sensitive near the geomagnetic equator. Regression analysis also was used to locate and evaluate velocity variations due to propagation under the auroral (or austral) zone (Refs. 4 and 5).

6.2.4 Diurnal Behavior

Unfortunately, Omega signals vary in time as well as in space. For a navigation signal attribute, one would prefer something that varies only with position in a mathematically simple way. However, the spatial variation of phase depends on path orientation, ground conductivity, etc., in a rather complex way. The effect of spatial variations can be simplified by selecting data for two clearly distinct periods: path-day and path-night. The situation becomes more complicated if paths of mixed illumination are considered.

In this discussion some old data will be used. The reader may well wonder why. The reason is that "honest" amplitude measurements of Omega signals have not been made for perhaps two decades. To a radio physicist, an amplitude measurement should be independent of noise. As discussed in Chapter 12, this means that the receiver front end should not limit the signals and, ideally, coherent detection should be employed. The last equipment to do this properly incorporated vacuum tubes! Nevertheless, some very good measurements were made — including those to be presented. Modern practice is to "measure" amplitude based on an estimate of noise and the resultant phase variance of the Omega measurement. This is more than adequate to study the characteristics of modal interference using signal measuring equipment on aircraft flying radial paths from transmitting stations. In an engineering sense, it has some advantage in that the newer technique addresses the same signal after limiting that an actual receiver would process. However, for this discussion, we return to the more fundamental quantities.

Figure 6.2-6 (from Ref. 21) shows the phase over a path between Forestport, NY and Balboa, Panama Canal Zone, which was operated during early system development. The time period of these observations was selected so that sunrise occurs simultaneously over both ends of the basically north-south path. Several features are apparent. Although abrupt, the phase changes do not occur infinitely fast. This suggests that the ionosphere has some effective time constant in its response to the "instantaneous" change in illumination. Even more apparent is a post-sunrise dip. Thus conditions during path transition are not simple functions of illumination. Some radio physicists attribute this behavior to the temporary formation of a reflecting "C" layer of ionization at sunrise. Figure 6.2-7 shows amplitude variation over the same path although not at the same time of year. Note the marked fade at the end of sunrise (near 1200 UT).

Figure 6.2-8 shows the phase of signals over the predominantly east-west path between Hawaii and Forestport, NY. One would expect that the segment-by-segment behavior of the signal over this path could be inferred from Fig. 6.2-6. Starting just before sunrise, the first feature of note is the marked distinct variation from the nighttime level. In fact, the time of this onset can typically be determined to an accuracy of about one minute from a continuous recording (see Section 6.2.1). This abrupt departure from night is clearly a result of an abrupt sunrise — not a gradual ionospheric lowering related to solar zenith angle change. Following this sudden shift, the sunrise phase transition, especially, exhibits a continuous ramp. This is as expected as transition proceeds during solar transit through the mid-path. There is a slight phase deviation at the end of sunrise as one would expect from segment contributions inferred from the north-south path in Fig. 6.2-6. Continuing in time, one notes a phase decrease roughly corresponding to variation of the solar zenith angle during the day. More precisely, the minimum phase is noted to occur six minutes after the average zenith angle minimum. If the solar zenith angle is regarded

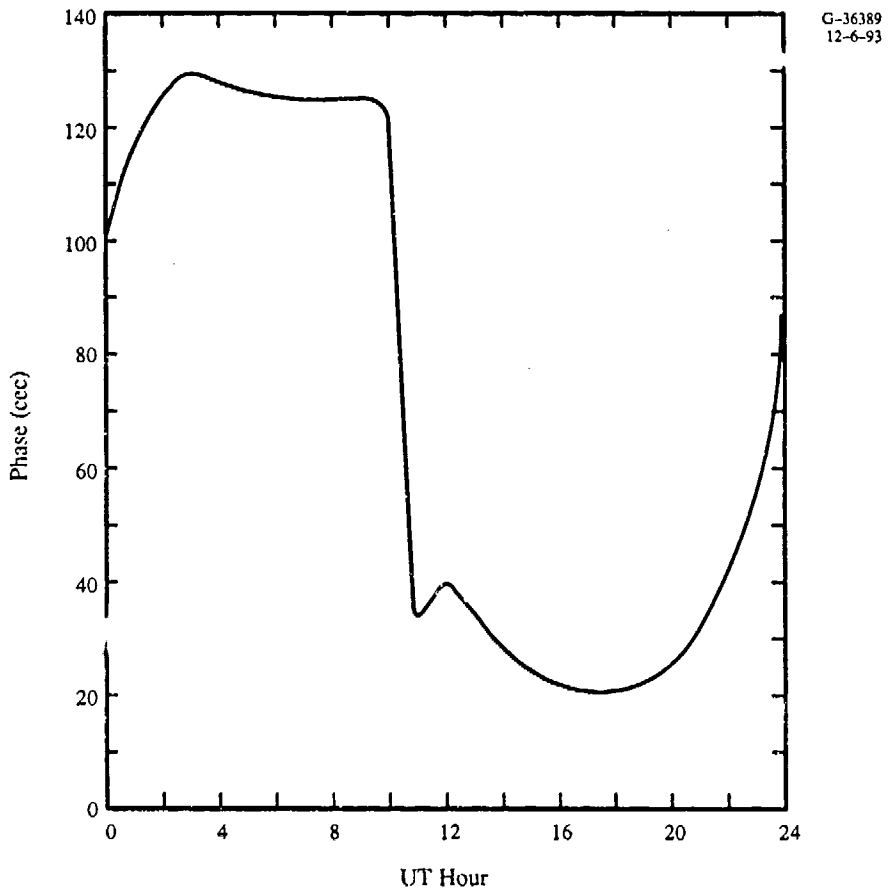

Figure 6.2-6 Diurnal Variation for a North-South Path (Balboa (Transmitter) to Forestport, NY, April 1963) Near the Equinox, 10.2 kHz

as an effective forcing function, the effective ionospheric time constant during the day is shown to be six minutes. We will see this number again and it is important as a measure of how fast the ionosphere could respond to the unexpected as, for example, from a solar flare. Continuing in time, one proceeds through the sunset transition returning to the nominal night level. In particular, Fi[illegible] 2-8 indicates that the night level is not immediately reached but requires over an hour after the solar [illegible]umination of the ionosphere is ended. This suggests another means of measuring the ionospheric time constant at night. Figure 6.2-9 shows amplitude over the same path but not at the same time of year. It, too, exhibits qualitatively the behavior one would expect from using the north-south observation to model incremental changes. Note that the minimum signal amplitude occurs just after sunrise rather than in mid-day. Over a variety of paths, the signal amplitude is about 4 dB below nominal day level for about an hour at the end of sunrise. As one hour out of 24 is about 5 percent of the time, the sunrise fade is the proper 95 percent design point for Omega signal amplitude (Ref. 6).

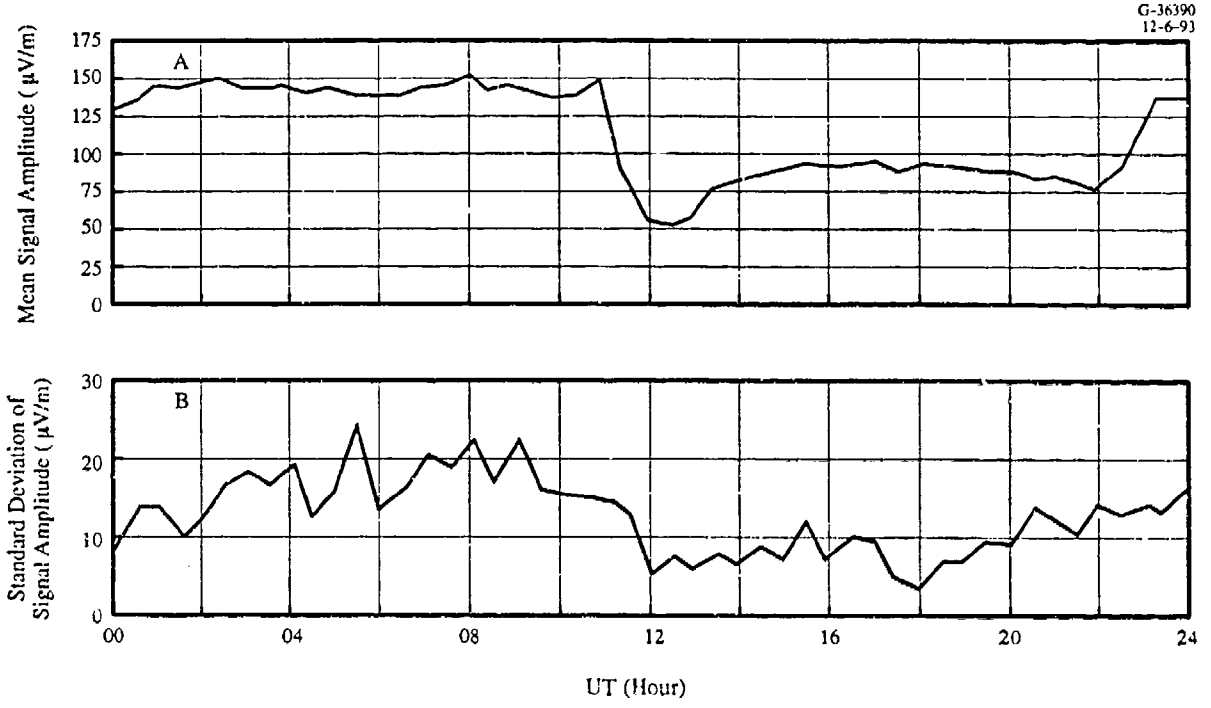

Figure 6.2-7 Plot of Mean Signal Amplitude (A) and Corresponding Standard Deviation (B) for the 10.2 kHz Signal Received at Farfan, Canal Zone, from Forestport, NY, 27 November–21 December 1962.

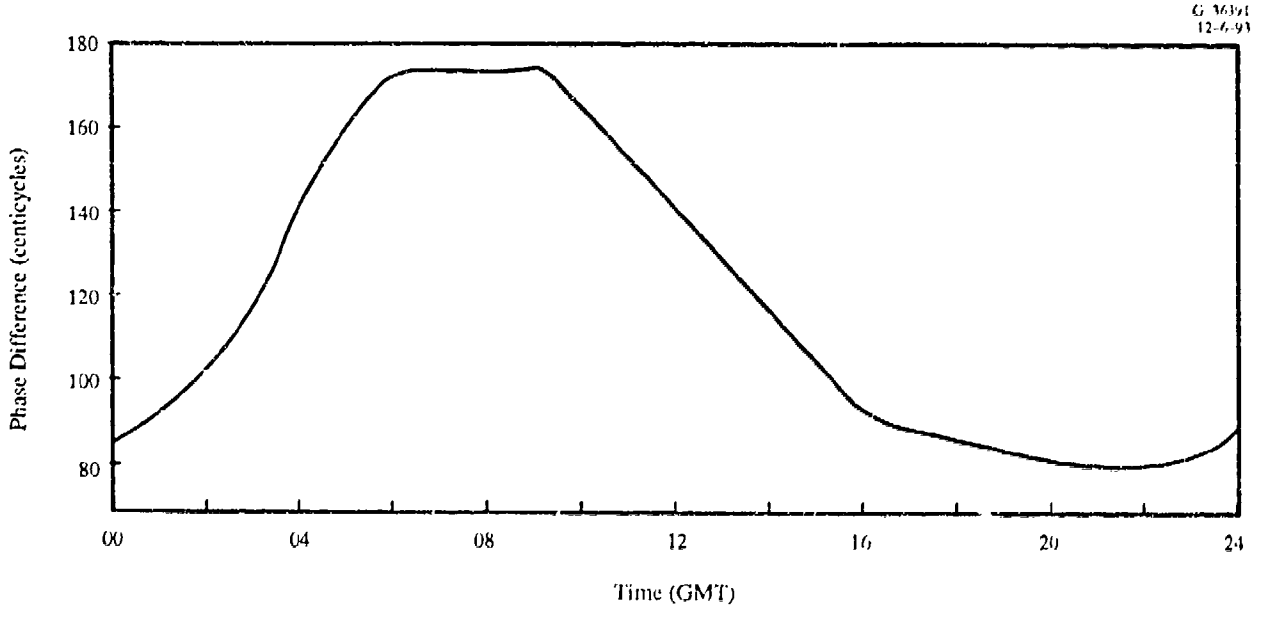

Figure 6.2-8 Average 10.2 kHz Phase of the Haiku, HI Transmitted Signal Received at Forestport, NY, 17–24 May 1966

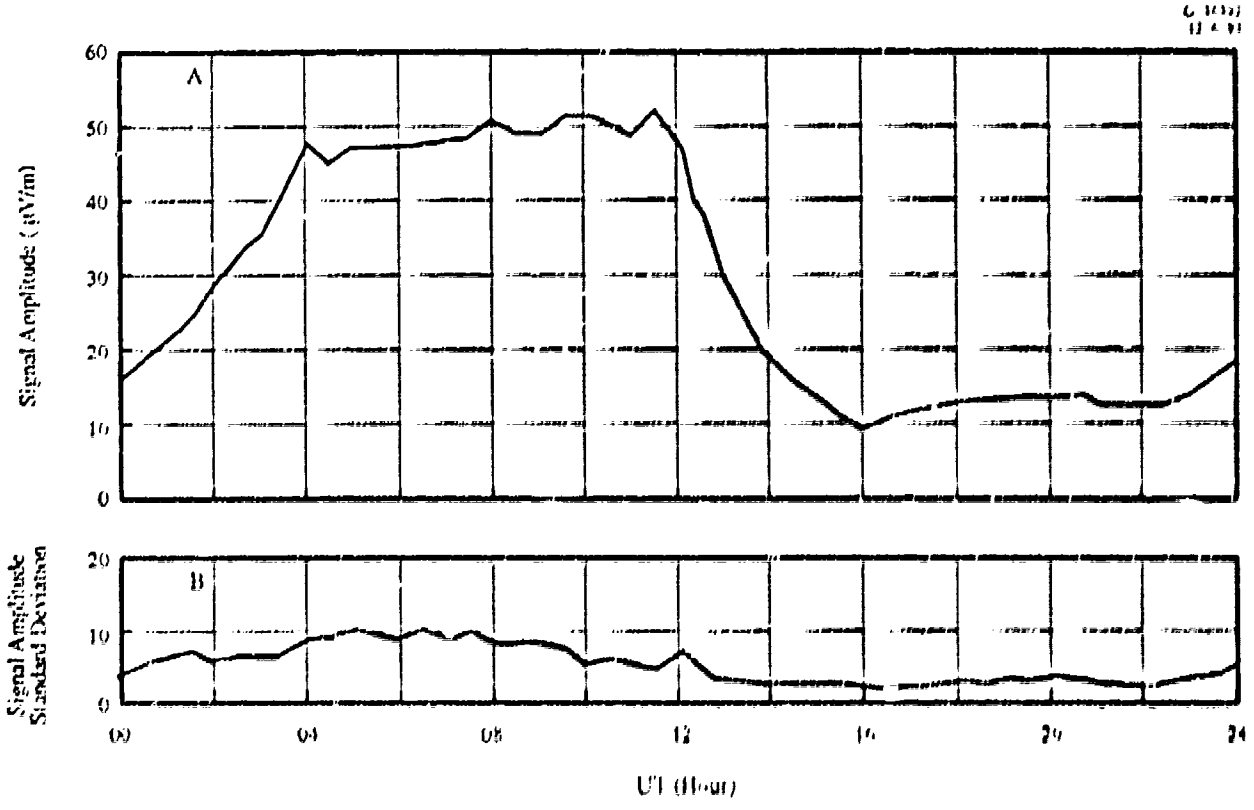

Figure 6.2-9 Plot of Average Field Strength (A) and Corresponding Standard Deviation (B) for the 10.2 kHz Signal Received at Rome, NY, Transmitted from Haiku, Hawaii, 24 October – 10 November 1962.

Ordinarily, one thinks of a "trapezoidal" diurnal phase change. The trapezoid is more "square" on north-south paths and less so on east-west paths. This is a rather imperfect model. Not only is there always marked "curvature" during the day, but the slope on the trapezoidal legs is not constant. For example, a path westward from Omega Norway starts with a slow diurnal variation that substantially increases as the path becomes more nearly north south near the equator. There is also an unusual "double" diurnal effect can occur on very high latitude paths (see Ref. 36, App. B). It is, however, a direct result of the individual path segment contributions.

A clarification is needed on the "daytime" phase previously introduced in the spatial discussion. The data clearly indicate phase changes slowly but continuously during the day. A "daytime" phase value can be obtained by "adjusting" the data to correspond to a situation in which a path is normally illuminated everywhere. One can get very clever and use the average adjustment as a regression variable. If done correctly, one would expect this to be unimportant. In practice, regression shows the adjustment to be basically

correct. As the adjustment is more nearly reflective of seasonal, rather than diurnal, change, this indicates that there is little seasonal variation other than that indicated by the zenith angle. (Arctic areas could be an exception to this but seasonal change becomes somewhat indistinguishable from the day night changes modeled by spatial theory.)

We should further note that the foregoing addresses rather precise measurements of amplitude and phase. Most users of automatic equipment do not see these signal components but only the resultant fix after Propagation Corrections (PCs) are applied. Clearly, a small error in transition time on a PC can yield a large error in prediction during a transition – particularly on a north south path. While the repeatability of phase measurements is very good during transitions, the difficulty of modeling suggests a strategy of "de weighting" them during rapid transitions.

Note that this section has addressed the diurnal variation of signals which are continuously dominated by the first propagation mode. This is the usually prevailing case and the case which must prevail for the signals to be useful. Sections 6.3.8 and 6.6 discuss the case of modal interference. Several examples of observed phase variation, normal and with interference, are given in Section 6.6.

6.3 COVERAGE LIMITATIONS

Section 6.2 addresses "normal behavior" as associated with useful signals. This section, too, addresses "normal" behavior as those characteristics common to most signals under some conditions (places or times), though not those associated with the usual desirable behavior. The distinction is that the signals discussed here cannot be used for navigation. Although less commonly encountered, these limitations on signal use are important in much the same way that it is important to keep a rotten apple out of a pie. Omega offers great redundancy. Indeed, the strength and character of Omega signals are such that even useful signals are typically received at 10.2 kHz alone (Refs. 7, 8, and 9). But it is necessary to know which signals to use and which to "de select."

Operationally, coverage limitations easily divide into two classes: (1) those that preclude measurement of the signal and (2) those that do not. The latter type are especially insidious. There are instances where a strong signal is received, but is of no value for navigation. There are circumstances where the received phase may be a *random number* even though the amplitude permits accurate measurement. Since a user may not be able to detect problem signals based only on received information, *a priori* coverage restrictions have been developed to provide guidance on the safe use of signals. Also, in some circumstances, receivers can be programmed to detect and avoid use of unsafe signals.

Circumstances that preclude adequate measurement of signals are those that yield an inadequate signal-to-noise ratio (SNR). The root cause may be low signal strength or high noise (or interference). These conditions are serious in that Omega navigation may be precluded, but at least provide no misinformation. It would be extraordinarily incompetent for any person or equipment to process phase values under conditions allowing inadequate measurement. Observability (in terms of SNR) is easily evaluated at the receiver (Chapter 12).

Signal self-interference is potentially dangerous in that the user cannot be guaranteed any means to determine the condition locally. Self-interference includes modal interference and long-path interference between signals received over the long as well as the short ares of the great-circle path. While this section introduces coverage limitations based on physics, expectations, and observations, Chapter 10 describes a wide array of coverage tools that have been developed for guidance regarding signal prediction.

6.3.1 Noise and Interference

Any platform — ship, aircraft, or land vehicle — will generate both noise and interference. Noise and interference may also be generated by nearby sources off the platform itself. For example, arc welders in shipyards are troublesome, as are some equipments used at aircraft gates. Additionally, lightning associated with thunderstorms contributes a background noise level worldwide.

Of these, most signal-to-noise coverage assessments consider only the thunderstorm-generated noise, which serves as a general background level. It is manifestly impossible to know in advance the proximity to an arc welder or the particular imperfections of an installation. Worldwide noise data can be obtained from CCIR tables or, better, from a thunderstorm center-based approach (Refs. 10, 11, and 12). One characteristic of thunderstorm-generated noise is that it is highly impulsive. Indeed, a processing gain of about 12 dB can be obtained by discriminating against the noise spikes (cf. Chapter 12). All worldwide noise data represent statistical *averages*. Statistically, at some place and time, whatever is specified will be exceeded.

The distinction between noise and interference is one of coherence. Theoretically, a harmonic of a local power frequency might exceed the level of an Omega signal and thus capture phase tracking in a receiver. In practice, power frequencies are rarely very stable — especially on vehicles — and harmonics do not tend to stay within tracking bandwidths long enough to be troublesome.

Generally, a discussion of how to reduce local noise and interference sources is out of place in this section. However, system personnel should be aware that the problems are quite real. While a proper response to a user may well be "clean up the installation," this may not prove easy. However, locally generated noise and interference can usually be adequately reduced.

6.3.2 Amplitude Limitations

The typical standard deviation of the amplitude, or "field strength," of an Omega signal at a fixed time of day is about 1 dB. There is considerable day-night variation and a "fade" of about 4 dB at sunrise, but ordinarily the received field strength is very stable (Ref. 6).

Field strength is usually not only stable, but high. Attenuation rates are low — sometimes lower than 1 dB/Mm. As will be noted in following sections, one can usually detect an increase in field strength near the antipode of station due to focusing on the spherical earth. A significant limitation is self-interference due to signal propagation over the long path more than halfway around the world.

One of the few circumstances that limits Omega usage due to field strength alone is when signals propagate over regions of the earth's surface with extremely low conductivity. Only two areas of the world have sufficiently low conductivity and are large enough to be notable limitations. From a signal propagation viewpoint, Greenland can be well approximated as a bowl of ice about 3000 m thick. Attenuation rates can reach 30 dB/Mm when the ice pack is illuminated by the sun. This acts as a "switch" to turn off Omega signals. Antarctica is similar to Greenland in this sense. A caution regarding theoretical studies of signals over these areas is that the effective ground conductivities are not well known — especially as the skin depth of Omega signals over Greenland can reach 1 km. It is also true that the electrical permittivity becomes important at very low conductivity and this, too, is not well known. (cf. Chapter 5).

Several of the coverage "holes" speculated for Omega are in areas closely adjacent to Greenland and Antarctica (Ref. 13). These are instances where a geometrically needed signal is severely attenuated passing over ice while the noise comes from an equatorial direction and suffers little attenuation. Note that the problem of signal reception at, say, the South Pole is essentially one of receiver design and clean installation. Noise and signals all come from outside the region and are affected equally.

6.3.3 Near Field

Within the near-field region close to stations, the modal structure is complex. In a sense, this can also be thought of as a modal interference region although it is best to think of the near field as an area in

which the skywaves and groundwave interfere. An example of structure in this region has already been presented (Fig. 6.2-4). This area is conventionally omitted from coverage. It is usually approximated by a circle of radius 1 Mm centered on the transmitting station. Although the detailed size and shape does vary from day to night, station to station, and frequency to frequency, this simple approximation has sometimes been applied in coverage evaluations because the coverage area varies with the square of the signal range; thus less than one percent of the possible coverage area is affected.

Signal use within the near field but closer to a station than the skywave-groundwave interference itself is possible. Propagation within this region is essentially groundwave and thus quite stable and predictable. There are three complications: (1) signal levels are high, thus possibly causing phase shift with amplitude in poorly designed receivers; (2) fix geometry often depends sensitively on position, thus possibly causing problems in inadequately designed automatic receivers; and (3) at ranges less than a wavelength, both the inductive and static field contributions need to be included in phase predictions. It may be noted that station monitors routinely operate very satisfactorily at about one wavelength. Operational regions of predominantly groundwave reception include Honolulu and Pearl Harbor, Hawaii (Omega Hawaii), the Bass Strait (Omega Australia), and Japanese and Korean coastal waters near Tsushima (Omega Japan).

6.3.4 Modal Interference

Modal interference limitations occur exclusively on night paths. Beyond the near field, the first mode is always dominant on short (< 20 Mm), full-day paths.

An example where modal interference extends great distances out from stations has already been shown [Fig. 6.2-5]. Sometimes, as in the case of Liberia, the interference is sufficient that Mode 1 never dominates at any range between certain westbound azimuths from the station. At other stations, Mode 1 may eventually dominate.

Interference is much more severe for equatorial stations than from those at high latitude. For comparison, Liberia is on the geomagnetic equator, while Norway and North Dakota are at high geomagnetic latitudes. A number of stations are sited near 21° geomagnetic latitude. For these, limitations arise almost immediately when propagating westbound toward the geomagnetic equator. In these cases, particularly at 13.6 kHz, exclusion of signal use also extends several thousand kilometers eastward and toward the equator. These eastward limitations are generally due to Mode 3 (second TM mode; see Chapter 5), propagation; not Mode 2 (first TE mode; see Chapter 5) as is the more common limitation.

Modal interference can also arise on a signal that is nominally undisturbed after the near field, but then becomes disturbed at some range. An example of this is the signal from North Dakota to the South Pacific. Due to the high geomagnetic latitude of the station, the excitation of Mode 1 is much favored over Mode 2 and clean signals propagate over the North Pacific. However, as the azimuth becomes more southwesterly and ranges extend beyond Hawaii over the geomagnetic equator, the second mode can eventually dominate. While some investigators favor explanations incorporating modal conversion at or near the geomagnetic equator, this is not necessary to explain the observed interference. A calculation using path averaging (WKB) techniques* explains the observations well — at least at 10.2 kHz. However, there are some instances where mode conversion unquestionably occurs — particularly during transitions on the higher-frequency VLF signals.

Modern full-wave propagation theory can yield predictions in excellent agreement with observation. The problem is that the model parameters, particularly electron density gradient and height, must be those that actually prevailed on a given day of observation. The "usual" parameters are likely to produce results that are somewhat "wrong" compared with any specific set of observations. Calculations indicate that the characteristic signal amplitude minima are more severe if the ionospheric height is chosen higher. However, the major effect of varying ionospheric height is to "stretch" the predicted pattern horizontally. Thus, a height change could shift the computed minima from, for example, ranges of 1, 2, and 3 Mm to 1.1, 2.2, and 3.3 Mm, respectively. Generally, calculations with relatively minor changes in the ionospheric height can yield good agreement with observation. Thus, the important feature of computed signal profiles is the prediction of any interference indications and the nominal magnitude. The precise location of the interference region is rarely of concern since, if a minimum is located at one point today, it will likely be somewhere else tomorrow as the ionospheric height fluctuates. However, it will exist somewhere in the area.

6.3.5 Antipode

The first of two coverage limitations arising from the spherical nature of the earth is the existence of an antipodal region directly opposite each transmitting station (cf. Fig. 5.4-3). The signal from each station arrives at its respective antipode from all paths and, indeed, a build up of field strength is

*See Chapter 5 for an explanation of these techniques.

experimentally observed in this region as shown in Fig. 6.3-1.* The phase in the vicinity of the antipode is, however, complicated. In the same way that the near field region around a station itself is eliminated from coverage, an antipodal region is also excluded. The coverage guidance given in Chapter 10 indicates that a circular region within 1 to 2 Mm of the antipode is excluded. The assessment aid PACE, noted in Chapter 11 and described more fully in Appendix C, also uses an exclusion radius in this range that corresponds roughly to the exclusion area employed for the near field.

6.3.6 Long Path

The second limitation introduced by the spherical shape of the earth is that for each receiving site and each short arc of the great-circle path, there is a corresponding signal path over the longer arc. This is a distinct limitation separate from the antipode in that the self-interfering signal is received over only one

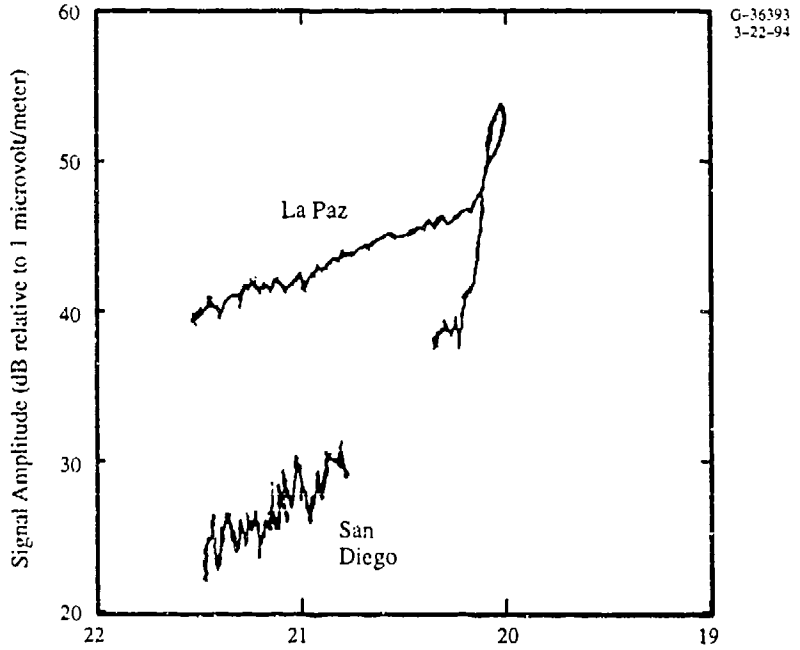

Figure 6.3-1 Omega La Reunion 13.6 kHz Signal Amplitude (108°, 152° long path radials) on a Flight From La Paz, Mexico to San Diego, CA via the La Reunion Antipode on 27 September 1979

*These data were measured as part of the North Pacific Validation Project. A flight was conducted from La Paz, Mexico (in Baja, California Sur) to San Diego, CA, via the La Reunion antipode. An amplitude buildup when flying both to and from the antipode is marked. Detailed analysis is complicated by bearing differences (on the two legs of the flight) and the fact that antipodal measurements necessarily include propagation over transitional paths.

path, the "long path." Owing to differences in attenuation between day and night and between westbound and eastbound signals, this limitation can be severe. The limitation will usually occur during the short-path day especially on west-bound paths near the equator. At times, the short-path signal from Liberia can be dominated by a long-path signal traveling 80 percent of the earth's circumference as compared with only 20 percent for the short path. If the long-path signal dominates, lines-of-position (constant phase contours) behave oppositely from the sense expected from vehicle motion. That is, when moving away from the transmitting station, one is moving toward the source of the dominant signal.

Long-path limitations are *the* most important restrictions on Omega signal usage when the short-path is fully in day. Signal coverage guidance indicates long-path limitations at 10.2 kHz which are particularly severe for Liberia (cf. Chapter 10).*

6.3.7 Modal Interference Signatures and Cycle Jumps

As already stated, modal interference can be particularly insidious simply because there is no completely reliable and predictable signature. There are locations where given signals may have cycle slips or jumps but, over a specific few days of observations, nothing unusual may occur. A marked spatial interference pattern (approximately constant in time) may exist but an aircraft or vessel may be moving more or less at constant distance from the station and not experience anomalies. It is also possible to be navigating in a region where Mode 2 is completely dominant. In Omega coverage nomenclature, this is also referred to as a "Modal Interference Region" although there is no longer any active modal competition. The "interference" in this case is with proper navigation. The phase velocity is not that associated with Mode 1, so that Propagation Corrections (PPCs) ar not valid, and unpredictable cycle slips or jumps may occur at sunrise and sunset transitions.

Certain indications, or characteristics, of modal interference may be used to validate coverage in a region.§ These indications may also prove effective within a given receiver to protect against inadequate coverage guidance or detect anomalous propagation conditions.

One of the most obvious characteristics of modal interference is a variation of amplitude with distance along a station radial. Four examples have been previously shown (Figs. 6.2-2 to 6.2-5). One

*Reference 14, a detailed study of signals available at one location, shows, on single displays for each station, the theoretical long- and short-path field strengths for idealized day and night conditions. Perusal of this reference will provide insight on not only long-path interference, but modal interference in general as well as antipodal field strength buildup.

§See Chapter 9 for a description of the ADI/PDADI algorithms that are used to detect modal interference (and other anomalies) in hourly phase, phase-difference, and SNR data.

other case exists: that where Mode 2 becomes completely dominant. In this case there would be no sign of modal interference after Mode 2 becomes dominant. In this case, phase would vary regularly, suggesting that a navigator in the region at the particular diurnal period could not detect the signal limitation. However, an investigator conducting a number of radial flights in adjacent regions would be able to identify the area as one of Mode 2 dominance and therefore not suitable for general use of the particular Omega signal. This is done by starting the analysis on a favorable radial from the station, that is, one where modal interference is known not to occur. As other radials are then examined while the azimuth from the station into the region is varied, one notices first an increase in modal interference and then a gradual decrease. This is explained as moving from a region of Mode 1 dominance, through active competition, into a region of Mode 2 dominance. This approach is used in the regional validation program to identify areas of modal interference, however, it requires amplitude measurements over a number of radials.*

Another tool for evaluation of modal interference is observation of diurnal phase variation. If Mode 1 is completely dominant, a diurnal phase variation will be very regular, as shown in Figs. 6.2-6 and 6.2-8. If not, one may first notice some irregularities developing in the transitions and, if there is a change in dominance, cycle jumps or cycle slips. How this happens may be explained theoretically under idealized circumstances. Figure 6.3-2 shows an idealized amplitude and phase variation over a long east-west mid-latitude path. As can be seen, the amplitude ramps upward during sunset to a nighttime value slightly higher than the daytime value. Phase varies regularly over a complete cycle during the transition. The phasor display in the center panel of the figure reflects this behavior. In this case, a second mode might be said to vary from near zero amplitude during the day to a negligible amplitude at night. The phase of this second mode would typically vary over about two cycles.

Let us now consider the phasor sum of contributions from two modes where they compete. Before summing the modes, however, we must specify the relative phasing. This we cannot do since the relative phasing depends on minor ionospheric variations along path which change from day to day. Hence, we consider three possible phase relationships leading to behavior illustrated in Figs. 6.3-3 and 6.3-4.

Figure 6.3-3 illustrates the circumstance where Mode 1 remains dominant for three different values of Mode 1 – Mode 2 phase difference (day). Noticeable fine structure is seen on the transition and the final night phase is somewhat perturbed by the interfering mode. However, these perturbations can usually be accepted operationally. Figure 6.3-4 shows the situation where Mode 2 can dominate at night. Depending on relative phasing, the phasor sum may be such that the locus encircles the origin

*Sometimes, data from other than true radials can also be used, although, this is best done with caution and only with supporting full-wave computations to multiple points along the path.

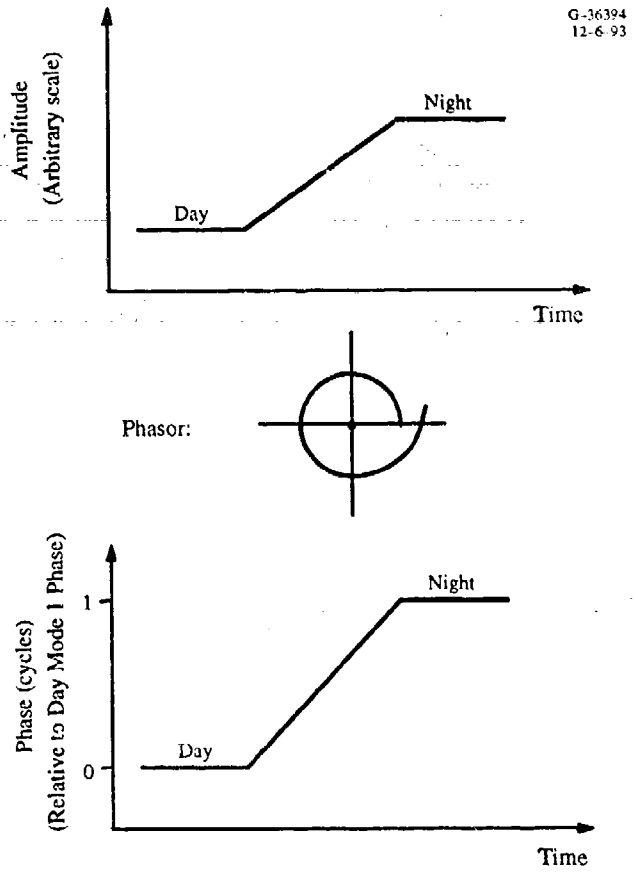

Figure 6.3-2 Sunset Diurnal Variation — Mode 1 Only

anomalously, corresponding to a cycle jump, passes directly through the origin corresponding to perfect anti-phasing of the component modes, or encircles the origin once, as is usual. Since the particular behavior depends on the relative phasing of the two modes and the relative phase value is essentially a random quantity, the occurrence of cycle jumps is random. The most extensive studies of cycle slippage have been conducted by Taguchi using, especially, measurements in Kagoshima (southern Japan). Measurements of Omega Hawaii at Kagoshima show cycle slips and jumps during transitions much as would be expected for a dominant Mode 2 at night but dominant Mode 1 during the day.

Figure 6.3-5 (from Ref. 15), shows the occurrence of cycle slips and jumps on the 10.2 kHz Omega Australia signal at Kagoshima. Kagoshima is roughly on the boundary between Mode 1/Mode 2 dominance at night. As can be seen, cycle slips and jumps occur throughout the year at night and much of the time during transitions.

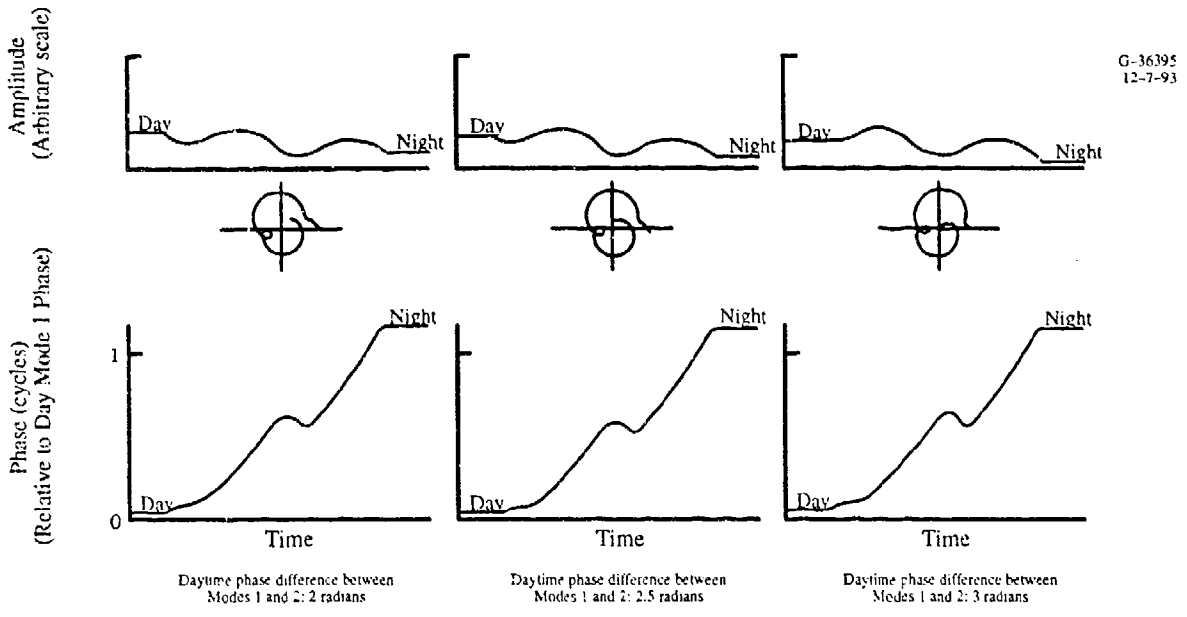

Figure 6.3-3 Sunset Diurnal Variation — Mode 1 Dominant over Mode 2

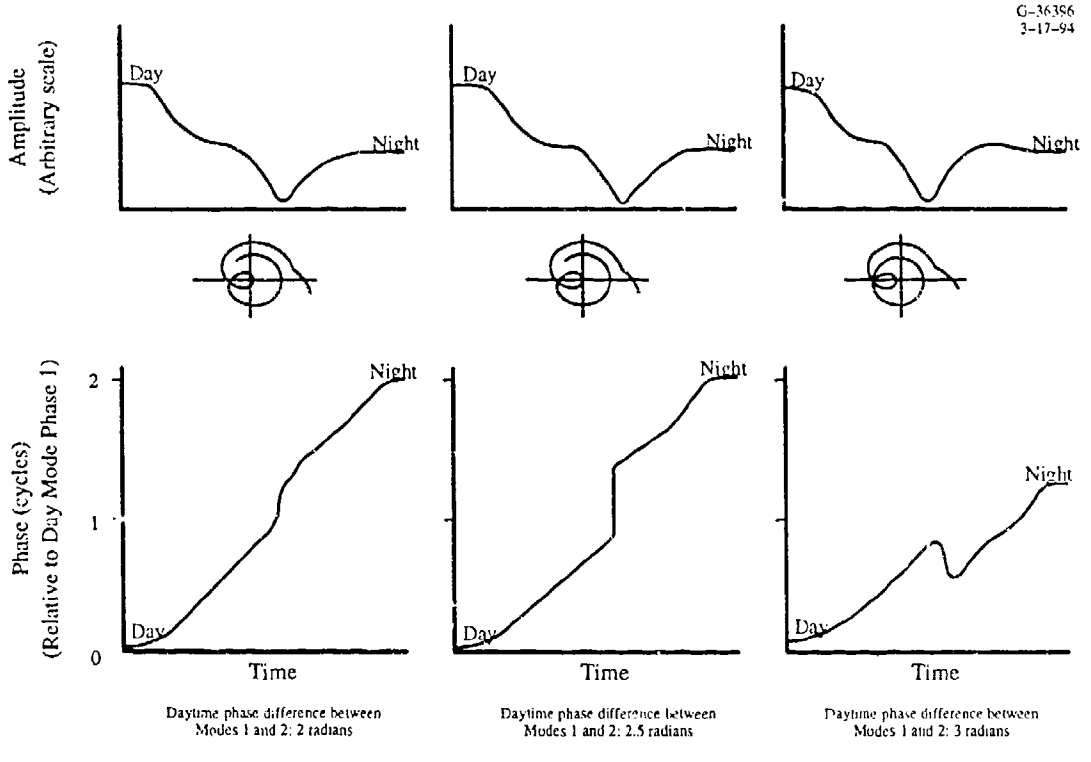

Figure 6.3-4 Sunset Diurnal Variation — Change of Mode Dominance from Mode 1 to Mode 2

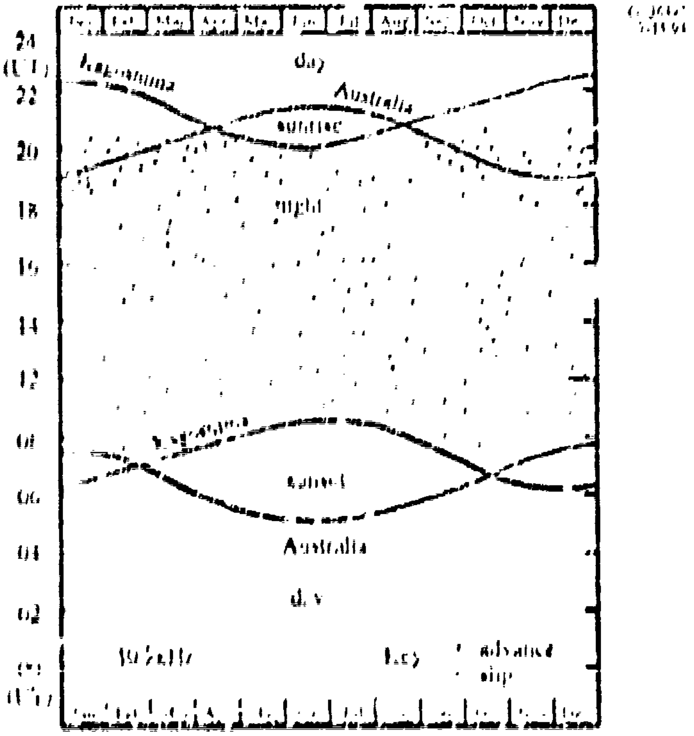

Figure 6.5-2 Cycle Jumps on the Omega Australia Signal as Received at Kagoshima, 10.2 kHz, 1964

The operational importance of cycle slippage should not be underestimated. A receiver [illegible] reliably and continuously into the wrong lane (see Chapter 4 for a discussion of "lanes"). Signals with a competing mode structure that can lead to cycle slippage must be excluded from the navigational solution. If a cycle jump occurs, the line of position error will be about eight miles. As long as the desired mode is dominant, the maximum line of position error due to interference from a single signal will come from a phase distortion of slightly under 25 cecs — that is, about two miles.

A practicing navigator, using only synthesized position developed by [illegible], can sometimes detect modal interference. An example of this situation occurred with [illegible] receivers on [illegible] to Brazil at night using the signal from [illegible]. This is a Mode 2 dominant signal, which one would ordinarily deselect. However, it is strong and geometrically useful. With dual Omega receivers, the aircraft operators navigating the [illegible] deselected [illegible] on one receiver but [illegible] the other. When the receiver using [illegible] jumped in position, a cycle jump was indicated and [illegible] was deselected. If no jump occurred, navigation continued with the assurance that the error was reasonable. Techniques of this type may be incorporated into Omega receiver design.

The existence of simultaneous transmissions at several frequencies is of great value in detecting modal interference, both for analysis and receiver signal processing. The added redundancy alone would make these transmissions valuable for anomaly detection. However, the gain for detecting modal interference is considerably greater because of the interrelationships of signal propagation at the various frequencies [cf. Section 6.5]. Modal interference results from certain resonance conditions in the earth-ionosphere waveguide (see Chapter 5). Thus, a given null at one frequency generally does not occur at the location or time of the same null at a different frequency. It might happen that, say, the fifth null at one frequency is coincident with the fourth of another. But there are still three more frequencies from each station. The probability that the same character of interference occurs on all frequencies from a station at the same time and place is vanishingly small.

We may apply the multi-frequency procedure to the detection of modal interference from diurnal variation. Detection is more difficult based on data at a single frequency alone as such behavior (see Fig. 6.3-3) can appear similar to possible combinations of effects of other factors — especially if the diurnal variation of a phase difference from propagation over two paths is being studied. However, the physics of diurnal irregularities as shown in Fig. 6.3-3 suggests that these will not occur at the same time on different frequencies. Diagnosis is enhanced by knowing that deviations between frequencies are likely due to modal interference while deviations due to other causes tend to affect all frequencies similarly. Section 6.6 expands on these observations and includes sample data.

Most modern receivers incorporate sophisticated proprietary software to detect signal anomalies. Some of these methods, which are based on system operation and physics, include:

1. Phase rate — If a signal exhibits a phase rate of change that is inconsistent with movement or anticipated diurnal change, particularly if it is changing inconsistently with signals from the same station at other frequencies, then modal interference is likely.
2. Amplitude imbalance — Other stations generally radiate about the same power at all frequencies. If there is a failure, power at 10.2 and 13.6 kHz especially will probably be maintained, if possible. Received signal imbalances may indicate modal interference — although they could also indicate locally generated electromagnetic interference at one frequency but not the others.
3. Fix inconsistency — If fixes obtained using one particular signal are inconsistent with those using all other signals, an anomalous signal is indicated.

A historical footnote is that many Omega receivers were developed and sold before specific guidance on coverage limitations had been developed or disseminated. Competent designs tended to be as well sufficient as possible by using redundancy to detect anomalous coverage conditions. Many of the

empirically developed techniques are now being reinvented in conjunction with the development of the Global Positioning System, GPS, under the general heading of Receiver Autonomous Integrity Monitoring (RAIM).

6.3.8 Validation Program

An experimental program was conducted principally in the 1980s to "validate" Omega coverage, i.e., to confirm or modify then-existing coverage predictions (Ref. 16). The effort targeted seven specific oceanic areas in sequential efforts conducted one to two years apart, each incorporating dedicated flights and aircraft measurements. Fixed-site land-based measurements were coordinated with the flight program. Maritime data were often used. The program is discussed further in Chapter 8.

Validation analysis attempted to determine spatial boundaries for modal interference and other boundaries between useful signals and self-interfering signals, such as long-path. Field strength was also measured to determine coverage limitations due to signal-to-noise ratio. A major guide to planning the validations and analysis was signal prediction using full-wave models. While measurement occasionally indicated slight variations in coverage from those predicted, the theoretical methods were mostly verified. The various validations are extensively documented and form an invaluable database (Refs. 17, 18, 19, 20, 21, 22, and 23).

6.4 ANOMALOUS SIGNAL BEHAVIOR

In addition to minor random variations and major predictable diurnal changes, the ionosphere may respond to solar flares. Solar flares are occasional massive eruptions on the surface of the sun. They are associated with sunspots but are not predictable with any degree of certainty. Ordinarily, solar flares emit X-rays that impinge on the sunlit portion of the ionosphere and may cause a *Sudden Ionospheric Disturbance* (SID). Some flares may emit protons that are also incident on the earth but, being charged particles, the earth's magnetic field carries them to enter the ionosphere near the poles on both the sunlit and dark sides. The effect on the ionosphere is theoretically called a *Polar Cap Absorption* (PCA) event although no substantial absorption occurs at Omega frequencies.* Collaterally, the earth's magnetic field may be disturbed.

---

* The distinction is reflected in the use of term *Polar Cap Disturbance* (PCD) by forecasters in warning broadcast services such as WWV to distinguish the VLF phenomena, the historical term comes from the use of riometers at higher frequencies to detect short wave fades in the Arctic.

These events are common, especially near the maximum of the sunspot cycle. However, statistically, they cause little degradation in the inherent Omega signal repeatability up to the 95th percentile. Above that level, deviations associated with flares are dominant (cf. Section 6.4.4). Thus they are important for analysis of navigational safety if not typical navigational accuracy.

6.4.1 Sudden Phase Anomalies (SPAs)

Sudden Phase Anomalies, SPAs, are the observed result on an Omega phase measurement of an SID that occurs on at least a portion of the affected propagation path. To some extent, the terms are used interchangeably. The excessive X-radiation causes additional ionospheric ionization, thus lowering the effective height and resulting in a phase advance. Since the x-rays arrive suddenly, the onset is abrupt. We have already seen (Section 6.2.4) that the ionosphere has an effective time constant, thus we expect the observed SPA to reflect the ionospheric response to the sudden stimulus. However, without using x-ray data measured above the ionosphere, one cannot tell to what extent an SPA reflects the fast build up and decay of x-rays from the sun as opposed to an ionospheric response to a sudden impulse.

Operationally, SPAs are important beyond their statistical effects due to their unpredictability and fast onset. The possibility of an SPA introduces a limit on pseudo differential techniques wherein the normally long autocorrelation time of phase fluctuations is exploited by using present measurements to predict the immediate future. For example, Omega can be used in conjunction with GPS to detect sudden satellite anomalies — but not to better accuracy than could be caused by the phase excursion from a Sudden Phase Anomaly. (This would be a RAIM issue for a combined GPS/Omega receiver [see Chapter 12].) The effect on ordinary fix accuracy is best analyzed on a case by case basis as the observed effect depends on location and illumination. If all paths are dark, there will be no effect. If all paths are of equal length, symmetrically distributed, and illuminated, there will also be little or no effect. Also, the probability of SPA occurrence varies greatly throughout the sunspot cycle.

An extensive synoptic study of SPAs was published in 1973 based on observations over North America from 1961 to 1970 (Ref. 24). The measurements were geographically restricted and were also partially made during very early system operation in a master secondary mode. While the fundamental physics and signal response profiles have presumably not changed, some allowances should be made to project the results to modern operation and to more average sunspot conditions. A necessary feature of the older data is its time resolution of about one minute that is necessary for the study of SPAs. Modern practice is to record hourly or, sometimes, every six minutes.

The synoptic study was structured to determine shape including rates of onset and recovery as well as maximum error. Figure 6.4-1 shows a typical SPA in the presence of noise while the approximating shape is shown in Fig. 6.4-2. Although the approximating shape is grossly idealized, controls within the study indicated that it is much better than might be expected. Five hundred SPAs with magnitudes greater than 5 secs were studied using observations at 10.2 kHz.

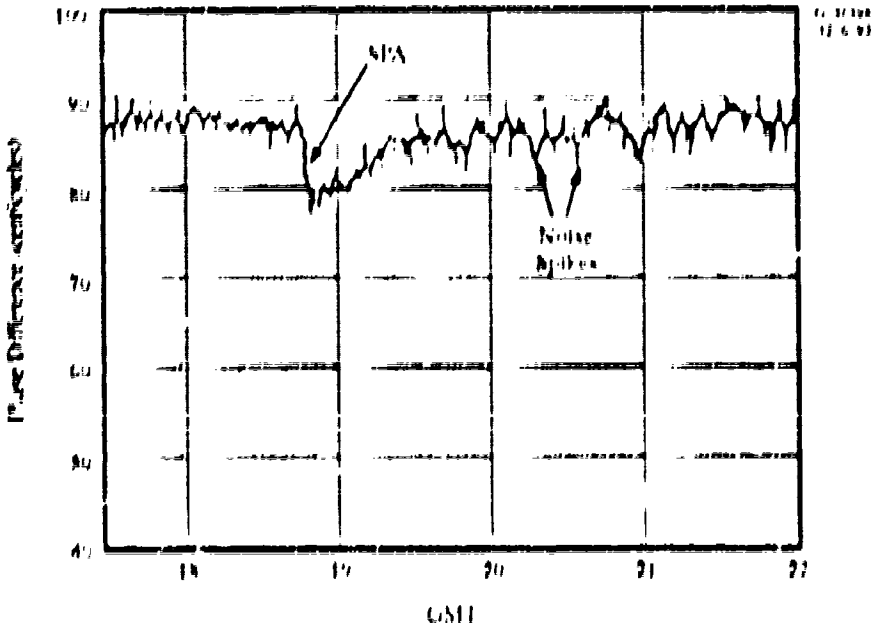

Figure 6.4-1 Typical VLF Phase Disturbance Caused by Solar X-ray Flare

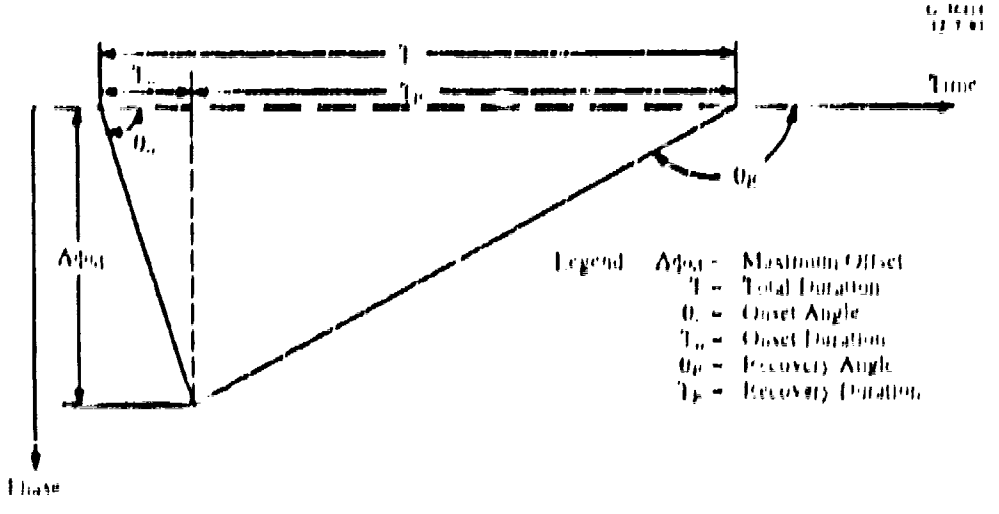

Figure 6.4-2 Idealized SPA Shape

Results of this study indicate that a rather abrupt phase variation occurs reaching a maximum effect in about six minutes with a total duration being about 45 minutes. Typical offsets are about 15 cec on paths of average length. Typical phase rates of change during onset are 3.5 cec/minute with maximum observed rates of 8 cec/minute. Maximum phase deviations of about one cycle are apparently quite rare. The typical rate of occurrence of SPAs varied with sunspot number, from a nearly vanishing probability at low solar activity to an occurrence probability of about once per day (somewhere on earth) when the sunspot number is about 85.

6.4.2 Polar Cap Disturbances (PCDs)

A *Polar Cap Disturbance* is the result on Omega propagation of a PCA event. As noted, this disturbance is due to protons emitted by some solar flares that are directed by the earth's magnetic field into the Arctic and Antarctic regions. The effect is restricted to signals propagating under the ionosphere within these regions. Unlike x-rays, which travel from sun to earth almost instantaneously, protons take from a few hours to a day to reach the vicinity of the earth. Compared with an SPA, the PCD is gradual with the phase variation corresponding to the differential proton flux near 6 MeV (Ref. 25). After the arrival of the first protons, the maximum phase deviation occurs within a few hours while recovery may take one to five days or longer.

Primary studies of PCD effects date from 1972 and 1975 (Refs. 26 and 27). Of these, the 1972 study is the more synoptic with the 1975 work addressing primarily modeling of the events. A problem is that PCDs are relatively rare. The 1972 work was based on only 15 events observed from June 1969 through July 1970. Existing data at a one-hour sampling rate should be more than adequate to greatly expand the compiled statistics. However, the general nature of the PCD effect on Omega signals is now understood.

The typical Omega phase deviation due to a PCD looks very much like that of an SPA but with a time scale in days instead of tens of minutes, i.e., the time scale of evolution is about two orders of magnitude slower than for SPAs. Typical duration is two to three days. Typical maximum phase deviation is about 30 cec although the largest observed have been nearly one cycle on nearly trans-polar paths. Phase variation over the duration of a PCD is shown in Fig. 6.4-3. A key feature is that the evolution of a PCD is sufficiently slow that warning notices are issued through special alert channels.

An apparently surprising feature of PCDs is that day and night perturbations appear to be nearly equal. The deposition of proton energy in the polar ionosphere yields roughly uniform ionization levels independent of local illumination.

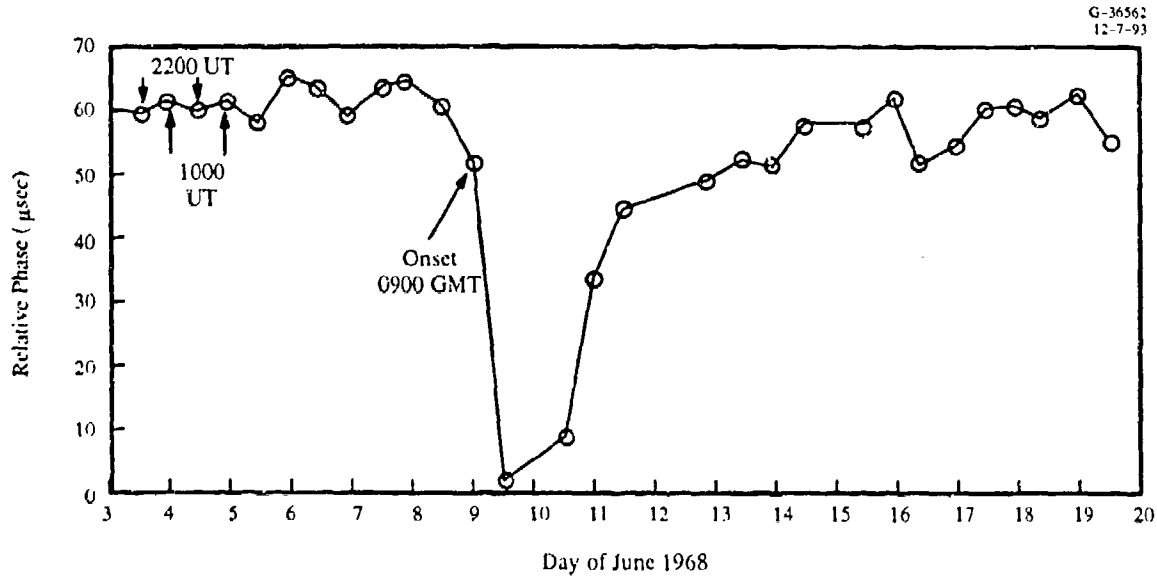

Figure 6.4-3 Effect of a PCD on the Norway Station Signal Phase as Received in Hawaii

As with SPAs, the effects of PCDs on practical navigation are best assessed on a case-by-case basis. For example, the approximate symmetry in signal arrival azimuths in the polar regions suggests that navigation at the magnetic poles will be nearly unperturbed by a PCD. The problem will be most severe where use may be made of a trans-polar signal. This circumstance is especially likely in the North Atlantic or North Pacific. In these locations the usual solution is to heed notices and deselect the trans-polar signal. While the resulting geometry is less favorable, there is reasonable assurance that the signals used will not be significantly perturbed. An alternative is use of the Composite Technique as described in Section 6.5.

6.4.3 Other Anomalous Disturbances

SPAs and PCDs are by far the most characteristic and important disturbances encountered in Omega use. Other anomalous effects may also occur — some recognized and others not. Anything that affects the radiation incident on the ionosphere or the geomagnetic field can cause a pervasive effect on Omega signals.

Operationally minor but measurable phase deviations are associated with *meteor showers* (Ref. 28). Effects have been noticed only during major showers and only when a path was on the leading side of the earth in its revolution around the sun (0600 local time).

Eclipses have predictable effects, which are ignored in phase predictions, thus requiring the issuing of alerts. Eclipses also afford unique opportunities to study ionospheric response to relatively slow

variations in illumination (Ref. 29). *Geomagnetic storms* are generally pervasive events that can affect Omega signals. These are caused by disturbances to the interplanetary magnetic field, resulting in a general disruption of the earth's magnetic field. They may be accompanied by the precipitation of relativistic electrons in the auroral zones, thus lowering the ionospheres in these zones. As these events lack a characteristic signature and the magnitude is typically less than about two standard deviations of the nominal scatter, they are not typically recognized and do not particularly degrade nominal navigation. The effect is mainly a lowering of the received signal phase which may be accompanied by some instability.

One notable aspect of some geomagnetic storms accompanying PCDs is that the effective polar regions may be enlarged with the auroral zones moving toward the equator. In severe events, related effects (such as aurora) have been observed as far from the poles as New Mexico.

6.4.4 Error Comparison

The relative importance of navigation as it relates to safety and efficient routing cannot be properly assessed as it depends on specific details of a given circumstance: traffic, route structure, and, especially, the use of the information at hand. Operational results depend on what is done with information, not the inherent quality of the information itself. For example, NOTAMs can influence action as well as self-consistency checks within receivers (RAIM). While acknowledging that any error comparison will necessarily be too general to be of any specific use, Fig. 6.4-4, from Ref. 31, shows the expected fix errors due to various causes including typical day-to-day scatter, SPAs, and PCDs, but not predictive errors. Predictive errors are large enough to obscure most of the SPA, PCD, and nominal errors. One airline flew for tens of thousands of hours before ever noticing a deviation that could be associated with an ionospheric disturbance.

6.5 COMPOSITE TECHNIQUES

As long as Mode 1 is dominant, phase changes tend to occur equally on all frequencies. The phase changes may be either due to anomalous events or nominal day-to-day diurnal changes. Since SPAs occur when the path is mostly in day, Mode 1 is generally dominant. Also, signals that could be affected by PCDs are usually Mode 1-dominated since modal interference rarely occurs in the polar regions where PCDs originate. Thus the tendency for similar phase changes on Omega frequency signals is particularly notable during SPAs and PCDs. Even spatial variations with ground conductivity tend to be highly correlated between frequencies.

Conveniently, variations are not only highly correlated, but are nearly the same, centicycle for centicycle. This means that the difference frequencies (e.g., 13.6 – 10.2 = 3.4 kHz) are little affected by

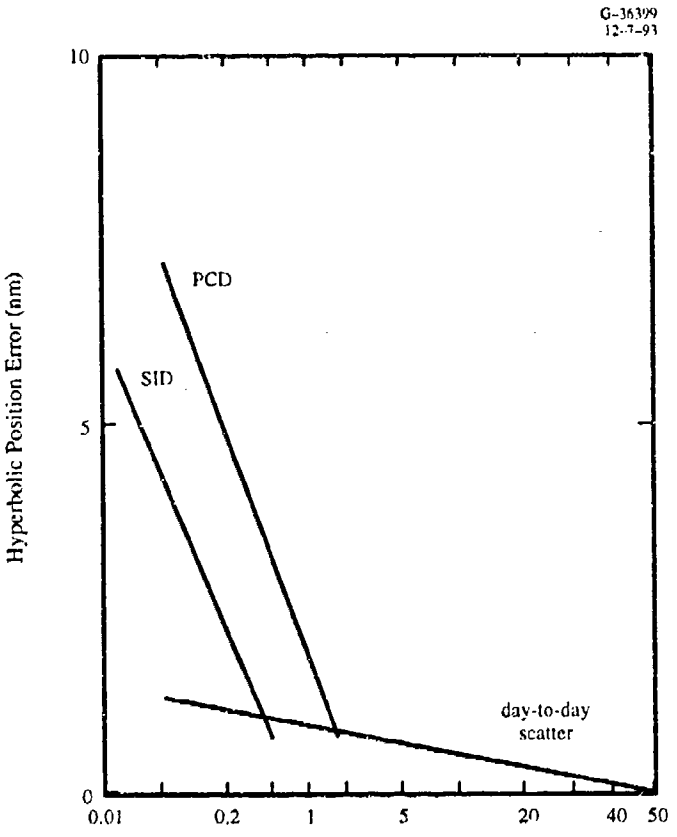

Figure 6.4-4 Percentage Probability that Position Displacement Exceeds Value on Ordinate

anomalous perturbations, day/night variation, or even poor modeling of ground conductivity. Unfortunately, a phase error of, say, 1 cec at 3.4 kHz is spatially equivalent to a phase error of 4 cec at 13.6 kHz. Further, the equivalence is not quite exact nor is it constant in space. Nevertheless, at certain times and under certain conditions, it is better to use the 3.4 kHz difference frequency directly rather than navigate on the individual carrier frequencies.

A technique to exploit the dispersive correlation between different frequencies was developed by J.A. Pierce and called *Composite Omega* (Ref. 32). It is equivalent to an optimum linear combination of phases at two or more frequencies but was developed from the fact that, for waveguides containing mostly neutral particles, the product of the signal phase velocity and group velocity is constant. Empirically, two optimizations are possible: minimum sensitivity to diurnal chang. and minimum sensitivity to anomalous variations in ground conductivity. The former optimization gives the possibility of building a receiver without elaborate propagation predictions; the latter option offers the prospect of better accuracy.

One study indicated that the composite phase was more accurate than the phase of the best carrier signal only in the Arctic regions under disturbed conditions (Ref. 33). However, Pierce made extensive measurements in Cambridge, Massachusetts, indicating the composite phase is more stable. Undoubtedly composite techniques offer advantages under some conditions.

Closely related to composite is use of multiple frequencies for analysis. This method of analysis is addressed in the following section.

6.6 MULTI-FREQUENCY MULTI-SITE OBSERVATIONS

Except for modal effects, one expects signal variations at Omega frequencies to follow each other. Use of decorrelation has already been mentioned in Section 6.3.8 as a means of detecting modal interference. This section provides some observations showing normal behavior and those resulting from modal interference. Comparisons are made both between different frequencies over the same path and also between observations of signals at the same frequency over reciprocal paths. Reciprocal paths are those over which one transmitted signal can be observed near a second station while, also, the signal of the second station can be observed near the first.

Three pairs of observed monthly data sets are to be presented — six data sets in all. Each set (figure) contains the same type of information. At the top of each figure is a graph showing diurnal phase variation of 10.2, 11⅓, and 13.6 kHz. Curves are shown both for the predicted and for the observed monthly average. Ideally, the difference between the observed and predicted phase should be zero. Any nonzero amount indicates there would be associated navigational error. Most likely these differences would be due to prediction bias but, on a more limited set of observations, could be due to abnormal propagation conditions. Also of special interest are the differences between observations at the same time but at different frequencies. Under normal conditions, one expects these differences to be nearly constant with, perhaps, some slow diurnal variation. Any fast hour-to-hour change suggests possible interference. This is also true if the observed hour-to-hour behavior is particularly erratic; however the diagnosis tends to be confirmed if the various frequencies do not fluctuate together. One final feature of the plots is that when data are shown over two ends of a reciprocal path, they are displayed in the same sense, namely with phase delay positive. Conventionally, phase differences are shown in "alphabetical order," e.g., A B not B A.

The first pair considered is Norway and Hawaii. The plot from Norway shows variation of the Hawaii signals while that from Hawaii shows variations of the Norwegian signals (Figures 6.6-1 and

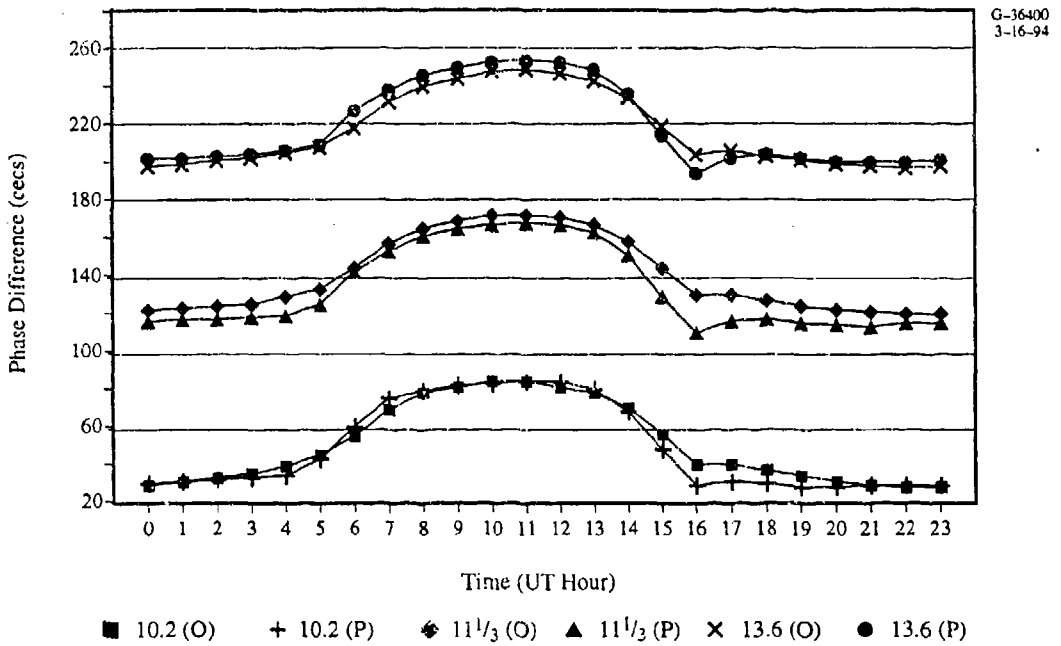

Figure 6.6-1 Phase of 10.2, 11⅓, and 13.6 kHz Hawaii Station Signals Received at the Norway Station Monitor – July 1989

6.6-2). The several frequencies received at one site can be compared or, alternatively, those at the same frequency can be compared at opposite ends of the path. In either case, variations of the several frequencies are similar. There are no abrupt shifts from hour to hour beyond a maximum variation of a few centicycles. This is as would be expected from a path which is Mode 1 dominant at all frequencies and in both directions. Predictions on this high latitude trans-arctic path in local summer are generally good but with some bias near 1600 UT when the sun rises on the north-south portion of the path near Hawaii.

Figure 6.6-3 shows North Dakota signals received in Liberia. Variation is generally smooth with rather high prediction biases at night. This is a typical example of a plot in which all signals can be used for navigation. Figure 6.6-4, which presents the reciprocal conditions of the Liberian signal received in North Dakota is quite different. Noon at mid-path is around 1500 UT so that signal variation during the day is again smooth. However, the situation deteriorates as the Liberian end of the path becomes dark. The Liberian signals are unusable throughout most of North America at night due to modal interference. This phenomenon is suggested by the data in that many difference frequency averages were not computed during transitions due to inconsistency. Furthermore, the computed difference frequency average for 10.2 – 13.6 kHz abruptly shifts between 0600 and 0700 UT. Taken together, this pair of figures illustrates the non-reciprocity of modal interference.

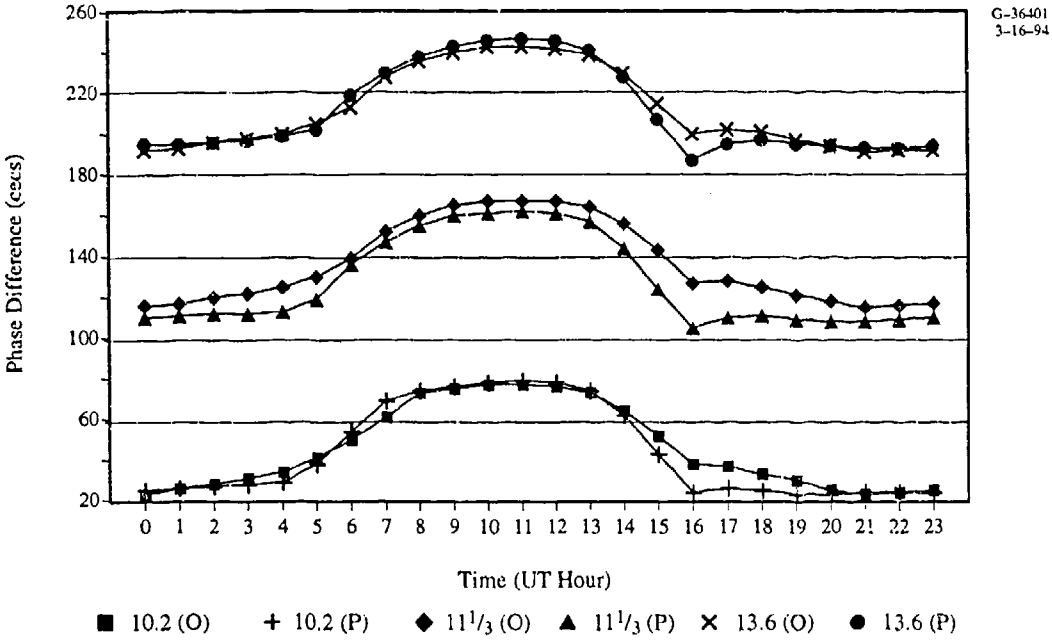

Figure 6.6-2 Phase of 10.2, 11⅓, and 13.6 kHz Norway Station Signals Received at the Hawaii Station Monitor – July 1989

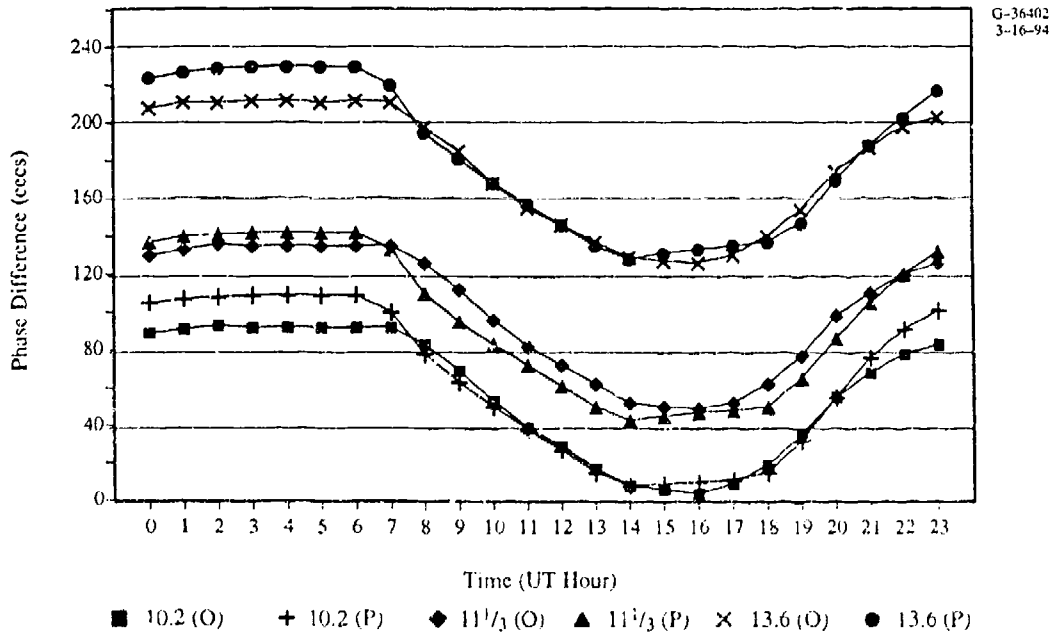

Figure 6.6-3 Phase of 10.2, 11⅓, and 13.6 kHz North Dakota Station Signals Received at the Liberia Station Monitor – January 1989

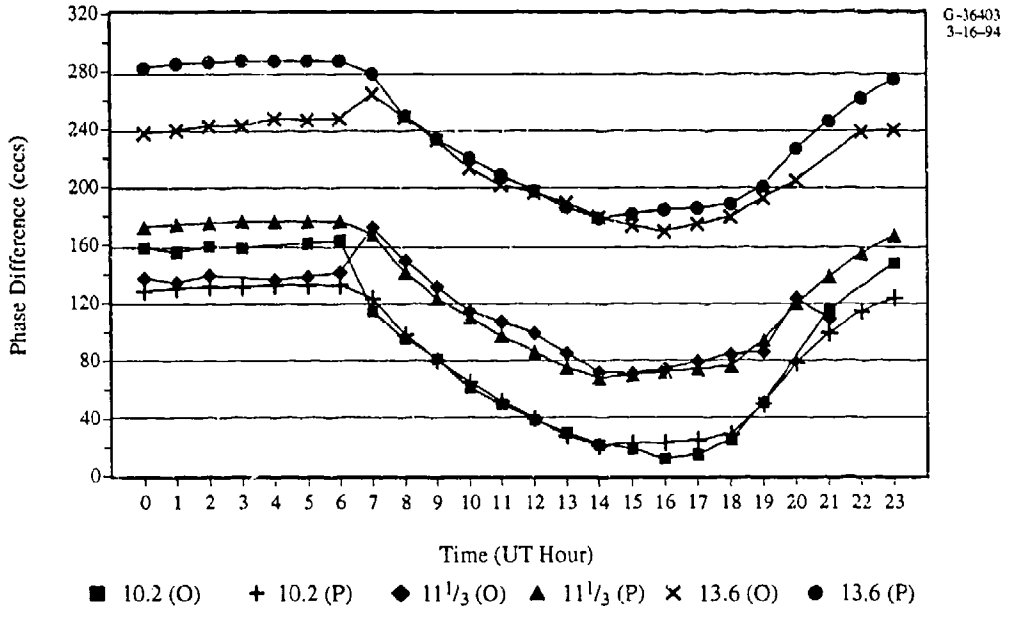

Figure 6.6-4 Phase of 10.2, 11⅓, and 13.6 kHz Liberia Station Signals Received at the North Dakota Station Monitor – January 1989

The third data pair is Japan and Liberia (Figures 6.6-5 and 6.6-6). When observed in Japan, the Liberian signals all vary smoothly and similarly throughout the 24-hour day with the exception of a few missing data points. The predictions biases are again quite large except at 10.2 kHz. These are the characteristics of Mode 1-dominant signals albeit signals rather poorly predicted. The behavior of Japan signals received in Liberia (Fig. 6.6-6) is quite different. Something is clearly anomalous—but what? Superficially, many of the jagged variations look similar on the various frequencies. However, close scrutiny indicates this is not always so. For example, the downward shift at 0300 UT occurs at the higher frequencies but not at 10.2 kHz. More clearly, correlation breaks down from 1700 UT on. The frequencies do not vary together nor are they smooth. We suspect interference—but what kind? Depending on time of day, we expect either modal interference or long-path interference on this path. Noon at mid-path is between 0800 and 0900 UT. The data at this time exhibit comparative stability but the diurnal behavior indicates a curvature in the *wrong sense*. In all likelihood, the long-path signals completely dominate those over the short path at this time and are reasonably stable. At other times, Mode 2 or long-path may be either actively competing with the short-path Mode 1 signal or may be dominant but differ from the Mode 1 prediction by about a half cycle. In this case, the processing used here* leads to a jagged cycling between lanes.

*The processing algorithm lanes the data by choosing the appropriate whole cycle value which, together with the observed fractional part, must be within 50 cec of the predicted value.

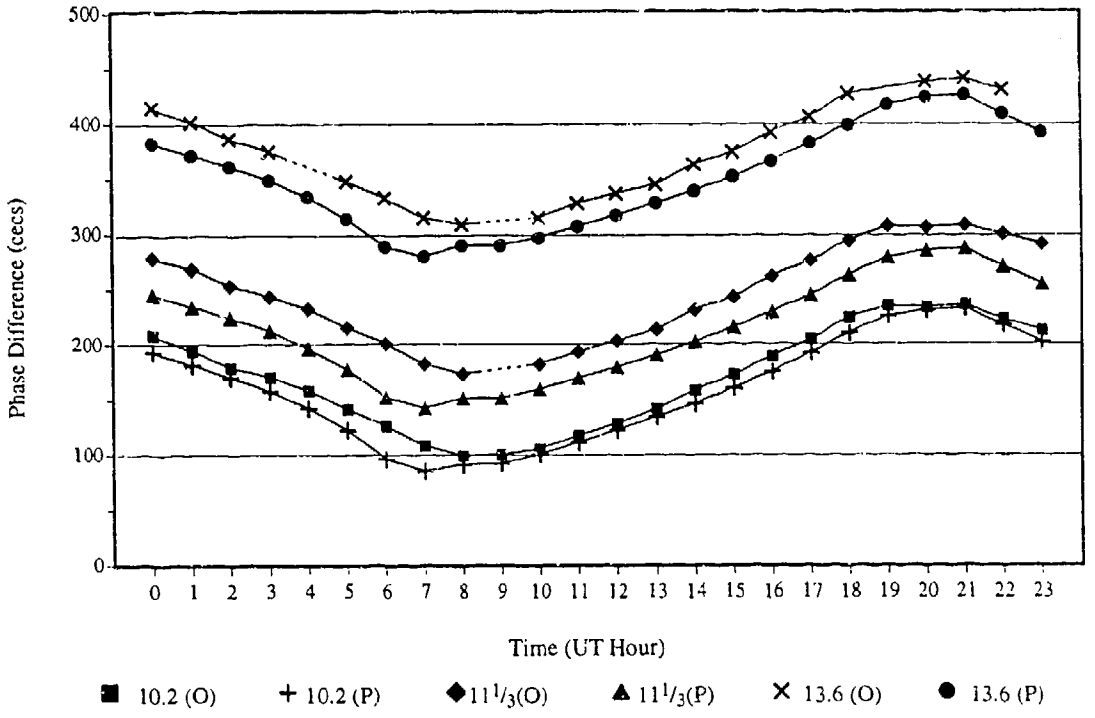

Figure 6.6-5 Phase of 10.2, 11⅓, and 13.6 kHz Liberia Station Signals Received at the Japan Station Monitor – March 1989

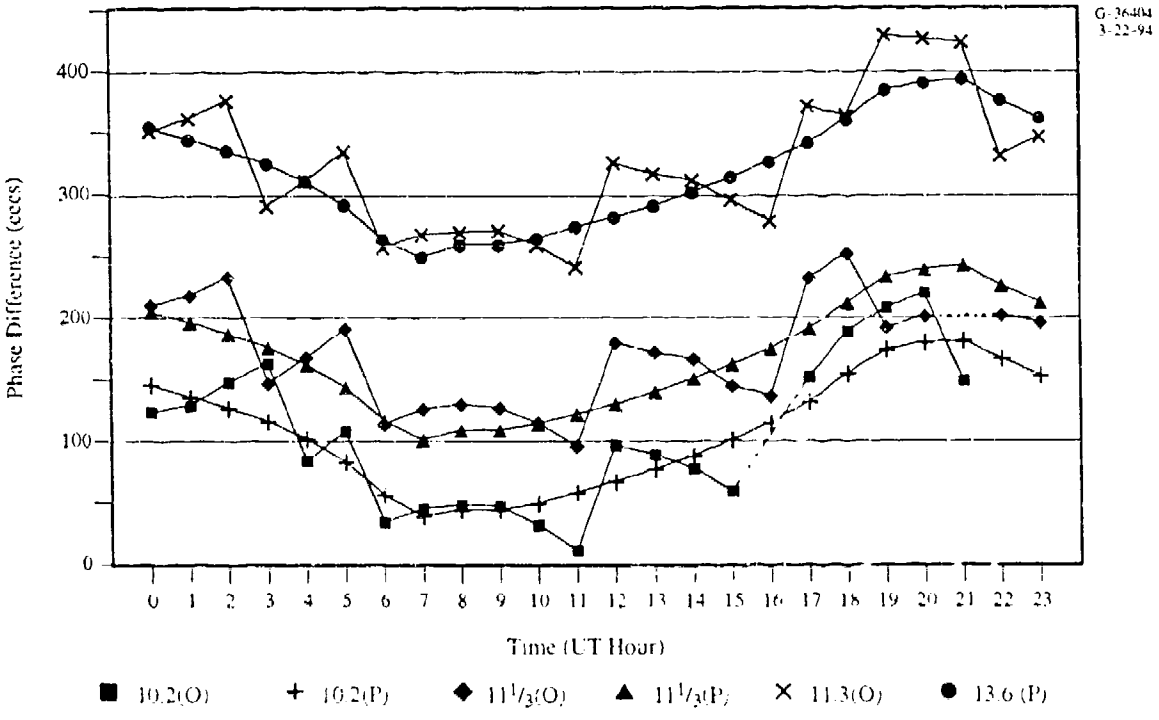

Figure 6.6-6 Phase of 10.2, 11⅓, and 13.6 kHz Japan Station Signals Received at the Liberia Station Monitor – March 1989

The several figures in this section are illustrative of data from modern monitor operation. While the hour sampling may seem relatively coarse and indeed does tend to obscure some diurnal behavior, it is not a fundamental limitation. Details of diurnal variation depend on the details of solar illumination which varies throughout the year. Whatever conditions need to be investigated will, sooner or later, occur on the sampled hour.

6.7 THEORY vs. EXPERIMENT

The title of this section was chosen to alert the reader that there may be differences between theory and observation. As always, provided the observations are well made, the problem is theory, not reality. As Einstein said, "No number of experiments can prove a theory true. But it only takes one to prove it false." That said, theory and experiment complement each other well in this area. A few problems, however, deserve explicit mention.

Ground conductivity is not well known — especially in Greenland and Antarctica where it is very important. Also important in these regions is the electrical permittivity, which is not well known either. Indeed, it is appropriate to modify conductivity maps to match observation especially in these regions.

Full-wave computations assume a smooth ionosphere whereas the ionosphere is known to be rough. Roughness will affect higher modes more than Mode 1. However smooth models have been used to predict observed amplitude measurements. Thus the ionospheric heights used to calibrate the models are those for a smooth model, not a more realistic rough one, with the result that ionospheric heights may be somewhat low.

Ionospheric profiles during transitions are unknown and may not simply be intermediate between day and night. Also, when a terminator affects a path, severe asymmetries in the direction of propagation may be introduced. This brings the great-circle path approximation into question. If the change of impedance at the earth's surface/ionosphere is sufficiently abrupt, modal conversion is conceivable. Modal conversion at the terminator unquestionably occurs at the higher frequencies in the VLF range especially near the equator, but the extent of its effect at 10.2 kHz is not clear. Modeling of the transition ionosphere is an area of great challenge and promise for improving operational accuracy.

6.8 TRENDS

This section addresses general tendencies of Omega signals. However, the reader is cautioned that the best approach in any specific situation is to check coverage predictions. Available predictions

are discussed in Chapter 10. Also, full-wave codes may be executed for the specific paths in question using a variety of ionospheric profiles. As a result of the Omega Validation Program, there is an extensive database of observations which may bear directly on specific questions.

Theoretical expectations for Omega are discussed in Section 5.5.3. Generalities on Omega propagation are dangerous as very often one can find exceptions when observing some station on some frequency at some time and place. With that caveat, some of the more likely features are given in the following paragraphs.

Attenuation rates (cf. Chapter 5) are higher during the day than at night and higher to the west than to the east. The differences can be quite marked. Equatorial attenuation to the east at night may be less than 1 db/Mm while that for propagation to the west is over 6 db/Mm. Attenuation rates are also higher with lower ground conductivity. A major case is propagation over extremely low ground conductivity such as Greenland and Antarctica where attenuation may be near 30 db/Mm during the day but about half that at night. At many receiving sites, these circumstances combine to form an effective "switch" to turn off a signal when it passes over the fresh-water ice during the Arctic (Antarctic) summer.

Phase velocity is not particularly sensitive to ground conductivity under most conditions. The phase shift for a signal passing over the continental United States is equivalent to a distance difference of only about 0.5 nm from that for the same signal passing over an equivalent region of sea water. However, the dependence becomes very important at low ground conductivity. Phase velocity varies little with direction during the day — only a few parts in 10^4. At night, the variation is marked, especially to the west. However, the variation is moot in cases where a higher mode dominates.

Significant modal interference is restricted to propagation at night and to signals propagating to the west near the equator. A region of Mode 2 interference typically exists on west-bound equatorial or trans-equatorial signals. The area may be vast, as for the signals transmitted by the Liberia station which lies close to the geomagnetic equator, or relatively localized as with North Dakota signals propagated across the equator to Australia. An additional limitation sometimes occurs on propagation to the east, particularly at 13.6 kHz, due to Mode 1/Mode 3 interference. A particularly severe example is La Reunion signals propagating to the central and eastern Indian Ocean.

Long-path signal dominance or interference (with the short path) may occur when the west-bound short path is sunlit. It arises because the westbound attenuation rates during the day are high while the rates for the eastbound signal at night are low. The most severe limitation is on the Liberian signal which is dominated by the long path over South America during short-path day — a 4:1 or 5:1 short-path/long-path

length ratio. At 10.2 kHz the long-path La Reunion signal in the continental United States is virtually dominant for the entire 24-hour day. The location of long-path boundaries is particularly uncertain.

SPAs and PCDs are both associated with rapid phase advances followed by slow recoveries. However, the time scales differ by about two orders of magnitude with SPAs typically persisting for 45 minutes compared to a duration of two to three days for PCDs. SPAs are restricted to signals propagating over the illuminated half of the earth; PCDs occur on signals propagating through the polar regions. The probability of either event nearly vanishes during the minimum of the solar sunspot cycle. During more active periods, about one SPA per day is observed somewhere in the world and perhaps one PCD per month.

6.9 PROBLEMS

6.9.1 Sample Problems

1. An individual reports using the 13.1 kHz unique frequency from North Dakota for frequency determination at a facility on Terminal Island (Los Angeles port area) for some years. However, the signal routinely drops out between 0730 and 0800 (local time) every morning and is also lost intermittently throughout the day. What is wrong?

Answer:

Since the problem has existed for a long time, station outages are not the problem. Also, the path is benign. The location should be well beyond the skywave-groundwave interference region and the daytime conditions argue against modal interference. While the propagation conditions could be further checked by fullwave calculations, the fixed time of occurrence strongly suggests local interference. Propagation problems tend to vary with time of day and season and certainly do not follow the advent of Daylight Saving Time! Local interference is especially likely near heavy equipment, as in this industrial area. It also likely to follow the local work schedule, e.g., start first thing in the morning and recycle throughout the day on demand (compressors, air conditioners). Tell the user to "clean up" the receiving site. (Note that, if there is a specific remote source of interference not on the North Dakota azimuth, it may be possible to orient a loop to null out the interference.)

2. Fishermen operating in the Labrador Sea several hundred miles west of Cape Farewell, Greenland, report that they experienced a two- to three-mile error when using Norway. This was a pervasive problem throughout the month of June when they were fishing. What was the problem?

Answer:

While it is true that people have been routinely flying over this area on trans-Atlantic routes for years and nothing has been reported, the magnitude of the error is not such that it would necessarily be noted in an aircraft. The fishermen, working in the area for a month, probably would notice. The path from Norway to this area is a real prediction challenge. It passes somewhat tangentially beneath the auroral zone which could be a cause of prediction error — but if so would likely have been observed over much of the U.S. and Canadian east coasts. A key is that the observations were made in June when Greenland is illuminated. Attenuation is very high. But the fishermen did not report a reception problem — they reported a position problem. The fact that the positional error was constant rules out long path interference, which is also ruled out by general experience in North America.

The phase velocity over the Greenland ice mass is also highly anomalous. This brings up the possibility of either of two fundamental problems. An abrupt change in surface impedance along a path can lead to modal conversion. This, in turn, could lead to interference and spatial perturbation in their fishing area. However, like most interference problems, it would not be likely to be steady over a large area.

The other possibility of a fundamental problem is an "off-path" effect that violates the usual great-circle path approximation. Very possibly the signal is propagating east of the ice pack and then rounding Cape Farewell to reach the fishing area. This type of condition has been observed over waters off Antarctica and reported by Barr (Ref. 34). (Note: This example is hypothetical; no such errors have been reported — but they yet could be.)

3. The tuna fleet reports problems off Ecuador and Peru using Liberian signals both during the day and at night. What is the problem?

Answer:

This problem is real and occurred before coverage limitations were widely understood. In that area, the Liberian signal is modally disturbed at night and received by long path during the day. It is useless and must be deselected.

6.9.2 Problems to be Solved by Reader

1. A user of a manual receiver in the U.S. Gulf Coast off Houston, Texas reports that the North Dakota – La Reunion line-of-position varies backward. That is, lanes decrease as the user moves away from North Dakota. What's wrong?

2. A user in southern Japan reports cycle jumps on Australia during the sunrise transition. The location is east of the predicted nighttime interference boundary, that is, in an area predicted to be Mode 1 at all times. What's wrong?

3. In central South America, an Omega user reports a problem flying in the daytime using Liberia. The route lies to the east of the predicted long-path interference boundary. What's wrong?

4. A user reports generally weak signals when flying in the U.S. midwest in the afternoon in August. What's wrong?

6.10 ABBREVIATIONS/ACRONYMS

ADI	Anomalous Data Identification
cec	Centicycle
C-layer	Region of the ionosphere at altitudes between about 50 and 70 km above the earth's surface
CCIR	International Radio Consultative Committee
dB	Decibel
D-region	Region of the ionosphere at altitudes between 70 and 90 km above the earth's surface
GPS	Global Positioning System
Hz	Hertz
kHz	Kilohertz
km	Kilometer
m	Meter
MeV	Million electron volts
Mm	Megameter or 1000 kilometers
NOTAM	Notice to Airmen
PCA	Polar Cap Absorption event
PCD	Polar Cap Disturbance event
PDADI	Phase-difference Anomalous Data Identification
PPC	Propagation Correction
RAIM	Receiver Autonomous Integrity Monitoring
RMS	Root-mean-squared
SID	Sudden Ionospheric Disturbance
SNR	Signal-to-Noise Ratio

SPA	Sudden Phase Anomaly
UT	Shortened form of UTC
UTC	Coordinated Universal Time
VLF	Very low frequency
WKB	Wenzel-Kramers-Brillouin technique for combining eigenstates on an inhomogeneous path
WWV	Call sign for time-disseminating radio station in Ft. Collins, CO

6.11 REFERENCES

1. Swanson, E.R., and Bradford, W.R., Diurnal Phase Variation at 10.2 kHz, Naval Electronics Laboratory Center Report 1781, August 11, 1971.
2. Swanson, E.R., Propagation Etfects on Omega in AGARD-CP-209 (Propagation Limitations of Navigation and Positioning Systems), published February 1977, pp. 15–1 to 15–21.
3. Swanson, E.R., Gimber, R.H., and Britt, J.E., Calibrated VLF Phase Measurements: Simultaneous Remote and Local Measurements of 10.2 kHz Carrier Phase Using Cesium Standards, *Proc. 4th Ann. DoD Precise Time and Time Interval (PTTI) Strat. Plan. Mtb.,* 14–16 November 1972. pp. 232–248.
4. Swanson, E.R., VLF Phase Prediction, *VLF-Propagation: Proceedings from the VLF-Symposium,* Sandefjord, Norway, 27–30 October 1971, Norwegian Institute of Cosmic Physics Report 7201, January 1972, pp. 8.1–8.36.
5. Morris, P. and Swanson, E.R., New Coefficients for the Swanson Propagation Correction Model, *Proc. 5th Ann. Mtg of the Int'l Omega Assoc.,* Bergen, Norway 5–7 August 1980. pp. 26–1 – 26–24.
6. Swanson, E.R., Electromagnetic Field Strength Measurements at 10.2 Kilocycles per Second, U.S. Navy Electronics Laboratory Research Report 1239, September 13, 1964.
7. Swanson, E.R., A New Approach to Omega Coverage Diagrams, *Proc. 8th Ann. Mtg. of the Int'l Omega Assoc.*, 18–22 July 1983, Lisbon, Portugal. pp. 20–1 – 20–24. (ISSN: 0278-9396).
8. Swanson, E.R., Omega Coverage: Accuracy at Specified Times, *Proc. 9th Ann. Mtg. of the Int'l Omega Assoc.*, 6–10 August 1984, Seattle, Washington, pp. 19–1 – 19–10. (ISSN: 0278-9396).
9. Swanson, E.R., On Omega Signal Availability at 10.2 kHz, *Proc. 9th Ann. Mtg. of the Int'l Omega Assoc.*, 6–10 August 1984, Seattle, Washington pp. 25-1 (ISSN: 0278-9396).
10. Maxwell, E.L. and Stone, D.L., 10 Kc/s Atmospheric Noise Predictions, DECO Electronics, Inc., May 1965, 51 pp.
11. Maxwell, E.L. and Stone, D.L., VLF Atmospheric Noise Predictions, DECO Electronics, Inc., 15 April 1966, 90 pp.
12. Stone, D.L., Croghan, R.D., and Crail, A.C., Computer Program Operational Manual for Atmospheric Noise Predictions, Westinghouse Georesearch Laboratory, Report No. 70-1H2-VLFNO-R2, June 1970.

13. Swanson, E.R., Omega possibilities: Limitations, options and opportunities, *Navigation*, vol. 26, no. 3, pp. 188–202, Fall 1979.

14. Swanson, E.R., Omega Coverage in India: A Case Study, Naval Electronics Laboratory Center TR 1974, 15 January 1976, 46 pp.

15. Taguchi, K., Suenaga, M., Yamashita, M., Transequatorial Omega Wave Receptions in the Western Pacific and Australia, *Proc. of the Int'l Omega Assoc.*, Munich, 10–14 Oct. 1988. pp. 22–1 – 22–6.

16. Doubt, R.J., Omega Navigation System Regional Validation Program, *Navigation, 31*, 3, 155.

17. Karkalik, F.G., Omega Validation Over the Water Pacific Area, *Navigation, 25*, 4, p. 395.

18. Karkalik, F.G., Sage, G.F., and Vincent, W.R., Western Pacific Omega Validation, USCG Rept. ONSOD 01-78. Vols. I and II.

19. Campbell, L.W., Servaes, T.M., and Grassler, E.R., Omega Validation in the North Atlantic, *Proc. of the 5th Annual Meeting of the Int'l Omega Association*, 4–7 August 1980, Bergen, Norway, pp. 24–1 – 24–23.

20. Levine, P.H., and Woods, R.E., North Pacific Omega Navigation System Validation, USCG Rept. CG-ONSOD-01–81, 31 December 1981, 327 pp. (ADA 212 105).

21. Watt, T., Results of the South Atlantic Omega Validation, *8th Annual Meeting of the Int'l Omega Association*, 18–22 July, Lisbon, Portugal, (ISSN: 0278-9396), pp. 17–1 – 17–9.

22. Swanson, E.R. and Kugel, C.P., Indian Ocean Validation, Omega Navigation System Center Rept. CG-ONSCEN-02-87, 1987, 179 pp. AD-A194458.

23. Hildebrand, V., *South Pacific Omega validation analysis*, Report No. CG-ONSCEN-02-89, August 1989.

24. Swanson, E.R., and Kugel, C.P., A synoptic study of sudden phase anomalies (SPAs) affecting VLF navigation and timing, *Proc. 5th Annual NASA and Dept of Defense Precise Time and Time Interval (PTTI) Planning Meeting*, 4–6 December 1973, pp. 443–471. NASA Pub. X814-74-225.

25. Sauer, H.H., Spjeldvik, W.N., and Steele, F.K., Relationship between long-term phase advances in high-latitude VLF wave propagation and solar energetic particle fluxes, *Radio Science, 22*, 3. (May-June 1987), pp. 405–424.

26. Martin, J.N., Omega Phase Variations During PCA Events, Naval Electronics Laboratory Center Technical Report 1835, 17 August 1972 (AD 764 521).

27. Argo, P.E., Modeling Omega PCA Phase Advances, Naval Electronics Laboratory Center TR 1950, 1 May 1975, 37 pp.

28. Chilton, C.J., LF phase perturbation associated with meteor shower ionization, *JRG*, 66, 2 (1961).

29. Swanson, E.R., The Solar Eclipse of 11 July 1991, *Proc 15th Ann. Mtg. of the Int'l Omega Assoc., Sanur, Bali, Indonesia*, 24–28 September 1990. pp. 11–1 – 11–4.

30. Air Force Geophysical Laboratory, AF Systems Command, USAF, *Handbook of Geophysics and the Space Environment*, A.S. Jursa, Editor, 1985, [ADA 167000].

31. Swanson, E.R., The distribution pattern of Omega observations, *J. (British) Inst. Navigation*, vol. 32, no. 2, pp. 276–278, May 1979.

32. Pierce, J.A., The use of composite signals at very low radio frequencies, Harvard Univ., Dep. Eng. Appl. Phys., Tech. Rept. 552, February 1968.

33. Swanson, E.R. and Hepperley, E.J., Composite Omega, Naval Electronics Laboratory Center Report 1657, 23 October 1969, (AD863791).

34. Barr, R., Preliminary results of the implementation of recommendations for improving Omega navigation in Antarctica, *Proc of the 14th Ann. Mtg. of the Int'l Omega Assoc.* Long Beach, 2–6 October 1989. pp. 16–1 – 16–6.

35. Swanson, E., and Dick, M., Propagational Assessment and VLF Navigation Signals in North America and the North Atlantic, NELC TR-1944, February 1975.

36. Morris, P. and Gupta, R., New Approach to Omega PPCs, CG-ONSCEN-03-89, ADA 215 610, November 1989.

CHAPTER 7

SYSTEM SYNCHRONIZATION PROCEDURES

Chapter Overview *— This chapter provides an overview of the basic principles of Omega system synchronization and the procedures used to synchronize the stations in the network. Following the chapter introduction in Section 7.1, the principles of system synchronization are reviewed in Section 7.2. These principles include both internal and external synchronization components, data sources, and the computational algorithm. Section 7.3 describes the operational procedures used to implement the weekly Omega synchronization process. Section 7.3 also traces the improvement in system synchronization performance as external measurements were incorporated into the synchronization procedure over a period of several years. Problems, including worked-out examples and those to be solved by the reader, are in Section 7.4. Abbreviations and acronyms used in the chapter are given in Section 7.5, followed by the cited references listed in Section 7.6.*

7.1 INTRODUCTION

7.1.1 Overview of Omega System Synchronization

Omega is a very low frequency radionavigation system composed of eight transmitting stations located in the United States and six other nations. At each station, continuous-wave (CW) signals are transmitted on five common frequencies and one station-unique frequency. The signal frequencies are time-shared among the stations so that a given frequency is transmitted by only one station at any given time.

The Omega signal transmission format is illustrated in Fig. 7.1-1. Across each of the eight rows in the figure is a ten-second sample of the signal frequencies transmitted by a particular station. Important features of this time/frequency multiplex format are:

- Four common signal frequencies are transmitted: 10.2, $11\frac{1}{3}$, 13.6, and 11.05 kHz
- One unique signal frequency is transmitted by each station
- An interval of 0.2 second separates each of the eight transmissions
- The transmission periods vary in length.

These features permit users to uniquely associate a given station and signal frequency as well as resolve lanes with reduced ambiguity (compared to a single frequency) and provide multi-spectral information on a given path.

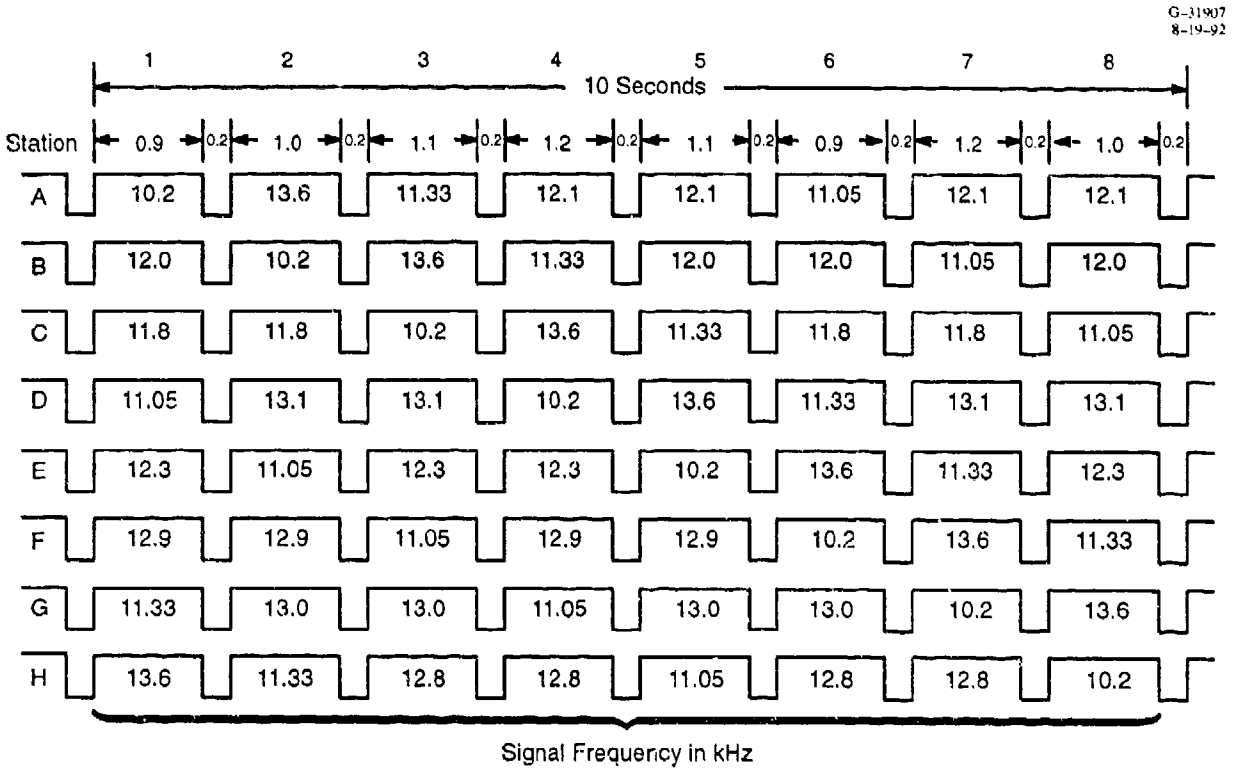

Figure 7.1-1 Omega Signal Transmission Format

A more basic property of the system not evident in Fig. 7.1-1 is that the signals transmitted by all stations are *phase-synchronized*. For example, the zero phase point on a given cycle of the 10.2 kHz signal transmitted from Norway occurs (in principle) exactly 1.100000 seconds before the zero phase point on a cycle of the 10.2 kHz signal transmitted from Liberia. For a sinusoidally varying Omega signal, the zero phase point (closely related to the station epoch) is the point at which the vertical electric field vanishes, in increasing from negative to positive values. In practice, slight deviations exist in phase synchronism from station to station at the submicrosecond level and even occasionally at the microsecond level.

It is important to differentiate between the two commonly used meanings of the word "synchronize." In connection with receiver signal acquisition, synchronize (sometimes called pattern synchronization) means to align the receiver with the Omega signal format *at the scale of seconds*. In other words, mis-synchronization means an alignment error or more than about one second. *System* synchronization, however, refers to alignment of signals at the *microsecond* scale. Phase synchronization usually implies a cycle-by-cycle match-up of two signals at the same frequency. Most receivers are not independently phase-synchronized to the transmitted signals, although they *become* phase-synchronized, with the use of control circuitry such as a phase locked loop (see Chapter 12).

At any given common frequency, Omega signals from each station are synchronized to each other to within an accuracy of about one centicycle, which is very nearly one microsecond (at 10.2 kHz).* Moreover, the stations are also synchronized to within one microsecond of the UTC epoch (a specific time marker). Time-synchronization at each station is measured with respect to the station epoch, the point in time (repeated every 30 seconds) at which all station signal frequencies are aligned at the common zero phase point. Thus, the Omega epochs at all stations have an average value (the Omega system time) that is well within one microsecond of the UTC epoch and a scatter of about 1 microsecond.

On a scale of seconds, however, Omega and UTC time formats are significantly shifted due to the injection of "leap" seconds. At 0000 UT on 1 January 1972, the Omega and UTC formats were identical (on the scale of seconds). Since that time, however, leap seconds have been introduced into the UTC format on a nearly annual basis, but not into the Omega format due to substantial coordination and procedural difficulties. Thus, as of 31 December 1993, Omega time leads UTC by 18 seconds.

In principle, the overall Omega synchronization methodology is based on the optimization of two independent processes:

- Internal synchronization
- External synchronization.

Each of these processes is supported by a characteristic type of measurement(s) and historically different objectives.

Internal synchronization is designed to keep the station epochs aligned as closely as possible. This process relies on "reciprocal path" phase measurements between pairs of stations. For purposes of basic radionavigation, it is important only that the signals at a given frequency are radiated simultaneously from each station's antenna. For hyperbolic navigation, the actual "time" of this transmission epoch is unimportant since its value cancels out in the navigation processing. For mobile receivers operating in the rho-rho-rho mode of navigation, a sufficient amount of phase information is collected to determine position/position change so that the difference between the transmission epoch and the receiver's internal time/phase is not needed but can be computed/estimated if desired. The mean of all station epochs relative to UTC defines Omega system time. For internal synchronization, the performance measure is the combined RMS error of each station epoch relative to Omega system time.

* Phase and time units are often used interchangeably, since there is a one-to-one relationship between the two quantities through the time measure of a wave period at a given frequency.

External synchronization refers to the simpler process of aligning Omega system time with the external UTC time base. This process is supported by measurements of station epoch relative to UTC as derived from received GPS or Loran-C signals. Alignment of Omega system time and UTC is useful as an alternative means of globally disseminating UTC epoch and for receivers relying on the interoperability of multiple navigation system sensors (see Chapter 12). In principle, strict adherence by each station to an external reference source obviates the need for internal synchronization. Because of possible failures in external timing information, however, a more robust approach is used which retains both processes.

The system synchronization procedure involves a weekly cycle of collecting daily internal and external measurements, computing and disseminating station phase and frequency offsets, and insertion of the clock corrections by each station. Internal synchronization data consists of daily reciprocal path measurements at two frequencies on four paths/station. External synchronization data comprise daily Omega station epoch measurements relative to Loran-C signals (for some Omega stations) and GPS signals (for all stations). These data are processed by the synchronization computer program (SYNC3) which is executed by both Japan's Maritime Safety Agency (JMSA) and the U.S. Coast Guard's Omega Navigation System Center (ONSCEN). The program's weekly outputs, i.e., optimal estimates of the phase and frequency offsets for each station's on-line and back-up clocks, are reversed (in sign) and issued as both one-time and cumulative corrections. Each station then inserts these corrections at specific times over the following week according to an established procedure.

7.1.2 Historical Overview of Omega Synchronization

Prior to 1966, experimental Omega transmitting stations (see Chapter 2) operated in the master/secondary mode in which one or more secondary stations synchronized their transmissions to the designated master transmitting station signal. Signal receivers within 10 to 30 km of the secondary station monitored the master station transmissions and fed the information to the secondary station which transmitted in a subsequent segment. This method of synchronization is similar to other wide-area radionavigation systems, such as Loran and Decca. With the advent of precise cesium frequency standards, independent synchronization of each station, known as the absolute mode, became feasible. The absolute mode of operation enhanced the accuracy of the system because fewer propagation paths, each of which introduced error, were involved in any combination of secondary station signals. It also improved reliability, since the failure of any one station did not affect the capability of other stations to transmit synchronized signals. During 1966–1967, a four-station network (Norway, Trinidad, Hawaii, and Forestport) commenced operations in the absolute mode, an event that marked the beginning of the modern Omega system (Chapter 2).

During the first few years of operation in the absolute mode, the stations were synchronized using a procedure developed by J.A. Pierce (Ref. 1). In this scheme, each station recorded the signal phase of the other stations and subtracted the best estimate of the inter-station propagation times/phases to determine the station's own phase correction. This method, however, contained an inherent instability that allowed a station's timing error to grow. For this and other reasons (Ref. 2) a centralized procedure evolved in which all reciprocal paths in the network were analyzed to determine each station's phase corrections. Initially, the analysis was conducted at the Naval Electronics Laboratory Center (now the Naval Command, Control, and Ocean Surveillance Center).

In the early 1970s, synchronization control moved to the newly formed Omega Navigation System Operations Detail (ONSOD). More advanced processing of the reciprocal path data led to least squares estimates of the phase offsets, computation of frequency offsets, as well as tracking the time history of the on-line and off-line cesium standards. In January 1975, a more sophisticated synchronization algorithm was developed and implemented as a computer program entitled SYNC2. This algorithm was based on a Kalman estimation technique applied to reciprocal path data using clock error models. By inherently accounting for the dynamics of the timing sources, SYNC2 was more adaptive and accurate than previous approaches. From 1970 to about 1976, system synchronization was conducted as an internal process, with SYNC2 maintaining an RMS synchronization accuracy of 3 to 5 microseconds. The system drifted with respect to UTC, however, at one time reaching a maximum of 29 microseconds (Ref. 2).

Several methods of external synchronization were explored and tested prior to 1976. These methods included Omega signal monitoring by the U.S. Naval Observatory (USNO), time transfer using television stations, portable clock measurements at the Omega stations, and station monitoring of locally available Loran-C signals. USNO monitoring continued but was limited by the uncertainty in the propagation corrections (PPCs) predicted for the monitored paths. Loran-C signal monitoring provided a more accurate technique and was available at four of the Omega stations: Norway, Hawaii, North Dakota, and Japan. Through an established network of monitoring and control, USNO maintained reasonably accurate weekly records of the epoch of each Loran-C chain with respect to UTC. Thus, by subtracting the propagation time delay from the local Loran-C transmitting stations, UTC was transferred to the four Omega stations.

SYNC2 was upgraded (to Version 2) in 1976 to incorporate Loran-C and other external measurements into the synchronization algorithm. In October of 1977, Japan's Maritime Safety Agency (JMSA)

assumed primary responsibility for Omega system synchronization computation and control. For purposes of redundancy and cross-checking, ONSCEN continued to perform a parallel computation of synchronization corrections. SYNC2 was again upgraded (Version 3) in 1979 to address noted problems (such as error covariance buildup) and incorporate other modifications.

In 1985, the availability of GPS satellites for sufficiently long daily periods provided a very convenient *global* source of UTC information. As a final revision, SYNC2 was modified (Version 4) to incorporate GPS timing receiver measurements at all stations. By the close of 1988, operational GPS measurements at all stations were fully incorporated into the system synchronization procedure and long-standing timing biases in the stations not accessible to Loran-C were removed.

The SYNC2 software was originally written in FORTRAN IV and hosted on a Honeywell 6000 series mainframe. Later revisions were made using FORTRAN 77 code and compiler. In about 1985, the program was hosted on a Data General minicomputer and compiled and executed under AOS. In 1993, the program was restructured, rewritten in C, and renamed SYNC3. SYNC3 maintains much of the original functionality of SYNC2, but exploits advances in computer technology, software engineering, and developments in the analysis of Omega data (Ref. 6).

7.2 SYNCHRONIZATION PRINCIPLES

The Omega system synchronization algorithm is structured to control two synchronization processes inherent in system operations: internal synchronization and external synchronization. The internal synchronization process attempts to maintain simultaneous signal transmission by the stations to permit navigation/position location for Omega-only receiving systems. Inevitably, there is a departure from simultaneous signal transmission in which epochs from some stations are earlier or later than others. In such cases, it is convenient to define a "pseudo-epoch" that is the mean value of all the station epochs at any given instant. The evolution of these pseudo-epochs defines a time scale called *Omega system time* (sometimes referred to as *mean* Omega system time). The process of external synchronization seeks the coincidence of Omega system time with the Coordinated Universal Time (UTC) epoch to permit the dissemination of UTC and the inclusion of Omega into interoperable receiving systems with multiple navigation sensors having a common UTC time base.

7.2.1 Internal Synchronization

Figure 7.2-1 illustrates the concept of Omega system time relative to UTC. In Fig. 7.2-1a, the relatively shifted waveforms transmitted by each station indicate the variation from a common signal

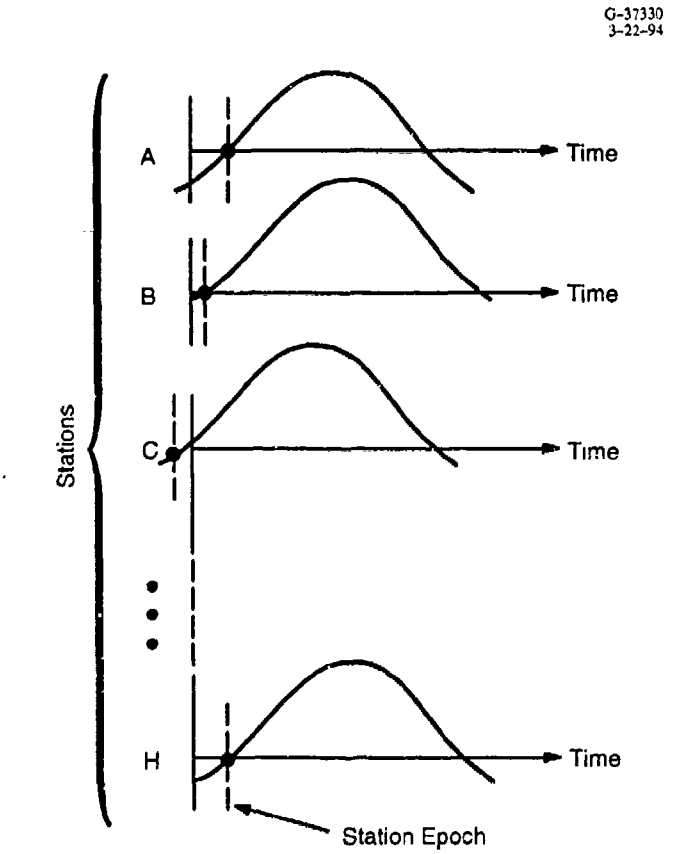

a) Comparison of Station Epochs

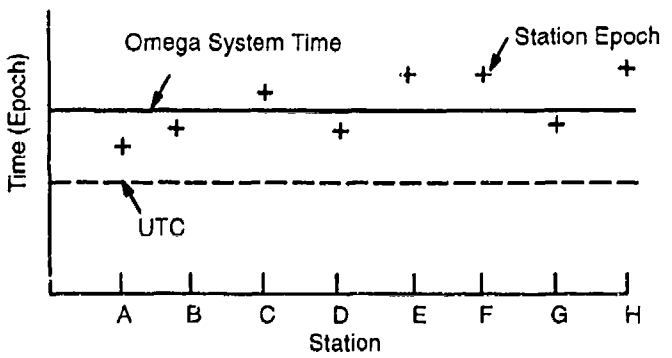

b) Omega System Time and UTC

Figure 7.2-1 Illustration of Station Epochs, Omega System Time, and UTC

transmission "time." Transmission time is quantified by the identification of an *epoch*, the occurrence of an actual, repeatable event, defined with respect to a universal time base such as UTC. Omega station epoch may be defined (see Chapter 3 for a more precise definition) as the occurrence of the waveform zero crossing as the signal increases from negative to positive values. Signal waveforms and the associated epochs for each station are illustrated in Fig. 7.2-1a relative to an arbitrary time origin. Actual epoch shifts are typically only a few hundredths of a cycle so that no cycle ambiguity occurs. Fig. 7.2-1b depicts a possible distribution of station epochs, the corresponding Omega system time, and the associated UTC epoch.

The internal synchronization process relies on phase measurements made on *reciprocal paths*. Reciprocal paths are sub-ionospheric propagation paths (over the surface of the earth) in which the locations of the transmitting station and receiver are (approximately) exchanged. Reciprocal paths for which these measurements are available couple station monitors and remote stations. These measurements are slightly complicated by the fact that they are referenced to the local transmitting station (and thus are actually phase-*difference* measurements). Reciprocal path measurements are used because their difference approximates the difference in synchronization error between the stations at both ends of the reciprocal paths. To see this, consider reciprocal paths for stations A and B. The phase measurement at the monitor local to station A is

$$\phi(\mathrm{B}, \mathrm{A}_m) - \phi(\mathrm{A}, \mathrm{A}_m) \tag{7.2-1}$$

where $\phi(X, Y)$ is the phase of station X at monitor Y, and the subscript m identifies the monitor local to the designated station. Similarly, the phase measurement at the monitor local to station B is

$$\phi(\mathrm{A}, \mathrm{B}_m) - \phi(\mathrm{B}, \mathrm{B}_m) \tag{7.2-2}$$

The actual phase ϕ may be decomposed as a sum of three terms:

- The predicted phase, ϕ_{pred}
- The error in the predicted phase, $\delta\phi_{\mathrm{pred}}$
- The synchronization error, $\delta\phi_{\mathrm{sync}}$

It should be noted that the predicted phase (and its error) depend on the *path*, whereas the synchronization error depends only on the *station* from which the signal was transmitted. With this decomposition, Eq. 7.2-1 may be written

$$\phi_{\text{pred}}(\text{B}, \text{A}_m) + \delta\phi_{\text{pred}}(\text{B}, \text{A}_m) + \delta\phi_{\text{sync}}(\text{B}) - \phi_{\text{pred}}(\text{A}, \text{A}_m) - \delta\phi_{\text{pred}}(\text{A}, \text{A}_m) - \delta\phi_{\text{sync}}(\text{A}) \tag{7.2-3}$$

Similarly, Eq. 7.2-2 may be written

$$\phi_{\text{pred}}(\text{A}, \text{B}_m) + \delta\phi_{\text{pred}}(\text{A}, \text{B}_m) + \delta\phi_{\text{sync}}(\text{A}) - \phi_{\text{pred}}(\text{B}, \text{B}_m) - \delta\phi_{\text{pred}}(\text{B}, \text{B}_m) - \delta\phi_{\text{sync}}(\text{B}) \tag{7.2-4}$$

The reciprocal path value, R(A,B), is the difference in the station monitor measurements expressed by Eqs. 7.2-3 and 7.2-4, i.e.,

$$R(\text{A}, \text{B}) = C + \delta\phi_{\text{pred}}(\text{B}, \text{A}_m) - \delta\phi_{\text{pred}}(\text{A}, \text{B}_m) + 2(\delta\phi_{\text{sync}}(\text{B}) - \delta\phi_{\text{synch}}(\text{A})) \tag{7.2-5}$$

where

$$C = \phi_{\text{pred}}(\text{B}, \text{A}_m) - \phi_{\text{pred}}(\text{A}, \text{B}_m) - (\phi_{\text{pred}}(\text{A}, \text{A}_m) - \phi_{\text{pred}}(\text{B}, \text{B}_m))$$

The predicted quantities that make up C involve the nominal values and PPCs (defined in Chapter 9) which are well-known so that C can be tabulated and subtracted from R(A,B).

The basic assumption in processing the reciprocal path measurements is that the *differences* in prediction error on reciprocal paths, which for the above example is

$$\delta\phi_{pred}(B, A_m) - \delta\phi_{pred}(A, B_m)$$

can be neglected. This is generally a good assumption, since the predictions for each of the two reciprocal paths differ relatively little (0 to 5 cecs) and therefore the errors differ even less (0 to 2 cecs). With this assumption, the difference in synchronization errors between stations B and A is

$$\delta\phi_{\text{sync}}(\text{B}) - \delta\phi_{\text{synch}}(\text{A}) = \frac{1}{2}R'(\text{A}, \text{B}) \tag{7.2-6}$$

where $R'(A,B) = R(A,B) - C$.

Since the internal synchronization process relates to excursions of each station epoch from Omega system time, the quantity obtained from the reciprocal path measurements (Eq. 7.2-6) may be written

$$\delta\phi_{B\Omega} - \delta\phi_{A\Omega} = \frac{1}{2}R'(A,B) \tag{7.2-7}$$

where $\delta\phi_{X\Omega}$ is defined to be the phase variation of station X's epoch from Omega system time. The sign is defined so that if $\delta\phi_{X\Omega}$ is positive, the epoch of station X is late with respect to Omega system time.

Effective reciprocal path phase measurement relations expressed in Eq. 7.2-7 are given for a *single* time. To incorporate the dynamics of the process into the synchronization algorithm, daily phase measurements over a week are processed to determine the (assumed linear) rate of change of phase excursion from Omega system time as well as the (assumed linear) rate of divergence or convergence of Omega system time from UTC. Since the time rate of change of phase is frequency, this independent set of measurements is called reciprocal path *frequency* measurements. Here, the word "frequency" refers to the time derivative of phase (a small fraction of a Hertz in magnitude) and not to the radiated signal frequency. A relation similar to Eq. 7.2-7 for stations A and B is given for the reciprocal path frequency measurements:

$$\delta f_{B\Omega} - \delta f_{A\Omega} = \frac{1}{2}\dot{R}'(A,B) \tag{7.2-8}$$

where the dot indicates time derivative and $\dot{R}'(A,B) = \dot{R}(A,B)$ to a good approximation since C is a function of the phase predictions that vary little from day to day (at the same hour) over a week.

7.2.2 External Synchronization

Measurements used for the external synchronization process are much more direct than the reciprocal path measurements required for internal synchronization. The external synchronization data consist of measurements of the difference between the Omega epoch and UTC epoch* at each station. In the case of Loran-C, the actual readings are adjusted to account for the propagation time of the signal, the coding delay, and the difference between the reference station chain timing and UTC as determined by

*When the two epochs are in perfect agreement at the microsecond scale, the Omega epoch leads the UTC epoch by exactly 18.000000 seconds (as of 01 January 1994).

USNO. For GPS timing receiver measurements, little or no adjustment or processing is required. Thus, for example, at station X the external measurement is

$$E(X) = \delta\phi_{X\mathrm{U}}$$

Here, the variation is written in terms of phase, although it can also be written in terms of time through the relation $\tau = 1/f \leftrightarrow 1$ cycle = 100 centicycles (cec). The variation of each station epoch from UTC can be decomposed into the excursion from Omega system time, $\delta\phi_{X\Omega}$, and the difference between Omega system time and UTC, $\delta\phi_{\Omega\mathrm{U}}$, i.e.,

$$E(X) = \delta\phi_{X\Omega} + \delta\phi_{\Omega\mathrm{U}} \tag{7.2-9}$$

The dynamics of the external synchronization process are incorporated into the synchronization algorithm in much the same way as for internal synchronization. Daily measurements of $E(X)$ over the seven days of the computation week are fit to a straight line whose slope is the frequency offset of station X's Cesium standard. Using the same decomposition as for Eq. 7.2-9 above yields

$$\dot{E}(X) = \delta f_{X\Omega} + \delta f_{\Omega\mathrm{U}} \tag{7.2-10}$$

To isolate the quantities $\delta\phi_{\Omega\mathrm{U}}$ and $\delta f_{\Omega\mathrm{U}}$, the mean values of Eqs. 7.2-9 and 7.2-10 are taken over all stations, resulting in the relations

$$\delta\phi_{\Omega\mathrm{U}} = 1/8 \sum_{X=\mathrm{A}}^{\mathrm{H}} E(X) \tag{7.2-11}$$

and

$$\delta f_{\Omega\mathrm{U}} = 1/8 \sum_{X=\mathrm{A}}^{\mathrm{H}} \dot{E}(X) \tag{7.2-12}$$

In deriving Eqs. 11 and 12, the definitions of Omega system time and Omega system frequency (see Fig. 7.2-1) were invoked, i.e.,

$$\sum_{X=\mathrm{A}}^{\mathrm{H}} \delta\phi_{X\Omega} = 0 = \sum_{X=\mathrm{A}}^{\mathrm{H}} \delta f_{X\Omega}$$

7.2.3 State Estimation

Using a state space formulation, the states of the system can now be defined and related to the reciprocal path measurements. The first eight states correspond to $\delta\phi_{X\Omega}$ where X = A, B, . . . H. The ninth state is $\delta\phi_{\Omega U}$, which is the variation of the Omega system time epoch from UTC. States 10 through 17 correspond to the time derivatives of states 1 through 8, i.e., $\delta\dot{\phi}_{X\Omega} = \delta f_{X\Omega}$. These states correspond to the variation of each station's frequency from the Omega system frequency, which is the mean of the station frequencies. The last state is $\delta f_{\Omega U}$, which is the time derivative of the phase variation of the Omega system time from the UTC epoch.

The reciprocal path data for one pair of stations is related to the corresponding two system states as in Eq. 7.2-7. Similarly, the average of the external measurement data is related to the ninth state as in Eq. 7.2-11. In general, the measurement data vector, z, may be related to the system state vector, $\delta\Phi$ (containing the 18 states) through the measurement matrix, H, as

$$z = H\delta\Phi + v \tag{7.2-13}$$

where v is the zero-mean measurement noise vector. Since there are about thirty reciprocal path phase measurements (per signal frequency), the first thirty components (rows) of Eq. 7.2-13 yield the internal measurements. For these components, the H-matrix contains 1s and −1s in the first eight columns, depending on the measurement set. The next component is just the average of the external measurement data, i.e., Eq. 7.2-11. The subsequent thirty components are reciprocal path *frequency* measurements similar to the example for two states given in Eq. 7.2-8. The last component is the Omega system frequency offset measurement given by Eq. 7.2-12.

With the system as now defined, the optimal discrete Kalman estimate of the state vector at a discrete time t_k is given as

$$\delta\hat{\Phi}_k(+) = \delta\hat{\Phi}_k(-) + K_k\left[z_k - H_k\delta\hat{\Phi}_k(-)\right] \tag{7.2-14}$$

where the "+" in parentheses refers to the state estimate at time t_k *after* the measurements are made and the "–" to the state estimate at time t_k *before* making the measurements. The quantity K_k is the Kalman gain which controls the relative importance of the new information in the measurement at t_k (the bracketed quantity). In other words, the estimate of the state after the measurement is given by the state estimate before the measurement modified by the new information in the measurement at t_k. The Kalman gain is given by

$$K_k = P_k(+)\, H_k^T\, R_k^{-1} \tag{7.2-15}$$

where P_k (+) is the covariance matrix associated with the state estimation error after the measurement at t_k and R_k is the covariance matrix associated with the measurement noise error (see Eq. 7.2-13), i.e.

$$P_k(+) = E[(\delta\Phi_k(+) - \delta\hat{\Phi}_k(+))(\delta\Phi_k(+) - \delta\hat{\Phi}_k(+))^T];\ R_k = E(v_k v_k^T)$$

Note, from Eq. 7.2-15, that the "magnitude" of the Kalman gain increases as the norm of P_k (+) increases and decreases as the norm of R_k increases. This behavior follows from the fact that a large covariance matrix norm means the system states are not well-estimated and thus, more weight is given to the most recent measurement (high Kalman gain). On the other hand, a large norm for R_k means that the measurements are very noisy and unreliable so that little weight should be given to the most recent measurement (low Kalman gain). The covariance matrix is updated as

$$P_k^{-1}(+) = P_k^{-1}(-) + H_k^T R_k^{-1} H_k$$

This expression means that, for large measurement errors (large norm for R_k), the updated covariance matrix changes little. For small R_k, however, the inverse of the updated covariance matrix is large compared to the covariance matrix inverse prior to the measurement. This means that small measurement errors lead to a reduction in the norm of the updated covariance matrix relative to its value before the measurement. Thus, the uncertainty in the updated state is reduced as a result of small measurement errors.

7.2.4 Computation of Synchronization Adjustments

The synchronization algorithm is implemented by a computer program designated SYNC3. The overall SYNC3 structure consists of the following three components:

- Input data preprocessor (PRESYNC3)
- Computational engine (SYNC3)
- Database.

The input data preprocessor and the computational engine perform the processing and both components interface with the database. Several additional utility programs are included in the interface code because of standard DOS memory constraints (< 640 kBytes).

The purpose of the input data preprocessor, PRESYNC3, is to read the input data from the weekly status reports submitted by each of the eight Omega stations. Each station's weekly status report contains the reciprocal path data for internal synchronization, external synchronization data and other

operational information. PRESYNC3 reads this data from files on the hard disc, parses the data into data structures, performs preliminary data reduction, validity and reasonableness checks, computes the timing measurements, and initiates the program to write the data to the database. A status report for each station monitor is available after the data is processed.

The SYNC3 program is organized to process the daily measurement set via an optimal Kalman filter to obtain the synchronization corrections (referred to as CORR and ACCUM). This procedure includes the following stages:

- Processing a week's worth of station monitor measurement data
- Retrieving supporting data from the database
- Comparing/verifying current week's cesium clock serial numbers with those of the previous week
- Processing the measurements sequentially to obtain the Kalman estimates
- Generating the synchronization messages for each Omega station.

Any mismatch between previous and current Cesium clock serial numbers is identified and/or rectified by the program. The iterative expressions presented in Section 7.2.3 are processed using Bierman's UD algorithm (Ref. 5). SYNC3 provides eight predefined plots and seven predefined tables that can be viewed interactively to permit analysis of the current data run. Further information on SYNC3 operation is contained in Ref. 7.

The SYNC3 software system runs on an IBM-PC compatible computer with an 80386 microprocessor under the MS-DOS operating system. No extended or expanded memory is required. The program consists of approximately 15,000 source lines of C code developed using the Borland C++ compiler (version 3.0). The Paradox relational database (version 3.5) supports SYNC3 processing. Most of the tables in the database are temporary tables used for plotting. Data is displayed and plotted within Paradox while the C programs are running. The Paradox engine (version 2.0) is used to interface the C programming language with the Paradox database.

SYNC3 permits six different input modes (combinations) for the station timing data. The initial phase covariance for a new on-line clock is 1 μsec^2 and the initial frequency covariance is 0.04 $(\mu sec/day)^2$. After the filter has reached statistical steady state, switching to an input mode with less data available for several weeks does not affect the performance of the SYNC3 Kalman filter. During the period with less available data, filter covariance begins to grow, but quickly decays when that timing data is available again. Especially in the presence of GPS data, the phase and frequency covariance terms recover quickly.

The principal outputs of the program are the updated state vector estimates (see Eq. 14). In particular, states 1 through 8 represent the estimated phase offsets (in microseconds) of the eight Omega stations from Omega system time. The corrections implemented by the stations are just the negative values of the resulting numerical outputs for the states. In similar fashion, states 10 through 17 yield the estimated station frequency offsets (in microseconds/day) from the Omega system frequency. These output state values are divided by –6 to obtain the four-hour ACCUM adjustments applied to the station on-line clock units. Note that states 9 and 18 correspond to no actual adjustment or correction, but the measurements involving those states are certainly used in computing all the other corrections/adjustments.

The output quantities described above, which are based on the Kalman estimation algorithm presented in Section 7.2.3 apply strictly to the on-line clock units at each station. Each of the two station back-up clock units serves as an immediate replacement in the event of failure of the back-up unit. To minimize any weekly differences between the on-line and back-up units, both back-up units are aligned ("scoped") to the on-line clock unit once per day.* Remaining divergences from the on-line clock over the period of a day are removed by adjusting (through the insertion of ACCUMs) the back-up clock units at each station every four hours. Although the procedure is the same, the ACCUMs for the back-up units are the result of a SYNC3 calculation separate from the Kalman estimates of Section 7.2.3. Instead, the phase shifter readings over the nine-week period prior to the current date are fitted to a straight line using a least-squares technique. The negative of the resulting slope (in microseconds per four-hour period) is then the ACCUM correction for the particular back-up clock unit for the succeeding week.

7.3 SYNCHRONIZATION OPERATIONS

The weekly collection of data and calculation of station synchronization corrections constitute one of the most important functions of Omega operations. As noted in Section 7.1.2, Japan's Maritime Safety Agency (JMSA) has led the operational generation of system synchronization corrections since about 1977. The Omega Navigation System Center (ONSCEN) performs back-up calculations of synchronization corrections to ensure computational accuracy and integrity.

The overall synchronization process consists of determining the station phase and frequency offsets and applying the computed corrections at each station. The phase and frequency offsets are obtained

*New Timing and Control Subsystem equipment being installed (May 1994) at the stations includes the Omega Signal Generator (OMSGEN) and the Omega Signal Controller (OMSCON). Instead of using the oscilloscope method, alignment of the back-up clock units to the on-line units is now made by inserting the difference in the OMSGENS into the OMSCON. All information regarding these differences is transmitted to the other subsystem units via a communication ring.

from daily reciprocal path phase measurements and satellite timing measurements. As noted above, this weekly data is independently processed by both JMSA and ONSCEN to verify the final results. JMSA issues directives to the stations where the corrections (some of which are applied throughout the week) are initiated within a few hours of receipt.

7.3.1 Measurement Input Data

The internal synchronization process is supported by reciprocal path data that is obtained from station monitor phase data. The phase data at each station monitor is collected for four remote stations whose phase is referenced to that of the local station. The remote transmitting station and monitor receiver constitute a *path* (actually, a *short* path), which, together with the measurement time, define a *path-time*. Both the paths and the path-times are carefully chosen to be anomaly-free, i.e., the predicted signal behavior is not modal, long-path, etc. (see Chapters 5 and 6) so that the data can supply maximum information on station synchronization differences. In most cases, path-times are chosen so that the path lies fully on the day side of the earth (although long-path reception is sometimes a danger when the short path is fully illuminated). In selecting or revising path-times, the principal criterion is that the random phase error (standard deviation over a month's worth of daily measurements at a fixed hour) be as small as possible. Additional information is provided by using phase data at both 10.2 and 13.6 kHz, which is averaged prior to processing by the Kalman filter.

Table 7.3-1 shows the measurement path-times for both internal and external synchronization data. The station monitors are listed across the top and the remote stations whose signals are monitored are given in the leftmost column. For the internal measurements at the Omega stations, the phase is always referenced to the station local to the station monitor. Note that the first eight rows are symmetric about the diagonal from upper left to lower right. This symmetry arises because of the need to make measurements at both ends of a reciprocal path at the same time. In some cases, daily measurement times (UT hours) change throughout the year, especially on polar paths, where path illumination changes substantially over the year. In the case of Loran-C and GPS measurements, the receiver is located at the Omega station itself. Note that Loran-C measurements are available at only four stations, whereas GPS data is recorded at all stations.

The synchronization data is compiled by each station and submitted to JMSA and ONSCEN every Monday in the form of a weekly station data report. This report presents the daily measurement data, both internal (10.2 and 13.6 kHz phase for four path-times) and external (Loran-C and GPS), for the eight days from the previous Monday to the most recent measurement. External measurement data, whose daily measurement times are given in Table 7.3-1, are in units of microseconds. All other (phase) measurements are

Table 7.3-1 Path-times for Synchronization Measurements

TRANSMITTING STATION	STATION MONITOR							
	NORWY	LIDER	HAWAI	NSDAK	REUNI	ARGE2	AUSTS	JAPAN
A		1300	0500 (Oct-Mar) 1700 (Apr-Sep)		1100			1800
B	1300			1600	1000	1500		
C	0500 (Oct-Mar) 1700 (Apr-Sep)			2000			2400	0100
D		1600	2000			1700		1100 (Oct-Mar) 2200 (Apr-Sep)
E	1100	1000				1800	0500	
F		1500		1700	1800		0900	
G			2400		0500	0900		0400
H	1800		0100	1100 (Oct-Mar) 2200 (Apr-Sep)			0400	
Loran-C	1200		1800					0400
GPS	0816	0846	0916		0616	0646	0716	0746

given in 0.01 cycle (centicycle (cec)) corresponding to the given frequency. The report also provides the phase shifter (clock) readings in microseconds for the on-line and each of the back-up (primary and secondary) clock units. The readings are made after the back-up clock units are aligned to the on-line units (see Section 7.2.4) for the current Monday. The remaining portion of the report describes any anomalies or discrepancies from routine operations, including:

- *Cesium status changes* — any change in precedence (on-line, primary back-up, secondary back-up) is noted, including the changed units, date/time of change, and phase shifter readings at the time of change.
- *Off-air periods* — normally refers to periods when transmitter operation has ceased so that no reciprocal path measurements are available but clock units remain active so that external measurements continue as well as ACCUM insertions for all clock units.
- *Reduced power periods* — generally do not affect synchronization measurements.
- *Signal anomalies* — reports of any sudden ionospheric disturbance or polar cap disturbance events during the week, including starting and ending times as well as the time of peak disturbance; reciprocal path data is excluded during these events although external data is presumably unaffected.

Further information regarding message format and content is given in Ref. 4.

7.3.2 Computational Output Data and Directives

The calculation of synchronization corrections commences after all weekly station data reports are received by JMSA and ONSCEN. The computation is not lengthy, but requires careful checking of inputs and outputs and possibly several re-executions. The central result of the calculation is the updated optimal estimate of the state vector. The first eight states describe the phase/time excursions of the station clocks from Omega system time. To offset these excursions, the negative value of these computed state values must be inserted into each station's on-line clock unit. The directive message from JMSA to each station contains the correction value in microseconds, which is entered into all on-line and back-up clock units at the next designated insertion time following receipt of the directive message. Table 7.3-1 gives the allowed insertion times for each station. The insertion times for each station differ so that system users do not experience a sudden "jump" in phase/time that might lead to a jump in a position track.

Similarly, states 10 through 17 define the frequency excursions of the station clocks from the Omega system "frequency." Thus, even though, in principle, the corrections from the first eight states reset the system, the non-zero drifts in the clocks imply that the stations will begin to diverge from synchronization soon after the corrections are made. The negative values of the frequency excursion states (States 10 through 17) are intended to offset the expected divergence. It is not feasible to implement a continuous time-linear phase change into the clock units, so the frequency offset is approximated as a series of incremental phase changes at fixed time intervals. This is the basis for the four-hour ACCUM insertions. For a given station's on-line clock, the ACCUM is computed as the negative of the corresponding frequency excursion state (in microseconds per day) divided by six (since there are six four-hour intervals in a day). The ACCUM values for each station clock unit are also contained in the JMSA directive message. Insertion of these values (which may or may not differ from the previous week's ACCUM values) commences at the first insertion time of the next UT day following receipt of the directive message. Table 7.3-2 indicates the six insertion times at four-hour intervals for each station. As noted above, these are staggered to "smooth out" any change in Omega system time. Also shown in Table 7.3-2 are the daily alignment or "scoping" times at each station, when the back-up clock units are aligned with the on-line units (see Section 7.2.4 and Chapter 3).

7.3.3 Synchronization Performance

As a system, Omega has remained well-synchronized throughout its operational history. Internally, the system has been synchronized to within about 5 microseconds since a centralized operations center was set up in 1971 under the auspices of the U.S. Coast Guard's Omega Navigation System

Table 7.3-2 Daily ACCUM Insertion and Scoping Times

UT HOUR*

STATION	00	01	02	03	04	05	06	07	08	09	10	11	12	13	14	15	16	17	18	19	20	21	22	23
A	16				16				16				16				16				16			
B	46				46				46				46				46				46			
C		16				16				16				16				16						
D		46				46				46				46				46						
E			16				16				16				16				16					
F			46				46				46				46				46					
G				16				16				16				16				16				
H				46				46				46				46				46				

* For each entry, the number refers to a measurement 16 (46) minutes after the hour at the top of the column. ACCUM insertion times occur at all indicated times; scoping times are designed by a shaded entry.

Operations Detail. Prior to that time, only two of the currently operating stations were transmitting and, in practice, the system was more experimental than operational, including the synchronization method. Also during this period, the system was not intentionally referenced to any external time scale.

Between 1971 and 1976, external synchronization was an *ad hoc* process that relied on USNO measurements of the North Dakota signal and portable clock measurements. Determining the Omega system time offset relative to UTC from the USNO data was inaccurate due to the uncertain propagation delay (computed from the available PPCs) between the station source and the receiver. A substantial bias error in the PPCs could therefore have resulted in a fixed offset for many months. On the other hand, portable clock measurements were very accurate but were made relatively infrequently due to the considerable logistics and cost involved. Though accurate initially, the effect of the portable clock measurement would begin to decay one week after the measurement was made and the routine weekly data sources (with their built-in biases) would again "steer" Omega system time after a few weeks. As noted in Section 7.1.2, Omega system time deviated by as much as 29 microseconds from the UTC epoch during this period.

Beginning in 1976, Loran-C timing equipment was installed at four of the Omega transmitting stations: Norway, Hawaii, North Dakota, and Japan. This equipment is used to detect the signal from the Loran-C station closest to each of the four Omega stations and compare its epoch with the local on-line clock unit. Before being used in the synchronization algorithm processing, the Loran-C timing data is corrected for the following effects:

- Deviation of the chain master station epoch from UTC
- ECD (at master station)

- Emission/coding delay (if signal is from a secondary station)
- Propagation delay (including ASF) from Loran-C station to timing receiver antenna at Omega station
- Antenna factor 180° phase shift (5 μsec) for loop antenna)
- Antenna-to-receiver cable delay
- Multi-coupler delay
- Receiver delay
- Time to standard zero crossing (nominally 30 μsec).

Except for the first correction, the above corrections are essentially fixed from week-to-week so that they are lumped together as a single correction term. The deviation of the chain master station epoch from UTC varies daily and is published in the USNO Series 4 Bulletin.

Since the combined accuracy of these corrections is within a microsecond, the four (northern hemisphere) stations making the Loran-C measurements have been held to UTC with an RMS error of about one microsecond (Ref. 2). Before 1985, however, it is now believed that the southern hemisphere station epochs, which were not externally referenced, deviated from UTC by as much as 3 microseconds (Ref. 2).

The discrepancy between the stations with and without external data sources can be traced to the PPCs. The only "connection" between these two types of stations is through the reciprocal path measurements. As shown in Section 7.2.1, the reciprocal path measurements isolate the station pair synchronization difference only to within the difference of the reciprocal path PPC errors. Though small, these errors are characterized as mostly *biases* (random component is small). Thus, they can persist for months, undetected by the internal synchronization measurements. Evidence for these biases emerged during the relatively infrequent portable clock visits to the stations and, in fact, efforts were made to correct these PPCs based on concurrent portable clock measurements at several stations. These efforts were not entirely successful due to the relatively short-term portable clock visits.

More direct indications of the biases between the externally linked and internally linked stations were obtained when GPS timing equipment was installed at all stations during the period 1985 to 1988. Figure 7.3-1 shows a plot of the daily differences between UTC epoch and the Liberia station epoch for the last three months of 1985 (Ref. 2). The data in the plot is taken from measurements of Liberia's on-line clock unit relative to GPS (which is essentially aligned to UTC). These measurements were not incorporated into the synchronization algorithm until Monday, 4 November 1985, when all measurements (internal and external) for the previous week were processed. The weekly computation was performed on Tuesday, 5 November, and the corrections were issued later that day. The next insertion time

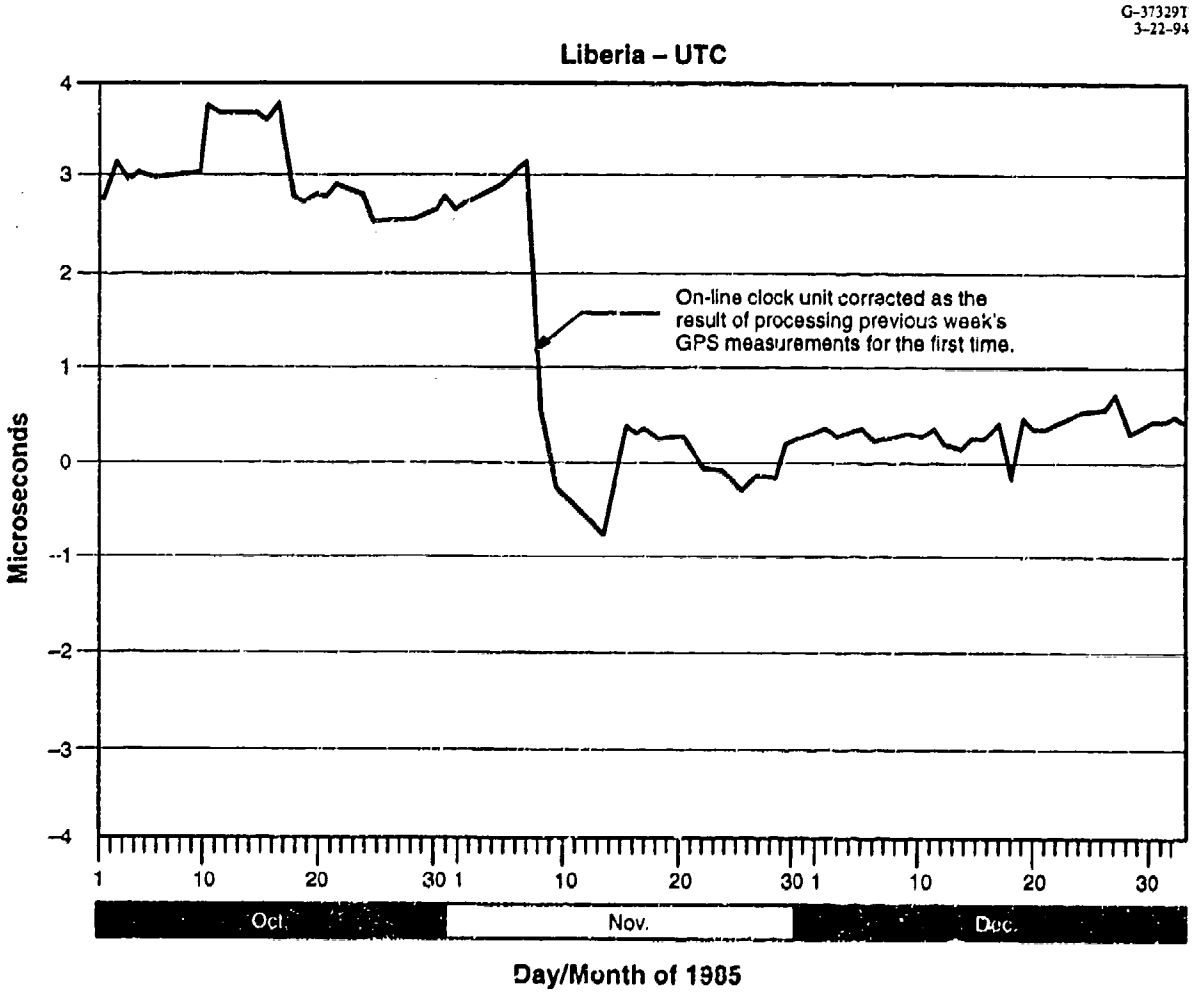

Figure 7.3-1 Variation of Liberia Station On-line Clock Epoch with Respect to UTC During Period When Liberia GPS Measurements were First Included in Synchronization Computation

following Liberia's receipt of the directive message was on 6 November 1985. The Liberia correction was large (about –3 microseconds) and the measurements shown in the figure reflect this correction.

Figures 7.3-2 and 7.3-3 provide more insight on the dynamical behavior of synchronization corrections. These figures display synchronization data from the period when GPS measurements from the Argentina station were first incorporated into the weekly synchronization computation. Figures 7.3-2a and 7.3-2b show the first eight states of the system synchronization model, i.e., the on-line clock

*This is opposite to the convention in which epoch difference A–B implies that A starts a counter and B turns it off; in this case, positive A–B means that A is *earlier* than B.

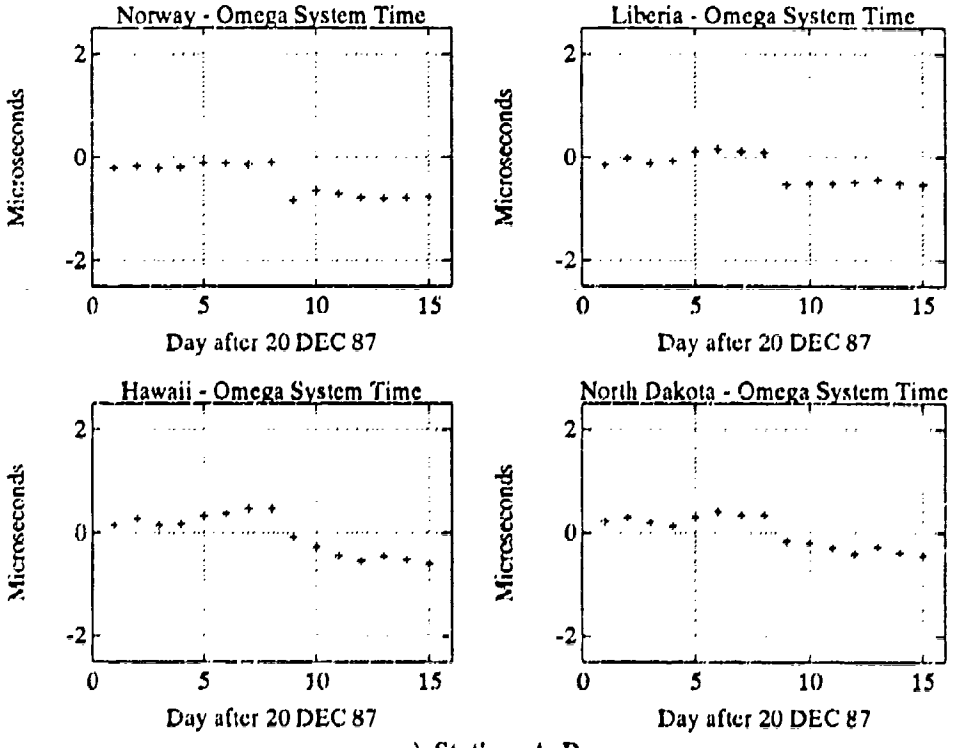

Figure 7.3-2 Station Epochs Relative to Omega System time for the Period 21 December 1987 through 04 January 1988

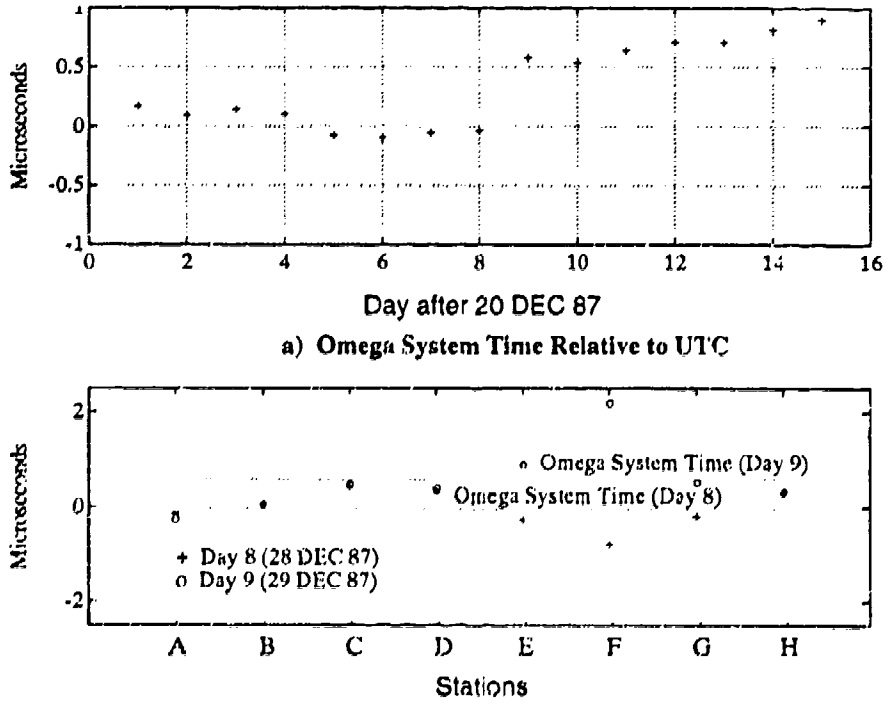

Figure 7.3-3 Omega System Time and Station Epoch Relative to UTC for the Period 21 December 1987 to 04 January 1988

unit at each of the eight stations relative to Omega system time. The sign convention for the time epochs is such that positive values mean the station on-line clock unit is *late* (i.e., occurs at a later and therefore greater UTC time value) with respect to Omega system time.*

The weekly computation was performed on Day 8 of the plot, i.e., Monday, 28 December 1987, using new data recorded daily from 21–28 December 1987. This data did *not* include GPS measurements from Argentina. However, the synchronization computation on the *next* Monday, 4 January 1988, did include Argentina GPS data recorded daily from 28 December 1987 to 4 January 1988. At this time, the synchronization algorithm "knew" that the on-line clock unit at the Argentina station was about 3 microseconds late with respect to the UTC epoch (see Fig. 7.3-3b and Fig. 7.3-4). Moreover, this new information meant that Omega system time was also late with respect to UTC, but not as late as the Argentina station (see Figs. 7.3-3a and 7.3-3b). Thus, the upper right panel of Fig. 7.3-2b shows the Argentina station epoch with respect to UTC shifting from a somewhat negative value on Day 8 to a large positive value on Day 9. Note that this does not reflect an actual change in time epoch but rather a dramatic increase

in the accuracy of the *information* regarding the position of the Argentina station's epoch. Also note that the discrepancy with respect to Omega system time continued to widen throughout the week up to the weekly computation date, Day 15 (4 January 1988). This happened because the directive information (corrections and ACCUMS) for that week were the result of calculations based on data from the previous week which did not include Argentina GPS measurements. Thus, the ACCUM insertions drove the Argentina on-line clock in the direction (toward later times) that the previous data indicated.

The new information regarding the Argentina station epoch had ramifications throughout the system since knowledge of Omega system time had changed significantly. With respect to UTC, however, Figure 7.3-3b shows that little changed at those stations (A, B, C, D, H) for which GPS/Loran-C external measurements had been recursively processed by the algorithm over an extended history. On 4 January 1988, the new correction/ACCUM computations based on the Argentina GPS measurements were issued as JMSA directives and implemented by the stations after this date. These corrections (and, to a lesser degree, the ACCUMs) are responsible for the dramatic shift in the Argentina station epoch with respect to UTC shown in Fig. 7.3-4. By May 1988 GPs measurements from all stations were being used in the synchronization computation and Omega system time generally fell within 0.5 microsecond of UTC (Ref. 2).

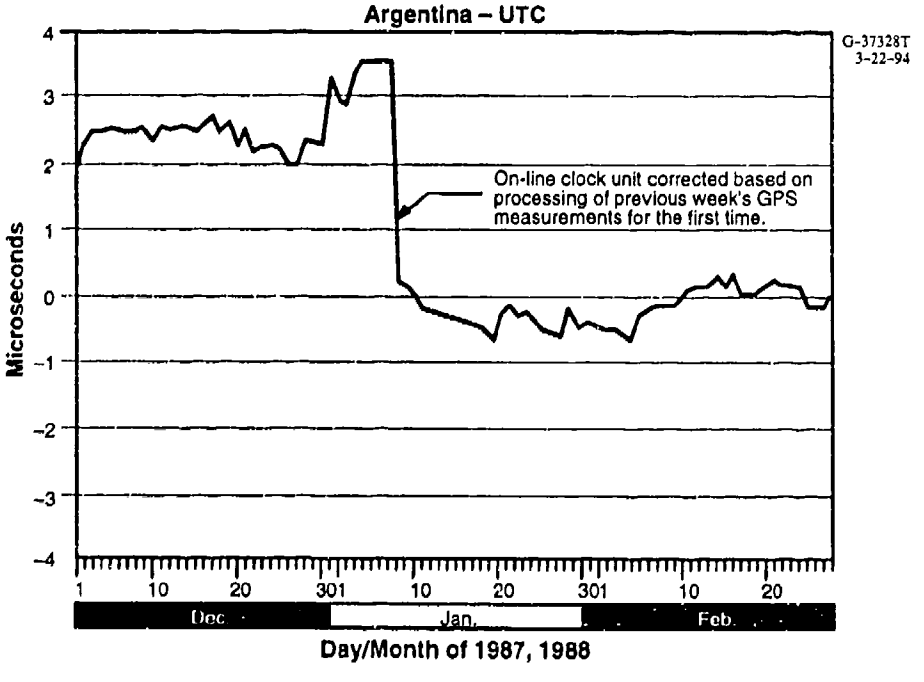

Figure 7.3-4 Variation of Argentina Station On-line Clock Epoch with Respect to UTC During Period When Argentina GPS Measurements were First Included in Synchronization Computation

7.4 PROBLEMS

7.4.1 Sample Problem

1. The following table gives accurate external data on offsets of each station's on-line clock unit relative to UTC ($\delta\phi_{XU}$) in microseconds.

Station	$\delta\phi_{XU}$ (μsec)
A	–3.3
B	+2.2
C	–0.6
D	–0.2
E	+1.5
F	–3.8
G	0.7
H	–1.1

   a. What is the offset of Omega system time relative to UTC?
   b. What is the offset of the Norway Station relative to Omega system time?

Answer:

   a. Eq. 7.2-11 shows that adding all $\delta\phi_{XU}$ and dividing by 8 yields $\delta\phi_{\Omega U}$, the offset of Omega system time relative to UTC, i.e., **–0.575 microsecond**
   b. From Eq. 7.2-9, we see that

$$\delta\phi_{AU} = \delta\phi_{A\Omega} + \delta\phi_{\Omega U}$$

From the table above, $\delta\phi_{AU}$ = –3.3 μsec and from part (a), $\delta\phi_{\Omega U}$ = –0.575 μsec. Thus, $\delta\phi_{A\Omega}$ = **–2.725** μsec.

7.4.2 Problems to be Solved by Reader

1. With the data table in Problem 1 of Section 7.4.1 and a similar table for δf_{XU}, is sufficient information available to estimate the projected state vector and thereby issue directive messages? If so, why are reciprocal path measurements still used?
2. Suppose the synchronization computation results in the estimate:

$$\hat{\delta f}_{B\Omega} = -0.32 \text{ μsec/day}$$

What is the appropriate ACCUM directive for Station B?

7.5 ABBREVIATIONS/ACRONYMS

A	Norway
ACCUM	Accumulative correction value inserted every 4 hours
AOS	Data General's Advanced Operating System
APR	April
ARGE2	Argentina's station monitor
AUST$	Australia's station monitor
B	Liberia transmitting station
C	Hawaii transmitting station; also a programming language
C++	An object-oriented programming language
CW	Continuous wave
cec	Centicycle
CORR	Weekly phase correction inserted into all clock units at each station
D	North Dakota transmitting station
DEC	December
E	East (referring to coordinates); La Reunion (referring to transmitting stations)
F	Argentina transmitting station
FORTRAN	FORmula TRANslation code; an older version was designated as IV, newer version is 77
G	Australia transmitting station
GPS	Global Positioning System
H	Japan transmitting station
HAWAI	Hawaii's station monitor
IBM-PC	International Business Machines personal computer
JAPAN	Japan's station monitor
JMSA	Japan's Maritime Safety Agency
kHz	Kilohertz
LIBER	Liberia's station monitor
MAR	March
MS-DOS	Microsoft Corporation's Disk Operating System
N$DAK	North Dakota's station monitor
NORWY	Norway's station monitor
OCT	October
ONSCEN	Omega Navigation System Center
ONSOD	Omega Navigation System Operations Detail
Paradox	A database management system produced by Borland

PPC	Propagation correction
PRESYNC3	Input data processor to SYNC3
REUNI	La Reunion's station monitor
RMS	Root-mean-squared
SEP	September
SYNC2	Name of Omega synchronization program used from 1975 to 1993
SYNC3	Name of Omega synchronization program used since 1993; also the name given to the computational engine of the synchronization program
UD	Upper Diagonal
USNO	U.S. Naval Observatory
UT	Shortened form of UTC
UTC	Coordinated Universal Time

7.6 REFERENCES

1. Pierce, J., Palmer, Watt A., and Woodward, R., Omega: A Worldwide Navigation System, System Specification and Implementation, Second Edition, Prepared for the U.S. Navy Department, Bureau of Ships, and submitted through the Office of Naval Research, Published by Pickard & Burns Electronics, Waltham, MA, May 1966.

2. Vannicola, V., and McManus, H., The evolution of synchronization in the world-wide Omega Navigation System, *Proceedings of the Twentieth Annual Precise Time and Time Interval (PTTI) Meeting*, Vienna, VA, November 1988.

3. Vannicola, V., private communication, October 1991.

4. Department of Transportation/U.S. Coast Guard, Omega Navigation System Operations Manual, COMDTINST M 16566.1A, December 1988.

5. Bierman, G., *Factorization Methods for Discrete Sequential Estimation*, Academic Press, Inc., London, 1977.

6. Covino, J., Noseworthy, G., and Casswell, R., SYNC3: A modern approach to Omega synchronization, *Proceedings of the Eighteenth Annual Meeting of the International Navigation Association*, Orlando, FL, October 1993.

7. Covino, J., Final SYNC3 (Version 2.0) User's Guide, Synetics Corporation, October 1993.

CHAPTER 8

DATA COLLECTION/ANALYSIS/PROCESSING PROCEDURES

Chapter Overview — This chapter describes the Omega signal data collection and analysis efforts that support the mission of the Omega Navigation System Center (ONSCEN). Section 8.1 reviews the goals and history of the Omega Signal Monitoring Program in terms of its two components: the Long-term Omega Monitor Program and the Omega Regional Validation Program. The network of land-based signal monitors supporting the Long-term Omega Monitor Program is described in Section 8.2. Section 8.3 explains the procedures used at ONSCEN for processing, analyzing, and storing the signal data recorded at the network monitors. Finally, Section 8.4 presents an overview of the Omega Regional Validation Program and the individual regional projects that make up this program. Problems, including worked-out examples and those to be attempted by the reader, are included in Section 8.5. Abbreviations and acronyms used in the chapter are given in Section 8.6 and references cited in the chapter are found in Section 8.7.

8.1 INTRODUCTION

8.1.1 Omega Signal Monitoring Program

Signals radiated at the current Omega frequencies have been received, recorded, and analyzed since well before the Omega system was declared operational. These early recordings demonstrated the repeatability and usability of the signals for navigation (see Chapter 2). As Omega grew into an operational system, signal monitors formed an integral part of the system configuration, playing key roles in signal performance evaluation, station integrity checks, and system synchronization.

In the early 1970s, an Omega Signal Monitoring Program was established by the Omega Navigation System Operations Detail (ONSOD) with two broad objectives:

- Develop and maintain a worldwide, long-term (multi-year) Omega signal data collection activity using land-based monitors for system performance evaluation, system synchronization, station signal specification integrity, propagation correction (PPC) model calibration, and operational data analysis
- Implement a series of short-term regional data collection activities using both air- and surface-based monitors to supplement the worldwide land-based monitor data in verifying/validating Omega signal coverage predictions

The program to carry out the first objective is referred to in this chapter as the Long-term Omega Monitor Program and the corresponding program to implement the second objective is termed the Omega Regional Validation Program. A time-line for the Omega Signal Monitoring Program, indicating major sub-programs and other events, is shown in Fig. 8.1-1.

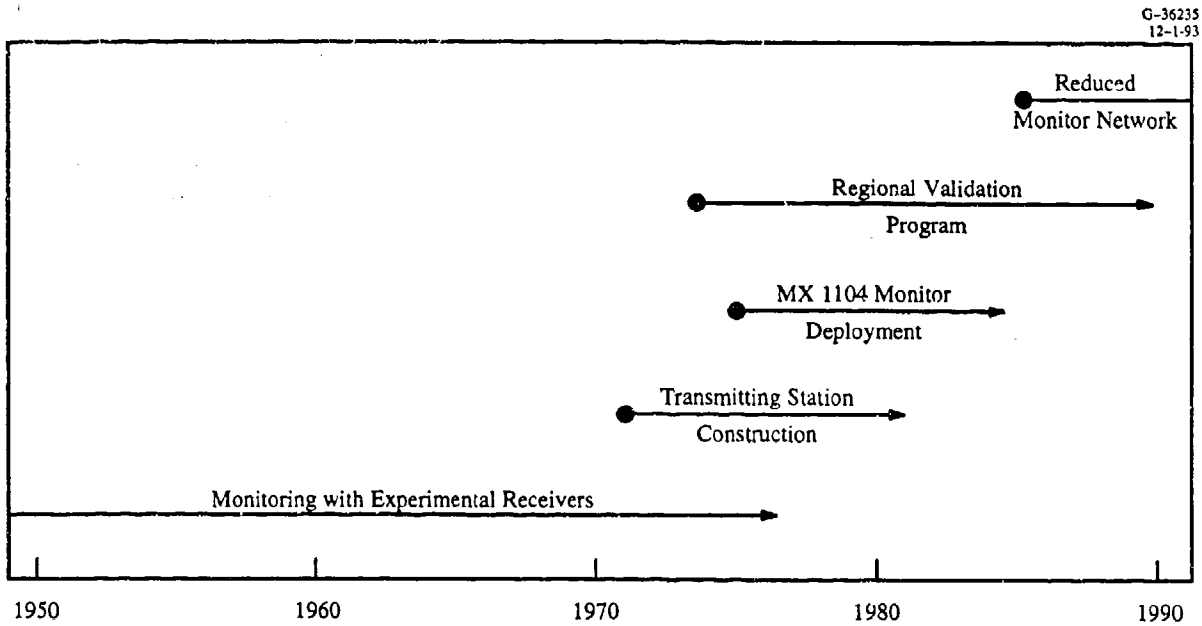

Figure 8.1-1 Omega Signal Monitoring Program Phases and Activities

True to its name, the Long-term Omega Monitor Program has continued from the early 1970s to the present (1994). Until about 1978, the program utilized, for the most part, signal monitor equipment developed by or for U.S. Navy Laboratories. As stations were constructed and brought on-line in the mid-1970s, station monitors were established at sites 20 to 50 km from the transmitting station antenna. These monitors were used for testing initial signal transmissions and synchronizing the signal epochs at each station to a common reference time. At that time, the "non-station" monitors were a collection of experimental receivers, used for a variety of special-purpose applications.

In the late 1970s, ONSOD launched an effort to develop a receiver system, specially designed to monitor Omega signals. The resulting units, built by Magnavox and designated as the MX 1104 series, serve as the basic measurement instrumentation for the modern long-term monitoring program. Until the late 1980s, the data was recorded with MFE cassette tape recorders on tapes that were mailed monthly to ONSOD. The monitor receivers designed for use at the Omega stations are MX 1104 units modified to operate in the high signal environment of the local station and perform precise single-path timing measurements. These units include both LS (local site) and MS (monitor site) receiving systems. Based on earlier studies of phase error models (Ref. 15), monitors were located at sites spaced at intervals of about 1500 km, corresponding to a correlation distance obtained from phase error measurements. The plan/schedule for establishing sites and deploying these monitors was guided partly by the need for

diversified data to calibrate the PPC model and partly by the needs of the Omega Regional Validation Program. The network of fixed monitor sites reached a maximum size in the mid-1980s and the decline in subsequent years stemmed from a need to consolidate existing data (in preparation for a re-calibration of the PPC model) and the completion of the regional validation program. Since the latter 1980s, a reduced monitor network of approximately 20 to 25 sites has operated to support system synchronization and performance evaluation through operational data analysis.

8.1.2 Long-term Omega Monitor Program -- Data Acquisition

The network of fixed Omega monitors consists of receiving systems whose measurement data serve two broad purposes. The two purposes are uniquely identified with the following two types of monitor sites:

- Station monitors (in the vicinity of a transmitting station) supplying information used for system synchronization and performance evaluation/operational data analysis
- Remote monitors (distant from any transmitting station) providing data used for system validation and PPC model calibration/refinement.

Whereas the station monitors form a generally fixed network (although the sites are occasionally relocated by no more than a few tens of kilometers), the remote monitor site configuration changes in response to PPC model calibration or validation program needs. Figure 8.1-2(a) illustrates the network of 56 fixed monitor sites (filled circles) that existed at the peak of the MX 1104 Monitor Deployment Program (see Fig. 8.1-1). These sites include both the station monitors and remote monitors used to support earlier validation/model calibration efforts. In most cases, a site established to support a regional validation project can also be used as a data source for subsequent PPC calibration work. When a regional validation project is completed and the focus shifts to another region, the previous site may be retained, if its data is deemed critical for PPC model calibration or system performance evaluation. For example, the monitor site in Tahiti was established to support the South Pacific validation effort but, because it was set up in the absolute synchronized mode of operation and is well separated from other remote monitor sites, it was retained to monitor and evaluate system performance for several more years following the validation tests in the South Pacific.

After the last regional validation project (Mediterranean), the monitor network was reduced in size and scope to reflect the needs of a mature system, i.e., inter-station synchronization data reporting and operational data analysis, with less emphasis on PPC model calibration and signal coverage validation. To satisfy these needs, the station monitors became the "nucleus" of the reduced monitor network,

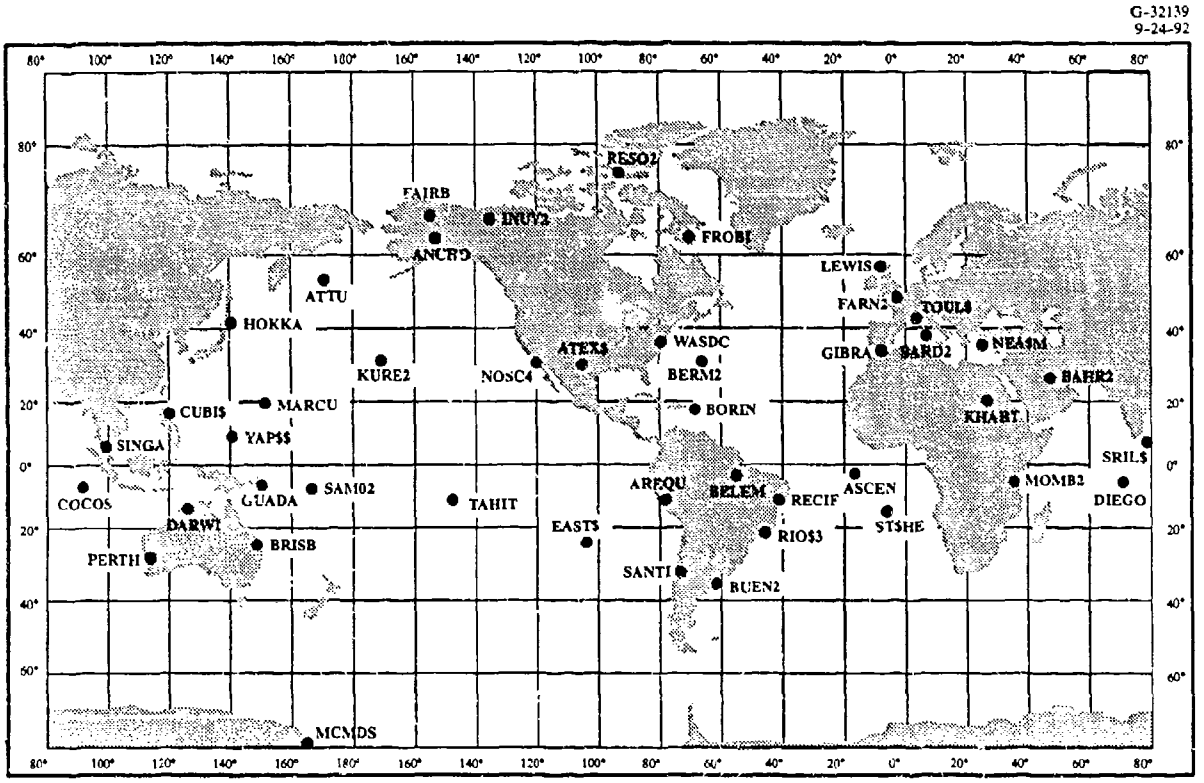

a) Remote Monitor Network — 1987

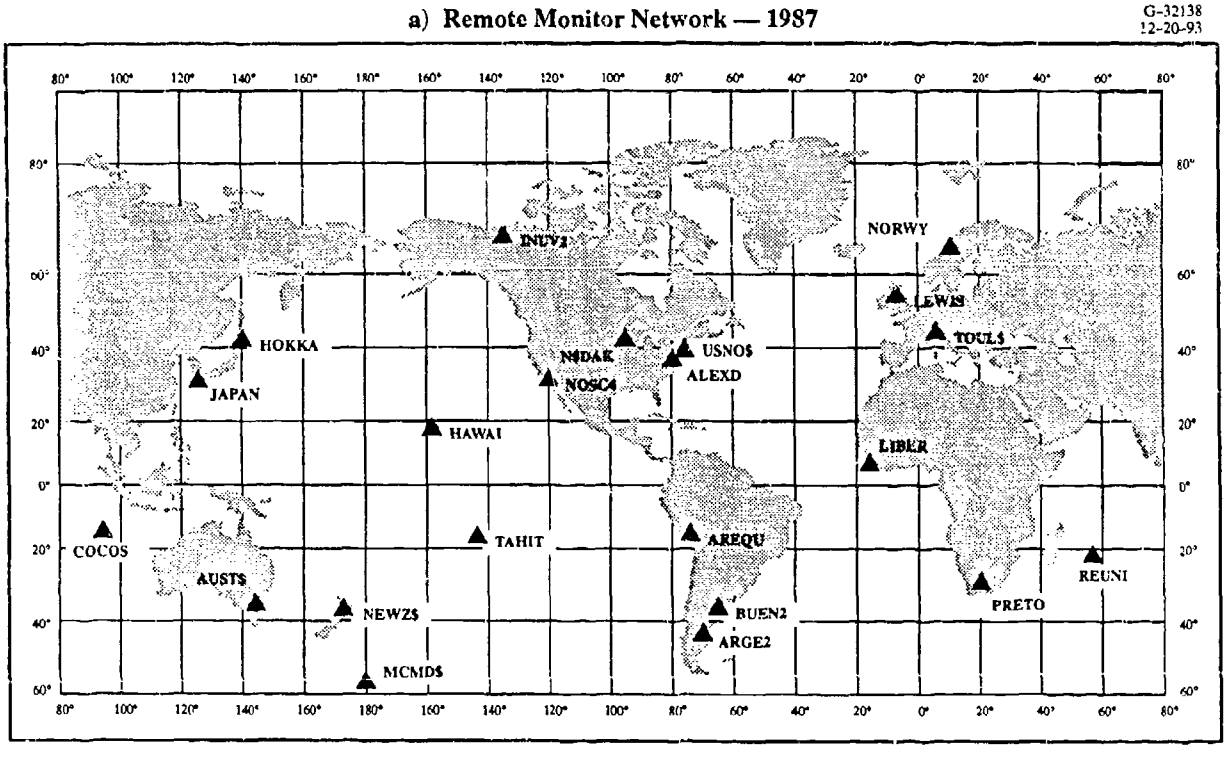

b) Reduced Monitor Network — 1993

Figure 8.1-2 Omega Monitor Network Sites

which is supplemented by additional monitors. Because of their unique location or accessible time/frequency support equipment, these additional monitors provide data that serves as a sensitive indicator of system operational performance. Figure 8.1-2(b) illustrates the 22 site locations (triangles) for the reduced monitor network as of June 1992.

The signal data measured by the MX 1104 monitor is recorded on a disk recorder collocated with the monitor. This data includes signal phase and signal quality number (related to signal-to-noise ratio (SNR)) at the three Omega frequencies of 10.2, 11⅓ and 13.6 kHz. Ancillary data, such as error codes and time constants is also included with the signal data. Normally, the data is recorded every hour on the hour, although occasionally it is recorded more frequently. A block format, providing signal phase and quality number for all eight stations and three frequencies, is used for the recorded data. A month's worth of data that has been recorded hourly is collected on diskette and mailed to ONSCEN.

Upon receipt by ONSCEN, the data blocks are validated, edited, re-formatted, combined with other blocks, and stored as sketched in Fig. 8.1-3. Diagnostic procedures are applied to validate the data, including immediate checks regarding block header information and later checks involving plots of the processed data. Data block editing may occur in the re-formatting procedures, although the data values themselves are not altered. The data is formatted and stored so as to be accessible to PPC model calibration routines and operational data analysis.

The procedures for handling data used to support system synchronization are somewhat different. At each station, 10.2 and 13.6 kHz phase data on selected paths at designated "control" times (see Chapter 7) are read from the monitor display (measured at the MS unit) and sent via message to Japan's Maritime Safety Agency (MSA) and ONSCEN. As explained in more detail in Chapter 7, this data helps to determine the relative phase offset of the received station signals. The data recorded on disk at each station monitor has the same format as that for the remote monitors. Figure 8.1-3 illustrates the data flow for both the station monitors, which provide data to support both system synchronization and non-operational objectives, and the remote monitors, which support only non-operational requirements.

8.1.3 Long-term Omega Monitor Program — Data Analysis

The data analysis conducted as part of the Long-term Omega Monitor Program is, of course, tied directly to program objectives and goals. As discussed in Section 8.1.1 and indicated in Figure 8.1-1, the principal program objectives in the "post-validation" period are to support both system synchronization and performance evaluation. Performance evaluation is mainly accomplished through operational data analysis but the evaluation results sometimes indicate the need to re-evaluate and re-calibrate the current

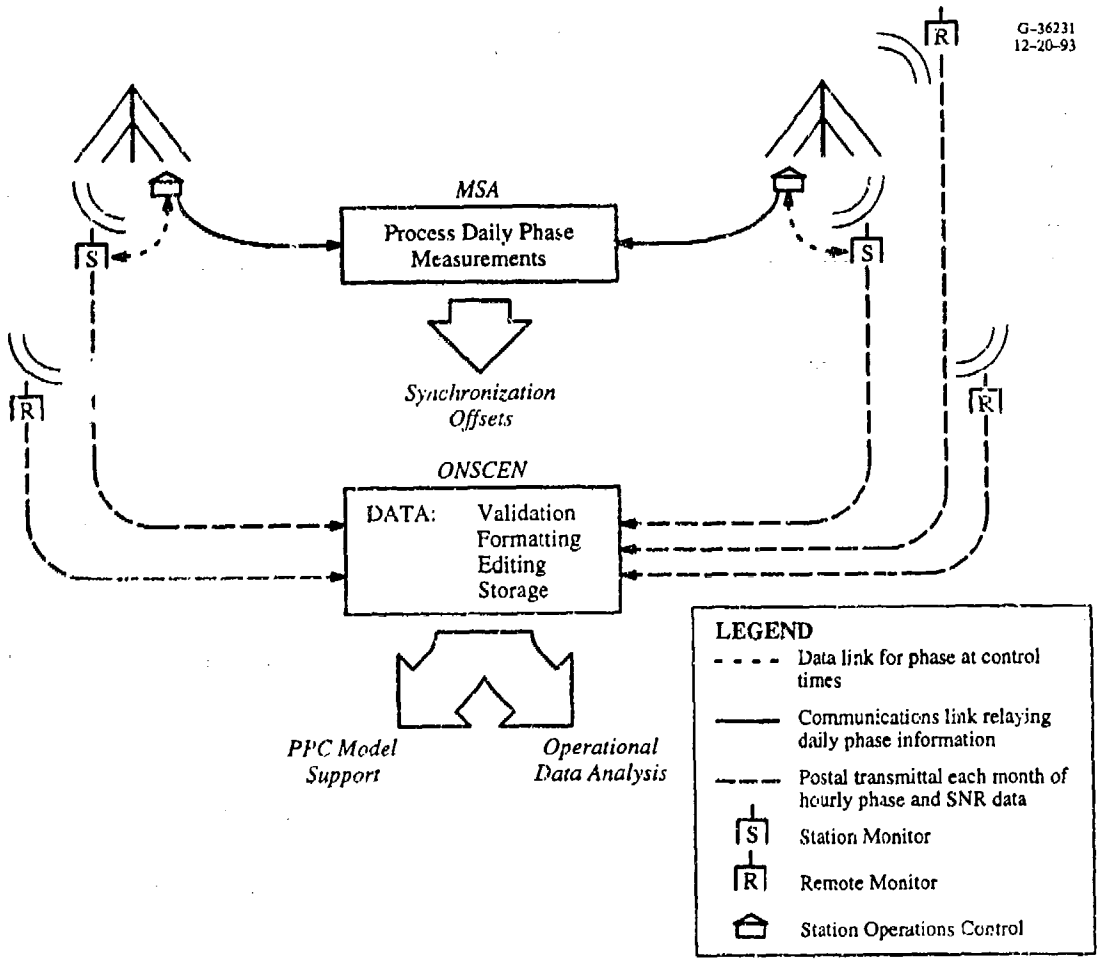

Figure 8.1-3 Data Acquisition and Analysis for Long-term Monitoring Program

PPC model. This need is shown in Fig. 8.1-3 in terms of remote monitor data that is used to support PPC model evaluation/calibration efforts as well as operational data analysis.

The particular type of monitor data required to support PPC model calibration is mostly phase, although quality number/SNR data is required for identification/rejection of anomalous data. Both phase data (from monitors whose phase reference is very precise) and phase difference data (from monitors whose phase reference is relatively imprecise) may be used for model calibration. Before applying the model calibration procedure, the data is screened to eliminate suspected anomalies, i.e., those with time profile signatures characteristic of modal interference (substantial presence of higher-order modes; see Chapter 5), long-path (signal arriving via the longer of the two great-circle arcs connecting a station

and receiver), low SNR, etc. The data is then down-sampled since the model cannot be simultaneously calibrated over *all* measurements (which amount to at least several hundred thousand). Finally, the data is laned, i.e., assigned the estimated whole cycle value for the particular measurement. The resulting data is then used to calibrate the linear PPC model coefficients. Certain non-linear parameters intrinsic to the PPC model are determined from continuous data usually obtained from strip chart recordings at the station monitors.

Virtually all hourly data recorded at both station and remote monitors is used in operational data analysis (ODA). The basic idea is to provide a time profile of phase and SNR data serving as a reference to validate newly acquired data, diagnose monitor equipment problems, investigate user-reported anomalies, and evaluate system performance. Prior to entry into the reference database, the raw data is re-formatted, edited, and laned. The reference information includes, for each monitor site, plots and statistics for the average diurnal phase and SNR profiles over each month at frequencies of 10.2, 11⅓, and 13.6 kHz. Predicted phase, computed using the most recent PPC model, is also included in the reference information. With this comprehensive information on the Omega monitor sites, operational data analysis can be applied to determine the extent of degraded signal behavior, e.g., month-hour combinations for which signals exhibit modal interference, long-path dominance, or low SNR, as well as the relative degree of position error.

8.1.4 Regional Validation Program

In general, the validation of Omega system performance in a given region consists of confirming or modifying, if necessary, predicted signal coverage, system availability, and position accuracy in the region. To test the accuracy of the system predictions, various types of measurement data are required including signal amplitude, signal phase, electromagnetic noise, and phase/position accuracy at most of the common Omega frequencies. To determine the appropriate coverage information, measurements are made using Omega monitor receivers on a mix of fixed and mobile platforms. Some signal coverage parameters, such as SNR, are equally well determined at either fixed or mobile monitors, while others, such as modal interference, can be unambiguously determined only from recordings on rapidly moving platforms, i.e., aircraft.

The validation regions are typically ocean areas including portions of surrounding land masses encompassing some 50 to 75 million square kilometers. The enormous size of these regions together with the need to measure the signals from eight stations at four common frequencies over 24 hours during all months of the year greatly constrains the scope of any experimental program with limited resources. Thus, the validation projects focused on locations, signals, and times that were expected to be

critical, in the sense of marginal coverage, availability, or position accuracy. Where possible, measurements were also made under conditions in which the model predictions are expected to be weak, because of either necessary model simplifications or uncertain geophysical parameters.

The validation program was carried out region by region over a 14-year period from 1977 to 1991, as indicated in Table 8.1-1. During this period, the project goals, approach, methods, and measurement technology evolved considerably. When the program was initiated in 1977, the immediate objective was to determine whether Omega would serve as a suitable replacement for Loran-A (whose phaseout was being considered) in the western Pacific Ocean area. Later, the program objectives were generalized to include testing the predictions of the model-based coverage diagrams. In particular, it was recognized that the coverage parameter describing modal interference could not be determined from fixed monitor sites (since its effects can mimic those of high noise conditions) so that the predictions of modal interference could only be tested with measurements on airborne platforms used in the regional validation projects. Thus, the later validation projects emphasized airborne measurements along radial paths from stations whose signals were expected to exhibit modal interference for certain hours of the day. Validation of modal interference (MI) predictions is facilitated by the relative insensitivity of MI to time of year, i.e., month (although it does depend strongly on time of day) so that the measurements could adequately test for modal predictions over the typical project span of a few weeks.

Table 8.1-1 Omega Regional Validation Projects

PROJECT/REGION	TIME PERIOD*
Western Pacific Ocean — I	1975–1978
Western Pacific Ocean — II†	1986–1990
North Atlantic Ocean	1978–1980
North Pacific Ocean	1977–1981
South Atlantic Ocean	1980–1983
Indian Ocean	1983–1987
South Pacific Ocean	1985–1987
Mediterranean Sea	1987–1991

* From beginning of short-term data collection to final documentation.

† The second phase extended work done during the first phase by including validation of Omega Australia signal behavior as well as measurement/analysis of modal interference and long-path propagation on all signals in the region.

Measurement data for the validation projects were obtained using a variety of equipment and platforms. The platforms included both short-term (a few days to several weeks) and long-term ground sites, shipboard installations, and dedicated aircraft. As part of the Long-term Omega Monitor Program, the long-term monitor sites were usually established with the dual purposes of supporting the validation project for the region in which the monitor was located and providing new data for PPC model calibration. The equipment used in the validation program varied from project to project but generally consisted of MX 1104 receivers (ground sites), MX 1105 receivers (shipborne units), specially configured receiver systems for the aircraft test bed, Cesium standards (for stable time reference), and supporting navigation equipment used as a position reference for both air and marine craft.

The analysis for each region was typically carried out by first synthesizing the data from the various platforms and receivers that were located in common geographic regions/cells and recording the same station signals at approximately the same time. The data was extensively processed and compared with predictions from theoretical models. During the coordinated tests, when all receivers/platforms were concurrently operating, ground site data was often collected at 6-minute intervals, rather than hourly. This permitted detection of temporally anomalous events, such as sudden phase anomalies (SPAs), and lane slips due to quasi-parallel path-terminator conditions.

As each regional validation project was completed, a final report was published describing the data collection effort and a summary of the system performance in the region including any variances from the standard predictions (see Refs. 2 through 9). In addition to analysis of the carefully controlled test data, the document included operational reports from both marine and air users to verify the operational capabilities implied by the test results. In most cases, approval of the final report was followed by a brief note in the Federal Register that the designated region had undergone validation and was "declared operational for Omega navigation." In this way, the validation program became a vehicle to extend step-by-step the system's officially declared operational area.

8.2 LONG-TERM OMEGA SIGNAL MONITORS

8.2.1 Objectives

For purposes of description, the term "long-term Omega signal monitor" refers collectively to the signal monitor equipment, the fixed ground site location/facility, and the recorded data associated with each of the installations contributing to the Long-term Omega Monitor Program. In contrast to the

shorter-term goals of the Regional Validation Program monitors, the objectives of these long-term monitors are to provide signal data to support:

- Evaluation/tracking of transmitting station performance
- System synchronization
- PPC model calibration/refinement
- Assessment of Omega signal coverage and accuracy.

The first two objectives of the long-term monitors listed are operational in nature and will probably remain as objectives throughout the lifetime of the Omega Monitor Program. The last two objectives support long-term programs to improve Omega accuracy (through improved phase prediction) and signal coverage specification; the continued need for these programs is periodically evaluated by the Omega Navigation System Center.

8.2.2 Historical Development

The 1966 Omega Implementation Committee Report (see Chapter 2) recommended placement of Omega signal monitor sites at transmitting stations to determine synchronization offsets. In the late 1960s and early 1970s, monitors not co-located at transmitting stations were used for research purposes, including determination of signal structure and ionospheric parameters, and utilization procedures for navigation. Later, as transmitting stations came on line, these monitors were used to verify that sufficient signal combinations were available to declare the Omega Navigation System operational within specific regions. The station monitors served the dual purpose of Omega system performance monitoring and transmitter synchronization.

In planning the deployment of the non-station monitors, an important consideration is the ideal separation of the monitor sites. Limited resources clearly constrain the lower limit on site separation, but intersite distances that are too large preclude a global characterization of signal behavior. A quantitative basis for site separation was sought which could be modified by logistical, political, and economical considerations. The prime consideration for selecting a quantitative basis, or model, was the phase error resulting from use of the PPCs. Thus, the ideal spatial distribution of monitor sites was based on the spatial correlation of phase prediction errors. Phase prediction error data from existing monitor sites having a range of intersite distances were used to determine a correlation "cutoff" distance (usually referred to as, simply, correlation distance). The correlation distance, which is independent of direction from the monitor site, thus defines the radius of a circle surrounding each monitor site as illustrated in Fig. 8.2-1. According to the correlation model, points inside each circle would yield phase errors which are reasonably well-correlated with those of the monitor site at the center of the circle.

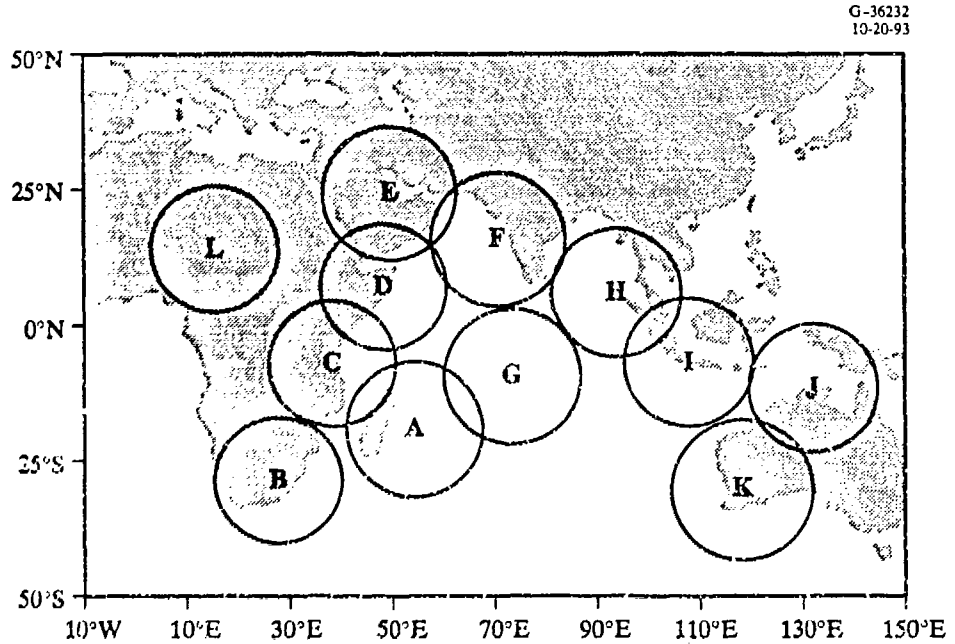

Figure 8.2-1 Example Monitor Site Spacing and Signal Correlation Distance

To determine a set of monitor sites for a region, circles (with radius equal to a correlation distance) are drawn about initial points in the region and then "shuffled" until the total overlap and uncovered region is minimized. Within each circle, several candidate monitor sites are selected based on logistical/political considerations, amount and quality of probable technical support, estimated degree of electromagnetic interference, and projected costs. Subsequent negotiations with host nation government officials and private parties determine the actual location of the site, duration of the monitoring, data sharing arrangements, etc. Figure 8.2-1 illustrates application of the method to the Indian Ocean region (focusing on major trade routes) using a correlation distance of 750 nm (1389 km). Circles are centered on probable site locations.

Implementation of the monitor plan proceeded slowly throughout the 1970s, primarily because of a scarcity of operational monitoring equipment, a lack of uniformity among the available monitor equipment, and data recording in the form of strip charts, thus requiring time-consuming, labor-intensive manual data entry for subsequent processing. Just prior to the introduction of the "standard" monitor receiver (described below), long-term Omega monitors, consisting of equipment from a variety of manufacturers, numbered about twenty.

Magnavox Advanced Products and Systems Company was contracted by the U.S. Coast Guard to develop an Omega receiving system to accurately measure phase without performing any of the usual navigation functions. The result was the MX 1104 monitor receiver which detects signal phase on three frequencies (10.2, 11⅓, and 13.6 kHz) and provides an estimate of "single-path" signal phase. The MX 1104 also outputs data in a phase-difference format. As a replacement for the earlier hodge-podge of equipment, the MX 1104 served as a common sensor for monitoring and permitted compilation of a uniform and consistent database. Following acquisition and deployment of the MX 1104 receiver, the network of Omega monitors expanded until the mid 1980s, when a total of 56 monitor sites including eight station monitor sites were operational (see Table 8.2-1 and Fig. 8.1-2(a)).

As the collection of phase and phase-difference recordings (referred to historically as the MASTERFILE) became dominated by the more consistent MX 1104 data, the resulting database could be reliably used for its intended applications. In the late 1970s, the most important of these applications was the calibration of the propagation correction (PPC) model. The PPC model is a semi-empirical phase prediction model based on both theory, which provides the analytical structure, and observed data, which ties the model to precise numerical values at known positions and measurement times. The PPC model structure was developed by a Naval Electronics Laboratory Center (NELC; now called Naval Command, Control, and Ocean Surveillance Center or NCCOSC) group headed by E. Swanson (Ref. 11). A version of the model was calibrated at frequencies of 10.2, 11⅓, and 13.6 kHz in about 1971 using data mostly from measurements made in the 1960s (Ref. 12). By 1980, a sufficiently diverse amount of historical and recent (MX 1104) data had been assembled to perform a re-calibration of the earlier model, which had been slightly revised. The data consisted primarily of phase difference data on signals at the three principal frequencies from the existing Omega stations (as well as from earlier, experimental stations), but excluding the Australia station, which was not yet on-air. The model calibrated with this data (known as the 1980 PPC Model) has been widely used in constructing published PPC tables as well as for algorithms utilized in Omega receiver/processor software (Ref. 13).

Following the 1980 PPC Model calibration, the Long-term Omega Monitor Program continued to acquire data in support of PPC model development and calibration, but other applications also began to make increasing use of the data. The regional validation program, which began in 1977, generally relied on aircraft measurements and short-term monitoring using both land-based and marine platforms to validate predictions in the region of interest. Beginning around 1980, data from monitor sites near and within the validation region of interest were included in the overall analysis and interpretation effort. The long-term Omega monitor data analyzed included SNR, for comparison with coverage predictions,

Table 8.2-1 Omega Monitor Network Sites: January 1987

MONITOR SITE	LOCATION	MONITOR SITE	LOCATION
ANCHO	Anchorage, Alaska, U.S.	KHART	Khartoum, Sudan
AREQU	Arequipa, Peru	KURE2	Kure Island (U.S.)
ARGEN	Trelew, Argentina	LEWIS	Butt of Lewis, U.K.
ASCEN	Ascension Island (U.K.)	LIBER	Brewerville, Liberia
ATEX$	Austin, Texas, U.S.	MARCU	Marcus Island (Japan)
ATTU$	Attu, Alaska, U.S.	MCMD$	McMurdo, Antarctica (U.S.)
AUST$	Carrajung, Australia	MOMB2	Mombasa, Kenya
BAHR2	Manama, Bahrain	NEA$M	Nea Makri, Greece
BELEM	Belem, Brazil	NEWZ$	Lower Hutt, New Zealand
BERM2	Bermuda (U.K.)	N$DAK	Dickey, North Dakota, U.S.
BORIN	Borinquen, Puerto Rico, U.S.	NORWY	Hestmannen, Norway
BRISB	Brisbane, Australia	NOSC4	San Diego, California, U.S.
BUEN2	Buenos Aires, Argentina	PERTH	Perth, Australia
COCOS	Cocos Islands (Australia)	PRETO	Pretoria, South Africa
CUBI$	Cubi Point, Philippines	RECIF	Recife, Brazil
DARWI	Darwin, Australia	RESO2	Resolute Bay, Canada
DIEGO	Diego Garcia (U.K.)	REUNI	La Reunion Island (France)
EAST$	Easter Island (Chile)	RIO$3	Rio de Janiero, Brazil
FAIRB	Fairbanks, Alaska, U.S.	SAM02	Pago Pago, American Samoa
FARN2	Slough, U.K.	SANTI	Santiago, Chile
FROBI	Frobisher Bay, Canada	SARD2	Sardinia (Italy)
GIBRA	Gibraltar (U.K.)	SINGA	Singapore
GRAND	Rio Grande, Argentina	SRIL$	Colombo, Sri Lanka
GUADA	Honiara, Guadalcanal, Solomon Is.	ST$HE	St. Helena Island (U.K.)
HAWAI	Wahiawa, Hawaii, U.K.	TAHIT	Tahiti (France)
HOKKA	Hokkaido, Japan	TOUL$	Toulon, France
INUV2	Inuvik, Canada	WASDC	Washington, DC, U.S.
JAPAN	Tsushima, Japan	YAP$$	Yap, Western Caroline Island (U.S.)

and phase/phase-difference, whose diurnal behavior yields clues regarding the presence of modal interference and long-path signal propagation. This data quickly became an integral part of the regional validation data collection effort and, later, the selection of new deployment regions for the long-term monitors were based on the regional validation schedule. Following the commencement of operations at Omega Australia in 1982, the monitored data for this signal was rapidly processed and analyzed to determine its time-dependent navigation utility in various parts of the world.

After reaching its peak size in the mid-1980s, the network of Omega monitors began to be scaled back in the late 1980s. This was partly due to a reduction in the scope of both the PPC model calibration database compilation and the regional validation program. Two important contributing factors, however, were that the buildup of measurement data began to exceed the capacity of the designated processing system and (partly because of the data overload) equipment failures were frequently not detected for extended periods of time. Thus, the long-term Omega monitor program in the late 1980s became focused on fewer sites with higher-quality data that was more rapidly processed. At monitor sites where precise UT time was available, exact single-path phase errors could be computed, leading to better estimates of Omega position accuracy. The operational objectives, including system synchronization, PCD detection, and system performance evaluation were also re-emphasized. As of June 1993, the Omega monitor network comprised a total of 22 sites (see Table 8.2-2 and Fig. 8.1-2(b)).

Table 8.2-2 Omega Monitor Network Sites: June 1993

MONITOR SITE	LOCATION	MONITOR SITE	LOCATION
ALEXD	Alexandria, Virginia	LIBER	Monrovia, Liberia
AREQU	Arequipa, Peru	MCMD$	McMurdo, Antarctica
ARGE2	El Tehuelche, Argentina	N$DAK	Dickey, North Dakota
AUST$	Carrajung, Victoria, Australia	NEWZ$	Wellington, New Zealand
BUEN2	Buenos Aires, Argentina	NORWY	Utskarpen, Norway
COCOS	Cocos Island, Australia	NOSC4	San Diego, California
HAWAI	Wahlawa, Oahu, Hawaii	PRETO	Pretoria, South Africa
HOKKA	Hokkaido, Japan	REUNI	Riviere des Plules, La Reunion
INUV2	Inuvik, NWT, Canada	TAHIT	Tahiti, French Polynesia
JAPAN	Ozaki, Tsushima Island, Japan	TOUL$	Toulon, France
LEWIS	Butt of Lewis, U.K.	USNO$	USNO, Washington, DC

8.2.3 Omega Monitor Modes and Data Types

Currently, the Long-term Omega Monitor Network comprises MX 1104 receiver systems, each of which consist of a receiver/processor unit, an antenna coupler unit, and a disk recorder unit. A crucial part of the receiving system is the reference oscillator, or clock, associated with the receiver/processor unit. The accuracy (stability) of the clock (oscillator) defines the *mode* of monitor and the *type* of data obtained. The reference oscillator internal to the MX 1104 has relatively low stability, but external oscillators of higher precision are easily attached to the MX 1104, effectively bypassing the internal oscillator.

The three basic monitor modes/types are listed in Table 8.2-3. Although mode and type are used synonymously, "mode" generally characterizes the stability of the reference oscillator, whereas "type" (numbered 1, 2, or 3) usually refers to the resulting data (see Chapter 9, Section 9.4.2). Note that the table contains headings for both frequency and time references. For Types 2 and 3, the distinction is immaterial, but for Type 1 data, the clock employed by the receiver in making the measurement must not only be stable, but *synchronized* to UTC. The three types of data are defined as follows:

Type 1 — Phase data referenced to a highly stable clock (such as a Cesium frequency standard) and phase/time-synchronized to the Omega station signals

Type 2 — Phase data referenced to a highly stable clock (such as a Cesium frequency standard)

Type 3 — Phase difference data, i.e., differences in signal phase between pairs of station signals accessible to the receiving system

Type 1 data is available at only a relatively few sites where external equipment, such as a cesium frequency standard or a satellite timing receivers, are available to maintain phase coherence and accurate time reference. Phase/time synchronization can be maintained through external means because the signal waveform transmitted by each Omega station is synchronized (approximately) to Coordinated Universal Time (UTC), which serves as a reference for most high-precision standards and navigation satellites. This type of data is the only source of phase error (observed phase — predicted phase) information over a single station-to-receiver path. Type 2 data, which is somewhat more common than Type 1 data, permits analysis of single path diurnal phase *behavior* (since it is referenced to a stable source), but not single station phase error. Type 3 data results when no high-stability reference (1 part in 10^{12} or better) is coupled with the receiver/processor so that only phase-difference measurements are meaningful.

Table 8.2-3 Omega Monitor Modes/Types

MODE (TYPE)	FREQUENCY REFERENCE		TIME REFERENCE	
	DEVICE	STABILITY	EPOCH	UNCERTAINTY
(1) Absolute	Cesium*	$< 10^{-12}$	UTC	~ 1 microsecond
(2) High-Stability Reference	Cesium*	$< 10^{-12}$	(none)	
(3) Low-Stability Reference	Crystal	$< 10^{-7}$	(none)	

* The Cesium Standard is the most common device satisfying the listed stability criterion, but other standards, such as Rubidium, which satisfy the stability criterion, are also used.

For the purposes of PPC model calibration, Type 2 as well as Type 3 data on single paths must be differenced, since an "exact" datum* is required to determine the linear model coefficients. The phase-difference measurements are less desirable, from the viewpoint of PPC model calibration, than the absolute mode measurements providing single-path phase data, since differences introduce additional noise (day-to-day fluctuations (at a fixed hour) on *two* paths) and reduce observability by subtracting modeled phenomena common to the two paths. Some Type 1 data was used in PPC Model calibrations prior to 1990, although it was extremely small compared to the phase difference component.

Type 2 data can be used directly (without differencing) for system performance evaluation and signal coverage analysis. Such analysis is possible because, aside from a fixed (unknown) offset, the reference phase diverges negligibly from the transmitted phase over a period of days or weeks. Thus, the diurnal behavior of a signal can be analyzed for signs of modal interference or long-path. Type 1 data also permits this kind of analysis, and, in addition, allows direct measurement of single-path phase error, since the reference phase offset is effectively zero. A collection of single-path phase errors at a monitor site can be used to directly determine the position error that would be incurred by a receiver operating in the range-only navigation mode in the vicinity of the monitor site.

An important source of Type 1 data is the station monitor receiver. In terms of equipment available at the site itself, the station monitors actually operate in the low-stability reference mode, i.e., the receivers are equipped with a medium-precision crystal oscillator so that only phase-difference measurements can be accurately made. For the station monitors, however, one of the paths is the very short

*The precision implied here refers to the fractional part of the cumulative phase, which is the only meaningful part of the measurement; the integer part is generally predicted reliably from assumed wave number values (see Chapters 9 and 4).

one (15 to 50 km) from the local station to the station monitor. This path is so short that the phase is assumed to be well-approximated by the free-space phase (although recent measurements indicate that this approximation may be less accurate than previously assumed (Ref. 14)). Since the phase for this short path is assumed to be a known constant (independent of time), the phase difference data is easily adjusted to describe entirely the path to the remote station. High time-resolution data from strip-charts at the station monitors are used to establish the nonlinear parameters of the PPC model which govern diurnal phase behavior and other time-dependent features.

8.2.4 MX 1104 Monitor Description

Figure 8.2-2 is a functional block diagram of the principal components of the Magnavox MX 1104 receiver system. The principal components of the system are:

- Antenna coupler unit
- Receiver/processor unit
- Data recording unit.

The antenna coupler unit consists of a whip antenna which senses the signal (and noise) in a relatively wide bandwidth, a pre-amplifier which amplifies both signal and noise, and a shielded cable, which transfers the signal from the antenna to the receiver. The antenna, which is of the E-field "blade-type," has an approximate bandwidth of 4 kHz and is mounted vertically. This antenna orientation is chosen so that the receiver responds preferentially to the linearly polarized, vertical Mode 1 electric field of the Omega signal. The pre-amplification boosts the signal (and noise) to overcome losses in the long cable (50 to 100 m).

The principal functions of the receiver/processor unit are to filter and amplify the signal, perform signal detection and tracking, extract and process the signal phase, and display the data. The receiver is of the "RF-tuned" type in which the signal is processed at its received frequency, rather than down-converted to a lower frequency prior to processing, as in heterodyned-type systems. The RF-tuning method was selected to eliminate phase distortions due to frequency down-conversions.

The receiver "front-end" is designed primarily to reduce/eliminate noise and isolate the signal without introducing "self-noise." This is accomplished by passing each (station/frequency) signal through a 100 Hz bandpass filter, a 100 mV/m limiter, and a multi-stage amplifier. The signals are associated with the appropriate Omega station through a signal acquisition/synchronization process in which the pulse widths at each frequency are measured and compared to the transmission format. The bandpass filter

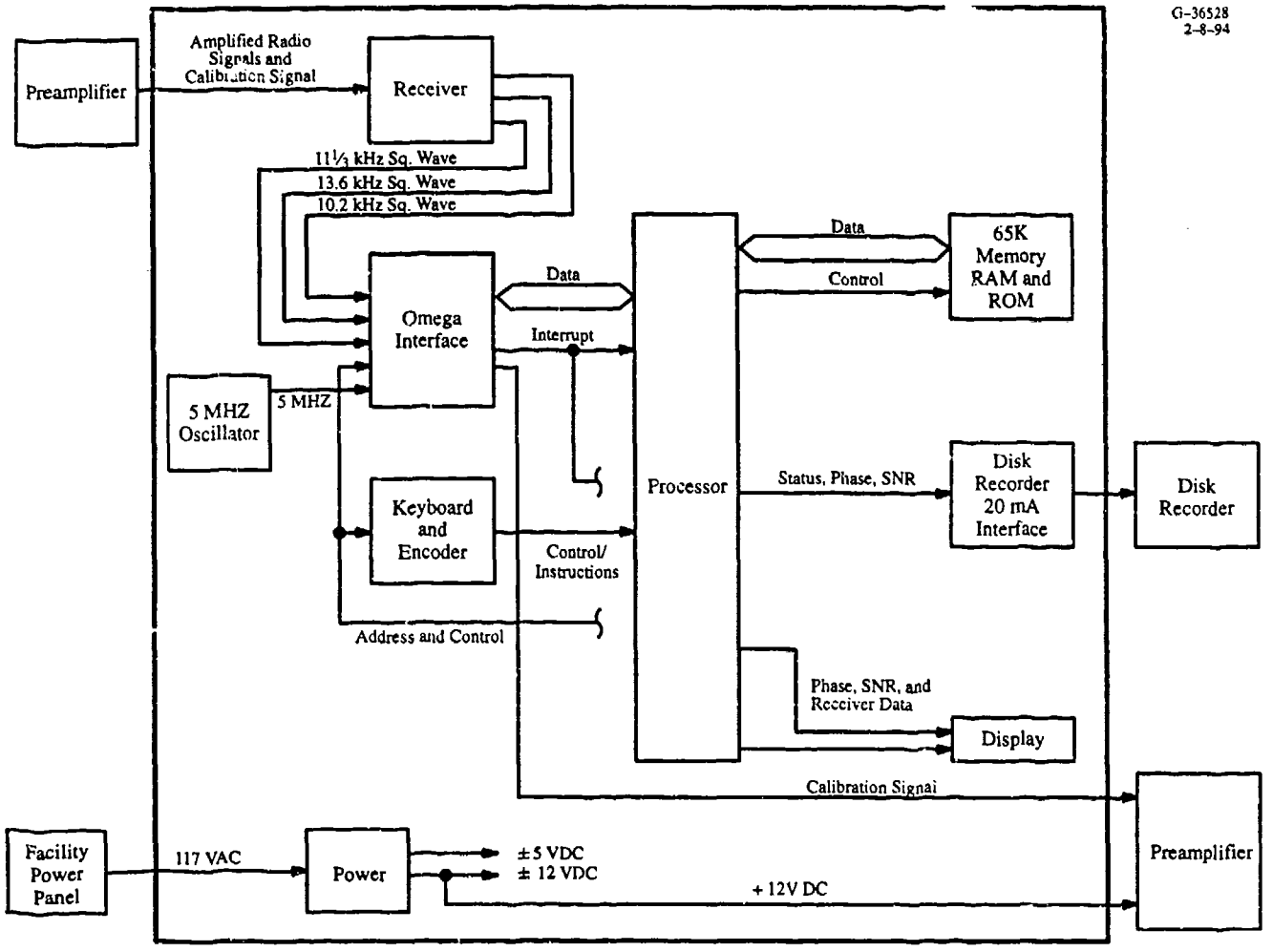

Figure 8.2-2 Magnavox MX 1104 Omega Receiver Components

reduces the flat-spectrum noise and the limiter excludes the high noise level impulses ("sferics"). The multi-stage amplifier is designed to minimize intermodulation products (internal phase noise).

In the detection stage of the receiver, the analog signal is first converted to a digital form using a 8-bit A/D converter. The time base for the resulting digitized signal is provided by the (internal or external) reference oscillator/clock which is typically at a frequency of 1 MHz. The "phase" of the signal is initially measured as the number of clock pulses from a reference point/interrupt to the next zero-crossing of the digitized signal. In the "absolute" mode of operation, a 120 mV calibration signal, which is generated by the receiver and injected at the antenna via a separate cable, is used to correct for the delay time through the antenna cable and receiver. The calibration signal is injected into the time/frequency slot corresponding to an operator-selected station whose signal is expected to be very weak and unusable.

The phase of each signal (identified by station/frequency) is controlled by an individual phase-locked loop. Each phase-locked loop is second-order to provide feedback control for both phase and phase rate of change. When averaged over several cycles, the phase-locked loop yields a smoothed estimate of the phase, depending on the time constant selected for the loop (1 to 5 minutes). In the most common mode of operation, the time constant is determined from the loop "error," i.e., the difference between the estimated and measured phase over one loop cycle. Thus, if the loop error is large or doesn't converge, the signal is "noisy" and the time constant is extended; conversely, a small loop error means a stable, noise-free signal and a short time constant. The cosine of the loop error (phase angle) is averaged and becomes the so-called "linear" estimate of signal-to-noise ratio (SNR). See Chapters 4 and 12 for additional information on phase-locked loops.

Phase and other data measured by the MX 1104 is sent to the receiver display, which is refreshed every 10 seconds. The display allows several options for data presentation, including selected phase difference readings, phase with respect to the reference clock for one or more stations/frequencies, and SNR, both as a linear estimate and the "true" value (in dB). The receiver-internal conversion from the linear estimate of SNR to its value in dB is obtained from a calibration of the receiver using a fixed signal level and variable noise level. Since the flat-spectrum noise generator used in the SNR calibration does not include "impulsive" noise, the dB-value form of the SNR datum may not be valid in the presence of a large impulsive noise component. This is true even though the receiver limiter "cuts off" large impulsive noise spikes since the noise level statistics (which influence the SNR calibration) change with the inclusion of the impulsive component. Finally, the receiver also displays diagnostic data such as error codes and estimates of internal oscillator drift.

The fixed-format data sent to the recorder is processed (averaged/smoothed) substantially more than the data displayed on the receiver CRT. The recorded phase and SNR data are the result of filtering/smoothing the instantaneous data values over the internal time constants. Phase data transferred to the recorder also passes through a triangular filter that weights each data group one time constant before and after the recording time by one-sixth and the data at the recording time by two-thirds. This filtering removes anomalous shifts in the data which may occur at the time of recording. Until the late 1980s, a cassette tape recorder was an integral part of the monitor equipment suite. A cassette tape typically held one month's worth of hourly phase and SNR data on the three primary Omega signal frequencies. To improve the reliability and maintainability of the recording function a disk recording system was acquired for all monitors beginning about 1989.

8.2.5 Monitor Site Operations

A uniform set of procedures have been established by ONSCEN for routine operations at all long-term monitor sites. These procedures include:

- Identification of monitor operational status
- Communications with ONSCEN regarding monitor operations or equipment malfunction
- In the case of an equipment malfunction, identification and removal of defective component
- Removal/replacement of data disk and submittal to ONSCEN.

These procedures are intended not only to make monitor operation as simple and routine as possible, but also to ensure uniformity of data collection and minimize operator-induced errors.

Long-term Omega monitors are frequently installed at a facility where other electronic equipment is also being operated. This arrangement is advantageous since the facility normally maintains proper environmental control (e.g., temperature and humidity) for electronic equipment and the personnel assigned to oversee the monitor are generally familiar with radio-type equipment. Oversight personnel are requested to make daily spot checks of the monitor equipment to insure normal operation.

If a problem with the monitor equipment is noted, diagnostic error codes may be entered from the keyboard to determine the general nature of the problem and, in some cases, the identification number of the faulty board. The problem symptoms and diagnostic results are communicated to ONSCEN usually by message or facsimile. ONSCEN's response may be a request to return a component, make an adjustment, or perform another diagnostic test. Returned components (normally circuit boards) are immediately replaced with functioning units to minimize monitor off-air time. ONSCEN sends the defective components to the manufacturer for repair or replacement.

At the end of a month, the data disk from the recorder is mailed to ONSCEN. A supply of disks is retained at the monitor site facility so that a new one can be inserted immediately after removing the old one. This procedure ensures a minimal loss of data during data transfer. The disk capacity is actually sufficient to hold more than a month's worth of data, but the monthly period is retained because:

- The capacity of the earlier cassette tape recorder unit was only slightly more than a month's data
- Longer periods increase the possibility that an undetected receiver error may render the data useless over a greater length of time.

Because some of the monitor sites ely remote, the mailing times vary from a few days to several weeks. As a result, ONSCEN attempts to screen the data quickly for any apparent receiver error so that the site can be notified of the error and the procedure for correcting it as soon as possible. The most direct way to detect an error is to scan the header line of the block format. Codes identifying system-detected errors are inserted in column six of the header line. These error codes, which are listed in Table 8.2-4, also appear on the MX 1104 display but may not be noted by monitor site personnel. Frequently, receiver malfunctions are not detected by the system. These errors are usually only determined through an analysis of the data itself. Some typical errors that may be detected in the data are: no diurnal variation in the phase for all channels may indicate a broken antenna wire, or incorrect diurnal variation on each channel (not physically realizable for the indicated station/frequency), an indicator that the receiver has probably become de-synchronized.

Table 8.2-4 MX 1104 Error Codes

ERROR CODE	PROBABLE CAUSE	CORRECTIVE ACTION
01	Checksum failure for the PROMs on Board 3 (Memory Board)	Replace Board 3
02	Failure of Control Processor Unit (CPU) on Board 4	Replace Board 4
03	Instability of 5 MHz Oscillator	Replace 5 MHz Oscillator
04	Failure of digital interface self-test on Board 7	Replace Board 7
08	Checksum failure for the memory (daughter board) on Board 7 (digital interface)	Replace the daughter board on Board 7

8.2.6 Current Monitor Network

The current Omega Monitor Network comprises the 22 monitor sites listed in Table 8.2-2 and portrayed in Fig. 8.1-2. Nearly a third of these sites (8) are station monitors, which effectively operate in the absolute mode, as explained in Section 8.2.3. Of the remaining 14 monitors, four are operated in the absolute mode, providing Type (1) data. Four other monitors operate in the high-stability reference mode (using Cesium standards) and the remaining six are low-stability reference mode monitors, utilizing only the internal MX 1104 oscillator. This network of monitors provides a good mix of monitor modes and a reasonably uniform geographic dispersal of sites.

Although the data from the current network sites may see some use in the support of PPC model improvement and signal coverage verification, most of its application will be to support system synchronization, system performance evaluation, and anomalous event detection. System performance evaluation requires a quantitative determination of: (1) how tightly each station maintains synchronization with respect to system time/UTC, (2) the adherence of each station's transmitted waveform to the signal specification, and (3) the relative amount of unscheduled off-air time. For synchronization, the station monitors provide system-internal measurements of phase as a critical adjunct to external time reference measurements. High-resolution data from the station monitors on certain polar paths is constantly checked for possible polar cap disturbance (PCD) events. A positive PCD indication on one path must be confirmed by positive indications on all polar paths before a PCD warning is publicly issued. Data from certain station monitors can now be readily accessed by modem. This data is acquired through the Remote Data Acquisition (RDA) system, recently implemented by ONSCEN and USNO. The RDA system, comprising a digital communication system and interface units, can retrieve/display phase, phase-difference, SNR, antenna current, and station timing information relative to GPS. The most recent data may be accessed as well as data for any hour over the preceding 45 days. Phase-difference data averaged over a five-day window (within the preceding 45 days) may also be obtained.

8.3 MONITOR DATA PROCESSING AND ANALYSIS

Monthly Omega signal data from the long-term Omega monitor sites are collected and processed by ONSCEN. Although monitor site personnel occasionally request permission to copy and analyze the monthly data prior to submittal to ONSCEN, most of the data collection and analysis is performed by ONSCEN staff. This single focal point for the data processing and analysis activities ensures uniformity and minimizes errors in the resulting data.

An illustration of the steps in the overall data processing procedure is portrayed in Fig. 8.3-1. Sections 8.3.1 and 8.3.2 describe the functions shown in the figure.

8.3.1 Initial Data Processing

Each monitor data file (resident on the data disk forwarded to ONSCEN) comprises a series of monitor data blocks which are normally recorded each hour on the hour. These data blocks contain signal data valid over the duration of approximately one time constant prior to the recording time.

An example of a monitor data block is portrayed in Fig. 8.3-2. Each block contains seven lines of character data. The header line (line 1) contains eight information fields as described in the figure. The descriptions are generally self-explanatory. Field five designates the presence of the triangular filter (see

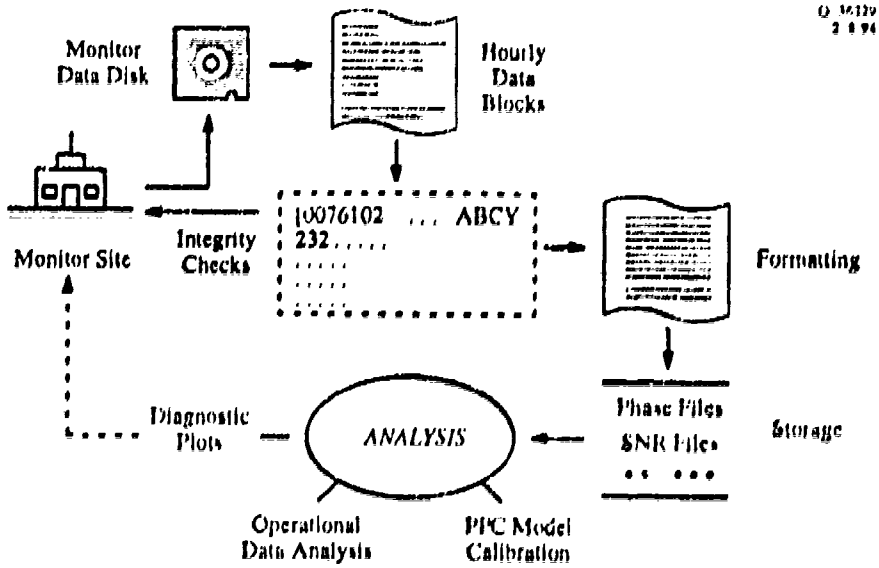

Figure 8.3-1 Monitor Data Processing and Analysis

Section 8.2.4). The error codes for Field six are given in Table 8.2-4. Note that for the station monitors, Fields five and six are reversed and two digits are allowed for an expanded set of error codes. The stations are listed in positional order so that, for example, if the signal from Station C (Hawaii) is being recorded, a C would be shown in the third position; if C is not being recorded, an X would appear in the third position, and, finally, if C were chosen as the calibrate channel, a Y would appear in the third position. The time constants (1 to 5 minutes) for each signal are tied to the same positional order. For example, if a Y appeared in the sixth position in the received signal list, a 1 would appear in the sixth position in the time constant list, since the calibrate signal is strong and requires only the shortest possible time constant to detect its phase.

Each of the next three lines contains the signal phase data for the eight Omega stations at a single frequency, i.e., Line two for 10.2 kHz data, Line three for 11⅓ kHz data, and Line four for 13.6 kHz data. Each line contains eight three-digit phase values corresponding to the station signal list given in the header line. As noted in the figure, the rightmost two digits are the phase values (with respect to the reference oscillator) in centicycles and the leftmost digit is the lane value. The lane value digit is arbitrarily assigned by the receiver, and has no inherent physical meaning. With a high-stability reference oscillator, this lane value can be used to track lane changes between any two hours (as long as the receiver is not restarted in the interim) and thus trace out the correct diurnal phase variation (correct to within an undetermined phase bias). With a low-stability reference oscillator, this procedure can only be applied

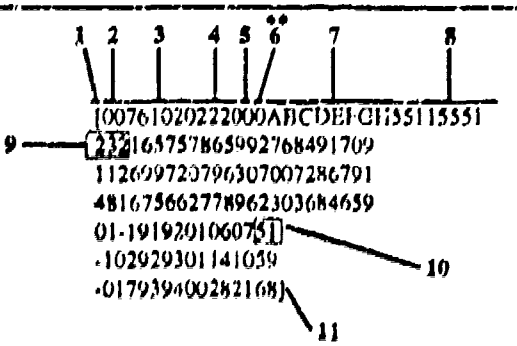

Item	Description
1.	Control start character ([).
2.	Monitor site identification code (00).
3.	Date in year, month, and day (761020).
4.	UT time in hours and minutes (2220).
5.	Filter flag. (0 = none; 1 = triangular filter) (0).
6.	Error code (0 = none; 1 to 9) (0).
7.	Station — A letter designation (A–H) indicates the station is being recorded. An X indicates the station is not being recorded. Y indicates the station signal is displaced by the calibration channel.
8.	Time constant for each station signal. The time constant is from 1 to 5 minutes.
9.	Signal phase of the first station recorded. The first character represents the least significant digit of lane count. The next two characters represent phase in centicycles. The example shows station A at 10.2 kHz.
10.	Signal-to-noise ratio quality index ("linear" scale) of station H at 10.2 kHz.
11.	Termination character (])

** Station monitor recorded data has blocks 5 and 6 reversed and allows two characters for the error code

Figure 8.3-2 Example of Monitor Data Block

to *differences* in the lane values between two signals recorded concurrently. In these cases the entire three-digit phase values are differenced (using 1000s-complement arithmetic).

Similarly, each of the final three lines contains the "signal quality" index for each of the three frequencies in the same order as phase. Each line contains eight two-digit values corresponding to the station signal list given in the header line. These indices are given with respect to the so-called "linear" scale (00-99) for signal quality. As noted in Section 8.2.4, these values are just the averaged cosine of the loop error resulting from the phase lock loop processing.

As a first step in monitor data processing, the data block header line is scanned by a pre-processor routine to detect possible faults. For example, the control start character may be absent or the site ID

code may not match that for the originating site as indicated by the mailing label. The pre-processor also checks for the correct number of characters per line and the total number of lines in the data block. Where possible, corrections for data block errors are implemented manually. If an error introduces an ambiguity that cannot be resolved, the data block is rejected.

Normally, the recording time in the header line is checked to see if it is *on* the hour (i.e., 00 minutes) and if the hour increments correctly through subsequent data blocks. Occasionally, however, other recording times are valid. For example, during certain validation tests, the data is recorded every 10 minutes over a period of a few days. The calibration channel assignment is also checked to ensure that it is not inadvertently changed over the month. Sometimes, however, ONSCEN directs the site to change calibration channels, based on analysis of the data or on operational requirements. Since the triangular filter ensures a more stable measurement of signal parameters, the filter field in the header line is checked for an ON status for most monitor operating conditions. Any non-zero error codes are noted and passed on to ONSCEN technicians who monitor the equipment/component history at each site. Based on the indicated error code, historical data, and other information, ONSCEN communicates an additional inquiry or corrective action to the monitor site. Finally, the calibration channel quality number is checked to see if it exceeds 90. A smaller number might indicate excess noise or a damaged antenna cable.

8.3.2 Data Formatting and Storage

For each monitor, the raw data blocks for a given month and year which are accepted by the pre-processor program are combined and reformatted, as illustrated in Fig. 8.3-3. The data is processed by means of a software utility (known as Program CRUNCH) which allows the following output format options:

- Raw data (no processing)
- Separate phase/SNR/frequency files
- Parsed data files.

The format for the raw data is illustrated in Figure 8.3-2. This option simply retains the original data format and effectively involves no processing.

The format for the second option, which is illustrated in the upper right portion of Fig.8.3-3, organizes the raw data for a given monitor/month/year into six files specified by frequency (10.2, $11\frac{1}{3}$, or 13.6 kHz) and data type (phase or SNR quality number). Thus, for example, file HAWAI0392.S2 contains SNR quality number data at $11\frac{1}{3}$ kHz from the HAWAII monitor site collected during March 1992. Within each

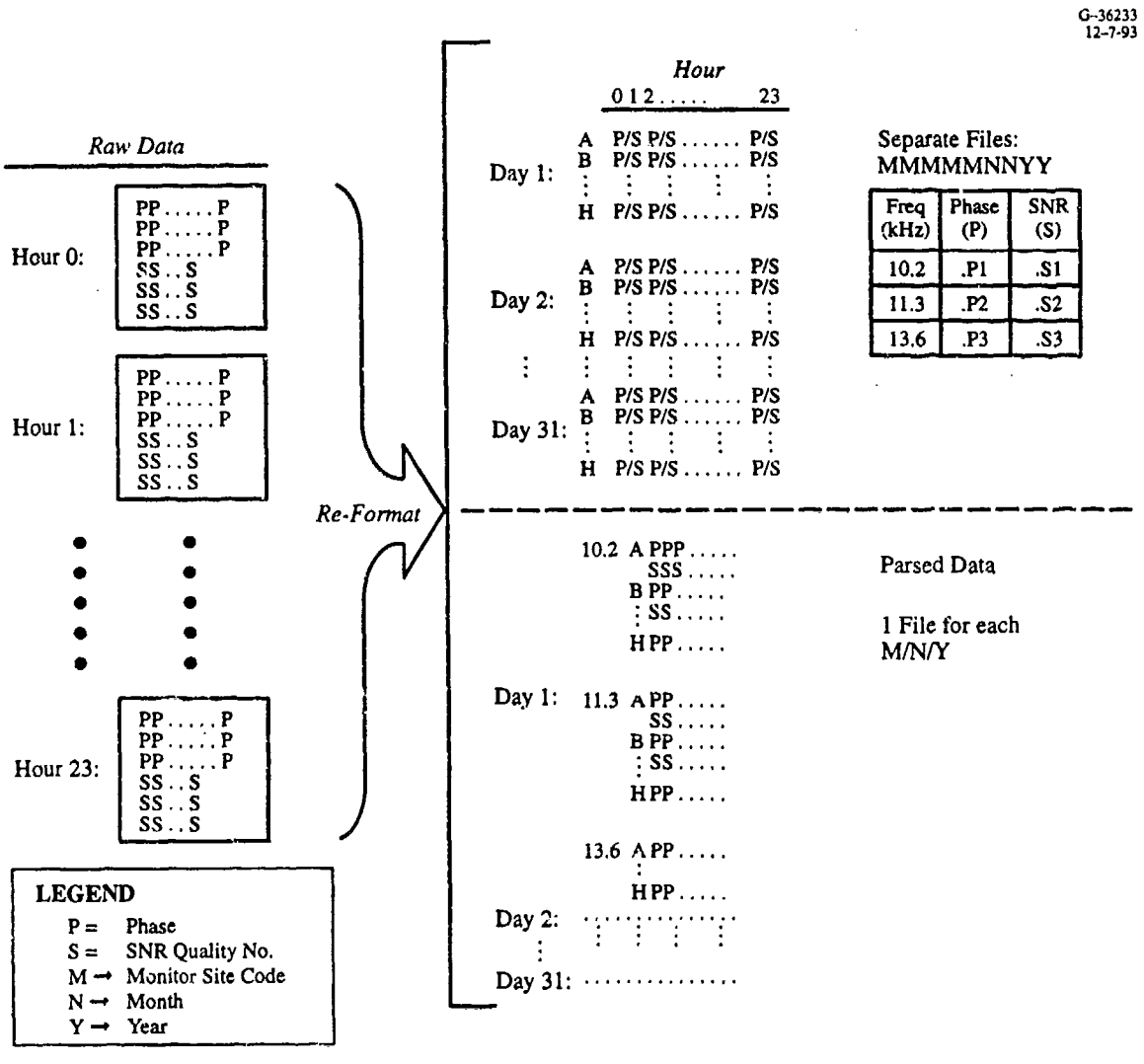

Figure 8.3-3 Monitor Data Reformatting Options

file, the data is listed as 24 columns, corresponding to UT hour, and 28 to 31 groups of eight-row data corresponding to station signals A, B, . . . , H for each day of the month.

The parsed data file format is illustrated in the lower right portion of Fig. 8.3-3. Each of these files contains both phase and SNR data for all frequencies for each day of a given month at a given monitor site. The corresponding filenames, e.g., REUNI1191, for this data format contain all the necessary information so that no file extension is needed. The data in each file is again arranged in 24 columns and 28 to 31 groups of rows corresponding to day of the month. Within each group of rows, the data is formatted as three subgroups (corresponding to frequency) which is further divided into eight two-row

units. Each two-row unit corresponds to a station signal with the first row containing the phase data and the second row containing the SNR quality number.

The files described above constitute the basic structure for storage of monitor data. Although subsequent processing stages may be considered as data analysis/applications, two procedures, implemented by programs ODAEDIT and SNRAVG, are routinely and systematically applied to the data. The inputs and outputs for these two programs are illustrated in Fig. 8.3-4. Note that not all of the program output options are routinely selected.

ODAEDIT processes the separate phase/frequency files according to an input file of selection options. These options include the desired phase-difference pairs (sometimes called "LOPs") at a given monitor site. The phase-difference values are obtained by differencing the appropriate raw signal station phase data which is referenced to the internal (or external, if present) receiver clock. The monitor site name and month/year is input to the routine via the list of input filenames.

The XEVENT files shown in Fig. 8.3-4 supply information on anomalous event occurrence so that measurements made concurrent with these events may be appropriately flagged. The event-concurrent measurements are flagged — not deleted — so that subsequent analyses may choose to delete or accept these measurements, based on an assumed level of user knowledge regarding event occurrence. The particular events for which the XEVENT files provide information are Sudden Ionospheric Disturbances (SIDs), Polar Cap Disturbances (PCDs), transmitting station outages, and monitor outages. Signal data recorded concurrently with these events are flagged as shown in Table 8.3-1. Other flags are

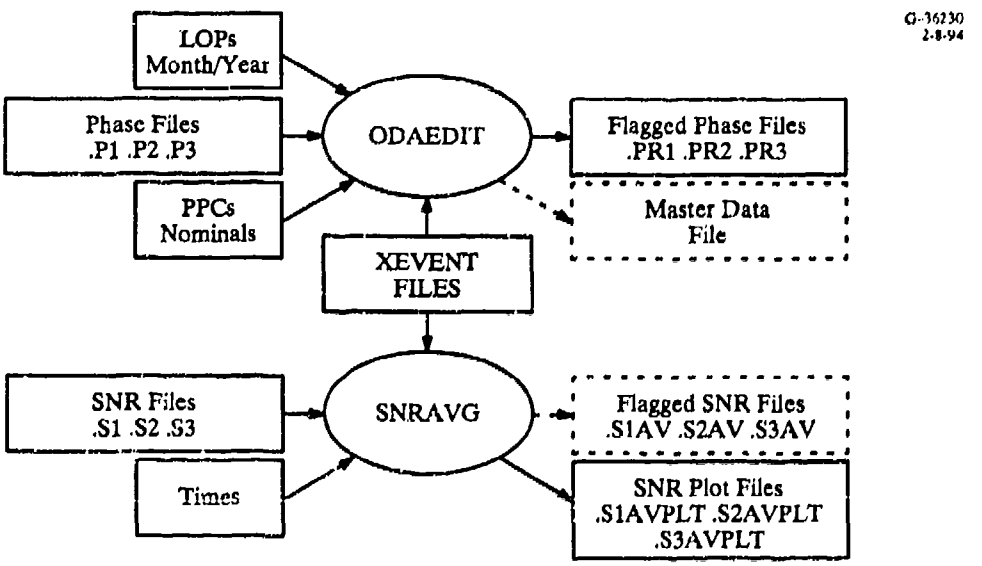

Figure 8.3-4 Routine and Special-Purpose Data Processing/Storage

assigned as a result of ODAEDIT processing. When evaluating the statistics of the daily measurements taken at a given hour (for a given monitor site/LOP/frequency/month/year), two types of outliers are identified. The Q-flag is assigned to a measurement if either of the following conditions hold:

- The measured value is more than two standard deviations from the mean of all previously unflagged measurements at the given hour
- The measured value is more than eight centicycles from the mean of all previously unflagged measurements at the given hour.

Table 8.3-1 Daily Measurement Flags

FLAG	DESCRIPTION
S	Measurement concurrent with an SID event
P	Measurement concurrent with a PCD event
D	One of the two stations making up the LOP pair was off-air at the time of the measurement
M	The monitor was not operational at the time of the measurement
Q	Outlier (more than two standard deviations or eight centicycles from the mean unflagged value at the given hour)
L	Data from a set of unlagged daily measurements which are too variable (standard deviation > 15 cec)
I	Insufficient data (fewer than 7 unlagged daily measurements for the month at a given hour)

If an outlier flag is assigned in the processing, the statistics are re-computed until either no outliers are assigned or if fewer than 7 unflagged daily measurements remain (for the given hour). When the re-computation cycle is completed, an L-flag is assigned to all remaining measurements if the standard deviation of the remaining unflagged daily measurements is 15 centicycles or greater. If, after the above flagging procedures are applied, fewer than 7 unflagged daily measurements remain for the given hour, the I-flag is attached to all remaining measurements for that hour.

The ODAEDIT output which is routinely produced consists of data files containing both observed and predicted information for a given site/LOP/month/year/frequency. In each file, the data is again formatted as 24 columns, corresponding to UT hours 00-23. The information given in each row includes, for each UT hour,

- The number of unflagged daily measurements
- The mean LOP value, averaged over the unflagged daily measurements
- The predicted LOP values, computed for Days 7 and 22 of the month and averaged.

The filenames for the output data files consist of a five-character monitor site name, two-digit month, two-digit year, and the two stations making up the LOP. The file extension contains the characters "PR" followed by the digits 1, 2, or 3, indicating 10.2, 11⅓ or 13.6 kHz, respectively. When files with common site/LOP/month/year are combined for all three frequencies, the resulting information is used to generate plots and special tables.

Like ODAEDIT, SNRAVG processes the separate SNR/frequency files according to an input file of selection options. These options include the station signals for which SNR is desired (usually excluding the calibrate channel) at a given monitor site. No SNR differencing option is available for this process. The monitor site name and month/year is input to the routine via the list of input filenames.

Two types of files are output by SNRAVG. The first type, which is written only for special-purpose applications, has a monthly block format (24 columns with the rows corresponding to days of the month), consisting of observed SNR quality numbers for a given station at a site/month/year/frequency. Following each block, two rows of data are provided which contain, for each UT hour,

- The number of unflagged daily measurements
- The mean SNR quality number for the given station, averaged over the unflagged daily measurements.

Each file contains eight such blocks (with the two summary rows appended to each block) corresponding to the eight station signals (including any station which happens to serve as a calibrate channel). This type of file is used for data analysis and is given a filename which consists of a five-character monitor site name, two-digit month, and two-digit year. The file extension contains the characters "SXAV," where "X" is 1, 2, or 3, corresponding to frequencies 10.2, 11⅓, or 13.6 kHz, respectively.

The second type of file, which is routinely written by SNRAVG, contains only the information listed in the two rows appended to each station signal block in the SXAV-type file (see the two bullets above). The file thus consists of eight pairs of rows, each pair corresponding to a station signal. This second type of file is used for ODA plotting and is given the extension "SXAVPLT," where, again, "X" is 1, 2, or 3, corresponding to frequencies 10.2, 11⅓, or 13.6 kHz, respectively. Because the SNR quality number has a nonlinear relationship to the SNR expressed in dB, the averaged quality number, converted to dB, is not the same as that obtained by first converting each SNR quality number to dB and then averaging.

Aggregation of all .PRX and .SXAVPLT files for a given site produces a series of plots and special tables which collectively serves as a hard-copy "dossier" of information for a given monitor site. This is described further in Section 8.3.5.

The predicted LOP values at a monitor site are simply the difference between the nominal LOP value (which depends on frequency) and the PPC (which depends additionally on time). The PPCs currently used (1993) are based on the 1980 PPC Model (see Chapter 9). Since the nominal LOP value contains the full cumulative phase difference information (in units of nominal wavelengths), the predicted LOP value has an integer part (number of nominal wavelengths) and a fractional part. The observation, however, provides valid information only on the fractional part. Thus, the observational data is "laned" by assuming that the full predicted value is within 0.5 cycle of the observed value at each hour. This assumption allows an unambiguous assignment of a full lane number (integer part of the phase value in cycles) to the observation for each hour. To reduce data storage, the minimum lane number over the 24-hour monthly average is subtracted from each laned observation average. This also ensures that all observed LOP averages are positive.

The principal reason for applying the procedure described above is *not* to establish correct lane, but to correctly juxtapose the hourly observed LOP values so that the shape of the diurnal is physically reasonable. For example, if the fractional part of the monthly average observed LOP value at hour h is 0.47 (cycle) and the value at hour h+1 is 0.98, then, without *a priori* guidance, one wouldn't know whether the phase increased by 0.51 cycle during the hour or decreased by 0.49 cycle (to –0.02 cycle which is equivalent to 0.98 cycle) over the same period. In this case the predictions (using the PPCs) supply the overall guidance, with the basic assumption that the predictions are within 0.5 cycle of the observed phase or phase-difference value. When this assumption is invalid (as occasionally happens on transition paths longer than 10 Mm), the LOP diurnal behavior is not correct. An alternative is to use the third least significant digit in the raw data. As noted in Section 8.3.1, when the phase values in a data block are differenced (to construct an LOP value), this third digit retains its validity as a lane reference from hour-to-hour or day-to-day. In unusual circumstances, where the propagation conditions change faster than the receiver time constant, the receiver may "slip" a lane and thereby yield the wrong third digit value. Another possibility is that the receiver may be shut down (power off) and restarted between hourly measurements, thus resetting the lane number difference relationship.

An optional output of the ODAEDIT program is a series of specially formatted monthly blocks of data making up the "Master Data File." This output format is used primarily for PPC model calibration and in response to special requests. The blocks contain the daily measured phase (two digits) at each UT hour for a given site/LOP/frequency/month/year. Each block corresponds to a unique file having a filename consisting of the five-character monitor site name, followed by the month (two digits), the last two digits of the year, and the two letters of the station pair (LOP). The file extension consists of "MF," followed by a single digit: 1 — 10.2 kHz, 2 — 11⅓ kHz, and 3 — 13.6 kHz. A sample file block is shown in Fig. 8.3-5.

```
8307136  JAPAN  CHH0B    323.082    815  34.32471  129.20641 DDDD        NN        DDD    813.040     .891
 -84   -83   -84   -85   -87   -90  -101  -114  -127  -140  -154  -164  -168  -170  -171  -171  -156  -127  -111   -98   -85   -87   -88   -85
 -84   -83   -84   -85   -88   -91  -102  -115  -128  -141  -155  -165  -168  -170  -171  -171  -160  -130  -114  -100   -86   -87   -88   -86
  0M    0M    0M    0M  803    0M    0M    0M    0M    0M    0M    0M  898  898  896    0M    0M    0M    0M    0M  807    0M    0M  798
 795  764S  790S  796S  800   806   816   832   856   880   886   890   898   901   898   900    0M    0M    0M    0M    0M  804   799   795
 794  791Q   794   797   801   806   817   838   864   879   891   895   891   886   882   887  878S   865   842   821   808   804  794S   797
 796   795   796   798   802   808   818   835   861   876   888   894   897   895   895   896   884   877   841   823   806   805   801   798
 796   795   796   798   802   807   819   834   851   867   876   883   887   895   900   902   893   870   847   822   808   807  797S   798
 795   794   795   797   802   804   816   834   856   880   889   896   899   898   898   905   890   872   837   819   806   805   802   797
 795   795   796   798   802   806  808S  827S  847S   873   890   903   906   911   910   907   891   869  831Q   818   807   805   801   798
 794   793   795   798  794S   804   812  824Q  859S   871   880   890   894   893   893   890   879   866   838   820   805   804   801   797
 795   795   795   798   802   807   816   836   869   890   898   909  911Q   911   913   913   902  883Q   841   819   806   805   801   799
 775S  794   796   799   802   805   815   826   850   865   873   880  882Q   883  879Q   883   876   857   839   819   805   803   798  782Q
 772Q  776S  789Q   795   801   805   812   829   870   880   891   898   898   897   901   903   893   875   847   820   807   806   801   797
 795   794   795   797   802   806   813   837   863   879   884   888   893   894   887   889   881   871   844   824   808   806   800   795
 791Q    0D    0D   796   801   802  809Q   826   953  996Q     5     7     6     5     0   992   981   957   943   921   905   905   902   898
 896   895   896   898   902   906   913   938   958   981   988   990   992   996   993   991   985   964   941   921   908   906   901   897
 893   893   895   898   902   906   911   932   968   978   984   988   986   986   987   986   981   965   945   919   906   904   900   896
 894   893   894   898   901   905   915   937   968   977   989     0     3     8    10    10     3   981   943   922   906   906   901   898
 896   894   894   896   900   906   912   940   952   967   979   988   992   995   997   997   990   961  934Q   922   907   906   901   896
 893   893   895   896   901   906   914   940   971   985   995     3     2     3     2     5   999   979   942   921   906   905   901   897
 895  887S  892Q   897   901   905   912   929   960   972   982   991   997     4     8    11     1   972   941   923   904   904   898   897
 894   894   894   897   900   906   916  926Q   961   979   989   996   996   993   992   989   980   963   940   917   904   903   900   897
 893   893  891S   896   900   904   916   937   966   985   998    10   14Q   15Q    12    10     5   977   941  913Q   905   904   900   897
 894   892   893   896   900   904   917   934   957   972   980   988   994   993   991   991   983   969  953Q  919S   906   904   900   896
 893   892   894   896   899   906   914   938   963   981   991   997   999     5     9    14     6   983  968Q    22     7     5     0   997
 995   994   994   997     0     7    18   27S   52S    66    81    86    85    82    82    88    82    62    46    21     8     5     0   995
 991Q  993   994   996     0     6    18    29   91Q  102Q   105   108   101   100   102    99    92    69   58Q    25    1S     2     1   998
 994   992  991Q  993Q   999     5    15    34   84Q   97Q   104   103   105   100    92    90    85    64    40    22     8     6     0   996
 992Q  993   994   998   997     5    16   47Q    73    88    99   101    97   100    95    91    84    59    44    20     4     4     1   996
 994   993   994  979S   998     1    14    34    69    82    97   102    97    94    88    83    81    63    40    17     4     5     0  989S
 988S  991Q  993   996     1     6    16    38   83Q    90    99   110   109   109   109   108   100    63    46    18     6   997  986S  989Q
 993   985S  993  993Q     0     6    11   52Q    68   82S    98   100    92    85   79Q    0D    0D    70    38    0D    0D     4   997   997
 992Q  993   995   996     0     6    16    40   56S    79    95   107   106   103    99    99    94    77    50    21     7     5     0    0M
   11    10    11    13    14    14    12    12    12    13    14    14    13    15    14    14    12    12    12    13    14    14    12    14
   12    13    13    13    16    16    16    12    11    13    16    16    15    15    15    15    15    16    12    13    14    16    15    13
 97.3  96.9  96.8  95.7  93.5  92.6  94.4  89.1  75.3  71.4  74.8  78.6  80.4  81.6  82.6  83.2  77.9  67.9  77.1  85.7  86.6  90.3  95.6  96.1
 98.2  98.2  98.3  96.7  96.4  94.0  95.2  87.4  71.8  70.5  70.6  73.8  77.9  79.9  80.0  80.2  75.9  68.7  79.6  87.4  88.3  91.1  96.2  97.5
   .9    .8    .6   1.0    .7   1.5   2.5   4.1   6.7   6.3   7.9   8.2   5.9   7.9   8.1   8.7   7.2   6.0   3.1   1.7   1.1   1.0   1.1   1.1
   .9    .7    .6    .8   1.1   1.3   2.0   3.7   6.1   7.3   8.2   7.6   6.0   7.6   8.9   9.7   9.1   7.6   3.3   2.2   1.4   2.1   1.1    .8
```

Figure 8.3-5 Sample Master Data File Block

The header line of the file block (see the sample block in Fig. 8.3-5) contain the year, month, frequency, and monitor site name. The two characters corresponding to the station signa: ıake up the phase difference measurement are followed by a third character indicating the station "local" to the monitor. A zero in the following field indicates the measurement was made "on" the UT hour. The character in the following field is a block flag indicating the quality of the data block as a whole. This flag is no longer used by ONSCEN in assessing data quality. The following real number is the nominal value of the LOP in cycles at the appropriate frequency. The nominal value is followed by the normal illumination depression (NID) in units of centicycles. The use of the NID in the 1980 calibration is discussed in Chapter 9. The NID is followed by the monitor site's latitude (positive is North) and longitude (positive is East) in degrees. The next 23 columns give the day/night flags for UT hours 00–23. "D" means both of the paths making up the LOP are fully illuminated (in day); "N" means both paths are in night. The last two figures in the header line are the day phase "error" (cecs) and night phase "error" (cycles), respectively, where "error" refers to the difference between the averaged observed value (separately for each "D" or "N" day/hour measurement) and the nominal value. These two values are no longer used by ONSCEN.

The next two rows in the Master Data File block list the PPCs (1980 PPC Model) for each UT hour for the first and second half-month (the 7th and 22nd of the month). The following rows list the raw phase-difference data (in cecs) for each UT hour and each day of the month. The next two rows provide the number of unflagged measurements for each half-month at each UT hour. The phase errors (observed – predicted; in cecs) for each hourly set of unflagged measurements for each half-month are given in the next two rows. The final two rows yield the standard deviations (in cecs) for each hourly set of unflagged measurements for each half-month.

ODAEDIT also provides as a "printer" output the information in a given Master Data File Block with additional statistics and data summaries, as shown in Fig. 8.3-6. Much of this information is specially prepared for use with the 1980 and earlier PPC model calibrations but is no longer used by ONSCEN.

8.3.3 Quarterly Monitor Report

To assist in managing the Long-term Omega Monitoring Program and coordinating the activities of the monitor installation teams, the data processing staff, and the data analysts, a report is prepared each quarter, providing the most recent information on the monitor program. This report, which is published by the Analysis and IRM Branch of the Signal Analysis and Control Division at ONSCEN, was formerly published monthly, but as monitoring activities have become more controlled, less frequent reports are needed. The distribution of the report coincides with a meeting of all Signal Analysis and Control and Engineering Division personnel with monitor-related duties.

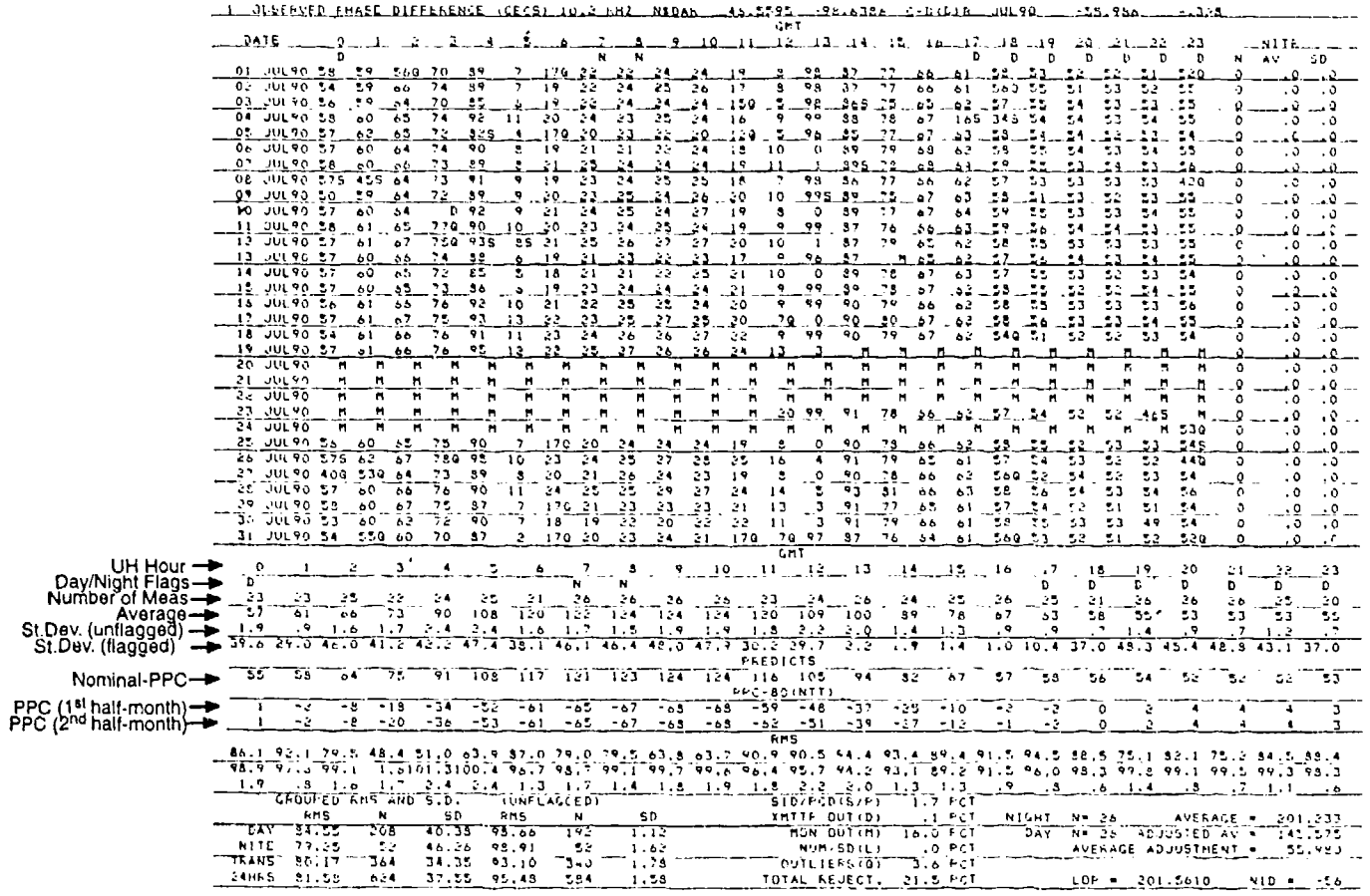

Figure 8.3-6 Sample "Printer" Output of Master Data File Block

The report commences with a map showing the locations of all active monitor sites. This is followed by a summary report of monitor site activities for the last 12 months (see the sample summary in Fig. 8.3-7). The activities are indicated by a table of monitor sites (rows) and the immediately previous 12 months (columns). Abnormal activities are listed as codes in three separate categories:

- General — monitor site established/disestablished; equipment status, etc.
- Data Disk Received — data not recorded on-hour, receiver mis-synchronized, less than 7 days of good data, etc.
- Data Disk not Received — late delivery expected, equipment problems suspected, etc.

The summary report is followed by a site-by-site list of communications with each monitor during the quarter. The communications items concern mostly reports on equipment health status, replacement components shipment status, requests to insert appropriate calibration channel, ID codes, etc. The communications report is followed by a status report on monitor site installations and/or removals. The monitor report usually concludes with a list of spare MX 1104 monitors and their operational status. During the final

					1991							1992			
SITES-	ID	CAL	CLK	CODE	JUN	JUL	AUG	SEP	OCT	NOV	DEC	JAN	FEB	MAR	APR	MAY	JUN
ALEXD-	90	(H)	ABS		*	E6	*	*	*	*	*	*	*	*	*	*	*
AREQU-	02	(A)	Cs5		*	*	*	E6	*	*	*	*	*	*	*	*	*
ARGE2+	65	(A)	Int		*	*	*	*	*	*	*	*	*	*	*	*	*
AUST$+	22	(A)	Int		*	*	*	*	*	*	*	*	*	*	*	*	*
BUEN2-	10	(A)	Cs5		*	*	*	E6	E4	E4	E3	E3	E8	E0	*	*	E6
COCOS-	15	(D)	Cs5	NO	*	*	*	*	*	*	*	*	*	*	*	*	*
HAWAI+	29	(F)	Int		*	*	*	*	*	*	*	*	E0	*	*	*	*
HOKKA-	31	(F)	Int		E6	*	*	*	*	*	*	E6	*	*	*	*	*
INUV2-	32	(F)	Int		*	*	E6	E4	E4	E4	E3	E3	E0	E0	*	*	*
JAPAN+	33	(B)	Int		*	*	*	*	*	*	*	*	*	*	*	*	*
LEWIS-	24	(C)	Int	NO	E4	E4	E4	*	*	*	*	*	E7	E0	*	*	*
LIBER+	45	(C)	Int		*	*	*	*	*	*	*	*	MV				
LIBE2+	43	(H)	Int										NP	E0	*	*	*
MCMD$-	44	(B)	Int		*	E7	E7	E7	E7	E7	E7	E7	E7	E7	E7	E7	E7
N$DAK+	51	(E)	Int		*	*	*	*	*	*	*	*	*	*	*	*	*
NEWZ$-	50	(B)	ABS		E4	E4	E4	*	*	*	*	*	*	*	*	*	E6
NORW2+	54	(G)	Int		NP	*	*	*	*	*	*	*	*	*	*	*	*
NOSC4-	52	(B)	Int		E4	E4	E4	*	*	*	*	*	*	*	*	*	*
PRETO-	68	(H)	ABS		*	*	*	*	*	*	*	*	*	*	*	*	E6
REUNI+	38	(D)	Int		*	*	*	*	*	*	*	E6	*	*	*	E6	E8
TAHIT-	66	(B)	Cs5	NO	E4	*	*	E4	*	*	E6	*	E6	E6	*	*	*
TOUL$-	85	(C)	Int	NO	*	*	*	*	E6	*	*	*	*	*	*	*	*
USNO$-	99	(H)	ABS		*	*	*	*	E0	*	*	*	*	*	*	*	*
DATA DISK RECEIVED--------					19	18	19	19	18	19	21	21	18	17	21	21	21
DATA DISK NOT RECEIVED----					3	4	3	3	4	3	1	1	4	5	1	1	1
TOTAL OPERATIONAL SITES--					22	22	22	22	22	22	22	22	22	22	22	22	22

LEGEND

GENERAL
MV= Monitor site was moved
NP= New Monitor site position.
NO= Site equipment not owned by ONSCEN
WD= Site withdrawn - Equipment returned to ONSCEN
E5= Awaiting return of equipment - NOT counted as operational site

DATA DISK RECEIVED
E1= Data no good, out of sync
E2= Data not recorded on the hour or within (+/- 6 min.)
E3= Data no good, possible equipment problems
E6= Less than one week of usable data received for the month
E8= Data no good, incorrect format or no data on tape

DATA DISK NOT RECEIVED
E0= Data disk not received, reason unknown
E4= Data disk not received, known equipment problems
E7= Data disk not received, expected later

Figure 8.3-7 Sample Monitor Data Summary Report

quarter of the year, a special table at the end of the report summarizes the data processing over the calendar year, including the fraction of "good" data received and processed.

8.3.4 Diagnostic Analysis

Although many of the malfunctions of the Omega monitoring equipment or operator errors can be detected by observing the receiver operation or scanning the error codes in the raw data header block, a sizable fraction of such errors remain undetected. To identify these problems and ensure phase data integrity, predicted and observed phase/phase-difference data are sampled and plotted. Specifically, the phase/phase-difference data provided in the .PRX files (see Section 8.3.2) are plotted as a function of UT hour.

A sample phase plot for the "G-D" LOP at the North Dakota station monitor is presented in Fig. 8.3-8. To within a constant phase bias, this plot shows the phase profile on the single path from the Australia transmitting station to the North Dakota station monitor. The "O" values in the figure plot correspond to the observed phase data with lane numbers obtained from the corresponding predicted values. The "P" values in the figure are predicted phase values obtained by subtracting the appropriate PPC (from the .PRX file) from the nominal value. This procedure automatically yields a full lane count for the predicted value and the lane number for the observed value is chosen so that it is within 0.5 cycle

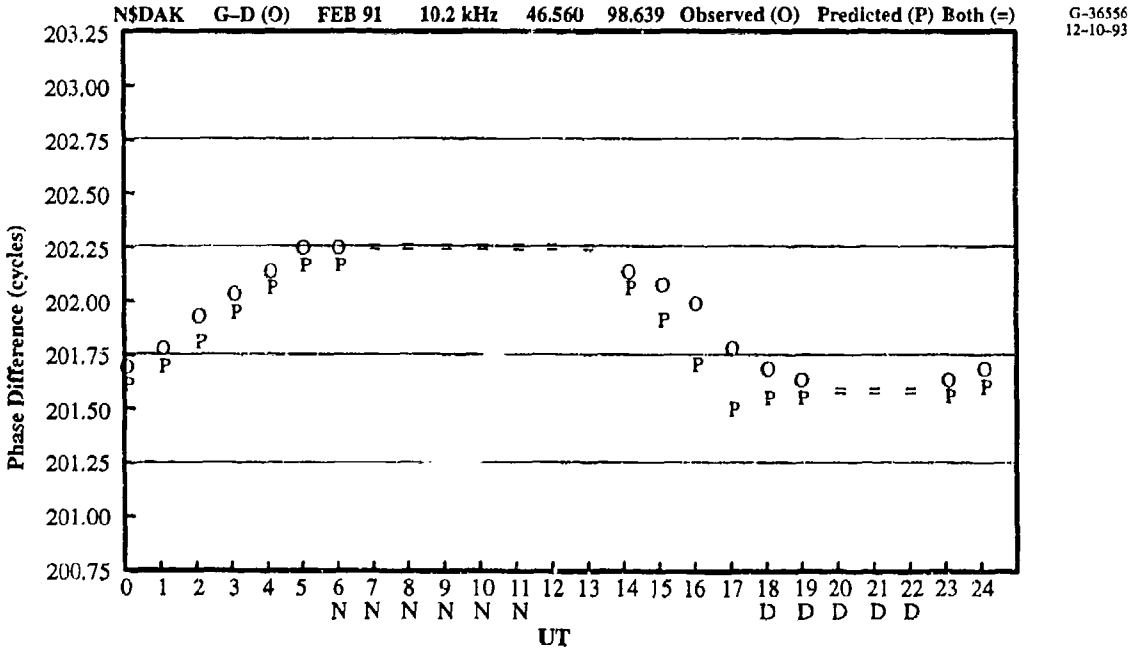

Figure 8.3-8 Sample Phase Plot for Data Diagnosis: Observed and Predicted 10.2 kHz Australia Station Signals as Received at the North Dakota Station Monitor – February 1991

of the predicted value. Where the "O" and "P" values overlap (are nearly equal), a "=" appears in the figure plot. Monitor name, LOP, time (year, month), frequency, and monitor location (latitude, longitude) are displayed at the top of the plot. The plot abscissa (labeled "GMT") also indicates the "LOP illumination" in which both paths of the LOP are in day ("D") or both are in night ("N").

A data plot such as this is useful for rapidly diagnosing certain types of monitor problems. For example, the observed values could lie along a straight line, parallel to the abscissa, thus not following the diurnal variation indicated by the predictions. This condition might indicate, for example, a severed antenna connection. Another possibility is that the "O" values could trace out a "sawtooth" shape, having an envelope which tends to follow the predictions. This result might suggest a malfunctioning oscillator with a "drift" rate greater than 1 cec/10-second Omega pulse. In other cases, a normal diurnal profile may be obtained, but not at all like the predicted diurnal variation. In these cases, the receiver has become mis-synchronized so that, for example, A → D, B → E, etc. This possibility is easily verified by consulting plots of other LOPs at the same site/month/year/frequency.

8.3.5 Operational Data Analysis

Operational data analysis (ODA) refers to a rather general set of activities, procedures, documentation, and databases that are used to provide information mostly on observed Omega signal behavior at the long-term Omega monitor sites. Specifically, ODA information is used to support:

- Omega system performance evaluation
- Reference/archive functions
- Signal usability classification
- Monitor fault analysis.

ODA supports Omega system performance evaluation by providing data that can be used to determine: (1) the utility of the "signal in space" from each transmitting station at the monitor sites, and (2) the reliability of signal transmission, in terms of off-air fraction (as measured, not as reported), and consistency/continuity of signal level and phase stability. Although the monitor sites represent a small spatial sample compared to the actual global usage, the data from these sites provides a useful check on the signal coverage predictions (see Chapter 10). Evaluating station reliability based on the monitored signal depends on the first item of performance evaluation listed above, i.e., the utility of the propagated signal. Station performance is best evaluated by combining the ODA information with direct information, such as antenna current levels, obtained through a remote data access (RDA) link to each station.

As a reference/archive source, ODA information can be used to identify anomalous signal propagation paths at a monitor site. Two commonly employed techniques are frequency tracking and reciprocal path analysis.

Frequency tracking refers to comparison of measured or predicted phase/phase-differences values at several frequencies. Frequency tracking is built on the assumption that, when Omega signal propagation to a monitor is not subject to self-interference, the measured diurnal signal phase for a given station will only differ from frequency to frequency by a bias, i.e., by a frequency-dependent shift.

Reciprocal path analysis is based on the assumption that the observed phase at either end of a "reciprocal path" should be nearly identical except for anisotropic (direction-dependent) propagation effects. Examples of reciprocal path measurements are phase measurements of Hawaii at the North Dakota station monitor and measurement of North Dakota at the Hawaii station monitor. The anisotropic propagation effects are generally small and are (approximately) incorporated into the PPC Model. Thus, reciprocal path difference measurements and predictions at the same frequency should track closely. If they do not, an anomalous path condition such as modal interference or long-path propagation is indicated.

8.4 OMEGA REGIONAL VALIDATION

By the late 1970s, the Omega Navigation System transmitting station network, with seven of the eight stations operational, was nearing completion. At this time, the U.S. Coast Guard and U.S. Navy initiated a wide-ranging program to validate the predicted coverage, accuracy, and availability of the Omega system. The overall validation effort, termed the Omega Regional Validation Program, was designed to determine worldwide system effectiveness through investigations of Omega performance in the seven regions portrayed in Fig. 8.4-1: the Western Pacific, North Atlantic, North Pacific, South Atlantic, Indian Ocean, South Pacific, and Mediterranean.

During its life, validation program objectives evolved as insight into Omega signal propagation increased. For example, the initial validation project in the Western Pacific sought to determine whether sufficient signal was available to declare the system operational there, and whether Omega could replace the LORAN-A system in the region. Also the initial validation projects (see Table 8.1-1) placed emphasis on SNR and GDOP as measures of system availability and effectiveness and on the collection of local phase data for PPC model refinement. However, by the mid-1980s the significant contribution of modal interference and long-path signal dominances phase interference on Omega signal usability had become apparent and use of the Omega Navigation System had shown that, at least for receiving systems using

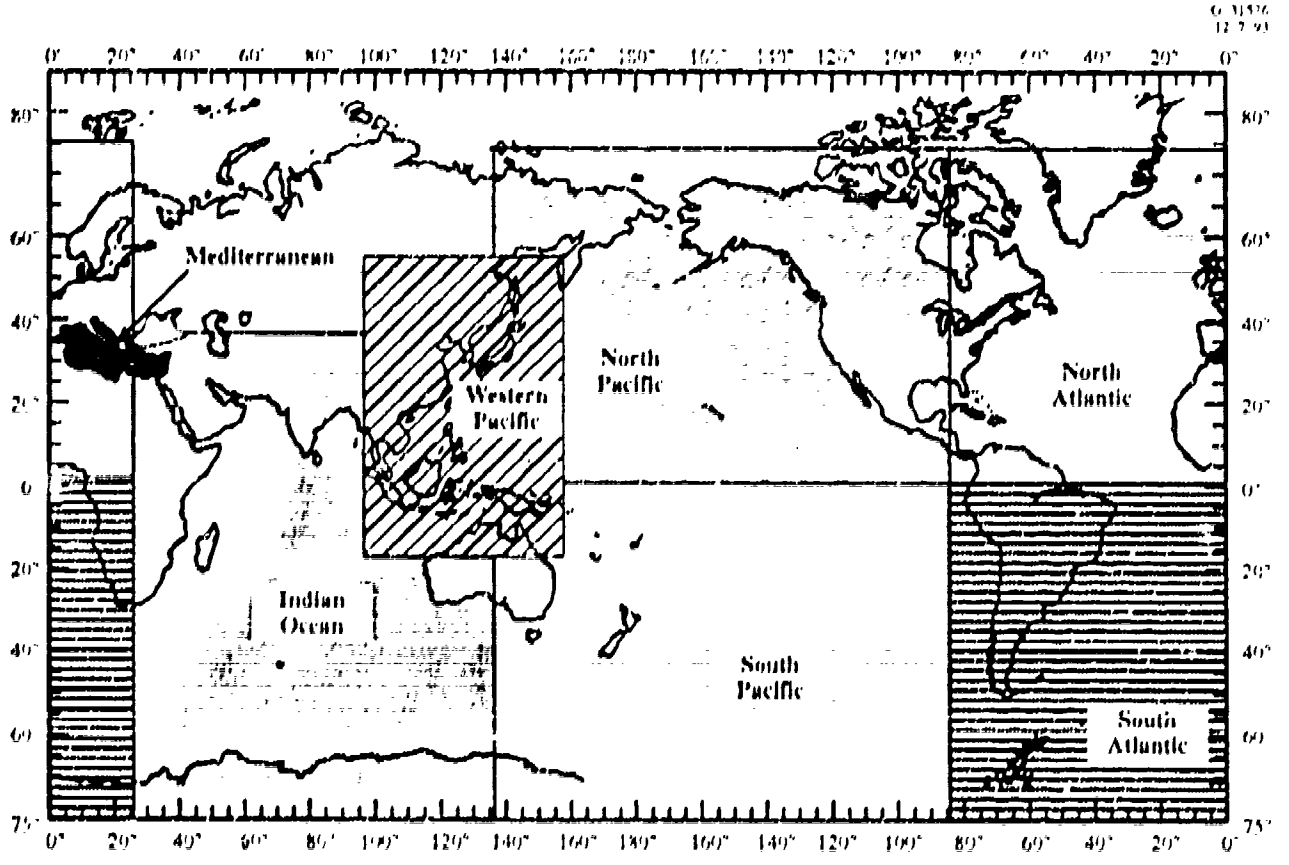

Figure 8.4-1 Omega Validation Regions

advanced signal processing techniques, SNR was sufficient to allow worldwide Omega operation. These developments resulted in a shift from the previous validation emphases of operational declarations and PPC refinement to an emphasis on validating the theoretical predictions of anomalous phase behavior. In other words, "validation" became a means of gathering information and conveying to the user the appropriate way to use Omega (e.g., which signals to deselect) as a function of time in the region of interest.

8.4.1 Methodology

System validation is, in general, a process of confirming or modifying, if necessary, established coverage, accuracy, and availability predictions for a given region of the globe. To verify and/or test these predictions, various types of data are required, including signal field strength, signal-to-noise ratio, single station phase vs. distance data, diurnal phase data, phase difference data, and the resulting fix

information. These data must necessarily be collected in a somewhat controlled environment, i.e., under carefully planned test conditions.

Figure 8.4-2 provides an overview of the methodology employed in the seven regional validation projects. First, theoretical models are employed to predict signal levels, SNRs, and phase behavior within a region. Next, spatial boundaries outlining area of significant signal behavior are determined. Such areas include regions of marginal signal coverage or high prediction uncertainty, e.g., modal signal region. Based on this theoretical guidance, test plans are generated for data collection using short-term land, ship, and airborne monitor platforms. These data as well as data from long-term Omega monitor sites are then analyzed and used to confirm/modify existing signal coverage predictions. Finally, a report is produced which documents the project including the test plan, data sources, analyses, and results.

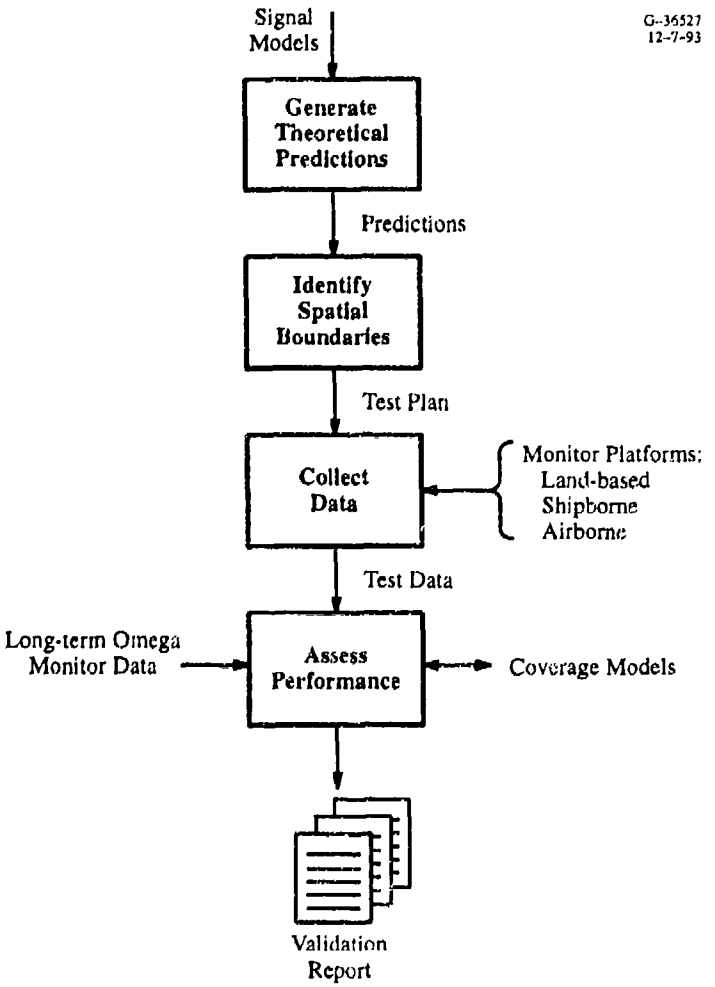

Figure 8.4-2 Overview of Validation Project Methodology

Four types of monitor platforms were used to provide validation project data:

- Airborne
- Shipborne
- Short-term land-based
- Long-term Omega monitor sites.

The first three types of platforms were used to collect data over the comparatively short duration (few weeks/months) of an individual validation project targeted for a specific region. The last platform type refers to sites of the Long-term Omega Monitor Network used to supplement the data collected from the short-term platforms.

Table 8.4-1 summarizes the types of data collected for the validation projects and indicates typical platform instrumentation. Data collected by airborne platforms include signal amplitude and noise measurements from calibrated receivers (see e.g., Ref. 7) as well as position-fix accuracy (see e.g., Ref. 4) from comparison of Omega and INS-derived position. In some cases Cesium reference clocks were used in combination with the Omega receiving system to measure single-path signal phase behavior. Signal amplitude and background noise data were also obtained from short-term land-based sites using calibrated receivers while Long-term Omega monitor sites provided SNR and phase/phase-difference data. Finally, shipborne receivers supplied SNR and position-fix data (through comparisons of Omega and TRANSIT-derived position — Ref. 5). Ship and airborne transits through a validation region also served to sample the spatial coverage of individual Omega station signals accessible to the region.

Figure 8.4-3 shows the flight paths used by the test aircraft for the Western Pacific (Phase II) Omega Validation Project. The configuration of these flight paths was strongly dictated by the predicted spatial modal interference patterns for the Japan and Australia transmitting stations.

Table 8.4-1 Validation Test Data Summary

PLATFORM	TYPICAL INSTRUMENTATION	DATA
Short-term land-based site	"Calibrated" MX 1104 receiver	Signal amplitude/phase VLF atmospheric noise
Shipborne	MX 1105 receiver	SNR Position-fix accuracy
Airborne	Calibrated receivers wave analyzers, high-precision frequency standards, and operational navigation receivers	Signal amplitude/phase SNR VLF atmospheric noise Position-fix accuracy
Long-term Omega monitor site	MX 1104 receiver	Phase/phase-difference SNR

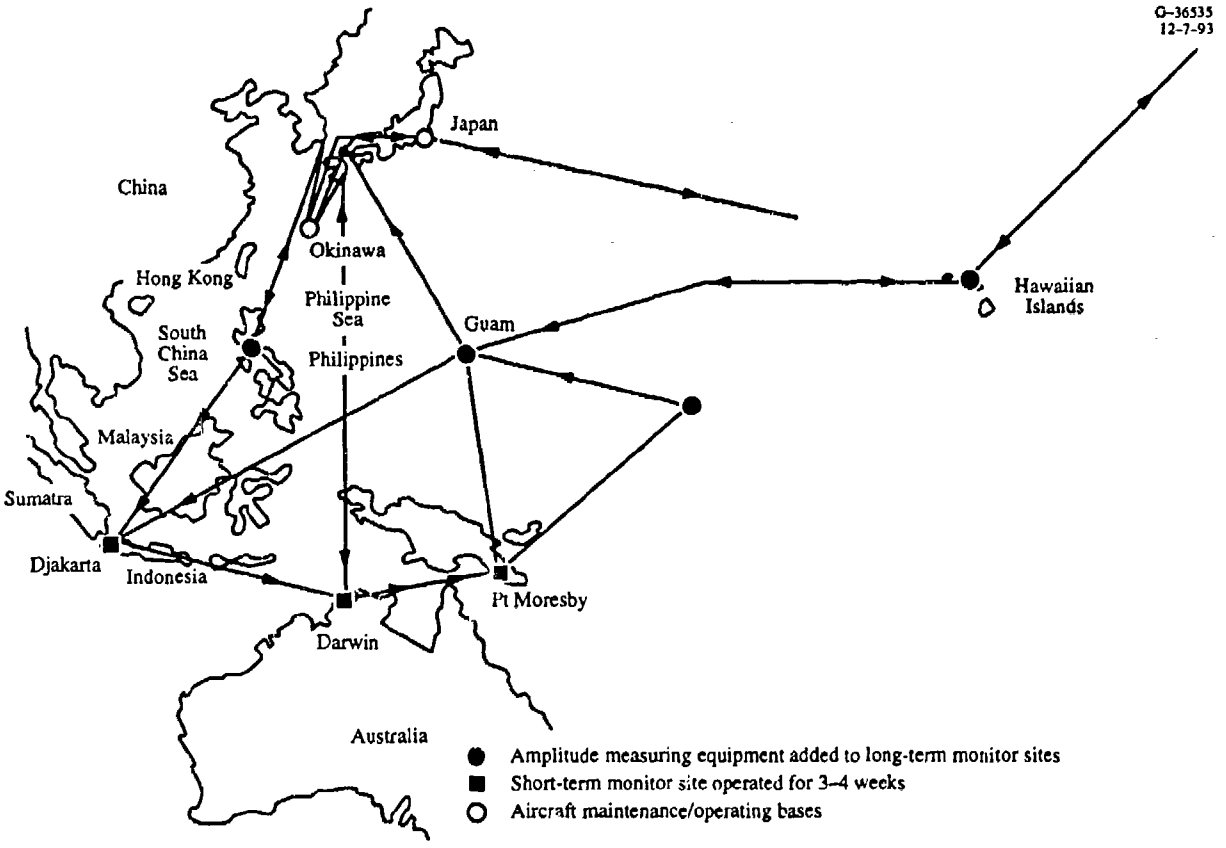

Figure 8.4-3 Western Pacific Omega Validation Test Program Aircraft Flight Paths and Fixed Monitor Sites

8.4.2 Documentation

As a part of each Regional Validation Project, a report was issued documenting test procedures, data, models and analyses, and results (Refs. 2 through 9). The content and scope of these reports changed over the period of the Validation Program in consonance with the changes in the goals/emphases of the validation effort. In the remainder of this section, summaries are given for each of the seven Validation Projects.

Western Pacific — This project was conducted in two phases as indicated in Table 8.1-1. The main goal of the first effort (Ref. 2) was to determine if Omega coverage and accuracy was adequate to replace LORAN-A in the region. This question was answered in the affirmative. Evaluations were made of phase and position-fix accuracy for the region and a map was developed showing LOP coverage at 10.2 kHz. The second phase of this effort (Ref. 9) was undertaken after the Australia transmitting

station became operational. Data collection and analyses focused on validating theoretical predictions of the extent and location of self-interference areas within the validation region. In the main, the theoretical self-interference predictions were found to be correct. Recommendations were made for changes to the boundaries of several modal areas based on the data analysis.

North Atlantic — This effort (Ref. 3), like the Western Pacific Validation Project, was initially planned to evaluate Omega as a replacement for LORAN-A in the region. With completion of the LORAN-A phase-out, the effort was redirected to focus on determining Omega performance in the region. It was found that Omega signals did meet marine/aviation navigation requirements by using a combination of 10.2 and 13.6 kHz signals to provide adequate coverage for this area. Data collection resources were concentrated on times (hour/month) consistent with available theoretical coverage predictions, i.e., local summer noon and local winter midnight. Sufficient data were obtained to locate the predicted eastern boundary (through the eastern U.S.) of the modal interference area associated with the Argentina station. Modal and long-path boundaries (through the North Atlantic airlanes) were also located for the Liberia and La Reunion station signals, respectively.

North Pacific — This validation effort (Ref. 4) showed that Omega provides excellent navigation fix accuracy and coverage in the region particularly north of Hawaii. This is achieved through a combination of good GDOP and exceptional signal coverage both spatial and temporal. As part of the analysis for this effort, models were developed describing modern Omega receivers. These enabled the coverage results, validated in this region for local summer noon and winter midnight, to be extrapolated to all months and hours. The effort also confirmed the predictions of modal interference associated with the Hawaii station signals and the long-path behavior in this region of signals from the Argentina transmitting station.

South Atlantic — For this effort (Ref. 5) theoretical coverage predictions were available for an expanded set of hours/months — 0600 and 1800 UT and February, May, August, and November — at 10.2 kHz. Data collected for the validation indicated good Omega coverage and accuracy at both 10.2 and 13.6 kHz. Analysis of self-interference of signals from the Liberia station suggested corrections to the predicted modal signal boundary for these signals.

Indian Ocean — This effort (Ref. 6) was the first in which theoretical predictions of self-interference were available at both 10.2 and 13.6 kHz. Emphasis was placed on evaluation of total Omega system performance at all frequencies. Good Omega coverage and accuracy were found in most of the region. The data confirmed theoretical predictions of 13.6 kHz modal signals from the Liberia station and supported the need to generate a more densely sampled set of modal predictions for 10.2 kHz Japan signals.

South Pacific — For this effort (Ref 7.), greatest emphasis was placed on validation/correction of self-interference predictions — particularly interference associated with trans-equatorial and low-latitude signal paths. Analyses of the collected data indicated that Omega signal availability and accuracy were adequate for navigation purposes. Relative to self-interference, the data confirmed most predictions of modal signal behavior at 10.2 and 13.6 kHz and suggested small changes to the near-station modal boundaries associated with the Japan and Hawaii station signals. Adjustments were also suggested for the predicted boundaries for long-path propagation, but accurate placement of the boundaries could not be determined based on the available data.

Mediterranean — This final validation project provided ONSCEN with an a opportunity to utilize the Omega system availability methodology/model (see Chapter 11 and Appendix C). Frequency-tracking analyses for the data collected during this validation effort confirmed the self interference predictions for both 10.2 and 13.6 kHz signals, and the effect of the "Greenland shadow" on reception of the North Dakota station signal in the eastern Mediterranean. The data also confirmed that sufficient signal combinations were available in both the eastern and western Mediterranean for navigation purposes. From analyses of the GDOP and phase errors associated with these signal combinations during the times at which they are available, Omega was found to meet the system design goal (2 to 4 nm position accuracy) with a 95% availability in both the eastern and western Mediterranean.

8.5 PROBLEMS

8.5.1 Sample Problems

1. Briefly discuss the conditions under which a signal could exhibit self-interference. Why would differencing reciprocal path phase data serve to indicate self-interference?

Solution:

a. Modal interference and long-path-dominant signal propagation are the most common forms of self-interference. Both types of interference depend on the direction of propagation of the signal, i.e., if the effect occurs on a given transmitter-receiver path, it generally does not occur if the transmitter and receiver are reversed. If propagation is normal, the signal phase recorded on the two reciprocal paths appears very similar. Thus, the reciprocal path difference will result in small values. Because of the direction dependence, however, if one of the reciprocal paths exhibits self-interference, the other reciprocal path is not likely to, so that differencing will yield large values over the time period of interest, e.g., over a diurnal period.

2. Suppose you are a project leader in the Regional Validation Program and have arranged for equipment to measure Omega signal amplitude at several short-term land-based sites. You need to measure the noise in some bandwidth, but can only use an MX 1104 receiver, since the amplitude-measuring equipment cannot make the required measurement. With only simple, inexpensive attenuators (devices that reduce signal amplitude) at your disposal, how can you use the MX 1104 to measure noise in the signal bandwidth, at least for those cases in which the SNR is not too low?

Solution

a. If the variable signal attenuators are connected between the pre-amplifier and the receiver front-end, they primarily act to reduce the signal level since the noise in the signal bandwidth is assumed to be dominated by the signal. By adjusting the attenuators, the output SNR, as estimated from the output of the phase-locked loop, can be set to 0 dB (or some specified positive number). This means that the signal and noise levels are equal in a 100 Hz bandwidth and since the signal amplitude is independently measured, the noise level (100 Hz BW) is readily determined.

8.5.2 Problems to be Solved by Reader

1. Raw MX 1104 phase data from a monitor site shows a value of 649 at hour 01 and 497 at hour 02 on a single-path measurement *without* a stable clock reference. If no predictions are available, can you tell whether the phase increased or decreased during the hour? If predictions *were* available and showed a phase increase, how would you reconcile this with the observed data? Would such a discrepancy normally occur with *phase-difference* measurements? Why?

2. Most Omega receivers employ a PPC model for adjusting received signal phase. Describe why signals affected by self-interference cannot be corrected by this model. What can a user do about signals with self-interference?

8.6 ABBREVIATIONS/ACRONYMS

PPC	Propagation Correction
ONSCEN	Omega Navigation System Center
SNR	Signal-to-Noise Ratio
ODA	Operational Data Analysis
UT	Universal Time, i.e., Greenwich Mean Time
µsec	microsecond

PCD	Polar Cap Disturbance
dB	decibels
LOP	Line-of-Position
XEVENT	File containing time/duration of anomalous events during which all signal measurements are flagged
SID	Sudden Ionspheric Disturbance
GDOP	Geometric Dilution of Precision

8.7 REFERENCES

1. Wenzel, CDR R., Omega System Status Update, Proceedings of the Thirteenth Annual Meeting of the International Omega Association, Munich, Federal Republic of Germany, October 1988.
2. Karkalik, F., Sage, G., and Vincent, W., Western Pacific Omega Validation, Vols I and II, Report No. ONSOD 01-78, April 1978.
3. Campbell, L., Servaes, T., Grassler, E., North Atlantic Omega Navigation System Validation, Report No. CG-ONSOD-01-80, July 1980.
4. Levine, P. and Woods, R., North Pacific Omega Navigation System Validation, Report No. CG-ONSOD-01-81, December 1981.
5. Watt, T., Bailie, G., and Sutphen, M., South Atlantic Omega Validation, January 1983.
6. Swanson, E. and Kugel, C., Indian Ocean Omega Validation, Report No. CG-ONSCEN-02-87, 1987.
7. Hildebrand, V., South Pacific Omega Validation Analysis, Report No. CG-ONSCEN-02-89, August 1989.
8. Wenzel, CAPT R., and Kugel, C., Mediterranean Sea Omega Validation Analysis, Report No. CG-ONSCEN-02-91, May 1991.
9. Hildebrand, V., Western Pacific Omega Validation Analysis, Report No. CG-ONSCEN-03-90, August 1990.
10. Wenzel, CAPT R., Vannicola, V., Casswell, R., McManus, H., ONSCEN's Operational Data Analysis Program, Proceedings of the Fifteenth Annual Meeting of the International Omega Association, Sanur, Bali, Indonesia, September 1990.
11. Swanson, E., and Brown, R., Omega Propagation Prediction Primer, NELC Technical Note TN 2102, 1972.
12. Morris, P., and Cha, M., Omega Propagation Corrections: Background and Computational Algorithm, Report No. ONSOD 01-74, December 1974.
13. Morris, P,. and Swanson, E., New Coefficients for the Swanson Propagation Correction Model, Proceedings of the Fifth Annual Meeting of the International Omega Association, Bergen, Norway, August 1980.
14. Vannicola, V., Private Communication, October 1991.
15. Calvo, A.B., Omega monitor network deployment study, TASC TR-343-5, January 1974.

CHAPTER 9

SIGNAL PHASE PREDICTION MODEL

Chapter Overview -- Omega navigation is fundamentally based on measurement of the Omega signal phase, but this phase must be "corrected" for signal propagation effects before it can be used for navigation. This chapter explains the need and basis for the signal phase corrections, known as Propagation Corrections (PPCs), and describes the prediction model used to calculate the PPCs. Section 9.1 summarizes the major technical issues in the chapter and provides a brief historical sketch of PPC model development. The basic relationships among cumulative phase, received phase, lanes, and distance over the earth are explained in Section 9.2. This section also discusses how the received signal phase is transformed into the "nominal" phase model through use of the signal phase prediction model, often referred to as, simply, the PPC model. Section 9.3 presents an overview of PPC model structure and computational flow in terms of path definition, sub-model classification, and temporal modification. Calibration and evaluation of the semi-empirical PPC model with respect to signal phase measurements at Omega monitor sites are described in Section 9.4. Also in this section, the signal prediction performance of various PPC models with respect to several measurement databases are compared and discussed. Section 9.5 is an appendix which provides a thorough treatment of the PPC model, including its semi-empirical form, representation of basic physical processes, and spatial/temporal structure. Problems, including worked-out examples and those to be attempted by the reader, are included in Section 9.6. Abbreviations and acronyms used in the chapter are given in Section 9.7 and references cited in the chapter are found in Section 9.8.

9.1 INTRODUCTION

9.1.1 Basis for a Signal Phase Prediction Model

The principles of Omega signal usage for navigation are based on the premise that the phase of a signal received from a transmitting station is closely related to the station-receiver distance (see Chapter 4). Ideally, changes in Omega signal phase, as measured on a moving platform, bear a fixed linear relationship to corresponding changes in the position of the platform over the surface of the earth. With this idealization, navigation and positioning are relatively simple procedures that involve only the signal frequency and station locations, in addition to the phase measurement.

In the case of Omega, however, signals propagate to very long ranges and are substantially influenced by spatial and temporal variations in the electromagnetic and geophysical properties of the earth and ionosphere. These effects on the received signal phase lead to a marked departure from a linear dependence on distance, thus greatly complicating use of the signals for navigation. To make the signals

usable for navigation, the complex propagation effects must therefore be eliminated or reduced. Assuming that this elimination or reduction is possible, how can it be most reliably and effectively achieved? Over the years, several methods have been developed for eliminating or reducing the complex signal propagation effects on navigation and positioning. These methods may be categorized as:

- *Internal* — Corrections are derived from the characteristics of the received signals (at one or more frequencies)
- *External* — Corrections are derived from external sources.

One of the internal methods that was used in earlier-generation receivers consists of simply subtracting the signal phases at two of the frequencies (e.g., 10.2 and 13.6 kHz) transmitted from the same station. To eliminate propagation effects, this procedure (which is similar to the method for resolving lanes) relies on the assumption that propagation effects at the two frequencies are completely correlated. In reality, the propagation effects at the two frequencies are only partially correlated, so that the complexity of the resulting signal is lessened but far from eliminated. A related, but improved internal method is to take the appropriate linear combination of the signal phases at the two frequencies, i.e., the combination that minimizes the variation over 24 hours (diurnal variation). This technique, known as Composite Omega (Ref. 1), reduces the diurnal variation, but does little to reduce the spatial variation, i.e., the wide range in phase behavior exhibited by equal-length paths during the same time period over substantially different electromagnetic and geophysical environments.

The external methods used to reduce the effects of the propagation path environment on signal phase include primarily real-time corrections (broadcast locally) or predicted corrections in the form of published tables or algorithms. Real-time corrections are provided by differential Omega systems (see Chapter 4) in certain local areas. These corrections are supplied to the receiver via a data link (usually an LF beacon) based on the processing of observed signals at a central, surveyed monitor site. Corrections are accessible to receivers in the local area, i.e., within about 200 to 500 nm of the monitor site. Predicted phase corrections, known as propagation corrections or PPCs, are available as published tables or computational algorithms. PPCs are computed from semi-empirical models of VLF signal phase, incorporating both signal propagation theory and observational data from worldwide monitor sites. PPCs are generally considerably more accurate than the internal methods described above but less accurate than real-time differential corrections (in the local areas where they apply). Compared to differential corrections, PPCs have the advantage that they apply globally (with varying degrees of accuracy). For these reasons, application of PPCs is currently the most common method of reducing the undesired effects of the signal propagation environment on the received Omega signal phase.

9.1.2 Principal Features of Propagation Correction (PPC) Models

A PPC model is essentially a description of how the phase of the Omega signal changes with distance and time between the generation of the signal at the transmitting station and its detection at the Omega receiver. A complete theoretical description of the propagation of the signal, accounting for its intermediate interaction with the earth and ionosphere signal environment is not only extraordinarily complex, but also insufficiently accurate for phase prediction. This inaccuracy is due partly to the assumptions and approximations made to derive expressions for the field quantities and partly to the uncertainty in the physical values of ground/ionosphere electromagnetic parameters. The other extreme is a purely empirical approach, in which only measurements of signal phase at fixed points in space and time are used: it is not reliable when extended beyond the spatial and temporal specifications of the measurements. Intermediate between these two types of models is the semi-empirical model, which combines all the essential elements of signal propagation theory with actual measurements of signal phase. A semi-empirical model is well-suited for Omega signal phase calculations, since it is substantially simpler and generally more accurate than a purely theoretical calculation and its range of application is much greater than a purely empirical model.

As mentioned in Section 9.1.1, the PPC is a predicted time- and space-dependent quantity which, when combined with a phase measurement, removes the complexities and non-linearities due to interaction of the signal with the propagation environment. In [illegible] the PPC transforms the measured phase value into one that follows the so-called "nom[illegible]se variation." This means that if a receiver records phase data at increasingly distant [illegible]itting station and the appropriate PPC is applied at each point, the resulting phase will [illegible]n distance with slope given by the nominal wave number. In the nominal model of phase [illegible]ation, the cumulative signal phase is a linear function of distance from the transmitting station for all possible receiver locations and times. The PPC model, then, attempts to characterize the variation of the actual (expected) phase from the corresponding nominal phase.

Because the nominal phase makes up most (about 99%) of the cumulative phase for typical paths, as illustrated in Fig. 9.1-1, the PPC is a comparatively small quantity, varying from about -2.0 to +2.0 cycles at 10.2 kHz and slightly more for the higher frequencies. Thus, the PPC can be thought of as a correction that eliminates the "perturbation" represented by the departure of the true phase from the nominal phase value; this perturbative property has implications for modeling (see Section 9.5). Besides having a relatively small magnitude, the PPC has a slow spatial variation, compared to the nominal phase (see Fig. 9.1-1). This property has the very important practical consequence that a PPC can be applied without precise knowledge of position. In fact, if this were not the case, Omega could not

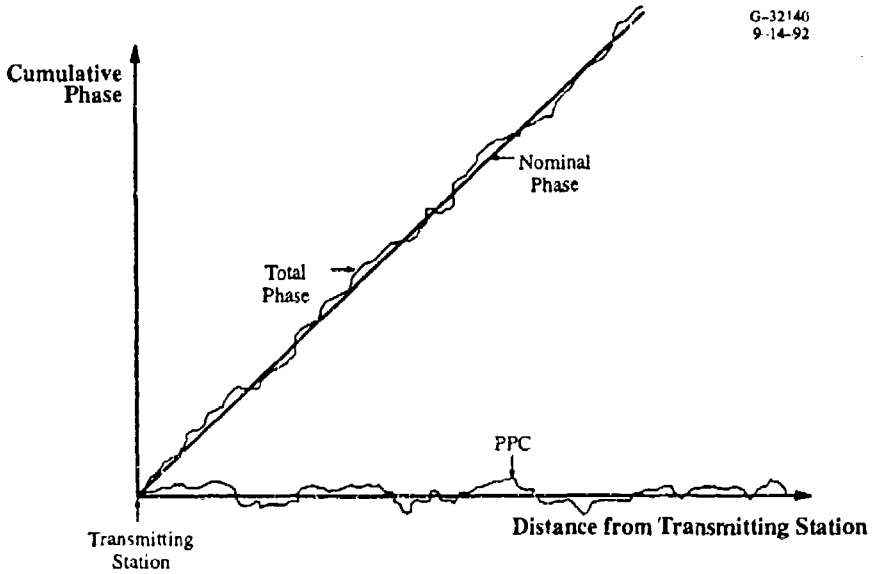

Figure 9.1-1 Comparative Spatial Variation of Nominal Phase and PPC

effectively be used as a navigation system, since precise knowledge of position would be necessary to compute the PPC which, in turn, is used to compute position! Because of the relatively low sensitivity to spatial position, the PPC can be applied to measurements with position uncertainties as large as 65 km with practically no resulting position accuracy degradation.

Keep in mind that the PPC is a *predicted* quantity and thus, when combined with an actual phase measurement, does not always remove the phase nonlinearities due to propagation effects. These imperfections lead to *PPC errors* or *phase prediction errors* in which combination of the erroneous PPC and the phase measurement result in an incorrect nominal phase value that, in turn, produces navigation/position errors. An *exact* PPC differs from the usual PPC definition in that it is the result of a measurement of actual signal phase (e.g., at a monitor site) subtracted from the nominal signal phase. Thus, in Fig. 9.1-1, the curve marked Total Phase is the *predicted* phase when the PPC curve (shown along the bottom axis) is predicted, but the Total Phase is the *observed* phase when the PPC curve is exact.

PPC models are structured to represent the predicted phase variation (from the nominal phase) of a transmitted signal at a given point in space and time as a double sum of incremental phase values. First, the path over the earth, between the transmitter and receiver, is broken into path segments, about 65 km in length. The incremental phase variation at each segment is expressed as a sum of component phase variations due to various electromagnetic/geophysical effects, such as ground conductivity and relative

sun angle. These component phase variations, defined as sub-models, are products of mathematical functions (functional forms) of the governing parameters (such as geomagnetic bearing angle) and linear model coefficients. The total phase variation for a path is the sum over the incremental phase variation at each segment of the path.

The mathematical functions specified by each sub-model are approximate representations of the analytical/observational behavior of the phase as obtained from theoretical calculations or experimental results. These calculations are based on an important class of full-wave models, known as waveguide-mode models, in which the signal field is expressed as a sum over the modes of the waveguide. In most cases, the "dominant" mode is the lowest phase velocity transverse magnetic mode, which is usually known as Mode 1 (see Chapter 5). Except for signals that propagate over very short paths or along westerly directed nighttime paths, the Mode 1 component usually dominates the total signal behavior at Omega frequencies. It also happens that Mode 1 signal phase behavior (in terms of quantities such as ground conductivity and geomagnetic field components) is much simpler than that for higher-order modes. For these two reasons, the functional forms used in PPC models are approximations to the Mode 1 behavior derived from waveguide-mode models. This is an important point, because it implies that, where (in both space and time) Omega signals are not adequately represented by Mode 1-dominated behavior, PPCs cannot be applied. This is the principal reason why signal coverage products (see Chapter 10) portray 'modal" regions and times (those for which the signals from a given station are not expected to be dominated by Mode 1 behavior) as unusable for Omega navigation.

Because Omega signal phase on a transmitter-receiver path differs dramatically between path-night and path-day, the functional forms for the sub-models are separately specified for "local maximum day" and "local maximum night." This means that separate functional forms are obtained as approximations to waveguide-mode model calculations for short paths in which the local ionosphere has:

- *Minimum Effective Reflection Height* -- corresponding to local maximum day, when the sun is directly above the local ionosphere
- *Maximum Effective Reflection Height* -- corresponding to local maximum night, when the sun is directly above the antipode* of the local ionosphere.

For intermediate times (or, equivalently, sun angle), a linear combination of the local maximum day and local maximum night sub-models are invoked. The linear combination is implemented through interpolation or evolution functions that depend on several parameters in addition to sun angle. The characteristics of these functions are important, since phase can change rapidly over periods of less than an hour.

*Point on the earth opposite to (through the center of the earth) the point in question.

As defined above, a sub-model is the product of a functional form (one or more mathematical functions including the domain of application) and a linear model coefficient. The linear model coefficients are not known *a priori* and are inserted into the semi-empirical model framework to partially account for the errors incurred in approximating the full theoretical model structure. Thus, for example, if the linear dependence postulated by the semi-empirical model were completely correct and in full agreement with noise-free measurements, the coefficients would all be unity (or a single, fixed number). Because the linear model does not fully describe the phase variation in terms of the geophysical and electromagnetic parameters in the signal propagation environment, the linear model coefficient set is not characterized by a single number and must be determined through calibration. Model calibration consists of determining the appropriate linear model coefficients (and, in some cases, embedded nonlinear parameters) that best "fit" a large number of phase or phase difference measurements recorded at Omega monitor sites throughout the world. Thus, although it is structured by theoretical principles, the semi-empirical PPC model is strongly "data driven," which heightens the need for high-quality data in the calibration. When fully calibrated (i.e., when all coefficients are satisfactorily determined), the model performance is measured by the RMS phase prediction error over measurements both inclusive and exclusive of those used in the calibration. If the model is sufficiently robust, i.e., if the calibration data represents a suitable cross section of the expected operating environment, the test performance will be comparable to the calibration performance.

9.1.3 Historical Development of PPC Models

The importance of PPCs was recognized from very early in Omega's history. J.A. Pierce was the first to propose simple corrections based on day/night considerations (Ref. 2). The Naval Electronics Laboratory (now known as Naval Command, Control, and Ocean Surveillance Center (NCCOSC)) began an extensive theoretical and experimental investigation of Omega signal propagation prediction in the 1960s, which laid the groundwork for a semi-empirical Omega phase prediction model. E.R. Swanson of NOSC led the development effort which resulted in a model based on path segmentation and waveguide-mode theory (Ref. 3). A rudimentary form of the model was produced in the late 1960s but the first widely disseminated model documentation appeared in 1974 (Ref. 4) after the U.S. Coast Guard had taken over responsibility for Omega system engineering, operations, and user support. In 1980, a major re-calibration of the 1974 PPC model structure was undertaken using three-frequency data acquired from a global distribution of monitor sites (Ref. 5) The only major change to the model structure was the addition of a long-term time sub-model. This sub-model was intended to capture the effect of assumed ionosphere "hardening" (increased ionization) by a fixed percentage increase each year (due to a corresponding growth in industrial emissions) thus leading to a

long-term exponential increase in phase variation. By 1989 this sub-model had exceeded the projection of its calibration time frame (Ref. 6), i.e., continued use would have lead to increased, rather than reduced, phase prediction error. As a result, the Omega community was notified that the sub-model should be effectively deleted (Ref. 7).

The PPCs based on the 1980 PPC model calibration showed a significant improvement over those of the 1974 model. However, subsequent usage and experimentation revealed some shortcomings in addition to those that may be due to the predicted long-term year-dependent variation. Most of the reported large errors resulting from the model's predictions were associated with transition paths, i.e., a sunrise/sunset terminator lies between the transmitter and receiver. The source of these large errors was found to be in the specification of the sunrise/sunset phase onset time. In other words, all-night or all-day phase behavior (for a given path) changes relatively little, but if the path is undergoing sunrise or sunset transition, the changes in phase can be large and sudden. An error in specifying the time of onset for these changes can lead to large phase errors during and beyond transition as shown in Fig. 9.1-2. The transition onset time specified by the 1980 PPC Model is believed to have a large uncertainty because:

- No explicit transition sub-model with calibration coefficients is invoked
- No transition phase data was used for model calibration.

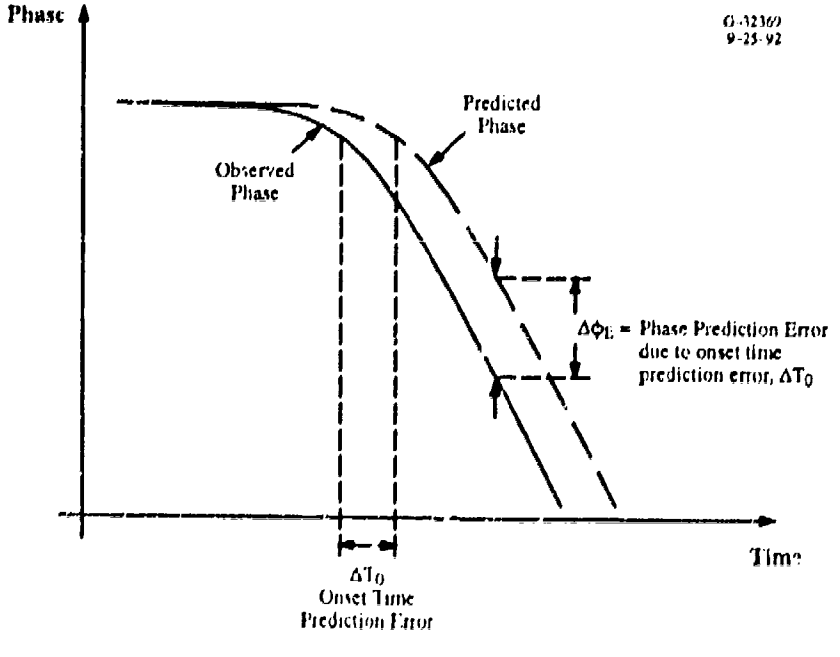

Figure 9.1-2 Phase Prediction Error Due to Sunrise Onset Time Prediction Error

Because of these limitations in the 1980 PPC Model, the Omega Navigation System Center (ONSCEN) initiated an effort to develop a new PPC model structure. The result of this effort is referred to as the 1993 PPC Model. It is specifically tailored to fit observed transition (where the path is part night and part day) phase profiles through the use of sunrise/sunset onset/recovery time parameters (Ref. 8). The 1993 PPC Model has been calibrated for 10.2 kHz signals using mostly 1988 data from 16 monitor sites uniformly distributed over the globe (Refs. 10 and 20–26). Though based on a set of path-limited measurements, the calibration results give preliminary indications that the 1993 PPC Model is accurate and robust.

9.1.4 Use of PPC Models

A candidate PPC model/algorithm undergoes rigorous testing and evaluation and, if successful, is authorized by ONSCEN for use by the general public. The existence of a new PPC model is generally communicated through informal channels, e.g., papers presented at the International Navigation Association (formerly the International Omega Association; see Chapter 2) or at navigation-oriented symposia. Upon request, ONSCEN provides a package containing a documentation of the PPC model/algorithm, a hard copy of the source code, copies of the executable and source codes in magnetic medium, and a program user guide (Ref. 27).

Omega receiver manufacturers make up an important segment of PPC model users. The manufacturers' software engineers normally revise the algorithm only to the extent that the code "fits" the particular computing environment used by the receiver/processor. For example, the spatial resolution of the ground conductivity map may be reduced due to data storage requirements or an exponential-type functional form may be approximated by a piecewise linear function. The basic structure of the algorithm is usually unaffected by these changes, however.

9.1.5 Outline of Chapter

The basic concepts involving cumulative phase and distance over the earth are outlined in Section 9.2. This section includes a discussion of the nominal phase model and multi-frequency PPCs.

Section 9.3 presents an overview of the generic structure of the PPC model. The description is intentionally general, making it applicable to most, if not all, PPC models in use. Included in this section are the structural components of PPC models, including sub-models, path domains, and time dependence.

PPC model calibration is covered in Section 9.4. This section covers data preparation, linear and nonlinear model parameter determination, and model performance.

A more detailed description of PPC model structure is included as an appendix in Section 9.5. This section addresses the physical basis for a generic PPC model and the technical issues involved in its development.

Section 9.6 contains problems related to the material presented. Both sample problems (with solutions) and problems to be solved by the reader are given.

Abbreviations and acronyms are briefly defined in Section 9.7. References called out in the Chapter text are listed in Section 9.8.

9.2 BASIC CONCEPTS

Omega propagation corrections (PPCs) are those predicted phase values which, when applied to the Omega signal phase measurement, provide a linear phase versus distance relationship. The relationship of the "true" signal phase to the measured signal phase is explored in Section 9.2.1. The PPC is a computed quantity that provides an estimate of the actual received phase at a given location and time with respect to a reference, or nominal, phase. The nominal phase model is described in more detail in Section 9.2.2. The PPC is described in terms of the "true" and the nominal phase values in Section 9.2.3.

9.2.1 Signal Phase and Laning

Given that an Omega transmitting station generates a signal at a precisely controlled frequency,

i.e., $A \sin(2\pi ft)$; [A = amplitude f = frequency; t = time] ,

then the signal observed at some distant point is given by

$$B \sin (2\pi(ft - \phi)) \; ; \; [\phi = \text{phase}]$$

where $|B| < |A|$. For a plane electromagnetic wave having a source at $\mathbf{r} = 0$, the phase is given by

$$\phi = \mathbf{k} \cdot \mathbf{r} \; [\; \mathbf{k} = \text{wave vector} \; ; \; \mathbf{r} = \text{position vector} \;].$$

The magnitude of the wave vector is called the wave number and is equal to the reciprocal of the wavelength (λ)*, i.e.,

$$| \mathbf{k} | = \text{wave number} = 1/\lambda \qquad (9.2\text{-}1)$$

*An alternative definition of the wave number used in many texts is $k = 2\pi f/c = 2\pi/\lambda$.

The electromagnetic field of the Omega signal propagates as shown in Fig. 9.2-1 in the comparatively thin shell (about 0.01 earth radius) between the earth and the ionospheric D-region. Thus, the wave may be treated as confined to the surface of a spherical earth, so that, between two points on the surface, the wave travels along the arc of a great circle. In the plane of the great circle, only a single angular coordinate is required to define the point of phase measurement and corresponding wave number, so that the phase is given by

$$\phi = k_\theta \, r_\theta \quad [\, k_\theta \ = \text{angular wave number} \ ; \ r_\theta = \theta \, R_E \,] \tag{9.2-2}$$

where θ is the angle (in radians) subtended by the transmitter-receiver path at the center of the earth and R_E is the earth's average radius. A similar expression is obtained for the phase of a signal propagated over a non-spherical (e.g., spheroidal) earth.

The expression for phase, given by Eq. 9.2-2, is sometimes known as the cumulative phase. Thus, for example, if the wavelength is 30 km and the distance from the transmitting station is 3015 km, the cumulative phase is

$$\phi = (1/30)\ (3015) = 100.5 \text{ cycles}$$

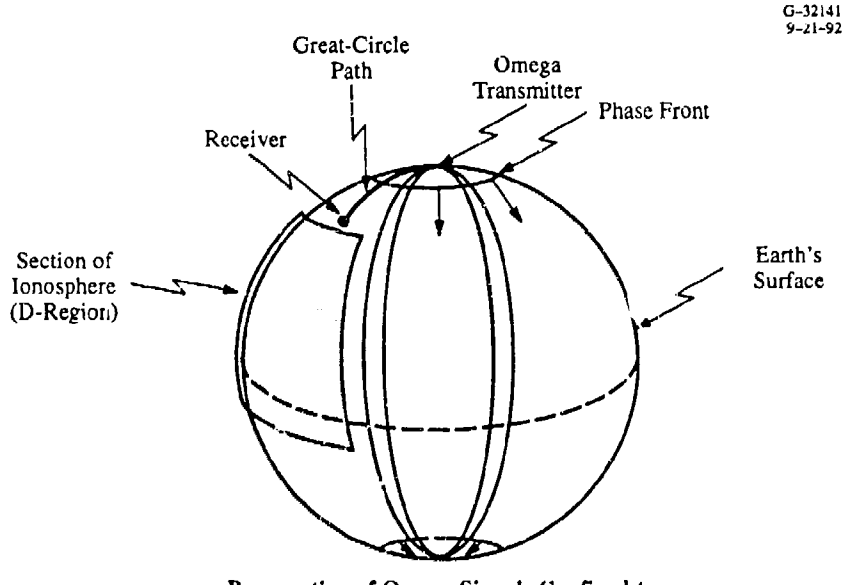

Figure 9.2-1 Idealized Propagation Environment for Omega Signals

The cumulative phase is composed of an integer part (100 in this example) and a fractional part (0.5 in this example). Since cycles of a single-frequency wave "look alike," an Omega receiver cannot directly measure the whole number of cycles developed by the wave over the path from the transmitting station, i.e., the integer part of the cumulative phase.* Thus, in the above example, an Omega receiver would measure 0.5 cycle (or, equivalently, 180° or π radians) but the same measurement would result if the integer part of the cumulative phase were 2, 87, or 234 cycles. This can be illustrated by noting that the received signal is alternately expressed as

$$B \sin (2\pi(ft + n + \alpha)) = B \sin (2\pi(ft + \alpha))$$

for any integer value of n. These findings may be summarized by noting that

- In terms of wavelength, the cumulative phase is composed of an integer part (whole number of cycles) and a fractional part
- The Omega receiver measures only the fractional part of the cumulative phase
- Since the total cumulative phase is important for navigation/positioning, the integer part must be obtained from external information.

The external information referred to includes approximate knowledge of the transmitting station-receiver path distance or, in the case of moving receiver, precise knowledge of the transmitting station-receiver distance at an earlier time.

If a marker is made at the station and at each wavelength on the station-receiver path, the spatial intervals between markers serve to define lanes, over which the phase varies from 0 to 2π radians (see also Chapter 4). More generally, a lane is defined as the largest spatial interval (a signal wavelength, in this case) that can be unambiguously related to a difference in phase measurements at a single frequency. Over the two-dimensional surface of the earth, these lanes form annuli, one wavelength wide, that are centered at the transmitting station. Lanes can be numbered or otherwise identified so that the problem of determining the integer part of the cumulative phase is equivalent to the problem of determining the appropriate lane. The uncertainty regarding the integer part of the cumulative phase is known as lane ambiguity.

As an example of the application of PPCs, consider two successive measurements of the phase of a transmitting station signal using a receiver attached to a moving vehicle (see Fig. 9.2-2). Suppose the

*In principle, one could infer the number of cycles from the pulse envelope arrival time measurement (assuming the Omega receiver is time-synchronized to the station timing standard) but, because of the narrow bandwidths involved, the measurement is very imprecise.

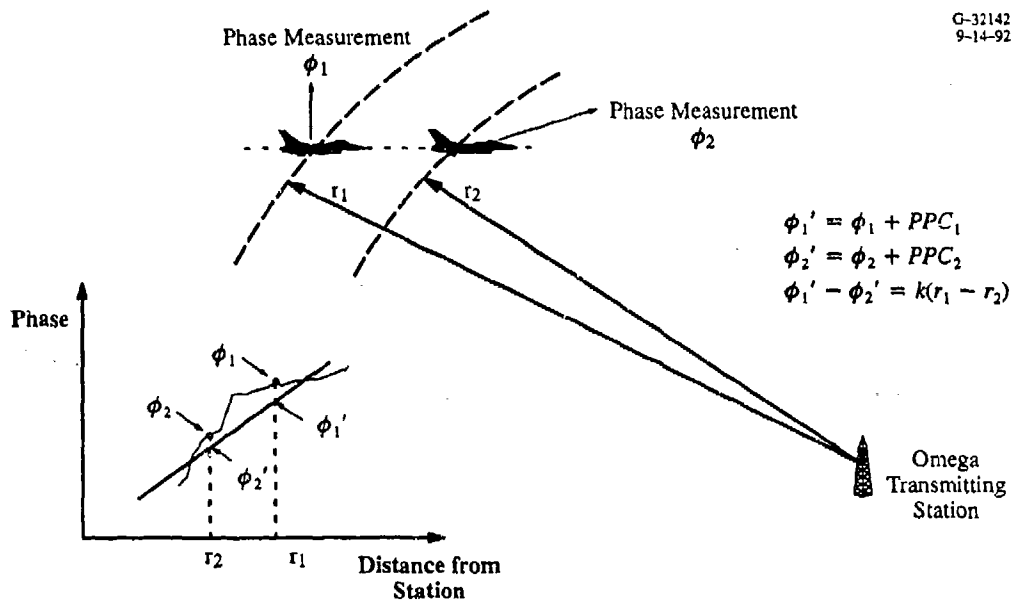

Figure 9.2-2 Application of PPC's to Two Phase Measurements

two raw phase measurements are labeled ϕ_1, ϕ_2 and that ϕ_1 is made when the vehicle is at distance r_1 from the transmitting station and ϕ_2 is made when the vehicle is at distance r_2 from the transmitting station. When the appropriate PPCs (which are functions of position and time) are added to each raw phase measurement, i.e.,

$$\phi_1' = \phi_1 + PPC_1 \; ; \; \phi_2' = \phi_2 + PPC_2,$$

the resulting phase change is proportional to the change in distance from the transmitting station, i.e.,

$$\phi_2' - \phi_1' = k(r_2 - r_1). \tag{9.2-3}$$

The proportionality constant k is the wave number, defined by Eq. 9.2-1. In general, the raw phase measurements, ϕ_2 and ϕ_1, do not have a difference which is proportional to the the station range difference, $r_2 - r_1$. If the range difference, $r_2 - r_1$ does not exceed a wavelength, there is no lane ambiguity, and no external information is required. The relationship expressed by Eq. 9.2-3 permits the straightforward application of navigation or position-fixing procedures (see Chapter 4).

9.2.2 Nominal Model

The reduction of the phase measurement to a linear function of distance can be traced back to the time when navigational charts were used for manual plotting of Omega lines of position (lines of

constant phase difference between two stations' signals). It is much easier to plot these lines of position (LOPs) if the phase (difference) is linearly related to the distance (difference) from the transmitting station. The particular wave number used to construct the charts is known as the "nominal" wave number, which is simply the ratio of the cumulative "idealized" phase developed by a signal to the distance over which the signal is propagated.

In free space (a vacuum with no other interactions), the wave number is given in terms of signal frequency (f) by

$$k_0 = f/c \tag{9.2-4}$$

where $c = 2.99793 \times 10^5$ km/sec is the speed of light (*in vacuo*). The nominal wave number is given in terms of k_0 as

$$k_{NOM} = 0.9974\ k_0$$

which is an intermediate value between observed night and day 10.2 kHz wave numbers* on seawater paths. For modeling purposes, the numerical value of the nominal wave number is not critical; it is only important that the value be "near" the average over all time and space conditions. As a practical matter, it is important that all navigation algorithms used in conjunction with PPC algorithms use the same value of k_{NOM} for the assumed nominal wave number. Reference 19 supplies information regarding the origin of the numerical value of k_{NOM}/k_0.

Note that the nominal wave number depends only on frequency (through Eq. 9.2-1) and is independent of space and time or any other parameter. In the example leading to Eq. 9.2-3, the fixed wave number k has a value equal to k_{NOM}. Table 9.2-1 lists the nominal wave numbers for the common Omega frequencies.

Table 9.2-1 Nominal Wave Numbers for the Common Omega Frequencies

FREQUENCY (kHz)	WAVELENGTH (LANEWIDTH) (km)	NOMINAL WAVE NUMBER (km^{-1})
10.2	29.3914	0.03394
11.05	27.1305	0.03676
$11\frac{1}{3}$	26.4523	0.03771
13.6	22.0436	0.04525

*k_{NOM} is actually much closer to the average day wave number; this is the basis for the laning procedure discussed in Section 9.4.

The nominal phase is a cumulative phase defined as

$$\phi_{NOM} = k_{NOM}\, D \tag{9.2-5}$$

where D is the distance between transmitting station and receiver over the earth. D is usually computed with a fair degree of precision since the nominal phase makes up about 99% of the total cumulative phase. As a result, D is computed as the transmitting station-to-receiver distance over an ellipsoidal model of the earth.*

9.2.3 PPCs as Corrections to the Nominal Model

With the cumulative phase (ϕ) and nominal model as described above, the PPC at position, $\mathbf{r}$, time, t, and frequency, f, is given by (the origin of the coordinate system is assumed to be at the transmitting station)

$$\text{PPC}\ (\mathbf{r},t,f,) = \phi_{NOM}\ (\mathbf{r},f) - \phi\ (\mathbf{r},t,f,) \tag{9.2-6}$$

where the nominal phase is given by Eq. 9.2-5. Note that, for a fixed frequency, the PPC and the measured phase both depend on the vector position coordinates (indicated by $\mathbf{r}$) and the time, t, whereas the nominal phase depends only on the range, D, over the surface of the earth from the transmitting station. For a spherical earth, the range, D, is given in terms of $|\mathbf{r}|$ and the earth's radius, R_E by

$$D = 2\ R_E\ \arcsin(|\mathbf{r}|/(2R_E))$$

Since the nominal phase accounts for about 99% of the predicted phase, the PPC has a typical magnitude between –2 and +2 cycles. The PPC is usually specified to a resolution of 0.01 cycle (centicycle (cec)), which is well below the PPC accuracy (5 to 12 cec) and is on the order of the phase resolution of most receivers. This resolution also corresponds approximately to the system synchronization error (1 cec ≈ 1 μsec at 10.2 kHz).

As noted in Section 9.1.2, the PPC is usually defined as a predicted quantity, so that the cumulative phase, ϕ, appearing in Eq. 9.2-6 is the predicted phase. If ϕ is chosen to label the *observed* phase, then the PPC, defined by Eq. 9.2-6, is exact. Of course, when an observed value of ϕ is used, the integer part must be obtained from external sources.

In contrast to the nominal phase which is computed using the nominal model described in Section 9.2.2, the expected phase is obtained from a very complex model described in Section 9.3. This

*A reference spheroid, such as WGS-72 or WGS-84, is commonly used.

model accounts for the various electromagnetic/geophysical properties of the earth and ionosphere which influence the wave propagating between the transmitting source and the receiver. In this model, as in the real world, the properties of the path are not constant but vary along the path, i.e., the path is said to be inhomogeneous. Since the wave number, k, depends on the electromagnetic properties of the earth's surface and the ionospheric D-region (which serve to reflect VLF waves), k also varies along the path. Thus, for a real, inhomogeneous signal path, the expression for the cumulative phase is given by

$$\phi = \int_C k(\mathbf{r})\, ds \tag{9.2-7}$$

where $\mathbf{r}$ is the position vector for some point on the path and ds is an element of path length. The integration contour, C, corresponds to the signal path over the surface of the earth between transmitter and receiver. If the wave number is constant over C, then Eq. 9.2-7 reduces to Eq. 9.2-2. For real paths, the wave number is most strongly influenced by the local illumination condition of the ionosphere, i.e., day or night. If the point on the surface of the earth identified by position vector $\mathbf{r}$ is in local day (i.e., the sun is a few degrees below the horizon to directly overhead), then k is normally slightly smaller than its nominal value. For points on the path in a local night condition, k is larger than its nominal value. Other local parameters, such as ground conductivity and certain components of the geomagnetic field, also affect k but to a smaller degree.

Figure 9.2-3 shows a typical diurnal (24-hour) observed phase profile (measured with respect to a precise time or frequency standard) in which the path illumination conditions, nominal phase, and two sample exact PPC values are identified. The figure illustrates the higher (retarded) phase during path night and the lower (advanced) phase in path day with a total diurnal shift of about 0.65 cycle. Since the phase is a function of effective ionospheric height, which varies with the relative sun angle (solar zenith angle), the observed phase exhibits a "bowl-shaped" profile during the day with less variation at night. The phase profile changes from day (night) to night (day) behavior during path transition when the sunset (sunrise) terminator cuts the path. The figure illustrates the time independence of the nominal phase and the consequent time dependence of the exact PPC values. Note that if the observed phase profile shown in the figure were the same as the predicted phase for all 24 hours, then the exact PPCs would be identical to "regular" PPCs, since the PPC, or prediction, error is zero.

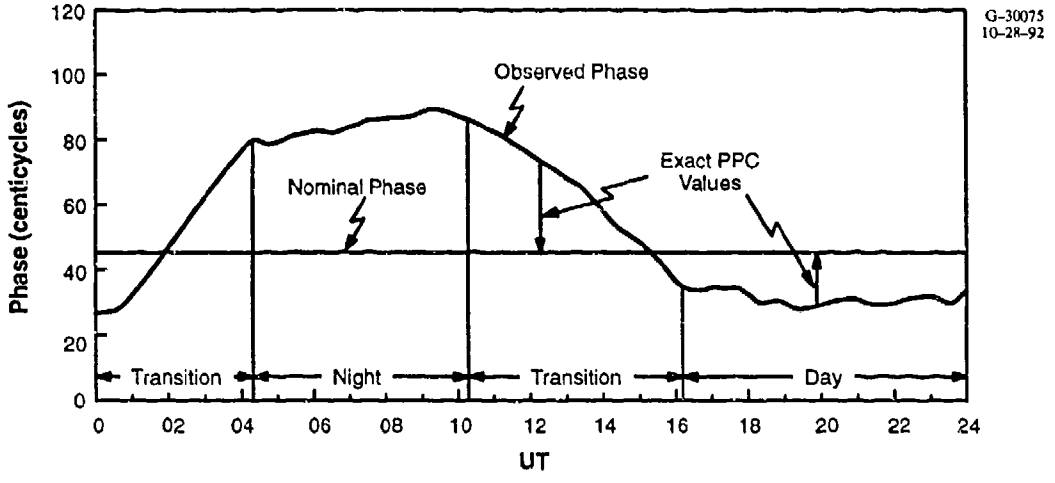

Figure 9.2-3 Typical Diurnal Profile of the Phase of an Omega Signal Recorded at a Fixed Site

9.2.4 Applicability of the PPC Model

Although the model for the expected phase (known as a PPC model) is fairly comprehensive, it is limited to certain signal path propagation conditions, including

- Short-path propagation, i.e., the signal must arrive at the receiver via the shorter of the two great-circle arcs joining transmitter and receiver
- Mode 1 dominance, i.e., the signal behavior must be effectively described by the signal's Mode 1 component (in a waveguide-mode model of VLF signal propagation (see Chapter 5))
- Off-path effects, i.e., the signal must not be significantly influenced by geophysical conditions laterally displaced from the short great-circle path.

The first condition is frequently violated when the receiver is west of the transmitting station and the short-path is fully illuminated by the sun. The second condition holds for most daytime paths (except for very short paths (<1,000 km)) and easterly propagating nighttime paths. The condition is nearly always violated for westerly propagating nighttime paths transiting the geomagnetic equator. The third condition holds for most paths and times except, for example, those for which the path and terminator cross at a very shallow angle or the seawater portion of the path passes close to a low conductivity region (e.g., Greenland).

The propagation conditions for which the PPC model is not applicable are identified by modern signal coverage products described in Chapter 10. Since the PPC model computes corrections for any given path and time, these coverage products should be consulted to determine the usable signals prior to calculation of PPCs.

9.2.4 Multi-frequency PPCs

The structure and form of a PPC model usually apply to more than one Omega signal frequency. However, the linear model coefficients, which are initially unspecified, are determined from calibration with observed data that shows them to be highly dependent on frequency. Other embedded, nonlinear model parameters also generally depend on frequency. Thus, although a calibrated PPC model/algorithm usually refers to a frequency-specific object, a fully calibrated model is a generalized algorithm that applies to more than one frequency. More importantly, a fully calibrated model is computed for the appropriate frequencies using the same (or very similar) database.

During the development of Omega, model calibrations have been performed at a single frequency and the resulting coefficients presented. For example, the PPC model developed in 1971 (Ref. 3) was re-calibrated in 1976 (Ref. 9) at 10.2 kHz using data from monitor sites in the Mediterranean region (including southern Europe and northern Africa). Although this re-calibration improved the accuracy of the 10.2 kHz PPCs relative to those predicted by the 1971 model, it did little to improve accuracy for most receiving systems which use combined phase information at two or more of the common Omega signal frequencies. This is because the 1971 PPC model was calibrated at three frequencies (10.2, 11 1/3, and 13.6 kHz) on essentially the same database. Moreover, certain relationships between the PPCs at the three frequencies were enforced in the calibration, so that, for example, prediction errors at 10.2 kHz (for a given time and location) are partially "compensated" by prediction errors at the other two frequencies.

As an example of a technique that combines multi frequency phase information, consider a simple difference frequency system (13.6 kHz phase – 10.2 kHz phase). When the difference in PPCs is added to the difference frequency measurement, correlated prediction errors in the PPCs will subtract, thereby leaving a smaller residual error than if the PPCs at the two frequencies were derived independently (e.g., using different databases). Similarly, if the 10.2 kHz PPCs are changed ("improved") without changing the other frequency PPCs, the combined frequency accuracy will be limited by the prediction accuracy of the most poorly predicted of the other frequency PPCs.

A second example of a frequency combining phase processing system is Composite Omega (Ref. 1). With this technique, a composite phase value is computed as a linear combination of 10.2 and 13.6 kHz signal phase measurements. The composite phase value has the advantage that its diurnal (day to night) phase shift is very small – smaller than the 13.6 and 10.2 kHz frequency difference shift. Because many of the early Omega receiver mechanizations used a composite phase technique, the multi frequency PPC model calibrations (1971 and 1980) ensured that no error was introduced by the

PPCs into the composite phase value. Single-frequency PPC model calibrations do not maintain the composite phase invariance.

Based, in part, on the above reasons, it is preferable to perform multi-frequency PPC model calibrations using primarily the same phase measurement database (paths and times). The size and diversity of the database, as well as the number of frequencies, is determined by the scope of the measurement program and other practical considerations. As a general rule, however, the greatest diversity in paths, times, and frequencies is the most desirable from the viewpoint of PPC model calibration.

9.3 OVERVIEW OF PPC MODEL STRUCTURE

The models used as the basis of PPC calculations have evolved with the increase in knowledge of VLF wave propagation effects and ionospheric processes. Diurnal changes were recognized from the earliest experiments as the principal contributor to phase variation on a fixed-length path. In the Omega Implementation Committee Report (Ref. 2), which served as the primary basis for development of the Omega system, a need and procedure were outlined for the development of diurnal phase corrections by means of "compensation graphs." Later, the Navy Electronics Laboratory (now the Naval Command, Control and Ocean Surveillance Center (NCCOSC)) identified additional phenomena contributing to the variation of the phase from a fixed (path length- and frequency-dependent) value. Based on results from complex, theoretical models of wave propagation, these effects were quantified and linked together within the framework of a semi-empirical model. This semi-empirical model was calibrated using recorded measurements of the signal phase from the relatively few Omega stations in existence prior to 1972 (see Chapter 2). In the 1970s, as new Omega stations were constructed and signal monitoring programs initiated, the database of phase and phase difference measurements was greatly expanded. Consequently, the PPC model was refined and re-calibrated several times during this period, although its essential semi-empirical character remained largely the same. Development of a PPC model is more than of academic interest, since the phase prediction (PPC) error is the largest component of the Omega position error budget. Thus, in a very real sense, the semi-empirical model used to compute PPCs is a central determinant of Omega system accuracy.

The essential features of PPC models have changed relatively little during the evolution of the Omega System and are not extraordinarily complex when reduced to a set of procedures, analytical expressions, and computational flows. However, the development of existing model structures,

including the rationale for path domains, temporal structure, and the relationship to full-wave waveguide-mode models of signal propagation, requires a lengthy discussion that may distract the reader from the basic ideas of phase prediction. As a result, this section presents a brief overview of the structure and computational flow for a generic PPC model, and the details of the model structure and the basis for its development are addressed in Section 9.5.

Figure 9.3-1 illustrates the overall structure and computational flow for a generic PPC model. The figure indicates that the basic elements of the PPC model structure and computational sequence may be organized in terms of the following functional categories:

- *Path Definition* — Set-up of path between transmitting station and receiver and definition of path domains
- *Sub-model Classification/Calculation* — Assignment of sub-models to the appropriate path domain
- *Temporal Modification* — Multiplication of excitation and phase velocity sub-models by evolution/diurnal functions that depend on time
- *PPC Calculation* — Aggregation of modified sub-model contributions and synthesis with reference and nominal phases to determine phase variation and PPC.

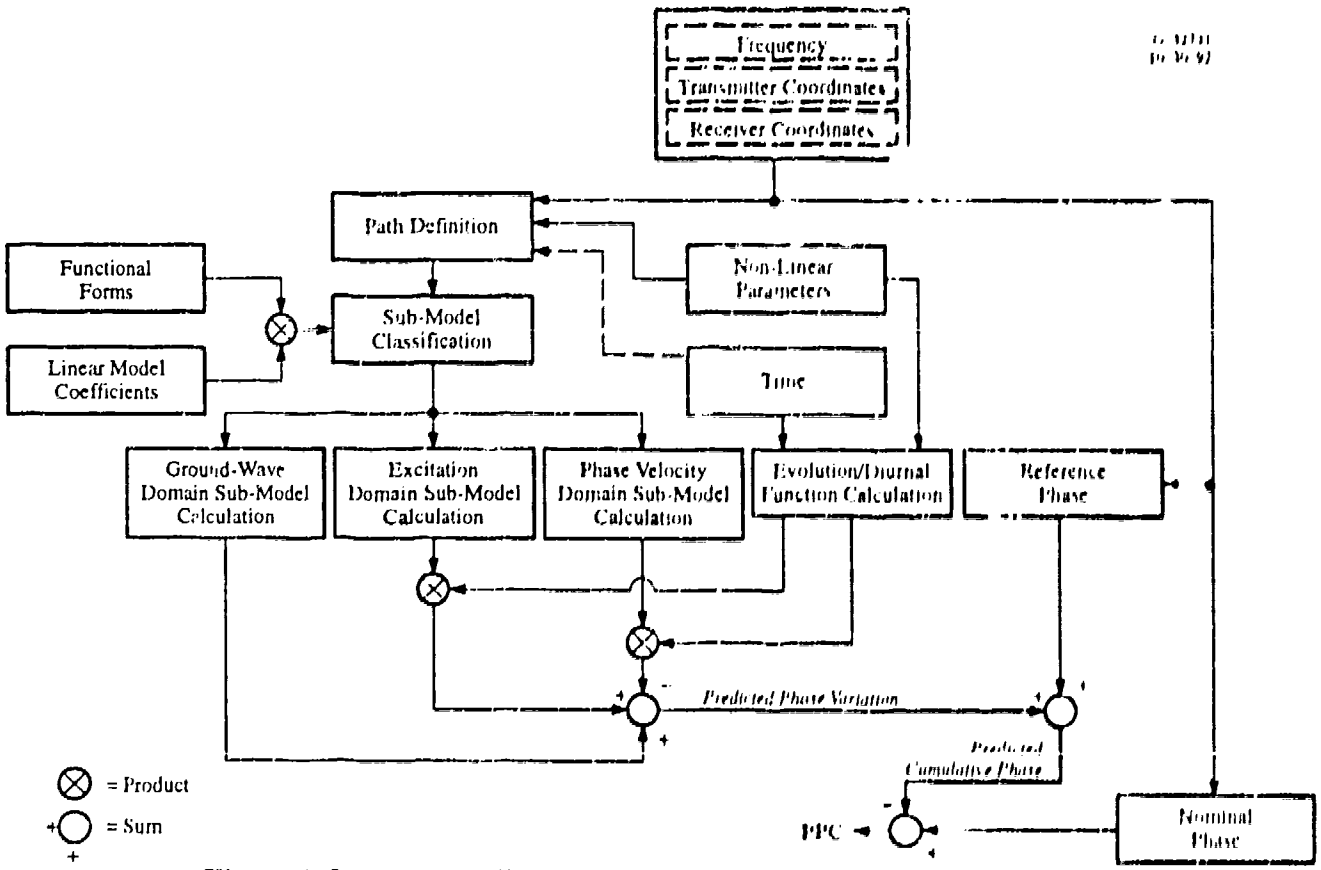

Figure 9.3-1 Overall PPC Model Structure/Computational Flow

These four functional categories of model structure and computational flow are described further in the following paragraphs.

As indicated in Fig. 9.3-1, definition of the signal propagation path requires several inputs. These inputs, which include transmitting station and receiver coordinates and the signal frequency (and for some models, time), determine how the path is partitioned to facilitate calculation of the predicted phase.

For the inhomogeneous paths encountered in the use of Omega signals, the predicted phase is expressed by the integral form given in Eq. 9.2-6. Actual calculations approximate this integral by a sum over path segments, i.e.,

$$\phi = \sum_i k_i \Delta r_i \tag{9.3-1}$$

where k_i is the wave number for segment i and Δr_i is the length of the path segment. Figure 9.3-2 shows the segmentation for a typical path. An individual segment, which is shown in more detail in Fig. 9.3-3, is approximately 60 km in length. In the end path regions, only the ground conductivity of the segment is specified, since the Mode 1 wave vector is not influenced by the ionosphere in these portions of the path (see Section 9.5). For the mid path region, the local properties of both the earth's surface and the D region of the ionosphere at the segment's lower and upper boundaries, respectively, are specified.

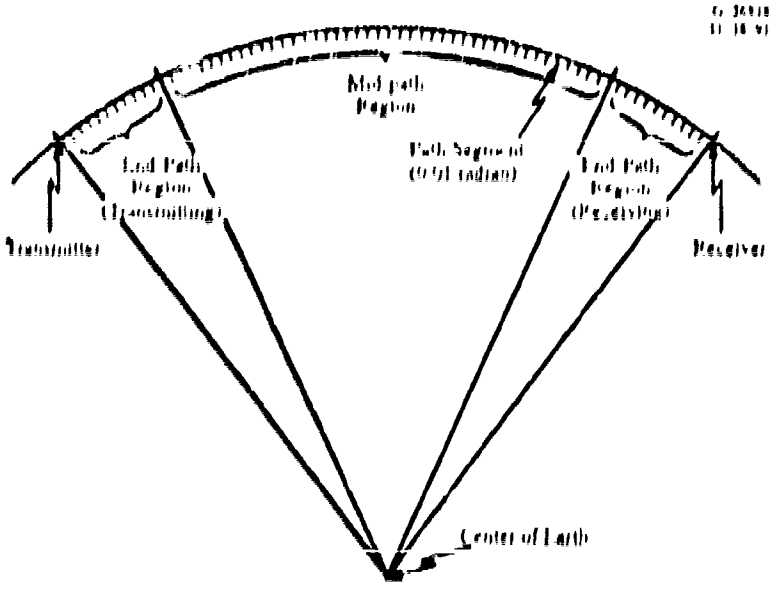

Figure 9.3-2 Path Segmentation for the Phase Calculation

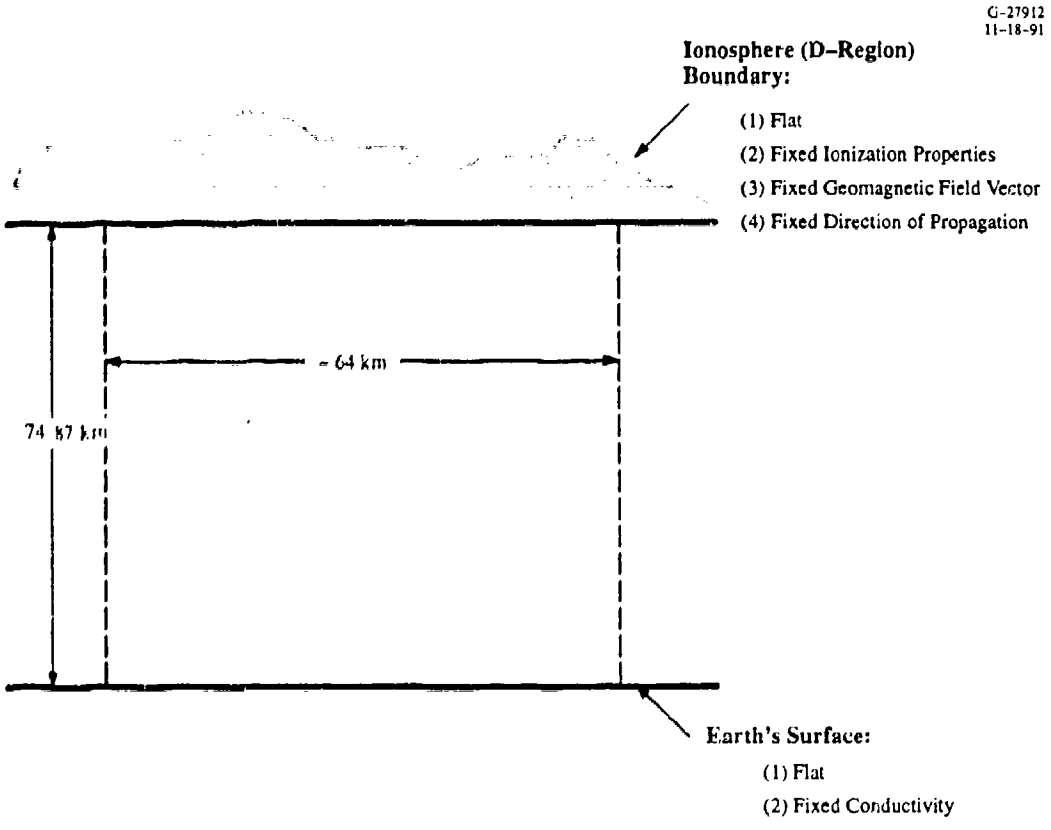

Figure 9.3-3 Model of a Typical Path Segment

The wave field associated with the transmitted signal and sensed by the Omega receiver interacts with the earth's surface and ionosphere (the waveguide boundaries) in a way that depends on the relative position along the path. Path domains are those portions of the path that have similar wave-boundary interactions and, therefore, invoke the same sub-models. The domains are referenced by the type(s) of sub-models invoked therein, i.e.,

- Ground-wave domain
- Excitation domain
- Phase velocity domain.

As shown in Fig. 9.3-4, the ground-wave domain comprises the two end-path regions. [In some of the PPC Model literature, the end-path region near the transmitter is called the excitation region and the end-path region near the receiver called the de-excitation region.] Since, in this domain, the wave only interacts with the earth's surface (lower boundary of the earth-ionosphere waveguide), the

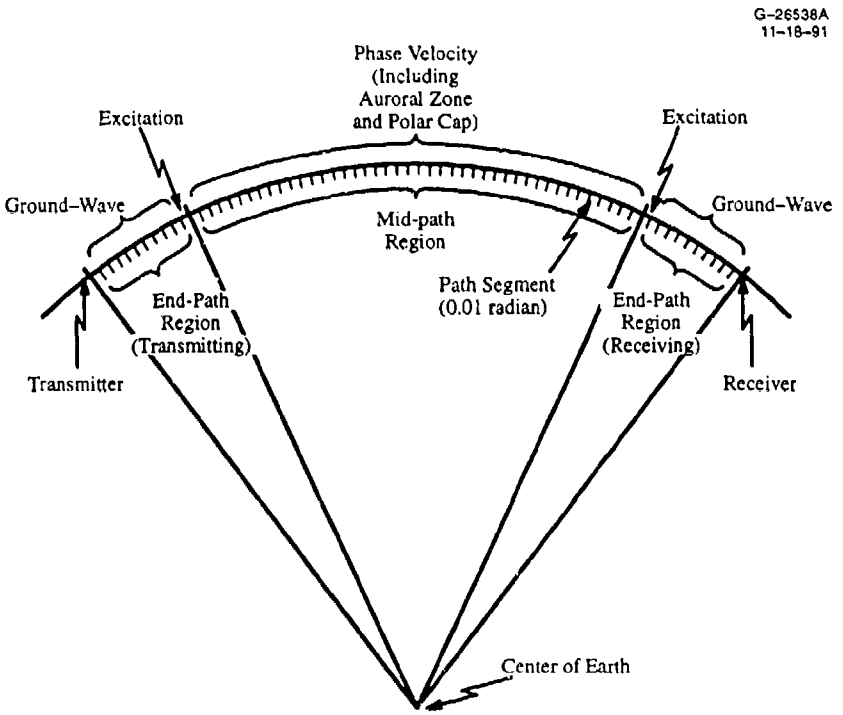

Figure 9.3-4 Path Domains/Segmentation Corresponding to Unique Sets of Sub-models

corresponding sub-models depend only on ground conductivity. The size of the ground-wave domain is fixed in most PPC models but in the 1992 PPC model, the extent of this domain varies with the local illumination condition and frequency. This somewhat indirect dependence of the domain definition on time is expressed in Fig. 9.3-1 by the dashed arrow of the time input to the path definition.

The excitation domain shown in Fig. 9.3-4 comprises that region of a path where the Mode 1-launched wave first (or finally) sets up the field structure that characterizes its general behavior in the earth-ionosphere waveguide. The nomenclature derives from the waveguide-mode model of VLF wave propagation in which a source wave is "excited" (to various degrees) in the earth-ionosphere waveguide. The degree of excitation depends on the signal wavelength and frequency, the size (height) of the waveguide, and the electromagnetic properties of the internal medium, and the boundaries of the waveguide. Thus, an excitation phase is said to be introduced in the propagated signal field where the wave first "sees" the ionosphere. Reciprocal arguments show that an excitation phase is introduced near both the transmitting source and the receiver.

For the vast majority of paths used in navigating with Omega signals, the phase velocity domain constitutes more than 80 percent of the path. This domain corresponds to the mid-path region (see Fig. 9.3-4) where the signal interacts with both the ionosphere and the earth's surface. In this domain, the

phase/unit path length is specified by the wave number, as in Eq. 9.1-3. The phase velocity depends on three parameters (which are, in general, coupled): ground conductivity, geomagnetic latitude, and geomagnetic bearing. Included in the phase velocity sub-models are those that describe the local wave number behavior in spatial regions with "anomalous" ionospheric height profiles, i.e., the auroral zones and polar caps.

For each path segment in a particular domain, the sub-models appropriate to that domain are computed as the products of functional forms and linear model coefficients. Functional forms are simple analytic forms that approximate the theoretical dependence of signal phase on geophysical and electromagnetic parameters, such as ground conductivity or geomagnetic latitude. Linear model coefficients are introduced to partially account for the approximation and linearization error incurred in establishing the functional forms. The linear model coefficients are determined by comparing the expression for the model prediction with the observed phase data (see Section 9.4).

Time dependence is introduced through those sub-models that characterize the time-varying ionosphere. Since ionospheric properties are required for sub-model calculation in the excitation and phase velocity path domains, only sub-models in these domains are modified to account for universal time, as shown in Fig. 9.3-1. Modification occurs through multiplication of the sub-model by the evolution/diurnal function. This function is effectively a means of interpolating between sub-models defined for "local maximum day" (sun directly over the segment) and "local maximum night" (segment at opposite point of the globe from local maximum day). The function depends on the local sun angle, known as the solar zenith angle (computed from the input year, month, day, hour, and minute) and certain non-linear parameters that are determined from calibration/experimentation (see Sections 9.4 and 9.5).

The sub-models for the ground-wave domain and the modified sub-models for the excitation and phase velocity domains are combined to produce the predicted phase variation for the input path, frequency, and time, as shown in Fig. 9.3-1.* To obtain the predicted cumulative phase for the path, the phase variation is combined with the reference phase, which for some models is the free-space phase and for other models is the nominal phase (see Section 9.1). The reference phase provides the principal information regarding the integer part of the cumulative phase in cycles. Note that the reference phase depends only on basic path information (transmitting station and receiver coordinates) and frequency. Finally, the PPC is computed as the difference between the nominal and predicted cumulative phase for the path/frequency/time.

*Note that the phase velocity sub-models are multiplied by –1 prior to combining with other sub-models as shown in Fig. 9.3-1 and explained in Section 9.5.

9.4 PPC MODEL CALIBRATION

The PPC Model, described in Sections 9.3 and 9.5, normally specifies the model structure, including the path segmentation, the types of sub-models used and where they are invoked, etc., but not the actual values of the model coefficients or embedded parameters. Comparison of the model with recorded phase measurements determines the numerical values of the model coefficients/parameters.

In this section, calibration of the PPC Model is explained by first outlining the overall calibration procedure. The nature and collection of the data that serves as input to the calibration procedure is then described. The model calibration itself is then presented as a three-step procedure:

- Preparation of model calibration database
- Implementation of the model calibration procedure
- Evaluation of the PPC model performance.

These topics are covered in general terms in the five sub-sections below.

9.4.1 Specification of Model Calibration Procedure

The basic idea of model calibration is to adjust certain free parameters/coefficients so that the predicted phase "best" matches the observed phase. Recall from Section 9.2.3 that the principal aim of a PPC model is to accurately predict the observed phase for a given path/time. Thus, if ϕ (path,time) is the observed phase for a given path/time and ϕ(path,time) is the predicted phase, then, in general,

$$\phi(\text{path, time}) = \hat{\phi}(\text{path, time}) + v(\text{path, time}) \tag{9.4-1}$$

where v is the prediction, or residual, error for the path/time. The "best" $\hat{\phi}$ is one that minimizes the function

$$MF = \sum_{\text{path/time}} | v |^2 = \sum_{\text{path/time}} | \phi - \hat{\phi} |^2$$

where the sum is over all path/times in the calibration database. If ϕ is taken to mean a vector of observed phase values (for a given collection of path/times), $\hat{\phi}$ is the corresponding vector of predictions, and v is the associated residual error vector, then the minimization function, MF, may be written

$$MF = v^T v = \left(\phi - \hat{\phi}\right)^T \left(\phi - \hat{\phi}\right) \tag{9.4-2}$$

The predicted phase vector may be written

$$\hat{\phi} = H\,(z_1, z_2, \ldots)\; C + \phi_0 \tag{9.4-3}$$

where H is the measurement matrix, z_1, z_2, . . . are embedded (usually non-linear) parameters, C is the coefficient vector, and ϕ_0 is the free space phase vector. The elements of H are functions of the path parameters and time, in addition to the embedded parameters. In contrast, the elements of the free space phase vector, ϕ_0, are a function only of signal frequency and path length. The objective of calibration is to choose the parameters z_1, z_2, . . . and the coefficient vector, C, so that

$$MF = \left(\phi - \left(H\; C + \phi_0\right)\right)^T \left(\phi - \left(H\; C + \phi_0\right)\right) \tag{9.4-4}$$

is minimized. Since H's dependence on the embedded parameters is highly non-linear, there is no simple analytical scheme to find the z_1, z_2, . . . that minimize MF. Normally, these parameters are determined using a combination of physical considerations and comparison of phase predictions (using candidate sets of reasonable parameters) with observations under the same conditions.

For a given set of embedded parameters, the coefficient vector, C, can be determined as a least squares estimate, i.e., one that minimizes Eq. 9.4-4. The form of the weighted least squares estimate for C is

$$C = \left(H^T\, R^T\, R\; H\right)^{-1}\; H^T\, R^T\, R\; \phi \tag{9.4-5}$$

where R is a diagonal weighting matrix associated with the observation vector ϕ. In response to a change in the embedded parameters $z_1, z_2, \ldots$, the measurement matrix, $H\,(z_1, z_2, \ldots)$ changes, C changes as prescribed by Eq. 9.4-5,and the predicted phase, $\hat{\phi}$, changes in accordance with Eq. 9.4-3.

9.4.2 Description of Phase Measurement Data

The observational data employed in PPC Model calibration generally comprises fixed-site measurements of signals from Omega transmitting stations. These measurements are of three kinds, depending on the type of reference oscillator, or clock, associated with the signal receiving system:

(1) Phase data referenced to a highly stable clock (such as a cesium frequency standard) and phase-synchronized to the Omega station signals

(2) Phase data referenced to a highly stable clock (such as a cesium frequency standard)

(3) Phase difference data, i.e., differences in signal phase between pairs of station signals accessible to the receiving system.

Type 1 data is available at only a relatively few sites where external equipment, such as a cesium frequency standard and a satellite signal receiver are available to maintain phase coherence. Phase synchronization can be maintained through external means because the signal waveform transmitted by each Omega station is synchronized (approximately) to Coordinated Universal Time (UTC), which serves as a reference for most high-precision standards and navigation satellites. This type of data is the only source of phase error (observed phase – predicted phase) information over a single station-to-receiver path. Type 2 data, which is somewhat more common than Type 1 data, permits analysis of single path diurnal phase behavior (since it is referenced to a stable source), but not single-station phase error. Signal receiving systems are limited to phase difference (Type 3 data) measurements when no highly stable reference (better than one part in 10^{12}) is available. For data of Types 2 and 3, only the difference in single-path phase error can be used for model calibration.

Since receiving systems providing Types 2 and 3 data are less sophisticated and require less attention than those providing Type 1 data, most of the data used in calibrations of PPC models have been of the phase difference type. These types of measurements are less desirable than Type 1 measurements providing single-path phase data, since they are inherently noisier (incorporating day-to-day fluctuations (at a fixed hour) on two paths) and reduce observability by subtracting modeled phenomena common to the two paths. Some Type 1 data has been used in PPC Model calibrations prior to 1990, although it has been extremely small compared to the phase difference component. In contrast, however, the Type 1 data used for the 1993 PPC Model calibration accounted for more than 50 percent of the calibration database.

An important source of Type 1 data is the network of monitors associated with each Omega station. Like most of the Omega monitor receivers at remote (non-station) sites, the station monitor receivers are equipped with only a medium-precision crystal oscillator so that only phase-difference measurements can be accurately made. For the station monitors, however, one of the paths is the very short one (15 to 50 km) from the local station to the station monitor. This path is so short that the phase is assumed to be well-approximated by the free-space phase (although recent measurements indicate that this approximation may be less accurate than previously assumed (Ref. 13)). Since the phase for this short path is assumed to be a known constant (independent of time), the phase difference data is easily adjusted to describe entirely the path to the remote station. Figure 9.4-1 depicts the locations of the current (1994) Type 1 monitor sites, including the 8 station monitors, Lower Hutt, New Zealand, and Pretoria, South Africa. Similarly, Fig. 9.4-2 shows locations of phase difference monitor sites that were operational in January 1987.

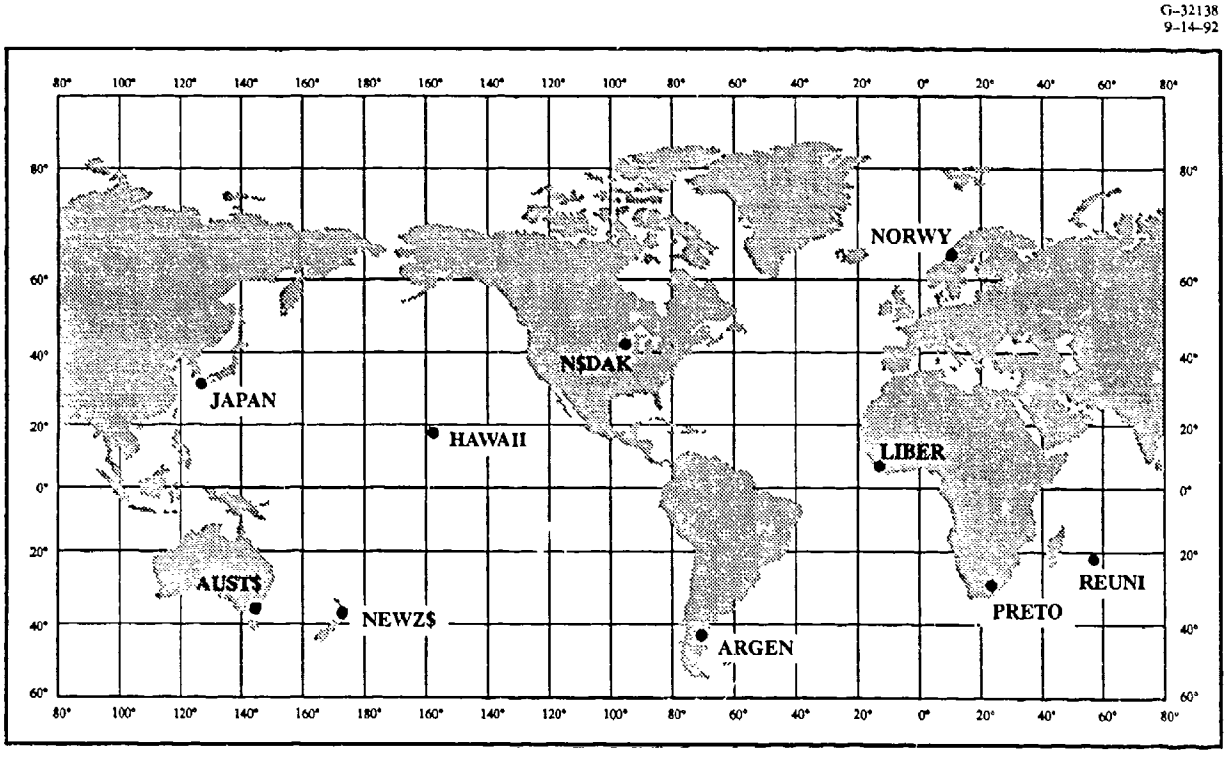

Figure 9.4-1 Site Locations for Type 1 Omega Monitors — 1988

To establish the implicit parameters that govern many of the time-dependent features of the model, high time-resolution data is required. Historically, this data has been obtained from continuous, paper strip-chart recordings of phase or phase difference. This data permits detection and tracking of rapid changes in phase (phase difference) that may accompany the onset or recovery of path transition. Because this data is most readily susceptible to manual scrutiny, comprehensive analysis of all such data is impractical.

The linear model coefficients can be systematically determined by means of a process often called "regression." In this scheme, a relatively small number of coefficients (e.g., 20 to 60) are determined from a database consisting of several hundred to several thousand measurements. Inspection of phase measurements from a variety of paths suggests that data recorded at hourly intervals provide sufficient time resolution of the typical diurnal phase profiles, while providing independent measurements. As a result, hourly data have served to provide the principal database for determining linear model coefficients since 1971. For consistency, these measurements are recorded "on" the UT hour, so that they represent an average over a receiver time constant (typically 1 to 3 minutes).

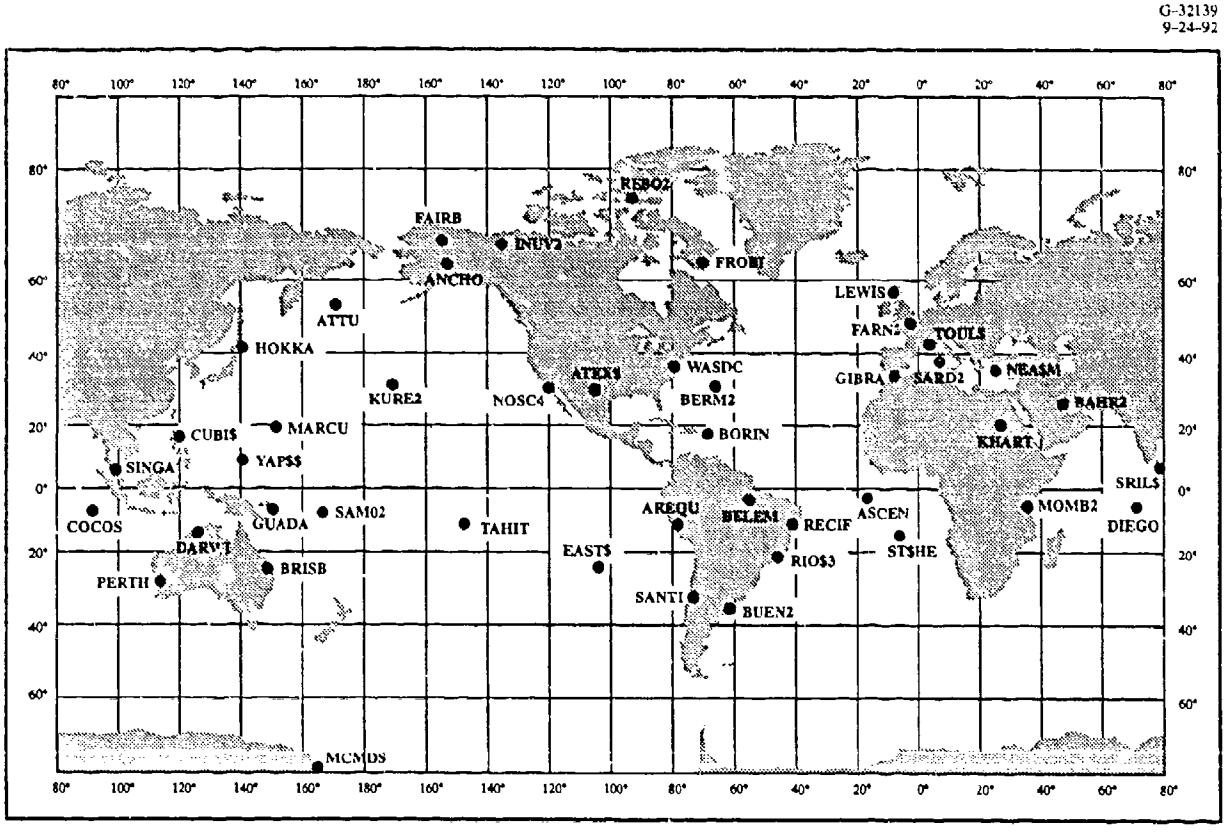

Figure 9.4-2 Site Locations for Types 2 and 3 Omega Monitors — January 1987

9.4.3 Preparation of Model Calibration Database

When the data of the type described in Section 9.4.2 becomes available, preparation of the model calibration database can proceed. This preparation task is crucial to the model calibration procedure and involves a substantial effort, which can be broken down into three primary stages:

- Identification and screening of anomalous data
- Down-sampling and secondary editing of data
- Attaching appropriate lane number to data samples.

Descriptions of these three stages follow.

Identification and Screening of Anomalous Data — Since the PPC model is composed of sub-models that are based on short-path Mode 1 signal phase behavior, it is critically important to ensure that, to the extent possible, phase data used to calibrate the model result from measurements of

short-path Mode 1 signals. The phase data must also result from measurements of signals whose signal-to-noise ratio (SNR) is high enough for adequate phase tracking. Signal data that do not meet these requirements are referred to as anomalous data and must be eliminated from the database to avoid corrupting calculation of the coefficients of the Mode 1-based PPC Model.

Identification of anomalous data is difficult and, in many cases, requires an experienced analyst to evaluate individual diurnal plots of phase or phase difference. For relatively small calibration efforts (e.g., a few hundred observations), such manual editing is feasible, but for larger efforts (e.g., those exceeding a thousand observations), the assistance of an automated procedure is necessary. For the 1993 PPC Model, an Anomalous Data Identification (ADI) algorithm is used that employs both theoretical predictions of signal behavior and certain statistical descriptors (known as "data indicators") of the observed data. Based on approximately one month's worth of phase or phase-difference data at a given hour and the two neighboring hours, ADI classifies the data as either normal or anomalous. If anomalous, the data is given a path quality assignment based on the the data indicators and the signal prediction appropriate to the path, as shown in Table 9.4-1 for single-path phase data. If conflicts arise between the data indicators and the path prediction, override tests are performed at neighboring hours to confirm the observational findings.

Table 9.4-1 ADI Phase Data Indicators for Anomalous Path Quality Assignments

Data Indicator (DI)	DI Criterion For Anomalous Assignment	Anomalous Path Quality Assignment
Day-to-day standard deviation of phase at a fixed hour	Value > 10 cec	Modal (Mode competition) or Low SNR
Day-to-day average phase (bias) error for path-night hours	Value > 20 cec	Modal (Higher-order mode dominance or cycle slip)
Slope of hour-to-hour phase profile for path-day or mixed-path hours	Sign of slope opposite to that predicted	Long-path
Day-to-day average SNR at a fixed hour	Value < −25 dB	Low SNR

Down-sampling and Secondary Editing of Data — Averaging of selected data, such as that specified for several of the data indicators, is necessary to reduce the originally supplied database to a manageable amount of information for the calibration software. Thus, it is not necessary to have the calibration database specify data for each day (and all 24 hours), since the phase at a fixed hour changes little from day to day. However, there is a slow change in phase throughout the year (at a fixed hour), so that, for example, averaging hourly phase over 60 days would eliminate much of the annual variation. A

compromise is generally taken to be 15 to 30 days, although, for some paths (long range paths traversing high latitudes), the phase change over these short periods is significant.

For the calibration database used in the 1993 PPC Model calibration, the data unit is a 15-day (first half-month and second half-month) average of the data for a given UT hour and is assumed to be representative of the observed data at the 7th and 22nd of each month, respectively. The variance of the data over the 15-day sample primarily indicates the day-to-day variation, although a certain amount of long-term seasonal variation is unavoidably included.

The data unit for the 1980 PPC Model calibration database is formed by averaging all data samples appropriate to a given path illumination condition. Thus, for example, for the calibration of the day linear model coefficients (entirely separate from the calibration of night linear model coefficients), the data unit is the average of all daytime path phase differences (and phase for a few single paths) at a given monitor site. In the case of the 1980 PPC Model calibration, a daytime path is one in which the maximum solar zenith angle is less than about 74° (depending on frequency; see Section 9.5.6 and Ref. 4). Prior to averaging, the predicted time dependence for day paths (referred to as the normal illumination depression (NID)) is subtracted to reference the data to a fixed, time independent value. In applying this procedure, the assumption is made that the time dependence is accurately known (from previous regression results) so that no error is introduced into the "data" read by the calibration programs. Error that is introduced in this way may be minimized through an iterative process. For calibration of night linear model coefficients, the data unit is similarly obtained as the result of all nighttime path phase differences (and phase for a few single paths) at each monitor site. Here, a nighttime path is one in which the minimum solar zenith angle is greater than about 99°. Since the 1980 PPC Model assumes no time dependence for nighttime paths, the night calibration data undergoes no NID-type processing prior to input to the calibration programs. Transition paths, i.e., those paths and times that do not conform to the definition of daytime or nighttime paths, were not included in the 1980 PPC Model calibration.

Because of the extensive averaging performed to obtain a data unit in the 1980 PPC Model calibration, the resulting observation vector (see Eqs. 9.4-1 and 9.4-2) is relatively small (a few hundred) and no further reduction is required. For the 1993 PPC Model calibration, however, only the 15-day fixed-hour averaging is performed, so that the observation vector is extremely large (10,000 to 20,000). For typical calibration databases, the observation vector contains about 250 to 450 data units/path, representing observations at different times (hour/month/half month). The measurement matrix, H, (see Eq. 9.4-3) manifests its time dependence through the evolution functions, as explained

Sections 9.3 and 9.5. However, since the path is the same for these 250 to 450 rows of H, elements that are zero (indicating no corresponding conductivity level on the path) will not change. The important point is that, for a given path, Eq. 9.4-3 specifies a substantial number of relations that differ relatively little from each other. A linear system having this property exhibits serious instabilities in the calibration procedure. The problem, known as "excessive near-parallelism," is heuristically illustrated in Fig. 9.4-3 for a space of two coefficients.

Thus, the temporally dense 1993 calibration database is reduced in the temporal dimension to ensure a stable solution for the coefficients. The reduction is performed by "down-sampling" the database according to specific rules. The essential idea is to select a set of observation times for each path such that the solar zenith angles (χ) corresponding to each time in the set span the range of possible χ as completely and uniformly as possible. This ensures that the rows of H for a given path will be as distinct (or "independent") as possible. This down sampling procedure reduces the observation vector to a manageable size (a few thousand).

For both the 1980 and 1993 PPC Model calibrations, the calibration database at this point undergoes a second level screening for anomalous data. Although the first-level screening eliminates 80 to 90 percent of the anomalous data, the second-level screening is necessary to remove inconsistencies and questionable data. Deletion of *all* observations for a given path effectively removes the path from the path limited database represented by H (Eq. 9.4-3) and is therefore made only when the data behavior supporting its removal is compelling.

Attaching Appropriate Lane Number to Data Samples -- The final, but perhaps the most important, step in preparing the calibration database is the assignment of the correct lane number

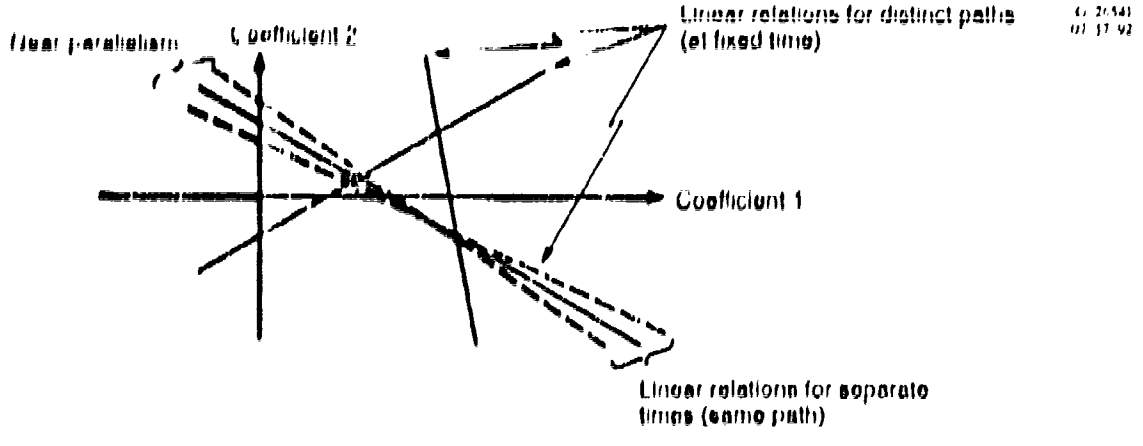

Figure 9.4-3 Heuristic Illustration of Excessive Near-Parallelism Found in Temporally Dense Calibration Data

(integer part of the phase) to the observed phase or phase difference. Laning arises because measurements of signal phase normally refer only to the fractional part of the phase. The integer part of the cumulative phase (lane) is almost never directly measured and therefore, theoretical predictions (assumed correct to within a cycle) are normally used.

In some applications, the lane number associated with the signal phase is not critically important, but, for model calibration purposes, attaching the correct lane number to the fractional part of the signal phase is absolutely crucial. This can be understood by noting that mislaning by a single lane is the same as injecting a 100 cec error into the data, thus significantly altering the computed coefficients and greatly increasing the RMS fit error.

Normally, lanes (for the case of phase measurement) are counted as the number of free-space wavelengths ($1/k_0$) or nominal wavelengths ($1/k_{NOM}$) from the transmitter to the receiver over the surface of the earth. The cumulative phase (see Eq. 9.2-6), measured in units of cycles or lanes, is thus a large number (100 to 600 for typical 10.2 kHz paths), whereas the scale of interest for PPCs is from about −2 to +2 cycles with a resolution of 0.01 cycle (centicycle).

Moreover, the actual phase measurements provide information on only the fractional part of the cumulative phase, so that the integer part must be estimated based on knowledge of the free-space or nominal phase and other information. This estimate is combined with the known fractional part to give an estimate of the cumulative phase (correct to within an integer number of lanes). From this number, the free-space or nominal phase is subtracted, thus providing a relatively small number between about −2.xx and +2.xx cycles for use in calculating the linear model coefficients.

The basic goal of laning, then, is to correctly assign the integer part of the cumulative phase to the measured fractional part. In all known laning techniques, the assignment is primarily based on the assumption that the nominal phase is a good approximation to the cumulative phase over daytime paths. For the 1980 PPC Model calibration, the lane assignment (closest to the nominal) is made for the daytime portion of the diurnal phase or phase difference profile and then tracked through successive differences to establish the lane assignment for other portions of the profile. The laning algorithm for phase data in the 1993 PPC Model calibration assigns the closest nominal lane for path/times having a maximum path solar zenith angle (MPSZA) of less than 70°. For path/times with larger MPSZA, the previously laned measurement that is "closest in time" (see Ref. 10) determines the lane assignment. The relative diurnal differences for phase difference data are generally smaller than for phase data, so that phase difference laning is more robust. The 1993 PPC Model calibration algorithm for phase difference assigns

"reference lane values" to each of the paths in a given path pair, depending on its path illumination condition (day, night, or transition).

9.4.4 Implementation of the Model Calibration Procedure

As explained in Section 9.4.1, PPC models are calibrated by determining two types of parameters: linear model coefficients and non-linear embedded parameters associated with the time variation. The linear model coefficients are calculated by means of a systematic computational procedure, whereas the embedded parameters are determined by empirical means.

The linear model coefficients are often referred to as the day/night coefficients since they provide a measure of the relative contribution of each sub-model for local maximum day and local maximum night (see Section 9.5). In the 1980 PPC Model calibration, separate calculations of the day and night coefficients were required since the corresponding day and night databases are entirely separate. Only a single execution is necessary for the day/night coefficient calculation in the 1993 PPC Model calibration scheme since the time dependence is included in the H matrix (see Eq. 9.4-3).

Both 1980 and 1992 model calibrations determined coefficients that minimized the mean square residual error (see Eqs. 9.4-2 and 9.4-4) and thus evaluated the expression, Eq. 9.4-5, for the coefficient vector, C. For the 1980 calibration, the observation vector, ϕ, has only a few hundred elements (since the time dependence was completely removed from the calibration input) so that the calculation of C is straightforward. In the case of the 1993 calibration, the number of elements in ϕ is about an order of magnitude larger so that calculation of C is non-trivial. The major computational problem is the matrix inversion appearing in Eq. 9.4-5. With a database of about 2500 data units, the 1993 PPC Model calibration used a high-end workstation and an efficient SVD algorithm to calculate C.

PPC model calibrations are usually performed for both weighted and unweighted measurement sets. The resulting calculations of C generally differ significantly only if the measurement data is relatively scarce or if the distribution of weights falls into widely separate domains. The weighting is implemented by use of the diagonal matrix R, appearing in Eq. 9.4-5. In the 1980 calibration, the elements of the diagonal weighting matrix R^TR were chosen to be the number of measurements (at different times) averaged to obtain the calibration data unit. For the 1993 calibration, the elements of the diagonal weighting matrix R are given by

$$R_{ii} = \left(1-\left(\mathrm{Min}(\sigma_i, 15)/15\right)^2\right) m_i/m_{\max} \; ; \; i = 1, 2, \ldots, n \; ; \; n = \text{number of data units}$$

where σ_i is the RMS variation of the daily phase measurements (in cccs) from a best-fitting linear ramp to the daily phase measurements for the half-month/hour corresponding to the i^{th} data unit, m_i is the number of unflagged daily measurements for the i^{th} data unit, m_{max} is the maximum number of days in the half-month. This weighting reflects both the data variation over the days of the half-month at a fixed hour and the relative number of measurements.

In addition to the computed coefficients, coefficient estimation variances are calculated to determine the degree of uncertainty associated with each coefficient. In the 1980 calibration, the estimation variance was used as a criterion for retaining or eliminating single-term sub-models, e.g., those associated with the geomagnetic equatorial region or long-term time dependence. The coefficient estimation variances computed as part of the 1992 calibration provided a means of determining whether the computed coefficients or theoretically derived values (from full-wave modeling) should be used in the PPC algorithm. If the coefficient estimation variance exceeds a certain threshold, the corresponding coefficients are too large and unstable. In this context, unstable means that, given a slightly different set of observed data, the coefficients change substantially. In such cases, the coefficients were fixed at theoretical values (see Ref. 8).

In performing a calibration, it is often necessary to fix (or "freeze") certain coefficients and "float" other free coefficients that are determined through the least-squares procedure and the chosen data set. For example, if a previous calibration run has established that coefficients associated with one or more sub-models have high coefficient estimation variance, these coefficients would likely be fixed at theoretical values in subsequent executions. When a mixture of free and fixed coefficients are specified, the dimensionality of the calibration problem is reduced by the number of fixed coefficients. In this case, a reduced coefficient vector, C', is defined which contains only the free coefficients, and an associated reduced measurement matrix, H', is formed containing only the columns associated with the free coefficients. The elements of the corresponding reduced observation vector are then given by

$$\phi_i' = \phi_i - \sum_j H_{ij} C_j$$

where the sum is over the indices of the fixed coefficients. The reduced vector of free coefficients is then given (for the unweighted case) by

$$C' = \left(H'^T H'\right)^{-1} H'^T \phi' \qquad (9.4\text{-}5)$$

9.4.5 PPC Model Performance

The performance of a PPC model is usually measured in terms of its predictive accuracy. For certain applications, other performance criteria, such as executable code size or algorithm processing speed may be important or even critical, but for most applications, the correct prediction of phase is the primary performance issue.

Recalling the discussion from Section 9.1.2, practical implementation of the PPC is possible only because the spatial variation of the PPC is small compared to that for the nominal phase. Thus, the PPC may be applied with little or no error with position uncertainties as large as 65 km. Usually this is no problem, since necessity of lane resolution limits the position uncertainty to well within 65 km; however, it does provide a practical lower bound for PPC accuracy (~0.1 – 1 cec).

Compared to spatial variations, temporal variations of the phase constitute a much greater limitation on the PPC accuracy. The prediction degradation is not primarily due to noise (which also has spatial and temporal variations) but presumably to day-to-day fluctuations in the ionosphere. These variations are characterized by the standard deviation of the observed phase over about 15 consecutive days (half-month) at a fixed hour; this standard deviation is referred to as the *random* component of phase error. This component was computed as part of the 1993 PPC Model calibration (see Section 9.4.3 and Ref. 10). The error in the predicted phase as measured using a stable, synchronized reference source at a known, surveyed monitor site for a given time is referred to as the *bias* error and is defined as

BIAS ERROR = OBSERVED PHASE – PREDICTED PHASE

The bias error may be viewed as an average of the observed minus predicted phase values over an approximate 15-day period at a fixed hour. From this viewpoint, the random error is a measure of the scatter about the bias error (average value), assuming the predicted phase for a half-month is adequately represented by the prediction at the "mid-point" (7th and 22nd day of the month).

Atmospheric noise at VLF originates primarily from lightning discharges associated with thunderstorms. These discharges act as "wideband" VLF radiation sources that propagate to long ranges, as do Omega signals. The noise sensed by an Omega user's antenna reduces the effective signal-to-noise ratio (SNR) in the receiver's front-end bandwidth and causes an error in the phase detected by the receiver. The phase error due to a finite SNR* is generally much smaller than either the bias or random components of the phase error as shown in Fig. 9.4-4. The data in the figure is derived

*The relationship between phase error standard deviation and SNR is given in Ref. 15, Appendix A.

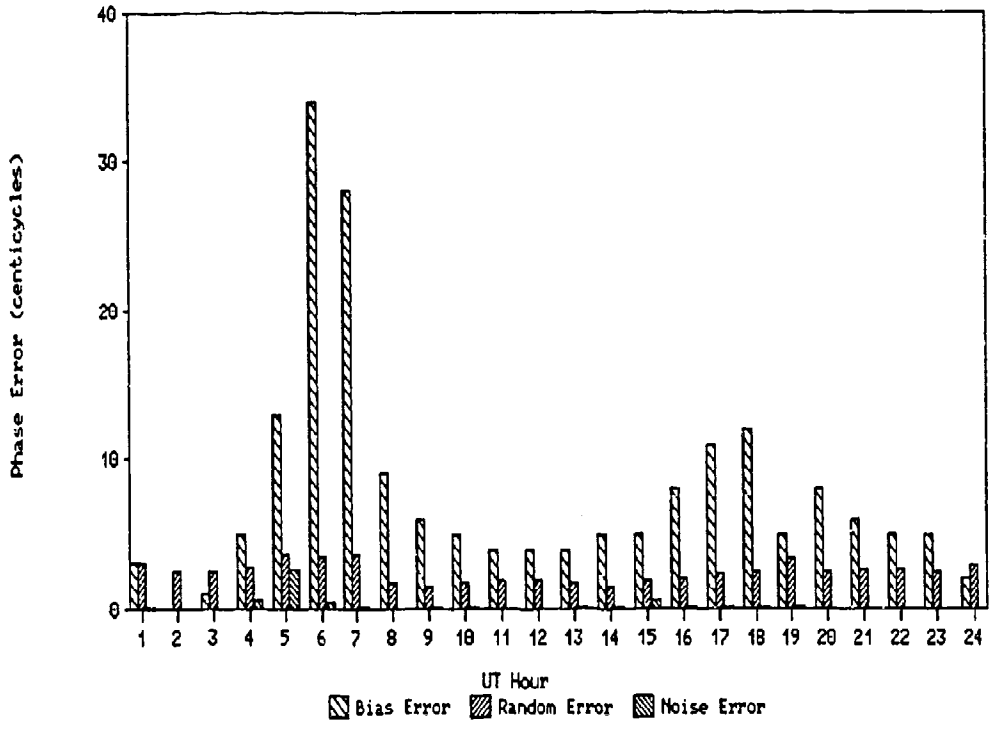

Figure 9.4-4 Phase Error Components for the 10.2 kHz Liberia Signal at the Norway Station Monitor Site — April 1988

from hourly measurements of the 10.2 kHz Omega signal phase at a monitor site near the Norway station during April 1988. The bias error is computed based on the 1980 PPC Model predictions and the random error is the standard deviation of the set of approximately 30 measurements at each UT hour. The phase error due to noise is derived from concurrent SNR measurements, which effectively indicate the noise environment over a receiver time constant (1 to 5 minutes). The general property indicated by the figure is that

BIAS ERROR > RANDOM ERROR >> ERROR DUE TO NOISE

As a result of this property, the phase error due to noise is usually neglected in compilations of phase error.

For the bias error, the RMS statistic is most commonly used for performance evaluation or comparison, although other statistics, such as mean error and relative fraction of "large errors" (e.g., those with magnitude greater than 20 cec) are also used. The random error is defined as a standard deviation so that it may be combined (in a root-sum-squared sense) with the RMS bias error to yield a total error.

Table 9.4-2 compares the phase prediction performance of several PPC Models as measured over several different databases. The figures in the table that indicate performance over the 1980 or 1971 calibration databases are obtained from Ref. 5. The entries for the "selected MASTERFILE" database is from Ref. 5 and the performance figures for the 1992 calibration database are from Ref. 10. As noted in the table and in Section 9.4.3, the category of day paths includes those whose maximum solar zenith angle is less than about 74°.* Similarly, night paths are those having a minimum solar zenith angle of about 99°.

The Pierce model contains only two sub-models (base velocity night and day) and the figures shown are based on the original phase velocity estimates (see Ref. 5) although two sub-model fits to other databases yield slightly different coefficients and slightly improved performance figures. The 1976 European "model" is really the 1971 model specialized to the European theater so that predictions in Europe exhibit good performance (see Ref. 9) while the *global* prediction accuracy is low. The Megatek model (Ref. 17) is a highly simplified PPC model but is unique in that it includes an empirically derived frequency dependence and an algorithm to reduce SID-induced phase errors (see Chapter 6). With some

Table 9.4-2 Performance Comparison of PPC Models on Day and Night Paths for 10.2 kHz Omega Signals

PPC MODEL	DATABASE	RMS BIAS ERROR (cec)	
		Day*	Night§
Pierce (Approx.)	1980 Calibration	13.4	14.3
1971–NOSC	1971 Calibration	5.2	4.9
1971–NOSC	1980 Calibration	6.9	10.0
1976 European		14.0	10.4
1979 Interim		7.3	12.7
1980–NOSC		5.7	6.3
Megatek (Approx.)		13.6	15.0
1980–NOSC	Selected MASTERFILE†	7.7	10.8
1980–NOSC	1992 Calibration	7.8	7.5

* Day paths are defined as those with a maximum mid-path solar zenith angle of less than about 74°.

§ Night paths are defined as those with a minimum mid-path solar zenith angle of greater than about 99°.

† Phase difference data samples (20,000-day and 30,000-night) from a subset of the ONSOD MASTERFILE (1982) comprising 3 path pairs from each of 16 monitor sites; anomalous data removed.

*For path-pairs associated with phase difference measurements (accounting for most of the data in Table 9.4-3), *both* paths must meet the maximum solar zenith angle requirement for day or the minimum requirement for night.

exceptions, the table shows that PPC model performance on day paths is better than that for night paths, reflecting the greater inherent instability of the nighttime ionosphere. It is important to note that the last two sets of performance figures in the table include the additional scatter due to random error. Thus, whereas the first seven sets of figures in the table include only a few hundred data points that represent average values over the appropriate illumination condition, the last two sets contain several thousand data points, corresponding to individual measurements. The difference in the 1980 PPC Model performance figures for the 1980 and 1992 calibration databases is accounted for by a 4 to 5 cec time variation of the observations averaged to form a data point in the 1980 calibration database. Time variations in this range were computed for the 1992 calibration database.

The figures in Table 9.4-2, which apply mostly to phase difference measurements, indicate performance for day and night paths but exclude the illumination condition with the largest path population — transition. Although day, night, and transition conditions are roughly equally represented among single-path phase measurements, data involving transition paths (all paths not conforming to the day or night definition) make up a large fraction (about 75 percent (Ref. 16)) of all phase difference measurements. This is because, on average, a pair of paths occupies a larger longitude interval than a single path and is thus less likely to be contained within a day or night hemisphere. Thus, Table 9.4-2, like many of the early papers documenting PPC model performance, does not indicate system performance over a representative set of illumination conditions.

In contrast, Table 9.4-3 lists performance figures for measurement databases including samples for all illumination conditions. The data units specified in these databases are not time-averaged, as are the data units in the first seven entries of Table 9.4-3, and include diurnal sampling intervals of 1 to 6 UT hours. The database labeled "Magnavox" (Ref. 18) is a collection of 122 phase difference data units selected from a sample of 3 to 4 path pairs from each of 15 monitor sites (those in the ONSOD MASTERFILE in 1985) recorded at 0000, 0600, 1200, and 1800 UT. The data unit consists of a 15-day (half-month) average of phase difference measurements recorded at one of these four UT hours, so that it does not include the full time variation implicit in the other figures in the table. The rather large RMS errors listed for this database may be due to the inclusion of anomalous measurement data that was not explicitly removed. For the other entries in Table 9.4-3, the RMS prediction error is generally much greater than that given in Table 9.4-2 because:

- The prediction error for measurements involving transition paths is substantially greater than for those involving all-day or all-night paths
- When sampled uniformly over hour, the number of phase difference measurements involving transition paths is much larger than for other path illuminations.

Table 9.4-3 Performance Comparison of PPC Models Under All Illumination Conditions for 10.2 kHz Omega Signals

PPC MODEL	DATABASE	RMS BIAS ERROR (cec)
1980–NOSC	Selected MASTERFILE*	13.6
1980–NOSC	Magnavox§	17.5
1985–Magnavox		12.3
1980–NOSC	1993 Calibration	12.8
1993		8.7

* Phase difference data samples (200,000 measurements) from a subset of the ONSOD MASTERFILE (1982) comprising 3 path pairs from each of 16 monitor sites (all hours); anomalous data removed.

§ 122 phase difference data units (each unit representing an average of about 15 measurements at a fixed hour) from a subset of the ONSOD MASTERFILE (1985) comprising 3 to 4 path pairs from each of 15 monitor sites at 0000, 0600, 1200, and 1800 UT; anomalous data apparently not moved.

A direct comparison of the performance of the 1980 and 1993 PPC Models with respect to path illumination condition using the entire 1993 phase database is shown in Table 9.4-4. The first column lists the random error, which represents the time variation of the measurements over about 15 days at a fixed hour. The second and third columns show the 1980 and 1993 PPC Model results for RMS bias error and the total error, which is root-sum-squared combination of the random and bias errors. In this case, day paths are defined as those having a maximum solar zenith angle of about 98°, which, therefore, includes many paths classified as transition in earlier PPC Model documentation (e.g., Refs. 4 and 5).

Table 9.4-4 Performance Comparison of 1980 and 1993 PPC Models by Path Illumination Condition Using the Entire 1993 Phase Database for 10.2 kHz Signals

PATH ILLUMINATION CONDITION	RMS RANDOM ERROR (cec)	RMS BIAS ERROR/ TOTAL ERROR (cec)	
		1980 Model	1993 Model
Day*	4.4	11.3/12.1	7.3/8.5
Night§	5.0	10.2/11.4	7.0/8/6
Transition†	6.2	14.4/15.7	9.2/11.1
24-hour	5.3	12.1/13.9	7.9/9.2

* Day paths are defined as those with a maximum mid-path solar zenith angle of less than about 98°.

§ Night paths are defined as those with a minimum mid-path solar zenith angle of greater than about 98°.

† Transition paths are defined as those which are not classified as either day or night.

Thus, the performance of paths satisfying the day illumination condition is reduced relative to that computed for the earlier day-path definition (maximum path solar zenith angle less than about 74°). Of the three path illumination categories, night paths exhibit the best performance since their phase profiles show the least temporal variation and the anomalous path/times (most commonly occurring during path night) are removed.

The RMS error figures for the 1993 PPC Model are significantly lower than those for the 1980 PPC Model partly because the 1993 Model was "fit" to a subset of the database* for which the performance figures are given. To test the robustness of the 1993 PPC Model, bias and random errors were computed for a database containing different observations than those in the calibration database. In this test database, the *paths* were the same, but the observation times were different than those in the calibration database. Performance figures for the 1993 PPC model on this database are within 0.5 cec of those shown in Table 9.4-4.

9.5 APPENDIX: DEVELOPMENT OF PPC MODEL STRUCTURE

Though PPC models have evolved as the Omega system has developed, many essential features of these models have changed relatively little. In this section, a generic PPC model structure will be described, although, where appropriate, specific models will be identified.

9.5.1 Physical Basis of the Model Structure

The PPC, as described in Section 9.2, is defined as the variation of the "true," or expected, phase from the nominal phase (see Eq. 9.2-7). Thus, the calculation of the PPC involves the calculation of the nominal phase and the expected phase. The nominal phase, as described in Section 9.2.2, is calculated in a straightforward fashion, although it may involve computatio[illegible] of distance over an ellipsoidal earth. Thus, determination of the PPC involves predominantly calcu[illegible] of the expected phase. VLF signal phase, as measured over long signal paths, is a complex fun[illegible] numerous parameters, thus requiring a model of the propagating wave interacting with the earth-ionosphere electromagnetic environment.

The clearest understanding of the model structure is obtained by first considering the spatial "picture," i.e., a representation of the signal path between a source (transmitting station) and a point at which the signal field is sensed (receiver at or near the surface of the earth). One can use a variety of models, or paradigms, to describe the signal field structure as the propagating wave interacts with the earth and ionosphere on its way from the transmitting source to the receiver. In this development, it is

*The 1993 PPC calibration database comprised a set of measurements that are about 10 percent of the total database size.

convenient to use both the "wavehop" and "waveguide-mode" representations of signal wave propagation (see Chapter 5) to guide the physical picture and understanding of the process.

The electromagnetic wave launched by the Omega antenna has approximate cylindrical symmetry (with a vertical axis of symmetry) near the antenna. At greater ranges (e.g., more than about 10 km) from the antenna, the wave takes on a more spherical character. Finally, when the wave begins to interact with the ionospheric *D*-region (at ranges greater than 70 km), it locally resembles a plane wave (see Fig. 9.5-1). A plane wave is characterized by a wave vector, **k**, (see Section 9.2.1), in addition to the signal frequency. In the wavehop model, a plane wave reflects from the ionosphere (via a scattering process) and from the ground as it propagates between the earth and ionosphere (Fig. 9.5-2). Since the wave has a spherical character prior to interacting with the ionosphere, there is a nearly continuous spectrum of wave vectors corresponding to plane waves interacting with the ionosphere. However, only certain wave vectors give rise to "self-reinforcing," or resonant, field structures in the earth-ionosphere waveguide (see Chapter 5). These wave vectors make up a discrete spectrum that is directly associated with the spectrum of waveguide modes. As shown in Fig. 9.5-1, the wave vector which makes the

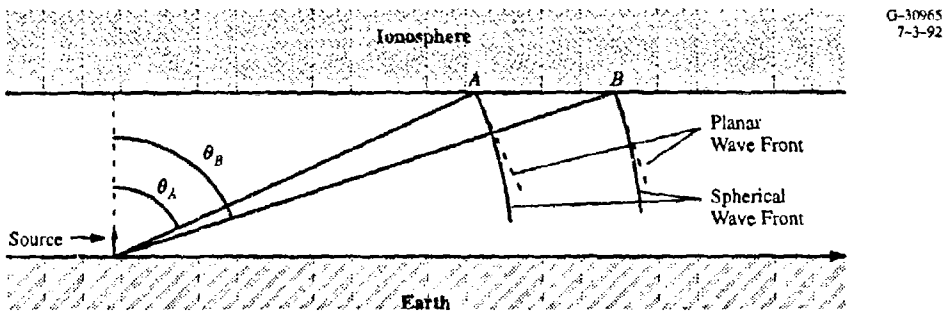

Figure 9.5-1 Plane Waves as Approximations to Spherical Waves When Encountering the Ionosphere

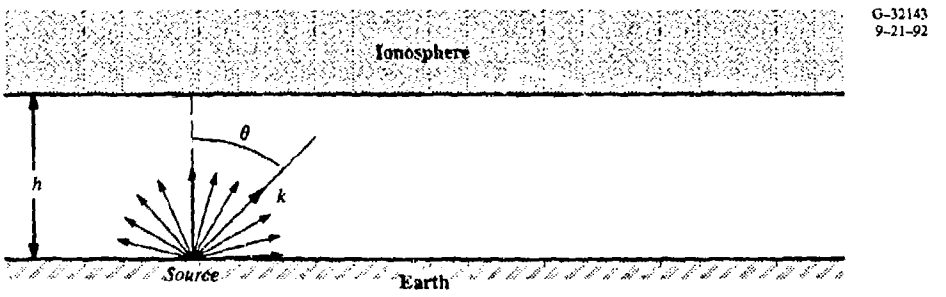

Figure 9.5-2 Continuous Spectrum of Wave Vectors Associated with Plane Waves Prior to Interaction with the Ionosphere

smallest angle to the ground is associated with the mode which normally survives to the longest ranges. Physically, this may be understood by noting that this wave suffers the fewest reflections from the ionosphere and the ground for a given distance over the earth. Each reflection reduces the wave energy so that the wave with the fewest reflections will generally have the greatest amplitude at a given range. The wave vector with the smallest launch angle (relative to the local tangent to the earth) is identified with "Mode 1," the lowest phase velocity TM mode (see Chapter 5). The properties of this mode, as noted in Sections 9.1 and 9.2, is the primary basis for the PPC model structure.

The point at which the Mode 1 wave vector intersects the ionosphere (see Fig. 9.5-3) is important because it determines the net ionospheric effect on the phase for all receiver locations "downstream" of the intersection point (known as the first point of ionospheric interaction (FPII)). Reciprocity arguments can be used to show that a similar wave vector configuration exists at the receiver. Thus, as shown in Fig. 9.5-3, a "Mode 1" wave vector is incident at the receiver from the ionosphere at the last point of ionospheric interaction (LPII). Between these two points of ionospheric interaction (which constitutes the majority of most paths), the wavefronts spread so that both upgoing and downgoing waves are present and the net wave vector is locally parallel to the ground.

Based on the above discussion, one can see that the portions of the ionosphere associated with the end-path regions, i.e., between the transmitting source and the FPII and the LPII and the receiver, will have little or no effect on the signal phase. In the end-path regions, only those electromagnetic properties of the earth's surface (i.e., ground conductivity) influence the signal phase detected at the receiver. For that portion of the path between the end-path regions, i.e., the mid-path region, both the ionosphere and the earth's surface influence the signal. Since the ionospheric properties (such as conductivity) change from day to night (and with relative position of the sun), time dependence of the signal phase is

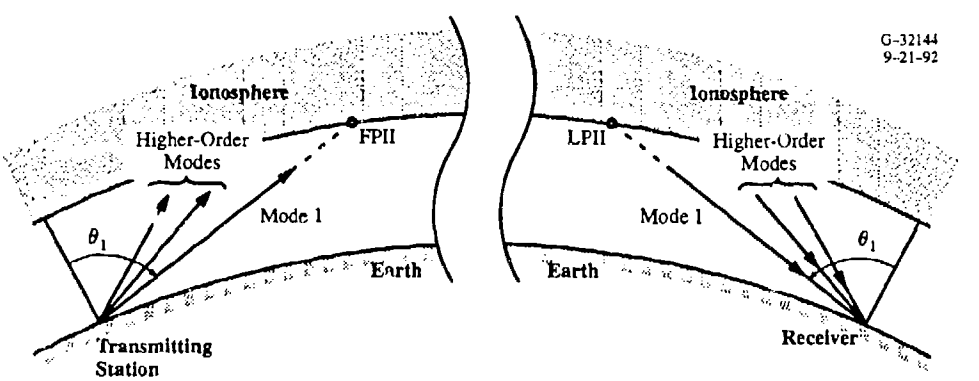

Figure 9.5-3 Transmitting Station-Receiver Signal Propagation Geometry Showing Transmitted and Received Mode 1 Wave Vectors

controlled by the ionosphere and, in particular, that portion of the ionosphere in the mid-path region. Since the geomagnetic field controls, to a large degree, the dynamics of the charged particles in the ionosphere, the local properties of this field in the mid-path region also greatly influence the phase at the receiver. The effects of the ionosphere and the earth's surface are thus conveniently organized in terms of "domains," which are presented in Section 9.5.4.

9.5.2 Path Definition and Phase Calculation

For the inhomogeneous paths encountered in the use of Omega signals, the predicted phase is expressed by the integral form given in Eq. 9.2-6. Actual calculations approximate this integral by a sum over path segments, i.e.,

$$\phi = \sum_i k_i \Delta r_i \qquad (9.5\text{-}1)$$

where k_i is the wave number for segment i and Δr_i is the length of the path segment. Figure 9.3-2 shows the segmentation for a typical path. An individual segment, which is shown in more detail in Fig. 9.3-3, is approximately 60 km in length. In the end-path regions, the segment serves to specify only the ground conductivity, since the Mode 1 wave vector is not influenced by the ionosphere in these portions of the path. For the mid-path region, the segment is associated with the local properties of both the earth's surface and the D-region of the ionosphere, which serve as boundaries of the space in which the signal is propagated.

In the waveguide-mode model of VLF signal propagation, each segment may be considered a homogeneous rectangular waveguide, i.e., one in which the boundaries are approximately straight and the geophysical/electromagnetic properties of the boundaries are approximately constant (see Chapter 5). In this homogeneous waveguide, the total electromagnetic field may be expressed as a sum of modal components, each of which has an associated phase and amplitude which are known functions of the boundary parameters. The vertical component of the electric field is expressed as a product of several complex quantities with a resultant amplitude and phase. The resultant phase is the sum of two terms: a "phase velocity" term (equivalent to the wave number expression for the phase defined in Eq. 9.2-6) and an excitation term. The excitation factor describes the efficiency with which the mode is excited by the waveguide. Thus, using the waveguide-mode model, the expression for the phase (Eq. 9.5-1) is modified to include the excitation factor phase, ϕ_e, i.e.,

$$\phi = \sum_i k_i \Delta r_i + \phi_e \qquad (9.5\text{-}2)$$

In principle, k_i and ϕ_e for the mid-path segments are derived from the modes of the homogeneous waveguide represented by the segment. The specific parameters associated with the signal modes are

based on the local properties of the waveguide boundaries. Because use of the FPC model presumes that the Mode 1 component dominates the total signal, the phase of the Mode 1 component (as a function of the boundary parameters) at each segment is obtained from the waveguide-mode model of signal wave propagation. For the segments in the end-path regions, a VLF ground-wave model of signal phase is appropriate.

9.5.3 Physical Parameters and Sub-models

The primary geophysical and electromagnetic quantities describing the earth-ionosphere waveguide affect the phase of the signal radiated by a ground-based source. The effects occur as the result of wave interactions with the waveguide boundaries whose properties are defined by:

- *Ground conductivity (VLF)* — over the entire path
- *Geomagnetic field vector (at D-region altitudes)* — in mid-path regions
- *Path orientation* — in mid-path region
- *Effective ionospheric reflection height* — in mid-path region.

Over most of the range of ground conductivity values, lower ground conductivities tend to increase the phase above its nominal behavior for both the mid-path and end-path regions. The component of the geomagnetic field vector that predominantly affects phase variation is the "dip" angle, i.e., the angle of the field vector below the horizon (see Fig. 9.5-4). With a dipole model of the geomagnetic field (see Fig. 9.5-5), a one-to-one relationship exists between the dip angle and the geomagnetic latitude for a given location. Another parameter closely associated with the geomagnetic latitude is the direction, or bearing of a path with respect to geomagnetic north (see Fig. 9.5-4). The effective ionospheric height for wave reflection is not an explicit parameter but is so important that the phase variation from the nominal is separately modeled for various values of height. For example, the phase behavior as a function of geomagnetic latitude and bearing is very different for ionospheric heights associated with day and night. In certain spatial regions, the effective ionospheric reflection heights diverge widely from "normal" values so that separate functional behavior is specified. The auroral zones and polar caps (see Fig. 9.5-6) are examples of regions with ionospheric heights that require special descriptions of phase behavior.

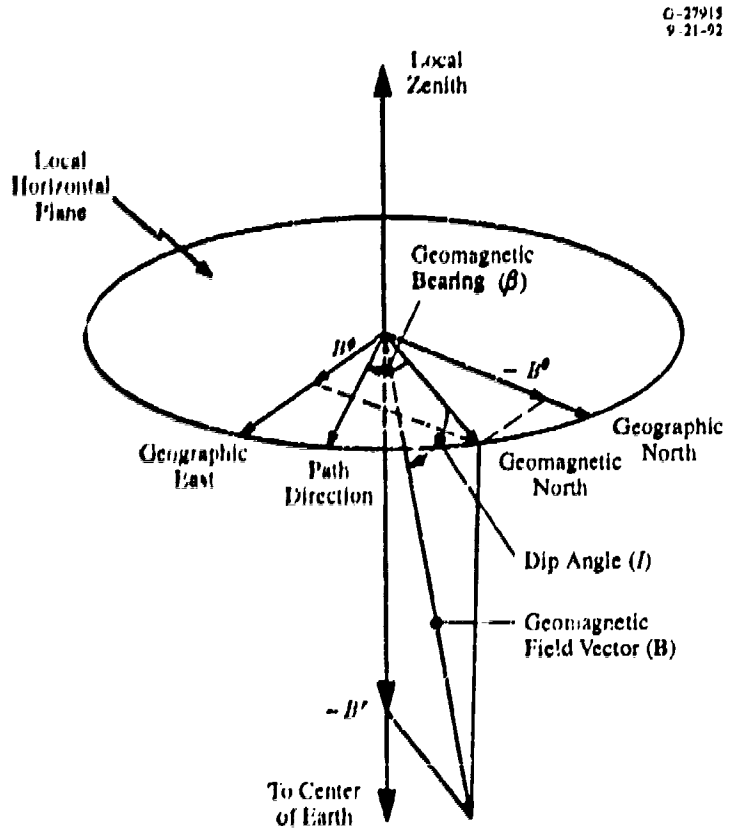

Figure 9.5-4 Path Direction and Components of the Geomagnetic Field Vector in Local Geographic Coordinate System

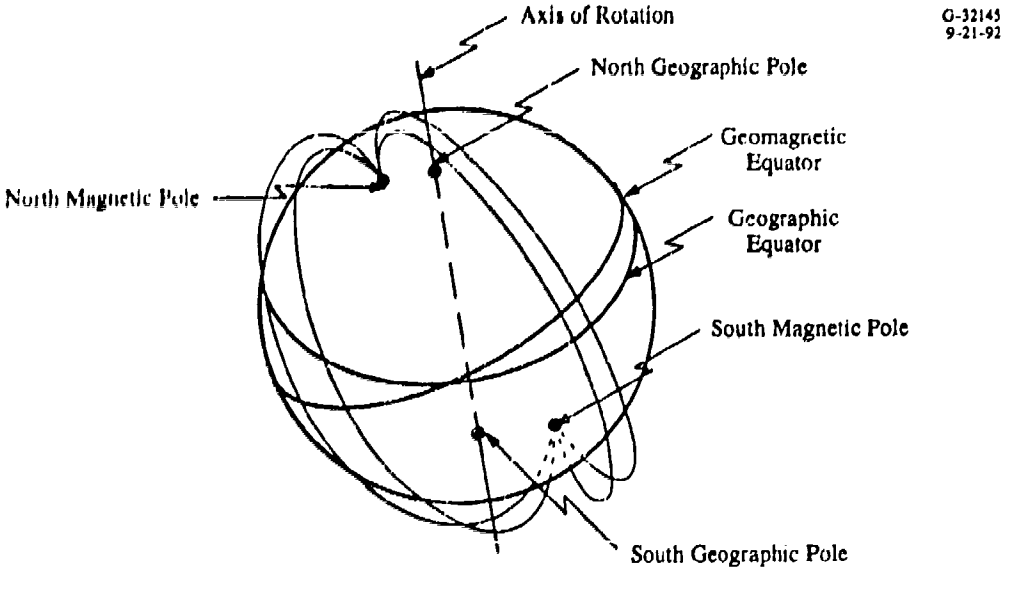

Figure 9.5-5 The Geomagnetic Field

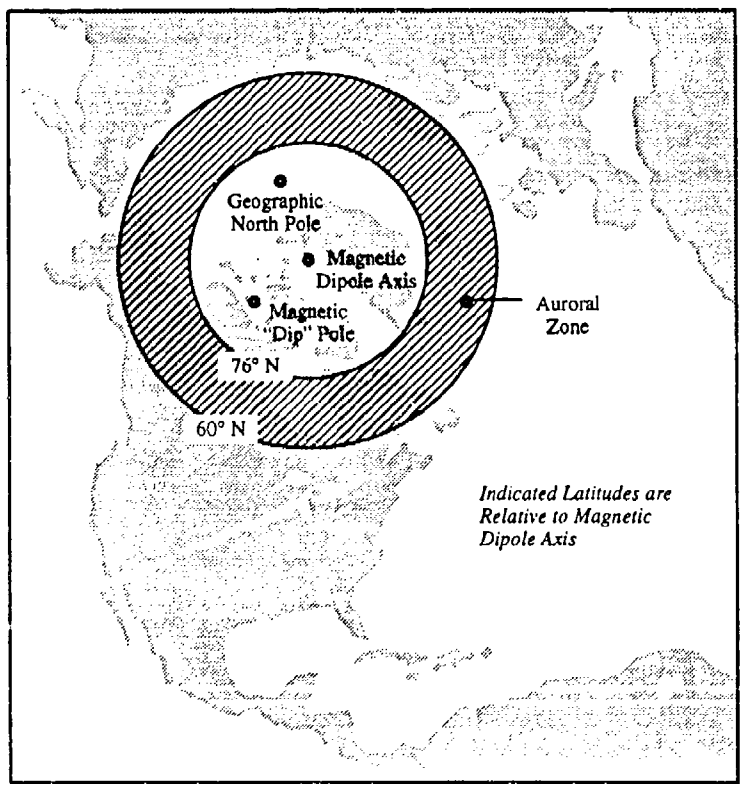

Figure 9.5-6 Effective Auroral Zone for VLF Propagation

Because the analytical form of the signal phase behavior in terms of the boundary parameters obtained from theoretical models is quite complex, *sub-models* have been developed to simplify and isolate the phase dependence in terms of one or two geophysical and electromagnetic boundary parameters. The basis for this simplification is that the wave number and excitation factor phase appearing in Eq. 9.5-2 are fairly well approximated by reference or nominal values, e.g., $k_0 L$ approximates the cumulative phase over a path of length L (k_0 is the free-space wave number) to within a few percent when the signal is Mode 1-dominated. For the conditions under which this approximation is reasonable, first-order corrections to the wave number and excitation factor phase may be used. To clarify this procedure, suppose that the wave number for a given segment is a function of one lower-boundary parameter (ground conductivity, σ) and one upper-boundary parameter (dip angle, I, of the geomagnetic field vector with respect to the local horizon). Then, to first order, the wave number is expressed as

$$k = k_0 + \left(\frac{\partial k}{\partial \sigma}\right)_0 \Delta\sigma + \left(\frac{\partial k}{\partial I}\right)_0 \Delta I \qquad (9.5\text{-}3)$$

where k_0 is the wave number for some initial conditions (e.g., seawater conductivity, zero dip angle), the partial derivatives of wave number (evaluated at the initial conditions) are determined from theoretical calculations, and $\Delta\sigma$, ΔI are incremental changes in conductivity and dip angle, respectively.

In actual practice, the "first-order" terms, e.g., the second and third terms of Eq. 9.5-3, are obtained using entities known as sub-models. A sub-model describes the theoretical phase variation (from the reference value) due to one or two geophysical/electromagnetic boundary parameters. To facilitate the calculation, the description is given in terms of *functional forms*, which are analytic or tabular functions approximating the indicated theoretical behavior. This approximation error and the linearization error implicit in Eq. 9.5-3 is at least partly accounted for by *linear model coefficients* that multiply each functional form. The sub-models are thus implemented as the product of the functional forms and the linear model coefficients. The linear model coefficients are determined by comparing the expression for the model prediction with the observed phase data. Once determined, the linear model coefficients indicate the relative contribution of the associated sub-model to the total phase variation.

First, consider the sub-models associated with the wave number (i.e., those depending on path length) in Eq. 9.5-2. Motivated by Eq. 9.5-3, the wave number for the I^{th} segment, k_I, is expressed in terms of the sub-models associated with each appropriate geophysical/electromagnetic parameter, i.e.,

$$k_I = k'_{0I} + \sum_J k_{IJ} \tag{9.5-4}$$

where k'_{0I} is the reference wave number at segment I, k_{IJ} is the wave number for the J^{th} sub-model at the I^{th} segment and the sum is over all sub-models applicable to segment I. Thus, Eq. 9.5-2 becomes

$$\phi = \sum_I k'_{0I}\,\Delta r_I + \sum_I \sum_J k_{IJ}\,\Delta r_I + \phi_r \tag{9.5-5}$$

For the mid-path segments, the wave number sub-models are obtained from precise calculations of Mode 1 signal parameters, specifically phase velocity. Plots or tabulations of Mode 1 phase velocity (v) are usually in terms of the relative phase velocity variation (from the free-space wave propagation velocity) per unit wavelength, i.e.,

$$(v/c - 1)/\lambda$$

where c is the speed of light (*in vacuo*) and λ is the free space wavelength (see Fig. 9.5-7). This quantity (which has wave number units) is computed as a function of the geophysical parameter(s) associated with each sub-model. The functional forms are obtained as approximations (involving one or more

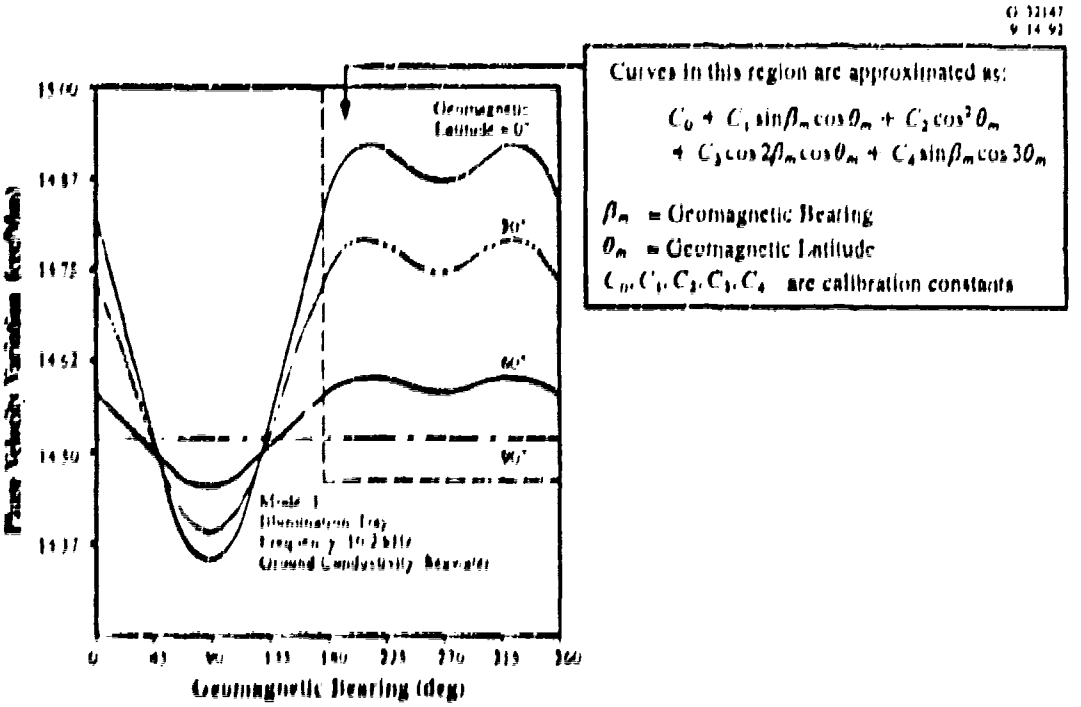

Figure 9.5-7 Day Phase Velocity Variation Over Seawater as a Function of Geomagnetic Latitude and Bearing: Theory-based Plot and Sub-model Approximation

"simple" functions) to the computed data. Figure 9.5-7 provides a simple example of a sub-model approximation to the theoretical behavior of day phase velocity variation over seawater as a function of geomagnetic bearing (β_m) and latitude (θ_m) for $\beta_m > 180°$. A similar form is obtained for $\beta_m < 180°$, although the value of the calibration constant c_1 would change. Recalling that a sub-model is implemented as the product of linear model coefficient and a functional form, a phase velocity sub model at segment i is expressed as

$$CF_i = (v_i/c - 1)/\lambda = (v_i/c - 1)k_0 \qquad (9.5\text{-}6)$$

where C is the linear model coefficient (in units of cycles/Megameter(Mm)) associated with dimensionless functional form F_i (having magnitude between 0 and 1) evaluated at path segment i, and k_0, the free space wave number, is the reciprocal of the wavelength, λ. The wave number corresponding to phase velocity v_i is $k_i = f/v_i$ where f is the signal frequency. Using this relationship and Eq. 9.5-6 yields

$$k_i = k_0/(1 + CF_i/k_0) \qquad (9.5\text{-}7)$$

Now, the phase velocity v_i appearing in Eq. 9.5-6 is typically close to c, e.g., for daytime north-south paths over seawater, v_i is about 1.004 c. As a result, the magnitude of $v_i/c - 1$ is typically much smaller than 1 so that Eq. 9.5-6 implies that $CF_i << k_0$. With this result, the denominator of Eq. 9.5-7 may be expanded to yield

$$k_i = k_0(1 - CF_i/k_0 + \ldots) \tag{9.5-8}$$

Thus, to a good approximation, k_i is given by $k_0 - CF_i$. In general, there are a number of phase velocity sub-models, e.g., those associated with different ground conductivity values or ranges of geomagnetic bearing. Thus, Eq. 9.5-8 is generalized to the form

$$k_i = k_0 - \sum_j C_j F_{ij} \tag{9.5-9}$$

where the sum is over the phase velocity sub-models applicable to segment i. Comparison of Eqs. 9.5-4 and 9.5-9 suggests the use of the free-space wave number k_0 as the reference wave number. The comparison also indicates that $k_{ij} = -C_j F_{ij}$ so that Eq. 9.5-5 becomes

$$\phi = k_0 L - \sum_i \sum_j C_j F_{ij} \Delta r_i + \phi_e \tag{9.5-10}$$

where L is the path length. The phase due to the ground-wave sub-model is a function of path length and thus also may be expressed as a wave number form (Eq. 9.5-9).

The excitation factor phase is not a function of path length but has a relationship to the excitation sub-models which is similar to that for the phase velocity sub-models. Thus, precise calculations of Mode 1 signal parameters also include excitation factor phase as a function of the appropriate geophysical parameters such as ground conductivity and path bearing (geomagnetic). Approximations to these functional relationships by simple functions or data tables give the functional forms for the excitation sub-models. Thus, for the j^{th} excitation functional form and the i^{th} segment

$$C_j' F_{ij}' = \phi_e$$

where the prime indicates quantities (linear model coefficients and functional forms) belonging to the excitation sub-models. Thus, Eq. 9.5-10 becomes

$$\phi = k_0 L - \sum_i \sum_j C_j F_{ij} \Delta r_i + \sum_j C_j' F_{ij}' \tag{9.5-11}$$

9.5.4 Sub-model Domains

As noted above, the wave field associated with the transmitted signal and sensed by the Omega receiver interacts with the earth's surface and ionosphere (the waveguide boundaries) in a way that depends on the relative path position. Path domains are those portions of the path that have similar wave-boundary interactions and therefore invoke the same sub-models. The domains are referenced by the type(s) of sub-models invoked therein, i.e.,

- Ground-wave domain
- Excitation domain
- Phase velocity domain.

As shown in Fig. 9.3-4, the ground-wave domain comprises the two end-path regions.* Since, in this domain, the wave only interacts with the earth's surface (the lower boundary of the earth- ionosphere waveguide), the corresponding sub-models depend only on ground conductivity. Table 9.5-1 (from Ref. 8) lists the ten conductivity levels and corresponding conductivity values (in mho/m) which are believed to adequately characterize the worldwide surface conductivities at VLF. Also listed are the corresponding permittivity values relative to the permittivity of free space.

Table 9.5-1 Earth's Ground Conductivity Levels and Associated Conductivity/Permittivity Values

LEVEL	CONDUCTIVITY (mho/m)	RELATIVE PERMITTIVITY
1 (Ice Cap)	1.0×10^{-5}	10.0
2	3.2×10^{-5}	10.0
3	1.0×10^{-4}	15.0
4	3.2×10^{-4}	15.0
5	1.0×10^{-3}	15.0
6	3.2×10^{-3}	15.0
7	1.0×10^{-2}	20.0
8	3.2×10^{-2}	20.0
9	1.0×10^{-1}	45.0
10 (Seawater)	4.0	81.0

The size of the ground-wave domain is fixed in most PPC models but in the 1993 PPC model, the extent of this domain varies with the local illumination condition. This is because the point of interaction between the Mode 1-launched wave and the ionosphere (see Fig. 9.5-3) depends on the ionization profile of the local ionosphere, i.e, the effective wave reflection height at the point of interaction. Thus,

*In some of the PPC Model literature, the end-path region near the transmitter is called the excitation region and the end-path region near the receiver called the de-excitation region.

the point of wave-ionosphere interaction depends on the local time at or near the interaction point. As a result of this dependence, the distance from the transmitting station (or the receiver) to the first wave-ionosphere interaction point typically ranges between 350 and 850 km. The precise range of this interaction point is an implicit parameter in the 1993 PPC Model and is discussed further in Section 9.5.6. A simple bias sub-model is invoked in this domain (and in all other domains) to align the zero-point of the diurnal phase with the nominal wave number.

In the 1980 PPC Model, the ground-wave domain extends to about 700 km, independent of the local illumination condition. In this regime, a "base velocity" sub-model is invoked which is similar to the 1993 bias sub-model in the sense that it serves as a correction to the nominal phase. In an earlier version of the 1980 model, a long-term year-dependent sub-model was also invoked in this domain.

Table 9.5-2 compares the ground-wave sub-models for the 1993 and 1980 PPC Models. This table indicates the portion (path segment) of the domain in which each type of sub-model is invoked, the type of functional form used for the sub-model, and the intended effect captured or described by the sub-model. In the 1993 PPC Model, the cumulative ground-wave phase is well-approximated by a linear function of distance (see Fig. 9.5-8)*, so that the functional form (invoked at each segment) is constant.

Table 9.5-2 Ground-wave Sub-models

Sub-Model Category		Where invoked	Type of Functional Form	Effect Captured by Sub-model
1980 Model	1	All segments	Constant	"Base velocity" term; similar to bias term in 1993 PPC Model*
1993 Model	1	All segments and path regions		Ground-wave phase contribution for each of 7 conductivity levels
	2			"Bias term" for correction to free-space wave number reference*

* Sub-model does not strictly describe ground-wave phase contributions; rather it represents a path-length-dependent bias common to all domains.

The excitation domain comprises that region of a path where the Mode 1-launched wave first (or finally) sets up the field structure which characterizes its general behavior in the earth-ionosphere waveguide. The nomenclature derives from the waveguide-mode model of VLF wave propagation in which a source wave is "excited" (to various degrees) in the earth-ionosphere waveguide. The degree of excitation depends on the signal wavelength/frequency, the size (height) of the waveguide, and the

*In Fig. 9.5-9 (from Ref. 14), the ground-wave phase is plotted as a function of logarithmic distance; as a function of linear distance, however, the phase behavior is very nearly linear.

electromagnetic properties of the internal medium and the boundaries of the waveguide. Thus, an excitation phase is said to be introduced in the propagated signal field where the wave first "sees" the ionosphere. Reciprocity arguments show that an excitation phase is introduced near both the transmitting source and the receiver.

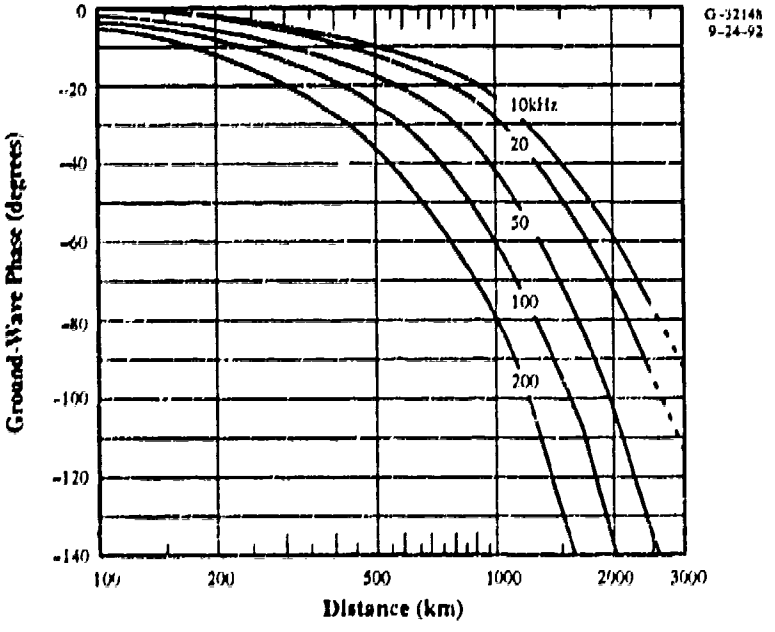

Figure 9.5-8 Ground-wave (Norton Surface Wave) Phase over Seawater as a Function of Distance from Source

For the 1993 PPC model, the excitation domain is taken to be the segment within each end-path region which borders the mid-path region (see Fig. 9.3-4). At these segments, the Mode 1-launched wave begins (or ends) its local interaction with the ionosphere. Thus, the excitation sub-models exhibit a coupled dependence on the ground conductivity and the ionospheric parameters, including geomagnetic latitude and bearing. "Coupled" means that the sub-model functional form cannot be written as a product of functions which depend only on one of the parameters, e.g., $F_j(\sigma, I) \neq g(\sigma)\, h(I) \Rightarrow \sigma$ and I are coupled with respect to F_j where σ and I are the ground conductivity and magnetic dip angle used in Eq. 9.5-3.

The excitation domain for the 1980 PPC model includes the entire end-path region. The ground conductivity throughout both end-path regions is assumed to contribute to the excitation of the signal, although the ionospheric contribution is computed at isolated points in the end-path regions. Thus, the conductivity-dependent excitation sub-model (which is de-coupled from the ionosphere-dependent

forms) is summed over each end-path region but invoked at the segments bordering the mid-path region. The excitation sub-models which depend on the geomagnetic field quantities (geomagnetic bearing and dip angle) are invoked at the second and next-to-last segments of the path. The excitation domain sub-models for the 1980 and 1993 PPC Models are compared in Table 9.5-3.

Table 9.5-3 Excitation Sub-models*

Sub-Model Category		Where Invoked	Type of Functional Form	Effect Captured by Sub-model
1980 Model	1	Last segment in xmtr. endpath region and last segment in rcvr. end-path region§	Power-law dependence on conductivity level (1–10) averaged over end-path region segments	Excitation factor phase due to ground conductivity throughout each end-path region
	2	Second path segment and next-to-last path segment	Constant	Separate bias term for excitation factor phase dependence
	3		Bilinear combinations of β_m and I for various ranges of β_m	Mode 1 excitation factor phase due to geomagnetic field (β_m and I)
1993 Model	1	Last segment in xmtr. endpath region and first segment in rcvr. end-path region	Constant and Fourier-type functions of β_m and θ_m	Mode 1 excitation factor phase behavior in terms of β_m and θ_m for day and night at each of 7 conductivity levels
	2		Products of Fourier-type functions of β_m and θ_m	Mode 1 excitation factor phase behavior in terms of β_m and θ_m for day-only at each of 7 conductivity levels
	3		Products of Fourier-type and Gaussian functions of β_m and θ_m.	Mode 1 excitation factor phase behavior in terms of β_m and θ_m for night-only at each of 7 conductivity levels

* In this table, β_m is the geomagnetic bearing measured clockwise from geomagnetic north; θ_m is the geomagnetic latitude assuming an earth-centered dipole representation of the geomagnetic field; I is the dip angle (see Fig. 9.3-6).

§ Sub-model is actually computed over each complete end-path region but invoked (i.e., included in the phase calculation) at segments bordering the mid-path region.

For the vast majority of paths used in navigating with Omega signals, the phase velocity domain constitutes more than 80 percent of the path. This domain corresponds to the mid-path region (see Fig. 9.3-4) where the signal interacts with both the ionosphere and the earth's surface. In this domain, the phase/unit path length is specified by the wave number, as in Eq. 9.5-1.

In the 1993 PPC Model, there are two kinds of phase velocity sub-models: those that depend on ground conductivity and those that do not. For the conductivity-dependent phase velocity sub-models, the phase variation (through the wave number or phase velocity) depends on three coupled parameters: ground conductivity, geomagnetic latitude, and geomagnetic bearing. This coupling increases the number of phase velocity sub-models required for characterization of the phase variation, although the increase is partially compensated by limiting the number of effective conductivity levels to seven. The conductivity-independent sub-models are those that describe the local wave number behavior in spatial regions having "anomalous" ionospheric height profiles, i.e., the auroral zones and polar caps.

The coupling between the conductivity and ionospheric parameters is assumed to be weak in the 1980 PPC Model, so that separate sub-models are specified for conductivity and other parameters in the phase velocity domain. Because of the strong coupling between the dip angle and geomagnetic path bearing, however, the corresponding sub-models are coupled in the 1980 PPC Model. The sub-models for the auroral zones and polar caps are identical for the 1993 and 1980 PPC Models. Table 9.5-4 provides a comparison of the phase velocity domain sub-models used in the 1980 and 1993 PPC Models.

Table 9.5-4 Phase Velocity Sub-models*

Sub-Model Category		Where Invoked	Type of Functional Form	Effect Captured by Sub-model
1980 Model	1	All segments	Constant	"Base velocity" term; similar to bias term in 1993 PPC Model§
	2	All segments in mid-path region	Products of Fourier-type functions of β_m and power-law functions of (0.9–0.573I/λ)	Mode 1 phase velocity (wave number) behavior in terms of β_m and I for seawater cond.
	3		Constant	Phase velocity (wave number) variation (from seawater) at each of 7 cond. levels
	4	Segments with $\lvert\theta_m\rvert > 1$ radian	Gaussian forms centered at 2 θ_m-values with same effective widths	Auroral zone ionospheres at $\lvert\theta_m\rvert$ = 65° and 69° with the same 1-σ width of 2°
	5	Segments with $\lvert\theta_m\rvert > 1.0821$ radian	Linear form increasing toward pole	Polar Cap ionosphere increasing in height poleward from $\lvert\theta_m\rvert$ = 62°
1993 Model	1	All segments in mid-path region	Constant	"Bias term" for correction to free- space wave number reference§
	2		Constant and products of Fourier-type functions of β_m and θ_m	Mode 1 phase vel. (wave number) behavior in terms of β_m and θ_m for day and night at each of 7 conductivity levels
	3		Products of Fourier-type functions of β_m and θ_m	Mode 1 phase vel. (wave number) behavior in terms of β_m and θ_m for day-only at each of 7 conductivity levels
	4		Products of Fourier-type functions of β_m and exponential functions of θ_m	Mode 1 phase vel. (wave number) behavior in terms of β_m and θ_m for night-only at each of 7 conductivity levels
	5	Segments with $\lvert\theta_m\rvert > 1$ radian	Same as 1980 PPC Model	Same as 1980 PPC Model
	6	Segments with $\lvert\theta_m\rvert > 1.0821$ radian		

* In this table, β_m is the geomagnetic bearing measured clockwise from geomagnetic north; θ_m is the geomagnetic latitude assuming an earth-centered dipole representation of the geomagnetic field; I is the dip angle (see Fig. 9.3-6).

§ Sub-model does not strictly describe phase velocity contributions; rather it represents a path-length dependent bias common to all domains.

9.5.5 Time Dependence

Up to this point, the discussion of the PPC model structure has primarily focused on the "spatial" component of the predicted phase calculation. For the boundary parameters of interest at Omega frequencies, the time dependence is introduced solely through the action of solar illumination of the ionosphere. The only time-dependent quantities mentioned so far, the effective ionospheric reflection

height and the extent of the ground-wave regions, are dependent on the local solar illumination. Thus, the sub-models which depend on the ionospheric height (i.e., those in the phase velocity and excitation domains) contribute to the time dependence of the predicted phase. Because Omega paths are typically long and the phase variation is highly sensitive to the local illumination condition (or ionospheric height), the time variable is of equal importance to the space variables in the prediction of signal phase.

The excitation and phase velocity sub-models described in Section 9.5.5 contain approximate forms for the components of the signal phase as a function of one or more geophysical/electromagnetic parameters. As derived from theory, these sub-models are given for two extreme states of the ionosphere:

- Local maximum day (sun directly overhead)
- Local maximum night (sun directly overhead at the antipode (opposite point on the earth)).

For intermediate states of the ionosphere, special functions (known as evolution or diurnal functions) appropriately combine the above-defined local maximum day and local maximum night sub-models. These intermediate states correspond to different times of day/year* in which the relative earth-sun position causes different ionization profiles in the ionosphere. The functional forms for local maximum day and local maximum night are sometimes very different and sometimes the same, depending on the functional behavior of the phase in terms of the underlying geophysical parameter. The linear model coefficients for local maximum day and local maximum night are nearly always different, however, to capture the differences in the day and night phase behavior.

To understand how the day and night sub-models are combined to produce a phase prediction at an arbitrary time, a greatly simplified model is considered to illustrate and clarify the underlying procedure. This simplified model specifies:

- A single mid-path sub-model with:

  functional form F_D and linear model coefficient C_D for local maximum day

  functional form F_N and linear model coefficient C_N for local maximum night
- A single segment of length Δr for the mid-path located at the equator during one of the equinoxes
- An end-path region fixed in size with no sub-models invoked.

*The quiet ionosphere has a relatively slow systematic change from day-to-day (at the same hour) over a year; random day-to-day fluctuations about this long-term variation are significant, however, and result in a random phase error of about 3 to 6 cec.

Using this simplified model and path, the predicted phase at the receiver (relative to the phase of the transmitted signal) when the sun is directly overhead (local maximum day) is

$$\phi_D = k_{NOM}\,\Delta r + C_D\,F_D \tag{9.5-12}$$

and 12 hours later (at local maximum night), the phase prediction is given by

$$\phi_N = k_{NOM}\,\Delta r + C_N\,F_N \tag{9.5-13}$$

where k_{NOM} is the nominal wave number (see Section 9.2.2). Since the phase velocity is greater for day paths than night paths (see Chapter 5), the day wave number is smaller than the night wave number (recall from Section 9.5.3 that phase velocity = frequency/wave number). Thus, the day phase, ϕ_D, is smaller than the night phase, ϕ_N, by an amount known as the *diurnal shift*. If the single sub-model invoked on the single mid-path segment is chosen to be the bias (1993 PPC Model) or base velocity (1980 PPC Model), then $F_D = F_N = 1$, and the diurnal shift is given by

$$\phi_N - \phi_D = C_N - C_D \tag{9.5-14}$$

For times other than local maximum day or local maximum night, the cumulative phase for this path is given by

$$\phi = k_{NOM}\,\Delta r + (C_N - C_D)\,f + C_D \tag{9.5-15}$$

where f is an interpolation function that varies with the *solar zenith angle*, i.e., the relative degree of solar illumination on the ionosphere of the 1-segment path (see Fig. 9.5-9). Note that, for consistency with Eqs. 9.5-12 and 9.5-13, the function f in Eq. 9.5-15 must have the value 1 for local maximum night and 0 for local maximum day. The function f is called the diurnal function in descriptions of the 1980 PPC Model and is related to the evolution function defined by the 1993 PPC Model.

The diurnal function shown in Fig. 9.5-10 for 10.2 kHz was obtained (Ref. 11) by means of a simplified photoionization model coupled with experimental observations. The function is plotted in terms of $\cos\chi$ (χ = solar zenith angle) and is divided into three illumination categories: night, transition, and day. The constant value ($f = 1$) at night means that no night variation in phase is predicted by this model for local solar zenith angles (χ) varying from 180° (local maximum night) to about 99°. A steep decline in the function occurs during transition, which is defined for $\chi = 99°$ to about 74°, although this latter number varies with frequency. During transition, a "dynamic" diurnal function and sunrise/sunset

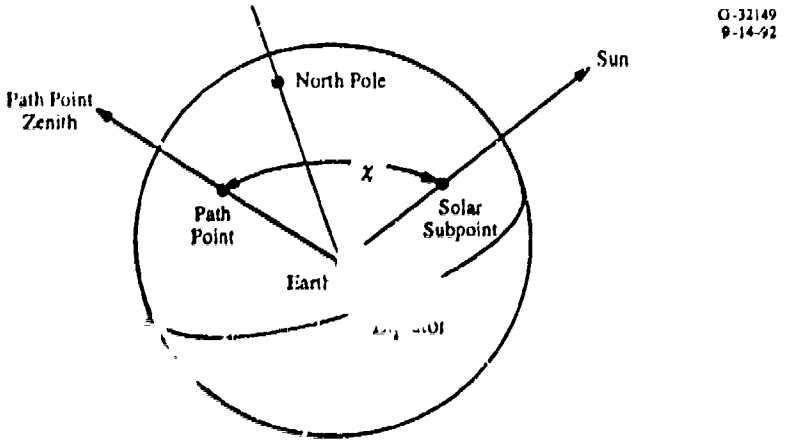

Figure 9.5-9 Solar Zenith Angle (χ)

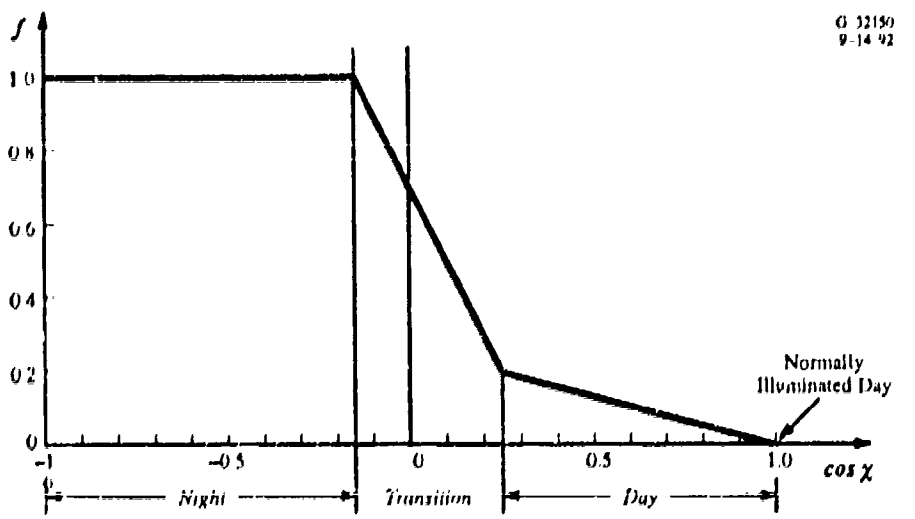

Figure 9.5-10 Diurnal Function *f* in Terms of cos χ (χ = Solar Zenith Angle) for 10.2 kHz

"dumps" are also invoked in the 1980 PPC Model. The dynamic diurnal function, *g*, is obtained from a differential relation analogous to a continuity equation for free electrons/ions in the ionospheric D region.* The "static" diurnal function, *f*, serves as the driving function for this dynamical relation. Also included in the dynamical relation for *g* is an impulsive-type forcing function describing the dynamics of weakly attached electrons which are rapidly injected into the transition ionosphere. The

*The continuity equation used as the basis for this calculation assumes a linear electron loss dependence, whereas most current work suggests a quadratic loss dependence (Ref. 12).

time profiles for these injections, known as "dump schedules," are specified separately for sunrise and sunset. During the day illumination, the diurnal function is given by a decreasing linear function of $\cos\chi$, approaching zero for normally illuminated day. This portion of the diurnal function (which has a substantially smaller slope than that for transition) gives rise to the familiar "bowl-shaped" daytime phase profile for a full (multi-segment) path illustrated in Fig. 9.2-3.

For the 1993 PPC Model, separate daytime and nighttime evolution functions are defined. The daytime evolution function (E_D), illustrated in Fig. 9.5-11a for 10.2 kHz, describes the time variation of sub-models associated only with daytime phase behavior, while the nighttime evolution function (E_N), illustrated in Fig. 9.5-11b, describes the time variation of sub-models associated only with nighttime phase behavior. The daytime evolution function "turns on" at a threshold solar zenith angle χ_{THR} of 98.0°, which was determined from analysis of continuously recorded data. The steep rise between $\chi = \chi_{THR}$ and $\chi = 84.3°$ ($\cos\chi = 0.1$ *) is better fit by a linear function than by the logarithm of a Chapman function (as discussed in Ref. 8). Between $\chi = 84.3°$ and $\chi = 0°$ ($\cos\chi = 1$), the evolution function behaves linearly with $\cos\chi$, suggesting multiple layers or a broad spectrum of photoionization energies. The nighttime evolution function varies linearly with $\cos\chi$ from $\chi = 180°$ to $\chi = \chi_{THR}$ based on observed "clean" (Mode 1-dominant) nighttime phase behavior and satellite data on solar radiation scattered through the geocorona (Ref. 8). For sub-models which apply to both daytime and nighttime ionospheres (same functional forms), the two evolution functions are linearly combined to yield

$$E_0 = 1.8e^{-\sigma_1 E_D} - 0.9e^{-\sigma_2 E_N}$$

where $\sigma_1 = 0.69315$ and $\sigma_2 = 0.1178$. This form resembles the diurnal function when plotted as a function of $\cos\chi$.

As noted above, the diurnal and evolution functions depend on certain experimentally determined parameters. For the diurnal function, these include day and night time constants, and the sunrise/sunset dump schedule profile. The evolution functions depend on three implicit parameters: (1) the threshold solar zenith angle, (2) the daytime ionospheric response time, and (3) the nighttime ionospheric response time; these are a subset of the more general onset/recovery time parameters (ORTP) which control the time dependence of the phase. The remaining ORTP define the size of the end-path regions, and thus effectively, the size and position of the ground-wave, excitation, and phase velocity domains.

---

* The breakpoint for E_D (see Figure 9.5-11a) varies with frequency; thus, for 10.2 kHz, E_D ($\cos\chi = 0.1$) = 0.5850, for $11^1/_3$ kHz, E_0 ($\cos\chi = 0.05$) = 0.5850, and for 13.6 kHz, E_D ($\cos\chi = 0.0$) = 0.5850.

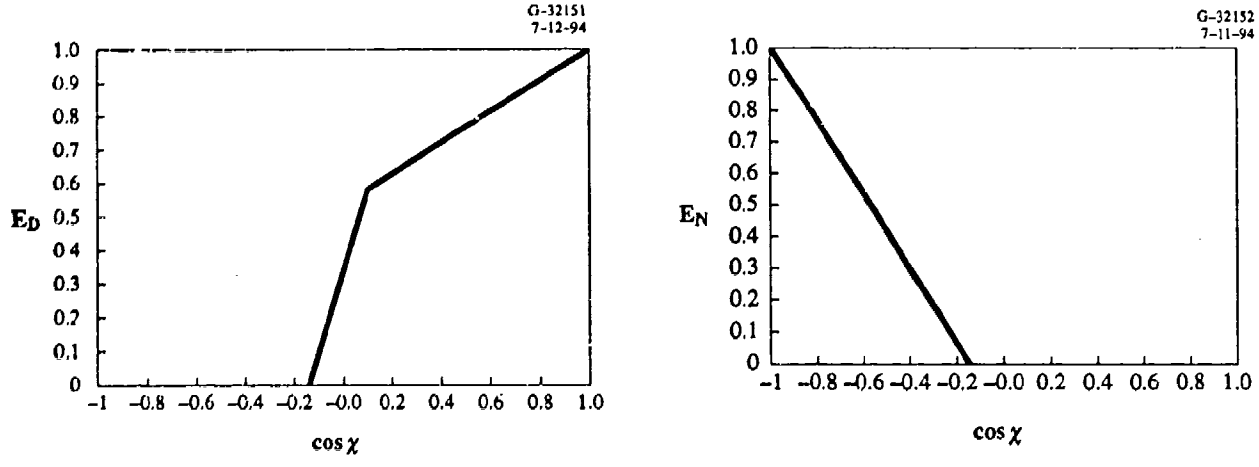

a) Daytime b) Nighttime

Figure 9.5-11 Evolution Functions for 10.2 kHz Used in 1993 PPC Model

9.5.6 Summary of Model Structure

The PPC model structure may be summarized by inspecting the general expression for the path cumulative phase, incorporating both spatial and temporal effects. The simple model/path considered in Sec. 9.5.6 to illustrate the time dependence of the phase, given by Eq. 9.5-15, is easily generalized. For a model containing a mix of separately or identically defined local maximum day and local maximum night sub-models and a multi-segment path, the phase is obtained by inserting the time-dependent form of Eq. 9.5-15 into the time-independent expression for the phase given by Eq. 9.5-11. The resulting expression for the predicted cumulative phase for an Omega signal at a given frequency for a specified path at time t is given by

$$\phi(t) = k_0 L - \sum_i \sum_j \left[\left(C_{N_j} F_{N_{ij}} - C_{D_j} F_{D_{ij}} \right) f_i(t) + C_{D_j} F_{D_{ij}} \right] \Delta r_i$$

$$+ \sum_i \sum_j \left[\left(C'_{N_j} F'_{N_{ij}} - C'_{D_j} F'_{D_{ij}} \right) f_i(t) + C'_{D_j} F'_{D_{ij}} \right] + \sum_i \sum_j C_j F_{ij} \Delta r_i \qquad (9.5\text{-}16)$$

In the above expression, the first term gives the free-space contribution, which accounts for about 99% of the cumulative phase. The first double sum specifies the contribution from the phase velocity domain, with index i referring to the path segment (and thus, indirectly, the spatial coordinates) and index j identifying the particular sub-models. Note that the linear model coefficients for local maximum day

(C_{D_j}) and local maximum night (C_{N_j}), are associated with sub-model j but independent of segment (spatial position). The functional forms for local maximum day ($F_{D_{ij}}$) and local maximum night ($F_{N_{ij}}$), however, depend on both spatial position and the invoked sub-model. The diurnal function, f, depends on the time, t, and the spatial position of the path segment through the solar zenith angle. Since the phase velocity sub-models have the dimensions of wave number (and f is dimensionless), they are multiplied by the segment length, Δr_i. The second double sum in the above expression gives the contribution from the excitation domain. This portion of the expression is similar to that of the phase velocity domain except that different (and far fewer) spatial segments are involved and, of course, the sub-model functional forms are different. Also note that the path segment length is not included as a factor since excitation is not a "wave number-like" quantity. The last double sum represents the ground-wave domain contribution in which the sub-models are explicitly time-independent since the Mode 1-launched/received wave does not interact with the ionosphere in this domain. The sub-models in this domain behave as wave numbers and so must be multiplied by the path segment length, Δr_i.

9.6 PROBLEMS

9.6.1 Sample Problem with Solution

1. An aircraft is flying due east at 400 knots (nautical miles/hour). An Omega receiver on board the aircraft measures the phase of a 10.2 kHz signal transmitted from a station located exactly southwest of the aircraft's current position. Assume that phase measurements are effectively made every 2 minutes with respect to a stable oscillator/clock.

   a. Do the successive phase readings increase or decrease?

   b. What is the lane width of the signal?

   c. How many times per hour would the aircraft cross lane boundaries?

   d. For fastest crossing of lane boundaries, which direction should the aircraft travel (maintaining the same speed)?

   Assume that the PPC at the first lane boundary crossing is 5 cecs and the PPC at the next lane boundary crossing is 10 cecs.

   e. Does the phase measured by the receiver at the second lane boundary crossing change by more than one cycle or less than one cycle with respect to the phase measurement at the first lane boundary crossing?

   f. Using the free-space wave number, find the actual distance the aircraft travels when the *measured* phase change is one cycle.

1. Solution:

a. Since the station is to the southwest of the aircraft, "away" from the station would encompass all aircraft headings northwest (315°) clockwise through southeast (135°). The aircraft is heading east which is within this range and so is moving away from the station. Since the aircraft receiver measures phase with respect to a stable clock, the phase will be correct to within an additive constant. Thus, the phase reading (proportional to distance within an additive constant) will increase as the aircraft moves away from the station.

b. For this "direct-ranging" case, the lanewidth is just the free-space signal wavelength, which is just c/f, where c is the speed of light in free space and f is the frequency. Thus, for this 10.2 kHz signal,

$$\text{lanewidth} = (2.99793 \times 10^5 \text{ km/sec}) / 10{,}200 \text{ Hz}$$
$$= 29.3915 \text{ km}$$

c. Since the station is assumed to have an exact southwest bearing (225°) from the aircraft, the lane boundaries (lines of constant range) are locally approximated by straight lines extending from southeast (135°) to northwest (315°). Since the aircraft is headed due east, it crosses the lane boundaries at 45°, so that the distance between lane boundaries is (lanewidth) $\cdot \sqrt{2}$, where the lanewidth is computed in (b). In terms of km/hr, the aircraft speed is 740.8 so that the number of lane boundary crossing/hour is

$$(740.8 \text{ km/hr}) / (29.3915 \cdot \sqrt{2}) \text{ km} = 17.8 \text{ (1/hr)}$$

In other words, the aircraft crosses a full lane in slightly more than 3 minutes. Since the time constant is 2 minutes, the receiver is not likely to slip lanes.

d. The fastest (or shortest) crossings of the lanes are those with tracks perpendicular to the lane boundaries. Since the lane boundaries extend from southeast to northwest, the fastest crossing (at fixed aircraft speed) is from southwest to northeast or northeast to southwest.

e. From Eq. 9.2-3 (and the one immediately preceding it in Section 9.2.1), the nominal form of the measurements at the two successive lane boundaries is (phase quantities in cycles) given by:

$$\phi_1' = \phi_1 + PPC_1 = \phi_1 + 0.05$$

$$\phi_2' = \phi_2 + PPC_2 = \phi_2 + 0.10$$

where ϕ_1 and ϕ_2 are the measured phase values at the first and second lane boundary crossing, respectively. Thus

$$\phi_2' - \phi_1' = \phi_2 - \phi_1 + 0.05 \qquad (9.6\text{-}1)$$

or

$$\phi_2 - \phi_1 = \phi_2' - \phi_1' - 0.05 \qquad (9.6\text{-}2)$$

Now, since the nominal phase values at the lane boundaries differ by a cycle (by definition), Eq. 9.6-2 yields

$$\phi_2 - \phi_1 = 1.0 - 0.05 = 0.95$$

Thus, the measured phase values differ by less than a cycle.

f. Since we are told that the measured phases at the successive lane boundaries differ by one cycle, Eq. 9.6-1 yields

$$\phi_2' - \phi_1' = 1.0 + 0.05 = 1.05 \qquad (9.6\text{-}3)$$

For the case in which the aircraft track and the signal propagation differ in direction by an angle, θ, Eq. 9.2-3 becomes

$$\phi_2' - \phi_1' = k\,(r_2 - r_1)\cos\theta$$

This result, coupled with Eq. 9.6-3 yields

$$k\,(r_2 - r_1)\cos\theta = 1.05. \qquad (9.6\text{-}4)$$

Since the wave number, k, may be approximated by the free-space wave number, k_0, and $\theta = 45°$, Eq. 9.6-4 becomes

$$r_2 - r_1 = 1.05 \,/\, \left(k_0 \,/\, \sqrt{2}\right).$$

k_0 is just the reciprocal of the free-space wavelength (computed in (b)), so that Eq. 9.6-5 becomes

$$r_2 - r_1 = 1.05 \cdot (29.3915 \text{ km}) \cdot \sqrt{2} = 43.64 \text{ km}$$

9.6.2 Problems to be Solved by Student

1. Suppose a receiver and a transmitting station (both on the surface of a spherical earth) have an angular separation of 60°.

   a. What is the angular separation in radians?

   b. If the radius of the spherical earth is assumed to be 6367 km, what is the distance (in km) between the transmitting station and receiver over the surface of the earth? This is the path length.

   If the station transmits 12 kHz signals,

   c. Find the wavelength of the signals.

   d. Find the free space wave number for the signals.

   e. Find the nominal wave number for the signals.

f. What is the nominal value of the cumulative phase at the receiver?

g. If, at a given time, the exact PPC is known to be zero, what is the observed value (in principle) of the cumulative phase at the receiver?

The cumulative phase can be separated into an integer part and a fractional part.

h. Which part can be measured by a conventional Omega receiver that is phase-synchronized to the transmitted signal?

2. Suppose a researcher wishes to add a set of sub-models describing the effects of a Sudden Ionospheric Disturbance (SID) to the 1993 PPC Model.

a. To which path domain would these sub-models primarily apply?

b. Would other path domains be affected?

An SID effectively depresses the daytime ionosphere, thus making the path even more "day-like" than normal. Assume that the functional form is taken to be a constant and the linear model coefficient is positive.

c. As a term in the expression for predicted phase, what is the sign of the resulting sub-models?

d. Assuming the sub-models only apply to segments having ground conductivity levels of 7 and 10, how many sub-models would be needed?

9.7 ABBREVIATIONS/ACRONYMS

ADI	Anomalous Data Identification
D-region	Ionospheric layer 70 to 90 km above the earth's surface from which Omega/VLF signals are scattered/reflected
FPII	First Point of Ionospheric Interaction
kHz	Kilohertz
km	Kilometer
LF	Low Frequency
LOP	Line of Position
LPII	Last Point of Ionospheric Interaction
MASTERFILE	A master database of phase and phase-difference measurements resident at ONSCEN
MPSZA	Maximum Path Solar Zenith Angle
NCCOSC	Naval Command, Control and Ocean Surveillance Center

NID	Normal Illumination Depression
ONSOD	Omega Navigation System Operations Detail
ONSCEN	Omega Navigation System Center
ORTP	(Sunrise/Sunset) Onset/Recovery Time Parameter
PCD	Polar Cap Disturbance
PPC	Propagation Correction
RMS	Root Mean Squared
SID	Sudden Ionospheric Disturbance
SNR	Signal-to-noise ratio
SVD	Single-valued Decomposition
TM	Transverse Magnetic (waveguide mode)
UT	Universal Time (short for UTC)
UTC	Coordinated Universal Time
VLF	Very Low Frequency
WGS-72	World Geodetic Spheroid reference published in 1972
WGS-84	World Geodetic Spheroid reference published in 1984

9.8 REFERENCES

1. Pierce, J., The Use of Composite Signals at Very Low Radio Frequencies, Harvard University Engineering and Applied Physics Division Technical Report 552, February 1968.

2. Pierce, J., Palmer, W., Watt, A., and Woodward, R., Omega: A Worldwide Navigational System, System Specification and Implementation, Second Edition, Prepared for the U.S. Navy Department, Bureau of Ships and submitted through the Office of Naval Research, Published by Pickard & Burns Electronics, Waltham, MA, May 1966.

3. Swanson, E., and Brown, R., Omega Propagation Prediction Primer, NELC Technical Note TN 2102, 1972.

4. Morris, P., and Cha, M., Omega Propagation Corrections: Background and Computational Algorithm, Report No. ONSOD 01-74, December 1974.

5. Morris, P., and Swanson, E., New coefficients for the Swanson propagation correction model, *Proceedings of the Fifth Annual Meeting of the International Omega Association*, Bergen, Norway, August 1980.

6. Swanson, E., Long-term variations in Omega signals, *Proceedings of the Fourteenth Annual Meeting of the International Omega Association*, Long Beach, CA, October 1989.

7. Wenzel, CAPT R., McManus, H., Casswell, R., and Vannicola, V., The 1980 Omega PPC Model time term should not be used, *Proceedings of the Fifteenth Annual Meeting of the International Omega Association*, Sanur, Bali, Indonesia, September 1990.

8. Morris, P. and Gupta, R., New Approach to Omega PPCs, Report No. CG-ONSCEN-03-89, November 1989.

9. Tolstoy, A., New coefficients for the Swanson PPC Model as utilized by Omega at 10.2 kHz, Report No. ONSOD-01-76, October 1976.

10. Morris, P., 1990 PPC Model Calibration for 10.2 kHz Signals, Report No. CG-ONSCEN-01-92, February 1992.

11. Swanson, E. and Bradford, W., Diurnal Phase Variation at 10.2 kHz, NELC TR 1781, August 1971.

12. Banks, P. and Kockarts, G., *Aeronomy (Parts A and B)*, Academic Press, New York, 1973.

13. Vannicola, V., Private Communication, October, 1991.

14. Watt, A., *VLF Radio Engineering*, Pergamon Press, Oxford, 1967.

15. Morris, P., Omega System Availability as a Global Measure of Navigation Accuracy, Report No. CG-ONSCEN-05-90, September 1990 (National Technical Information Service No. ADA 229492).

16. Gupta, R., Creamer, P., and Morris, P., Assessment of Omega phase-difference errors, *Proceedings of the Seventh Annual Meeting of the International Omega Association*, Arlington, VA, USA, October 1982.

17. Levine, P., Tests of a simple Omega phase model including solar flare effects, *Proceedings of the Fifth Annual Meeting of the International Omega Association*, Bergen, Norway, August 1980.

18. Maenpa, J., The 1985 Magnavox Omega phase propagation correction model, *Proceedings of the Tenth Annual Meeting of the International Omega Association*, Brighton, U.K., July 1985.

19. Pierce, J.A., Annual Progress Report #60, Havard Craft Laboratory, July 1961.

20. Morris, P.B., Calibration of the 1992 PPC Model at 10.2 kHz, TASC Technical Information Memorandum TIM-5919-22, March 1993.

21. Morris, P.B., Preparation of the PPC93 Calibration Database, TASC Technical Information Memorandum TIM-6989-1-1, October 1993.

22. Morris, P.B., PPC93 Calibration, TASC Technical Engineering Memorandum EM 2979, November 1993.

23. Morris, P.B., 1993 PPC Model Prediction Performance Evaluation, TASC Engineering Memorandum EM-2980, January 1994.

24. Morris, P.B., and Van Ruitenbeek, A.J., Calibration of the 1992 Omega PPC propagation correction model at 10.2 kHz. In *Proceedings of the Seventeenth Annual Meeting, International Omega Association*, Amsterdam, Netherlands, August 1992.

25. Casswell, R.M., and Morris, P.B., Calibration of the 1993 Omega propagation correction model. In *Proceedings of the Eighteenth Annual Meeting, International Navigation Association*, Orlando, FL, October 1993.

26. Morris, P.B., and Casswell, R.M., Evaluation of the 1993 Omega propagation correction model, *Proceedings of the 1994 Position, Location, and Navigation Symposium (PLANS '94)*, Las Vegas, NV, April 1994.

27. Morris, P.B., 1993 PPC Prediction Program (PPC93) User Guide, TASC Technical Information Memorandum TIM-6989-2-1, December 1993.